Combined Psychophysical and Neurophysiological Tools for Mechanism-Based Observation of

Impaired Nociceptive Processing

Boudewijn van den Berg

Combined Psychophysical and Neurophysiological Tools for Mechanism-Based Observation of Impaired Nociceptive Processing

Gecombineerde psychofysische en neurofysiologische technieken voor mechanisme-gebaseerde observatie van disfunctionele nociceptieve verwerking

Boudewijn van den Berg

This work was supported by the Netherlands Organisation for Scientific Research (NWO) through the NOCICEPT project, which is part of the NeuroCIMT Perspectief Programme (NWO project number: 14905). The work was carried out at:

UNIVERSITY OF TWENTE. | TECHMED CENTRE

Chair Biomedical Signals and Systems
Faculty of Electrical Engineering,
Mathematics and Computer Science
University of Twente, the Netherlands

Cover: Boudewijn van den Berg, using neural style transfer (Golnaz Ghiasi, Honglak Lee, Manjunath Kudlur, Vincent Dumoulin, Jonathon Shlens. Exploring the structure of a real-time, arbitrary neural artistic stylization network. Proceedings of the British Machine Vision Conference, 2017.).

Back: Photograph by Marieke Bosman.

Printed by: Ipskamp Printing B.V.
Layout: Boudewijn van den Berg
ISBN: 978-90-365-5354-4
DOI: 10.3990/1.9789036553544

For access to the digital version of this book, scan the QR-code.

Combined Psychophysical and Neurophysiological Tools for Mechanism-Based Observation of Impaired Nociceptive Processing

DISSERTATION

to obtain
the degree of doctor at the Universiteit Twente,
on the authority of the rector magnificus,
prof. dr. ir. A. Veldkamp,
on account of the decision of the Doctorate Board
to be publicly defended
on Friday 3 June 2022 at 16:45 hours

by

Boudewijn van den Berg

born on the 8th of January, 1993

in Gouda, The Netherlands

This dissertation has been approved by:

Supervisors

dr. ir. Jan R. Buitenweg

prof. dr. ir. Peter H. Veltink

Graduation committee:

Chair/Secretary

prof. dr. J. N. Kok	University of Twente

Supervisors

dr. ir. Jan R. Buitenweg	University of Twente
prof. dr. ir. Peter H. Veltink	University of Twente

Committee Members

prof. dr. ir. M. J. A. M. van Putten	University of Twente
prof. dr. R. J. A. van Wezel	University of Twente
prof. dr. A. Mouraux	Catholic University of Leuven
C. D. Mørch MSc PhD	Aalborg University

Contents

Summary

Pain has an enormous impact on patients with chronic pain. Under healthy conditions, pain is caused by the activation of nociceptive Aδ- and C-fibers following actual or potential tissue damage. The nociceptive signal reaches the brain following transmission by secondary and tertiary neurons in the dorsal horn and the thalamus. Transmission of this signal can be facilitated or inhibited in the dorsal horn by top-down control. The combined activation of sensory-discriminative and emotional-affective brain areas by the nociceptive input signal creates the experience of pain. Patients with chronic neuropathic pain experience pain as a result of spontaneous activity and associated sensitization of neurons in the nociceptive system. Patients with chronic nociplastic pain experience pain as a result of sensitization and decreased inhibition of neurons in the nociceptive system.

Diagnosis of nociplastic pain is complicated and usually takes several years. Treatment of neuropathic and nociplastic pain is challenging and relief is often not sufficient. A mechanism-based approach could enable early diagnosis and effective treatment of neuropathic, nociplastic and mixed pain patients. Therefore, the goal of this thesis is 'to develop combined psychophysical and neurophysiological tools for mechanism-based observation of impaired nociceptive processing'. The strategy in this thesis is to combine psychophysical methods with neurophysiological techniques to provide mechanism-based information on nociceptive function.

Part I of this thesis describes the technical development and exploration of a method to observe nociceptive processing using intra-epidermal electric detection thresholds and evoked potentials. This is implemented by combining an adaptive psychophysical method of limits to measure the detection threshold with intra-epidermal stimulation for preferential stimulation of nociceptive afferents, and an EEG recording setup to measure cortical activity evoked by stimulation. To differentially activate peripheral and central mechanisms, single- and double-pulse electric stimuli are used with one or more settings for inter-pulse interval.

In **Chapter 2,** a single-trial EEG approach based on linear mixed regression is outlined to analyze the effect of stimulus properties on the evoked potential while accounting for between-subject variability, potential threshold drift and habituation. Importantly, this chapter provided a method to analyze evoked brain activity during measurement of nociceptive detection thresholds using an adaptive psychophysical algorithm, by incorporating all potentially confounding trial parameters into a single linear mixed model.

In **Chapter 3,** the combination of intra-epidermal detection probability and evoked potentials is measured in healthy participants to study feasibility of the method. Relations between intra-epidermal stimulus properties, detection thresholds and evoked potentials are explored using linear mixed regression. It is found that both outcomes are modulated by stimulus properties such as stimulus amplitude, number of pulses and the number of received stimuli. These observations suggest that we might quantify aspects of nociceptive processing, by measuring the effect of stimulus properties on detection probability and evoked brain activity.

The same method is used in **Chapter 4** to accurately quantify nociceptive system behavior using these outcomes in a large group of healthy subjects. The objectives are to study 1) which peaks are present in brain activity evoked by intra-epidermal electric stimulation, 2) the influence of filter settings on these peaks and their topography, 3) at which electrodes these peaks have the largest signal-to-noise ratio (SNR), 4) the number of trials required to achieve an acceptable SNR of these peaks and 5) the effect of intra-epidermal stimulus properties on both outcomes. This study allows us to explore how we might improve observation of intra-epidermal detection thresholds and evoked potentials and provides reference values for the effect of intra-epidermal stimulus properties on both outcomes in a healthy population. The workflow for the experiment and analysis developed in Chapter 4 provides the basis for subsequent clinical studies.

Part II of this thesis describes the exploration of feasibility and utility of this method in a clinical setting. In **Chapter 5,** this method is used in a sleep deprivation study at the Centre for Human Drug Research (Leiden, the

Netherlands) to study if intra-epidermal detection probability and evoked potentials can be used to identify and quantify altered nociceptive processing following sleep deprivation. Observation of altered nociceptive detection thresholds and evoked potentials following sleep deprivation in male and female populations shows that it is feasible to evaluate impaired nociceptive processing following sleep deprivation in a human population based on intra-epidermal detection thresholds and evoked potentials, while taking into consideration that most effects are sex-dependent and can only be observed in either a male or a female population.

In **Chapter 6**, this method is used to evaluate the feasibility of measuring intra-epidermal detection probability and evoked potentials in a group of patients with failed back surgery syndrome (FBSS) and a control group of healthy participants at the St. Antonius Hospital (Nieuwegein, the Netherlands). This first hospital study shows the applicability of the method in a dysfunctional nociceptive system, and the ability to observe altered nociceptive detection thresholds and evoked potentials in FBSS patients. The strongly increased nociceptive detection thresholds and reduced contribution of the pulse amplitude to the evoked potential implies that it is possible observe clinically relevant alterations of nociceptive function, which is a crucial step toward mechanism-based monitoring.

In **Chapter 7**, psychophysical and EEG features from healthy controls and FBSS patients are combined using machine learning methods to study which combination of outcomes is most effective for identifying impaired nociceptive processing in FBSS. It is found that mostly the psychophysical features (i.e., detection thresholds and psychometric slopes) contribute to classification, with only marginal gains by adding EEG features for classification, indicating that the information included in EEG data is mostly redundant with the psychophysical data. In summary, it is shown in Part II that it is possible to simultaneously measure intra-epidermal evoked potentials, detection thresholds and the effect of stimulus properties on both outcomes in a clinical setting, and that we might use these outcomes for the observation of impaired nociceptive processing. Nevertheless, it remains unclear how potential

impairment of nociceptive processing mechanism might be reflected in those outcomes.

Part III of this thesis describes the first steps in our exploration how intra-epidermal electric detection thresholds and evoked potentials could be interpreted, and how they might be used to identify impaired mechanisms in the nociceptive system. **Chapter 8** investigates if nociceptive detection thresholds and evoked potentials are biased by a response criterion, by comparison of detection thresholds measured using an adaptive Go-/No-Go (GN) procedure and using an adaptive 2-Interval Forced Choice (2IFC) procedure. It is found that the response criterion could have a major influence on stimulus detection behavior. The average P2 evoked potential is proportional to detection probability and shows dichotomous behavior with respect to stimulus detection, indicating that during these experiments, the P2 reflects conscious stimulus perception rather than the presence of sensory evidence itself. The notion that we can measure the potential influence of a perceptual criterion by comparing detection thresholds using a GN and a 2IFC procedure opens new avenues of research into the role of perception in nociceptive processing and (chronic) pain.

In **Chapter 9**, a theoretical framework to model detection behavior is presented. The detection probability is expressed as a function of a time-varying response criterion, a system impulse response function and spontaneous neural activity. Implications of this framework are 1) that the difference between the detection probability of single- and double-pulse stimuli can be used to probe the system impulse response function at several intervals and 2) that the absolute amplitude of psychometric parameters can inform us about the presence and amplitude of spontaneous neurophysiological activity. Retrospective analysis of data from FBSS patients in this chapter suggests that spontaneous neurophysiological activity is a potential explanation for the increased nociceptive detection thresholds and decreased psychometric slopes in patients.

Part IV of this thesis describes new techniques which could improve identification of impaired nociceptive processing in future projects. In **Chapter**

10 it is shown that we can use the phenomenon that conscious perception of a stimulus is associated with a P2 evoked potential, to measure perceptual thresholds based on brain activity. A deep neural network is used to perform a 2-interval forced choice procedure to determine which of two EEG intervals included evoked brain activity. The perceptual thresholds estimated using this procedure are similar to the thresholds estimated based on participant report. Further development of this method could lead to a procedure that is immune to potential simulation of symptoms and suitable for patients that are unable to reliably communicate their perception.

With the aims of reducing the influence of stimulus salience and perception and getting a larger SNR from sensory brain areas, **Chapter 11** introduces a novel approach to measure the nociceptive steady-state evoked potential (SSEP) based on frequency modulation of a series of intra-epidermal pulses. Multisine frequency modulation at frequencies of 3, 7 and 13 Hz elicits associated brain activity at the same frequencies. Further investigation in **Chapter 12** shows that multisine modulation of intra-epidermal pulses results in an activation at the fundamental stimulation frequencies in the secondary somatosensory cortex and potentially the primary somatosensory cortex. These results suggest that nociceptive SSEPs in response to intra-epidermal electric stimulation could be used to study activation of sensory-discriminative brain areas in response to a tonic nociceptive stimulus. The technique of evoking SSEPs in response to multisine modulated intra-epidermal stimulation provides a new method to study the neural processing from a neural firing rate in peripheral nociceptive afferents to an evoked cortical potential.

To conclude, the studies presented in this thesis show that the combined observation of intra-epidermal detection thresholds and evoked potentials allows for the observation of impaired nociceptive processing. Novel technologies that were invented during this thesis are still in a low technology readiness level but can aid observation of impaired nociceptive processing in future scientific and clinical applications.

Samenvatting

Pijn heeft een enorme impact op patiënten met chronische pijn. Onder gezonde omstandigheden wordt pijn veroorzaakt door de activering van nociceptieve Aδ- en C-vezels na feitelijke of potentiële weefselbeschadiging. Het nociceptieve signaal bereikt de hersenen na overdracht door secundaire en tertiaire neuronen in de dorsale hoorn en de thalamus. Transmissie van dit signaal kan worden vergemakkelijkt of geremd in de dorsale hoorn door top-down controle vanuit de hersenen. De gecombineerde activering van sensorisch-discriminerende en emotioneel-affectieve hersengebieden door het nociceptieve signaal creëert de ervaring van pijn. Patiënten met chronische neuropathische pijn ervaren pijn als gevolg van spontane activiteit en bijbehorende sensitisatie van neuronen in het nociceptieve systeem. Patiënten met chronische nociplastische pijn ervaren pijn als gevolg van sensitisatie en verminderde inhibitie van neuronen in het nociceptieve systeem.

Diagnose van nociplastische pijn is gecompliceerd en duurt meestal enkele jaren. Behandeling van neuropathische en nociplastische pijn is een uitdaging en de pijnverlichting is vaak niet toereikend. Een mechanisme-gebaseerde benadering zou een vroege diagnose en effectieve behandeling van neuropathische, nociplastische en gemengde pijnpatiënten mogelijk maken. Het doel van dit proefschrift is daarom 'het ontwikkelen van gecombineerde psychofysische en neurofysiologische technieken voor mechanisme-gebaseerde observatie van disfunctionele nociceptieve verwerking'. De strategie in dit proefschrift is om psychofysische methoden te combineren met neurofysiologische technieken om mechanisme-gebaseerde informatie over de nociceptieve functie te verschaffen.

Deel I van dit proefschrift beschrijft de technische ontwikkeling en verkenning van een methode om nociceptieve verwerking te observeren met behulp van intra-epidermale elektrische detectiedrempels en elektrische hersenactiviteit. Dit wordt gedaan door een adaptieve psychofysische methode om de detectiedrempel te meten te combineren met intra-epidermale stimulatie voor preferentiële stimulatie van nociceptieve zenuwvezels, en een EEG opstelling

om corticale activiteit te meten die wordt opgewekt door stimulatie. Om perifere en centrale mechanismen differentieel te activeren, worden elektrische stimuli met enkele en dubbele pulsen gebruikt met een of meerdere verschillende intervallen tussen beide pulsen.

In **Hoofdstuk 2** wordt een single-trial EEG techniek beschreven om het effect van stimuluseigenschappen op elektrische hersenactiviteit te analyseren, rekening houdend met variabiliteit tussen proefpersonen, potentiële verandering over de tijd, en gewenning. Belangrijk is dat dit hoofdstuk een methode biedt om de hersenactiviteit die wordt opgewekt tijdens het meten van nociceptieve detectiedrempels te analyseren, door alle relevante parameters op te nemen in een enkel lineair mixed model.

In **Hoofdstuk 3** wordt de combinatie van intra-epidermale detectiekans en hersenactiviteit gemeten bij gezonde deelnemers om de haalbaarheid van de methode te bestuderen. De relaties tussen intra-epidermale stimuluseigenschappen, detectiedrempels en elektrische hersenactiviteit worden onderzocht met behulp van lineaire mixed regressie. Het blijkt dat beide uitkomsten worden gemoduleerd door stimuluseigenschappen zoals stimulus amplitude, aantal pulsen en het aantal reeds ontvangen stimuli. Deze observaties suggereren dat we aspecten van nociceptieve verwerking kunnen kwantificeren door het effect van stimuluseigenschappen op detectiekans en elektrische hersenactiviteit te meten.

Dezelfde methode wordt in **Hoofdstuk 4** gebruikt om het gedrag van het nociceptieve systeem nauwkeurig te kwantificeren bij een grote groep gezonde proefpersonen. De doelstellingen zijn om te bestuderen 1) welke pieken aanwezig zijn in de hersenactiviteit die wordt opgewekt door intra-epidermale elektrische stimulatie, 2) de invloed van filterinstellingen op deze pieken en hun topografie, 3) bij welke elektroden deze pieken de grootste signaal-ruisverhouding hebben, 4) het aantal stimuli dat nodig is om een acceptabele signaal-ruisverhouding van deze pieken te bereiken en 5) het effect van intra-epidermale stimuluseigenschappen op beide uitkomsten. Deze studie stelt ons in staat om te onderzoeken hoe we de observatie van intra-epidermale detectiedrempels en elektrische hersenactiviteit kunnen verbeteren, en biedt

referentiewaarden voor het effect van intra-epidermale stimuluseigenschappen op beide uitkomsten in een gezonde populatie. De workflow voor het experiment en de analyse ontwikkeld in **Hoofdstuk 4** vormt de basis voor latere klinische studies.

Deel II van dit proefschrift beschrijft de verkenning van de haalbaarheid en bruikbaarheid van deze methode in een klinische omgeving. In **Hoofdstuk 5** wordt deze methode gebruikt in een slaapdeprivatiestudie van het Centre for Human Drug Research in Leiden om te onderzoeken of intra-epidermale detectiekans en hersenactiviteit kunnen worden gebruikt om veranderde nociceptieve verwerking na slaapdeprivatie te identificeren en te kwantificeren. Observatie van veranderde nociceptieve detectiedrempels en hersenactiviteit na slaapdeprivatie bij mannelijke en vrouwelijke populaties toont aan dat het haalbaar is om een disfunctionele nociceptieve verwerking na slaapdeprivatie in een menselijke populatie te evalueren op basis van intra-epidermale detectiedrempels en hersenactiviteit, rekening houdend met het feit dat de meeste effecten geslachtsafhankelijk zijn en alleen kunnen worden waargenomen bij een mannelijke of een vrouwelijke populatie.

In **Hoofdstuk 6** wordt deze methode gebruikt om de haalbaarheid te evalueren van het meten van intra-epidermale detectiekans en hersenactiviteit in een groep patiënten met Failed Back Surgery Syndrome (FBSS) en een controlegroep van gezonde deelnemers in het St. Antonius Ziekenhuis in Nieuwegein. Deze eerste ziekenhuisstudie toont de toepasbaarheid van deze methode in een disfunctioneel nociceptief systeem aan en demonstreert het vermogen van deze methode om veranderde nociceptieve detectiedrempels en hersenactiviteit bij FBSS patiënten te observeren. De sterk verhoogde nociceptieve detectiedrempels en verminderde bijdrage van de puls amplitudes aan de geobserveerde hersenactiviteit impliceert dat het mogelijk is om klinisch relevante veranderingen van de nociceptieve functie waar te nemen, wat een cruciale stap is in de richting van mechanisme-gebaseerde monitoring.

In **Hoofdstuk 7** worden psychofysische en EEG kenmerken van gezonde controles en FBSS patiënten gecombineerd met behulp van machine learning methoden om te bestuderen welke combinatie van uitkomsten het meest

effectief is voor het identificeren van disfunctionele nociceptieve verwerking in FBSS patiënten. Het blijkt dat vooral de psychofysische kenmerken (d.w.z. detectiedrempels en de helling van de psychometrische functie) bijdragen aan classificatie, met slechts marginale winsten door EEG kenmerken toe te voegen aan de classificatie, wat aangeeft dat de informatie in EEG kenmerken grotendeels redundant is met de informatie in de psychofysische kenmerken. Samenvattend, wordt in deel II aangetoond dat het mogelijk is om gelijktijdig intra-epidermale detectiedrempels en hersenactiviteit en het effect van stimuluseigenschappen op beide uitkomsten in een klinische omgeving te meten, en dat we deze uitkomsten kunnen gebruiken voor de observatie van disfunctionele nociceptieve verwerking. Desalniettemin blijft het onduidelijk hoe veranderde intra-epidermale detectiedrempels en hersenactiviteit geïnterpreteerd kunnen worden in termen van mechanismen in het nociceptieve systeem.

Deel III van dit proefschrift beschrijft de eerste stappen in onze verkenning hoe intra-epidermale detectiedrempels en hersenactiviteit kunnen worden geïnterpreteerd, en hoe ze kunnen worden gebruikt om verstoorde mechanismen in het nociceptieve systeem te identificeren. **Hoofdstuk 8** onderzoekt of nociceptieve detectiedrempels en hersenactiviteit beïnvloed worden door een responscriterium, door vergelijking van detectiedrempels gemeten met behulp van een adaptieve Go-/No-Go (GN) procedure en met behulp van een adaptieve 2-Interval Forced Choice (2IFC) procedure. Het blijkt dat het responscriterium een grote invloed kan hebben op de gerapporteerde stimulusdetectie. De grootste positieve piek in hersenactiviteit, de P2, is evenredig met de detectiekans en vertoont dichotoom gedrag met betrekking tot stimulus detectie, wat aangeeft dat tijdens deze experimenten de P2 bewuste perceptie weerspiegelt in plaats van de aanwezigheid van sensorische hersenactiviteit zelf. Het idee dat we de potentiële invloed van een perceptie criterium kunnen meten door detectiedrempels te vergelijken met behulp van een GN- en een 2IFC-procedure, opent nieuwe mogelijkheden voor onderzoek naar de rol van perceptie bij nociceptieve verwerking en (chronische) pijn.

In **Hoofdstuk 9** wordt een theoretisch raamwerk gepresenteerd om detectiegedrag te modelleren. De detectiekans wordt uitgedrukt als een

functie van een in de tijd variërend responscriterium, een impulsresponsie en spontane neurale activiteit. Implicaties van dit raamwerk zijn 1) dat het verschil tussen de detectiekans van enkele en dubbele puls stimuli kan worden gebruikt om de impulsresponsie van het systeem op verschillende momenten te onderzoeken en 2) dat de absolute amplitude van psychometrische parameters ons kan informeren over de aanwezigheid en amplitude van spontane neurofysiologische activiteit. Retrospectieve analyse van de gegevens van FBSS patiënten suggereert dat spontane neurofysiologische activiteit een mogelijke verklaring is voor de verhoogde nociceptieve detectiedrempels en verminderde helling van de psychometrische functie bij patiënten.

Deel IV van dit proefschrift beschrijft nieuwe technieken die de objectieve identificatie van disfunctionele nociceptieve verwerking zouden kunnen verbeteren. In **Hoofdstuk 10** wordt aangetoond dat we het fenomeen dat bewuste perceptie van een stimulus geassocieerd is met een P2 piek in de hersenactiviteit, kunnen gebruiken om perceptuele drempels te meten op basis van hersenactiviteit. Een diep neuraal netwerk wordt gebruikt om een 2-IFC procedure uit te voeren, waarin het neurale netwerk bepaalt welke van twee EEG intervallen de hersenactiviteit in reactie op een nociceptieve stimulus bevat. De perceptuele drempels die met deze procedure worden geschat, zijn vergelijkbaar met de drempels die worden geschat op basis van gerapporteerde stimulus perceptie. Verdere ontwikkeling van deze methode zou kunnen leiden tot een procedure die immuun is voor mogelijke simulatie van symptomen en geschikt is voor patiënten die hun perceptie niet betrouwbaar kunnen communiceren.

Met het doel om de invloed van stimulus salience te verminderen en om activiteit uit sensorische hersengebieden te kunnen meten met een hogere signaal-ruisverhouding introduceert **Hoofdstuk 11** een nieuwe techniek, waarin we nociceptieve steady-state hersenactiviteit opwekken en meten door middel van frequentiemodulatie van een reeks intra-epidermale pulsen. Frequentiemodulatie met meerdere sinussen bij frequenties van 3, 7 en 13 Hz wekt bijbehorende hersenactiviteit op dezelfde frequenties op. Verder onderzoek in **Hoofdstuk 12** laat zien dat frequentiemodulatie van intra-epidermale pulsen met een multisinus resulteert in een activatie van de

fundamentele stimulatiefrequenties in de secundaire somatosensorische cortex en mogelijk ook de primaire somatosensorische cortex. Deze resultaten suggereren dat steady-state hersenactiviteit opgewekt door middel van intra-epidermale elektrische stimulatie kan worden gebruikt om activering van sensorisch-discriminerende hersengebieden te bestuderen in reactie op een tonische nociceptieve stimulus. Deze techniek biedt een nieuwe methode om nociceptieve verwerking te bestuderen van een neurale vuursnelheid in perifere nociceptieve zenuwvezels tot opgewekte corticale hersenactiviteit.

In conclusie, laten de studies gepresenteerd in dit proefschrift zien dat de gecombineerde observatie van intra-epidermale detectiedrempels en hersenactiviteit het mogelijk maakt om disfunctionele nociceptieve verwerking te observeren. Nieuwe technologieën die tijdens dit proefschrift zijn ontwikkeld, bevinden zich nog in een laag Technology Readiness Level, maar kunnen helpen bij het observeren van disfunctionele nociceptieve verwerking in toekomstige wetenschappelijke en klinische toepassingen.

Artist's impression of low back pain, drawn in the style of Amadeo de Souza-Cardoso using neural style transfer.

Chapter 1

General Introduction

"What is your friend: the things you know, or the things you don't know. First of all, there's a lot more things you don't know. And second, the things you don't know is the birthplace of all your new knowledge! So if you make the things you don't know your friend, rather than the things you know, well then you're always on a quest in a sense. You're always looking for new information in the off chance that somebody who doesn't agree with you will tell you something you couldn't have figured out on your own! It's a completely different way of looking at the world. It's the antithesis of opinionated."

Jordan B. Peterson

This dissertation is about the development of combined psychophysical and neurophysiological tools for mechanism-based observation of impaired nociceptive processing in patients with chronic pain. At least 10% of the world's population suffers from chronic pain (Jackson, Stabile, & McQueen, 2014), which is often caused by maladaptive nociceptive processing mechanisms. Clinicians struggle to select treatments and monitor progress, as it is difficult to observe the underlying mechanisms that generate pain in individual chronic pain patients, and hard to measure the effect of treatments on these mechanisms. In particular, it remains difficult to selectively activate the part of the nervous system involved in nociceptive processing and pain, and identify maladaptive nociceptive processing based on quantitative outcome measures. These measures are often biased by temporary psychological states and therefore inadequate for observing the underlying physiological mechanisms of chronic pain. The development of new tools for researchers and clinicians to observe mechanisms that underly the generation of chronic pain in individual patients can support early diagnosis and effective treatment.

This introduction starts by discussing the processes that generate pain, and potential mechanisms underlying chronic pain. The methods that are currently available to study maladaptive nociceptive processing in chronic pain are reviewed, to arrive at a more accurate description of the challenges for this project. Subsequently, the starting points that were available to support the development of tools for observation of maladaptive nociceptive processing at the start of this project are described, to arrive at a strategy for solving these challenges.

1.1 Nociception and Pain

1.1.1 Pain

Pain is defined as "an unpleasant sensory and emotional experience associated with, or resembling that associated with, actual or potential tissue damage" (Raja et al., 2020). For clinical and scientific purposes, pain is subdivided by the International Association for the Study of Pain (IASP) in three classes: nociceptive, neuropathic and nociplastic pain. Almost all of us have experienced nociceptive pain, which is pain arising from actual or potential tissue damage and plays a crucial role in protecting the body. In fact, the rare group of people born without sensitivity to nociceptive pain often dies at a young age due to illnesses and injuries that go unnoticed (Linton, 2005).

For the two other types, neuropathic and nociplastic pain, the functional relevance for survival is less evident. Neuropathic pain is caused by damage to the nociceptive or somatosensory system, resulting in a projected sensation of pain in the body parts innervated by the affected nerves (Jensen et al., 2011). Nociplastic pain is caused by altered nociception with no evidence of actual or threatened tissue damage or evidence for disease or lesion of the somatosensory system and was often labeled as neuropathic pain until recently (Kosek et al., 2016). Both types of pain remain poorly understood and often play a major role in long recurring episodes of pain, persisting past normal healing time.

1.1.2 Chronic Pain

When pain persists or recurs for more than 3 to 6 months, this pain is usually regarded as chronic pain (Merskey, 1986; Treede et al., 2015). It is estimated that each year about one out of ten people develops chronic pain (Jackson, Stabile, & McQueen, 2014), and that chronic pain accounts for 15% to 20% of physician visits (Koleva, Krulichova, Bertolini, Caimi, & Garattini, 2005; Mäntyselkä et al., 2001). The economic impact of chronic pain is large due to absenteeism and risk of leaving the labor market (Phillips, 2009). For example, it was estimated that 1 million working days are lost annually in Denmark due

to chronic pain (Eriksen, Sjøgren, Bruera, Ekholm, & Rasmussen, 2006) and that $61 billion per year is lost in productivity due to common pain conditions in the US alone (Stewart, Ricci, Chee, Morganstein, & Lipton, 2003). The source of chronic pain can be mainly nociceptive in nature, but is in many cases neuropathic (e.g. spinal cord injury, carpal tunnel syndrome, multiple sclerosis, HIV, diabetic polyneuropathy, sarcoidosis), nociplastic (e.g. fibromyalgia, complex regional pain syndrome) (Cohen, Vase, & Hooten, 2021), or a combination of both (also known as mixed pain). Chronic pain remains difficult to treat and about 40% of chronic pain patients receives inadequate treatment for the pain (Breivik, 2006). Treatments for chronic pain with a neuropathic and nociplastic origin are often ineffective as the underlying mechanisms are poorly understood. Observation of nociceptive processing before and during treatment can improve our understanding of underlying mechanisms and the development of effective new treatments. In the next sections, the basic mechanisms of nociception and pain, and potential mechanisms of chronic pain are briefly discussed. Note that the content is certainly not exhaustive but focuses on the theory and ideas relevant for this thesis. Note that a more comprehensive overview of what is currently known about nociception and pain can be found in Wall and Melzack's Textbook of Pain 6th Edition (McMahon, Koltzenburg, Tracey, & Turk, 2013).

1.1.3 Neurophysiology of Pain

Nociceptive pain starts with the activation of peripheral nociceptive nerve fibers categorized as C- and Aδ-fibers. The unmyelinated C-fibers respond to thermal, mechanical, and chemical stimuli and are therefore considered polymodal. The myelinated Aδ-fibers are either polymodal (Type I) or sensitive to thermal and chemical stimuli (Type II) (Ringkamp, Raja, Campbell, & Meyer, 2013). These nociceptive nerve fibers are located in the skin in the epidermis, but also in the corneas, mucosa, and a variety of organs. The conduction velocity of Aδ-fibers is fast (Type I: 25-55 m/s, Type II: around 15 m/s) while the conduction velocity of C-fibers is slow (around 1 m/s). As a result, activation of Aδ-fibers rapidly results in a sharp pricking sensation, while the activation of C-fibers results in a slow burning sensation (Obi et al., 2007). A third type of nerve

fiber in the skin is the thickly myelinated Aβ-fiber which is even faster than Aδ-fibers (33-75 m/s) (Siegel & Sapru, 2005). Activation of these Aβ-fibers results in tactile sensations and can lead to inhibition of surrounding Aδ-fibers, known as gate-control (Wall, 1978).

The cell bodies of C-, Aδ- and Aβ-fibers in the skin are located in the dorsal root ganglia close to the spinal cord. Incoming signals from nociceptive C-, Aδ- and Aβ-fibers in the skin are transmitted by these nerve cells towards the dorsal horn in the spinal cord. The Aβ-fibers have a quick connection to the thalamic nuclei via the dorsal column-medial lemniscus pathway (Nosek, 1998). A part of the Aδ- and Aβ-fibers terminate together at wide-dynamic-range (WDR) neurons in lamina I and V of the dorsal horn. The Aδ-fibers also terminate at nociceptive specific neurons located mostly in lamina I and V. C-fibers terminate at nociceptive specific neurons located mostly in in lamina I and II (Todd & Koerber, 2013). The majority of these wide-dynamic-range and nociceptive specific neurons project towards the thalamic nuclei via the spinothalamic tract (for more details, see (Dostrovsky & Craig, 2013)). The thalamus works as a relay station, directing the flow of information from the spinal cord to the brain areas designated for processing of the incoming information.

A majority of studies suggest that somatosensory processing in the brain has a serial organization, where somatosensory information from the thalamus arrives sequentially at the primary somatosensory cortex (SI), secondary somatosensory cortex (SII), and the insular and anterior cingulate cortex (IC and ACC) (de Haan & Dijkerman, 2020; Hu, Zhang, & Hu, 2012; Inui, Wang, Tamura, Kaneoke, & Kakigi, 2004; Pons, Garraghty, Friedman, & Mishkin, 1987). In contrast, some studies suggest that nociceptive processing might be organized in parallel. While some thalamic nuclei are thought to project in parallel to the SI and SII (Liang, Mouraux, & Iannetti, 2011; Ploner, Schmitz, Freund, & Schnitzler, 1999), other nuclei project in parallel to the IC and ACC (Apkarian, Bushnell, Treede, & Zubieta, 2005; Price, 2000). Note that despite the potential difference in order, somatosensory and nociceptive processing both involve mostly the same brain areas. As such, it is difficult to distinguish nociceptive brain activity from somatosensory brain activity, and the existence of a unique

'pain matrix' in the brain remains highly debated (Iannetti & Mouraux, 2010). However, due to the differences in conduction velocity of activated peripheral nerve fibers, pathways towards the brain and the order of processing in the brain, somatosensory tactile stimuli lead to brain responses at earlier latencies than nociceptive electric of laser stimuli (Mouraux, 2010).

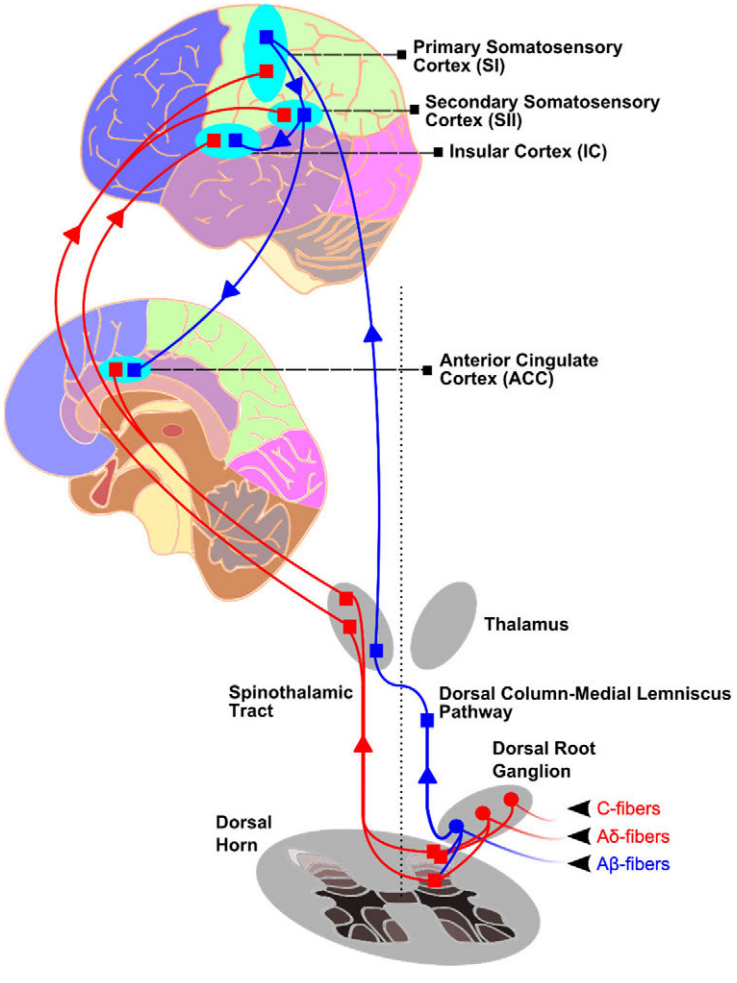

Figure 1.1: *Afferent pathways of the nociceptive system which connect peripheral nociceptive nerve fibers (Aδ- and C-fibers) to cortical areas involved in nociception including the ACC (sagittal view), SI, SII and IC (external view). Based on information from (Apkarian, Bushnell, Treede, & Zubieta, 2005; de Haan & Dijkerman, 2020; Dostrovsky & Craig, 2013; Hu, Zhang, & Hu, 2012; Inui, Wang, Tamura, Kaneoke, & Kakigi, 2004; Nosek, 1998; Ploner, Schmitz, Freund, & Schnitzler, 1999; Pons, Garraghty, Friedman, & Mishkin, 1987; Price, 2000; Todd & Koerber, 2013).*

It remains unknown how activity in these brain areas leads to either a non-painful sensory percept, or the experience of pain. However, studies do agree that brain areas can encode different aspects of the pain experience. Activation of the SI and SII underlies the perception of the sensory features of pain. Activation of the ACC and IC, regions of the limbic system, underlies the affective-motivational aspects of pain (Apkarian, Bushnell, Treede, & Zubieta, 2005). Due to the parallel nature of nociceptive processing in the brain, activation of affective-motivational brain areas does not require activation of sensory brain areas and vice-versa. This phenomenon, with profound consequences to our view of nociception and pain, has been supported by numerous studies of patients with brain lesions. For example, a patient who suffered a stroke in the SI and SII regions could still perceive an unpleasant feeling when presented with a noxious stimulus, but could not determine the exact location or timing of the stimulus (Ploner, Freund, & Schnitzler, 1999).

To sum up, pain is evoked through a series of events starting in peripheral nociceptive afferents and ending in the parallel activation of sensory cortices and affective brain areas (Figure 1.1). Whether a sensation is perceived as painful or not depends on both peripheral activation as well as central processing of the stimulus.

1.1.4 Descending Control of Nociception

One powerful mechanism of the body to regulate the sensation of pain, is descending control of nociception. The father of modern medicine Hippocrates observed that "when two pains occur together, but not in the same place, the more violent obscures the other" (Hippocrates, 400 BC). In the past decades, research has established that multiple descending pathways modulate spinal nociceptive processing. Descending inhibitory and facilitatory control in response to a noxious stimulus in human subjects is primarily regulated by two systems: 1) diffuse noxious inhibitory control (DNIC) by a feedback loop through an area in the medulla called the dorsal reticular nucleus and 2) top-down modulation via the periaqueductal gray (PAG) and the rostral ventromedial medulla (RVM).

The PAG-RVM system serves as a bidirectional top-down control that could either amplify or decrease nociceptive processing in the dorsal horn by modulating the neurotransmitter release by primary afferents and the activity of interneurons (Todd, 2010) or wide-dynamic-range neurons (Heinricher, Tavares, Leith, & Lumb, 2009). The mechanism of DNIC works via top-down connections from the dorsal reticular nucleus to wide-dynamic range neurons in the dorsal horn, which in turn project back to the dorsal reticular nucleus (Leone & Truini, 2019) to form a feedback loop. As it remains unclear in most human subject studies whether top-down inhibition of nociceptive processing following a conditioning stimulus takes place via DNIC or the PAG-RVM system, pain modulation is usually described in those studies using the general term 'conditioned pain modulation' (Yarnitsky, 2010).

1.1.5 Neuropathic Pain Mechanisms

When one cuts the wires of a telephone, the line is dead. However, when one blocks a branch of peripheral nerves, the patient often ends up with neuropathic pain originating from the bundle of nerves that was blocked. This is the paradoxical nature of neuropathic pain (Devor, 2013). Perhaps the most famous type of neuropathic pain is the pain experienced in a phantom limb following amputation. When an axon is cut during amputation or other types of nerve injury, the ending that is still connected to the body forms a swelling that is depleted of the normal myelin sheet. Since regrowth of the nerve is impossible as the limb has been amputated, regeneration fails and nerve endings form a tangled knot which is referred to as a nerve-end neuroma (Fried, Govrin-Lippmann, Rosenthal, Ellisman, & Devor, 1991).

The nerve-end neuroma is not only a sign of failed regeneration, but also a potential generator of neuropathic pain. When probed with percussion, a neuroma generates a large discharge of action potentials resulting in an intense stinging pain. However, the neuroma also generates spontaneous ectopic discharges in absence of mechanical stimulation (Wall & Gutnick, 1974). Spontaneous ectopic neural firing also occurs in other types of nerve injury such as sites of demyelination caused by neural entrapment (Burchiel, 1980).

Subsequent research showed that in addition to the discharges around the sites of neuroma or demyelination, a majority of ectopic discharges is generated by the cell bodies located in the dorsal root ganglion (Ma & LaMotte, 2007; Wall & Devor, 1983). While the aforementioned studies were conducted in animals, studies in patients with neuropathic pain confirmed that there is a direct relation between ectopic firing in peripheral afferents and pain in patients with neuropathy (Burchiel & Baumann, 2004; Ochoa, Campero, Serra, & Bostock, 2005), and that the dorsal root ganglia are a likely source of this spontaneous activity (North et al., 2019).

The description above is focused on neuropathic pain caused by dysfunction of peripheral nerve fibers. When central nerve fibers are blocked another type of neuropathic pain occurs, which is commonly referred to as central pain. Although the causes of central pain remain unknown, abnormal bursting activity has been observed in the thalamus of patients with central pain (Lenz, Kwan, Dostrovsky, & Tasker, 1989; Rinaldi, Young, Albe-Fessard, & Chodakiewitz, 1991), suggesting a similar role of spontaneous ectopic firing. The discovery that spontaneous firing underlies most clinical manifestations of neuropathic pain provides a valuable target for the diagnosis and treatment of neuropathic pain (Devor, 2013).

Two symptoms lead to additional difficulty in the lives of patients with peripheral or central neuropathic pain: allodynia and hyperalgesia. Allodynia is defined as the sensation of pain following a stimulus that would normally be non-painful, for example gently touching the skin. Hyperalgesia is defined as an increased amount of pain in response to stimuli that were already moderately painful. Both features are linked to the sensitization of peripheral neurons, referred to as peripheral sensitization, or the sensitization of central neurons involved in nociception, referred to as central sensitization. A state of peripheral sensitization is usually triggered by tissue injury and is induced by the release of inflammatory substances that change the properties of ion channels in peripheral neurons (Schaible, Ebersberger, & Natura, 2011). A state of central sensitization can be triggered by tissue injury and electrical nerve stimulation in a matter of minutes in an experimental setting (Woolf, 1983), which is rapidly reversed when nociceptor activity is silenced, e.g. by local

anesthesia (Gracely, Lynch, & Bennett, 1992; Pitcher & Henry, 2008; Sukhotinsky, Ben-Dor, Raber, & Devor, 2004). However, central sensitization can also be induced by spontaneous activity in peripheral neurons of patients with neuropathic pain (Devor, 2013). Unfortunately, it remains difficult to remove these sources of spontaneous ectopic activity driving the central sensitization in patients with neuropathic pain. Treatment of neuropathic pain is challenging, and pain relief is often not sufficient. **A mechanism-based classification and treatment approach would enable selection of effective treatments and improve the outlook for neuropathic pain patients (Baron, Binder, & Wasner, 2010).**

1.1.6 Nociplastic Pain Mechanisms

The term nociplastic pain was recently invented to describe chronic pain states without actual or threatened tissue damage, or injury to the somatosensory or nociceptive nervous system. Nonetheless, clinical evidence suggests that nociplastic pain should be seen as part of a continuum, in which nociplastic pain can occur in isolation, or in combination with nociceptive or neuropathic pain (Kosek et al., 2016). Nociplastic pain therefore includes a wide variety of chronic pain states, including diffuse sensitization (e.g., fibromyalgia), functional visceral pain (e.g., irritable bowel syndrome) and regional somatic sensitization (e.g., complex regional pain syndrome).

The common denominator in these chronic pain states is amplified processing and/or decreased inhibition of nociceptive input following maladaptive nociplastic changes (Fitzcharles et al., 2021). Decreased inhibition refers to a reduced effect of conditioned pain modulation in chronic pain patients (van Wijk & Veldhuijzen, 2010; Yarnitsky, 2010). Amplified nociceptive processing refers to the amplification of nociceptive signaling in peripheral nociceptive neurons, i.e. peripheral sensitization (Nielsen & Henriksson, 2007), or central nociceptive and wide-dynamic-range neurons, i.e. central sensitization (Nijs et al., 2021). Although decreased inhibition and sensitization occur in isolated nociplastic pain (e.g., fibromyalgia), both are also observed in combination with pain of nociceptive or neuropathic origin. Chronic pain states with a nociceptive

or neuropathic origin and nociplastic amplification or reduced inhibition of the pain are often referred to as mixed pain (Freynhagen et al., 2019). The remaining chronic pain states in which amplification or decreased inhibition occurs without apparent tissue or nerve injury are classified as nociplastic pain, leading to a rather diffuse set of conditions.

Diagnosis of nociplastic pain is complicated and takes a long time as physicians adhere to a diagnosis of exclusion for many conditions, with an average duration of 35 months in which the patient interacts with an average of 4.5 physicians (Clark, Paiva, Ginovker, & Salomón, 2013; Fitzcharles et al., 2021). **Identification of the underlying mechanisms could aid diagnosis and is crucial for the development of effective treatment strategies for nociplastic pain (Fitzcharles et al., 2021).**

1.2 Observation of Nociceptive Processing

An area of priority in pain research is the identification of biomarkers to objectively quantify nociceptive function, identify patients with a risk of developing chronic pain, and predict treatment outcomes (Cohen, Vase, & Hooten, 2021). Objective methods to quantify pain could be used to measure and compare the effect of several pain treatments and provide an important proof-of-concept in early-phase clinical trials. Methods to identify the type of pain (i.e., nociceptive, neuropathic or nociplastic) and preferably the exact underlying mechanisms (e.g., reduced DNIC, sensitization of wide-dynamic-range neurons, etc.) would provide an invaluable improvement in the clinical workup of patients, by identifying potential targets for treatment. Development of such methods requires 1) an appropriate stimulus to activate the nociceptive system, and 2) techniques to quantify the behavioral and neurophysiological response to stimulation and ideally to observe the various steps of nociceptive processing.

1.2.1 Nociceptive Stimulation

Researchers have been extremely resourceful in the invention of methods to stimulate the nociceptive system. Stimulation methods vary in terms of modality (chemical, mechanical, thermal, electrical), location (skin, muscle, visceral), activated types of nerve fibers (C-, Aδ- or Aβ-fibers) and temporal pattern (single pulse, repeated pulse, tonic, etc.). An overview of methods to stimulate nociceptive nerve fibers in the skin is provided in Figure 1.2. For investigation of the nociceptive system, an ideal stimulus should selectively stimulate nociceptive Aδ- and C-fibers, while stimulation should be safe, reproducible and quantifiable (Plaghki & Mouraux, 2003). Furthermore, a steep rise in stimulus intensity is important if one wants to investigate the latency of behavioral or neurophysiological responses (Inui & Kakigi, 2012).

Mechanical pressure stimulation can be used to generate a wide range of pain intensities and stimulus durations but lacks selectivity due to the activation of tactile Aβ-fiber afferents and it is difficult to apply a fast and precisely controlled stimulus using a conventional mechanical stimulator. Mechanical pinprick stimulation does allow application of a fast and precisely controlled stimulus, and pinprick-evoked responses have been shown sensitive to the experimental induction of secondary hyperalgesia (Iannetti, Baumgärtner, Tracey, Treede, & Magerl, 2013; van den Broeke, Lambert, Huang, & Mouraux, 2016). Nevertheless, mechanical pinprick stimulation is likely to co-activate tactile afferents. Contact heat or cold stimulation is able to selectively activate nociceptive fibers, but the rise in skin temperature is usually too slow for accurate measurement of behavioral or neurophysiological response latencies, although the recent advent of fast thermodes based on micro-Peltier elements might partially solve this problem (De Keyser, van den Broeke, Courtin, Dufour, & Mouraux, 2018). This problem can be circumvented by using laser stimulation, which allows for selective and quick activation of Aδ- and C-fibers in the skin (Plaghki & Mouraux, 2003). Therefore, laser stimulation is currently considered to be the best method for nociceptive stimulation, even though expensive equipment is required to perform the stimulation (Inui & Kakigi, 2012) and a relatively long inter-stimulus interval of 5 to 20 seconds is required

to prevent accumulation of heat and sensitization of the stimulated area (Mouraux, 2010).

A cheaper method for the quick and synchronized activation of afferent nerve fibers in the skin is electrical stimulation. Traditional transcutaneous electrical stimulation lacks selectivity as tactile Aβ-fibers have a lower electrical threshold than nociceptive Aδ- and C-fibers. However, this problem is circumvented by using a special electrode with small needles protruding into the epidermis of the skin (Inui & Kakigi, 2012; Inui, Tran, Hoshiyama, & Kakigi, 2002; Steenbergen et al., 2012). Validation studies in human participants (Mouraux, 2010) and simulations (Poulsen, Tigerholm, Meijs, Andersen, & Mørch, 2020) have confirmed the selectivity of intra-epidermal electric stimulation, provided that stimulus intensity is less than twice the detection threshold. A major benefit of electrical stimulation is that it allows for precise control of the temporal stimulus pattern, including the pulse shape, pulse amplitude, pulse width, number of pulses and the inter-pulse interval.

Measuring the effect of electrical stimulus properties on behavioral or neurophysiological outcomes could allow for the observation of nociceptive system behavior. Peripheral properties such as peripheral nerve fiber recruitment (Hugosdottir, Mørch, Andersen, Helgason, & Arendt-Nielsen, 2019) and the strength-duration relationship (Rollman, 1969) can be studied by varying the pulse amplitude and pulse width. Inhibition and facilitation of repeated nociceptive input can be explored by varying the number of pulses and the inter-pulse interval (Doll, Maten, Spaan, Veltink, & Buitenweg, 2016; Mouraux, Marot, & Legrain, 2014; van der Heide, Buitenweg, Marani, & Rutten, 2009).

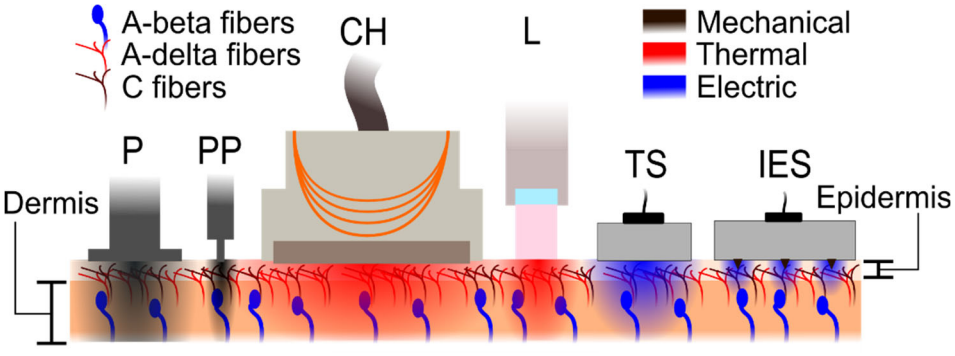

Figure 1.2: *Methods for mixed and selective stimulation of nociceptive nerve fibers in the skin. Mechanical pressure (P) and pinprick (PP) stimulation activate a mixed population of tactile and nociceptive afferents. Contact heat (CH) and laser (L) stimulation allow for selective activation of nociceptive afferents. Transcutaneous electric stimulation (TS) activates a mixed population of tactile and nociceptive afferents. Intra-epidermal electric stimulation (IES) selectively activates nociceptive nerve fibers at currents close to the detection threshold.*

1.2.2 Observation Methods

Pain is by definition a subjective experience and is therefore traditionally assessed based on the reported perception of patients. One of the most regularly reported outcomes in pain experiments is the perceived intensity of pain, measured using the Numeric Rating Scale (NRS) or the Visual Analogue Scale (VAS). Specific questionnaires have also been designed to measure multiple sensory and emotional aspects of the perceived pain, e.g. the McGill Pain Questionnaire (Melzack, 1975), or to assess pain in specific patient groups, e.g. the painDETECT questionnaire for patients with neuropathic pain (Freynhagen, Baron, Gockel, & Tölle, 2006). Although questionnaires can be used to measure the quality and intensity of the pain experience, they are inherently prone to response biases and provide little insight into the several steps of nociceptive processing.

Psychophysical methods to systematically assess alterations and reorganization of the nociceptive system have been developed within the framework of Quantitative Sensory Testing (QST) (Arendt-Nielsen & Yarnitsky, 2009). Methods of QST aim to assess the threshold and the magnitude of

sensory perception with respect to stimulus intensity to identify increased (hyper) or decreased (hypo) function. Within this framework, the sensory threshold is used to assess gain and loss of sensory function in terms of hyperesthesia and hypoesthesia. The pain threshold is used to assess gain and loss of nociceptive function in terms of hyperalgesia and hypoalgesia (Figure 1.3). Assessment of thermal and mechanical sensory and pain thresholds has already been applied on a large scale to document impaired nociceptive processing in several chronic pain syndromes (Maier et al., 2010), and is increasingly adopted by physicians as a diagnostic tool. A limitation of current QST methods is that the outcomes are influenced by a large number of factors including the stimulation instrument, room temperature, site of stimulus, size of stimulated area, stimulus velocity and inter-stimulus interval (Shy et al., 2003). The results are also dependent on psychological factors such as patient motivation, vigilance, and attention (Hansson, Backonja, & Bouhassira, 2007; Yarnitsky & Sprecher, 1994).

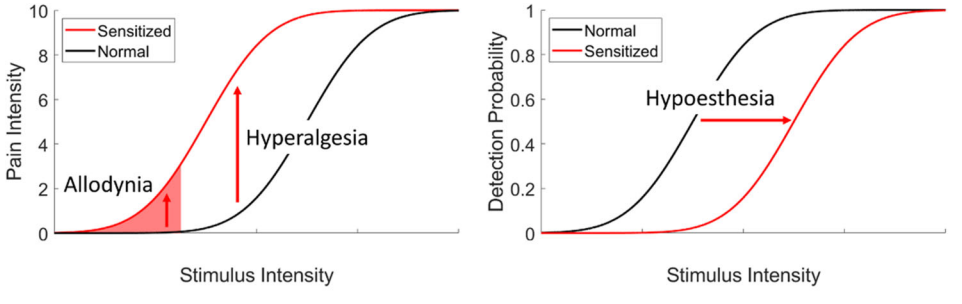

Figure 1.3: *Pain intensity scores and the pain threshold are used to assess gain and loss of nociceptive function in terms of allodynia, and hyperalgesia or hypoalgesia (left). The sensory detection probability and sensory threshold are used to assess gain and loss of sensory function in terms of hyperesthesia or hypoesthesia (right).*

Pain neuroimaging techniques enable new breakthroughs in pain science as functional neuroimaging can potentially be used to measure pain more 'objectively', to diagnose clinical pain conditions based on their underlying mechanisms and to quickly identify new pain-relieving drugs (Mouraux &

Iannetti, 2018). Neuroimaging techniques such as electroencephalography (EEG), magnetoencephalography (MEG), positron emission tomography (PET) and functional magnetic resonance imaging (fMRI) can be used to measure spontaneous and stimulus-evoked cortical activations. Although PET and fMRI provide a better spatial resolution, EEG and MEG provide a superior temporal resolution and allow for spatial reconstruction of sources if the data is of sufficient quality (i.e., sufficient spatial resolution and a high signal-to-noise ratio). A major benefit of EEG is that the costs are much lower than MEG, PET, or fMRI, making it a more attractive option for application in a clinical context.

Cortical nociceptive processing can be observed by measuring the average EEG response to a nociceptive stimulus, which is referred to as the evoked potential. The evoked potential in response to a nociceptive stimulus is defined by a succinct temporal pattern reflecting the activation of cortical areas, which has been repeatedly reproduced by studies using selective nociceptive stimulation (Legrain, Bruyer, Guérit, & Plaghki, 2003; Liang, Lee, O'Neill, Dickenson, & Iannetti, 2016; Mouraux, 2010). The observed cortical activity in response to a nociceptive stimulus applied to the hand dorsum starts with an early negative peak contralateral to the stimulated site (e.g., at T7-Fz) between 100 and 200 ms, which is referred to as the N1, sometimes preceded by an early positive peak, the P1. Subsequently, a second negative peak is observed at central electrodes (e.g., at Cz) between 200 and 300 ms, the N2, followed by a large positive peak between 300 and 500 ms, the P2.

A different approach to measure stimulus-evoked cortical responses is to use a series of stimuli that are applied at a specific frequency in order to generate a steady-state evoked potential (SSEP) (Regan, 1966). By continuous application of a series of stimuli, the effect of stimulus saliency is downregulated. Instead, the SSEP is thought to reflect entrainment of a network of cortical areas involved in sensory processing, or the superposition of transient cortical responses (Norcia, Appelbaum, Ales, Cottereau, & Rossion, 2015). Recent studies have demonstrated the possibility of eliciting nociceptive SSEPs, by applying blocks of laser or electric pulses to the skin at a single frequency (Colon, Nozaradan, Legrain, & Mouraux, 2012; Mouraux et al., 2011) or by

modulating skin temperature at a single frequency using a contact thermode (Colon, Liberati, & Mouraux, 2017).

The scalp topography of (steady-state) evoked potentials can be used for source localization in combination with a head conduction model and reconstruction techniques such as dipole source analysis (Scherg, 1990) and beamforming (Van Veen, van Drongelen, Yuchtman, & Suzuki, 1997). Source localization studies have shown that the P1 and N1 reflect the activation of suprasylvian sources involved in nociceptive processing and primarily the SII. On the other hand, sources for the N2 and P2 were primarily found in the ACC (Garcia-Larrea, Frot, & Valeriani, 2003). Note that this pattern of activation is not unique for nociceptive processing, as similar brain areas are activated by somatosensory stimuli (Mouraux & Iannetti, 2009), but can be used to assess nociceptive brain responses provided that nociceptive afferents are stimulated selectively.

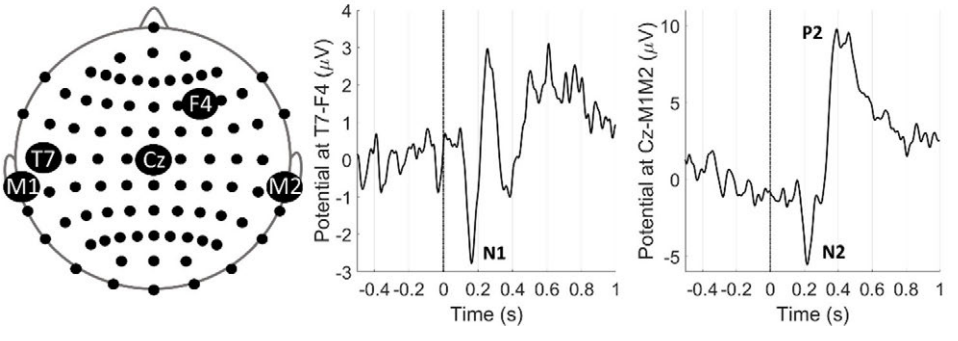

Figure 1.4: *The average evoked potential in a single participant, showing a cortical activation typical for nociceptive and somatosensory stimulation. An early negative peak (N1) is observed at electrodes contralateral to the side of stimulation. A second negative peak (N2) is observed at central electrodes, which is followed by a major positive peak (P2).*

1.3 Challenges and Goal

The research in this thesis was part of the NOCICEPT project, which stands for 'Neurophysiological Observation of Chronification: System Identification Concepts for Effective Pain Treatment'. This project aimed to develop a point-of-care applicable tool to monitor nociceptive processing for prevention and treatment optimization of chronic pain disorders. This is the first of three theses written in the context of this project, which describes the development of combined psychophysical and neurophysiological tools to observe impaired nociceptive processing in a clinical setting.

1.3.1 Challenge

Chronic pain is the result of impaired nociceptive processing leading to spontaneous ectopic activity, sensitization, and reduced inhibition. It remains difficult for clinicians to effectively treat neuropathic, nociplastic or mixed chronic pain, because it remains difficult to observe the underlying physiological mechanisms of chronic pain and the effect of treatments on those mechanisms. As such, a mechanism-based classification and treatment approach would enable selection of effective treatments and improve the outlook for patients with neuropathic chronic pain (Baron, Binder, & Wasner, 2010). Identification of the underlying mechanisms of nociplastic pain could also aid this diagnosis, occurring in isolation or in combination with neuropathic pain, and is crucial for the development of effective treatment strategies (Fitzcharles et al., 2021).

1.3.2 Goal

To address these concerns regarding the diagnosis of neuropathic and nociplastic pain, the goal of this thesis was to develop combined psychophysical and neurophysiological tools for mechanism-based observation of impaired nociceptive processing.

1.3.3 Starting Points

If we can make scientific progress, it is by standing on the shoulder of giants (reference to (Newton & Hooke, 1675)). This thesis builds forth on the significant progress made in pain research throughout the past century, and in particular on the expertise obtained through earlier projects in the research domain of Nociceptive and Somatosensory Processing at the University of Twente.

Observation of Time-Dependent Psychophysical Functions

Sensory and pain thresholds can be used to assess gain and loss of nociceptive function. Experimental techniques to allow simultaneous observation of multiple non-stationary psychophysical thresholds were developed by Doll (Doll, 2016). The method that was developed to measure time-dependent nociceptive detection thresholds in this earlier work (Doll, Veltink, & Buitenweg, 2015), also referred to as threshold tracking, was used as one of the starting points for this thesis.

Although QST methods are frequently used to study nociceptive processing, it remains difficult to observe the underlying mechanisms using these methods, as it is impossible to separate effects of peripheral and central processing mechanisms using a single threshold. However, some of the underlying mechanisms might be observed by presenting selective nociceptive stimuli with various temporal properties (e.g., pulse-width, inter-pulse interval, number of pulses) and measuring multiple nociceptive detection thresholds. To address these concerns regarding the observation of nociceptive processing, Doll et al. (Doll, 2016) developed a method to simultaneously estimate and track multiple nociceptive detection thresholds, referred to as threshold tracking.

Threshold tracking is an adaptive randomized psychophysical method of limits. Subjects are instructed to press-and-hold a response button, and to briefly release the button as soon as they perceive any sensation around the electrode that they ascribe to the application of a stimulus. A vector of 5 amplitudes with

a fixed step-size is initialized starting at zero or centered around an initial estimate of the detection threshold. The applied stimulus amplitude is chosen randomly from this vector. The vector is increased one step if the response button is not released (i.e., the stimulus is not detected), and the vector is decreased one step if the response button is released (i.e., the stimulus is detected) (Figure 1.5A). This process is repeated to obtain a sufficient number of stimulus-response pairs. This process can be used to track thresholds of multiple stimulus types simultaneously by using one vector of amplitudes per stimulus type, and randomly varying the order of stimulus types (Figure 1.5B). The detection threshold and slope of the psychometric function are estimated afterwards using logistic or probit regression (Figure 1.6).

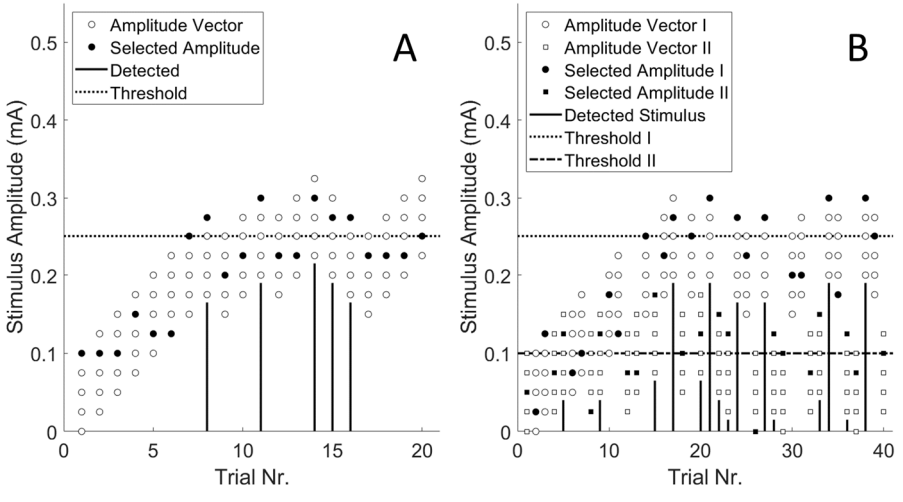

Figure 1.5: *Examples of threshold tracking with one stimulus type (A) and two stimulus types (B). For each stimulus type a vector of 5 stimulus amplitudes (open markers) is initialized starting from 0 or centered around an initial estimate of the detection threshold. One amplitude is selected randomly from the vector for stimulation (filled marker). If the stimulus was detected (indicated by lines), the vector is decreased by one step. If the stimulus was not detected, the vector is increased by one step.*

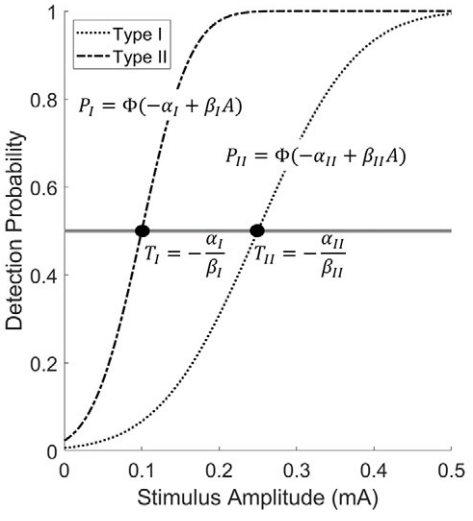

Figure 1.6: *The detection threshold and psychometric slope can be estimated based on the stimulus-response pairs using logistic or probit regression, where the psychometric function (Φ) is estimated to describe detection probability (P) in terms of stimulus parameters (e.g., the stimulus amplitude, A). The detection threshold (T), defined as the stimulus amplitude at which the detection probability is 50%, can be computed as a function of the regression coefficients. The slope of the psychometric curve is proportional to the regression coefficient (β).*

Threshold tracking is useful to observe altered nociceptive processing in terms of stimulus detection behavior of the participant. However, a limitation of threshold tracking is that this method still depends on the subjective interpretation of sensations by the participant, rather than directly measuring the neurophysiological activity related to nociception. Potentially, more objective outcomes could be obtained by directly measuring stimulus-evoked cortical potentials using electroencephalography.

Evoked Potentials in Response to Electrocutaneous Stimulation

Cortical nociceptive processing can be observed by measuring the evoked potential following a nociceptive stimulus. An exploration of the effect of nociceptive electric stimuli on the evoked potential was done by Van der Heide (van der Heide, 2009). Although nociceptive evoked cortical responses are regularly used in pain research to study regular and impaired nociception, it remains difficult to observe the underlying nociceptive mechanisms based on the average cortical response itself. Van der Heide explored the merits of cortical responses evoked by electrocutaneous single-pulse and pulse-train

stimulation for the observation of impaired nociceptive processing mechanisms.

First, Van der Heide et al. (van der Heide, Buitenweg, Marani, & Rutten, 2009) explored the effect of stimulus intensity and the number of electric pulses on the NRS and the evoked potential. In this work, it was shown that single-pulse and pulse-train nociceptive electric stimuli can be used to record evoked potentials and to observe cortical activity involved in sensory-discriminative (N1) and affective-motivational aspects (N2, P2) of nociceptive processing. It was shown that the NRS and evoked potential components are correlated with stimulus intensity and number of pulses. While the NRS and P2 increased linearly with respect to stimulus intensity, both outcomes increased non-linearly with respect to the number of pulses. This exploration demonstrated that it might be possible to identify properties of the nociceptive system (e.g., peripheral nerve fiber recruitment, temporal summation) by studying the relation between electrical stimulus properties and the evoked potential.

Second, it was also found that the effect of conditioned pain modulation was visible in the evoked P2 response for both single-pulse and pulse-train stimulation, and only in the evoked N1 response for pulse-train stimulation (van der Heide, 2009). In contrast, impaired nociceptive processing in patients with lumbosacral radiculopathy only affected the P1 and P2 responses to single-pulse stimuli. This exploration showed potential clinical utility assessing altered nociceptive processing based on evoked cortical responses to single- and multi-pulse nociceptive stimuli.

Several limitations of this approach need to be addressed before it can be used to assist diagnosis. In the work of Van der Heide, electric stimulation was not selective and the proportion of activated nociceptive and tactile afferents remained unknown. Furthermore, stimulus intensities were determined based on a combination of the pain and detection threshold. As both thresholds are subjective and show a high inter-individual variability among healthy and especially clinical populations (most notably the pain threshold (Cathcart & Pritchard, 2006)), the potential calibration error reduced significance of effects

on a group-level and would certainly impede interpretation of these results in an individual patient.

This problem of selective activation was addressed by Doll (Doll, 2016) by tracking the nociceptive detection threshold and limiting stimulus intensity to less than twice the detection threshold, which was suggested in earlier validation studies (Mouraux, 2010) as a rule of thumb for nociception selective intra-epidermal electric stimulation. In addition, this reduced the possible error in stimulus intensity calibration, as accurate estimates of the detection threshold remain available throughout the measurement. However, no EEG recording was used in the work of Doll, and it remains unknown if evoked potentials can be measured and analyzed during threshold tracking to directly assess the neurophysiological correlates of nociceptive stimulus perception.

1.3.3 Strategy and Outline

The strategy in this thesis is to combine psychophysical methods for the observation of nociceptive processing with neurophysiological techniques to provide objective mechanism-based information on nociceptive function. Intra-epidermal electric stimulation will be used to preferentially activate nociceptive afferents in the skin (Inui & Kakigi, 2012; Steenbergen et al., 2012). The threshold tracking method (Doll, Veltink, & Buitenweg, 2015) will be used to center stimulus amplitudes around the detection threshold, 1) to ensure preferential nociceptive stimulation and 2) to obtain an accurate estimate of nociceptive detection threshold (NDT) and potential threshold drift. The assessment of detection threshold is combined with recording of cortical evoked potentials using EEG, to obtain a direct measure of neurophysiological activation alongside subjective detection thresholds (Figure 1.7). These cortical evoked potentials might objectively inform us about potential dysfunctions of the nociceptive system by directly observing (altered) cortical activity involved in sensory-discriminative (N1) and affective-motivational aspects (N2, P2) of nociceptive processing. Both outcomes are used to observe peripheral and central nociceptive processing by varying the number of pulses and the inter-pulse interval of electric stimuli.

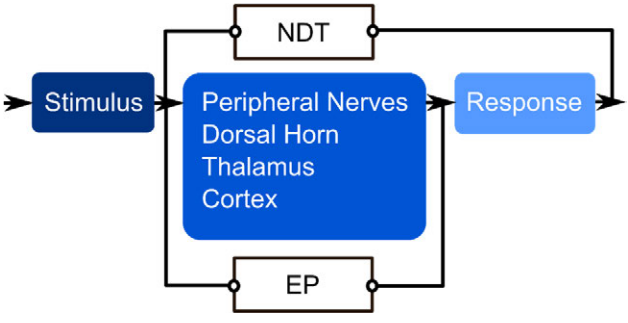

Figure 1.7: *A method for tracking of nociceptive detection thresholds (NDT) (Doll, Veltink, & Buitenweg, 2015) was used as a starting point, to observe nociceptive processing in terms of stimulus-response relations. In this thesis, this method is combined with EEG recording to directly measure the neurophysiological activity evoked by stimulation (evoked potentials, EP), alongside tracked detection thresholds.*

Technological development and exploration of method feasibility and results in healthy participants is treated in **Part I** of this thesis. The developed method is used healthy participants before and after sleep deprivation, to test if this method can be used to observe impaired nociceptive processing following sleep deprivation. The method is also used in healthy participants and patients with chronic pain in a clinical setting, to test if this method can be used to observe impaired nociceptive processing. This exploration of clinical feasibility and utility of the method is outlined in **Part II**. To develop a method for usage in a clinical setting, demonstration of feasibility and sensitivity to impaired nociceptive processing is not sufficient: researchers and clinicians should know how to interpret outcome measures in terms of physiological mechanisms. The first steps in our exploration how nociceptive detection thresholds and evoked potentials should be interpreted, and how they can be used to identify impaired mechanisms in the nociceptive system, are described in **Part III**. In addition, new techniques are developed that could improve identification of impaired nociceptive processing in future projects, which are presented in **Part IV**.

The research questions addressed in each part, and the technological and clinical steps in each chapter towards the goal 'to develop combined

psychophysical and neurophysiological tools for mechanism-based observation of impaired nociceptive processing', are outlined below.

Part I: Observation of nociceptive processing using intra-epidermal electric detection thresholds and evoked potentials

- *Can we quantify aspects of nociceptive processing?*
- *Can we objectively quantify aspects of nociceptive processing using evoked potentials?*

Chapter 2: Analysis of nociceptive evoked potentials during multi-stimulus experiments using linear mixed models

- Outline of a single-trial EEG method to deal with high-dimensional data, trial-to-trial variability and between subject variations in evoked brain activity.

Chapter 3: Simultaneous tracking of psychophysical detection thresholds and evoked potentials to study nociceptive processing

- Feasibility demonstration of recording and analysis of intra-epidermal evoked potentials during a psychophysical detection task in healthy participants.

Chapter 4: Observation of nociceptive processing: effect of intra-epidermal electric stimulus properties on detection probability and evoked potentials

- Baseline measurement of the influence of intra-epidermal electric stimulus properties on nociceptive detection probability and evoked potentials in healthy participants.
- Exploration of the influence of number of trials, recording electrodes and filter settings on the evoked potential waveform and signal-to-noise ratio.

Part II: Observation of impaired nociceptive processing in a clinical setting

- *Can we observe altered nociceptive processing in a clinical setting?*
- *Can we improve observation of altered nociceptive processing using evoked potentials?*
- *Can we improve observation of altered nociceptive processing using machine learning?*
- *Can clinicians start using the developed procedure for patient assessment?*

Chapter 5: Simultaneous measurement of intra-epidermal electric detection thresholds and evoked potentials for observation of nociceptive processing following sleep deprivation

- Evaluation of the sensitivity of intra-epidermal detection thresholds and evoked potentials to altered nociceptive processing following sleep deprivation in both sexes.

Chapter 6: Observing nociceptive detection thresholds and brain evoked potentials in failed back surgery syndrome patients

- Feasibility demonstration of recording and analysis of intra-epidermal evoked potentials during a psychophysical detection task in patients with failed back surgery syndrome.
- Evaluation of the sensitivity of intra-epidermal detection thresholds and evoked potentials to impaired nociceptive processing in failed back surgery syndrome.

Chapter 7: Combining psychophysical and EEG biomarkers using machine learning for improved observation of altered nociceptive processing in individual failed back surgery syndrome patients

- Outline of a machine learning method to combine psychophysical and EEG features for improved classification of failed back surgery syndrome.
- Identification of the most relevant features for the identification of failed back surgery syndrome.

Part III: Mechanisms for altered intra-epidermal detection thresholds and evoked potentials

- *Can we interpret nociceptive detection thresholds and evoked potentials in terms of nociceptive processing mechanisms?*
- *Can we interpret altered nociceptive detection thresholds and evoked potentials in a clinical setting?*

Chapter 8: Observation of nociceptive detection thresholds and cortical evoked potentials: go/no-go versus 2-interval forced choice

- Validation if nociceptive detection thresholds during a go/no-go task are biased by a response criterion.
- Validation if evoked potentials in response to near-threshold stimuli are altered by the presence of a response criterion.

Chapter 9: Psychophysical models for detection of single- and double-pulse electronociceptive stimuli: implications for interpretation of clinical observations

- Derivation of a theoretical framework to describe how central neurophysiological activity leads detection behavior, to explain the observed differences between healthy controls and patients with failed back surgery syndrome.
- Explanation why stimulus detection behavior might be altered in patients with failed back surgery syndrome.

Part IV: Novel technological steps for improved observation of impaired nociceptive processing

- *Can we invent new procedures to study nociceptive processing more objectively?*

Chapter 10: Estimation of perceptual thresholds based on the electroencephalogram using a deep neural network

- Demonstration of a method to automatically measure the perceptual threshold to any type of stimulus, solely based on EEG activity.

Chapter 11: Multisine frequency modulation of intra-epidermal electric pulse sequences: a novel tool to study nociceptive processing

- Demonstration of a method to directly modulate the pulse rate of nociceptive afferents in the skin with a multisine waveform through intra-epidermal electric stimulation.
- First recording of multisine nociceptive steady-state evoked potentials.

Chapter 12: Nociceptive intra-epidermal electric stimulation evokes steady-state responses in the secondary somatosensory cortex

- Exploration of the cortical sources and generation mechanisms of nociceptive steady-state evoked potentials in response to intra-epidermal electric stimuli.

Further clinical validation and application of the techniques presented in this thesis is clearly necessary and is part of follow-up research that is currently being done at the St. Antonius Hospital (Nieuwegein, the Netherlands) and the University of Twente (Enschede, the Netherlands) as part of the NOCICEPT project and will be continued in the NociTune project. Results of these validation and clinical application studies will be covered in the theses of colleagues Tom Berfelo and Niels Jansen.

1.4 References

Apkarian, A. V., Bushnell, M. C., Treede, R.-D., & Zubieta, J.-K. (2005). Human brain mechanisms of pain perception and regulation in health and disease. *European Journal of Pain, 9*(4), 463-463.

Arendt-Nielsen, L., & Yarnitsky, D. (2009). Experimental and Clinical Applications of Quantitative Sensory Testing Applied to Skin, Muscles and Viscera. *Journal of Pain, 10*(6), 556-572.

Baron, R., Binder, A., & Wasner, G. (2010). Neuropathic pain: diagnosis, pathophysiological mechanisms, and treatment. *The Lancet Neurology, 9*(8), 807-819.

Breivik, H., Collett, B., Ventafridda, V., Cohen, R., & Gallacher, D. (2006). Survey of chronic pain in Europe: prevalence, impact on daily life, and treatment. *European journal of pain, 10(4)*, 287-287.

Burchiel, K. J. (1980). Ectopic impulse generation in focally demyelinated trigeminal nerve. *Experimental Neurology, 69*(2), 423-429.

Burchiel, K. J., & Baumann, T. K. (2004). Pathophysiology of trigeminal neuralgia: new evidence from a trigeminal ganglion intraoperative microneurographic recording: Case report. *Journal of Neurosurgery, 101*(5), 872-873.

Cathcart, S., & Pritchard, D. (2006). Reliability of pain threshold measurement in young adults. *J Headache Pain, 7*(1), 21-26.

Clark, P., Paiva, E. S., Ginovker, A., & Salomón, P. A. (2013). A patient and physician survey of fibromyalgia across Latin America and Europe. *BMC Musculoskeletal Disorders, 14*(1), 188.

Cohen, S. P., Vase, L., & Hooten, W. M. (2021). Chronic pain: an update on burden, best practices, and new advances. *The Lancet, 397*(10289), 2082-2097.

Colon, E., Liberati, G., & Mouraux, A. (2017). EEG frequency tagging using ultra-slow periodic heat stimulation of the skin reveals cortical activity specifically related to C fiber thermonociceptors. *NeuroImage, 146*, 266-274.

Colon, E., Nozaradan, S., Legrain, V., & Mouraux, A. (2012). Steady-state evoked potentials to tag specific components of nociceptive cortical processing. *NeuroImage, 60*(1), 571-581.

de Haan, E. H. F., & Dijkerman, H. C. (2020). Somatosensation in the Brain: A Theoretical Re-evaluation and a New Model. *Trends in Cognitive Sciences, 24*(7), 529-541.

De Keyser, R., van den Broeke, E. N., Courtin, A., Dufour, A., & Mouraux, A. (2018). Event-related brain potentials elicited by high-speed cooling of

the skin: A robust and non-painful method to assess the spinothalamic system in humans. *Clin Neurophysiol, 129*(5), 1011-1019.

Devor, M. (2013). Neuropathic Pain: Pathophysiological Response of Nerves to Injury. In S. B. McMahon, M. Koltzenburg, I. Tracey, & D. C. Turk (Eds.), *Wall and Melzack's Textbook of Pain* (6th ed., pp. 861-888): Elsevier Saunders.

Doll, R. J. (2016). *Psychophysical Methods for Improved Observation of Nociceptive Processing.* University of Twente, Enschede.

Doll, R. J., Maten, A. C. A., Spaan, S. P. G., Veltink, P. H., & Buitenweg, J. R. (2016). Effect of temporal stimulus properties on the nociceptive detection probability using intra-epidermal electrical stimulation. *Experimental Brain Research, 234*(1), 219-227.

Doll, R. J., Veltink, P. H., & Buitenweg, J. R. (2015). Observation of time-dependent psychophysical functions and accounting for threshold drifts. *Attention, Perception, and Psychophysics, 77*(4), 1440-1447.

Doll, R. J., Veltink, P. H., & Buitenweg, J. R. (2015). Observation of time-dependent psychophysical functions and accounting for threshold drifts. *Attention, Perception, & Psychophysics, 77*(4), 1440-1447.

Dostrovsky, J. O., & Craig, A. D. (2013). Ascending Projection Systems. In S. B. McMahon, M. Koltzenburg, I. Tracey, & D. C. Turk (Eds.), *Wall and Melzack's Textbook of Pain* (6th ed., pp. 182-196): Elsevier Saunders.

Eriksen, J., Sjøgren, P., Bruera, E., Ekholm, O., & Rasmussen, N. K. (2006). Critical issues on opioids in chronic non-cancer pain: an epidemiological study. *Pain, 125*(1-2), 172-179.

Fitzcharles, M. A., Cohen, S. P., Clauw, D. J., Littlejohn, G., Usui, C., & Häuser, W. (2021). Nociplastic pain: towards an understanding of prevalent pain conditions. *Lancet, 397*(10289), 2098-2110.

Freynhagen, R., Baron, R., Gockel, U., & Tölle, T. R. (2006). painDETECT: a new screening questionnaire to identify neuropathic components in patients with back pain. *Curr Med Res Opin, 22*(10), 1911-1920.

Freynhagen, R., Parada, H. A., Calderon-Ospina, C. A., Chen, J., Rakhmawati Emril, D., Fernández-Villacorta, F. J., . . . Ciampi de Andrade, D. (2019). Current understanding of the mixed pain concept: a brief narrative review. *Curr Med Res Opin, 35*(6), 1011-1018.

Fried, K., Govrin-Lippmann, R., Rosenthal, F., Ellisman, M. H., & Devor, M. (1991). Ultrastructure of afferent axon endings in a neuroma. *Journal of Neurocytology, 20*(8), 682-701.

Garcia-Larrea, L., Frot, M., & Valeriani, M. (2003). Brain generators of laser-evoked potentials: From dipoles to functional significance. *Neurophysiologie Clinique, 33*(6), 279-292.

Gracely, R. H., Lynch, S. A., & Bennett, G. J. (1992). Painful neuropathy: altered central processing maintained dynamically by peripheral input. *Pain, 51*(2), 175-194.

Hansson, P., Backonja, M., & Bouhassira, D. (2007). Usefulness and limitations of quantitative sensory testing: Clinical and research application in neuropathic pain states. *Pain, 129*(3).

Heinricher, M. M., Tavares, I., Leith, J. L., & Lumb, B. M. (2009). Descending control of nociception: Specificity, recruitment and plasticity. *Brain Res Rev, 60*(1), 214-225.

Hippocrates. (400 BC). *Aphorisms* (W. H. S. Jones, Trans.).

Hu, L., Zhang, Z. G., & Hu, Y. (2012). A time-varying source connectivity approach to reveal human somatosensory information processing. *NeuroImage, 62*(1), 217-228.

Hugosdottir, R., Mørch, C. D., Andersen, O. K., Helgason, T., & Arendt-Nielsen, L. (2019). Preferential activation of small cutaneous fibers through small pin electrode also depends on the shape of a long duration electrical current. *BMC Neurosci, 20*(1), 48.

Iannetti, G. D., Baumgärtner, U., Tracey, I., Treede, R. D., & Magerl, W. (2013). Pinprick-evoked brain potentials: A novel tool to assess central sensitization of nociceptive pathways in humans. *Journal of Neurophysiology, 110*(5), 1107-1116.

Iannetti, G. D., & Mouraux, A. (2010). From the neuromatrix to the pain matrix (and back). *Experimental Brain Research, 205*(1), 1-12.

Inui, K., & Kakigi, R. (2012). Pain perception in humans: Use of intraepidermal electrical stimulation. *Journal of Neurology, Neurosurgery and Psychiatry, 83*(5), 551-556.

Inui, K., & Kakigi, R. (2012). Pain perception in humans: use of intraepidermal electrical stimulation. *Journal of Neurology, Neurosurgery and Psychiatry, 83*(5), 551.

Inui, K., Tran, T. D., Hoshiyama, M., & Kakigi, R. (2002). Preferential stimulation of Aδ fibers by intra-epidermal needle electrode in humans. *Pain, 96*(3), 247-252.

Inui, K., Wang, X., Tamura, Y., Kaneoke, Y., & Kakigi, R. (2004). Serial processing in the human somatosensory system. *Cereb Cortex, 14*(8), 851-857.

Jackson, T. P., Stabile, V. S., & McQueen, K. A. K. (2014). The Global Burden Of Chronic Pain. *ASA Newsletter, 78*(6), 24-27.

Jensen, T. S., Baron, R., Haanpää, M., Kalso, E., Loeser, J. D., Rice, A. S. C., & Treede, R. D. (2011). A new definition of neuropathic pain. *Pain, 152*(10), 2204-2205.

Koleva, D., Krulichova, I., Bertolini, G., Caimi, V., & Garattini, L. (2005). Pain in primary care: an Italian survey. *Eur J Public Health, 15*(5), 475-479.

Kosek, E., Cohen, M., Baron, R., Gebhart, G. F., Mico, J. A., Rice, A. S. C., . . . Sluka, A. K. (2016). Do we need a third mechanistic descriptor for chronic pain states? *Pain, 157*(7), 1382-1386.

Legrain, V., Bruyer, R., Guérit, J. M., & Plaghki, L. (2003). Nociceptive processing in the human brain of infrequent task-relevant and task-irrelevant noxious stimuli. A study with event-related potentials evoked by CO2 laser radiant heat stimuli. *Pain, 103*(3), 237-248.

Lenz, F. A., Kwan, H. C., Dostrovsky, J. O., & Tasker, R. R. (1989). Characteristics of the bursting pattern of action potentials that occurs in the thalamus of patients with central pain. *Brain Res, 496*(1-2), 357-360.

Leone, C., & Truini, A. (2019). The CPM Effect: Functional Assessment of the Diffuse Noxious Inhibitory Control in Humans. *J Clin Neurophysiol, 36*(6), 430-436.

Liang, M., Lee, M. C., O'Neill, J., Dickenson, A. H., & Iannetti, G. D. (2016). Brain potentials evoked by intraepidermal electrical stimuli reflect the central sensitization of nociceptive pathways. *Journal of Neurophysiology, 116*(2), 286-295.

Liang, M., Mouraux, A., & Iannetti, G. D. (2011). Parallel Processing of Nociceptive and Non-nociceptive Somatosensory Information in the Human Primary and Secondary Somatosensory Cortices: Evidence from Dynamic Causal Modeling of Functional Magnetic Resonance Imaging Data. *The Journal of Neuroscience, 31*(24), 8976.

Linton, S. (2005). *Understanding Pain for Better Clinical Practice: A Psychological Perspective*: Elsevier Health Sciences.

Ma, C., & LaMotte, R. H. (2007). Multiple Sites for Generation of Ectopic Spontaneous Activity in Neurons of the Chronically Compressed Dorsal Root Ganglion. *The Journal of Neuroscience, 27*(51), 14059.

Maier, C., Baron, R., Tölle, T. R., Binder, A., Birbaumer, N., Birklein, F., . . . Treede, D. R. (2010). Quantitative sensory testing in the German Research Network on Neuropathic Pain (DFNS): somatosensory abnormalities in 1236 patients with different neuropathic pain syndromes. *Pain, 150*(3), 439-450.

Mäntyselkä, P., Kumpusalo, E., Ahonen, R., Kumpusalo, A., Kauhanen, J., Viinamäki, H., . . . Takala, J. (2001). Pain as a reason to visit the doctor: a study in Finnish primary health care. *Pain, 89*(2-3), 175-180.

McMahon, S. B., Koltzenburg, M., Tracey, I., & Turk, D. C. (2013). *Wall and Melzack's Textbook of Pain* (6th ed.): Elsevier Saunders.

Melzack, R. (1975). The McGill Pain Questionnaire: Major properties and scoring methods. *Pain, 1*(3), 277-299.

Merskey, H. E. (1986). Classification of chronic pain: Descriptions of chronic pain syndromes and definitions of pain terms. *Pain*.

Mouraux, A., & Iannetti, G. D. (2009). Nociceptive Laser-Evoked Brain Potentials Do Not Reflect Nociceptive-Specific Neural Activity. *Journal of Neurophysiology, 101*(6), 3258-3269.

Mouraux, A., & Iannetti, G. D. (2018). The search for pain biomarkers in the human brain. *Brain, 141*(12), 3290-3307.

Mouraux, A., Iannetti, G. D., Colon, E., Nozaradan, S., Legrain, V., & Plaghki, L. (2011). Nociceptive Steady-State Evoked Potentials Elicited by Rapid Periodic Thermal Stimulation of Cutaneous Nociceptors. *The Journal of Neuroscience, 31*(16), 6079.

Mouraux, A., Iannetti, G. D., & Plaghki, L. (2010). Low intensity intra-epidermal electrical stimulation can activate Aδ-nociceptors selectively. *Pain, 150(1)*, 199-207.

Mouraux, A., Marot, E., & Legrain, V. (2014). Short trains of intra-epidermal electrical stimulation to elicit reliable behavioral and electrophysiological responses to the selective activation of nociceptors in humans. *Neuroscience Letters, 561*(Supplement C), 69-73.

Newton, I., & Hooke, R. (1675). [Isaac Newton letter to Robert Hooke].

Nielsen, L. A., & Henriksson, K. G. (2007). Pathophysiological mechanisms in chronic musculoskeletal pain (fibromyalgia): the role of central and peripheral sensitization and pain disinhibition. *Best Practice & Research Clinical Rheumatology, 21*(3), 465-480.

Nijs, J., George, S. Z., Clauw, D. J., Fernández-de-las-Peñas, C., Kosek, E., Ickmans, K., . . . Curatolo, M. (2021). Central sensitisation in chronic pain conditions: latest discoveries and their potential for precision medicine. *The Lancet Rheumatology, 3*(5), e383-e392.

Norcia, A. M., Appelbaum, L. G., Ales, J. M., Cottereau, B. R., & Rossion, B. (2015). The steady-state visual evoked potential in vision research: A review. *J Vis, 15*(6), 4.

North, R. Y., Li, Y., Ray, P., Rhines, L. D., Tatsui, C. E., Rao, G., . . . Dougherty, P. M. (2019). Electrophysiological and transcriptomic correlates of neuropathic pain in human dorsal root ganglion neurons. *Brain, 142*(5), 1215-1226.

Nosek, T. M. (1998). Brain Function: Somatic Sensibility. In *Essentials of Human Physiology* (pp. 22): Gold Standard Multimedia Incorporated.

Obi, T., Takatsu, M., Yamazaki, K., Kuroda, R., Terada, T., & Mizoguchi, K. (2007). Conduction Velocities of Aδ-fibers and C-fibers in Human Peripheral Nerves and Spinal Cord After CO_2 Laser Stimulation. *Journal of Clinical Neurophysiology, 24*(3).

Ochoa, J. L., Campero, M., Serra, J., & Bostock, H. (2005). Hyperexcitable polymodal and insensitive nociceptors in painful human neuropathy. *Muscle Nerve, 32*(4), 459-472.

Phillips, C. J. (2009). The Cost and Burden of Chronic Pain. *Reviews in pain, 3*(1), 2-5.

Pitcher, G. M., & Henry, J. L. (2008). Governing role of primary afferent drive in increased excitation of spinal nociceptive neurons in a model of sciatic neuropathy. *Experimental Neurology, 214*(2), 219-228.

Plaghki, L., & Mouraux, A. (2003). How do we selectively activate skin nociceptors with a high power infrared laser? Physiology and biophysics of laser stimulation. *Neurophysiol Clin, 33*(6), 269-277.

Ploner, M., Freund, H. J., & Schnitzler, A. (1999). Pain affect without pain sensation in a patient with a postcentral lesion. *Pain, 81*(1), 211-214.

Ploner, M., Schmitz, F., Freund, H. J., & Schnitzler, A. (1999). Parallel activation of primary and secondary somatosensory cortices in human pain processing. *J Neurophysiol, 81*(6), 3100-3104.

Pons, T. P., Garraghty, P. E., Friedman, D. P., & Mishkin, M. (1987). Physiological evidence for serial processing in somatosensory cortex. *Science, 237*(4813), 417-420.

Poulsen, A. H., Tigerholm, J., Meijs, S., Andersen, O. K., & Mørch, C. D. (2020). Comparison of existing electrode designs for preferential activation of cutaneous nociceptors. *Journal of Neural Engineering*.

Price, D. D. (2000). Psychological and Neural Mechanisms of the Affective Dimension of Pain. *Science, 288*(5472), 1769.

Raja, S. N., Carr, D. B., Cohen, M., Finnerup, N. B., Flor, H., Gibson, S., . . . Vader, K. (2020). The revised International Association for the Study of Pain definition of pain: concepts, challenges, and compromises. *Pain, 161*(9).

Regan, D. (1966). Some characteristics of average steady-state and transient responses evoked by modulated light. *Electroencephalography and Clinical Neurophysiology, 20*(3), 238-248.

Rinaldi, P. C., Young, R. F., Albe-Fessard, D., & Chodakiewitz, J. (1991). Spontaneous neuronal hyperactivity in the medial and intralaminar thalamic nuclei of patients with deafferentation pain. *J Neurosurg, 74*(3), 415-421.

Ringkamp, M., Raja, S. N., Campbell, J. N., & Meyer, R. A. (2013). Peripheral Mechanisms of Cutaneous Nociception. In S. B. McMahon, M. Koltzenburg, I. Tracey, & D. C. Turk (Eds.), *Wall and Melzack's Textbook of Pain* (6th ed., pp. 1-30): Elsevier Saunders.

Rollman, G. B. (1969). Electrocutaneous stimulation: Psychometric functions and temporal integration. *Perception & Psychophysics, 5*(5), 289-293.

Schaible, H.-G., Ebersberger, A., & Natura, G. (2011). Update on peripheral mechanisms of pain: beyond prostaglandins and cytokines. *Arthritis research & therapy, 13*(2), 210-210.

Scherg, M. (1990). Fundamentals if dipole source potential analysis. In Grandori, M. Hoke, & G. I. Romani (Eds.), *Auditory evoked magnetic fields and electric potentials* (pp. 40 - 69). Basel: Karger.

Shy, M. E., Frohman, E. M., So, Y. T., Arezzo, J. C., Cornblath, D. R., Giuliani, M. J., . . . Weimer, L. H. (2003). Quantitative sensory testing. *Neurology, 60*(6), 898.

Siegel, A., & Sapru, H. (2005). *Essential Neuroscience*: Lippincott Williams & Wilkins.

Steenbergen, P., Buitenweg, J. R., Trojan, J., van der Heide, E. M., van den Heuvel, T., Flor, H., & Veltink, P. H. (2012). A system for inducing concurrent tactile and nociceptive sensations at the same site using electrocutaneous stimulation. *Behavior Research Methods, 44*(4), 924-933.

Stewart, W. F., Ricci, J. A., Chee, E., Morganstein, D., & Lipton, R. (2003). Lost productive time and cost due to common pain conditions in the US workforce. *Jama, 290*(18), 2443-2454.

Sukhotinsky, I., Ben-Dor, E., Raber, P., & Devor, M. (2004). Key role of the dorsal root ganglion in neuropathic tactile hypersensibility. *European Journal of Pain, 8*(2), 135-143.

Todd, A. J. (2010). Neuronal circuitry for pain processing in the dorsal horn. *Nature Reviews Neuroscience, 11*(12), 823-836.

Todd, A. J., & Koerber, H. R. (2013). Neuroanatomical Substrates of Spinal Nociception. In S. B. McMahon, M. Koltzenburg, I. Tracey, & D. C. Turk (Eds.), *Wall and Melzack's Textbook of Pain* (6th ed., pp. 77-93): Elsevier Saunders.

Treede, R. D., Rief, W., Barke, A., Aziz, Q., Bennett, M. I., Benoliel, R., . . . Wang, S. J. (2015). A classification of chronic pain for ICD-11. *Pain, 156*(6), 1003-1007.

van den Broeke, E. N., Lambert, J., Huang, G., & Mouraux, A. (2016). Central Sensitization of Mechanical Nociceptive Pathways Is Associated with a Long-Lasting Increase of Pinprick-Evoked Brain Potentials. *Frontiers in Human Neuroscience, 10*.

van der Heide, E. M. (2009). *Neurophysiological Observation of the Nociceptive System Using Electrocutaneous Stimulation.* Universiteit Twente, Enschede.

van der Heide, E. M., Buitenweg, J. R., Marani, E., & Rutten, W. L. (2009). Single pulse and pulse train modulation of cutaneous electrical stimulation: a comparison of methods. *J Clin Neurophysiol, 26*(1), 54-60.

Van Veen, B. D., van Drongelen, W., Yuchtman, M., & Suzuki, A. (1997). Localization of brain electrical activity via linearly constrained minimum variance spatial filtering. *IEEE Trans Biomed Eng, 44*(9), 867-880.

van Wijk, G., & Veldhuijzen, D. S. (2010). Perspective on Diffuse Noxious Inhibitory Controls as a Model of Endogenous Pain Modulation in Clinical Pain Syndromes. *Journal of Pain, 11*(5), 408-419.

Wall, P. D. (1978). The gate control theory of pain mechanisms. A re-examination and re-statement. *Brain, 101*(1), 1-18.

Wall, P. D., & Devor, M. (1983). Sensory afferent impulses originate from dorsal root ganglia as well as from the periphery in normal and nerve injured rats. *Pain, 17*(4), 321-339.

Wall, P. D., & Gutnick, M. (1974). Properties of afferent nerve impulses originating from a neuroma. *Nature, 248*(5451), 740-743.

Woolf, C. J. (1983). Evidence for a central component of post-injury pain hypersensitivity. *Nature, 306*(5944), 686-688.

Yarnitsky, D. (2010). Conditioned pain modulation (the diffuse noxious inhibitory control-like effect): Its relevance for acute and chronic pain states. *Current Opinion in Anaesthesiology, 23*(5), 611-615.

Yarnitsky, D., & Sprecher, E. (1994). Thermal testing: normative data and repeatability for various test algorithms. *Journal of the Neurological Sciences, 125*(1), 39-45.

The NociTRACK AmbuStim stimulator, used to generate single- and double-pulse electric stimuli, drawn in the style of Amadeo de Souza-Cardoso using neural style transfer.

Part I:

Observation of Nociceptive Processing using Intra-Epidermal Electric Detection Thresholds and Evoked Potentials

"Divide each difficulty into as many parts as is feasible and necessary to resolve it."

René Descartes, Discourse on Method


NooiTRACK

Chapter 2

Analysis of Nociceptive Evoked Potentials during Multi-Stimulus Experiments using Linear Mixed Models

Published as:

Van den Berg, B., & Buitenweg, J. R. (2018). Analysis Of nociceptive evoked potentials during multi-stimulus experiments using linear mixed models. Proceedings of the 40th Annual International Conference of the IEEE Engineering in Medicine and Biology Society (EMBC), Honolulu, United States.

DOI: https://www.doi.org/10.1109/EMBC.2018.8513032

Abstract

Neural processing of sensory stimuli can be studied using EEG by estimation of the evoked potential using the averages of large sets of trials. However, it is not always possible to include all stimulus parameters in a conventional analysis, since this would lead to an insufficient number of trials to obtain the evoked potential by averaging. Linear mixed models use dependencies within the data to combine information from all data for the estimation of the evoked potential. In this work, it is shown that in multi-stimulus EEG data the quality of an evoked potential estimate can be improved by using a linear mixed model. Furthermore, the linear mixed model effectively deals with correlation between parameters in the data and reveals the influence of individual stimulus parameters.

2.1 Introduction

To study neural processing of sensory stimuli using EEG, the evoked potential (EP) must be estimated using a sufficient number of trials. To identify important parameters of stimulus processing, it is required to apply stimuli with multiple properties. However, experiments to gather the required data on human subjects cannot take too long and the number of stimuli is limited, which is problematic for the acquisition of sufficient trials. Often, stimulus selection methods are used for a more efficient probing of the stimulus parameter space. However, this results in different amounts of trials per stimulus property. Since the variance of the estimated EP depends on the amount of acquired trials, analysis of those trials using conventional averaging is impeded. This could be overcome by using an analysis method which is robust for variations in the amount of acquired trials. Such a method is provided by a linear mixed model (LMM), which deals with those variations by using dependencies within the data. This means that a lower number of trials is required to accurately estimate the effect of stimulus parameters with respect to averaging.

Recently, we have used EPs to study neural processing of single and double pulse nociceptive electrical stimuli around the detection threshold, which is defined as the stimulus amplitude at which 50% of the stimuli are detected. For optimal estimation of the probability that a stimulus is detected roughly equal amounts of detected and undetected stimulus-response pairs have to be acquired. To keep stimulus amplitudes around the detection threshold, we developed a method for simultaneous tracking of nociceptive detection thresholds (NDTs) for multiple types of stimuli (Doll, Buitenweg, Meijer, & Veltink, 2014). A single detection threshold is tracked by an adaptive randomized stimulus sequence which automatically varies the stimulus amplitude with respect to the amount of detected and undetected stimuli. Detection thresholds for multiple stimulus types are tracked by randomly interchanging the stimulus types (single-pulse and double-pulse) during stimulation, which is shown in Figure 2.1. Because NDTs change over time due to habituation of the nociceptive system, a wide variety of stimulus amplitudes is used throughout the experiment. Because of this variety, the data does not include equal amounts of trials per stimulus amplitude. This leads to a poor

estimation of the signal by averaging, which is shown in Figure 2.2. To extract and analyze the brain activity during detected and undetected stimuli, a more efficient method than averaging is required.

A tool which successfully accounts for the effects of multiple stimulus parameters simultaneously is the linear model (LM). Regression using a LM has the benefit over averaging that it allows for a large number of repeated measures without using many subjects, deals more efficiently with missing data and is flexible in modeling covariates and correlation structures. Although LMs are a popular statistical tool in fMRI research, they have been used by few researchers for EEG analysis, of which some interesting examples include (Hauk, Pulvermüller, Ford, Marslen-Wilson, & Davis, 2009) and (Smith & Kutas, 2015).

Recently Vossen et al. (Vossen, Van Breukelen, Hermens, Van Os, & Lousberg, 2011) used linear mixed models (LMMs) in EEG analysis to account for between-subject variations and habituation. A major difference with LMs is that LMMs attempt to model the distribution of random effects in the data, enabling subject-level and group-level intercepts and slopes. This provides a convenient way of modeling the dependence of EEG data within one subject or one group. Considering their efficiency in dealing with high-dimensional data, trial-to-trial variability, and between-subject variations, they provide an ideal tool for analysis of multivariate EEG data. In addition, they provide means to measure the influence of within-subject and between-subject variations simultaneously, which is useful in clinical studies.

In this work, it is demonstrated that a LMM enables the analysis of variations within EEG data with respect to stimulus intensity and stimulus properties, such as the variation of the EEG signals obtained during NDT tracking experiments. It will be shown that a LMM effectively reduces the amount of background activity and can be used to measure and test relations between stimulus parameters, psychophysical responses, and nociceptive EPs.

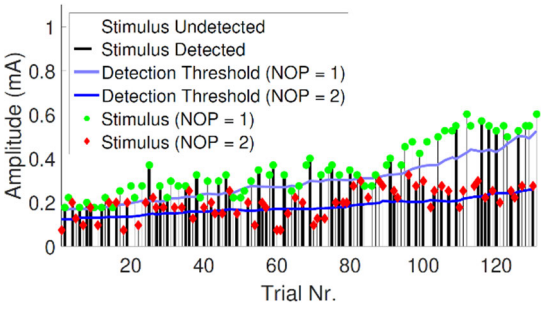

Figure 2.1: *Simultaneous tracking of NDTs for multiple stimulus types, with a varying number of pulses (NOP), by randomized stimulation around the nociceptive detection threshold (Doll et al., 2014). In this case, stimuli with a single pulse (NOP = 1) and a double pulse with 10 ms inter-pulse interval (NOP = 2) were used.*

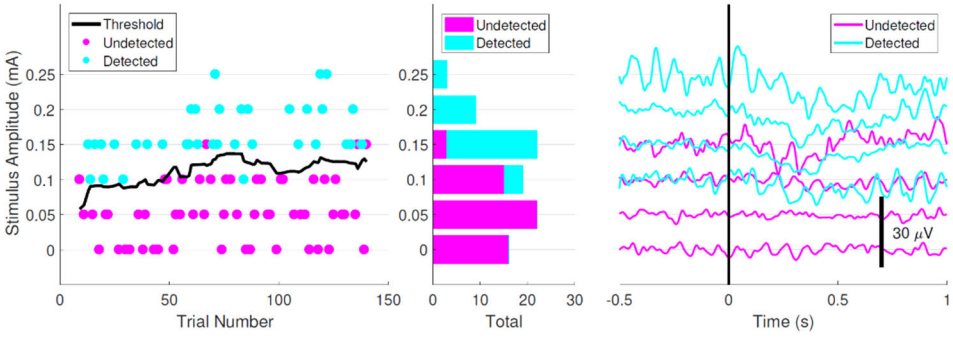

Figure 2.2: *Summary of data acquired from one of the subjects. The figure on the left shows the amplitudes of all detected and undetected double-pulse stimuli with respect to the NDT. The histogram in the middle shows that at most 25 times the same stimulus was used. This leads to a poor estimation of the EP by averaging, which is shown in the figure on the right.*

2.2 Method

2.2.1 Experiment

Single and double-pulse stimuli are applied to twelve healthy subjects (5 male, 7 female) via intra-epidermal electrocutaneous stimulation. Nociceptive detection thresholds are tracked by randomized application of stimuli around the detection threshold (Doll et al., 2014). A vector of 5 stimulus amplitudes with a step size of 0.025 mA is initialized, of which one amplitude is chosen randomly for the next stimulus of that type. During the experiment, all amplitudes in this vector are increased or decreased depending on the previous response of the subject. In total 171±24 trials were recorded for every stimulus type from each subject, with a variable amplitude. Figure 2.1 shows an example

of the paradigm. The institution's ethical review board approved all experimental procedures involving human subjects and all subjects provided written informed consent prior to participation.

2.2.2 EEG Data Recording and Pre-processing

EEG data was recorded continuously with a sampling rate of 1024 Hz at 64 Ag/AgCl electrodes placed on the scalp according to the international 10-20 system using a TMSi REFA amplifier. In this work, data from the Cz channel is analyzed. Signals are pre-processed using FieldTrip (Oostenveld, Fries, Maris, & Schoffelen, 2011), a Matlab toolbox for scientific EEG and MEG analysis. Contamination of the EEG by eye-blinks or movements is corrected using an independent component analysis algorithm (Delorme & Makeig, 2004). Trials for EP analysis are extracted from the EEG using a window ranging from 0.5 s before until 1.0 s after the stimulus, bandpass filtered from 0.1 to 40 Hz and baseline corrected using the interval ranging from -0.5 s to 0 s relative to stimulus onset. EEG data is downsampled to 200 Hz to increase computational speed.

2.2.3 Model Formulation

The statistical model should ideally include all relevant experimental parameters. However, the total amount of model parameters should be restricted to prevent overfitting. In this case, the detection of a stimulus (D) can be expected to be of major influence on the EP. Furthermore, another part of the activity might be directly related to the intensity of the pulse. Both pulses (P1 and P2) can cause an independent increase of brain activity. Brain activity can decrease over time with respect to the number of received stimuli (TRL) due to habituation. Additionally, effect sizes might be dependent on the subject. The LMM that is used to describe those modulations and random effects during the j-th trial of the i-th subject at time τ is shown in Equation (1).

$$y_{ij}(\tau) = \beta_{Int.}(\tau) + \beta_{P1}(\tau)x_{P1,ij} + \beta_{P2,ij}x_{P2,ij} + \beta_{D}(\tau)x_{D,ij} + \beta_{TRL}(\tau)x_{TRL,ij} + u_{Int.,i}(\tau) + u_{P1,i}(\tau)x_{P1,ij} + u_{P2,i}(\tau)x_{P2,ij} + u_{D,i}(\tau)x_{D,ij} + u_{TRL,i}(\tau)x_{TRL,ij} + \eta_{ij}(\tau) \quad (1)$$

Where:

- The single-channel EEG signal in one trial is $y_{ij}(\tau)$
- The stimulus parameters are $x_{P1/P2/D/TRL,ij}(\tau)$
- The general model intercept is $\beta_{Int.}(\tau)$
- The general model slopes with respect to stimulus parameters are $\beta_{P1/P2/D/TRL}(\tau)$
- The subject-specific model intercept is $u_{Int.,i}(\tau)$
- The subject-specific model slopes with respect to stimulus parameters are $u_{P1/P2/D/TRL}(\tau)$
- The model residual is $\eta_{ij}(\tau)$

2.2.4 Analysis and Statistical Testing

The model variables are centered and scaled based on their mean and standard deviation. Next, model coefficients are estimated for every point in time by optimization of the restricted maximum likelihood using Matlab (The MathWorks Inc., version 2015b). To verify model validity, the model residuals are assessed for normality along the entire EP interval. Significance of the model coefficients is tested against the null-hypothesis using a Wald t-test. To reduce the chance of false significance due to retesting, the requirement is imposed that a coefficient should be significant ($p<0.05$) for at least 4 subsequent time points. Furthermore, the residual is checked for normality along the entire interval.

2.3 Results

2.3.1 Reduction of Background Activity

Figure 2.2 shows that averaging data for every amplitude and stimulus type per subject results in estimated EPs where post-stimulus activity is difficult to distinguish from pre-stimulus activity due to the high amount of background activity. One way to obtain information about how the EP varies with respect to the stimulus amplitude is by pooling the data with respect to the amplitude and average over considerably larger sets of trials. Figure 2.3 shows EP waveforms computed by averaging over trials pooled for the three stimulus amplitudes with the largest number of trials. Although the estimated EPs show a clear variation with respect to stimulus amplitude, the pre-stimulus period shows that our estimate still contains a considerable amount of background activity. Figure 2.4 shows the average fit of a LMM on the same data. In this figure, the pre-stimulus period shows clearly less background activity.

For both figures, the percentage of explained variance was computed by dividing the variance of the model fit by the total variance on each point in time. In the case of averaging, the average was considered the model fit. A comparison between the amount of explained variance in Figure 2.3 and Figure 2.4 shows that the data from all trials using a LMM increases the amount of explained variance. A comparison between the significance returned by cluster-based permutation testing (Maris & Oostenveld, 2007) of the contrast (left) and the significance of the model coefficient (right), shows that testing the model coefficient results in a higher and more sustained significance of the effect of stimulus amplitude.

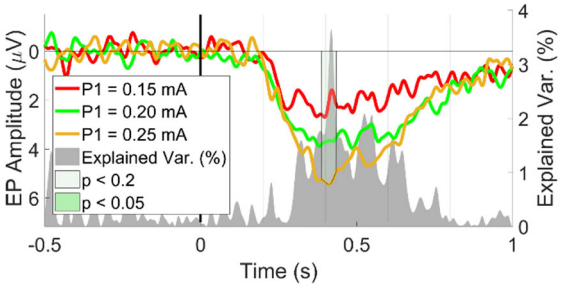

***Figure 2.3**: Grand averages of the EEG signal at Cz, pooled with respect to amplitude values with more than 300 trials. Significance is computed using cluster-based permutation testing (Maris & Oostenveld, 2007).*

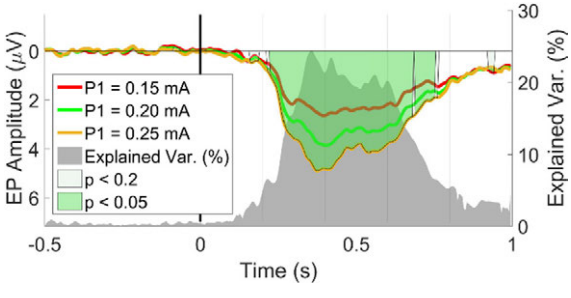

***Figure 2.4**: Average model fit for amplitude values with more than 300 trials at Cz, and the percentage of explained variance of the average model fit. Significance was computed by a Wald t-test of the model coefficient.*

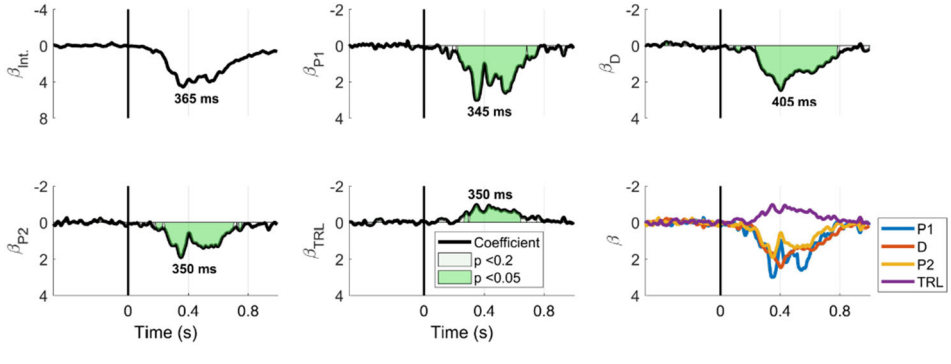

***Figure 2.5**: The model coefficients and their significance based on a Wald t-test at Cz. All coefficients are significant during the post-stimulus interval. The influence of the first pulse and second pulse is computed by the coefficients β_{P1} and β_{P2}. The influence of stimulus detection and the number of received stimuli is computed by the coefficients β_D and β_{TRL}.*

2.3.2 Influence of Stimulus Parameters

Model coefficients are shown in Figure 2.5. All coefficients show a significant modulation of the EP. The coefficients can be used to predict the variation of the EP with respect to the variation of a single parameter. In Figure 2.6 the variation of EP with respect to the pulse amplitudes and stimulus detection is predicted using the model. The Figures 2.3 and 2.4 both show a strong modulation by the stimulus amplitude. However, the prediction of the linear mixed model in Figure 2.6 mostly varies with respect to stimulus detection.

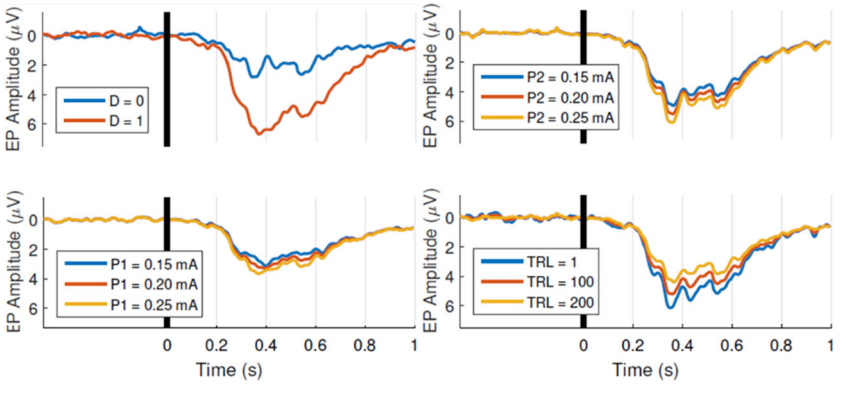

Figure 2.6: The effect of variation of stimulus detection (D), the pulse amplitude (P1 and P2) and the amount of received stimuli (TRL) with respect to the model intercept at Cz.

2.4 Discussion

2.4.1 Reduction of Background Activity

Figure 2.5 shows that evoked potentials which are estimated using a linear mixed model include less background activity and therefore provide a more accurate estimate of the stimulus-related electrophysiological activity. Furthermore, using a LMM increases the percentage of explained variance with respect to averaging by using a larger number of trials. This was successfully demonstrated in Figures 2.3 and 2.4, where an increase of the explained variance from 3.6% to 24.4% can be observed around 0.4 s. The significance

returned by a Wald t-test of the model coefficient shows a higher and more sustained significance of the effect of stimulus amplitude than cluster-based permutation testing. This demonstrates that for a multi-stimulus experiment a Wald t-test of the model coefficient is a more efficient statistical test than cluster-based permutation testing of the contrast.

2.4.2 Influence of Stimulus Parameters

The model shows significant modulation of the EP by all factors. As can be expected based on neurophysiology, the coefficient of the first pulse modulates an earlier part of the EP than the coefficient of the second pulse and the coefficient of stimulus detection.

A major part of the EP waveform is significantly modulated by the amount of received stimuli: due to habituation the EP will be lower with respect to stimuli of the same amplitude at the end of the experiment. While conventional averaging would not have enabled analysis of the influence of stimulus amplitude and the amount of received stimuli, the LMM successfully accounts for those effects.

Since stimulus detection is correlated with the pulse amplitude (i.e., a higher pulse amplitude results in an increased detection probability), the variation in the average EP in Figures 2.3 and 2.4 is likely confounded by stimulus detection. The model prediction in Figure 2.6 shows that the observed variation of the EP is mainly caused by stimulus detection, while changes in pulse amplitudes only result in minor changes of the EP. Conventional averaging might not have revealed these relations between stimulus parameters and the EP, since inclusion of all potential confounders in the analysis would not be possible due to a lack of trials.

2.5 Acknowledgments

The authors would like to thank M. Schooneman and R.J. Doll for acquiring the experimental data used in this study.

2.6 References

Delorme, A., & Makeig, S. (2004). EEGLAB: An open source toolbox for analysis of single-trial EEG dynamics including independent component analysis. *Journal of Neuroscience Methods, 134*(1), 9-21.

Doll, R. J., Buitenweg, J. R., Meijer, H. G. E., & Veltink, P. H. (2014). Tracking of nociceptive thresholds using adaptive psychophysical methods. *Behavior Research Methods, 46*(1), 55-66.

Hauk, O., Pulvermüller, F., Ford, M., Marslen-Wilson, W. D., & Davis, M. H. (2009). Can I have a quick word? Early electrophysiological manifestations of psycholinguistic processes revealed by event-related regression analysis of the EEG. *Biological Psychology, 80*(1), 64-74.

Maris, E., & Oostenveld, R. (2007). Nonparametric statistical testing of EEG- and MEG-data. *Journal of Neuroscience Methods, 164*(1), 177-190.

Oostenveld, R., Fries, P., Maris, E., & Schoffelen, J. M. (2011). FieldTrip: Open source software for advanced analysis of MEG, EEG, and invasive electrophysiological data. *Computational Intelligence and Neuroscience, 2011*.

Smith, N. J., & Kutas, M. (2015). Regression-based estimation of ERP waveforms: I. The rERP framework. *Psychophysiology, 52*(2), 157-168.

Vossen, H. G., Van Breukelen, G., Hermens, H., Van Os, J., & Lousberg, R. (2011). More potential in statistical analyses of event-related potentials: A mixed regression approach. *International Journal of Methods in Psychiatric Research, 20*(3), e56-e68.


NooiTRACK

Chapter 3

Simultaneous Tracking of Psychophysical Detection Thresholds and Evoked Potentials to Study Nociceptive Processing

Published as:

Van den Berg, B.*, Doll, R. J.*, Mentink, A. L. H., Siebenga, P. S., Groeneveld, G. J., & Buitenweg, J. R. (2020). Simultaneous tracking of psychophysical detection thresholds and evoked potentials to study nociceptive processing. *Behavior Research Methods*, 52(4), 1617-1628. **authors contributed equally*

DOI: https://www.doi.org/10.3758/s13428-019-01338-7

Abstract

Measuring altered nociceptive processing involved in chronic pain is difficult due to a lack of objective methods. Potential methods to characterize human nociceptive processing involve measuring neurophysiological activity and psychophysical responses to well-defined stimuli. To reliably measure neurophysiological activity in response to nociceptive stimulation using EEG, synchronized activation of nerve fibers and a large number of stimuli is required. On the other hand, to reliably measure psychophysical detection thresholds, selection of stimulus amplitudes around the detection threshold and many stimulus-response pairs are required. Combining both techniques helps quantifying properties of nociceptive processing related to detected and non-detected stimuli around the detection threshold.

Both techniques were combined in an experiment including 20 healthy participants to study the effect of intra-epidermal electrical stimulus properties (i.e., amplitude, single or double pulse and trial number) on the detection thresholds and vertex potentials. Generalized mixed regression and linear mixed regression were used to quantify the psychophysical detection probability and neurophysiological EEG responses, respectively.

It was shown that the detection probability is significantly modulated by the stimulus amplitude, trial number, and the interaction between stimulus type and amplitude. Furthermore, EEG responses were significantly modulated by stimulus detection and trial number. Hence, we successfully demonstrated the possibility to simultaneously obtain information on psychophysical and neurophysiological properties of nociceptive processing. These results warrant further investigation of the potential of this method to observe altered nociceptive processing.

3.1 Introduction

Identification of malfunctioning mechanisms in the nociceptive system of chronic pain patients is challenging, as it is difficult to quantify properties of nociceptive processing. Many investigators aim to observe properties of central nociceptive processing by measuring neurophysiological responses to cutaneous nociceptive stimuli. The processing of nociceptive stimuli can be divided into three steps: 1) activation of peripheral nociceptive nerve fibers by a stimulus, 2) processing of peripheral input into various central neural representations leading to 3) conscious detection, evaluation and subsequent actions (Dehaene & Naccache, 2001). Observing brain responses related to these steps in nociceptive processing could be useful to study the enhanced pain sensation in chronic pain patients, as plausible explanations include altered mechanisms of upstream nociceptive processing (Sandkühler, 2009) as well as altered brain mechanisms involving pain perception and regulation (Apkarian, Bushnell, Treede, & Zubieta, 2005). Therefore, to be able to study such changes in nociceptive processing using neurophysiological responses, a major step would be to establish methods to quantify stimulus-response relations.

If one wants to specifically study the nociceptive system, stimuli should activate nociceptive nerve fibers, i.e. Aδ and C fibers, selectively (Inui & Kakigi, 2011). One method which preferentially activates nociceptive nerve fibers is intra-epidermal electric stimulation (Inui, Tran, Hoshiyama, & Kakigi, 2002; Otsuru et al., 2009; Otsuru et al., 2010). To preferentially activate nociceptive nerve fibers using intra-epidermal electrical stimulation one has to apply stimulus intensities below twice the detection threshold (Mouraux, 2010).

Changes in the detection threshold, for example drifting (Fründ, Haenel, & Wichmann, 2011), can be observed using adaptive psychophysical methods (Doll, Veltink, & Buitenweg, 2015). Recently, a method was developed for simultaneously tracking the nociceptive detection threshold (NDT) for multiple properties of intra-epidermal electric stimuli, such as the number of pulses and the inter-pulse interval. Simultaneously observing the NDTs for different sets of stimulus properties can be used to characterize various aspects of nociceptive processing in terms of psychophysical (detection) thresholds (i.e.,

NDT) and slopes (i.e., the gradient of detection probability at the detection threshold). Using this method, the drift over time of the NDT and slope and variation of the detection probability with respect to the number of pulses, inter-pulse interval, and pulse-width was quantified (Doll, Maten, Spaan, Veltink, & Buitenweg, 2016). By tracking the NDT, it is possible to observe modulation of nociceptive processing, e.g. the effect of diffuse noxious inhibitory control by tracking NDTs during a cold pressor test (Doll, Buitenweg, Meijer, & Veltink, 2014) and an altered NDT up to several weeks after the application of capsaicin (Doll et al., 2016). The slope provides additional information about the reliability of stimulus detection by subjects (Gold & Ding, 2013). However, a major limitation of this tracking technique is that it is unknown if characteristics of the detection probability are related to psychological or physiological factors. For example, a changing NDT could either be interpreted as a changing subjective detection criterion, or as neuroplasticity of nociceptive processing.

More specific insights into nociceptive processing might be obtained by measuring neurophysiological activity in response to a stimulus using EEG, as this activity is thought to be related to the various central neural representations of the stimulus that contribute to stimulus perception (Mouraux, Iannetti, Baumgärtner, & Treede, 2015). Recently, it was shown that the amplitude of temporal components of the evoked potentials in response to suprathreshold intra-epidermal electrical stimulation can be used to observe altered central processing, such as central sensitization induced by capsaicin (Liang, Lee, O'Neill, Dickenson, & Iannetti, 2016) and by high-frequency stimulation of the skin (Manresa, Andersen, Mouraux, & van den Broeke, 2018). Recent studies demonstrate that the effect of stimulus properties on the evoked potential can be successfully quantified using linear mixed regression (LMR)(Van den Berg & Buitenweg, 2018; Vossen, Vossen, Marcus, Van Os, & Lousberg, 2013; Vossen, Van Breukelen, Hermens, Van Os, & Lousberg, 2011). Vossen et al. recently showed the potential of this technique to identify altered nociceptive processing by demonstrating altered habituation of the evoked potential to nociceptive stimuli in chronic low-back pain patients (Vossen, Vossen, Joosten, Van Os, & Lousberg, 2015).

Acquiring EEG during multiple threshold tracking allows for simultaneous observation of detection thresholds and corresponding evoked potentials in response to multiple types of stimuli while targeting nociceptive pathways by stimulating around the NDT. As such, combining both methods in a single experiment might create an improved method to observe (altered) nociceptive processing. Therefore, the aim of this work is to study the potential of this combination of techniques to explore how stimulus properties are reflected in NDTs and vertex potentials in healthy subjects.

Similar to earlier studies detection probability and the corresponding NDT are tracked in response to intra-epidermal stimuli. Responses to intra-epidermal stimuli with properties similar to those studies (Doll, Maten, Spaan, Veltink, & Buitenweg, 2016; Doll et al., 2016) are analyzed using generalized mixed regression to observe if effects of stimulus properties on the detection probability can be replicated. In addition, this study combines EEG responses with the existing method. A method of integrated analysis of those responses and the detection probability is outlined, in which LMR is used to explore if the evoked potentials observed during this experiment correlate to stimulus properties.

3.2 Methods

The data presented in this paper are acquired from a larger set involving various psychophysical and neurophysiological recordings with stimulation at multiple skin locations, during two occasions. For the purpose of this paper, the currently selected data involves recordings obtained during the first occasion. It contains EEG and stimulus-response pair data collected at three different skin locations: two adjacent locations on the participant's right forearm and one location on the left forearm.

3.2.1 Participants

After approval of the Medical Review and Ethics Committee (Foundation BEBO, Assen, the Netherlands) and in accordance with the declaration of

Helsinki, 20 healthy male participants were enrolled after providing written informed consent. Inclusion criteria were: 18 – 65 years old, body mass index between 19 and 30 kg m-2, good medical condition defined as absence of clinically significant findings in their medical history, physical examination, and vital signs. Exclusion criteria were illicit drug use, frequent caffeine use (> 8 units per day), smokers (> 10 cigarettes per day), extreme responders to capsaicin 1% topical cream (Numeric Rating Scale > 8 out of 10), skin abnormalities and abnormal blood pressure. Moreover, in a separate part of the study (not reported here), erythema or reddening of the skin was measured. As this cannot be measured in dark-toned skin, participants with dark toned skin (Fitzpatrick scale type V and VI) were excluded from the study. The use of over-the-counter medication within 3 days of measurements was not allowed. During the study, participants were to refrain from strenuous physical exercise, use of all (methyl)xanthenes, and alcohol. Participants unable to tolerate the assessments at screening were excluded. Participants received remuneration for participation and could withdraw at any time without jeopardizing the remuneration.

3.2.2 Stimuli

Participants were presented with intra-epidermal electrical stimulation on the anterior part of the left and right volar forearm, to generate a pinprick-like sensation. The electrode for stimulation consisted of an array of five interconnected microneedles serving as a compound cathode. Needles protruded 0.2 mm into the skin, allowing for preferential nociceptive stimulation. A 50 x 90 mm TENS electrode served as anode and was placed distally from the intra-epidermal electrode. Electric stimuli were administered using a custom built constant current stimulator (NociTRACK AmbuStim, University of Twente, Enschede, the Netherlands). The electric stimuli were cathodic rectangular pulses with two different settings (Figure 3.1A):

- A single 210 µs pulse
- A double 210 µs pulse with an inter-pulse interval of 10 ms

3.2.3 Procedure

Participants were seated in a comfortable chair directed towards a wall and were requested to focus on one point on the wall. The procedure started by probing the initial detection threshold with a normal staircase procedure and a step-size of 0.05 mA. Subsequently, stimulus amplitudes were chosen according to an adaptive staircase procedure allowing to stimulate near the detection threshold (Doll, Veltink, & Buitenweg, 2015), as is illustrated in Figure 3.1B. A set of seven equidistant stimulus amplitudes centered around the detection threshold was defined of which the upcoming stimulus was randomly selected. All amplitudes in the set were increased and decreased with a fixed step size of 0.05 mA after a non-detected stimulus and detected stimulus respectively. Single pulse and double pulse stimuli were presented in random order.

During the application of those stimuli, participants were instructed to hold a response button until stimulus detection. While non-detected, the stimulator continued to apply stimuli with a randomized inter-stimulus interval ranging between 3 and 10 seconds. After a stimulus was detected, participants were to release the button and to press the button again after about a second. This procedure was repeated until 100 stimulus response pairs (50 per stimulus type) were collected per skin location (approximately 10 minutes per location). Participants had a small break when the electrode was moved to a different location. A custom computer program (written in LabVIEW 2011, SP1) controlled all stimulation procedures, as well as the registration of stimulus amplitudes in mA, stimulation times in milliseconds, and responses to stimuli (i.e., detected, or non-detected).

3.2.4 Electroencephalography

EEG was recorded with a sample frequency 1024 Hz with a REFA amplifier (TMSi B.V., Oldenzaal, the Netherlands) using a 24-channel electrode cap (10/20 layout and mastoids) and additional leads on the earlobes with the common average as reference. Eye movements were recorded using bipolar electrodes placed at about 2 cm superior to the right eye outer canthus, and 2

cm inferior to the left eye outer canthus. Electrode impedances were kept below 5 kΩ.

EEG data was preprocessed using FieldTrip (Oostenveld, Fries, Maris, & Schoffelen, 2011). For each trial of the experiment, which is defined as the application of one stimulus, EEG epochs were extracted from 0.5 s pre- to 1 s post-stimulus (Figure 3.1D). Epochs were bandpass filtered between 0.1 and 30 Hz using a 2nd order Butterworth high-pass filter and a 6th order Butterworth lowpass filter, and baseline corrected using the 500 – 0 ms pre-stimulus interval. Epochs containing eye blink artefacts were removed using automatic rejection of epochs containing potentials larger than 3 times the standard deviation based on either the EOG or FPz channel. Stimulus-response pairs corresponding to those epochs were also removed from the dataset prior to statistical analysis.

3.2.5 Statistical Analysis

Data preparation and statistical analysis of the effects of stimulus properties on EPs was performed in MATLAB 2017b (MathWorks, Inc.). Statistical analysis of the effect of stimulus properties on the detection probability was performed in R using the lme4 toolbox (Bates, Mächler, Bolker, & Walker, 2015).

Effect of Stimulus Properties on Detection Probability

The effect of stimulus properties on the detection probability was evaluated using generalized linear mixed regression (GLMR) using a logit link function. The intercept, stimulus amplitude (AMP, in mA), type (TYP), trial number (TRL), stimulation location (LOC), and the interaction between the stimulus amplitude and stimulus type were included as fixed effects. First all fixed effects were included as random effects, grouped by subject. Subsequently random effects were excluded if this led to a lower model AIC. As a result, between-subjects random effects were included for the intercept, the stimulus amplitude, stimulus type, trial number, and location. The trial number variable was centered and scaled prior to analysis to speed up the estimation process. An

unstructured covariance matrix was used to model the random effects. The equation of the used GLMR model in Wilkinson notation is shown in (1).

$$ln\left(\frac{P_d}{1-P_d}\right) \sim 1 + AMP * TYP + TRL + LOC + (1 + AMP * TYP + TRL + LOC|S) \quad (1)$$

Type III Wald Chi-square statistics were used to test the main and interaction effects of the fixed effects. Confidence intervals of the regression parameters were based on the Wald z statistics. Threshold and slope estimates were obtained from the regression parameters. The logistic psychophysical curves representing the detection probability were computed by inverse-logit transformation of the regression parameters. Note that the guess rate and lapse rate were both assumed to be zero for robust estimation of psychometric function parameters.

Effect of Stimulus Properties on EEG

EEG data at the Cz-A1A2 derivation were used for modeling and analysis. The effect of stimulus properties on the EEG potential (U_EEG) was computed for every point in time using LMR (Figure 3.1E). The equation of the used LMR model in Wilkinson notation is shown in (2).

$$U_{EEG} \sim 1 + AMP * TYP * RES + TRL * RES + LOC * RES + (1 + AMP + RES + TRL|S) \quad (2)$$

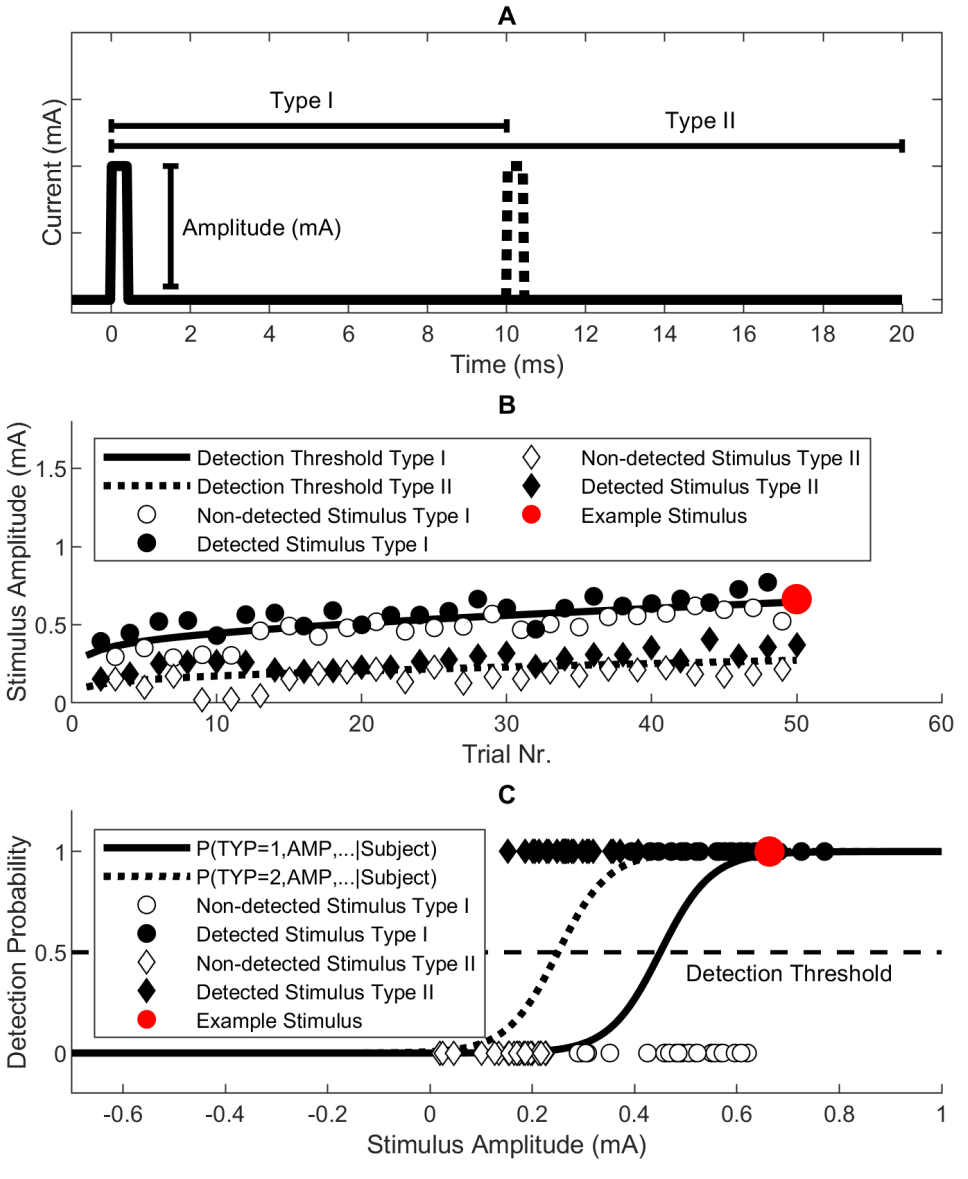

***Figure 3.1 (A-C)**: Workflow for simultaneous recording and analysis of NDTs and EEG. A. Stimulate using one or more types of phasic stimuli. B. Use an adaptive paradigm to stimulate close to the detection threshold and record whether a stimulus is detected. C. Use GLMR to compute the detection probability (P) as a function of stimulus properties, e.g., the stimulus type (TYP) and amplitude (AMP) and determine the detection threshold with respect to every stimulus.*

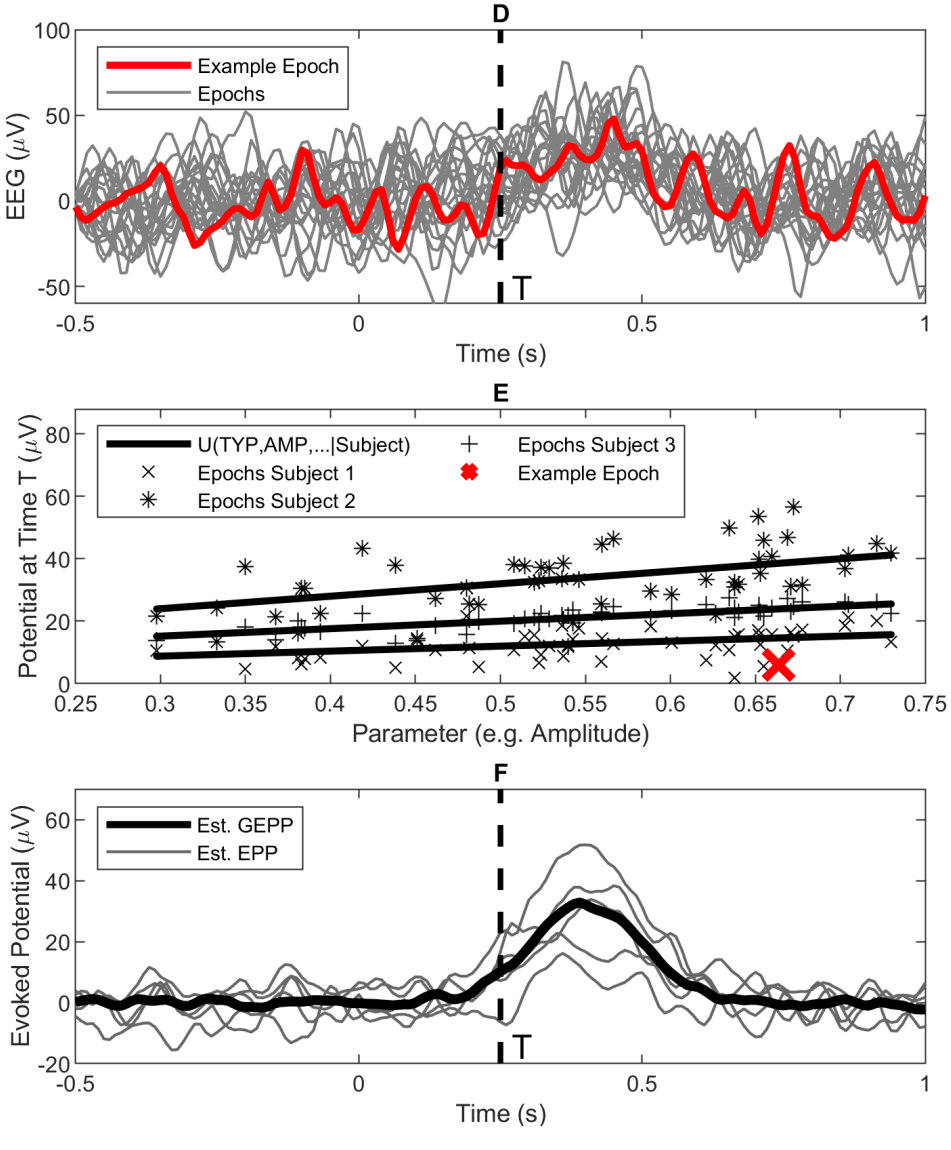

***Figure 3.1 (D-F)**: D. Record an EEG epoch for every stimulus. E. For every time-point T in the set of EEG epochs, use LMR to compute the potential (U) as a function of stimulus properties, e.g., the stimulus type (TYP) and amplitude (AMP). F. Use the obtained LMR for every point in time to predict the potential for a specific set of parameters over all subjects (grand evoked potential prediction, GEPP) or for specific subjects (evoked potential prediction, EPP). As an example, one stimulus and the corresponding results are shown in red.*

The stimulus amplitude (AMP, in mA), stimulus type (TYP), trial number (TRL) and the interaction between stimulus amplitude and stimulus type were included as fixed effects in the LMR model to study the effect of these parameters. Furthermore, stimulation location (LOC) was included to prevent potential confounding by the location or the order in which the locations were measured. An interaction of all those fixed effects with response (RES) as well as the main effect of response were included to account for differences in processing between detected and non-detected stimuli. Random effects grouped by subject (S) were chosen by first including all fixed effects and interactions, and subsequently excluding random effects if this led to a lower model AIC. An unstructured covariance matrix was used to model the random effects.

For every point in time, regression parameters were estimated by optimization of the restricted maximum likelihood. Normality of the model residuals was assessed by computing residual skewness and kurtosis along the entire epoch. Significance of the fixed effects in the LMR model was tested using the t-statistic with Satterthwaite's method for estimation of the degrees of freedom. Subsequently, significance values were corrected for positive dependence in time using Benjamini-Hochberg correction (Groppe, Urbach, & Kutas, 2011; Hochberg & Benjamini, 1995). Furthermore, LMR parameters were used to model the effect of trial parameters on the time-locked EEG, resulting in an evoked potential prediction (EPP) on the subject level and a grand evoked potential prediction (GEPP) on the group level (Figure 3.1F). This was done by filling out the LMR equation for each point in time using the corresponding trial parameters.

3.3 Results

A total of 20 participants participated in the experiment. One participant withdrew from the experiment and was replaced. A total of 7 measurements were excluded due to technical issues leaving 53 measurements available for analysis. After rejecting epochs with ocular activity, 216±52 stimulus response pairs and corresponding EEG epochs were available per participant in which 90.5% of the stimuli were estimated to be below two times the NDT.

Parameter	Parameter Estimate	95 % Confidence Interval	Effect χ^2(df)	Effect *p*
(Intercept)	-3.52	[-4.36 -2.68]	67.66 (1)	< .001
Stimulus amplitude	8.55	[6.78 10.32]	89.67 (1)	< .001
Stimulus type			0.39 (1)	.53
Double pulse	0.21	[-0.45 0.88]		
Location			3.18 (2)	.20
Second	-0.72	[-1.70 0.26]		
Third	0.12	[-1.04 1.28]		
Trial number	-0.42	[-0.58 -0.27]	27.58 (1)	< .001
Type × Amplitude			57.94 (1)	< .001
Double pulse	9.38	[6.96 11.79]		

***Table 3.1**: Regression parameter estimates of the fixed effects of the GLMR, corresponding confidence intervals and type III Wald statistics of the main effects. There is a significant increase of detection probability with respect to amplitude. There is a significant decrease of the detection probability with respect to the trial number, which results in an increase of the NDT. Furthermore, there is a significant positive interaction between stimulus type and amplitude, effectively resulting in a higher detection probability and lower NDT for double pulse stimuli.*

3.3.1 Effect of Stimulus Properties on Detection Probability

Table 3.1 presents the estimated log-odds for the parameters of the GLMR model with corresponding 95% confidence intervals and significance tests for the main effects. Stimulus amplitude, trial number, and the interaction between stimulus type and amplitude had a significant effect on the detection probability. However, there was no indication of the stimulation location and stimulus type having a significant effect on the intercept of the detection probability. The regression parameters were inverse-logit transformed to obtain the logistic psychophysical curves for both settings at the first stimulation area (Figure 3.2). The average NDTs for a single and double pulse stimulus were 0.50 and 0.22 mA, respectively. The slopes for single and double pulse stimuli were found to be 8.55 and 17.93 mA^{-1}, respectively. Adding a second pulse to the stimulus significantly decreased the NDT and significantly increased the detection slope ($p < .001$). The NDT increased with respect to the trial number. Effectively, the NDT for single pulse stimuli increases from 0.41 mA at the start of the experiment to 0.59 mA at the end of the experiment, while the NDT for double pulse stimuli increased from to 0.18 mA to 0.27 mA.

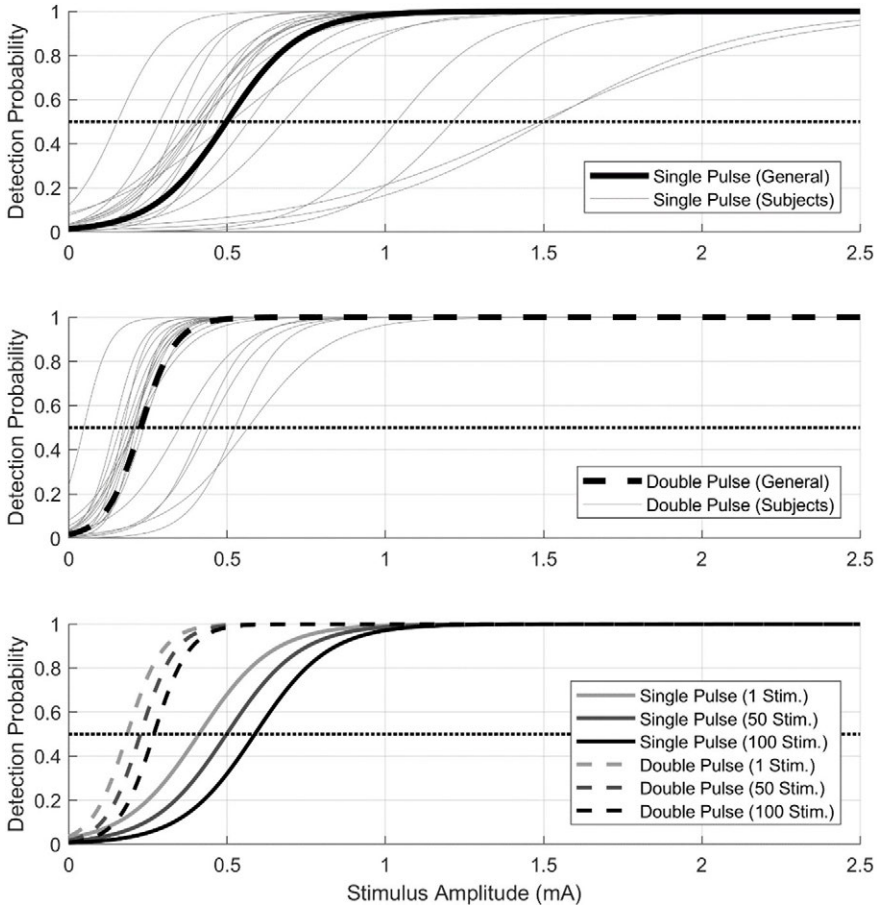

Figure 3.2: Logistic psychophysical curves modelling the detection probability were obtained by inverse-logit transformation of the regression parameters. The resulting general and subject-level detection probabilities for single and double pulse stimuli are shown in the first two figures and their variation with respect to the trial number is shown in the bottom figure. The first two figures show that the psychophysical curve of double pulse stimuli has a steeper slope and a lower NDT than the curve for single pulse stimuli. The bottom figure shows that the NDT increases with respect to the number of trials, where '1 Stim.' corresponds to the start, '50 Stim.' to the middle and '100 Stim.' to the end of the experiment.

3.3.2 Effect of Stimulus Properties on Evoked Potentials

To determine the effect of stimulus parameters on the evoked potential, LMR parameters were computed for every point in time at Cz-A1A2 based on the entire set of EEG epochs. The skewness and excess kurtosis of the model

residuals along the entire epoch are shown in Figure 3.3. The excess kurtosis has a maximum value over the entire epoch of 3.91, while the skewness has a maximum value over the entire epoch of 0.37.

Parameters and their significances are shown in Figure 3.4. Parameters of detected and non-detected stimuli appear to show a positive effect of amplitude, type and the interaction between amplitude and type on the evoked potential. However, none of these effects or their interactions with response is significant. A negative effect of trial number on the evoked potential was observed. This effect significantly interacts with response between 250 and 500 ms, as the effect of trial number is much larger for detected stimuli at these latencies.

Figure 3.5 shows the GEPP and EPPs of single pulse and double pulse detected and non-detected stimuli. For detected and non-detected stimuli there was a positive peak in the GEPP around 340 ms, and a late positive component between 500 and 1000 ms. The peak at 340 ms had a larger amplitude for detected stimuli (single pulse: 10.10 μV, double pulse: 11.75 μV) than for non-detected stimuli (single pulse: 4.89 μV, double pulse: 5.10 μV). Furthermore, there was a larger P340 amplitude for double pulse stimuli than for single pulse stimuli.

The effect of trial number on the GEPP is displayed in Figure 3.6. GEPPs corresponding to both detected and non-detected stimuli are decreasing with an increasing number of trials, with a major decrease between 200 ms and 900 ms. For detected stimuli, the P340 amplitude decreases from 14.37 μV at the first trial to 6.18 μV at the last trial (single pulse) and from 16.12 μV at the first trial to 7.27 μV at the last trial (double pulse). For non-detected stimuli, the P340 amplitude decreases from 6.56 μV at the first trial to 3.18 μV at the last trial (single pulse) and from 6.77 μV at the first trial to 3.41 μV at the last trial (double pulse).

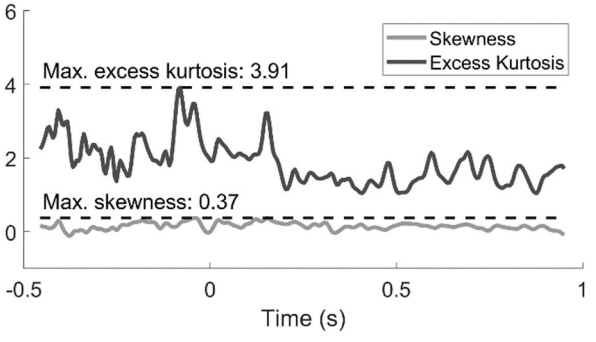

Figure 3.3: Skewness and excess kurtosis of LMR residuals over time.

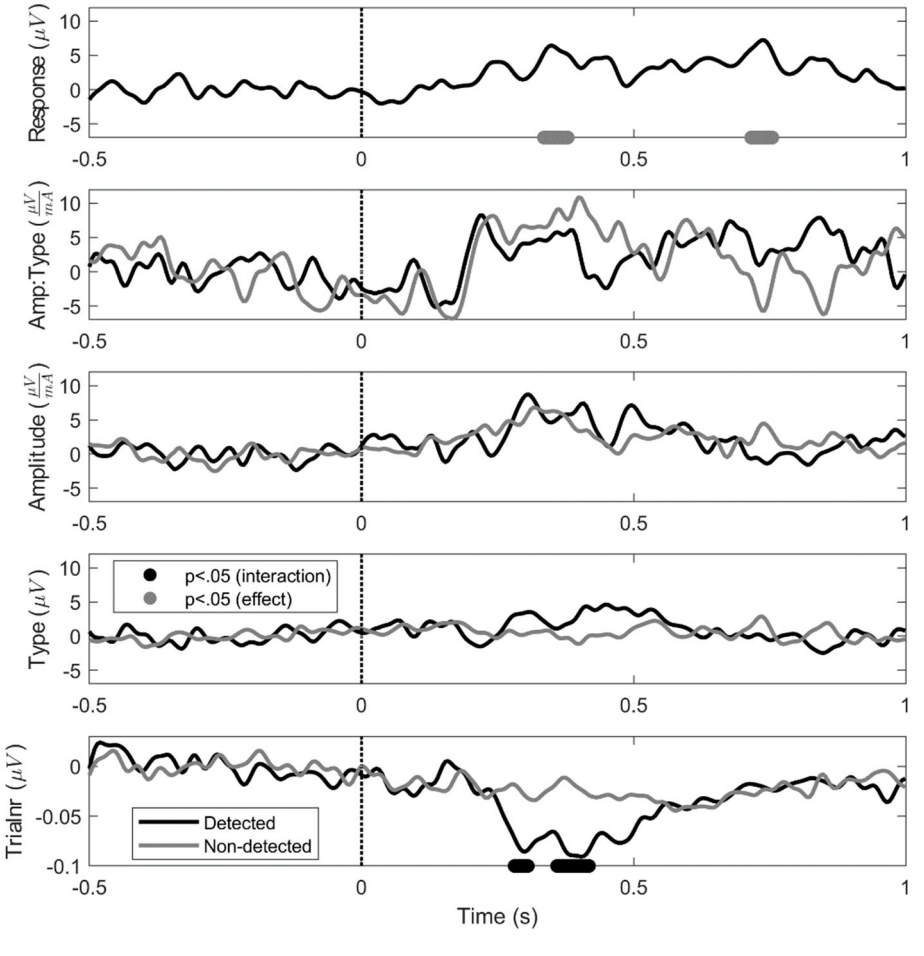

Figure 3.4: LMR parameters over time, which quantify the effect of each stimulus property on the evoked potential for detected (black) and non-detected (gray) stimuli. Gray and black dots below the curves respectively indicate an effect and an interaction with response that is significantly different than zero (p<0.05).

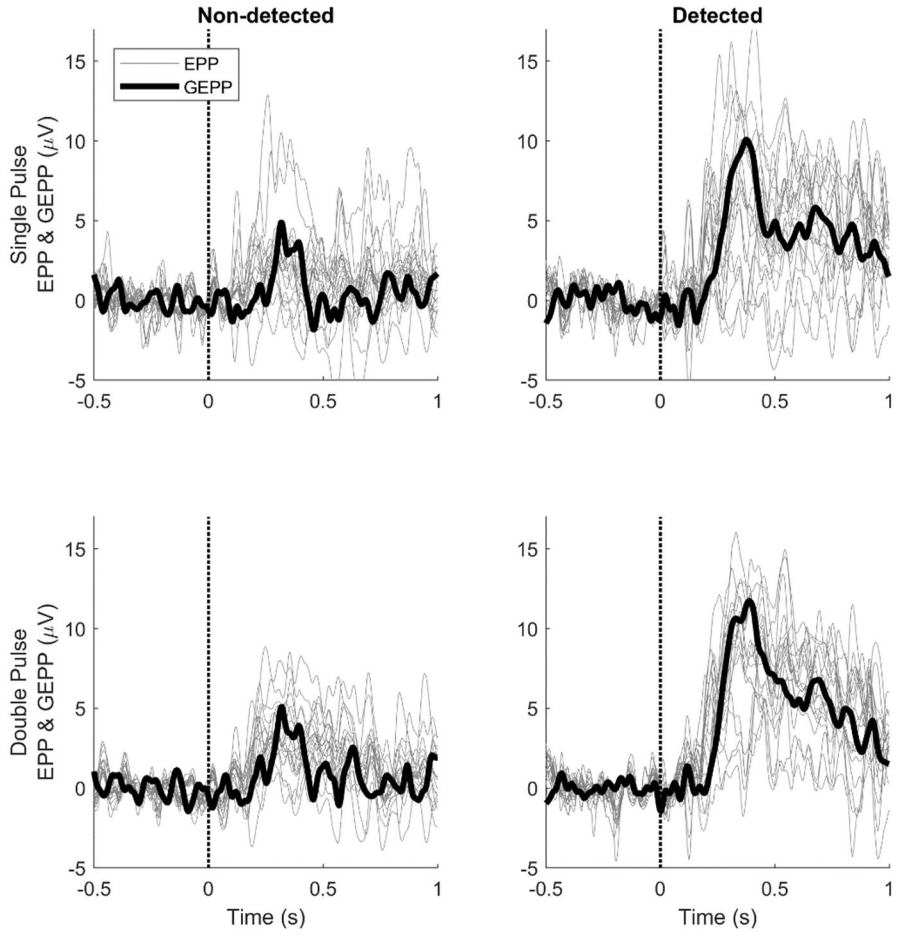

***Figure 3.5**: GEPPs and EPPs at Cz-A1A2 in response to stimuli with a stimulus amplitude equal to the NDT, computed using LMR. EPPs (gray) show the spread of subject responses, which is at its largest around 340 milliseconds. GEPPs show the responses on group level, with a peak around 340 ms and a late positive component between 500 and 1000 ms.*

The effect of stimulus amplitude on the GEPP is shown in Figure 3.7. Both non-detected and detected stimuli show some variation with respect to the stimulus amplitude. However, the GEPP in response to detected stimuli is larger than the GEPP in response to non-detected stimuli, regardless of using the same stimulus amplitude. For example, the amplitude of the GEPP for detected stimuli at 2 times the NDT is 12.98 μV (single pulse) and 14.45 μV (double pulse), while for non-detected stimuli at 2 times the NDT, this is 8.28 μV (single pulse) and 8.12 μV (double pulse).

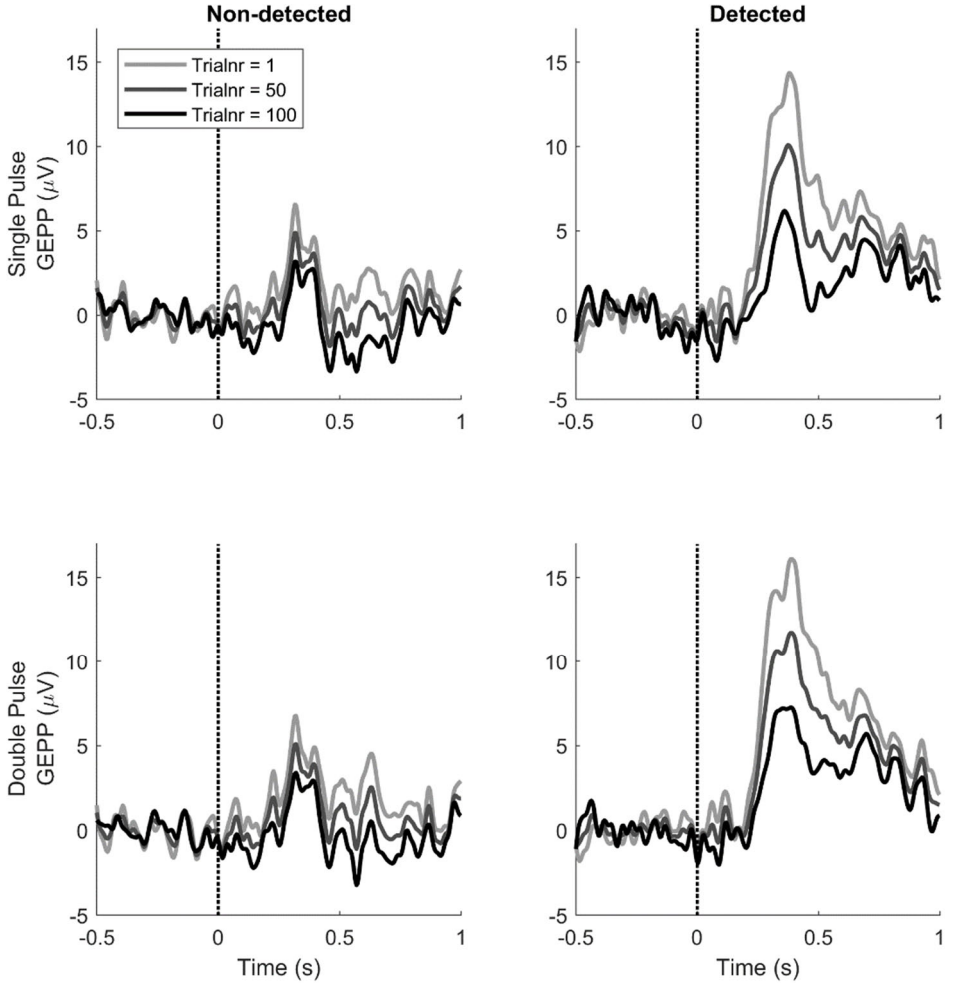

Figure 3.6: GEPPs in response to stimuli with a stimulus amplitude equal to the NDT after 1, 50 and 100 trials, computed using LMR. The GEPP varies the most around 340 ms with respect to detected stimuli.

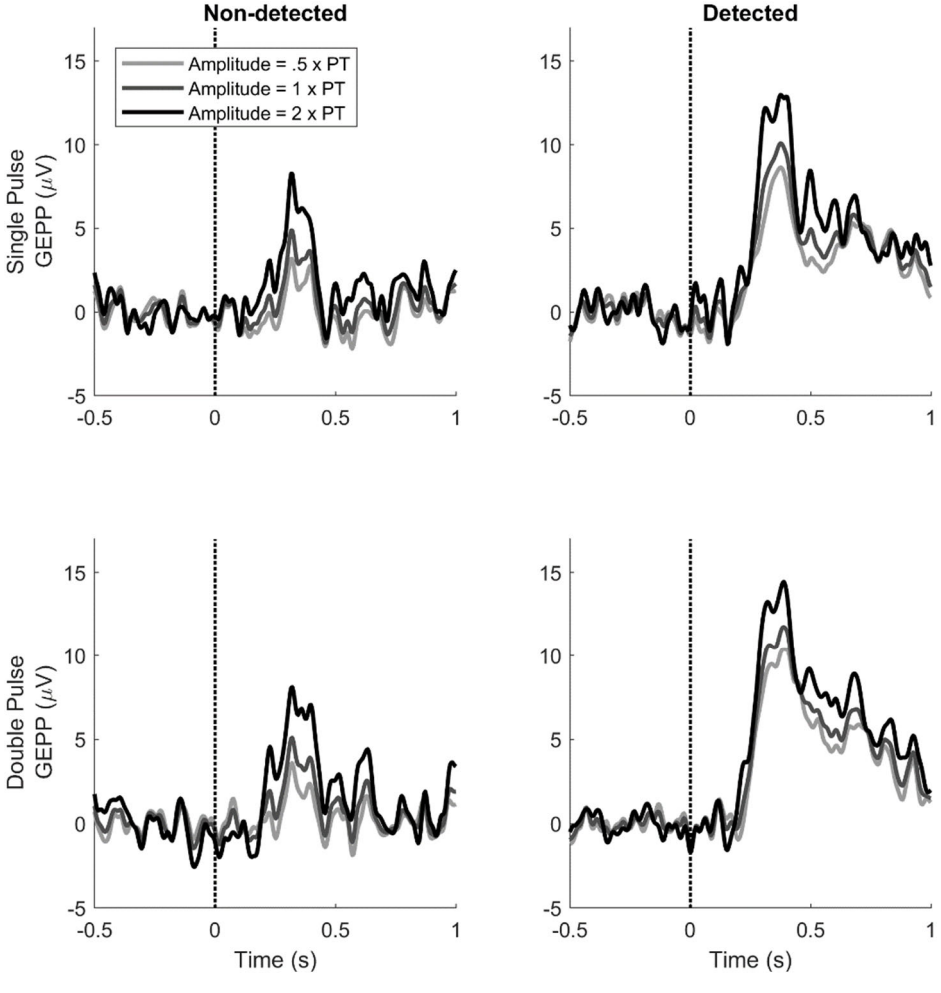

Figure 3.7: *GEPPs in response to stimuli with a stimulus amplitude of 0.5, 1.0 and 2 times the NDT. The GEPP varies the most around 340 ms for both detected and non-detected stimuli.*

3.4 Discussion

In this experiment, evoked potentials and NDTs with respect to nociceptive specific stimuli were simultaneously measured. The detection probability was tracked using an adaptive stimulus selection procedure aimed at stimulating close to the NDT, while EEG was recorded in response to every stimulus. Here, the same electrode was used and the effect of temporal stimulus properties on the NDT was quantified using the same method to track the detection threshold (Doll, Maten, Spaan, Veltink, & Buitenweg, 2016). The computed NDTs and slopes in this experiment are in a similar range to those reported earlier by Doll et al.

The evoked potentials were acquired and analyzed in combination with stimulus-response pairs. LMR was used to compute the effects of stimulus properties on the evoked potential. Evoked potentials in response to detected and non-detected stimuli were observed in the GEPPs and EPPs, as shown in Figures 3.5, 3.6, and 3.7. The evoked potential in response to detected stimuli shows a positive component with the peak amplitude near 340ms (i.e., P340), with a late positive component between 500 and 1000 ms.

The waveform and latency of the observed P340 appears to correspond to the P2 reported in literature (Legrain, Bruyer, Guérit, & Plaghki, 2003; Legrain, Guérit, Bruyer, & Plaghki, 2002). The P340 will be referred to as the P2 in the next sections. While others report a positive correlation between the stimulus amplitude and the P2 amplitude (Ohara, Crone, Weiss, Treede, & Lenz, 2004), this correlation was not significant here. As the detection threshold increased with the number of given stimuli, the stimulation amplitudes also increased (see Figure 3.2). As a result, the given stimulus amplitudes were only varied within a relatively small range around the detection threshold limiting the observability of this correlation. Regardless, a trend suggesting an increased P2 amplitude with increased stimulus amplitudes can be visually observed (see Figure 3.7). Potential correlation could be more accurately assessed in follow-up studies by increasing the range of stimulus amplitudes or by increasing the number of trials.

The observed late positive component between 500 and 1000 ms (see Figure 3.7) significantly different between detected and non-detected stimuli. The behavior and the latency of this component is similar to earlier reports of the P3b component (Legrain, Bruyer, Guérit, & Plaghki, 2003). Although this component is normally evoked by rare stimuli in an oddball paradigm, this component has also been obtained earlier in one-stimulus paradigms where subjects have to detect all stimuli (Polich, Eischen, & Collins, 1994). Based on these similarities with literature, the late positive component between 500 and 1000 ms will be referred to as the P3b in the next sections.

3.4.1 Effect of Stimulus Properties on Detection Probability and Evoked Potentials

The effect of stimulus properties on the evoked potentials was studied by computing the GLMR and LMR parameters in Table 3.1 and Figure 3.4, and predicting the GEPPs and EPPs in Figures 3.5, 3.6 and 3.7. In general, it can be observed that all GEPPs increase in amplitude when a stimulus is detected. The LMR parameter for response in Figure 3.4 shows that parts of the P2 as well as P3b are significantly modulated by stimulus detection. While the P3b appears to be exclusively present when a stimulus was detected, the P2 can be identified in responses to both detected and non-detected stimuli. This observation could mean that the P2 component contains information about an internal stimulus representation prior to the conscious detection of stimuli. However, it is important to note that this component could also be present due to false negative responses of the subjects, in which subjects did feel the stimulus but did not release the response button.

When comparing the NDTs and slopes corresponding to the single and double pulse stimuli, it was observed that the NDT was lower, and the slope was steeper for a double pulse stimulus than for a single pulse stimulus (see Figure 3.2). This is similar to earlier findings (Doll, Maten, Spaan, Veltink, & Buitenweg, 2016). There, it was hypothesized that a facilitating nociceptive mechanism is also involved in the processing of double pulses resulting in an even lower NDT for double pulse stimuli than would be expected based on the principle of

probability summation. The underlying physiology of this effect remains unknown and could include central (e.g. temporal summation, short-term synaptic plasticity (Zucker & Regehr, 2002) or peripheral (e.g. subthreshold or suprathreshold superexcitability (Bostock et al., 2005)) mechanisms. Even though such a difference was observed in NDT and slopes, no significant difference in P2 amplitudes for single and double pulse stimuli was observed here (see Figure 3.4). Potential explanations for this are discussed in Section 3.4.2. Regardless, the differences in nociceptive processing between single pulse and double pulse stimuli might be further studied in future work combining this technique with experimental pain models to study the individual contributions of specific inhibitory and facilitating mechanisms to this effect.

In Figure 3.6, it is shown that the GEPP around the P2 decreases with respect to the trial number. This effect can be observed most clearly on the GEPP in response to detected stimuli. Figure 3.4 shows that there is indeed a negative effect of trial number on the evoked potential, with a significant interaction with response. A similar effect is also observed for the detection probability in Figure 3.2 and a significant negative parameter for the effect of trial number on detection probability in Table 3.1. Such a negative effect of the number of received stimuli was shown in earlier studies on the evoked potential by Vossen et al. (Vossen, Vossen, Marcus, Van Os, & Lousberg, 2013; Vossen, Van Breukelen, Hermens, Van Os, & Lousberg, 2011) and on the NDT and detection probability by Doll et al. (Doll, Maten, Spaan, Veltink, & Buitenweg, 2016). In both studies this effect was referred to as habituation. This effect might be attributed to a decreasing attention to the stimuli or to a changing criterion for stimulus detection. Although the exact mechanism is unknown, estimating the effect of trial number on the evoked potential and the NDT is a relevant subject for further studies, as it could be a potential biomarker for several types of diseases, such as chronic low back pain (Vossen, Vossen, Joosten, Van Os, & Lousberg, 2015), fibromyalgia (Smith et al., 2008) and migraine (Valeriani et al., 2003).

In Figure 3.7 an increase of the GEPP with respect to stimulus amplitude is shown, corresponding to a positive LMR parameter for stimulus amplitude and the interaction between stimulus amplitude and stimulus type in Figure 3.4. As

both parameters were not significant, their true effect size for both detected and non-detected stimuli is to be evaluated in future studies. As such, recommendations for future studies for more accurate measurements of these effects are discussed in the next paragraph.

3.4.2 Recommendations for Simultaneous Tracking of Psychophysical Detection Thresholds and Evoked Potentials

This study was a first-time demonstration of the concept of simultaneous tracking of psychophysical detection thresholds and evoked potential. As no previous EEG data was available from such a study design, power considerations were not based on EEG data. Furthermore, no assumptions could be made regarding the evoked potential component latencies and therefore no tests could be defined a priori. Instead, EEG data was tested in an exploratory fashion at every latency, requiring temporal correction for retesting using Benjamini-Hochberg correction. Although this method guarantees our false discovery rate to remain below the set critical value (5%), this could reduce the power of potentially significant effects. As the range of amplitudes was relatively limited, potential effects of stimulus amplitude on the EP and interactions with stimulus type could not be found. If an effect exists, it might be observed by increasing the range of stimulus amplitudes. Furthermore, future studies might also improve the accuracy of estimated effect sizes by increasing the number of trials and subjects.

In addition, Figure 3.3 shows a relatively high excess kurtosis (max. 3.91) of the LMR residuals. A high kurtosis indicates that the residual distribution has fat tails associated to outlying values of EEG potential, which results in a loss of power in the statistical tests. Such outliers are likely caused by artefacts in EEG data (Delorme, Sejnowski, & Makeig, 2007). As in this study a high kurtosis remains despite rejection of EOG artefacts, potential improvement could be made by either 1) improved training of participants to prevent EEG artifacts or 2) enhanced detection of artefacts in EEG data. Furthermore, excessive EEG noise might obscure any small variations in the evoked potential with respect to stimulus parameters. As the set of stimuli comprised a relatively narrow

range of stimulus amplitudes around the detection threshold, EEG noise might have influenced significance of this parameter.

3.5 Conclusion

This study demonstrated a method to record NDTs and evoked potentials in response to stimuli around those thresholds and quantify the effect of stimulus properties on those measures. Threshold tracking made it possible to observe the time-course of the NDT and to center stimulation around the detection threshold to preferentially stimulate nociceptive nerve fibers. As evoked potentials are related to the central neural representations underlying stimulus perception, they could help to assess properties of nociceptive processing more objectively in a clinical context. This study quantified the effect of stimulus properties on healthy subjects as a proof of principle. However, the most interesting application of this method would be to study how nociceptive processing is modulated by experimental pain models, therapeutic interventions, and most importantly chronic pain. In the current study, the exact mechanisms of the observed effects of stimulus properties on evoked potentials remain unknown, and some of these effects were insignificant. Therefore, subsequent studies should focus on accurately documenting the effects of stimulus properties on NDTs and evoked potentials in healthy subjects and compare those to the effects under abnormal conditions. Besides shedding more light on nociceptive system behavior, this could be used to determine if combined NDT and evoked potential measurement provides a valid metric for alterations of the nociceptive system associated to chronic pain.

3.6 References

Apkarian, A. V., Bushnell, M. C., Treede, R.-D., & Zubieta, J.-K. (2005). Human brain mechanisms of pain perception and regulation in health and disease. *European Journal of Pain, 9*(4), 463-463.

Bates, D., Mächler, M., Bolker, B., & Walker, S. (2015). Fitting Linear Mixed-Effects Models Using lme4. *Journal of Statistical Software; Vol 1, Issue 1 (2015)*.

Bostock, H., Lin, C. S.-Y., Howells, J., Trevillion, L., Jankelowitz, S., & Burke, D. (2005). After-effects of near-threshold stimulation in single human motor axons. *The Journal of physiology, 564*(Pt 3), 931-940.

Dehaene, S., & Naccache, L. (2001). Towards a cognitive neuroscience of consciousness: basic evidence and a workspace framework. *Cognition, 79*(1), 1-37.

Delorme, A., Sejnowski, T., & Makeig, S. (2007). Enhanced detection of artifacts in EEG data using higher-order statistics and independent component analysis. *NeuroImage, 34*(4), 1443-1449.

Doll, R. J., Buitenweg, J. R., Meijer, H. G. E., & Veltink, P. H. (2014). Tracking of nociceptive thresholds using adaptive psychophysical methods. *Behavior Research Methods, 46*(1), 55-66.

Doll, R. J., Maten, A. C. A., Spaan, S. P. G., Veltink, P. H., & Buitenweg, J. R. (2016). Effect of temporal stimulus properties on the nociceptive detection probability using intra-epidermal electrical stimulation. *Experimental Brain Research, 234*(1), 219-227.

Doll, R. J., van Amerongen, G., Hay, J. L., Groeneveld, G. J., Veltink, P. H., & Buitenweg, J. R. (2016). Responsiveness of electrical nociceptive detection thresholds to capsaicin (8 %)-induced changes in nociceptive processing. *Experimental Brain Research, 234*(9), 2505-2514.

Doll, R. J., Veltink, P. H., & Buitenweg, J. R. (2015). Observation of time-dependent psychophysical functions and accounting for threshold drifts. *Attention, Perception, and Psychophysics, 77*(4), 1440-1447.

Fründ, I., Haenel, N. V., & Wichmann, F. A. (2011). Inference for psychometric functions in the presence of nonstationary behavior. *Journal of Vision, 11*(6), 16-16.

Gold, J. I., & Ding, L. (2013). How mechanisms of perceptual decision-making affect the psychometric function. *Progress in Neurobiology, 103*, 98-114.

Groppe, D. M., Urbach, T. P., & Kutas, M. (2011). Mass univariate analysis of event-related brain potentials/fields I: A critical tutorial review. *Psychophysiology, 48*(12), 1711-1725.

Hochberg, Y., & Benjamini, Y. (1995). Controlling the false discovery rate: A Practical and powerful approach to multiple testing. *J.Roy.Statist.Soc.*, *57*, 289-300.

Inui, K., & Kakigi, R. (2011). Pain perception in humans: use of intraepidermal electrical stimulation. . *J Neurol Neurosurg Psychiatry*.

Inui, K., Tran, T. D., Hoshiyama, M., & Kakigi, R. (2002). Preferential stimulation of Aδ fibers by intra-epidermal needle electrode in humans. *Pain, 96*(3), 247-252.

Legrain, V., Bruyer, R., Guérit, J. M., & Plaghki, L. (2003). Nociceptive processing in the human brain of infrequent task-relevant and task-irrelevant noxious stimuli. A study with event-related potentials evoked by CO2 laser radiant heat stimuli. *Pain, 103*(3), 237-248.

Legrain, V., Guérit, J. M., Bruyer, R., & Plaghki, L. (2002). Attentional modulation of the nociceptive processing into the human brain: Selective spatial attention, probability of stimulus occurrence, and target detection effects on laser evoked potentials. *Pain, 99*(1-2), 21-39.

Liang, M., Lee, M. C., O'Neill, J., Dickenson, A. H., & Iannetti, G. D. (2016). Brain potentials evoked by intraepidermal electrical stimuli reflect the central sensitization of nociceptive pathways. *Journal of Neurophysiology, 116*(2), 286-295.

Manresa, J. B., Andersen, O. K., Mouraux, A., & van den Broeke, E. N. (2018). High frequency electrical stimulation induces a long-lasting enhancement of event-related potentials but does not change the perception elicited by intra-epidermal electrical stimuli delivered to the area of increased mechanical pinprick sensitivity. *PLoS ONE, 13*(9).

Mouraux, A., Iannetti, G. D., Baumgärtner, U., & Treede, R. D. (2015). Evoked potentials in relation to pain perception. In A. V. Apkarian (Ed.), *The brain adapting with pain: Contribution of neuroimaging technology to pain mechanisms*: IASP Press.

Mouraux, A., Iannetti, G. D., & Plaghki, L. (2010). Low intensity intra-epidermal electrical stimulation can activate Aδ-nociceptors selectively. *Pain, 150(1)*, 199-207.

Ohara, S., Crone, N. E., Weiss, N., Treede, R. D., & Lenz, F. A. (2004). Amplitudes of laser evoked potential recorded from primary somatosensory, parasylvian and medial frontal cortex are graded with stimulus intensity. *Pain, 110*(1-2), 318-328.

Oostenveld, R., Fries, P., Maris, E., & Schoffelen, J. M. (2011). FieldTrip: Open source software for advanced analysis of MEG, EEG, and invasive electrophysiological data. *Computational Intelligence and Neuroscience, 2011*.

Otsuru, N., Inui, K., Yamashiro, K., Miyazaki, T., Ohsawa, I., Takeshima, Y., & Kakigi, R. (2009). Selective stimulation of C fibers by an intra-epidermal needle electrode in humans. *Open Pain J, 2*, 53-56.

Otsuru, N., Inui, K., Yamashiro, K., Miyazaki, T., Takeshima, Y., & Kakigi, R. (2010). Assessing A-delta Fiber Function With Lidocaine Using Intraepidermal Electrical Stimulation. *The Journal of Pain, 11*(7), 621-627.

Polich, J., Eischen, S. E., & Collins, G. E. (1994). P300 from a single auditory stimulus. *Electroencephalography and Clinical Neurophysiology/Evoked Potentials Section, 92*(3), 253-261.

Sandkühler, J. (2009). Models and Mechanisms of Hyperalgesia and Allodynia. *Physiological Reviews, 89*(2), 707-758.

Smith, B. W., Tooley, E. M., Montague, E. Q., Robinson, A. E., Cosper, C. J., & Mullins, P. G. (2008). Habituation and sensitization to heat and cold pain in women with fibromyalgia and healthy controls. *Pain, 140*(3), 420-428.

Valeriani, M., de Tommaso, M., Restuccia, D., Le Pera, D., Guido, M., Iannetti, G. D., . . . Cruccu, G. (2003). Reduced habituation to experimental pain in migraine patients: a CO2 laser evoked potential study. *Pain, 105*(1), 57-64.

Van den Berg, B., & Buitenweg, J. R. (2018). *Analysis Of Nociceptive Evoked Potentials During Multi-Stimulus Experiments Using Linear Mixed Models*. Paper presented at the 40th Annual International Conference of the IEEE Engineering in Medicine and Biology Society (EMBC), Honolulu, United States.

Vossen, C. J., Vossen, H. G., Joosten, E. A., Van Os, J., & Lousberg, R. (2015). Does habituation differ in chronic low back pain subjects compared to pain-free controls? A cross-sectional pain rating ERP study reanalyzed with the ERFIA multilevel method. *Medicine (United States), 94*(19).

Vossen, C. J., Vossen, H. G., Marcus, M. A., Van Os, J., & Lousberg, R. (2013). Introducing the event related fixed interval area (ERFIA) multilevel technique: A method to analyze the complete epoch of event-related potentials at single trial level. *PLoS ONE, 8*(11).

Vossen, H. G., Van Breukelen, G., Hermens, H., Van Os, J., & Lousberg, R. (2011). More potential in statistical analyses of event-related potentials: A mixed regression approach. *International Journal of Methods in Psychiatric Research, 20*(3), e56-e68.

Zucker, R. S., & Regehr, W. G. (2002). Short-term synaptic plasticity. *Annual Review of Physiology, 64*, 355-405.


NoodleTRACK

Chapter 4

Observation of Nociceptive Processing: Effect of Intra-Epidermal Electric Stimulus Properties on Detection Probability and Evoked Potentials

Published as:

Van den Berg, B., & Buitenweg, J. R. (2021). Observation of nociceptive processing: effect of intra-epidermal electric stimulus properties on detection probability and evoked potentials. *Brain Topography*, 34(2), 139-153.

DOI: https://www.doi.org/10.1007/s10548-020-00816-y

Abstract

Monitoring nociceptive processing is a current challenge due to a lack of objective measures. Recently, we developed a method for simultaneous tracking of psychophysical detection probability and brain evoked potentials in response to intra-epidermal stimulation. An exploratory investigation showed that we could quantify nociceptive system behavior by estimating the effect of stimulus properties on the evoked potential (EP).

The goal in this work was to accurately measure nociceptive system behavior using this method in a large group of healthy subjects to identify the locations and latencies of EP components and the effect of single- and double-pulse stimuli with an inter-pulse interval of 10 or 40 ms on these EP components and detection probability. First, we observed the effect of filter settings and channel selection on the EP. Subsequently, we compared statistical models to assess correlation of EP and detection probability with stimulus properties and quantified the effect of stimulus properties on both outcome measures through linear mixed regression.

We observed lateral and central EP components in response to intra-epidermal stimulation. Detection probability and central EP components were positively correlated to the amplitude of each pulse, regardless of the inter-pulse interval, and negatively correlated to the trial number. Both central and lateral EP components also showed strong correlation with detection.

These results show that both the observed EP and the detection probability reflect the various steps of processing of a nociceptive stimulus, including peripheral nerve fiber recruitment, central synaptic summation, and habituation to a repeated stimulus.

4.1 Introduction

A major challenge in the development of pain biomarkers is the complex nature of the pain experience, as it is determined by a significant amount of supra-spinal processing of the initial sensory input (Apkarian, Bushnell, Treede, & Zubieta, 2005). Developing methods to accurately measure the relation between a well-defined sensory input, brain activation, and pain perception might one day lead to more objective mechanism-based pain biomarkers. A well-defined nociceptive sensory input can be generated by preferential stimulation of nociceptive Aδ afferents in the skin using intra-epidermal electric stimulation (Inui, Tran, Hoshiyama, & Kakigi, 2002). This technique has been shown to preferentially activate nociceptive afferents when applied at less than two times the detection threshold (Mouraux, 2010; Poulsen, Tigerholm, Meijs, Andersen, & Mørch, 2020). Recently, we developed a method to concentrate stimulation around this (drifting) detection threshold, and measure stimulus-response pairs and evoked potentials in response to these nociceptive stimuli (van den Berg et al., 2020).

Based on acquired stimulus-response pairs, a psychometric function for the detection probability can be determined which is characterized by a detection threshold and a slope. Recent research has demonstrated that the detection threshold can be used to observe both short-term and long-term effects of experimental pain conditioning. Conditioned pain modulation by immersion of one foot in ice water resulted in a direct increase of the detection threshold of single-pulse intra-epidermal stimuli (Doll, Buitenweg, Meijer, & Veltink, 2014). On the other hand, 1-hour application of an 8% capsaicin patch resulted in a long-term increase of the detection threshold to intra-epidermal stimuli (Doll et al., 2016). More specifically, detection thresholds to single-pulse intra-epidermal stimuli were significantly increased on days 2 to 7 following capsaicin application, while detection thresholds to double-pulse intra-epidermal stimuli were significantly increased on days 7 to 28 after capsaicin application. The difference between both stimulus types was that by using two or more pulses, we also observed the effect of temporal summation on nociceptive processing, which lead to a significant decrease of the detection threshold and increase of

the slope in the case of double-pulse intra-epidermal stimuli (Doll, Maten, Spaan, Veltink, & Buitenweg, 2016).

Centering stimulus amplitudes around the detection threshold allows for the measurement of evoked potentials in response to nociceptive intra-epidermal stimulation. Earlier studies showed that intra-epidermal stimulation at twice the detection threshold results in an evoked potential waveform that is sensitive to experimental pain conditioning such as the intra-epidermal injection of capsaicin (Liang, Lee, O'Neill, Dickenson, & Iannetti, 2016) and high-frequency stimulation (Manresa, Andersen, Mouraux, & van den Broeke, 2018). Typically this evoked potential included an early contralateral negative peak around 150 ms referred to as the N1 (Mouraux, Marot, & Legrain, 2014), a central negative peak observed between 130-150 ms (Liang, Lee, O'Neill, Dickenson, & Iannetti, 2016) or 220-230 ms (Mouraux, Marot, & Legrain, 2014), and a central positive peak between 290-330 ms (Liang, Lee, O'Neill, Dickenson, & Iannetti, 2016) or 360-370 ms (Mouraux, Marot, & Legrain, 2014). This difference in latencies might be partly explained by the difference in filter settings used in both studies. Nevertheless, a systematic evaluation of the influence of filter settings on intra-epidermal evoked potential waveforms and topographies has not been done so far. Intra-epidermal evoked potential waveforms were also shown to be affected by the number of pulses, as the N1, N2 and P2 were shown to be larger and more reliable when multiple electric current pulses were applied, while the evoked potential latencies and response times remained the same (Mouraux, Marot, & Legrain, 2014). However, an evaluation of the influence of the interval between those pulses on the resulting evoked potential was not done yet.

After a technical pilot study (van den Berg et al., 2020), we designed a new study with the combined measurement of detection thresholds and evoked potentials to accurately quantify the effect of intra-epidermal stimulus properties, i.e. number of pulses and inter-pulse interval, on both outcome measures in healthy individuals. More specifically, we wanted to 1) confirm the presence of previously observed EP components in response to intra-epidermal electric stimulation, 2) determine at which scalp locations and which latencies the observed EP components are maximal and 3) analyze in detail how these

components and detection thresholds are influenced by intra-epidermal stimulus properties in healthy subjects, using (generalized) linear mixed regression models. After exploring the effect of various filter settings on the EP waveform, we investigated which model most effectively captures the data and studied the effect of detection, pulse amplitudes, trial number and the interaction between detection and trial number. In this way, we aimed to obtain new insights and directions for the design of future studies employing this method to study alterations in nociceptive function.

4.2 Methods

The experiments presented in this work include measurements of the detection threshold and the EEG with respect to intra-epidermal stimuli on a single occasion at the University of Twente, the Netherlands. All experiments were approved by the local Medical Review and Ethics Committee and in accordance with the declaration of Helsinki.

4.2.1 Participants

A total of 30 healthy participants (20 males and 10 females, age 23.0 ± 3.4, 4 left-handed) were included in this study. To be included, participants had to have an age between 18 and 40 years old. Exclusion criteria were skin abnormalities at the site of stimulation, diabetes, implanted stimulation devices, pregnancy, usage of analgesics within 24 hours before the experiment, the consumption of alcohol or drugs within 24 hours before the experiments, pain complaints at the time of the experiment, a medical history of chronic pain or any language problems that would impede communication with the participant. All participants provided written informed consent and received a monetary compensation of €20 for participation in the experiment.

4.2.2 Stimuli

Stimuli consisted of square-wave electrical current pulses generated by a constant current stimulator (NociTRACK AmbuStim, University of Twente, Enschede, The Netherlands) and were applied intra-epidermal to achieve preferential activation of Aδ-fibers (Inui, Tran, Hoshiyama, & Kakigi, 2002; Mouraux, 2010). Stimulation was applied using a custom-made electrode consisting of 5 inter-connected microneedles (Figure 4.1). A previous validation study of this electrode showed that stimulation resulted in a sharp pricking sensation (Steenbergen, 2012).

A previous study measuring the detection probability and detection thresholds in response to intra-epidermal stimulation observed a larger detection probability than would be expected based on probability summation for double-pulse stimuli with inter-pulse intervals on a range of 10 to 100 ms, which suggests that such stimuli are amplified by a facilitatory mechanism (Doll, Maten, Spaan, Veltink, & Buitenweg, 2016). In this study, we aimed to reproduce this increased detection probability of double-pulse stimuli, and to observe if this is related to an increase of evoked potential. As we wanted to remain well below the inter-pulse interval at which each pulse is observed individually of 200 ms (Lee, Mouraux, & Iannetti, 2009) and well above the time required for nerve repolarization we used inter-pulse intervals of 10 and 40 ms. As such, a total of three different settings was used:

- A single 210 µs pulse
- A double 210 µs pulse with an inter-pulse interval of 10 ms
- A double 210 µs pulse with an inter-pulse interval of 40 ms

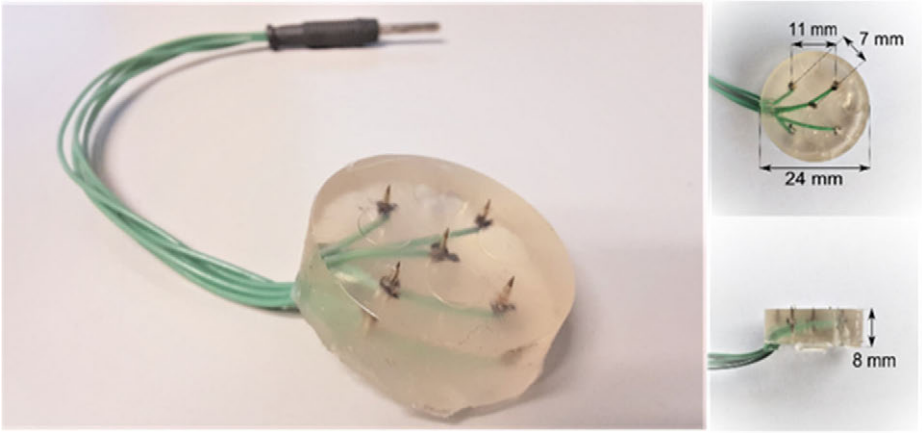

Figure 4.1: Electrode for intra-epidermal stimulation, consisting of an array of 5 inter-connected microneedles embedded in a flexible layer of silicone.

4.2.3 Procedure

Participants were seated in a comfortable chair and instructed to focus on the electrode. First, their initial detection threshold was approximated by a standard staircase procedure without inversion with a step size of 0.025 mA. Subsequently, nociceptive detection thresholds were tracked simultaneously for the 3 stimulus types on 30 participants, with a total of 150 stimuli per stimulus type per participant. Participants were instructed to press and hold a button, and shortly release the button as soon as they felt a sensation that they ascribe to the application of a stimulus. While the button was pressed, the stimulator applied stimuli to the participant. Stimulus amplitudes were chosen according to an adaptive staircase procedure designed to converge towards and track a time-dependent psychophysical threshold (Doll, Veltink, & Buitenweg, 2015). A set of five equidistant amplitudes with a step size of 0.025 mA was defined around the initial detection threshold, from which the next stimulus was randomly selected. A stimulus was identified as detected if the participant released the button within one second after the stimulus, and otherwise considered non-detected. This reaction time was measured internally by the stimulator as the time between stimulus onset and button release, with a resolution 35 microseconds. The set of equidistant amplitudes

was decreased by 0.025 mA if a stimulus was detected and increased by 0.025 mA if a stimulus was non-detected. Subsequently, the next stimulus was selected from the updated set of equidistant amplitudes and applied after a uniformly randomized interval of 4.3 to 5.3 seconds. This procedure was repeated until the end of the experiment.

4.2.4 Electroencephalography

The scalp EEG was continuously recorded with a sampling rate of 1024 Hz using a REFA amplifier (TMSi B.V., Oldenzaal, the Netherlands) at 128 Ag/AgCl electrodes with a common average reference. Electrodes were placed on the scalp according to the international 10/5 system (Oostenveld & Praamstra, 2001) and additional leads were placed on the earlobes. The participants were asked to fix their gaze at a spot on the wall and blink as few times as possible while they pressed the response button and hence received stimuli. Participants with excessive electrode impedance (>5 channels with >20kΩ) were excluded. Therefore, a total of 25 participants (16 males and 9 females, age 23 ± 3.6, 1 left-handed) were used for analysis.

EEG data was pre-processed using FieldTrip (Oostenveld, Fries, Maris, & Schoffelen, 2011), a Matlab toolbox for EEG and MEG signal processing. Contamination of the EEG by eye-blinks was corrected using an independent component analysis algorithm (Delorme, Sejnowski, & Makeig, 2007). Subsequently, epochs with excessive EMG activity or movement artefacts were removed by visual inspection. The first 15 epochs were removed as no reliable estimate of the detection threshold was available for those trials. Furthermore, epochs in which the stimulus amplitude exceeded two times the tracked individual detection threshold were excluded from analysis. Based on earlier observations that opercular sources are first activated contralateral with respect to stimulation and lateralized afterwards (Garcia-Larrea, Frot, & Valeriani, 2003), the channel topography for left-handed subjects was inverted such that uneven numbers correspond to the contralateral side and even numbers to the ipsilateral side with respect to stimulation.

Epochs for EP analysis were extracted from the EEG using a window ranging from 0.5 s before until 1.0 s after the stimulus. To compare EP waveforms in the current study, with those previously observed in literature in response to intra-epidermal stimulation, grand average waveforms, and topographies at Cz (average reference) and T7-Fz, bandpass filtered at 0.1 to 40 Hz, 0.5 to 45 Hz and 0.1 to 30 Hz and baseline corrected, were set side by side. Further analyses were performed using the waveforms bandpass filtered at 0.1 to 40 Hz to minimize signal loss and the potential bias induced by the high-pass filter (Acunzo, Mackenzie, & van Rossum, 2012).

Average latencies of three peaks in the EP were defined as follows. A first negative peak (N1) was defined as the most negative peak at T7-Fz between 130-170 ms after stimulus onset. A second negative peak (N2) was defined as the most negative peak at Cz between 170-300 ms after stimulus onset. Lastly, a positive peak (P2) was defined as the most positive peak at Cz between 300-500 ms after stimulus onset. To check if each of those peaks coincide with global peaks of EEG activity, peak latencies were compared with the butterfly plot and the global field power (Lehmann & Skrandies, 1980).

To systematically study on which locations the N1, N2 and P2 are best observed, the SNR was computed for each channel, where SNR was defined as in Equation (1), where $S(t)$ denotes the grand average potential at latency t and $\sigma_{baseline}$ denotes the standard deviation of the grand average from -0.5 to -0.3 s with respect to stimulus onset.

$$SNR = \frac{|S(t)|}{\sigma_{baseline}} \quad (1)$$

Subsequently, grand average EP waveforms were computed at derivations with a maximum SNR: T7-F4 at N1 and N2, and CPz-A1A2 at P2. The effect of intra-epidermal stimulus properties on these EP waveforms was studied using linear mixed regression, which is further outlined in Section 4.2.6.

4.2.5 Effect of Intra-Epidermal Stimulus Properties on Detection Probability

Statistical analysis of stimulus-response pairs was performed in R with the lme4 toolbox (Bates, Mächler, Bolker, & Walker, 2015). The effect of stimulus properties on the detection probability was estimated using logistic generalized linear mixed regression using a statistical model selected using the procedure outlined in Section 4.2.7. The track of individual and group level thresholds was estimated by performing generalized mixed regression over a moving window of 30 stimulus-response pairs. Subsequently, generalized mixed regression was performed over the entire dataset to establish accurate estimates of effect size and significance. The guess rate and lapse rate were both assumed to be zero for robust estimation of effect sizes. The trial number was centered and scaled to speed up the model estimation process. Estimates of the threshold and slope were obtained using the estimated effect sizes, and corresponding standard errors were approximated using the Delta procedure (Faraggi, Izikson, & Reiser, 2003; Moscatelli, Mezzetti, & Lacquaniti, 2012). Effect significance was assessed using type III Wald Chi-square statistics with a two-tailed test. As 26 tests are performed in this article, the significance level was set to 0.025/26≈0.001 after Bonferroni correction.

4.2.6 Effect of Intra-Epidermal Stimulus Properties on Evoked Potential

Statistical analysis of EEG data was performed in MATLAB 2017b (MathWorks, Inc.). The effect size of stimulus properties was evaluated using linear mixed regression (Van den Berg & Buitenweg, 2018). Regression parameters were computed for every point in time at CPz-A1A2 and T7-F4 using a statistical model selected using the procedure outlined in Section 4.2.7. Model variables were centered and scaled to speed up the estimation progress. Subsequently, effect sizes and their corresponding *t*-values were estimated for every point in time by optimization of the restricted maximum likelihood. At component latencies (153, 213 and 418 ms) significance of the effect sizes was assessed using the *t*-statistic with a two-tailed test using Satterthwaite's method for estimation of the degrees of freedom. Similar to the previous section, the significance level was set to 0.001 after Bonferroni correction.

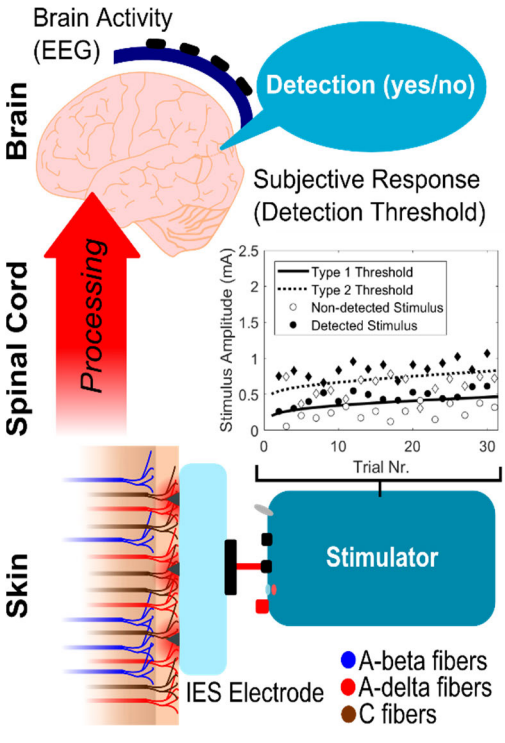

Figure 4.2: *We attempt to characterize nociceptive processing by simultaneously measuring the effect of intra-epidermal stimulus properties on psychophysical detection probability and brain evoked potentials. Multiple stimulus types (i.e., with a different number of pulses or inter-pulse interval) are generated with a varying amplitude close to the detection threshold. Stimuli preferentially activate nociceptive nerve fibers by using a specially designed needle electrode which protrudes into the epidermis of the skin using microneedles. Subject responses (detected or non-detected) and EEG corresponding to the applied stimuli are acquired and analyzed using (generalized) linear mixed regression to quantify the effect of stimulus properties on detection probability and evoked potentials.*

4.2.7 Model Selection

We compared several models for statistical analysis of the detection probability and EEG, based on the Akaike information criterion (AIC) (Akaike, 1974) and the Bayesian information criterion (BIC) (Schwarz, 1978). For both criteria a lower value indicates a better model fit, while accounting for overfitting. In the case that the AIC and BIC values did not agree on the same model, the value of the BIC was used to select a statistical model for further analyses.

The first model assumed that neurophysiological activity of both pulses was integrated by temporal summation, where the neurophysiological activity generated as a result of the first pulse amplitude (in mA, denoted by PU1) is summed with activity generated as a result of the second pulse amplitude with either 10ms IPI (in mA, denoted by $PU2_{10}$) or 40ms IPI (in mA, denoted by $PU2_{40}$). Furthermore, this signal could decrease with respect to the trial number (denoted by TRL) due to habituation effects.

The resulting generalized linear mixed regression model for computing detection probability in A was compared to models using a direct combination of the experimental parameters in B, C and D, where the response was modeled based on the stimulus amplitude (in mA, denoted by AMP), stimulus type (denoted by TYP) and the trial number. The random effect structure was grouped by subject (denoted by S) and included all model terms. An unstructured covariance structure was used to model the random effects. Models are written in Wilkinson notation (Wilkinson & Rogers, 1973), where random effects are written in between brackets and '| S' denotes that the random effects are grouped by subject.

$$\boldsymbol{ln\left(\frac{P_d}{1-P_d}\right) \sim 1 + PU1 + PU2_{10} + PU2_{40} + TRL + (1 + PU1 + PU2_{10} + PU2_{40} + TRL \mid S)} \quad \text{A}$$

$$ln\left(\frac{P_d}{1-P_d}\right) \sim 1 + AMP * TYP * TRL + (1 + AMP * TYP * TRL \mid S) \quad \text{B}$$

$$ln\left(\frac{P_d}{1-P_d}\right) \sim 1 + AMP * TYP + TRL + (1 + AMP * TYP + TRL \mid S) \quad \text{C}$$

$$ln\left(\frac{P_d}{1-P_d}\right) \sim 1 + AMP + TYP + TRL + (1 + AMP + TYP + TRL \mid S) \quad \text{D}$$

The first linear mixed regression model for analyzing EEG activity was based on the temporal summation model in A but included a term for additional brain activity evoked by stimulus detection which could increase or decrease with respect to the trial number (denoted by the interaction TRL*D). The resulting model in E was compared to the models based on combinations of experimental parameters in F, G, H, and I at the P2 latency (414 ms). The random effect structure was grouped by subject and included all model terms. A diagonal covariance structure was used to model the random effects.

$$\boldsymbol{U_{EEG}} \sim \mathbf{1} + \boldsymbol{PU1} + \boldsymbol{PU2_{10}} + \boldsymbol{PU2_{40}} + \boldsymbol{TRL} * \boldsymbol{D} + (\mathbf{1} + \boldsymbol{PU1} + \boldsymbol{PU2_{10}} + \boldsymbol{PU2_{40}} + \boldsymbol{TRL} * \boldsymbol{D} \mid \boldsymbol{S}) \quad \textbf{E}$$

$$U_{EEG} \sim 1 + AMP * TYP * TRL * D + (1 + AMP * TYP * TRL * D \mid S) \quad \text{F}$$

$$U_{EEG} \sim 1 + AMP * TYP * D + TRL * D + (1 + AMP * TYP * D + TRL * D \mid S) \quad \text{G}$$

$$U_{EEG} \sim 1 + AMP * TYP + TRL * D + (1 + AMP * TYP + TRL * D \mid S) \quad \text{H}$$

$$U_{EEG} \sim 1 + AMP + TYP + TRL + D + (1 + AMP + TYP + TRL + D \mid S) \quad \text{I}$$

4.3 Results

4.3.1 Model Selection

A functional model was compared to models directly based on the experimental parameters for statistical analysis of the detection probability and the EEG. Model AIC and BIC values are shown in Table 4.1. For the detection probability, the experiment-based model B including all effects resulted in the lowest AIC. For EEG data, the functional model E resulted in the lowest AIC. For both the detection probability and the EEG data, the functional models A and E resulted in the lowest BIC.

Detection Probability			EEG		
Model	**AIC**	**BIC**	**Model**	**AIC**	**BIC**
A	13444	**13591**	E	**25069**	**25177**
B	**13393**	14053	F	25389	25575
C	13413	13670	G	25107	25314
D	14015	14161	H	25105	25241
			I	25122	25215

Table 4.1: *AIC and BIC values for comparison of the functional models (A and E) with various experiment-based models. A lower AIC or BIC value indicates a better model fit while accounting for the number of parameters in the model.*

4.3.2 Effect of Intra-epidermal Stimulus Properties on Detection Probability

Subjects detected on average 46.7% of all applied stimuli with a reaction time of 546±161 ms. A typical example of a resulting tracked NDT in a single subject is shown on the left side of Figure 4.3. For each stimulus type, the NDT increased over time. Both thresholds for double pulse stimuli were almost equal, i.e., there was no difference of NDT with respect to the inter-pulse interval in this subject. Similar results are shown in the group level thresholds on the right in Figure 4.3, computed using the GLMR model over a 30-trial moving window (continuous lines) and over the entire dataset (dotted lines). Group level NDTs computed over the entire dataset increased over the trials and remained within the standard error of the mean (SEM) of NDTs computed over a 30-trial moving window. Once again, no difference was seen between NDTs of double pulse stimuli with 10 ms inter-pulse interval and those with 40 ms inter-pulse interval.

Observations in Figure 4.3 are supported by effect sizes and significances in Table 4.2. There was a significant positive effect size for each of the pulse amplitudes, indicating an increase in detection probability with respect to the pulse amplitudes. There was a significant negative effect size of trial number, indicating a decrease of detection probability with respect to the trial number. In Table 4.3, it is shown that there was indeed a significantly lower detection threshold ($p<0.001$) and steeper slope ($p<0.001$) for both types of double-pulse stimuli in comparison with a single-pulse stimulus. However, there was no significant difference in detection threshold or slope between double pulse stimuli with 10 or 40 ms inter-pulse interval.

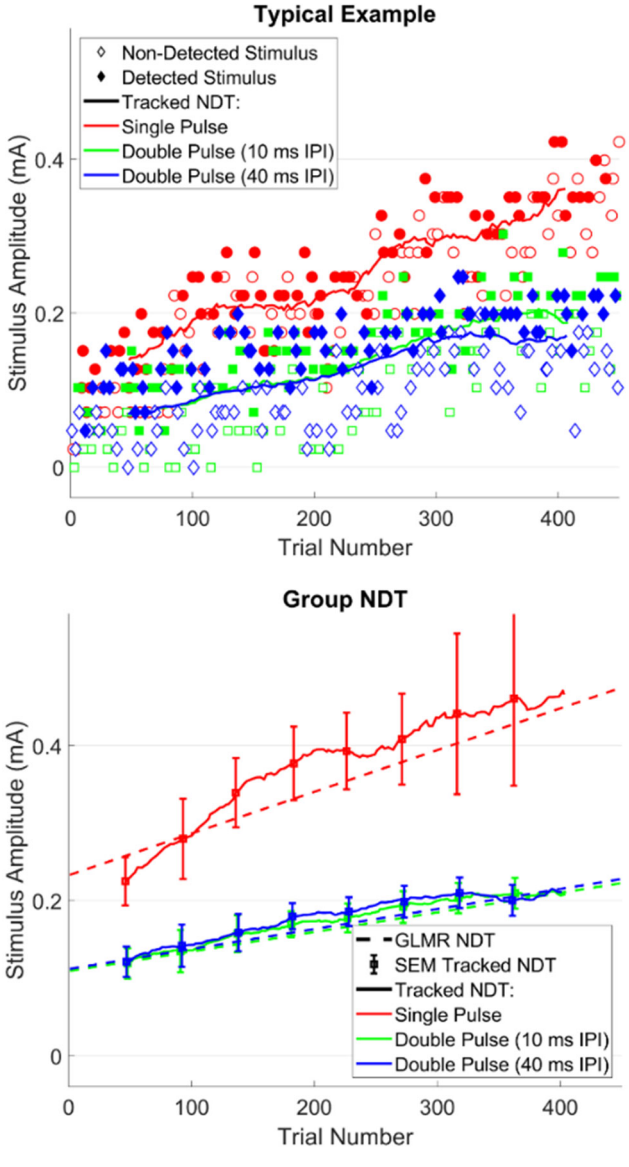

Figure 4.3: *A typical example of tracked nociceptive detection thresholds (NDTs) in a typical subject (top) and the group average NDTs (bottom). On the top, single-pulse stimuli, double-pulse stimuli with 10ms IPI, and double-pulse stimuli with 40ms IPI, are indicated by circles, squares, and diamonds respectively. On the bottom, both group level detection thresholds computed over a time window of 30 stimuli (tracked NDT) and computed over the entire experiment (GLMR NDT) are shown. The standard error of the mean (SEM) of tracked thresholds is indicated by bars. For each NDT, it can be observed that the threshold increased over time and that the threshold for double pulse stimuli was much lower. However, there was no difference in detection threshold with respect to inter-pulse interval (IPI).*

Stimulus Property	Effect Size	95% Confidence Interval	Effect χ^2	Effect *p*
(Intercept)	-3.70	[-4.32 -3.09]	139.61	**<.001**
Pulse 1 (PU1)	10.43	[7.14 13.72]	38.67	**<.001**
Pulse 2, 10ms IPI ($PU2_{10}$)	11.83	[9.03 14.63]	68.38	**<.001**
Pulse 2, 40ms IPI ($PU2_{40}$)	11.31	[8.61 14.01]	67.40	**<.001**
Trial number (TRL)	-0.0056	[-0.0074 -0.0038]	37.69	**<.001**

Table 4.2: *Effect of stimulus properties on the detection probability, computed using GLMR. All effect sizes and confidence intervals were rescaled to physical units (Int.: -, PU1: mA^{-1}, $PU2_{10}$: mA^{-1}, $PU2_{40}$: mA^{-1}, TRL: $trial^{-1}$). Significance was assessed using type-III Wald Chi-square statistics. All tested stimulus properties have a significant effect on the detection probability. The detection probability decreases with respect to trial number and increases with respect to the amplitude of the first pulse and of the second pulse with either 10ms or 40ms IPI.*

Stimulus Type	Threshold	95% Confidence Interval	Slope	95% Confidence Interval
Single-pulse	0.35	[0.33 0.52]	10.43	[7.20 13.66]
Double-pulse, 10ms IPI	0.17***	[0.14 0.20]	22.26***	[17.15 27.37]
Double-pulse, 40ms IPI	0.17***	[0.14 0.20]	21.74***	[16.42 27.06]

Table 4.3: *Detection thresholds (in mA) and slopes (in mA^{-1}) per stimulus type. There is a significantly ($p<0.001$, indicated by ***) lower detection threshold and steeper slope for each type of double-pulse stimulus in comparison to the detection threshold of single-pulse stimuli. There was no significant difference in detection threshold or slope between both types of double-pulse stimuli.*

4.3.3 Evoked Potential in Response to Intra-epidermal Stimuli

For comparison with previously observed EP waveforms in response to intra-epidermal stimulation in literature (Liang, Lee, O'Neill, Dickenson, & Iannetti, 2016; Mouraux, Marot, & Legrain, 2014), EP waveforms at the same channels and with the same filters as in those studies are shown in Figure 4.4A and Figure 4.4B. The N1 was located at 160 ms (1 to 30 Hz) and 162 ms (0.1 to 40 Hz and 0.5 to 45 Hz) at T7-Fz. The N2, was located at 180 ms (0.1 to 40 Hz) and 190 ms (0.5 to 45 Hz and 1 to 30 Hz) at Cz. The P2 was located at 390 ms (1 to 30 Hz), 408 ms (0.5 to 45 Hz) and 414 ms (0.1 to 40 Hz).

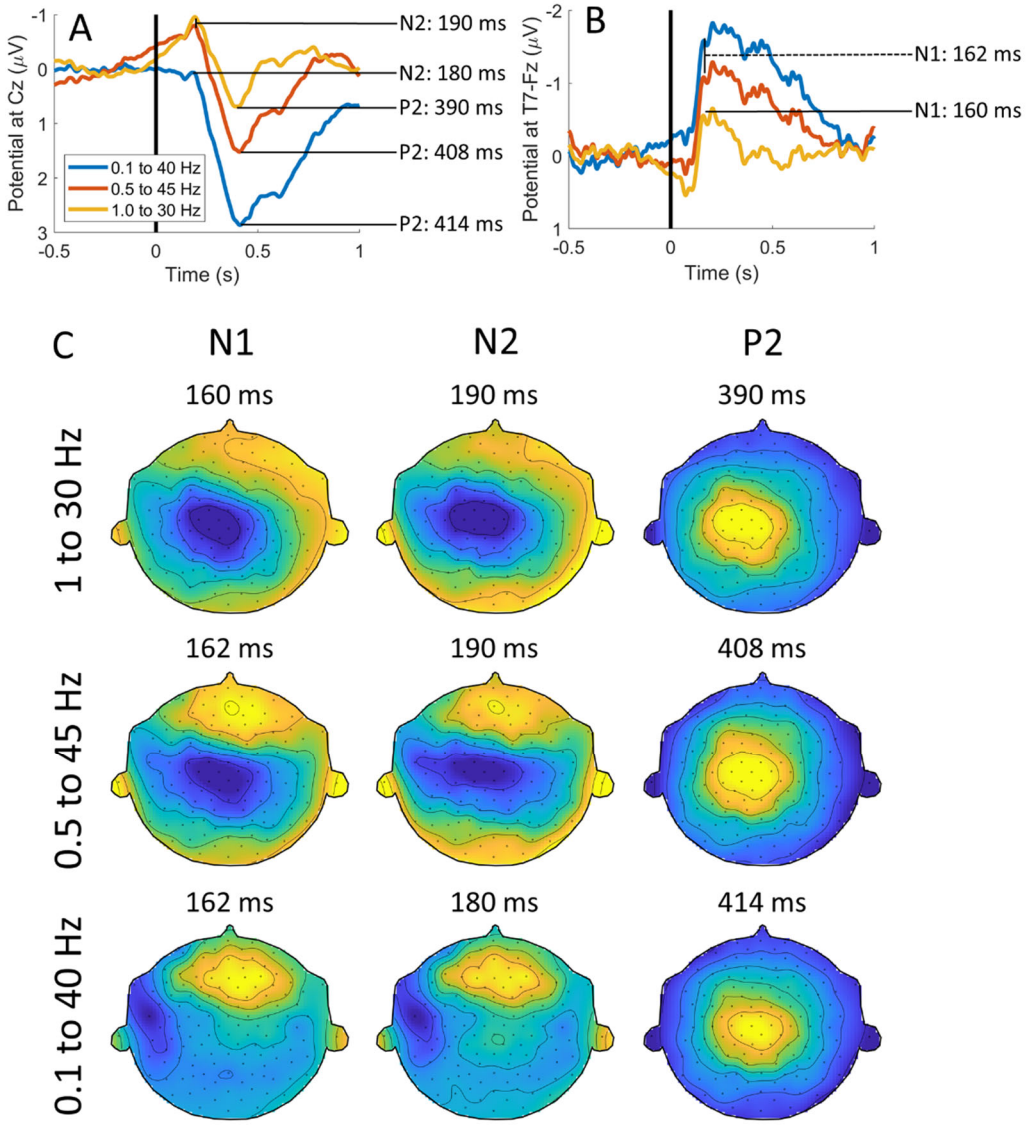

Figure 4.4: *A and B) Evoked potential at Cz (average reference) and T7-Fz band-pass filtered at 0.1 to 40 Hz, 0.5 to 45 Hz and 1 to 30 Hz, and latencies of the peaks in each of the EP waveforms. C) Evoked potential topographies at the latencies of N1, N2 and P2.*

Grand average EP topographies at these peak latencies are displayed in Figure 4.4C. Topographies of the N1 and N2 were similar to each other for all filter settings but differ per filter setting. The N1 and N2 both showed a central negative topography when using filters of 0.5 to 45 Hz and of 1 to 30 Hz. In contrast, the N1 and N2 showed a distinct contralateral topography when using filters of 0.1 to 40 Hz. The topography of the P2 was central and positive for all filter settings.

A butterfly plot of grand average EPs and the global field power (GFP) in response to the intra-epidermal electric stimuli is shown in Figure 4.5. The global field power showed a major peak around the P2 and a minor peak around the N1, each corresponding to local maxima in a subset of channels. However, the N2 did not appear to coincide with any peak of global field power or of any subset of channels.

For each latency, the 12 channels with the largest positive and negative potentials are shown in Table 4.4. In addition, the SNR of each channel was computed, which in this case correlated strongly with the potential (i.e., the channels with the largest potential also have a large SNR). The derivation with the largest potential at each latency was found by subtracting the most negative channel(s) from the most positive channel or vice-versa depending on polarity. Based on these considerations, T7-F4 and CPz-A1A2 were selected for further investigation of the EP.

For the selected channels, the SNR is shown as a function of the number of trials in Figure 4.6. For the N1 and N2, there is an initial peak of SNR after 60 trials. For the P2, there is an initial peak of the SNR after 34 trials. However, in both cases the SNR tends to increase with an increasing number of trials, with a maximum at 382 trials for the N1 and N2, and a maximum at 403 trials for the P2.

	N1 Channel	Value (µV)	SNR	N2 Channel	Value (µV)	SNR	P2 Channel	Value (µV)	SNR
1	F4*	0.83	*23.49*	T7*	-0.82	*18.36*	CPz**	3.33	*185.57*
2	T7*	-0.82	*18.22*	F4*	0.77	*21.76*	CCP1h***	3.31	*122.68*
3	FFC2h***	0.81	*17.41*	F1**	0.75	*14.41*	CP1**	2.99	*111.57*
4	F2**	0.79	*20.35*	F2**	0.72	*18.76*	Cz*	2.80	*97.37*
5	Fz*	0.77	*18.96*	FFC2h***	0.72	*15.42*	CCP2h***	2.78	*163.37*
6	FFC4h***	0.71	*15.24*	TTP7h***	-0.71	*20.61*	C1**	2.76	*91.46*
7	F1**	0.71	*13.65*	Fz*	0.70	*17.12*	A1*	-2.74	*36.57*
8	AFF2***	0.69	*19.38*	AFz***	0.67	*13.67*	CPP2h***	2.64	*111.59*
9	FC2*	0.68	*17.85*	FT9***	-0.63	*12.16*	CPP1h***	2.62	*92.24*
10	AFz***	0.68	*13.88*	AFF2***	0.63	*17.81*	CCP3h***	2.57	*91.15*
11	FT9***	-0.64	*12.24*	FFC4h***	0.62	*13.44*	A2*	-2.56	*30.74*
12	TTP7h***	-0.63	*18.36*	FC2*	0.59	*15.44*	CP2*	2.51	*126.85*

Table 4.4: *Grand average electrode potential and SNR at N1, N2 and P2. The electrodes with the largest potential values were also the electrodes with the largest SNR at N1 (F4) and P2 (CPz). Electrodes which are present in a regular 32-channel cap, 64-channel cap, and 128-channel cap (10-5 system) are denoted with *, ** and *** respectively.*

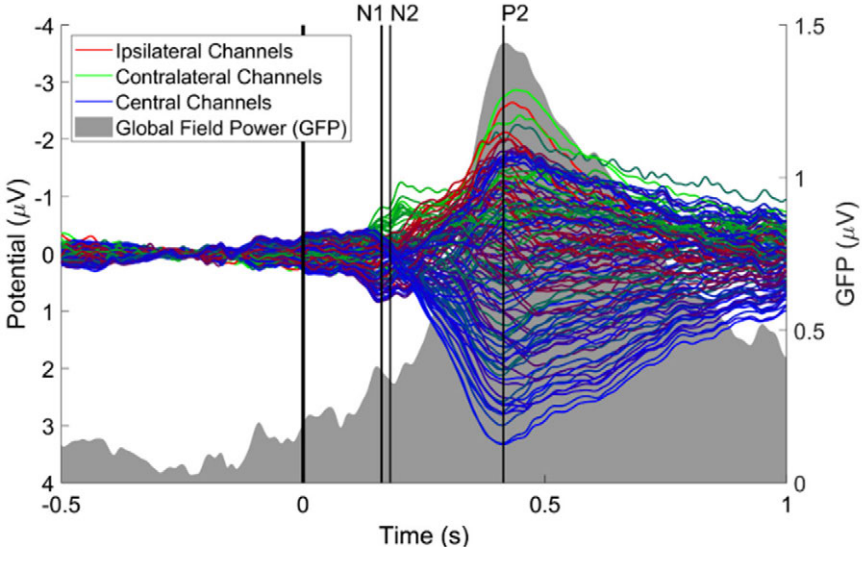

Figure 4.5: *Butterfly plot of the grand average potential and global field power (GFP) of EEG channels in response to intra-epidermal stimuli around the nociceptive detection threshold (<2×NDT). The N1 appeared to coincide with an early peak of the GFP, while the P2 coincided with the maximum of the GFP. The N2 did not coincide with any peak in the GFP or in the butterfly plot.*

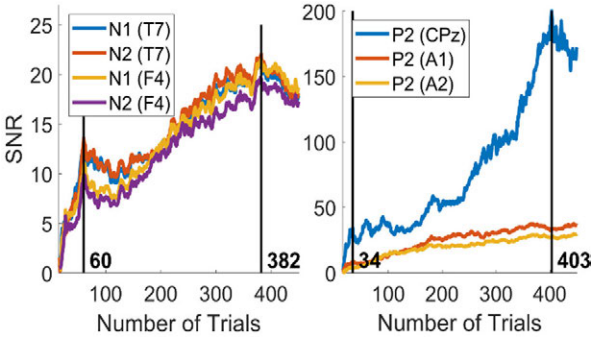

Figure 4.6: *Signal-to-noise ratio (SNR) of the evoked potential in the grand average of the channels T7 and F4 (for N1 and N2), and CPz, A1 and A2 (for P2). For N1 and N2, there is an initial peak of the SNR after 60 trials, and a maximum at 382 trials. For P2, there is an initial peak of the SNR after 34 trials and a maximum at 403 trials.*

4.3.4 Effect of Intra-epidermal Stimulus Properties on Evoked Potential

The grand average EP at T7-F4 and CPz-A1A2 is shown in Figure 4.7A and 4.8A respectively. At T7-F4 intra-epidermal stimuli elicited an early negative component with a peak around the N1 latency, followed by a small positive component. At CPz-A1A2, intra-epidermal stimuli elicited a clear positive component with a maximum close to the P2 latency.

The results of significance testing of stimulus properties at T7-F4 and CPz-A1A2 are shown in Table 4.5. At N1 and N2 only stimulus detection was significant. At P2 stimulus detection, each pulse amplitude and the interaction between detection and trial number were significant. For all significant effects, the effect sizes and *t*-values over time are displayed in Figure 4.7B (for T7-F4) and 4.8B-F (for CPz-A1A2). For T7-F4, the negative effect of detection was mostly concentrated around the N1. For CPz-A1A2, the positive effect of each pulse amplitude started before the P2 and lasted for several hundred milliseconds. The interaction between detection and trial number had a negative effect during the same time range as the pulse amplitudes. Detection had a positive effect starting before the P2 and lasting until the end of the epoch.

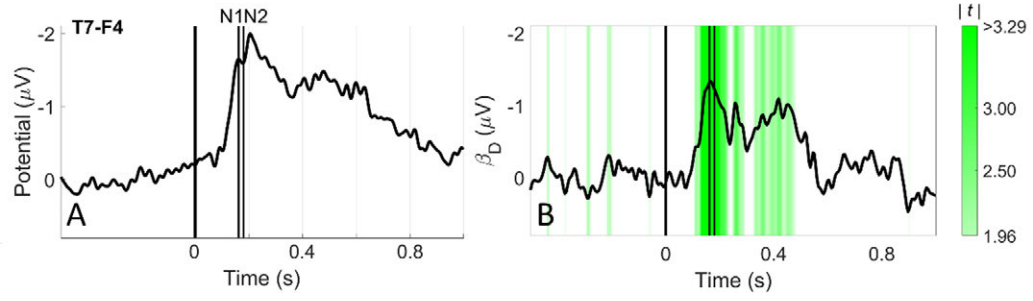

Figure 4.7: Grand average EP (A) and the effect of stimulus properties (B) at T7-F4. The corresponding t-values are shown in green on a scale of 1.96 (p=0.05 with inf. DOF) to 3.29 (p=0.001 with inf. DOF). At T7-F4 only stimulus detection had a significant effect on the EP at the N1 and N2 latencies.

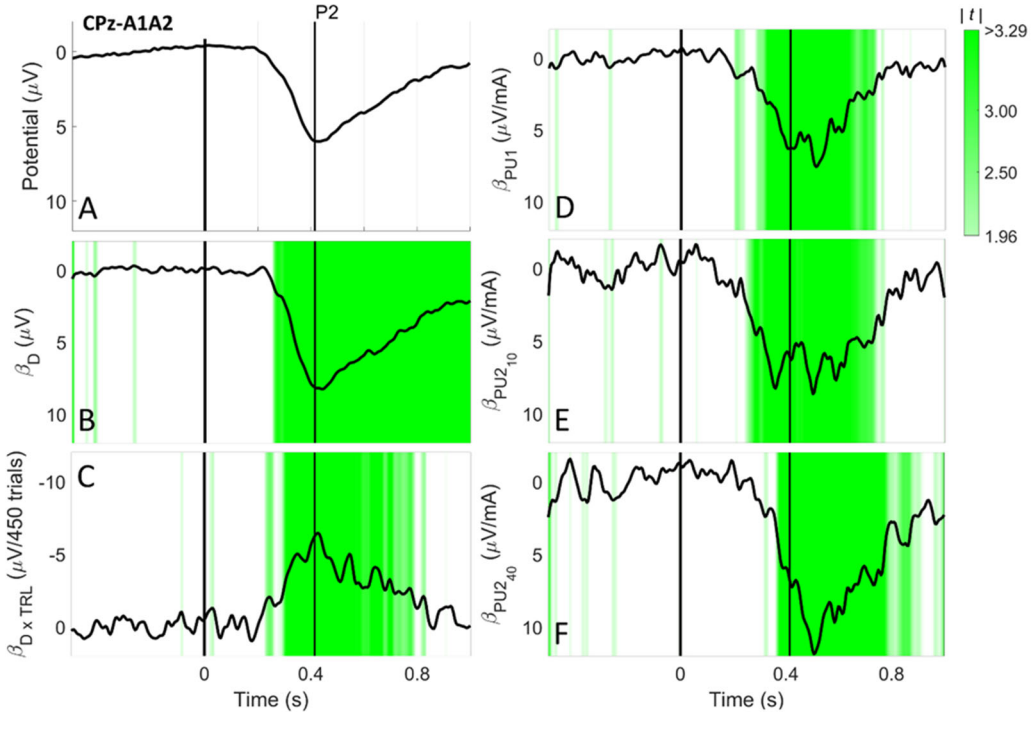

Figure 4.8: Grand average EP (A) and the effect of stimulus properties (B-F) at CPz-A1A2. The corresponding t-values are shown in green on a scale of 1.96 (p=0.05 with inf. DOF) to 3.29 (p=0.001 with inf. DOF). At CPz-A1A2 stimulus detection, the amplitude of each pulse and the interaction between detection and trial number had a significant effect on the EP at the P2 latency which lasted for several hundreds of milliseconds.

4.4 Discussion

We have simultaneously assessed neurophysiological and psychophysical effects of nociceptive intra-epidermal stimulation using a method to simultaneously measure EPs and detection thresholds in response to multiple stimulus types. Preferential activation of nociceptive afferents was achieved by stimulating at intensities close to the detection thresholds, and excluding trials from EEG analysis if the stimulus was larger than twice the NDT (Mouraux, 2010). We aimed to confirm the presence, location, and latency of EP components and to quantify the effect of intra-epidermal stimulus properties on those components.

4.4.1 Evoked Potential in Response to Intra-Epidermal Stimuli

The EP waveforms observed in this study correspond with those observed in previous studies using intra-epidermal stimulation (Figure 4.4A and 4.4B). Where an earlier study by Mouraux et al. (Mouraux, Marot, & Legrain, 2014) observed a N1 component in response to intra-epidermal stimulation around a latency of 150 ms, we observed a N1 component at the same derivation (T7-Fz) and with the same filter settings around 160 ms. Furthermore, Mouraux et al. observed a N2 component at Cz in the range of 220 to 230 ms and another study by Liang et al. (Liang, Lee, O'Neill, Dickenson, & Iannetti, 2016) observed a much earlier N2 component at the same channel in the range of 130 to 150 ms. The observed N2 component in the current study occurs at the same channel and filter setting at a latency in between those estimates, around 190 ms. For both the N1 and N2 the largest positive and negative potential values and SNR were found at F4 and T7 respectively. The SNR of both components at T7 and F4 was shown to increase with respect to the number of trials included in the grand average. However, after a steep increase of the SNR within the first 60 trials, the improvement of SNR flattens, potentially due to habituation effects and loss of attention.

The observed latencies of the P2 at Cz of 390 and 408 ms, are slightly later than those observed by Liang et al. (290 – 330 ms) and Mouraux et al. (360 – 370 ms) respectively. Although the observed amplitude is much lower than in studies

using heat pulses (Miyazaki et al., 1994; Treede, Kief, Hölzer, & Bromm, 1988), it is comparable to earlier nociceptive EP studies using intra-epidermal stimulation near the detection threshold (Mouraux, 2010; Van der Lubbe, Blom, De Kleine, & Bohlmeijer, 2017), indicating that this difference in potential might be due to stimulus intensity. The potential values in Table 4.4 show that during the observed P2, the largest positive potential value (and SNR) could be found at CPz, and the lowest negative potential value (and SNR) could be found at A1 followed by A2. The SNR of the P2 at CPz, A1 and A2 improved the most within the first 34 trials but kept increasing steeply until reaching a maximum close to the end of the experiment at 403 trials.

Although the observed EP waveform corresponds to previous studies using similar derivations and filter setting, it is clear from Figure 4.4 that filter settings have a profound influence on the EP waveform and topography. While the choice of a larger cutoff frequency for the high-pass filter enhances the N2 component at Cz, it strongly decreases amplitude of the P2. Furthermore, the filter setting has a profound influence on the observed topographies of N1 and N2. While the topographies of N1 and N2 in this study show a maximum around the vertex with a high-pass filter of 0.5 or 1 Hz, both topographies have a maximum contralateral to stimulation when using a high-pass filter of 0.1 Hz. In this work, we chose to minimize high-pass filter signal distortion, by choosing a relatively low high-pass filter cutoff frequency of 0.1 Hz (Acunzo, Mackenzie, & van Rossum, 2012).

When using a low high-pass filter cutoff frequency, the P2 amplitude is increased, but the N2 amplitude is severely reduced. Using this filter setting the observed global field power showed peaks only around the N1 latency and the P2 latency. Topographies of the N1 and N2 are almost identical, with a maximum at T7 and a minimum at F4. As such, it is questionable whether N1 and N2 identified in this study really represent independent components of brain activity. In the current study, it appears that the N2 rather arose from high-pass filter settings rather than physiological activity, as the high-pass filter essentially works as a signal differentiator resulting in peaks of opposite polarity before occurrence of the true effect, i.e. the P2 (Tanner, Morgan-Short, & Luck, 2015).

4.4.2 Effect of Intra-epidermal Stimulus Properties on Detection Probability

Intra-epidermal electric stimuli directly activate superficial afferents in the skin, rather than activating skin receptors (Inui & Kakigi, 2012; Inui, Tran, Hoshiyama, & Kakigi, 2002). As this signal is transduced by the relatively slow Aδ-fibers, rather than the fast Aβ-fibers, the reaction times to this type of stimulation are usually increased with respect to conventional transcutaneous electric stimulation. Correspondingly, the average reaction time in this study (546±161 ms) was markedly later than previously observed reaction times (Mouraux, 2010) to transcutaneous stimulation (283±47 ms) and intra-epidermal stimulation at twice the perceptual threshold (374±51 ms), but similar to laser stimulation (504±105 ms). As such, reaction times suggest preferential recruitment of Aδ-fibers.

Increasing the pulse amplitude directly enlarges the area of recruitment of peripheral afferent nerve fibers (Poulsen, Tigerholm, Meijs, Andersen, & Mørch, 2020). Increasing the number of pulses results in the generation of more action potentials. Central synaptic summation of these action potentials occurs in the spinal cord, where facilitatory or inhibitory effects could occur depending on the inter-pulse interval (Zucker & Regehr, 2002). Nociceptive processing adapts to repeated stimulus application, leading to a habituation of neurophysiological (Christmann, Koeppe, Braus, Ruf, & Flor, 2007) and psychophysical (May et al., 2012) responses. One of the aims was to probe each of these mechanisms by varying pulse amplitudes, the number of pulses and the inter-pulse interval of the applied stimuli. We started out by formulating and comparing multiple statistical models to study the effect of these stimulus properties. This included functional models explaining detection probability and EEG in terms of pulse amplitudes and trial number. It was found in Table 4.1 that both functional models (A and E) have the lowest BIC, indicating that among the tested models these models are the closest approximation of the true physiological behavior.

We found that nociceptive stimulus detection behaves according to theory, where the pulse amplitudes and trial number have a significant effect on the detection probability. The effects of pulse amplitudes observed in this study lie within the confidence interval reported in the earlier technical demonstration

of the method (van den Berg et al., 2020). As was expected based on the larger recruitment of peripheral afferents, the detection probability increased with increasing pulse amplitudes. Furthermore, we saw that addition of a second pulse with either 10 ms or 40 ms inter-pulse interval leads to a significant increase of detection probability (Figure 4.3, Table 4.2) similar to earlier observations by Doll et al. (Doll, Maten, Spaan, Veltink, & Buitenweg, 2016). This results in significantly lower detection thresholds and significantly steeper slopes for these double pulse stimuli (Table 4.3). However, there is no difference between double-pulse detection thresholds and slopes dependent on the inter-pulse interval, which was either 10 or 40 ms. Experiments in humans subjects measuring the compound sensory action potential in response to paired pulses indicate that peripheral sensory nerve fibers remain superexcitable up to approximately 20 ms after the first pulse and remain subexcitable from 20 to 100 ms after the stimulus (Kiernan, Mogyoros, & Burke, 1996). If these findings also hold for nociceptive afferents, one would expect a higher detection probability and lower threshold for double-pulse stimuli with an inter-pulse interval of 10 ms than for double-pulse stimuli with an inter-pulse interval of 40 ms. It turns the effect of adding a second pulse is similar regardless of the inter-pulse interval, resulting in similar detection thresholds for both stimulus types. As such, the effects of peripheral super- and subexcitability appear to be canceled out by a stronger central mechanism, such as the central temporal summation of both pulses (Zucker & Regehr, 2002).

The detection probability decreases over the number of trials, resulting in an increase of the detection threshold in Figure 4.3. In earlier studies, this effect was also found significant, but had a larger effect size (Doll, Maten, Spaan, Veltink, & Buitenweg, 2016; van den Berg et al., 2020). Altered habituation appears to play an important role in several types of chronic pain syndromes and is therefore an important phenomenon to observe when assessing nociceptive processing (Agostinho et al., 2009; Rodriguez-Raecke et al., 2014; Valeriani et al., 2003). Nevertheless, the neurophysiological mechanisms of this effect remain unknown, and this effect might be attributed to either an altered task performance, a shift of attention, learning or neuroplasticity.

4.4.3 Effect of Intra-epidermal Stimulus Properties on Evoked Potential

The effect of stimulus properties on the EP was shown in Table 4.5. Based on Figure 4.7B and 4.8B-F we could also observe at which latencies these effect sizes were largest. We did not find that the lateral potential at T7-F4 behaves according to the theory mentioned earlier. Instead, it was only significantly modulated by detection with its major effect size around the latency of N1. As such, we did not observe any significant encoding of physical properties of the stimulus (i.e., the pulse amplitudes) in the N1 or N2. It remains unknown if this absence of the effect of stimulus properties on lateral EP components is because these components do not encode any physical properties of a stimulus, or simply because the N1 and N2 are relatively small signals and easily obscured by background noise.

The potential at CPz-A1A2 around at P2 latency was not only modulated by detection, but also by the pulse amplitudes and the interaction between detection and trial number. The latter observation is consistent with earlier reports in literature, which show that the P2 represents multi-modal activity dependent on stimulus salience (Iannetti, Hughes, Lee, & Mouraux, 2008; Legrain, Iannetti, Plaghki, & Mouraux, 2011). As the pulse amplitudes and the trial number influence stimulus salience through the mechanisms discussed in last section, these properties were also expected to affect the P2. We saw that the contribution of the second pulse is equal or even larger than the contribution of the first pulse to the P2. This corresponds to the observation in last section, where the detection threshold is lowered by the addition of a second pulse and the effect size of both types of second pulse is actually larger than the effect size of the first pulse amplitude. As such, the observed increase in P2 amplitude is likely to be associated with similar facilitatory mechanisms as discussed in Section 4.4.2.

We also observed a significant effect of the interaction between detection and trial number on the P2 amplitude. As such, the P2 decreases with respect to trial number, but only in response to detected stimuli. Measuring this habituating behavior can be used to assess altered nociceptive processing. A decreased habituation of P2 amplitude over time or over the amount of repeated stimuli has been related to chronic pain in earlier literature in patients with migraine

(Valeriani et al., 2003), chronic low back pain (Vossen, Vossen, Joosten, Van Os, & Lousberg, 2015) and fibromyalgia (de Tommaso et al., 2011).

4.5 Conclusion

After a technical demonstration of combined threshold tracking and EP acquisition in an earlier study (van den Berg et al., 2020), we started this study to determine 1) which EP components can be observed during this procedure, 2) at which scalp locations these components are best observed and 3) to quantify the effect of stimulus properties on these components and detection thresholds in healthy subjects. We found that an N1 and N2 component can be observed with a maximum positive and negative potential at F4 and T7 respectively. The P2 component can be observed with maximum positive and negative potentials at CPz and A1 respectively. The P2 has a similar latency and topography regardless of filter settings. However, the N1 and N2 waveform and topography are heavily affected by the high-pass cutoff frequency. Using a larger cutoff frequency enhanced the N2 and shifted the topographies of N1 and N2 from contralateral to central, suggesting that the observed N2 could be an artifactual effect of high-pass filtering. Statistical analysis showed that the N1 and N2 components observed in this experiment mainly influence by stimulus detection, while the P2 as well as the detection probability of a stimulus are also significantly influenced by stimulus properties such as the pulse amplitudes and the trial number.

Measuring the effects of intra-epidermal stimulus properties on the detection threshold and the evoked potential simultaneously provides a way to measure brain activation and pain perception in response to a well-defined nociceptive input. The results in this study demonstrate that the various steps of processing of a nociceptive stimulus, including peripheral nerve fiber recruitment, central synaptic summation, and habituation to a repeated stimulus are reflected by the detection thresholds as well as the EP.

4.6 References

Acunzo, D. J., Mackenzie, G., & van Rossum, M. C. (2012). Systematic biases in early ERP and ERF components as a result of high-pass filtering. *J Neurosci Methods, 209*(1), 212-218.

Agostinho, C. M. S., Scherens, A., Richter, H., Schaub, C., Rolke, R., Treede, R. D., & Maier, C. (2009). Habituation and short-term repeatability of thermal testing in healthy human subjects and patients with chronic non-neuropathic pain. *European Journal of Pain, 13*(8), 779-785.

Akaike, H. (1974). A new look at the statistical model identification. *IEEE Transactions on Automatic Control, 19*(6), 716-723.

Apkarian, A. V., Bushnell, M. C., Treede, R.-D., & Zubieta, J.-K. (2005). Human brain mechanisms of pain perception and regulation in health and disease. *European Journal of Pain, 9*(4), 463-463.

Christmann, C., Koeppe, C., Braus, D. F., Ruf, M., & Flor, H. (2007). A simultaneous EEG-fMRI study of painful electric stimulation. *NeuroImage, 34*(4), 1428-1437.

de Tommaso, M., Federici, A., Santostasi, R., Calabrese, R., Vecchio, E., Lapadula, G., . . . Livrea, P. (2011). Laser-Evoked Potentials Habituation in Fibromyalgia. *The Journal of Pain, 12*(1), 116-124.

Delorme, A., Sejnowski, T., & Makeig, S. (2007). Enhanced detection of artifacts in EEG data using higher-order statistics and independent component analysis. *NeuroImage, 34*(4), 1443-1449.

Doll, R. J., Buitenweg, J. R., Meijer, H. G. E., & Veltink, P. H. (2014). Tracking of nociceptive thresholds using adaptive psychophysical methods. *Behavior Research Methods, 46*(1), 55-66.

Doll, R. J., Maten, A. C. A., Spaan, S. P. G., Veltink, P. H., & Buitenweg, J. R. (2016). Effect of temporal stimulus properties on the nociceptive detection probability using intra-epidermal electrical stimulation. *Experimental Brain Research, 234*(1), 219-227.

Doll, R. J., van Amerongen, G., Hay, J. L., Groeneveld, G. J., Veltink, P. H., & Buitenweg, J. R. (2016). Responsiveness of electrical nociceptive detection thresholds to capsaicin (8 %)-induced changes in nociceptive processing. *Experimental Brain Research, 234*(9), 2505-2514.

Doll, R. J., Veltink, P. H., & Buitenweg, J. R. (2015). Observation of time-dependent psychophysical functions and accounting for threshold drifts. *Attention, Perception, & Psychophysics, 77(4)*, 1440-1447.

Garcia-Larrea, L., Frot, M., & Valeriani, M. (2003). Brain generators of laser-evoked potentials: From dipoles to functional significance. *Neurophysiologie Clinique, 33*(6), 279-292.

Iannetti, G. D., Hughes, N. P., Lee, M. C., & Mouraux, A. (2008). Determinants of laser-evoked EEG responses: Pain perception or stimulus saliency? *Journal of Neurophysiology, 100*(2), 815-828.

Inui, K., & Kakigi, R. (2012). Pain perception in humans: Use of intraepidermal electrical stimulation. *Journal of Neurology, Neurosurgery and Psychiatry, 83*(5), 551-556.

Inui, K., Tran, T. D., Hoshiyama, M., & Kakigi, R. (2002). Preferential stimulation of Aδ fibers by intra-epidermal needle electrode in humans. *Pain, 96*(3), 247-252.

Inui, K., Tran, T. D., Hoshiyama, M., & Kakigi, R. (2002). Preferential stimulation of Aδ fibers by intra-epidermal needle electrode in humans. *Pain, 96(3)*, 247-252.

Kiernan, M. C., Mogyoros, I., & Burke, D. (1996). Differences in the recovery of excitability in sensory and motor axons of human median nerve. *Brain, 119 (Pt 4)*, 1099-1105.

Lee, M. C., Mouraux, A., & Iannetti, G. D. (2009). Characterizing the cortical activity through which pain emerges from nociception. *Journal of Neuroscience, 29*(24), 7909-7916.

Legrain, V., Iannetti, G. D., Plaghki, L., & Mouraux, A. (2011). The pain matrix reloaded: A salience detection system for the body. *Progress in Neurobiology, 93*(1), 111-124.

Lehmann, D., & Skrandies, W. (1980). Reference-free identification of components of checkerboard-evoked multichannel potential fields. *Electroencephalography and Clinical Neurophysiology, 48*(6), 609-621.

Liang, M., Lee, M. C., O'Neill, J., Dickenson, A. H., & Iannetti, G. D. (2016). Brain potentials evoked by intraepidermal electrical stimuli reflect the central sensitization of nociceptive pathways. *Journal of Neurophysiology, 116*(2), 286-295.

Manresa, J. B., Andersen, O. K., Mouraux, A., & van den Broeke, E. N. (2018). High frequency electrical stimulation induces a long-lasting enhancement of event-related potentials but does not change the perception elicited by intra-epidermal electrical stimuli delivered to the area of increased mechanical pinprick sensitivity. *PLoS ONE, 13*(9).

May, A., Rodriguez-Raecke, R., Schulte, A., Ihle, K., Breimhorst, M., Birklein, F., & Jürgens, T. P. (2012). Within-session sensitization and between-session habituation: a robust physiological response to repetitive painful heat stimulation. *Eur J Pain, 16*(3), 401-409.

Miyazaki, M., Shibasaki, H., Kanda, M., Xu, X., Shindo, K., Honda, M., . . . Kimura, J. (1994). Generator mechanism of pain-related evoked potentials following CO_2 laser stimulation of the hand: Scalp

topography and effect of predictive warning signal. *Journal of Clinical Neurophysiology, 11*(2), 242-254.

Mouraux, A., Iannetti, G. D., & Plaghki, L. (2010). Low intensity intra-epidermal electrical stimulation can activate Aδ-nociceptors selectively. *Pain, 150(1)*, 199-207.

Mouraux, A., Marot, E., & Legrain, V. (2014). Short trains of intra-epidermal electrical stimulation to elicit reliable behavioral and electrophysiological responses to the selective activation of nociceptors in humans. *Neuroscience Letters, 561*(Supplement C), 69-73.

Oostenveld, R., Fries, P., Maris, E., & Schoffelen, J. M. (2011). FieldTrip: Open source software for advanced analysis of MEG, EEG, and invasive electrophysiological data. *Computational Intelligence and Neuroscience, 2011*.

Oostenveld, R., & Praamstra, P. (2001). The five percent electrode system for high-resolution EEG and ERP measurements. *Clin Neurophysiol, 112*(4), 713-719.

Poulsen, A. H., Tigerholm, J., Meijs, S., Andersen, O. K., & Mørch, C. D. (2020). Comparison of existing electrode designs for preferential activation of cutaneous nociceptors. *Journal of Neural Engineering*.

Rodriguez-Raecke, R., Ihle, K., Ritter, C., Muhtz, C., Otte, C., & May, A. (2014). Neuronal differences between chronic low back pain and depression regarding long-term habituation to pain. *European Journal of Pain (United Kingdom), 18*(5), 701-711.

Schwarz, G. (1978). Estimating the Dimension of a Model. *The Annals of Statistics, 6*(2), 461-464.

Steenbergen, P., Buitenweg, J. R., Trojan, J., van der Heide, E. M., van den Heuvel, T., Flor, H., & Veltink, P. H. (2012). A system for inducing concurrent tactile and nociceptive sensations at the same site using electrocutaneous stimulation. *Behavior research methods, 44(4)*, 924-933.

Tanner, D., Morgan-Short, K., & Luck, S. J. (2015). How inappropriate high-pass filters can produce artifactual effects and incorrect conclusions in ERP studies of language and cognition. *Psychophysiology, 52*(8), 997-1009.

Treede, R. D., Kief, S., Hölzer, T., & Bromm, B. (1988). Late somatosensory evoked cerebral potentials in response to cutaneous heat stimuli. *Electroencephalography and Clinical Neurophysiology, 70*(5), 429-441.

Valeriani, M., de Tommaso, M., Restuccia, D., Le Pera, D., Guido, M., Iannetti, G. D., . . . Cruccu, G. (2003). Reduced habituation to experimental pain in migraine patients: a CO2 laser evoked potential study. *Pain, 105*(1), 57-64.

Van den Berg, B., & Buitenweg, J. R. (2018). *Analysis Of Nociceptive Evoked Potentials During Multi-Stimulus Experiments Using Linear Mixed Models*. Paper presented at the 40th Annual International Conference of the IEEE Engineering in Medicine and Biology Society (EMBC), Honolulu, United States.

van den Berg, B., Doll, R. J., Mentink, A. L. H., Siebenga, P. S., Groeneveld, G. J., & Buitenweg, J. R. (2020). Simultaneous tracking of psychophysical detection thresholds and evoked potentials to study nociceptive processing. *Behavior Research Methods*.

Van der Lubbe, R. H. J., Blom, J. H. G., De Kleine, E., & Bohlmeijer, E. T. (2017). Comparing the effects of sustained and transient spatial attention on the orienting towards and the processing of electrical nociceptive stimuli. *International Journal of Psychophysiology, 112*, 9-21.

Vossen, C. J., Vossen, H. G., Joosten, E. A., Van Os, J., & Lousberg, R. (2015). Does habituation differ in chronic low back pain subjects compared to pain-free controls? A cross-sectional pain rating ERP study reanalyzed with the ERFIA multilevel method. *Medicine (United States), 94*(19).

Wilkinson, G. N., & Rogers, C. E. (1973). Symbolic Description of Factorial Models for Analysis of Variance. *Journal of the Royal Statistical Society. Series C (Applied Statistics), 22*(3), 392-399.

Zucker, R. S., & Regehr, W. G. (2002). Short-term synaptic plasticity. *Annual Review of Physiology, 64*, 355-405.

A 128-channel EEG cap, drawn in the style of Amadeo de Souza-Cardoso using neural style transfer.

Part II:

Observation of Impaired Nociceptive Processing in a Clinical Setting

"Every human being has a right to freedom from pain to the extent that our knowledge permits health professionals to achieve this goal."

Ronald Melzack and Patrick D. Wall, The Challenge of Pain

Chapter 5

Simultaneous Measurement of Intra-epidermal Electric Detection Thresholds and Evoked Potentials for Observation of Nociceptive Processing Following Sleep Deprivation

Published as:

Van den Berg, B., Hijma, H.J., Koopmans, I., Doll, R.J., Zuiker, R.G.J.A., Groeneveld, G.J., & Buitenweg, J. R. (2022). Simultaneous measurement of intra-epidermal electric detection thresholds and evoked potentials for observation of nociceptive processing following sleep deprivation. *Experimental Brain Research*, 240(2), 631-649.

DOI: https://www.doi.org/10.1007/s00221-021-06284-5

Abstract

Sleep deprivation has been shown to increase pain intensity and decrease pain thresholds in healthy subjects. In chronic pain patients, sleep impairment often worsens the perceived pain intensity. This increased pain perception is the result of altered nociceptive processing. We recently developed a method to quantify and monitor altered nociceptive processing by simultaneous tracking of psychophysical detection thresholds and recording of evoked cortical potentials during intra-epidermal electric stimulation. In this study, we assessed the sensitivity of nociceptive detection thresholds and evoked potentials to altered nociceptive processing after sleep deprivation in an exploratory study with 24 healthy male and 24 healthy female subjects. In each subject, we tracked nociceptive detection thresholds and recorded central evoked potentials in response to 180 single- and 180 double-pulse intra-epidermal electric stimuli. Results showed that the detection thresholds for single- and double-pulse stimuli and the average central evoked potential for single-pulse stimuli were significantly decreased after sleep deprivation. When analyzed separated by sex, these effects were only significant in the male population. Multivariate analysis showed that the decrease of central evoked potential was associated with a decrease of task-related evoked activity. Measurement repetition led to a decrease of the detection threshold to double-pulse stimuli in the mixed and the female population but did not significantly affect any other outcome measures. These results suggest that simultaneous tracking of psychophysical detection thresholds and evoked potentials is a useful method to observe altered nociceptive processing after sleep deprivation but is also sensitive to sex differences and measurement repetition.

5.1 Introduction

Despite ample research efforts, there are only few biomarkers that can be used for objective monitoring and stratification of chronic pain patients. Patients with chronic pain often experience sensations of pain in response to a non-nociceptive input (i.e., allodynia), or an increased sensation of pain in response to a nociceptive input (i.e., hyperalgesia). A current challenge is to find biomarkers that can identify alterations in nociceptive processing leading to or involved in chronic pain on an individual level. The identification of such biomarkers could allow for patient stratification into functionally distinct groups, and may enable prediction of treatment efficacy per individual (Mouraux & Iannetti, 2018). Furthermore, the development of such mechanism-based biomarkers can make it possible to accurately quantify the effects of analgesic drugs on nociceptive processing, which may provide an important proof-of-concept tool in early phase clinical pharmacology studies.

Key aspects in many types of chronic pain, including fibromyalgia, headache and complex regional pain syndrome, are central sensitization (Woolf, 2011) and reduced endogenous modulation of nociceptive input (Edwards, 2005). Therefore, recent studies have focused on measuring the effect of central sensitization or reduced inhibition induced by experimental pain models, e.g., capsaicin induced secondary hyperalgesia (Lee, Zambreanu, Menon, & Tracey, 2008; Zambreanu, Wise, Brooks, Iannetti, & Tracey, 2005). One method to centrally alter pain perception is by depriving healthy individuals of sleep (Schuh-Hofer et al., 2013). In this model, both central sensitization and reduced endogenous inhibition are thought to increase pain perception (Herrero Babiloni et al., 2020). Various studies have demonstrated a close relation between sleep impairments and an increased sensitivity to pain stimuli. In healthy subjects, sleep deprivation has been shown to cause hyperalgesic responses and an altered evoked cortical response, i.e., a decreased amplitude and increased habituation of the P2 in laser evoked potentials (Schuh-Hofer, Baumgärtner, & Treede, 2015; Schuh-Hofer et al., 2013). Another recent study demonstrated impaired conditioned pain modulation and facilitation of temporal pain summation following 24 hours of total sleep deprivation in healthy subjects (Staffe et al., 2019). Impaired pain inhibition on one hand, and

enhanced pain facilitation on the other, have both been related to various chronic pain conditions such as musculoskeletal, visceral and neuropathic pain (Herrero Babiloni et al., 2020). These observations suggest that sleep deficiency leads to altered central nociceptive processing, and an associated increase in pain perception. The sleep deprivation model may therefore be ideal to generate biomarkers that aim to quantify altered central nociceptive processing in healthy volunteer- and chronic pain patient populations.

Recently, we developed a method for the characterization of both peripheral and central nociceptive processing by measuring the effect of nociceptive stimulus properties on detection probability and cortical evoked potentials (EPs). Nociceptive nerve fibers in the skin are activated using low-intensity intra-epidermal electric stimulation with cathodic square-wave pulses (Mouraux, 2010). Inhibition and facilitation of repeated nociceptive input are explored by varying the number of pulses and the inter-pulse interval (Doll, Maten, Spaan, Veltink, & Buitenweg, 2016; Mouraux, Marot, & Legrain, 2014; van der Heide, Buitenweg, Marani, & Rutten, 2009), based on the concept that central (e.g. temporal summation, short-term synaptic plasticity (Zucker & Regehr, 2002)) or peripheral (e.g. subthreshold or suprathreshold super-excitability (Bostock et al., 2005)) neural mechanisms can attenuate or amplify neural activation by a second pulse dependent on its time with respect to the first pulse.

During a single measurement session, single- and double-pulse stimuli are applied according to an adaptive method of limits to track corresponding nociceptive detection thresholds (Doll, Maten, Spaan, Veltink, & Buitenweg, 2016) while recording the electroencephalogram (EEG) to measure associated EPs (van den Berg et al., 2020). This combination of outcome measures potentially provides a unique insight into nociceptive processing. Nociceptive detection thresholds can be used to observe altered sensitivity (Doll et al., 2016; Gottrup, Nielsen, Arendt-Nielsen, & Jensen, 1998; Treede, Meyer, Raja, & Campbell, 1992). In addition, the reliability of detecting the corresponding stimulus level (i.e. the minimum needed for a subject to detect nociception) is quantified by the detection probability slope (Gold & Ding, 2013). EPs can be used as biomarker for altered nociception, such as in the case of central

sensitization (van den Broeke et al., 2015), attentional modulation (Legrain, Guérit, Bruyer, & Plaghki, 2002) and placebo analgesia (Wager, Matre, & Casey, 2006). We believe that both outcomes (i.e., EPs and nociceptive detection thresholds) measure different aspects of nociceptive processing and should be combined in a single experiment. After an initial demonstration that both techniques could be efficiently combined (van den Berg et al., 2020) we showed how the combined method may be used for studying the effect of intra-epidermal stimulus properties on nociceptive detection thresholds and EPs in a healthy population (van den Berg & Buitenweg, 2021).

This combined method was developed with the goal of identifying combinations of psychophysical and neurophysiological features that could aid diagnosis and stratification of chronic pain patients, and as a proof-of-concept tool to characterize the effects of (investigational) analgesics in early-phase clinical studies. Here, we examined if we could register altered nociceptive processing following sleep deprivation using this method in an exploratory study with 24 healthy male and 24 healthy female subjects. We study the feasibility of using the combination of nociceptive detection thresholds and EPs to observe altered nociceptive processing following sleep deprivation in both sexes.

5.2 Methods

The work presented here was part of a study at the Centre for Human Drug Research (Leiden, the Netherlands) in which also other nociceptive pain tasks were performed. During the first part of this study, 24 male subjects were included. During the second part, 24 female subjects were included. In each part subjects participated in a measurement session (described below) after a night of sleep deprivation (sleep deprived occasion) and after a normal night of sleep (control occasion) (Figure 5.1). On the sleep deprived occasion, subjects were deprived of their sleep by remaining awake a full night under supervision of a research assistant, after which the subjects participated in one measurement session in the morning. To ensure wakefulness of the subjects, they were closely monitored the entire night. To minimize the chance of creating a bias in

study results, the interactions between subject and research assistant were kept to a minimum at night. In addition, the morning measurements were performed by a different assistant than the assistant that monitored the subject(s) during the sleep deprivation night. On the control occasion, subjects participated to two measurement sessions following a normal night of sleep, one in the morning and one in the afternoon. Participants were asked to go to sleep between 22:00 and 23:00, and to wake up between 7:00 and 8:00, on the night preceding the control occasion. The order of both occasions was randomized. If the sleep deprived occasion preceded the control occasion, a minimum resting period of at least 5 days was required. In practice, this resting period was either 7 or 8 days on all occasions.

The study received approval from a Medical Review and Ethics Committee (Foundation BEBO, Assen, the Netherlands) before study start, and was performed in accordance with the declaration of Helsinki. All subjects provided written informed consent prior to any study assessments taking place. The study has prospectively been registered in the Dutch Trial Register (NTR) as NTR7517.

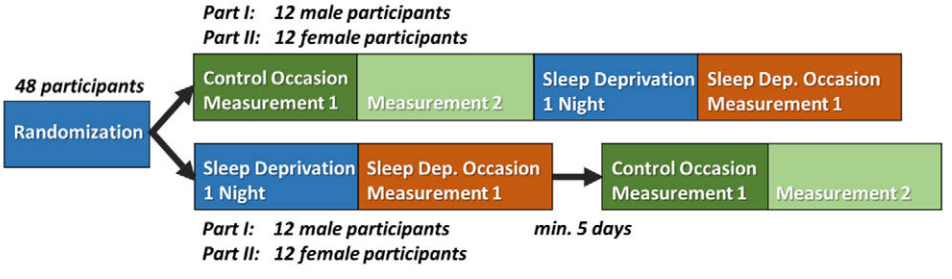

Figure 5.1: Participants were measured on two occasions: after a night of sleep deprivation (1 measurement) and after a normal night of sleep (2 measurements). If the sleep deprived occasion preceded the control occasion, a resting period of at least 5 days was used between both occasions.

5.2.1 Participants

A total of 24 healthy male (age 26.2 ± 2.1) and 24 healthy female (age 25.9 ± 3.0) participants were enrolled. Participants were recruited via media advertisement or from the subjects' database of the Centre for Human Drug Research, Leiden, the Netherlands. Inclusion criteria were an age between 23 and 35 years, to reduce the potential influence of age on outcome measures, and a body mass index between 18 and 32 kg/m2, to exclude underweight or extremely overweight individuals. Exclusion criteria were a history or symptoms of any significant disease, history or presence of sleep disorders, a change in time zones 7 days prior to the study period, average usage of tobacco products equivalent to or more than 10 cigarettes per day, average usage of (methyl)xanthines of more than 8 units per day and inability to refrain from usage during the study occasions. No usage of (illicit) drugs was permitted from 3 days prior to each study period until discharge. Consumption of alcohol or tobacco- and nicotine-containing products was not permitted from 24 hours prior to each scheduled visit until discharge. Participants underwent a urine drug screening and alcohol breath test on each arrival at the clinical research unit, i.e., before the start of each occasion. In addition, participants were not allowed to consume excessive amounts of caffeine, defined as more than 800mg per day, from 2 days prior to each visit. Participants fully abstained from using caffeine-containing products from 4 hours prior to each visit until discharge. No prescription medications and over-the-counter medications, except for contraceptive pill usage, were permitted within 14 days prior to the first occasion, or less than 5 half-lives, and during the course of the study. In addition, no vitamin, mineral, herbal, and dietary supplements were permitted within 7 days prior to the first occasion, or less than 5 half-lives, and during the course of the study.

To minimize a possible influence of the menstrual cycle on pain perception, females were required to use a reliable method of hormonal contraception at least 30 days before the first study day until the end of the study. Females were required to use their own hormonal anticonception (prescribed by their general practitioner of gynecologist) continuously during study participation or were only allowed to participate if the study days were more than 2 days after re-

start of contraceptive pill use or after bleeding withdrawal. This to prevent possible variations caused by the menstrual cycle. No side effects of hormonal contraception were reported.

5.2.2 Stimuli

Participants received intra-epidermal electric pulses applied by a constant current stimulator (NociTRACK AmbuStim, University of Twente, Enschede, the Netherlands). Intra-epidermal electric stimulation at intensities of less than twice the detection threshold preferentially activates Aδ-fibers in the skin (Motogi et al., 2016; Mouraux, 2010; Poulsen, Tigerholm, Meijs, Andersen, & Mørch, 2020). Stimuli were applied via an electrode attached to the volar lower arm at the side of the dominant hand (Figure 5.2). The electrode consisted of an array of 5 interconnected microneedles embedded in silicone, each needle protruding 0.5 mm from the electrode surface. Previous studies using this electrode showed that stimulation resulted in a sharp pricking sensation (Steenbergen, 2012), and similar latencies of response times and evoked N1, N2 and P2 peaks in comparison with earlier studies using intra-epidermal and laser stimulation (van den Berg & Buitenweg, 2021). In addition to single-pulse stimuli, double-pulse stimuli were used to observe potential effects of inhibition or facilitation of repeated nociceptive input (Doll, Maten, Spaan, Veltink, & Buitenweg, 2016; Mouraux, Marot, & Legrain, 2014; van der Heide, 2009). As such, two stimulus types were used in this study:

- A single 210 µs pulse
- A double 210 µs pulse with an inter-pulse interval (IPI) of 10 ms

5.2.3 Procedure

While seated in a comfortable chair, participants were instructed to focus their attention on the stimulation electrode, to reduce the potential influence of (variations in) spatial attention. First, a rough estimate of the detection threshold was obtained using a normal staircase procedure with a step size of

0.025 mA. The participant was instructed to hold a button, and to release the button as soon as a stimulus was perceived. Second, an accurate estimate of the detection threshold was obtained using an adaptive and randomized psychophysical method of limits, also referred to as 'threshold tracking', designed to estimate detection thresholds with a potential drift (Doll, Veltink, & Buitenweg, 2015). Participants were instructed to hold a button, and to briefly release the button when a stimulus was perceived. A vector of 5 stimulus amplitudes was initialized with a step size of 0.025 mA around the initial estimate of the detection threshold. For each stimulus, a value was randomly chosen from this vector. When the stimulus was detected, the vector was decreased by 0.025 mA. When the stimulus was not detected, the vector was increased by 0.025 mA. This process was repeated for a total of 180 single- and 180 double-pulse stimuli, during a time period of approximately 20 minutes. The interval between two consecutive stimuli was randomized with a uniform distribution of 2.5 to 3.5 seconds.

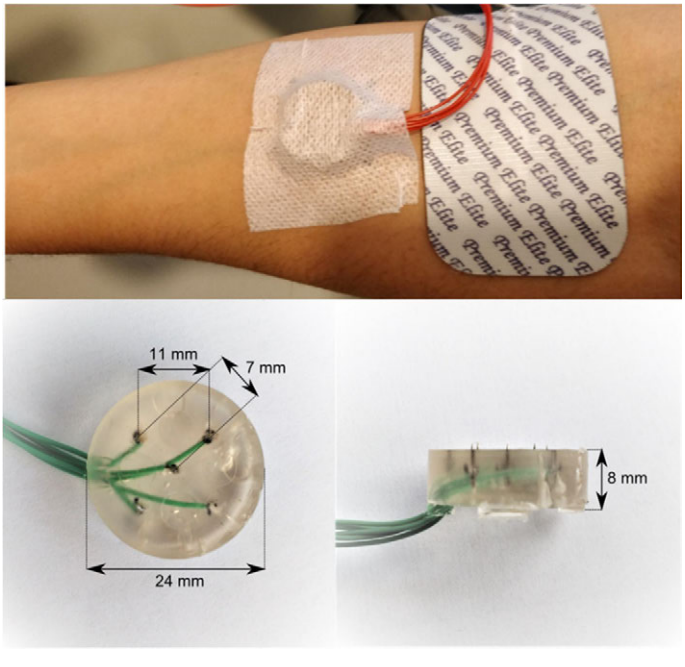

***Figure 5.2**: Electrode placement on the volar forearm on the side of the dominant hand (top), and electrode dimensions (bottom).*

5.2.4 Electroencephalography Recording

During the entire detection threshold tracking procedure, the scalp EEG was recorded at 32 Ag/AgCl electrodes located on the scalp according to the international 10/20 system. Electrode impedance was kept below 5 kΩ. To reduce eye blink and movement artefacts, participants were asked to fix their gaze at one spot on the wall and blink as few times as possible while pressing the response button and focusing their attention on the received stimuli.

5.2.5 Analysis

Effect of Stimulus Properties and Sleep Deprivation on Detection Probability

The effect of stimulus properties and sleep deprivation on the detection probability was analyzed for the male group, female group and the combination of both groups using a generalized linear mixed model in R, estimated using the lme4 (Bates, Mächler, Bolker, & Walker, 2015) and MASS toolboxes (Venables & Ripley, 2002). We used the statistical model in Equation (1), where the log-odds of stimulus detection ($\ln\left(\frac{P_d}{1-P_d}\right)$) is modulated by the effects and interaction of stimulus type (TYP), i.e., single- or double-pulse, stimulus amplitude (AMP) and condition (C) and by the effects and interaction of trial number (TRL) and condition (C). The guess rate and lapse rate were both assumed to be zero for robust estimation of effect sizes. We also added terms for measurement number (M) and occasion (O) to account for potential confounding. Condition, measurement, and occasion were modeled as categorical. All within-subject fixed effects were also included as random effects grouped by subject (S) to effectively account for differences between subjects (Barr, Levy, Scheepers, & Tily, 2013).

$$\ln\left(\frac{P_d}{1-P_d}\right) \sim 1 + AMP * TYP * C + TRL * C + M + O + (1 + AMP * TYP * C + TRL * C + M + O|S) \quad (1)$$

Before GLMR analysis of the dataset outliers were excluded, defined as measurements in which the detection threshold was estimated smaller than 0 or larger than 1.6 mA, or where the slope of the psychometric curve was estimated smaller than 0 or larger than 100 mA^{-1}. Effect significance was tested using a two-tailed type III test using Wald Chi-square statistics.

Detection thresholds and slopes were computed using the estimated model coefficients. Differences of detection thresholds and slopes between the sleep deprived measurement and the first control measurement and between both control measurements were tested by generating a posterior distribution of each model coefficient with 20000 samples using the ARM package in R (Gelman & Hill, 2006). Subsequently, these posterior distributions were used to compute the distribution, confidence intervals and significance of the (difference between) detection thresholds.

Preprocessing of EEG Data

The scalp EEG data was pre-processed using Fieldtrip (Oostenveld, Fries, Maris, & Schoffelen, 2011). Epochs were extracted from the EEG from 0.5 s before to 1.0 s after the stimulus. Eye blink and movement artefacts were identified and removed using independent component analysis (Delorme, Sejnowski, & Makeig, 2007), resulting in removal of 2 independent components on average. Epochs with excessive EMG activity were excluded from analysis based on visual inspection. Subsequently, epochs were bandpass-filtered from 0.1 to 40 Hz and baseline-corrected using the interval ranging from -0.5 s to 0.0 s relative to stimulus onset.

Grand Average Evoked Potential

The Cz-M1M2 derivation was used for analysis of the central EP, as previous studies showed that these channels (Cz, M1 and M2) have the largest SNR for intra-epidermal electric EPs in healthy participants, when using a 32-channel electrode configuration (van den Berg & Buitenweg, 2021). Grand average waveforms at the identified latency at the Cz-M1M2 derivation were computed

by averaging all trials separated by measurement number (1 or 2), stimulus type (single- or double-pulse) and condition (with or without sleep deprivation), resulting in 180 trials per average. A positive peak (P2) was defined as the most positive peak between 300 and 500 ms at Cz-M1M2 and selected for further analysis. The differences of average EP at Cz-M1M2 between the sleep deprived measurement and the first control measurement and between both control measurements were tested at the identified P2 latency (390 ms) using a two-tailed paired-sample *t*-test.

Effect of Stimulus Properties on Evoked Potential

The effect of stimulus properties and sleep deprivation on the EP at P2 latency was analyzed for the male group, female group and the combination of both groups using a linear mixed model in Matlab (version 2017b, MathWorks, Inc.). We used the statistical model in Equation (2), similar to the model for analysis of detection probability in Equation (1) but including a term for additional cortical activity evoked by stimulus detection (D) which could decrease with respect to the trial number (TRL), and also vary with respect to condition (C). Condition, stimulus detection, measurement and occasion were modeled as categorical. Significance of the effect coefficients was assessed using a two-tailed *t*-test using Satterthwaite's method for estimation of the degrees of freedom.

$$\mathrm{U_{EEG}} \sim 1 + \mathrm{AMP} * \mathrm{TYP} * \mathrm{C} + \mathrm{TRL} * \mathrm{D} * \mathrm{C} + \mathrm{M} + \mathrm{O} + (1 + \mathrm{AMP} * \mathrm{TYP} * \mathrm{C} + \mathrm{TRL} * \mathrm{D} * \mathrm{C} + \mathrm{M} + \mathrm{O}|\mathrm{S}) \quad (2)$$

5.3 Results

5.3.1 Exclusion of Outliers

In the first part of the study (males) 7 out of 72 measurements were excluded due to an incomplete measurement. For the analysis of EEG, 3 out of the remaining 65 measurements were excluded due to extreme noise caused by a faulty electrode. For the analysis of detection probability, 16 out of the

remaining 65 measurements were excluded due to poor task performance, defined as measurements in which the detection threshold was estimated smaller than 0 or larger than 1.6 mA, or where the slope of the psychometric curve was estimated smaller than 0 or larger than 100 mA^{-1}.

In the second part of the study (females) 4 out of 72 measurements were excluded due to an incomplete measurement. For the analysis of EEG, 3 out of the remaining 68 measurements were excluded due to extreme noise caused by a faulty electrode. For the analysis of detection probability, 2 out of the remaining 68 measurements were excluded due to poor task performance, defined as measurements in which the detection threshold was estimated smaller than 0 or larger than 1.6 mA, or where the slope of the psychometric curve was estimated smaller than 0 or larger than 100 mA^{-1}.

5.3.2 Effect of Stimulus Properties and Sleep Deprivation on Detection Probability

In the male group 7 out of 72 measurements were excluded due to technical problems with the measurement setup. The effect of stimulus properties and sleep deprivation on detection probability is shown in Table 5.1. The random effects covariance matrices associated with each generalized linear mixed model fit are available in Appendix I. In all groups, significant effects on the detection probability were observed for the intercept, amplitude, type, trial number and the interaction between amplitude and type. The detection probability increases with respect to the amplitude and decreases over the number of trials. The positive coefficients for type and the interaction between amplitude and type shows that addition of a second pulse to the stimulus increases detection probability. An additional significant effect of stimulus type is observed in the combined group, as well as male group only. The combination of both groups and the female group show an additional significant effect of measurement, and of the interaction between amplitude, type, and condition.

Detection thresholds derived from the coefficient estimates are shown in Table 5.2. For the combined group and the male group, the estimate of the detection threshold is significantly lower for both single-pulse and double-pulse stimuli

after sleep deprivation. The female group shows a similar non-significant trend after sleep deprivation. For the combination of both groups and the female group, the estimate of the detection threshold is significantly lower for both single-pulse and double-pulse stimuli during the second control measurement. The male group shows a similar non-significant trend during the second control measurement.

Detection probability slopes derived from the coefficient estimates are shown in Table 5.3. The slope appears to increase in all groups after sleep deprivation. However, this increase was only significant in the female group for double-pulse stimuli.

Stimulus Property	Coeff (All)	Coeff (M)	Coeff (F)	χ^2 (All)	χ^2 (M)	χ^2 (F)	*p* (All)	*p* (M)	*p* (F)
(Intercept)	**-3.50**	**-3.19**	**-3.44**	**172.51**	**80.24**	**69.25**	**<.001**	**<.001**	**<.001**
Amplitude (AMP)	**6.10**	**4.45**	**7.52**	**148.42**	**85.06**	**98.05**	**<.001**	**<.001**	**<.001**
Type (TYP)				**6.01**	**11.83**	0.66	**<.05**	**<.001**	.42
Type 2	**-0.39**	**-0.85**	-0.19						
Trial number (TRL)	**-0.52**	**-0.41**	**-0.62**	**108.89**	**26.88**	**104.33**	**<.001**	**<.001**	**<.001**
Measurement (M)				**5.90**	0.82	**4.33**	**<.05**	.37	**<.05**
Measurement 2	**0.64**	0.31	**0.77**						
Occasion (O)				2.22	0.97	2.10	.14	.32	.14
Occasion 2	0.30	-0.48	-0.32						
Condition (C)				0.11	1.64	0.01	.74	.20	.90
Sleep Dep.	0.14	0.85	0.08						
Amplitude x Type				**52.81**	**20.69**	**38.09**	**<.001**	**<.001**	**<.001**
Amplitude x Type 2	**6.69**	**5.74**	**7.81**						
Amplitude x Condition				1.09	0.82	1.07	.30	.36	.30
Amplitude x Sleep Dep.	1.23	1.14	1.88						
Type x Condition				0.10	1.40	0.70	.75	.23	.40
Type 2 x Sleep Dep.	-0.13	0.54	-0.60						
Trial number x Condition				0.06	0.06	0.16	.80	.81	.69
Trial number x Sleep Dep.	-0.02	-0.03	-0.04						
Amplitude x Type x Condition				**3.74**	0.52	**3.90**	**.05**	.47	**<.05**
Amplitude x Type 2 x Sleep Dep.	**3.18**	1.36	**5.19**						

***Table 5.1**: Effect of stimulus properties on the detection probability for the male group (M), the female group (F) and the combination of both (All), computed using GLMR. Significance was assessed using type-III Wald Chi-square statistics with one degree of freedom. All effect coefficients are expressed in log-odds per unit with the units mA^{-1} for amplitude and $(100\,trials)^{-1}$ for trial number. The numbers of measurement and occasion refer to the moments at which the procedure was conducted as described in Figure 5.1. Significant values (p<.05) are shown in bold.*

Stimulus Type	Thresh. (All)	Thresh. (M)	Thresh. (F)	95% CI (All)	95% CI (M)	95% CI (F)
Single-pulse, Control 1	0.57	0.72	0.46	[0.48 0.69]	[0.55 0.94]	[0.37 0.55]
Single-pulse, Control 2	**0.47***	0.65	**0.35***	[0.38 0.57]	[0.43 0.92]	**[0.31 0.41]**
Single-pulse, Sleep Dep.	**0.46***	**0.42****	0.36	**[0.38 0.58]**	**[0.28 0.62]**	[0.29 0.48]
Double-pulse, Control 1	0.30	0.40	0.24	[0.25 0.38]	[0.29 0.59]	[0.19 0.29]
Double-pulse, Control 2	**0.25***	0.37	**0.19***	[0.21 0.32]	[0.24 0.58]	**[0.16 0.22]**
Double-pulse, Sleep Dep.	**0.23***	**0.21*****	0.18	**[0.18 0.29]**	**[0.14 0.31]**	[0.14 0.24]

*Table 5.2: Detection thresholds for the male group (M), the female group (F) and the combination of both (All) per stimulus type (in mA). Control 1 and Control 2 refer to the first and second control measurement in Figure 5.1 respectively. Each significant difference of the sleep deprived measurement or the second control measurement with respect to the first control measurement is denoted with * (p<0.05), ** (p<0.01) and *** (p<0.001). Detection thresholds with a significant difference with respect to the first control occasion (p<.05) and associated confidence intervals are shown in bold.*

Stimulus Type	Slope (All)	Slope (M)	Slope (F)	95% CI (All)	95% CI (M)	95% CI (F)
Single-pulse, Control 1 & 2	6.11	4.45	7.52	[5.14 7.07]	[3.56 5.35]	[6.04 8.99]
Single-pulse, Sleep Dep.	7.32	5.59	9.42	[5.23 9.49]	[3.26 7.95]	[6.34 12.44]
Double-pulse, Control 1 & 2	12.79	10.18	15.33	[10.46 15.13]	[7.06 13.30]	[12.34 18.33]
Double-pulse, Sleep Dep.	17.18	12.66	**22.40***	[12.43 22.00]	[7.75 17.68]	**[15.80 28.84]**

*Table 5.3: Detection probability slopes for the male group (M), the female group (F) and the combination of both (All) per stimulus type (in mA^{-1}). Control 1 and Control 2 refer to the first and second control measurement in Figure 5.1 respectively. Each significant difference of the sleep deprived measurement with respect to the control measurements is denoted with * (p<0.05), ** (p<0.01) and *** (p<0.001). Slopes with a significant difference with respect to both control occasions (p<.05) and associated confidence intervals are shown in bold.*

5.3.3 Grand Average Evoked Potential

The difference between sleep deprived and control measurements for each group is shown in the time domain at the Cz-M1M2 derivation in Figure 5.3. For the combination of both groups and the male group, there was a significant decrease in maximum EP amplitude in response to detected single- and double-pulse stimuli after sleep deprivation. For the female group, there was no significant difference in maximum EP amplitude between sleep deprived on control measurements. For all groups, there was no significant difference in EP between both control measurements.

5.3.4 Effect of Stimulus Properties and Sleep Deprivation on Evoked Potential

The effects of stimulus properties and sleep deprivation on the EP at 390 ms latency on the Cz-M1M2 derivation were quantified by linear mixed regression based on Equation (2) and a *t*-test of each computed effect coefficient. Results for each group are shown in Table 5.4. The random effects covariance matrices associated with each linear mixed model fit are available in Appendix I. For each group, significant effects of stimulus properties on the EP were found for stimulus detection, trial number, amplitude and the interaction between amplitude and type. For the combination of both groups and for the male group, a significant interaction between sleep deprivation and stimulus detection was found. For this interaction between sleep deprivation and stimulus detection, effect coefficients of -1.28 and -2.21 were found for the combination of both groups and for the male group respectively, which means that the EP in response to detected stimuli decreased by -1.28 and -2.21 μV after sleep deprivation.

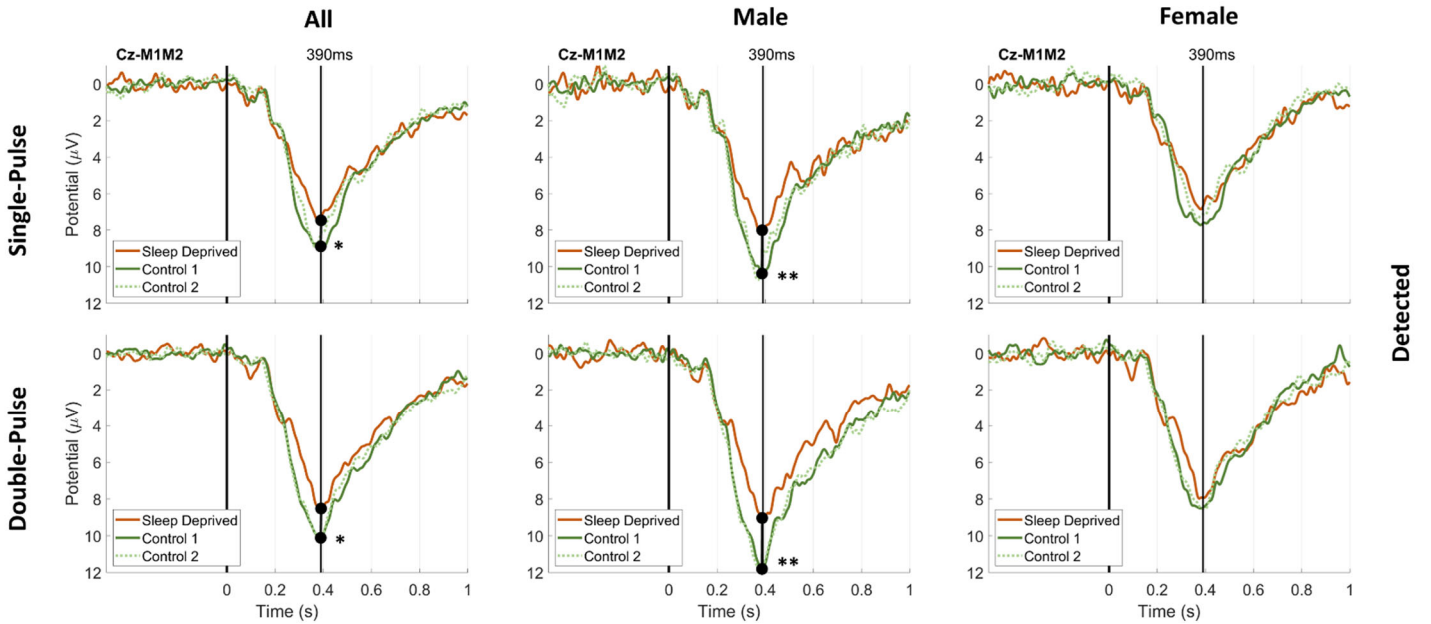

Figure 5.3a: *Grand average EP in each group in response to detected single-pulse and double pulse intra-epidermal stimuli at Cz-M1M2 for participants with normal sleep during a first and a second measurement (Control M1 and Control M2 respectively) and after 24 hours of sleep deprivation. There was a significant difference in maximum EP amplitude at Cz-M1M2 between the sleep deprived and the first control measurement for detected single- and double-pulse stimuli in the male group and the combination of both groups. Significance is indicated with * (p<.05) and ** (p<.01).*

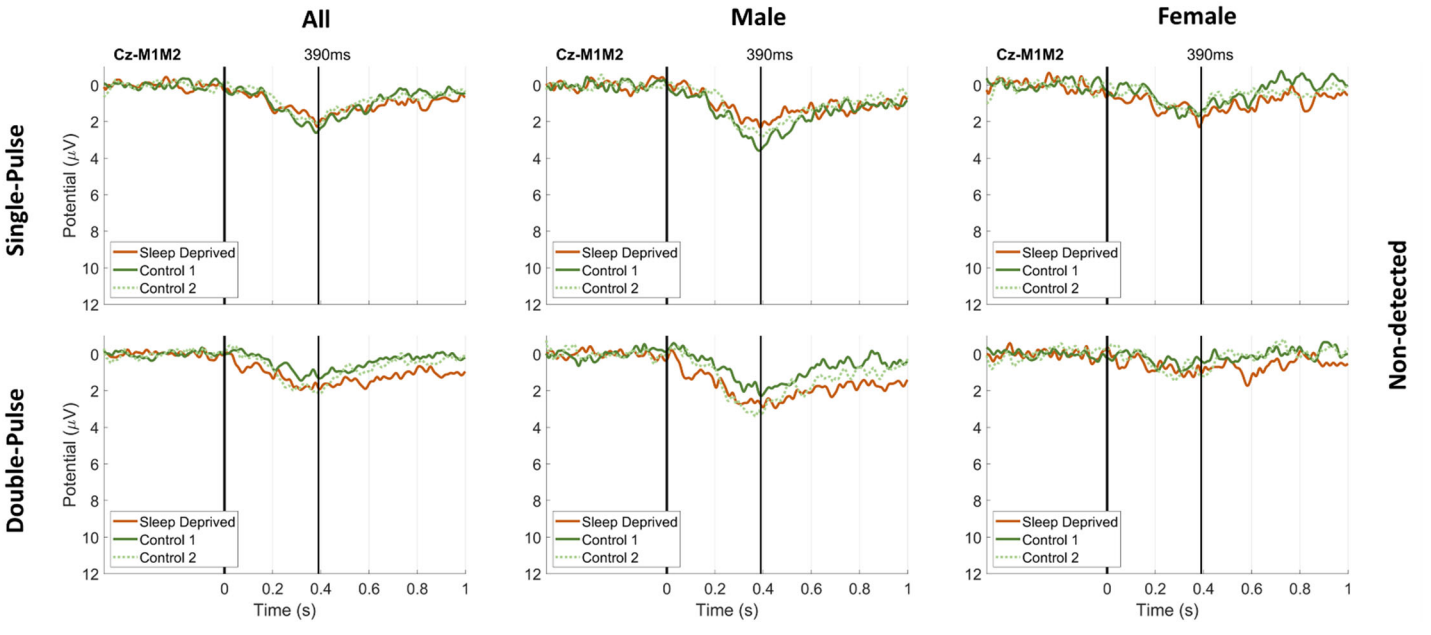

Figure 5.3b: *Grand average EP in each group in response to non-detected single-pulse and double pulse intra-epidermal stimuli at Cz-M1M2 for participants with normal sleep during a first and a second measurement (Control M1 and Control M2 respectively) and after 24 hours of sleep deprivation. There was a significant difference in maximum EP amplitude at Cz-M1M2 between the sleep deprived and the first control measurement for detected single- and double-pulse stimuli in the male group and the combination of both groups. Significance is indicated with * (p<.05) and ** (p<.01).*

Stimulus Property	Coeff. (All)	Coeff. (M)	Coeff. (F)	*t* (All)	*df*	*t* (M)	*df*	*t* (F)	*df*	p (All)	p (M)	p (F)
(Intercept)	0.89	1.61	0.06	1.54	*31.2*	1.49	*15.6*	0.12	*50.8*	.13	0.15	.91
Detection (D)												
Detected	**7.02**	**7.71**	**6.43**	**11.10**	***44.6***	**7.45**	***22.0***	**8.45**	***21.7***	**<.001**	**<.001**	**<.001**
Amplitude	**2.40**	**2.54**	**2.58**	**4.11**	***35.1***	**2.60**	***13.5***	**3.04**	***34.0***	**<.001**	**<.05**	**<.01**
Type												
Type 2	-0.37	-0.59	-0.50	-1.04	*108.3*	-1.05	*48.9*	-0.85	*29.8*	.30	.30	.40
Trial number (TRL)	**-0.57**	**-0.54**	**-0.65**	**-3.34**	***53.3***	**-2.30**	***27.1***	**-2.62**	***25.8***	**<.01**	**<.05**	**<.05**
Measurement (M)												
Measurement 2	-0.17	-0.76	0.18	-0.42	*23.4*	-1.22	*14.8*	0.37	*18.5*	.68	.24	.72
Occasion (O)												
Occasion 2	-0.44	-0.53	0.14	-1.38	*21.0*	-1.17	*13.5*	0.30	*13.5*	.18	.26	.77
Condition (C)												
Sleep dep.	-0.42	-1.57	0.03	-0.46	*29.8*	-1.05	*16.1*	0.02	*19.1*	.65	.31	.98
Amplitude x Type												
Amplitude x Type 2	**3.60**	**3.60**	**4.65**	**4.08**	***11.3***	**4.22**	***12.1***	**2.37**	***11.7***	**<.01**	**<.01**	**<.05**
Trial number x Detection												
Trial number x Detected	-0.55	-0.34	-0.72	-1.96	*43.7*	-0.84	*21.1*	-1.85	*23.4*	.06	.41	.08
Detection x Condition												
Detected x Sleep dep.	**-1.28**	**-2.21**	-0.99	**-2.39**	***45.3***	**-3.13**	***22.7***	-1.28	*23.3*	**<.05**	**<.01**	.21
Amplitude x Condition												
Amplitude x Sleep dep.	0.56	1.61	0.61	0.58	*25.4*	1.00	*14.0*	0.37	*11.7*	.57	.34	.72
Type x Condition												
Type 2 x Sleep dep.	0.36	0.44	-1.07	0.49	*44.0*	0.43	*31.1*	-0.98	*23.3*	.63	.67	.34
Trial number x Condition												
Trial number x Sleep dep.	-0.09	-0.65	0.20	-0.30	*44.0*	-1.52	*22.5*	0.45	*23.2*	.76	.14	.65
Amp. x Type x Condition												
Amp. x Type 2 x Sleep dep.	-1.29	-0.33	5.24	-0.97	*16.8*	0.25	*13.5*	1.54	*16.4*	.35	.81	.14
Trial num. x Det. x Cond.												
Trial num. x Det. x Sleep dep.	-0.45	-0.14	-0.69	-0.93	*45.9*	-0.21	*26.9*	-0.98	*21.8*	.36	.83	.34

Table 5.4*: The coefficient estimates, and corresponding t- and p-values for effects of stimulus properties on the EP at 390ms (Cz-M1M2) in the male group (M), the female group (F) and the combination of both (All). All effect coefficients are expressed in* μV *per unit with the units* mA^{-1} *for amplitude and* $(100\ trials)^{-1}$ *for trial number. The numbers of measurement and occasion refer to the moments at which the procedure was conducted as described in Figure 5.1. Significant values (p<.05) are shown in bold.*

5.4 Discussion

In search of a composite biomarker for altered nociceptive processing, we combined techniques to simultaneously measure detection thresholds and EPs in response to nociceptive intra-epidermal electric stimulation. We explored if this combination of techniques could be used to observe changes in nociceptive processing following sleep deprivation in a male and female population. We found that intra-epidermal electric detection thresholds and EPs both decreased after 24 hours of sleep deprivation in a combined group of healthy male and female subjects.

The effects of intra-epidermal electric stimulus properties on the detection probability were similar to the effects observed in previous studies (Doll, Maten, Spaan, Veltink, & Buitenweg, 2016; van den Berg & Buitenweg, 2021; van den Berg et al., 2020), supporting the validity of our results. Similar to these earlier observations on unchallenged healthy subjects, we observed a general positive effect of stimulus amplitude and the interaction between amplitude and type on detection probability (Table 5.1). Both effects indicate that the detection probability increased when the stimulus amplitude of single- or double-pulse stimuli increased, which is associated with an increased recruitment of peripheral nerve fibers at increased currents. The detection probability also increased following addition of a second pulse as a result of the temporal summation of neural activity elicited by both pulses, which was signified by the positive effect of stimulus type and the positive interaction between stimulus amplitude and stimulus type in generalized linear mixed regression (Table 5.1). The detection probability decreased over the number of trials, plausibly due to a decreased attention or physiological habituation to the stimulus. In addition, there was a significant interaction between stimulus amplitude, type, and sleep deprivation for the mixed population, suggesting that the effect of adding a second pulse on the detection probability is increased after sleep deprivation. This interaction suggests an increased facilitation or decreased inhibition of neural activity evoked by the second pulse following sleep deprivation. A potential explanation for increased facilitation of the second pulse is increased temporal summation, as originally defined by (Price, Hu, Dubner, & Gracely, 1977), which has also been shown to be increased following sleep deprivation

using modern temporal summation paradigms (Matre, Andersen, Knardahl, & Nilsen, 2016; Smith et al., 2019).

Nociceptive detection thresholds for intra-epidermal electric stimulation were decreased following sleep deprivation. These detection thresholds were computed from generalized linear mixed regression coefficients (Moscatelli, Mezzetti, & Lacquaniti, 2012), and statistically tested through Monte-Carlo simulation of detection threshold distributions. As a result, we found that in a mixed population (i.e., male, and female groups combined) detection thresholds for both types of stimuli decreased after sleep deprivation. Earlier studies have examined the effects of sleep deprivation using mechanical and thermal pain (detection) thresholds. Some of these studies support that pain thresholds are decreased following sleep deprivation, having observed a significant decrease in mechanical (Moldofsky & Scarisbrick, 1976; Moldofsky, Scarisbrick, England, & Smythe, 1975; Onen, Alloui, Gross, Eschallier, & Dubray, 2001) and heat pain thresholds (Kundermann, Spernal, Huber, Krieg, & Lautenbacher, 2004) due to sleep deprivation. However, not all studies found a significant correlation between pain thresholds and sleep deprivation (Drewes et al., 1997; Older et al., 1998). We demonstrated here that the nociceptive intra-epidermal electric detection thresholds to single-pulse and double-pulse stimuli were decreased in a mixed population, while noting that both detection thresholds were also significantly decreased during the second control measurement. As such, any repeated measures designs involving nociceptive detection thresholds should account for this effect by randomization of the measurement order.

Intra-epidermal stimulation evoked a cortical response with a maximum at 390 ms, which was decreased following sleep deprivation. The latency of this evoked response was similar to the P2 potential measured in response to nociceptive stimuli in previous studies (Liang, Lee, O'Neill, Dickenson, & Iannetti, 2016; Mouraux, Marot, & Legrain, 2014; van den Berg & Buitenweg, 2021). We used the Cz-M1M2 derivation to study the influence of sleep deprivation and stimulus properties on evoked cortical activity at this latency. We found a significant decrease of the P2 amplitude in response to detected single- and double-pulse stimuli after sleep deprivation, while the waveform

remained similar during both control measurements. Regression analysis showed a significant interaction between sleep deprivation and stimulus detection suggesting that sleep deprivation mainly resulted in a reduction of task-related cortical activity.

A decrease of P2 amplitude at Cz-M1M2 has also been related to reduced stimulus intensity and reduced stimulus salience in earlier studies (Iannetti & Mouraux, 2010; Ohara, Crone, Weiss, Treede, & Lenz, 2004), which appears contradictory to the notion that sleep deprivation causes hyperalgesia (Lautenbacher, Kundermann, & Krieg, 2006). A decreased P2 amplitude might reflect a decreased attention (Legrain, Bruyer, Guérit, & Plaghki, 2003), as a result of sleep deprivation. However, decreased attention appears contradictory to our observation that sleep deprivation results in a higher nociceptive detection threshold, which suggests that participants are more sensitive to nociceptive input following sleep deprivation. This simultaneous increase of sensitivity and decrease of measured cortical activity was also found in three recent studies assessing pain sensitivity (Azevedo et al., 2011; Ødegård et al., 2015; Schuh-Hofer et al., 2013). Hypotheses for this phenomenon in these studies include loss of attention or a reduction in cortical cognitive or perceptual mechanisms. However, a recent fMRI study suggests the reduction of cortical activity following sleep deprivation is associated with a reduction of stimulus evoked activity in the insula and the anterior cingulate cortex, which are both involved in the endogenous modulation of pain (Krause, Prather, Wager, Lindquist, & Walker, 2019). Although the origin of this phenomenon is reason of debate, it shows that detection thresholds and EPs are measuring distinct aspects of nociceptive processing and are useful to combine to study effects of sleep deprivation on nociception. Further experimental and modelling studies are necessary to better explain why an increased nociceptive sensitivity and a decreased EP are both observed following sleep deprivation in this and other studies.

To the best of our knowledge, this is the first study to examine the effect of sleep deprivation on nociceptive detection thresholds and EPs in both a male and a female population. In fact, few studies have been done to identify sex differences in nociceptive processing before and after sleep deprivation

(Eichhorn, Treede, & Schuh-Hofer, 2018; Smith et al., 2019). To start with, there was a large difference in detection task performance between males and females, as a total of 16 measurements had to be removed due to unreliable detection thresholds in the male group in comparison to only 2 measurements in the female group. This difference was also observed in the detection slopes (quantifying detection (un)certainty), which were lower for male subjects on all occasions. Furthermore, this difference between both groups was larger on the control occasion than on the sleep deprived occasion. The observed difference in task performance might be attributed to a greater sensitivity to noxious stimuli in females (Fillingim & Maixner, 1995). However, other sex-related differences in sensitivity, cognitive performance and attention cannot be excluded based on the current results.

Separate analysis of the results for a male and a female population suggests that outcomes are dependent on sex. While average detection thresholds decreased for both stimulus types in both groups, this decrease was only significant in the male population when analyzed in separate groups. On the other hand, only the female population showed an increased effect of double-pulse stimuli on detection probability following sleep deprivation, potentially associated with increased temporal summation of pulses. The grand average EP amplitude was significantly decreased after sleep deprivation in the male population and regression analysis showed a significant decrease in task-related activity following sleep deprivation in the male population only. Divergent sex-dependent effects of sleep deprivation on nociceptive processing and pain have been noted previously. Smith et al. (Smith et al., 2019) observed that a significant increase of capsaicin-induced secondary hyperalgesia following sleep deprivation only occurred in males, while a significant increase of nociceptive temporal summation following sleep deprivation mostly occurred in females. Furthermore, Eichhorn et al. (Eichhorn, Treede, & Schuh-Hofer, 2018) observed that the decrease in endogenous inhibitory control associated with sleep deprivation only occurred in females. From those results as well as ours, it is clear that there are not only significant differences in nociception and pain between the sexes (Bartley & Fillingim,

2013), but also that the effect of sleep deprivation on nociceptive processing and pain might depend on sex.

5.4.1 Limitations

There are several limitations that should be addressed before adopting this method in further clinical or pharmacological studies. This was an exploratory study, as this was the first study to examine intra-epidermal electric detection thresholds and EPs following sleep deprivation, and no prior data was available to formulate hypotheses and perform a sample size calculation. Although this study included a larger group of participants than earlier studies showing significant effects of sleep deprivation on nociceptive detection thresholds (ranging from 6 (Moldofsky & Scarisbrick, 1976) to 20 (Kundermann, Spernal, Huber, Krieg, & Lautenbacher, 2004) participants) or EPs (ranging from 12 (Schuh-Hofer, Baumgärtner, & Treede, 2015) to 33 (Ødegård et al., 2015) participants), this study might still lack sufficient power to observe some of the sex-dependent effects of sleep deprivation.

Several other choices in our current study design might have impacted study results and are important to address in potential follow-up studies. In the current study, the male and female population were recruited in two time periods with an interval of 1.5 years. As such, potential confounding by the time period in which the experiments were performed (e.g., COVID-19 risk mitigation measures, seasonal effects, and potentially other unknown factors) on the sex-dependent effects observed in this study, cannot be excluded. Follow-up studies should therefore recruit and test participants in the same time period. Females were required to use their own hormonal anticonception continuously during study participation to prevent an influence of potential hormonal variations caused by the menstrual cycle on pain perception (Kowalczyk et al., 2010). Nevertheless, this might limit generalizability of our current observations to females who do not take hormonal anticonception. The effect of hormones on nociceptive processing following sleep deprivation remains undocumented, and further studies are needed to provide more insight in the potential influence of hormones on sleep and nociception. Another potential bias in outcomes might have been introduced by the time gap between occasions. As in half of the subjects the second occasion was preceded

by a resting period of at least 5 days, while in the other half the second occasion was preceded by the first (separated by one night), this could have led to a bias in outcomes due to potential familiarization effects in the second half. Future experiments might avoid such a bias by including an equal resting period between each occasion. Experiments with male and female participants were performed by a mixed population of research assistants of both sexes. As the gender of the experimenter can influence reported pain measures (Aslaksen, Myrbakk, Høifødt, & Flaten, 2007; Kállai, Barke, & Voss, 2004; Levine & Lee De Simone, 1991), this could have led to additional variance of outcomes between subjects.

5.5 Conclusion

Observation of altered nociceptive detection thresholds and EPs following sleep deprivation in male and female populations shows that it is feasible to evaluate impaired nociceptive processing following sleep deprivation in a human population based on intra-epidermal detection thresholds and EPs. Some effects were only observed in either a male or a female population, such as a decrease of the intra-epidermal electric detection threshold or a decrease of the EP and might be sex dependent. The current results suggest that intra-epidermal electric detection thresholds and EPs could be helpful in exploring the link between sleep impairment and chronic pain in future studies. Nevertheless, it remains important to note that, like any method relying on participant report (e.g., questionnaires, quantitative sensory testing), nociceptive detection thresholds and EPs might be influenced by attention and learning processes. Developing nociception biomarkers that are unbiased by psychological states remains a current challenge for pain science. The possibilities of combining the sleep deprivation model with more objective measures of nociception and pain are exciting, as they allow to translate results from earlier pharmacological animal studies using sleep deprivation, e.g. (Gürel, Ural, Öztürk, & Öztürk, 2014; Skinner, Damasceno, Gomes, & De Almeida, 2011; Wodarski et al., 2015), to humans with potential applications in the identification of analgesic and sedative compounds.

5.6 Appendix

5.6.1 Appendix I

Covariance matrices of (generalized) linear mixed models.

	(Intercept)	Amplitude	Sleep dep.	Type 2	Trial number	Measurement 2	Occasion 2	Amplitude x Sleep dep.	Amplitude x Type 2	Type 2 x Sleep dep.	Trial number x Sleep dep.	Amplitude x Type 2 x Sleep dep.
(Intercept)	0.071	-0.043	-0.084	-0.015	0.000	-0.041	-0.021	0.143	0.078	0.037	-0.010	-0.125
Amplitude	-0.043	0.251	0.057	0.016	-0.012	0.018	-0.028	-0.210	0.148	-0.046	0.012	0.029
Sleep dep.	-0.084	0.057	0.179	0.015	-0.002	0.066	0.006	-0.389	-0.082	-0.050	0.016	-0.009
Type 2	-0.015	0.016	0.015	0.025	0.001	0.007	0.002	-0.023	-0.100	-0.038	0.002	0.080
Trial number	0.000	-0.012	-0.002	0.001	0.003	0.001	0.004	0.005	-0.022	0.004	-0.001	-0.005
Measurement 2	-0.041	0.018	0.066	0.007	0.001	0.070	-0.009	-0.076	-0.035	-0.008	0.004	0.013
Occasion 2	-0.021	-0.028	0.006	0.002	0.004	-0.009	0.041	0.016	-0.063	-0.011	-0.001	0.134
Amplitude x Sleep dep.	0.143	-0.210	-0.389	-0.023	0.005	-0.076	0.016	1.398	0.098	0.107	-0.038	0.694
Amplitude x Type 2	0.078	0.148	-0.082	-0.100	-0.022	-0.035	-0.063	0.098	0.847	0.141	-0.011	-0.402
Type 2 x Sleep dep.	0.037	-0.046	-0.050	-0.038	0.004	-0.008	-0.011	0.107	0.141	0.164	0.000	-0.419
Trial number x Sleep dep.	-0.010	0.012	0.016	0.002	-0.001	0.004	-0.001	-0.038	-0.011	0.000	0.006	-0.009
Amplitude x Type 2 x Sleep dep.	-0.125	0.029	-0.009	0.080	-0.005	0.013	0.134	0.694	-0.402	-0.419	-0.009	2.711

***Table 5.5**: Random effects covariance matrix of the generalized linear mixed model fit (Table 5.1) for the combination of the male and the female group.*

	(Intercept)	Amplitude	Sleep dep.	Type 2	Trial number	Measurement 2	Occasion 2	Amplitude x Sleep dep.	Amplitude x Type 2	Type 2 x Sleep dep.	Trial number x Sleep dep.	Amplitude x Type 2 x Sleep dep.
(Intercept)	0.171	-0.178	-0.213	-0.042	0.011	-0.124	-0.004	0.340	0.107	0.102	-0.029	-0.221
Amplitude	-0.178	0.577	0.222	0.069	-0.022	0.060	-0.027	-0.684	0.077	-0.191	0.031	0.216
Sleep dep.	-0.213	0.222	0.364	0.057	-0.018	0.148	-0.026	-0.748	-0.179	-0.155	0.046	0.133
Type 2	-0.042	0.069	0.057	0.052	-0.001	0.023	-0.005	-0.126	-0.225	-0.099	0.009	0.142
Trial number	0.011	-0.022	-0.018	-0.001	0.004	-0.001	0.001	0.041	-0.012	0.018	-0.003	-0.028
Measurement 2	-0.124	0.060	0.148	0.023	-0.001	0.139	-0.009	-0.134	-0.094	-0.011	0.016	0.044
Occasion 2	-0.004	-0.027	-0.026	-0.005	0.001	-0.009	0.047	0.054	0.006	-0.004	0.003	0.097
Amplitude x Sleep dep.	0.340	-0.684	-0.748	-0.126	0.041	-0.134	0.054	3.326	0.189	0.520	-0.093	0.566
Amplitude x Type 2	0.107	0.077	-0.179	-0.225	-0.012	-0.094	0.006	0.189	1.601	0.407	-0.037	-0.826
Type 2 x Sleep dep.	0.102	-0.191	-0.155	-0.099	0.018	-0.011	-0.004	0.520	0.407	0.509	-0.020	-1.296
Trial number x Sleep dep.	-0.029	0.031	0.046	0.009	-0.003	0.016	0.003	-0.093	-0.037	-0.020	0.012	0.026
Amplitude x Type 2 x Sleep dep.	-0.221	0.216	0.133	0.142	-0.028	0.044	0.097	0.566	-0.826	-1.296	0.026	6.909

***Table 5.6**: Random effects covariance matrix of the generalized linear mixed model fit (Table 5.1) for the female group.*

	(Intercept)	Amplitude	Sleep dep.	Type 2	Trial number	Measurement 2	Occasion 2	Amplitude x Sleep dep.	Amplitude x Type 2	Type 2 x Sleep dep.	Trial number x Sleep dep.	Amplitude x Type 2 x Sleep dep.
(Intercept)	0.127	-0.034	-0.073	-0.027	-0.008	0.014	-0.086	0.045	0.235	0.018	0.004	-0.156
Amplitude	-0.034	0.232	0.092	-0.020	-0.016	0.002	-0.080	-0.082	0.325	0.032	0.028	-0.063
Sleep dep.	-0.073	0.092	0.440	-0.006	0.001	0.104	-0.118	-0.556	0.095	-0.066	-0.004	-0.139
Type 2	-0.027	-0.020	-0.006	0.061	0.003	0.009	0.035	0.108	-0.184	-0.080	-0.012	0.298
Trial number	-0.008	-0.016	0.001	0.003	0.007	0.000	0.013	0.003	-0.060	0.000	-0.004	0.020
Measurement 2	0.014	0.002	0.104	0.009	0.000	0.115	-0.053	-0.150	0.058	-0.049	-0.006	-0.043
Occasion 2	-0.086	-0.080	-0.118	0.035	0.013	-0.053	0.235	0.137	-0.330	-0.034	-0.022	0.280
Amplitude x Sleep dep.	0.045	-0.082	-0.556	0.108	0.003	-0.150	0.137	1.591	-0.204	-0.067	-0.040	1.186
Amplitude x Type 2	0.235	0.325	0.095	-0.184	-0.060	0.058	-0.330	-0.204	1.592	0.153	0.049	-1.003
Type 2 x Sleep dep.	0.018	0.032	-0.066	-0.080	0.000	-0.049	-0.034	-0.067	0.153	0.210	0.027	-0.617
Trial number x Sleep dep.	0.004	0.028	-0.004	-0.012	-0.004	-0.006	-0.022	-0.040	0.049	0.027	0.018	-0.083
Amplitude x Type 2 x Sleep dep.	-0.156	-0.063	-0.139	0.298	0.020	-0.043	0.280	1.186	-1.003	-0.617	-0.083	3.571

***Table 5.7**: Random effects covariance matrix of the generalized linear mixed model fit (Table 5.1) for the male group.*

	(Intercept)	Amplitude	Amplitude x Sleep dep.	Amplitude x Type 2	Amplitude x Type 2 x Sleep dep.	Measurement 2	Occasion 2	Detected	Detected x Sleep dep.	Detected x Sleep dep. x Trial number	Detected x Trial number	Sleep dep.	Sleep dep. x Trial number	Trial number	Type 2	Type 2 x Sleep dep.
(Intercept)	5.608	-0.171	0.841	0.319	-0.422	-0.455	-0.330	0.060	-0.046	-0.561	0.805	-0.843	0.575	-0.790	-0.436	0.644
Amplitude	-0.171	3.109	-0.203	0.659	-0.663	-0.230	0.459	0.539	-0.321	0.669	-0.300	0.014	-0.674	0.251	-0.090	0.178
Amplitude x Sleep dep.	0.841	-0.203	8.642	0.357	-0.376	-0.338	-0.166	-0.076	0.136	-0.305	0.606	-0.941	0.429	-0.529	-0.454	0.788
Amplitude x Type 2	0.319	0.659	0.357	7.024	-0.856	-0.341	0.619	0.317	-0.035	0.551	-0.083	-0.414	-0.363	-0.047	-0.370	0.397
Amplitude x Type 2 x Sleep dep.	-0.422	-0.663	-0.376	-0.856	11.252	0.621	-0.451	-0.511	0.171	-0.268	-0.174	0.557	0.187	0.115	0.451	-0.570
Measurement 2	-0.455	-0.230	-0.338	-0.341	0.621	4.821	-0.260	-0.141	0.179	0.192	-0.348	0.603	0.090	0.068	0.228	-0.524
Occasion 2	-0.330	0.459	-0.166	0.619	-0.451	-0.260	2.736	0.114	0.266	0.708	-0.592	0.108	-0.761	0.507	0.206	-0.179
Detected	0.060	0.539	-0.076	0.317	-0.511	-0.141	0.114	8.231	-0.440	0.033	-0.160	-0.027	-0.172	0.087	0.110	0.030
Detected x Sleep dep.	-0.046	-0.321	0.136	-0.035	0.171	0.179	0.266	-0.440	5.490	0.050	0.067	-0.011	-0.041	-0.244	0.387	-0.213
Detected x Sleep dep. x Trial number	-0.561	0.669	-0.305	0.551	-0.268	0.192	0.708	0.033	0.050	5.077	-0.717	0.294	-0.781	0.602	-0.018	-0.096
Detected x Trial number	0.805	-0.300	0.606	-0.083	-0.174	-0.348	-0.592	-0.160	0.067	-0.717	3.011	-0.652	0.708	-0.864	-0.383	0.541
Sleep dep.	-0.843	0.014	-0.941	-0.414	0.557	0.603	0.108	-0.027	-0.011	0.294	-0.652	9.577	-0.331	0.474	0.506	-0.896
Sleep dep. x Trial number	0.575	-0.674	0.429	-0.363	0.187	0.090	-0.761	-0.172	-0.041	-0.781	0.708	-0.331	2.563	-0.618	-0.452	0.277
Trial number	-0.790	0.251	-0.529	-0.047	0.115	0.068	0.507	0.087	-0.244	0.602	-0.864	0.474	-0.618	1.491	0.163	-0.268
Type 2	-0.436	-0.090	-0.454	-0.370	0.451	0.228	0.206	0.110	0.387	-0.018	-0.383	0.506	-0.452	0.163	1.665	-0.727
Type 2 x Sleep dep.	0.644	0.178	0.788	0.397	-0.570	-0.524	-0.179	0.030	-0.213	-0.096	0.541	-0.896	0.277	-0.268	-0.727	5.818

***Table 5.8**: Random effects covariance matrix of the linear mixed model fit (Table 5.3) for the combination of the male and the female group.*

	(Intercept)	Amplitude	Amplitude x Sleep dep.	Amplitude x Type 2	Amplitude x Type 2 x Sleep dep.	Measurement 2	Occasion 2	Detected	Detected x Sleep dep.	Detected x Sleep dep. x Trial number	Detected x Trial number	Sleep dep.	Sleep dep. x Trial number	Trial number	Type 2	Type 2 x Sleep dep.
(Intercept)	2.025	-0.670	0.765	0.099	-0.089	-0.313	0.335	0.527	-0.095	-0.274	0.342	-0.522	0.106	-0.504	-0.344	0.462
Amplitude	-0.670	2.593	-0.665	0.148	0.374	-0.303	-0.139	-0.794	0.032	-0.022	0.039	0.279	0.191	0.146	-0.025	-0.354
Amplitude x Sleep dep.	0.765	-0.665	9.205	0.251	-0.400	-0.402	0.590	0.741	-0.069	0.217	-0.133	-0.832	-0.433	0.038	-0.293	0.604
Amplitude x Type 2	0.099	0.148	0.251	10.780	-0.559	-0.621	0.675	0.139	0.254	0.330	-0.329	-0.282	-0.312	0.218	-0.630	0.132
Amplitude x Type 2 x Sleep dep.	-0.089	0.374	-0.400	-0.559	19.056	0.111	-0.568	-0.605	0.236	-0.636	0.584	0.364	0.434	-0.605	0.574	-0.584
Measurement 2	-0.313	-0.303	-0.402	-0.621	0.111	3.995	-0.719	0.008	0.041	-0.091	-0.110	0.656	0.149	0.028	0.499	-0.241
Occasion 2	0.335	-0.139	0.590	0.675	-0.568	-0.719	3.519	0.260	0.170	0.565	-0.136	-0.793	-0.573	0.166	-0.512	0.405
Detected	0.527	-0.794	0.741	0.139	-0.605	0.008	0.260	6.927	-0.246	0.200	-0.443	-0.384	-0.365	0.288	-0.094	0.435
Detected x Sleep dep.	-0.095	0.032	-0.069	0.254	0.236	0.041	0.170	-0.246	5.857	0.158	-0.052	0.145	-0.444	-0.244	0.374	-0.620
Detected x Sleep dep. x Trial number	-0.274	-0.022	0.217	0.330	-0.636	-0.091	0.565	0.200	0.158	5.526	-0.729	-0.413	-0.844	0.770	-0.163	0.328
Detected x Trial number	0.342	0.039	-0.133	-0.329	0.584	-0.110	-0.136	-0.443	-0.052	-0.729	2.993	0.035	0.691	-0.890	-0.005	-0.130
Sleep dep.	-0.522	0.279	-0.832	-0.282	0.364	0.656	-0.793	-0.384	0.145	-0.413	0.035	5.838	0.471	-0.148	0.415	-0.671
Sleep dep. x Trial number	0.106	0.191	-0.433	-0.312	0.434	0.149	-0.573	-0.365	-0.444	-0.844	0.691	0.471	2.928	-0.587	-0.158	-0.063
Trial number	-0.504	0.146	0.038	0.218	-0.605	0.028	0.166	0.288	-0.244	0.770	-0.890	-0.148	-0.587	1.642	-0.098	0.296
Type 2	-0.344	-0.025	-0.293	-0.630	0.574	0.499	-0.512	-0.094	0.374	-0.163	-0.005	0.415	-0.158	-0.098	2.733	-0.720
Type 2 x Sleep dep.	0.462	-0.354	0.604	0.132	-0.584	-0.241	0.405	0.435	-0.620	0.328	-0.130	-0.671	-0.063	0.296	-0.720	5.888

***Table 5.9**: Random effects covariance matrix of the linear mixed model fit (Table 5.3) for the female group.*

	(Intercept)	Amplitude	Amplitude x Sleep dep.	Amplitude x Type 2	Amplitude x Type 2 x Sleep dep.	Measurement 2	Occasion 2	Detected	Detected x Sleep dep.	Detected x Sleep dep. x Trial number	Detected x Trial number	Sleep dep.	Sleep dep. x Trial number	Trial number	Type 2	Type 2 x Sleep dep.
(Intercept)	8.639	-0.442	0.936	0.256	0.392	-0.476	-0.303	-0.250	0.512	-0.531	0.787	-0.939	0.528	-0.832	-0.251	0.442
Amplitude	-0.442	6.528	-0.608	0.433	-0.548	-0.184	-0.029	0.732	-0.592	0.337	-0.116	0.381	-0.295	0.035	0.775	-0.140
Amplitude x Sleep dep.	0.936	-0.608	12.474	0.199	0.528	-0.369	-0.130	-0.384	0.649	-0.381	0.586	-0.935	0.489	-0.605	-0.327	0.492
Amplitude x Type 2	0.256	0.433	0.199	3.420	0.162	-0.329	0.454	0.219	-0.217	0.434	-0.020	-0.223	-0.434	-0.219	0.746	-0.146
Amplitude x Type 2 x Sleep dep.	0.392	-0.548	0.528	0.162	6.468	0.515	0.198	-0.277	0.274	0.159	-0.128	-0.231	0.227	-0.083	-0.115	-0.231
Measurement 2	-0.476	-0.184	-0.369	-0.329	0.515	5.186	0.082	-0.132	-0.038	0.431	-0.584	0.615	-0.015	0.463	-0.162	-0.490
Occasion 2	-0.303	-0.029	-0.130	0.454	0.198	0.082	2.800	-0.076	-0.363	0.559	-0.739	0.298	-0.828	0.645	0.450	-0.540
Detected	-0.250	0.732	-0.384	0.219	-0.277	-0.132	-0.076	9.650	-0.651	-0.089	-0.030	0.204	0.052	-0.028	0.742	-0.278
Detected x Sleep dep.	0.512	-0.592	0.649	-0.217	0.274	-0.038	-0.363	-0.651	4.750	-0.104	0.412	-0.617	0.508	-0.309	-0.693	0.772
Detected x Sleep dep. x Trial number	-0.531	0.337	-0.381	0.434	0.159	0.431	0.559	-0.089	-0.104	4.784	-0.736	0.495	-0.610	0.580	0.409	-0.235
Detected x Trial number	0.787	-0.116	0.586	-0.020	-0.128	-0.584	-0.739	-0.030	0.412	-0.736	3.131	-0.767	0.671	-0.939	-0.313	0.595
Sleep dep.	-0.939	0.381	-0.935	-0.223	-0.231	0.615	0.298	0.204	-0.617	0.495	-0.767	11.826	-0.543	0.734	0.240	-0.662
Sleep dep. x Trial number	0.528	-0.295	0.489	-0.434	0.227	-0.015	-0.828	0.052	0.508	-0.610	0.671	-0.543	2.925	-0.600	-0.480	0.543
Trial number	-0.832	0.035	-0.605	-0.219	-0.083	0.463	0.645	-0.028	-0.309	0.580	-0.939	0.734	-0.600	1.401	0.127	-0.412
Type 2	-0.251	0.775	-0.327	0.746	-0.115	-0.162	0.450	0.742	-0.693	0.409	-0.313	0.240	-0.480	0.127	1.969	-0.440
Type 2 x Sleep dep.	0.442	-0.140	0.492	-0.146	-0.231	-0.490	-0.540	-0.278	0.772	-0.235	0.595	-0.662	0.543	-0.412	-0.440	4.816

***Table 5.10**: Random effects covariance matrix of the linear mixed model fit (Table 5.3) for the male group.*

5.7 References

Aslaksen, P. M., Myrbakk, I. N., Høifødt, R. S., & Flaten, M. A. (2007). The effect of experimenter gender on autonomic and subjective responses to pain stimuli. *Pain, 129*(3), 260-268.

Azevedo, E., Manzano, G. M., Silva, A., Martins, R., Andersen, M. L., & Tufik, S. (2011). The effects of total and REM sleep deprivation on laser-evoked potential threshold and pain perception. *Pain, 152*(9), 2052-2058.

Barr, D. J., Levy, R., Scheepers, C., & Tily, H. J. (2013). Random effects structure for confirmatory hypothesis testing: Keep it maximal. *Journal of memory and language, 68*(3).

Bartley, E. J., & Fillingim, R. B. (2013). Sex differences in pain: a brief review of clinical and experimental findings. *British Journal of Anaesthesia, 111*(1), 52-58.

Bates, D., Mächler, M., Bolker, B., & Walker, S. (2015). Fitting Linear Mixed-Effects Models Using lme4. *Journal of Statistical Software; Vol 1, Issue 1 (2015)*.

Bostock, H., Lin, C. S.-Y., Howells, J., Trevillion, L., Jankelowitz, S., & Burke, D. (2005). After-effects of near-threshold stimulation in single human motor axons. *The Journal of physiology, 564*(Pt 3), 931-940.

Delorme, A., Sejnowski, T., & Makeig, S. (2007). Enhanced detection of artifacts in EEG data using higher-order statistics and independent component analysis. *NeuroImage, 34*(4), 1443-1449.

Doll, R. J., Maten, A. C. A., Spaan, S. P. G., Veltink, P. H., & Buitenweg, J. R. (2016). Effect of temporal stimulus properties on the nociceptive detection probability using intra-epidermal electrical stimulation. *Experimental Brain Research, 234*(1), 219-227.

Doll, R. J., van Amerongen, G., Hay, J. L., Groeneveld, G. J., Veltink, P. H., & Buitenweg, J. R. (2016). Responsiveness of electrical nociceptive detection thresholds to capsaicin (8 %)-induced changes in nociceptive processing. *Experimental Brain Research, 234*(9), 2505-2514.

Doll, R. J., Veltink, P. H., & Buitenweg, J. R. (2015). Observation of time-dependent psychophysical functions and accounting for threshold drifts. *Attention, Perception, and Psychophysics, 77*(4), 1440-1447.

Drewes, A. M., Rössel, P., Arendt-Nielsen, L., Nielsen, K. D., Hansen, L. M., Birket-Smith, L., & Stengaard-Pedersen, K. (1997). Sleepiness does not Modulate Experimental Joint Pain in Healthy Volunteers. *Scandinavian Journal of Rheumatology, 26*(5), 399-400.

Edwards, R. R. (2005). Individual differences in endogenous pain modulation as a risk factor for chronic pain. *Neurology, 65*(3), 437.

Eichhorn, N., Treede, R.-D., & Schuh-Hofer, S. (2018). The Role of Sex in Sleep Deprivation Related Changes of Nociception and Conditioned Pain Modulation. *Neuroscience, 387*, 191-200.

Fillingim, R. B., & Maixner, W. (1995). Gender differences in the responses to noxious stimuli. *Pain Forum, 4*(4), 209-221.

Gelman, A., & Hill, J. (2006). *Data Analysis Using Regression and Multilevel/Hierarchical Models*. Cambridge: Cambridge University Press.

Gold, J. I., & Ding, L. (2013). How mechanisms of perceptual decision-making affect the psychometric function. *Progress in Neurobiology, 103*, 98-114.

Gottrup, H., Nielsen, J., Arendt-Nielsen, L., & Jensen, T. S. (1998). The relationship between sensory thresholds and mechanical hyperalgesia in nerve injury. *Pain, 75*(2-3), 321-329.

Herrero Babiloni, A., De Koninck, B. P., Beetz, G., De Beaumont, L., Martel, M. O., & Lavigne, G. J. (2020). Sleep and pain: recent insights, mechanisms, and future directions in the investigation of this relationship. *Journal of Neural Transmission, 127*(4), 647-660.

Iannetti, G. D., & Mouraux, A. (2010). From the neuromatrix to the pain matrix (and back). *Experimental Brain Research, 205*(1), 1-12.

Kállai, I., Barke, A., & Voss, U. (2004). The effects of experimenter characteristics on pain reports in women and men. *Pain, 112*(1-2), 142-147.

Krause, A. J., Prather, A. A., Wager, T. D., Lindquist, M. A., & Walker, M. P. (2019). The Pain of Sleep Loss: A Brain Characterization in Humans. *The Journal of Neuroscience, 39*(12), 2291.

Kundermann, B., Spernal, J., Huber, M. T., Krieg, J.-C., & Lautenbacher, S. (2004). Sleep Deprivation Affects Thermal Pain Thresholds but Not Somatosensory Thresholds in Healthy Volunteers. *Psychosomatic Medicine, 66*(6).

Lautenbacher, S., Kundermann, B., & Krieg, J.-C. (2006). Sleep deprivation and pain perception. *Sleep Medicine Reviews, 10*(5), 357-369.

Lee, M. C., Zambreanu, L., Menon, D. K., & Tracey, I. (2008). Identifying Brain Activity Specifically Related to the Maintenance and Perceptual Consequence of Central Sensitization in Humans. *The Journal of Neuroscience, 28*(45), 11642.

Legrain, V., Bruyer, R., Guérit, J. M., & Plaghki, L. (2003). Nociceptive processing in the human brain of infrequent task-relevant and task-irrelevant noxious stimuli. A study with event-related potentials evoked by CO_2 laser radiant heat stimuli. *Pain, 103*(3), 237-248.

Legrain, V., Guérit, J. M., Bruyer, R., & Plaghki, L. (2002). Attentional modulation of the nociceptive processing into the human brain:

Selective spatial attention, probability of stimulus occurrence, and target detection effects on laser evoked potentials. *Pain, 99*(1-2), 21-39.

Levine, F. M., & Lee De Simone, L. (1991). The effects of experimenter gender on pain report in male and female subjects. *Pain, 44*(1), 69-72.

Liang, M., Lee, M. C., O'Neill, J., Dickenson, A. H., & Iannetti, G. D. (2016). Brain potentials evoked by intraepidermal electrical stimuli reflect the central sensitization of nociceptive pathways. *Journal of Neurophysiology, 116*(2), 286-295.

Matre, D., Andersen, M. R., Knardahl, S., & Nilsen, K. B. (2016). Conditioned pain modulation is not decreased after partial sleep restriction. *Eur J Pain, 20*(3), 408-416.

Moldofsky, H., & Scarisbrick, P. (1976). Induction of Neurasthenic Musculoskeletal Pain Syndrome by Selective Sleep Stage Deprivation. *Psychosomatic Medicine, 38*(1).

Moldofsky, H., Scarisbrick, P., England, R., & Smythe, H. (1975). Musculosketal Symptoms and Non-REM Sleep Disturbance in Patients with "Fibrositis Syndrome" and Healthy Subjects. *Psychosomatic Medicine, 37*(4).

Moscatelli, A., Mezzetti, M., & Lacquaniti, F. (2012). Modeling psychophysical data at the population-level: The generalized linear mixed model. *Journal of Vision, 12*(11), 26-26.

Motogi, J., Sugiyama, Y., Laakso, I., Hirata, A., Inui, K., Tamura, M., & Muragaki, Y. (2016). Why intra-epidermal electrical stimulation achieves stimulation of small fibres selectively: a simulation study. *Phys Med Biol, 61*(12), 4479-4490.

Mouraux, A., & Iannetti, G. D. (2018). The search for pain biomarkers in the human brain. *Brain, 141*(12), 3290-3307.

Mouraux, A., Iannetti, G. D., & Plaghki, L. (2010). Low intensity intra-epidermal electrical stimulation can activate Aδ-nociceptors selectively. *Pain, 150(1)*, 199-207.

Mouraux, A., Marot, E., & Legrain, V. (2014). Short trains of intra-epidermal electrical stimulation to elicit reliable behavioral and electrophysiological responses to the selective activation of nociceptors in humans. *Neuroscience Letters, 561*(Supplement C), 69-73.

Ødegård, S. S., Omland, P. M., Nilsen, K. B., Stjern, M., Gravdahl, G. B., & Sand, T. (2015). The effect of sleep restriction on laser evoked potentials, thermal sensory and pain thresholds and suprathreshold pain in healthy subjects. *Clinical Neurophysiology, 126*(10), 1979-1987.

Ohara, S., Crone, N. E., Weiss, N., Treede, R. D., & Lenz, F. A. (2004). Amplitudes of laser evoked potential recorded from primary

somatosensory, parasylvian and medial frontal cortex are graded with stimulus intensity. *Pain, 110*(1-2), 318-328.

Older, S. A., Battafarano, D. F., Danning, C. L., Ward, J. A., Grady, E. P., Derman, S., & Russell, I. J. (1998). The effects of delta wave sleep interruption on pain thresholds and fibromyalgia-like symptoms in healthy subjects; correlations with insulin-like growth factor I. *J Rheumatol, 25*(6), 1180-1186.

Onen, S. H., Alloui, A., Gross, A., Eschallier, A., & Dubray, C. (2001). The effects of total sleep deprivation, selective sleep interruption and sleep recovery on pain tolerance thresholds in healthy subjects. *Journal of Sleep Research, 10*(1), 35-42.

Oostenveld, R., Fries, P., Maris, E., & Schoffelen, J. M. (2011). FieldTrip: Open source software for advanced analysis of MEG, EEG, and invasive electrophysiological data. *Computational Intelligence and Neuroscience, 2011*.

Poulsen, A. H., Tigerholm, J., Meijs, S., Andersen, O. K., & Mørch, C. D. (2020). Comparison of existing electrode designs for preferential activation of cutaneous nociceptors. *Journal of Neural Engineering*.

Price, D. D., Hu, J. W., Dubner, R., & Gracely, R. H. (1977). Peripheral suppression of first pain and central summation of second pain evoked by noxious heat pulses. *Pain, 3*(1), 57-68.

Schuh-Hofer, S., Baumgärtner, U., & Treede, R. D. (2015). Effect of sleep deprivation on the electrophysiological signature of habituation to noxious laser stimuli. *European Journal of Pain, 19*(8), 1197-1209.

Schuh-Hofer, S., Wodarski, R., Pfau, D. B., Caspani, O., Magerl, W., Kennedy, J. D., & Treede, R. D. (2013). One night of total sleep deprivation promotes a state of generalized hyperalgesia: A surrogate pain model to study the relationship of insomnia and pain. *Pain, 154*(9), 1613-1621.

Smith, M. T., Jr., Remeniuk, B., Finan, P. H., Speed, T. J., Tompkins, D. A., Robinson, M., . . . Irwin, M. R. (2019). Sex differences in measures of central sensitization and pain sensitivity to experimental sleep disruption: implications for sex differences in chronic pain. *Sleep, 42*(2).

Staffe, A. T., Bech, M. W., Clemmensen, S. L. K., Nielsen, H. T., Larsen, D. B., & Petersen, K. K. (2019). Total sleep deprivation increases pain sensitivity, impairs conditioned pain modulation and facilitates temporal summation of pain in healthy participants. *PLoS ONE, 14*(12), e0225849.

Steenbergen, P., Buitenweg, J. R., Trojan, J., van der Heide, E. M., van den Heuvel, T., Flor, H., & Veltink, P. H. (2012). A system for inducing concurrent tactile and nociceptive sensations at the same site using

electrocutaneous stimulation. *Behavior research methods, 44(4)*, 924-933.

Treede, R. D., Meyer, R. A., Raja, S. N., & Campbell, J. N. (1992). Peripheral and central mechanisms of cutaneous hyperalgesia. *Progress in Neurobiology, 38*(4), 397-421.

van den Berg, B., & Buitenweg, J. R. (2021). Observation of Nociceptive Processing: Effect of Intra-Epidermal Electric Stimulus Properties on Detection Probability and Evoked Potentials. *Brain Topography*.

van den Berg, B., Doll, R. J., Mentink, A. L. H., Siebenga, P. S., Groeneveld, G. J., & Buitenweg, J. R. (2020). Simultaneous tracking of psychophysical detection thresholds and evoked potentials to study nociceptive processing. *Behavior Research Methods*.

van den Broeke, E. N., Mouraux, A., Groneberg, A. H., Pfau, D. B., Treede, R.-D., & Klein, T. (2015). Characterizing pinprick-evoked brain potentials before and after experimentally induced secondary hyperalgesia. *Journal of Neurophysiology, 114*(5), 2672-2681.

van der Heide, E. M., Buitenweg, J. R., Marani, E., & Rutten, W. L. (2009). Single pulse and pulse train modulation of cutaneous electrical stimulation: a comparison of methods. *J Clin Neurophysiol, 26*(1), 54-60.

van der Heide, E. M., Buitenweg, J. R., Marani, E., & Rutten, W. L. (2009). Single pulse and pulse train modulation of cutaneous electrical stimulation: a comparison of methods. (26(1)), 54-60.

Venables, W. N., & Ripley, B. D. (2002). *Modern Applied Statistics with S* (4 ed.): Springer-Verlag New York.

Wager, T. D., Matre, D., & Casey, K. L. (2006). Placebo effects in laser-evoked pain potentials. *Brain, Behavior, and Immunity, 20*(3), 219-230.

Woolf, C. J. (2011). Central sensitization: implications for the diagnosis and treatment of pain. *Pain, 152*(3 Suppl), S2-S15.

Zambreanu, L., Wise, R. G., Brooks, J. C. W., Iannetti, G. D., & Tracey, I. (2005). A role for the brainstem in central sensitisation in humans. Evidence from functional magnetic resonance imaging. *Pain, 114*(3), 397-407.

Zucker, R. S., & Regehr, W. G. (2002). Short-term synaptic plasticity. *Annual Review of Physiology, 64*, 355-405.

Chapter 6

Observing Nociceptive Detection Thresholds and Brain Evoked Potentials in Failed Back Surgery Syndrome Patients

Submitted as:

Berfelo, T.*, **Van den Berg, B.***, Krabbenbos, I.P., Buitenweg, J.R., Observing nociceptive detection thresholds and brain evoked potentials in persistent spinal pain syndrome type 2 patients.** **authors contributed equally **"Persistent spinal pain syndrome type 2" was recently introduced as a new terminology for "failed back surgery syndrome". In this chapter, we use "failed back surgery syndrome" for consistency within this dissertation.*

Abstract

The search for objective measures providing insight into key neural mechanisms underlying chronic pain, such as central sensitization, continues. Recently, we combined nociceptive detection thresholds (NDTs) with evoked potentials (EPs) to study neurophysiological activity related to the processing of electronociceptive stimuli. Results from healthy subjects measured at the University of Twente suggest that this combination (referred to as the NDT-EP method) can be used to observe nociceptive system behavior. The potential of intra-epidermal electrical stimulation to study nociceptive processing in chronic pain patients remains unexplored. The first step is an exploration of its feasibility in a clinical environment and its sensitivity to detect altered nociceptive processing in failed back surgery syndrome (FBSS) patients.

We explored the feasibility of observing nociceptive system behavior in seventeen healthy subjects (Central Sensitization Inventory (CSI)-score 14.6 ± 8.8) at the St. Antonius Hospital. Subsequently, we analyzed effects of the same intra-epidermal stimulus properties on NDTs and EPs in sixteen FBSS patients (CSI-score 44.6 ± 13.9).

Results demonstrated that it is possible to measure and evaluate intra-epidermal electric NDTs and EPs in FBSS patients at the hospital. We found that FBSS was associated with increased NDTs. Furthermore, we found that FBSS was associated with a reduced effect of pulse intensity on the EP.

Observation of nociceptive system behavior in a clinical environment indicates that outcome measures are observer and location independent. Altered NDTs and EP responses to stimulation suggest altered central nociceptive function in FBSS patients observed by the NDT-EP method but needs to be further explored in future studies.

6.1 Introduction

One out of five adults suffers from moderate-to-severe non-cancer chronic pain in Europe (Reid et al., 2011). Besides the fact that chronic pain has a major impact on patient-perceived health statuses, it also entails a significant economic burden on society and the healthcare system. Diagnosing and treating pain disorders is challenging since the underlying mechanisms responsible for persistence of chronic pain often cannot be identified clinically. There is increasing evidence that chronic pain is associated with altered processing of signals in the central and peripheral nervous system (Harte et al., 2018). Features of central sensitization, partly caused by ongoing nociceptive input, is present in nearly all chronic pain conditions, including failed back surgery syndrome (FBSS) patients (Groen, Beese, Van de Kelft, & Groen, 2016; Van Buyten, 2016).

In pain research, quantitative sensory testing (QST) methods are accepted and widely used non-invasive measures to identify central sensitization features and to characterize pain and sensory mechanisms (Arendt-Nielsen, 2015; Arendt-Nielsen & Yarnitsky, 2009; Backonja et al., 2013; Cruz-Almeida & Fillingim, 2014; Edwards, 2005; Harte, Harris, & Clauw, 2018; Pavlaković & Petzke, 2010; Pfau, Geber, Birklein, & Treede, 2012; Vuilleumier et al., 2015; Wylde et al., 2017). However, these measures for nociceptive processing are dependent on varying subjective criteria such as the pain threshold. Additionally, they are limited in their ability to assess neuroplastic changes (Arendt-Nielsen et al., 2018). Nowadays, we still cannot objectively observe key (patient-specific) characteristic malfunctions of the nociceptive system. Therefore, the search for objective measures providing insight into key neural mechanisms underlying chronic pain, such as central sensitization, continues.

Recently, we combined nociceptive detection thresholds (NDTs) with brain evoked potentials (EPs) to observe psychophysical and neurophysiological responses related to the processing of single- and double-pulse electronociceptive stimuli (van den Berg & Buitenweg, 2021; van den Berg et al., 2020). During the combined acquisition of NDTs and EPs, which we will refer to as the NDT-EP method, intra-epidermal nociceptive Aδ fibers are activated

using intra-epidermal electrical stimulation (IES) around the detection threshold. The detection probability and thresholds of each stimulus type are tracked using the subject's response (detected or non-detected) to each stimulus. Simultaneously, the stimulus-related neurophysiological response is captured using electroencephalography (EEG). In this way, we aim to develop a tool for quantification of the nociceptive function in pain patients towards identification of maladaptive underlying mechanisms. Experimental NDT-EP results from healthy subjects measured at the Technical Medical Center (TechMed Center) of the University of Twente have quantified the effect of stimulus detection, pulse amplitudes, and the number of trials on the EP (van den Berg & Buitenweg, 2021). Identification of such nociceptive system properties (i.e., peripheral fiber recruitment, central synaptic summation, and habituation) might enable mechanism-based monitoring of chronic pain disorders. However, it is still unknown whether it is feasible to successfully use IES detection thresholds and EPs in a clinical environment as a support for diagnostics. Additionally, the NDT-EP method has never been applied to chronic pain disorders, such as FBSS patients.

In this study, we investigated the feasibility of using the NDT-EP method in FBSS patients and secondary explored its sensitivity to altered nociceptive processing. The effect size of IES properties on NDTs and EPs is analyzed at a group level, of which significant parameters are subsequently analyzed for their sensitivity on an individual level to diagnosis, subject characteristics, and clinical features.

6.2 Methods

The study was a mono-center explorative cross-sectional study that was approved by the Medical Research Ethics Committees United (MEC-U, file number: NL66136.100.18), which was carried out in the Pain Clinics department at St. Antonius Hospital Nieuwegein, The Netherlands. Each participant underwent one session of the NDT-EP method, which was performed using the same procedure as earlier experiments at the TechMed Center of the University of Twente (METC Twente, file number: NL62721.044.17) (van den Berg &

Buitenweg, 2021). The session consisted of two measurements, one on each hand. Verbal and written informed consent were obtained before inclusion.

6.2.1 Subjects

Twenty healthy subjects and twenty FBSS patients were enrolled in the study. None of the healthy subjects (age above 18 years) took analgesic medication. The healthy subjects had no medical history of pathological (chronic) pain and no pain complaints at the time of the experiment.

The FBSS patients suffered from persistent radicular (radiating) leg pain. In the medical history, they were treated by medication, nerve blocks, and (at least once by) surgical intervention (i.e., laminectomy or spondylodesis) on the lumbar spinal cord (at level L3-S1). Most FBSS patients showed signs of central sensitization (i.e., allodynia or hyperalgesia) during a neurological examination. Symptoms of numbness, burning, and stabbing sensations in both the back and leg occurred in all of the patients, in which the pain in the leg was predominant. During a multidisciplinary approach with the anesthesiologist/pain specialist, neurologist, psychiatrist, and technical physician, the FBSS patients were qualified to be scheduled for a spinal cord stimulation treatment. Before the neurostimulator was intended to be implanted, the subjects participated in the measurement session using NDT-EP. On the day of the experiment, the patients were not treated by a nerve block or spinal cord surgery for at least three months. They were allowed to continue intake of strong opioids or anti-depressants, if necessary.

Exclusion criteria of the study were: participant's refusal during the study, inability to understand the instructions, lacking knowledge of the Dutch language, pregnancy, neurological disorders affecting sensory function (i.e., diabetes mellitus, polyneuropathy), and consumption of alcohol 24 hours before the measurement. Not completing the measurement and inadequate performance of the instructions were the exclusion criteria for data analysis.

6.2.2 Stimuli

An AmbuStim 1-channel stimulator applied cathodic stimulation, using a custom-made electrode with intra-epidermal needles. This IES-5 electrode contained an array of five interconnected 0.5 mm needles, which preferentially activate nociceptive (Aδ) afferents in the skin when stimulating at an intensity below twice the detection threshold (Doll, Maten, Spaan, Veltink, & Buitenweg, 2016; Doll, Veltink, & Buitenweg, 2015; Inui & Kakigi, 2012; Inui, Tran, Hoshiyama, & Kakigi, 2002; Mouraux, 2010; Steenbergen, 2013, 2014, 2012). A rectangular 9 x 5 cm TENS electrode served as an anode and was placed proximal to the IES-5 electrode at the wrist. A previous validation study of the IES electrode showed that stimulation resulted in a sharp pricking sensation (Steenbergen, 2012). Nociceptive detection thresholds were tracked for three different stimulus types: (1) a single 210 μs square-wave pulse, (2) a double 210 μs square-wave pulse with an IPI of 10 ms, and (3) a double 210 μs square-wave pulse with an IPI of 40 ms. The tracking procedure is described in the sections below.

6.2.3 EEG Recording

During the stimulation, electrical brain activity was recorded continuously with a sampling frequency of 1 kHz. This was performed using an ANT Neuro Waveguard EEG cap containing 64 Ag/AgCl electrodes (modified international 10-20 system (Stowell, 1984)) in combination with a TMSi 72-channel REFA EEG amplifier.

6.2.4 Procedure

The subject was asked to fill in a set of questionnaires, including the numeric rating scale (NRS) and the central sensitization inventory (CSI). The EEG cap was applied to the head. A ground electrode was placed on the forehead and earlobe electrodes were applied for re-referencing of CPz to CPz-A1A2. The scalp electrode impedance was verified and recorded to be below 5 kΩ for all channel electrodes. The subject was asked to focus their eyes on one point and

avoid muscular face movements (e.g., talking and swallowing). The stimulation electrodes were attached to the dorsum of the hand while the stimulator was held on the other hand. The side of the first measurement was randomized on the dominant or non-dominant hand and the side of the second measurement was subsequently on the complementary hand. The subject was familiarized with test stimuli and detection tasks for a few minutes before the start of each measurement. The initial thresholds were determined for each stimulus type using a normal stair-case procedure with a step-size of 0.05 mA.

During the measurement using the NDT-EP method, a total amount of 450 stimuli consisting of 150 stimuli for each stimulus type were applied to the subject. Detection thresholds for each stimulus type were tracked using the multiple threshold tracking (MTT) paradigm (Doll, Buitenweg, Meijer, & Veltink, 2014; Doll, Maten, Spaan, Veltink, & Buitenweg, 2016; Doll, Veltink, & Buitenweg, 2015). Thresholds for each stimulus type were tracked simultaneously by measuring the subject's response (detected or non-detected) to a randomized stimulus sequence. Stimuli of each type were presented in random order. The inter-stimulus interval was set on a uniform distribution of 2.5 to 3.5 seconds. The stimulus amplitude of those stimuli was chosen from an adaptive set of five equidistant amplitudes. Amplitudes in this set were increased and decreased with a fixed step size of 0.025 mA after a non-detected stimulus and detected stimulus, respectively. The subject was instructed to press a button to indicate stimulus detection by releasing the button as soon as any sensation was felt which was ascribed to the application of a stimulus. The subject was asked to continue the task after about half a second. If the button was released within 1000 ms after the stimulus, the stimulus was labeled as 'detected'. The stimulus was labeled as 'non-detected' if the button remained pressed. The EEG was recorded during the entire NDT-EP method.

6.2.5 Data Analysis

Mean and standard deviations of occasional subject characteristics (i.e., age, sex, BMI), pain intensity, and central sensitization measures (i.e., NRS and CSI) were calculated for each group.

6.2.6 Nociceptive Detection Thresholds

Data from the MTT paradigm in response to stimuli were preprocessed and analyzed in MATLAB (version 2015b; The MathWorks Inc, Natick, Massachusetts, US). Model computation and statistical analysis were performed in R using the 'lme4' (Bates, Mächler, Bolker, & Walker, 2015) and the 'MASS' libraries (Venables & Ripley, 2002).

Group-level detection probability (P_d) was analyzed using generalized linear mixed regression (GLMR) with a logit link function. In line with the previous study, the detection probability was modeled as a function of an intercept, amplitude of the first pulse (*PU1*), amplitude of the second pulse with 10 ms IPI ($PU2_{10}$), amplitude of the second pulse with 40 ms IPI ($PU2_{40}$), diagnosis (*DIAG*), trial number (*TRL*) and measurement number (*M*) as fixed effects (van den Berg & Buitenweg, 2021). An interaction with diagnosis of the subject (i.e., healthy control or FBSS) was included for the pulse amplitudes and trial number. Between-subject (*S*) random effects were included for every fixed effect and interaction. The guess rate and lapse rate were both assumed to be zero for robust estimation of effect sizes. The equation of the GLMR model in Wilkinson notation is shown in (1).

$$ln\left(\frac{P_d}{1-P_d}\right) \sim 1 + PU1 * DIAG + PU2_{10} * DIAG + PU2_{40} * DIAG + TRL * DIAG + M + (1 + PU1 * DIAG + PU2_{10} * DIAG + PU2_{40} * DIAG + TRL * DIAG + M|S) \quad (1)$$

Fixed effects and interactions were tested using type III Wald Chi-square statistics. Confidence intervals of the fixed effects were computed using a normal approximation to the distribution of the estimated parameters. Detection thresholds were computed based on the regression parameters and

assessed for significance using a z-test after approximation of the standard errors using the Delta procedure (Faraggi, Izikson, & Reiser, 2003; Moscatelli, Mezzetti, & Lacquaniti, 2012). First, detection thresholds were tracked over time by applying GLMR to a moving window of 30 stimulus-response pairs for each stimulus type. As the tracked detection thresholds each showed a linear trend, group-level detection probability, detection thresholds were subsequently analyzed by applying GLMR to the entire dataset.

6.2.7 Nociceptive Detection Thresholds on Individual Level

To explore the sensitivity of outcomes measures to altered nociceptive function on an individual level, mean effect sizes on the detection probability were computed on an individual level for all significant regression parameters (i.e., stimulus properties on detection probability and thresholds) of the GLMR model in healthy subjects and FBSS patients. Also, individual NDTs were calculated in response to each stimulus type and tested between groups using a two-sample t-test.

6.2.8 Nociceptive Detection Thresholds Related to Subject Characteristics

The significant regression parameters on nociceptive detection probability and thresholds derived from Equation (1) were analyzed concerning subject characteristics using a linear regression model. The regression parameters were modeled as a function of an intercept, diagnosis, age, sex, and BMI as fixed effects. Between-subject random effects were included for every fixed effect.

The same significant regression parameters were analyzed concerning clinical features for chronic pain using an additional linear regression model. These regression parameters were modeled as a function of an intercept, NRS-score, CSI-score, pain duration, duration FBSS, and medication intake as fixed effects. Between-subject random effects were included for every fixed effect.

6.2.6 Evoked Potentials

The EEG was preprocessed using FieldTrip, which is a MATLAB toolbox for signal processing (Oostenveld, Fries, Maris, & Schoffelen, 2011). Trials for the EP analysis were segmented using a fixed time window range from 0.5 s before the stimulus to 1.0 s post-stimulus. The data were offline band-pass filtered from 0.1 – 40 Hz and baseline-corrected using the period from -0.5 s to 0.0 s. Eye blinks (Delorme, Sejnowski, & Makeig, 2007) and muscular activity in the raw EEG data were evaluated and removed from each measurement using an independent component analysis algorithm in MATLAB (version 2015b; The MathWorks Inc, Natick, Massachusetts, US).

A butterfly plot was generated to have an overview of the grand average EPs for each EEG channel. The global field power (GFP) described the spatial standard deviation of all grand average EPs (Lehmann & Skrandies, 1980; Skrandies, 1990), which was used for latency identification and selection. The grand average EEG scalp topographies were plotted around the selected latencies at 190 ms and 440 ms post-stimulus based on GFP peaks. The grand average EPs were derived from two derivations: (1) CPz-A1A2 and (2) T7-F4 (van den Berg & Buitenweg, 2021). In line with the previous study, CPz-A1A2 was used to observe central EP components, while T7-F4 was used to observe contralateral EP components since T7 and F4 showed the largest signal-to-noise ratio for the N1 peak in a previous study using intra-epidermal electric stimulation (van den Berg & Buitenweg, 2021).

6.2.7 Effects of Stimulus Properties on the Brain Evoked Potential

The EP (U_{EEG}) was modeled as a function of stimulus parameters by an LMR model, for both derivations. Statistical analysis was performed in MATLAB 2017b (MathWorks, Inc.). In line with previous studies, the EP was modeled as a function of an intercept, the amplitude of the first pulse (*PU1*), the amplitude of the second pulse with 10 ms IPI ($PU2_{10}$) and 40 ms IPI ($PU2_{40}$), and interaction between the trial number (*TRL*) and stimulus detection (*D*) (van den Berg & Buitenweg, 2021). The effect of FBSS was modeled by adding an interaction of diagnosis (*DIAG*) with each of those parameters. Furthermore, measurement

number (*M*) was included to prevent potential confounding. Between-subject (*S*) random effects were included for every fixed effect and interaction. The equation of the LMR model in Wilkinson notation is given in (4).

$$U_{EEG} \sim 1 + PU1 * DIAG + PU2_{10} * DIAG + PU2_{40} * DIAG + D * TRL * DIAG + M + (1 + PU1 * DIAG + PU2_{10} * DIAG + PU2_{40} * DIAG + D * TRL * DIAG + M|S) \quad (2)$$

Effect sizes and their t-values of each regression parameter were calculated for every time point. Statistical t-tests were performed at the identified latencies (190 ms and 440 ms post-stimulus).

6.2.8 Brain Evoked Potentials and Effect Size of Stimuli on Individual Level

To explore the sensitivity of brain evoked potentials to altered nociceptive function on an individual level, mean effect sizes on the P440 were computed on an individual level for all significant regression parameters of the LMR model (i.e., stimulus types) in healthy subjects and FBSS patients. Besides, the individual average potential of the P440 was calculated in response to each stimulus type and tested between groups using a two-sample t-test.

6.2.9 Brain Evoked Potential Related to Subject Characteristics

The influence of significant regression parameters on the P440 was analyzed concerning subject characteristics using a linear regression model. These regression parameters were modeled as a function of an intercept, diagnosis, age, sex, and BMI. The role of these characteristics was estimated between every subject.

Additionally, the influence of significant parameters on the P440 was analyzed concerning clinical features of chronic pain using a linear regression model. The role of NRS-score, CSI-score, pain duration, duration FBSS, and medication intake was estimated between every subject. NRS-and CSI-scores were modeled numerically. Effect significance was assessed using a t-test.

6.3 Results

The subject's group characteristics are summarized in Table 6.1. In total seventeen healthy subjects (3 males, age: 35.9 ± 11.9 years) and sixteen FBSS patients (9 males; age: 50.1 ± 9.1 years) were enrolled for data-analysis. Three healthy subjects were excluded due to technical issues with the setup. Four FBSS patients were excluded from data analysis because the data was unusable. Two of these patients showed an inadequate performance of the instructions. The third patient was an outlier based on detection thresholds and reported to suffer from a differential diagnosis of an early-stage diabetic polyneuropathy in their feet. The last patient had a sensibility disorder since nerves were damaged after surgical intervention in olecranon bursitis.

None of the healthy subjects had a medical history of chronic pain, and nobody had pain complaints (NRS: 0.0 ± 0.0) during the experiment. Additionally, none of the healthy subjects were diagnosed with a neurological disorder. Healthy subjects reported a CSI-score lower than 40 (mean CSI-score 14.6 ± 8.8), indicating that they did not suffer from a central sensitization syndrome. In contrast, eleven out of sixteen FBSS patients suffered from a central sensitization syndrome (Table 6.1). On average, FBSS patients reported an NRS-score of 7.0 ± 2.1. Seven of the FBSS patients took pain medication on the day of the experiment. Note that average age, sex-ratio, and BMI differed from healthy controls. None of the female subjects were in their menstrual period.

6.3.1 Nociceptive Detection Thresholds

The group-level thresholds of all stimulus types are shown in Table 6.2. Mean NDTs from FBSS patients were higher than NDTs of healthy subjects, which was found for each stimulus type (Table 6.2). The regression parameters of the GLMR model which modulated the detection probability (and hence NDT) are outlined in Table 6.3. It was seen that the pulse amplitudes (Pulse 1; Pulse 2, 10ms IPI; Pulse 2, 40ms IPI) and the trial number (i.e., habituation of stimuli) modulated the detection probability in healthy subjects (Table 6.3). Additionally, the detection probability was significantly modulated by the interaction of these coefficients with the diagnosis of FBSS. The measurement number did not affect the detection probability.

Characteristics	Pain-free subjects *(N=17)*	FBSS *(N=16)*
Diagnosis	Control (Hospital)	FBSS (Hospital)
Age (*years*)	35.9 ± 11.9	50.1 ± 9.1
Sex (*M/F*)	3/14	9/7
BMI (*kg/m²*)	22.2 ± 2.8	25.8 ± 3.3
NRS-score	0.0 ± 0.0	7.0 ± 2.1
CSI-score	14.6 ± 8.8	44.6 ± 13.9
Pain duration (*years*)	-	13.4 ± 13.3
Duration FBSS (*months*)	-	47.5 ± 56.8
Medication intake (*N*)	0	7

Table 6.1: Mean and standard deviations from subject and pain characteristics.

	Pain-free Hospital		FBSS Hospital	
Stimulus types	**NDT**	**SE**	**NDT**	**SE**
Single-Pulse	0.33	0.03	0.83	0.09
Double-Pulse 10ms IPI	0.20	0.02	0.36	0.05
Double-Pulse 40ms IPI	0.20	0.02	0.40	0.05

Table 6.2: Mean NDTs and standard error (SE) in response to each stimulus type, for each group. Threshold differences between groups for each stimulus type.

Regression Parameter	Effect Size	95% Confidence Interval	Likelihood Ratio Test χ^2(df)	Effect p
(Intercept)	-4.27	[-5.10 -3.52]	103.47 (1)	**<.001**
Pulse 1	12.94	[8.69 17.21]	33.38 (1)	**<.001**
Pulse 2, 10ms IPI	8.71	[6.31 11.20]	43.61 (1)	**<.001**
Pulse 2, 40ms IPI	8.49	[6.17 10.87]	45.79 (1)	**<.001**
Trial Number	-2.21	[-2.79 -1.71]	64.13 (1)	**<.001**
Measurement Number	0.20	[-0.34 0.78]	0.52 (1)	.47
Diagnosis	1.66	[0.69 2.58]	11.78 (1)	**<.001**
Pulse 1	-9.80	[-14.26 -5.12]	17.14 (1)	**<.001**
Pulse 2, 10ms IPI	-4.56	[-7.37 -1.28]	8.17 (1)	**<.01**
Pulse 2, 40ms IPI	-5.06	[-7.65 -2.07]	12.12 (1)	**<.001**
Trial Number	1.22	[0.41 1.89]	10.02 (1)	**<.01**

Table 6.3: Regression parameters of the generalized linear mixed model. Each parameter modulated the detection probability, except for Measurement Number.

6.3.2 Nociceptive Detection Thresholds and Effect Size of Stimuli on Individual Level

The effect size and NDTs in response to significant regression parameters are depicted on an individual level in Figure 6.1 for both healthy subjects and FBSS patients. The effect sizes for each regression parameter related to the detection

probability differed significantly between the groups. The individual effect sizes and NDTs for FBSS patients who took medication were homogeneously distributed, which illustrated that NDT differences in FBSS patients were not caused by medication use on an individual level.

6.3.3 Effect of Subject and Pain Characteristics on Nociceptive Detection Threshold

Nociceptive detection probability and thresholds in response to the significant regression parameters of the GLMR model show relevant relationships with several characteristics, as demonstrated in Table 6.4. NDTs were significantly modulated by diagnosis for all stimulus types. Detection probability and thresholds were generally speaking not influenced by subject characteristics, such as age, sex, and BMI. Sex only played a significant role in NDTs for double-pulse stimuli. Strikingly, thresholds and effects on detection probability were modulated by NRS-score and CSI-score, but they were not significantly related to other patient features like pain duration, duration of FBSS, and medication intake.

6.3.4 Grand Average Brain Evoked Potentials

Grand average brain EPs for all EEG channels are visible in Figure 6.2. The butterfly plot illustrated that the applied stimuli caused clear waveforms post-stimulus on ipsilateral, contralateral, and central channels. Major GFP peaks were found at 190 ms and 440 ms post-stimulus. The GFP peak at 190 ms was mainly related to large deviations at the contralateral channels. These contralateral channels, including T7, contained a negative peak of the EP at 190 ms, referred to as N190. The GFP peak at 440 ms contained large deviations on central channels, including CPz. The positive peak at 440 ms was referred to as P440.

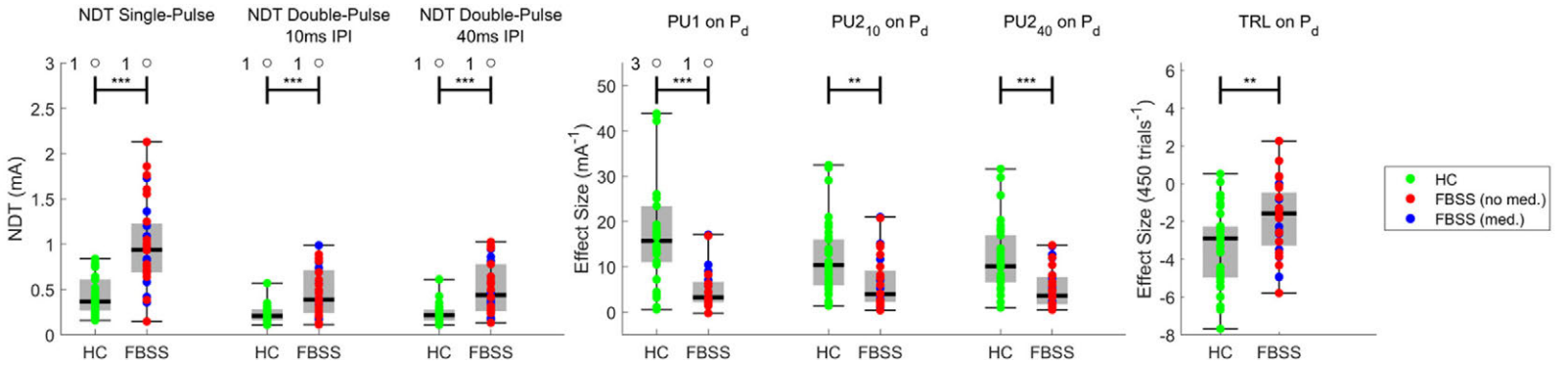

Figure 6.1: *Average NDTs and effect size of regression parameters on the detection probability for both pain-free subjects (HC) and failed back surgery syndrome patients (FBSS) on an individual level.*

Regression parameter	NDT Single-Pulse		NDT Double-Pulse 10ms IPI		NDT Double-Pulse 40ms IPI		Effect size Pulse 1 on P_d		Effect size Pulse 2 10ms IPI on P_d		Effect size Pulse 2 40ms IPI on P_d		Effect size Trial Number on P_d	
	Est	**p**	**Est**	**p**	**Est**	**p**	**Est**	**p**	**Est**	**p**	**Est**	**p**	**Est**	**p**
(Intercept)	-0.32	**<.001**	0.03	**<.001**	-0.01	**<.001**	27.16	**<.01**	14.68	**<.05**	17.11	**<.01**	-7.70	**<.001**
Diagnosis	0.39	**<.001**	0.17	**<.05**	0.20	**<.01**	-8.46	**<.01**	-2.83	0.25	-3.73	0.09	0.26	0.70
Age (*years*)	0.00	0.40	0.00	0.74	0.00	0.96	-0.07	0.50	-0.09	0.31	-0.07	0.38	0.04	0.07
Sex (*male*)	0.17	0.10	0.10	**<.05**	0.11	**<.05**	-1.30	0.61	-4.05	0.05	-3.52	0.06	0.65	0.25
BMI (kg/m^2)	0.03	0.34	0.01	0.36	0.01	0.15	-0.37	0.31	0.05	0.87	-0.11	0.66	0.12	0.13
(Intercept)	0.42	**<.001**	0.20	**<.001**	0.21	**<.001**	15.61	**<.001**	10.85	**<.001**	10.70	**<.001**	-3.31	**<.001**
NRS-score	0.12	**<.001**	0.05	**<.001**	0.05	**<.001**	-2.05	**<.001**	-1.67	**<.001**	-1.44	**<.001**	0.35	**<.01**
CSI-score	-0.01	0.08	0.00	**<.05**	0.00	0.07	0.18	0.13	0.17	0.06	0.14	0.09	-0.03	0.25
Pain duration (*years*)	0.01	0.30	0.00	0.36	0.00	0.68	-0.12	0.37	0.08	0.41	0.04	0.70	0.00	0.99
Duration FBSS (*months*)	0.00	0.15	0.00	0.15	0.00	0.06	-0.04	0.13	-0.01	0.50	-0.02	0.16	0.01	0.19
Medication intake	-0.05	0.78	0.09	0.16	0.05	0.37	-1.34	0.68	-0.95	0.70	-1.08	0.63	-0.19	0.79

Table 6.4: *Average NDTs and effect size on the detection probability related to subject and pain characteristics. The NDT values were log-transformed for significance testing.*

The distribution of the EP is illustrated by grand average scalp topography as depicted in Figure 6.2. The EP shifted over time from a contralateral distribution pattern at N190 to a central distribution pattern at P440. At N190, the area of the contralateral distribution pattern occurred near the channels T7 and F4. At P440, it was found that the central distribution pattern occurred around CPz, A1, and A2. In general, this was found for both healthy subjects and FBSS patients. Derivations of T7-F4 and CPz-A1A2 were selected for further EP investigation.

Grand average EPs in response to stimuli are displayed in Figure 6.2. Amplitudes from healthy subjects were proportional to FBSS patients. Using T7-F4 the latency of the maximum amplitude was at 190 ms for healthy subjects, while the latency of this peak was later for FBSS patients. Using CPz-A1A2 it was seen that the latency of the maximum amplitudes was at 440 ms for both groups.

6.3.5 Effects of Stimulus Properties to Brain Evoked Potentials

Relations between regression parameters of the LMR model and the brain EP at P440 using CPz-A1A2 derivation are summarized in Table 6.5. The EP was significantly modulated by stimulus detection, amplitude of single-and double-pulse stimuli, and trial number. The EP was significantly affected by the interaction of diagnosis (i.e., FBSS) with the amplitude of the first pulse and of a second pulse after 10 or 40 ms. The measurement number did not play a significant role.

The effect size of the second pulse on the EP and corresponding t-values in healthy subjects and FBSS patients are depicted over time using CPz-A1A2 derivation in Figure 6.3. Most strikingly, the negative effect of the interaction of diagnosis (i.e., FBSS) with stimulus amplitudes of double-pulse stimuli caused that the positive effect of stimulus amplitude on the EP in healthy subjects was canceled-out in FBSS patients. In other words, addition of a second pulse did not affect the EP amplitude in FBSS patients, while it significantly increased the EP amplitude in healthy subjects. In healthy subjects, the increase of the EP in response to the second pulse accordingly occurs during

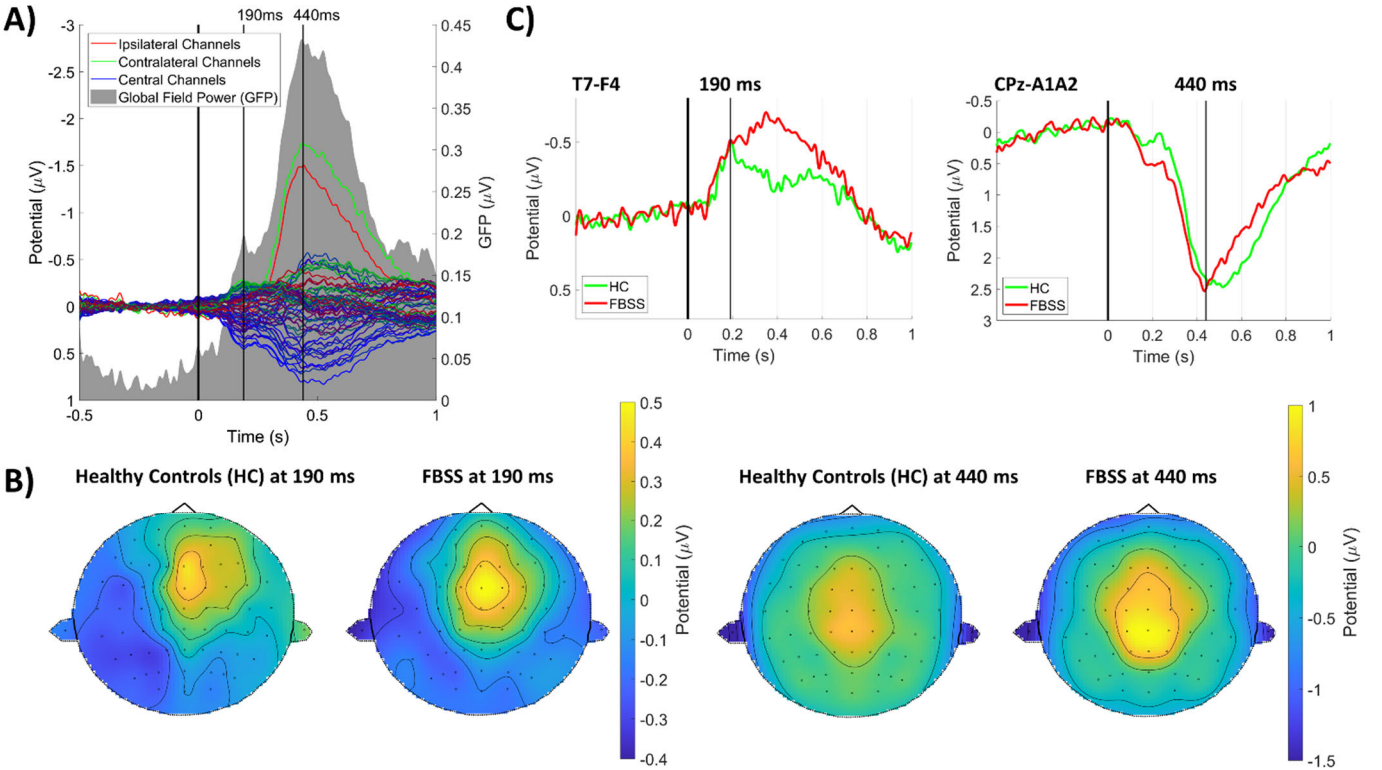

Figure 6.2: *(A) Butterfly plot from FBSS patients and healthy controls measured at the St. Antonius Hospital. The grand average EPs are derived from 64 channels and subdivided into three groups: ipsilateral, contralateral, and central channels. The global field power shows a peak at 190 ms and 440 ms post-stimulus. (B) Grand average scalp topographies from both healthy subjects (upper panels) and FBSS patients (lower panels). The distribution of the EP is displayed at 190 ms (left panels) and 440 ms (right panels) post-stimulus. (C) The grand average EP of the contralateral (left panel) and central (right panel) component is displayed using T7-F4 and CPz-A1A2, respectively.*

a few-hundred-milliseconds-window around 440 ms post-stimulus (Figure 6.3). In the same period in healthy subjects, stimulus amplitudes of single-pulse stimuli had a positive effect on the EP, and trial number a negative effect (Table 6.5). Stimulus detection had a positive effect on the EP in healthy subjects.

Using the T7-F4 derivation, it was shown that the N190 was significantly ($p<0.01$) modulated by stimulus detection only. This regression parameter had a negative effect on the EP for approximately 100 ms around the peak. All other parameters did not significantly affect the N190.

6.3.6 Brain Evoked Potentials and Effect Size of Stimuli on Individual Level

The average potential of the P440 and the effect of each pulse on the P440 on an individual level are depicted in Figure 6.4. The potential did not significantly differ between healthy subjects and FBSS on an individual level. However, the effect size of each pulse on the P440 was significantly lowered in FBSS patients.

Regression parameter	**Effect size**	**95% Confidence Interval**	**CPz-A1A2: P440**	
			t	**p**
(Intercept)	-1.97	[-2.71 -1.23]	-5.29	**<.001**
Detection	5.02	[3.70 6.33]	7.77	**<.001**
Detection × Trial Number	-0.29	[-1.52 0.94]	-0.48	0.636
Pulse 1	2.96	[1.78 4.14]	4.93	**<.001**
Pulse 2, 10ms IPI	4.16	[2.54 5.78]	5.19	**<.001**
Pulse 2, 40ms IPI	3.87	[2.57 5.16]	5.85	**<.001**
Trial Number	-1.76	[-2.64 -0.88]	-4.03	**<.001**
Measurement Number	0.18	[-0.51 0.87]	0.52	0.604
Diagnosis	1.88	[0.75 3.00]	3.32	**<.01**
Detection	-0.78	[-2.67 1.11]	-0.84	0.409
Detection × Trial Number	-0.13	[-1.93 1.67]	-0.14	0.886
Pulse 1	-1.72	[-3.16 -0.29]	-2.36	**<.05**
Pulse 2, 10ms IPI	-3.29	[-5.33 -1.26]	-3.36	**<.01**
Pulse 2, 40ms IPI	-3.06	[-4.58 -1.54]	-3.95	**<.001**
Trial Number	1.23	[-0.20 2.66]	1.72	0.090

***Table 6.5**: Relations between regression parameters of the LMR model and EP at P440 using CPz-A1A2 derivation.*

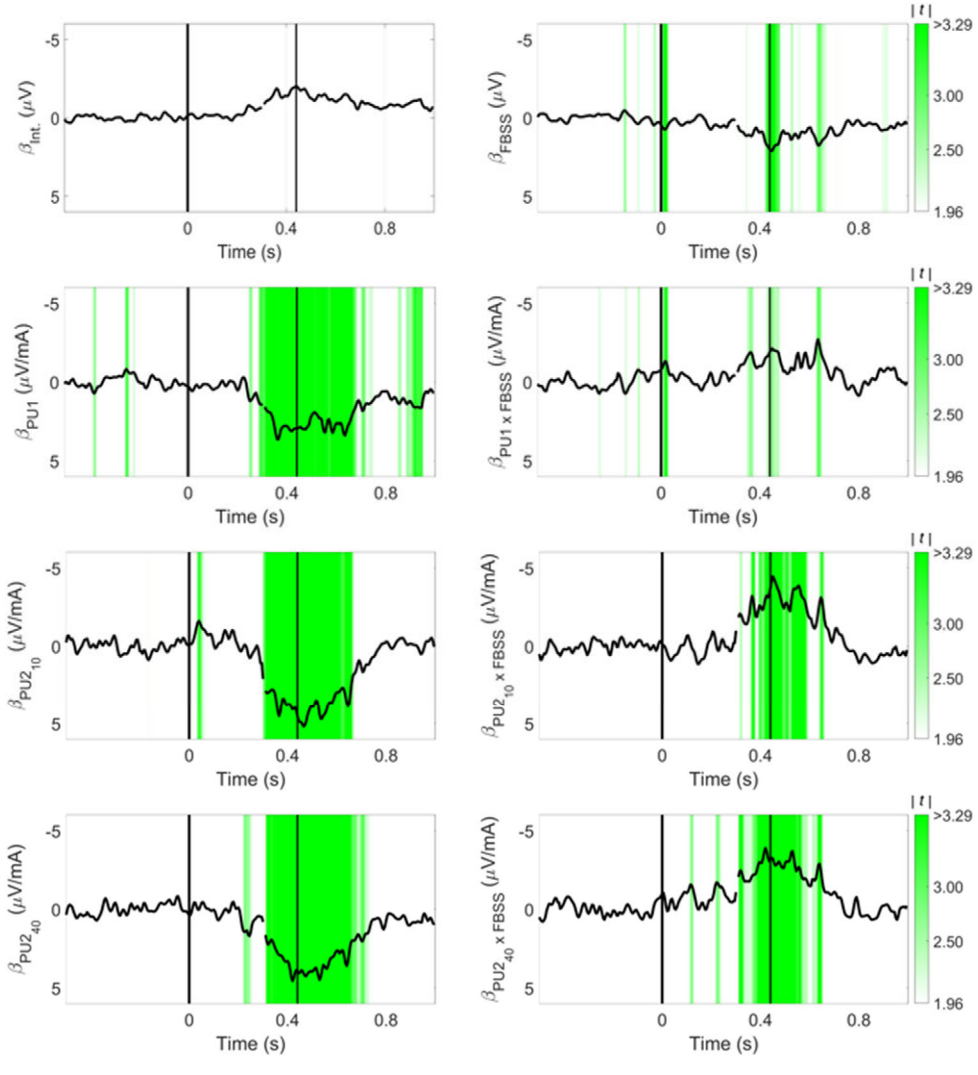

***Figure 6.3**: Significant regression parameters of the LMR model with their effect size and corresponding t-values.*

6.3.7 Effect of Subject and Pain Characteristics on Evoked Potentials

The influence of significant regression parameters on the P440 related to subject characteristics was shown in Table 6.6. For each stimulus type, the average P440 amplitude was mainly modulated by subject characteristics such as age, sex, and BMI. However, the average P440 amplitude was not sensitive to clinical features. In contrast, the effect of pulse amplitudes (Pulse 1; Pulse 2, 10ms IPI; Pulse 2, 40ms IPI) on the P440 was not significantly modulated by subject characteristics. Instead, the effect of pulse amplitudes on the P440 was strongly dependent on clinical features such as the NRS-score, CSI-score, and duration of FBSS. Medication intake did not affect the average P440 amplitude and effects of pulse amplitudes on the P440.

6.4 Discussion

In this study, we investigated the feasibility to record intra-epidermal electric detection thresholds and evoked potentials using the NDT-EP method in healthy subjects and FBSS patients at the hospital, followed by an exploration of its sensitivity to altered nociceptive processing. We explored the effect size of IES stimulus properties on NDTs and EPs at a group level. Significant parameters were analyzed for their sensitivity on an individual level to the diagnosis, subject characteristics, and clinical features

6.4.1 Feasibility of the NDT-EP Method

Results demonstrated that group-level NDTs for all stimulus types measured in healthy subjects at the Hospital were in line with those measured in the previous study (Table 6.2). By analyzing the effect of stimulus properties on the detection probability, it was found that detection probability was significantly affected by the same regression parameters as in previous laboratory studies on healthy subjects (van den Berg & Buitenweg, 2021). Regression parameters, such as stimulus amplitude for each stimulus type and the trial number showed again that they played an important role in the detection probability on intra-epidermal electric stimuli.

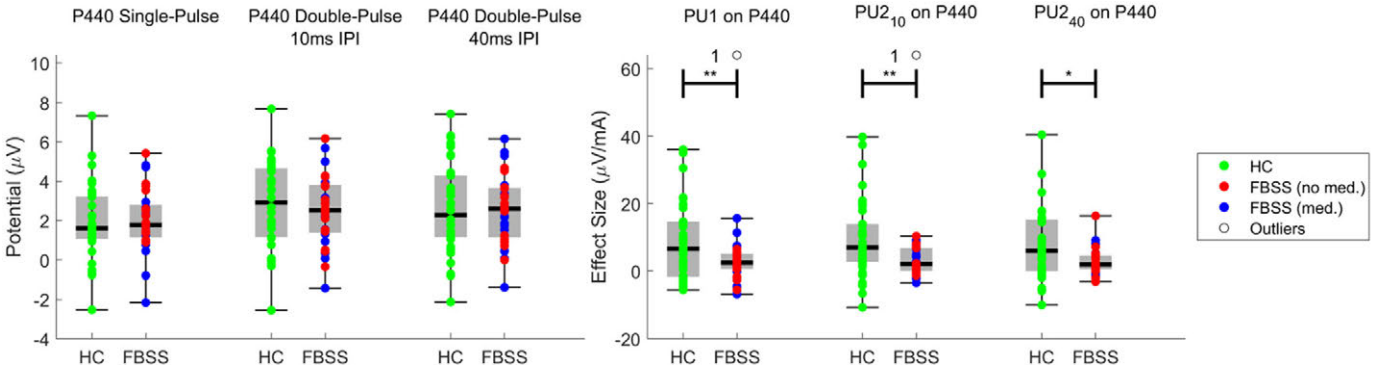

Figure 6.4: *The effect size and mean potential in response to regression parameters for all individual pain-free subjects (HC) and failed back surgery syndrome patients (FBSS).*

Regression parameter	**P440 Single-Pulse**		**P440 Double-Pulse 10ms IPI**		**P440 Double-Pulse 40ms IPI**		**Effect size Pulse 1 on P440**		**Effect size Pulse 2 10ms IPI on P440**		**Effect size Pulse 2 40ms IPI on P440**	
	Est	p	Est	p	Est	p	Est	p	Est	p	Est	p
(Intercept)	3.56	**<.05**	2.20	0.20	0.91	0.62	24.62	**<.01**	12.11	0.15	7.73	0.32
Diagnosis	1.55	**<.01**	0.85	0.18	0.61	0.36	-0.28	0.93	-3.38	0.28	-3.84	0.18
Age (*years*)	-0.08	**<.001**	-0.07	**<.01**	-0.06	**<.05**	-0.18	0.09	-0.12	0.27	0.01	0.93
Sex (*male*)	-1.28	**<.01**	-1.92	**<.001**	-1.34	**<.05**	-4.52	0.08	-5.08	0.06	-2.70	0.26
BMI (kg/m^2)	0.06	0.44	0.15	**<.05**	0.19	**<.05**	-0.39	0.28	0.12	0.74	0.00	1.0
(Intercept)	1.86	**<.001**	2.38	**<.001**	2.17	**<.001**	6.81	**<.01**	6.87	**<.01**	4.72	**<.05**
NRS-score	0.01	0.94	-0.13	0.30	-0.11	0.39	-1.64	**<.01**	-1.77	**<.01**	-1.51	**<.01**
CSI-score	0.00	0.85	0.04	0.11	0.04	0.16	0.25	**<.05**	0.31	**<.01**	0.29	**<.01**
Pain duration (*years*)	0.03	0.33	0.03	0.32	0.02	0.46	-0.14	0.29	-0.05	0.69	-0.05	0.66
Duration FBSS (*months*)	-0.01	0.20	-0.01	**<.01**	-0.01	0.05	-0.04	0.13	-0.05	**<.05**	-0.04	**<.05**
Medication intake	-0.29	0.64	-0.67	0.33	-0.32	0.65	-0.26	0.93	-2.50	0.42	-2.21	0.42

Table 6.6: *The P440 and EP in response to significant regression parameters of the linear regression related to subject characteristics using CPz-A1A2 derivation.*

To assess the feasibility of using the novel NDT-EP method in FBSS patients, this study had to deal with challenges from two sides. On the one hand, the applicability of the NDT-EP method in a dysfunctional nociceptive system, which was related to the performance of FBSS patients. On the other hand, the ability of the NDT-EP method to provide clinically relevant information about the malfunctional nociceptive system.

All twenty FBSS patients succeeded in completing the two NDT-EP method measurements. Four of them were excluded due to poor data quality, of which two patients appeared to suffer from a comorbid peripheral neurological disorder and two patients had an inadequate task performance. It is difficult to find an evidenced reason for their inadequate task performance, but attention seems to be relevant for detecting low-intensity stimuli. Over the whole, difficulties concerning measurement duration were reported by some FBSS patients, because they complained about attentional issues due to the pain from the sitting position. Although the effect of pain may influence attention, the effect of age cannot be ruled out. It might be possible that diagnosis and age-related issues are confounding.

6.4.2 Observing Altered Nociceptive Processing in FBSS Patients

The FBSS patients suffered from chronic pain (i.e., >3 months) in the back and leg(s). The mean pain duration was 13.4 years ranging from 3 to 54 years. During this period, FBSS patients were treated with medication in several categories, nerve blocks, and underwent at least one surgical spinal cord intervention. According to the NRS-score, the patients reported moderate to severe pain (Boonstra et al., 2016) in their back and leg(s) on the measurement day (7.0 ± 2.1). On the whole, the FBSS patients were assumed to suffer from a central sensitization syndrome since the mean CSI-score was 44.6 ranging from 18 to 65. Symptoms of numbness, burning, and/or stabbing sensations in the back and leg(s) were found in everyone, even without clinical somatic substrate. Along with the diffuse pattern of symptoms, the pathophysiology of FBSS is known to be extremely complex. The persistent interplay between nociceptive and neuropathic pain components is characterized by the chronification of back

pain (Blond, Mertens, David, Roulaud, & Rigoard, 2015). Strikingly, we found that FBSS demonstrated an increased mean NDT compared to healthy controls. The loss of sensitivity reflected by increased detection thresholds was also found in NDTs from the painful limb of FBSS patients without DRG stimulation (Berfelo, Doll, Krabbenbos, & Buitenweg, 2022). The relevance of FBSS modulating the detection probability was marked by a significant main effect of diagnosis along with the amplitude of each pulse and trial number. Here, the negative interaction between diagnosis and pulse amplitudes shows that the effect of each pulse amplitude on detection probability is less in FBSS patients, leading to lower psychometric slopes for single- and double-pulse stimuli, and suggesting less temporal summation of the neural activity evoked by each pulse. Additionally, effect sizes and NDTs measured on an individual level were significantly different between diagnosis groups. Generally speaking, NDTs and detection probability were not found to be modulated by subject characteristics or medication intake. Overall, the detection probability and NDTs were mainly associated with clinical features such as diagnosis and NRS-score. Therefore, this data indicates that NDTs might be sensitive to changes in nociceptive function as expressed in FBSS patients.

The effect of pulse amplitudes on the brain evoked potential in FBSS patients also shows a remarkable reduction with respect to the same effects in healthy subjects. There is a reduced contribution of pulse amplitudes to the P440 amplitude compared to healthy controls. In addition, the potential of the P440 was significantly modulated by the diagnosis. While the grand average EP of FBSS patients showed a similar amplitude as the control group, it should be noted that the stimulus intensities applied around the detection threshold were much higher in FBSS patients. This means that the grand average EP amplitudes would be lower in FBSS patients when correcting for stimulus intensity, which corresponds with the reduced sensitivity to pulse amplitudes in FBSS patients. On an individual level, the average potential of the P440 amplitudes did not significantly differ between the diagnosis groups for each stimulus type. By analyzing the average P440 amplitude related to subject characteristics, it was seen that it was significantly modulated by age, sex, and BMI. However, the significantly reduced effect size of each pulse amplitude on

the P440 in FBSS patients was not modulated by these subject characteristics. More interestingly, the effect of both pulse amplitudes on the P440 was significantly correlated with NRS-score, CSI-score, and FBSS duration. This implies that the reduced effects on P440 in FBSS patients were mainly reflected by clinical features and not by subject characteristics or medication intake. Future studies should overcome the heterogeneity of the FBSS group in this explorative study, and therefore, it is recommended to study the role of subject characteristics, e.g., age and gender, on nociceptive function, and subsequently, to include future FBSS patients based on subject and pain characteristics. Furthermore, it is advised to match individual patients with healthy controls based on similar subject characteristics.

6.4.3 Clinical Interpretation

The differences between pain-free subjects and FBSS patients might be features of central sensitization (i.e., widespread hyper-/hypoesthesia and loss of cortical coding). Average NDTs and P440 amplitudes, and the effects of pulse amplitudes on the detection probability and P440 amplitude were not modulated by medication intake. Instead, it might be assumed that increased NDTs (i.e., signs of widespread hypoesthesia) are related to central nociceptive malfunctions, since we activated peripheral nociceptors in a non-painful area. Moreover, the reduced sensitivity to pulse amplitude, which is significantly correlated with the subject's pain experience (i.e., NRS-score, CSI-score, and FBSS duration) supports that the peripheral nociceptive back pain has been moved centrally. This was possibly developed due to its increased persistent nociceptive afferent inflow (Blond, Mertens, David, Roulaud, & Rigoard, 2015; Chan & Peng, 2011). As a consequence, it is assumed that hyperexcitable central neurons and deficient inhibitory descending pathways might play a role in the chronification of pain in FBSS patients (Ossipov, Dussor, & Porreca, 2010). Several studies agreed that FBSS patients illustrate signs of altered central nociceptive processing possibly induced by changes in functional neural properties of primary afferent neurons (Blond, Mertens, David, Roulaud, & Rigoard, 2015; Chan & Peng, 2011). The current study added to this evidence of

altered central nociceptive processing in FBSS and showed that we might monitor these patients using a mechanism-based approach.

6.5 Conclusion

This study demonstrated the feasibility to record intra-epidermal electric detection thresholds and evoked potentials using the NDT-EP method in healthy subjects and FBSS patients at the hospital, the applicability of the NDT-EP method in a dysfunctional nociceptive system, and the ability to observe altered NDTs and EPs in FBSS patients. The strongly increased NDTs and reduced contribution of the second pulse to the brain potential imply that the NDT-EP method suggest that we might use this method to observe clinically relevant alterations of nociceptive function, which is a crucial step toward mechanism-based monitoring. Future research into subject characteristics, e.g., age and gender, related to nociceptive function is recommended and FBSS patients should be age- and gender-matched.

6.6 References

Arendt-Nielsen, L. (2015). Central Sensitization in Humans: Assessment and Pharmacology. In H.-G. Schaible (Ed.), *Pain Control* (pp. 79-102). Berlin, Heidelberg: Springer Berlin Heidelberg.

Arendt-Nielsen, L., Morlion, B., Perrot, S., Dahan, A., Dickenson, A., Kress, H. G., . . . Drewes, A. M. (2018). Assessment and manifestation of central sensitisation across different chronic pain conditions. *European Journal of Pain, 22*(2), 216-241.

Arendt-Nielsen, L., & Yarnitsky, D. (2009). Experimental and Clinical Applications of Quantitative Sensory Testing Applied to Skin, Muscles and Viscera. *Journal of Pain, 10*(6), 556-572.

Backonja, M. M., Attal, N., Baron, R., Bouhassira, D., Drangholt, M., Dyck, P. J., . . . Ziegler, D. (2013). Value of quantitative sensory testing in neurological and pain disorders: NeuPSIG consensus. *Pain, 154*(9).

Bates, D., Mächler, M., Bolker, B., & Walker, S. (2015). Fitting Linear Mixed-Effects Models Using lme4. *Journal of Statistical Software; Vol 1, Issue 1 (2015)*.

Berfelo, T., Doll, R.-J., Krabbenbos, I. P., & Buitenweg, J. R. (2022). Observing Altered Nociceptive Detection Thresholds in Patients With Persistent Spinal Pain Syndrome Type 2 With a Dorsal Root Ganglion Stimulator. *Neuromodulation: Technology at the Neural Interface*.

Blond, S., Mertens, P., David, R., Roulaud, M., & Rigoard, P. (2015). From "mechanical" to "neuropathic" back pain concept in FBSS patients. A systematic review based on factors leading to the chronification of pain (part C). *Neurochirurgie, 61 Suppl 1*, S45-56.

Boonstra, A. M., Stewart, R. E., Köke, A. J. A., Oosterwijk, R. F. A., Swaan, J. L., Schreurs, K. M. G., & Schiphorst Preuper, H. R. (2016). Cut-Off Points for Mild, Moderate, and Severe Pain on the Numeric Rating Scale for Pain in Patients with Chronic Musculoskeletal Pain: Variability and Influence of Sex and Catastrophizing. *Frontiers in Psychology, 7*(1466).

Chan, C.-w., & Peng, P. (2011). Failed Back Surgery Syndrome. *Pain Medicine, 12*(4), 577-606.

Cruz-Almeida, Y., & Fillingim, R. B. (2014). Can Quantitative Sensory Testing Move Us Closer to Mechanism-Based Pain Management? *Pain Medicine, 15*(1), 61-72.

Delorme, A., Sejnowski, T., & Makeig, S. (2007). Enhanced detection of artifacts in EEG data using higher-order statistics and independent component analysis. *NeuroImage, 34*(4), 1443-1449.

Doll, R. J., Buitenweg, J. R., Meijer, H. G. E., & Veltink, P. H. (2014). Tracking of nociceptive thresholds using adaptive psychophysical methods. *Behavior Research Methods, 46*(1), 55-66.

Doll, R. J., Maten, A. C. A., Spaan, S. P. G., Veltink, P. H., & Buitenweg, J. R. (2016). Effect of temporal stimulus properties on the nociceptive detection probability using intra-epidermal electrical stimulation. *Experimental Brain Research, 234*(1), 219-227.

Doll, R. J., Veltink, P. H., & Buitenweg, J. R. (2015). Observation of time-dependent psychophysical functions and accounting for threshold drifts. *Attention, Perception, and Psychophysics, 77*(4), 1440-1447.

Edwards, R. R. (2005). Individual differences in endogenous pain modulation as a risk factor for chronic pain. *Neurology, 65*(3), 437.

Faraggi, D., Izikson, P., & Reiser, B. (2003). Confidence intervals for the 50 per cent response dose. *Statistics in Medicine, 22*(12), 1977-1988.

Groen, G. J., Beese, U. H., Van de Kelft, E., & Groen, R. J. M. (2016). A Practical Approach to the Diagnosis and Understanding of Chronic Low Back Pain, Based on Its Pathophysiology. In E. van de Kelft (Ed.), *Surgery of the Spine and Spinal Cord: A Neurosurgical Approach* (pp. 359-381). Cham: Springer International Publishing.

Harte, S. E., Harris, R. E., & Clauw, D. J. (2018). The neurobiology of central sensitization. *Journal of Applied Biobehavioral Research, 23*(2), e12137.

Inui, K., & Kakigi, R. (2012). Pain perception in humans: Use of intraepidermal electrical stimulation. *Journal of Neurology, Neurosurgery and Psychiatry, 83*(5), 551-556.

Inui, K., Tran, T. D., Hoshiyama, M., & Kakigi, R. (2002). Preferential stimulation of Aδ fibers by intra-epidermal needle electrode in humans. *Pain, 96(3)*, 247-252.

Lehmann, D., & Skrandies, W. (1980). Reference-free identification of components of checkerboard-evoked multichannel potential fields. *Electroencephalography and Clinical Neurophysiology, 48*(6), 609-621.

Moscatelli, A., Mezzetti, M., & Lacquaniti, F. (2012). Modeling psychophysical data at the population-level: The generalized linear mixed model. *Journal of Vision, 12*(11), 26-26.

Mouraux, A., Iannetti, G. D., & Plaghki, L. (2010). Low intensity intra-epidermal electrical stimulation can activate Aδ-nociceptors selectively. *Pain, 150(1)*, 199-207.

Oostenveld, R., Fries, P., Maris, E., & Schoffelen, J. M. (2011). FieldTrip: Open source software for advanced analysis of MEG, EEG, and invasive electrophysiological data. *Computational Intelligence and Neuroscience, 2011*.

Ossipov, M. H., Dussor, G. O., & Porreca, F. (2010). Central modulation of pain. *The Journal of Clinical Investigation, 120*(11), 3779-3787.

Pavlaković, G., & Petzke, F. (2010). The Role of Quantitative Sensory Testing in the Evaluation of Musculoskeletal Pain Conditions. *Current Rheumatology Reports, 12*(6), 455-461.

Pfau, D. B., Geber, C., Birklein, F., & Treede, R.-D. (2012). Quantitative Sensory Testing of Neuropathic Pain Patients: Potential Mechanistic and Therapeutic Implications. *Current pain and headache reports, 16*(3), 199-206.

Reid, K. J., Harker, J., Bala, M. M., Truyers, C., Kellen, E., Bekkering, G. E., & Kleijnen, J. (2011). Epidemiology of chronic non-cancer pain in Europe: narrative review of prevalence, pain treatments and pain impact. *Curr Med Res Opin, 27*(2), 449-462.

Skrandies, W. (1990). Global field power and topographic similarity. *Brain Topography, 3*(1), 137-141.

Steenbergen, P., Buitenweg, J. R., Trojan, J., & Veltink, P. H. (2013). Reproducibility of somatosensory spatial perceptual maps. *Experimental brain research, 224(3)*, 417-427.

Steenbergen, P., Buitenweg, J. R., Trojan, J., & Veltink, P. H. (2014). Tactile localization depends on stimulus intensity. . *Experimental brain research, 232(2)*, 597-607.

Steenbergen, P., Buitenweg, J. R., Trojan, J., van der Heide, E. M., van den Heuvel, T., Flor, H., & Veltink, P. H. (2012). A system for inducing concurrent tactile and nociceptive sensations at the same site using electrocutaneous stimulation. *Behavior research methods, 44(4)*, 924-933.

Stowell, H. (1984). Event related brain potentials and human pain: a first objective overview. *Int J Psychophysiol, 1*(2), 137-151.

Van Buyten, J. P. (2016). Neurostimulation for the Management of Failed Back Surgery Syndrome (FBSS). In E. van de Kelft (Ed.), *Surgery of the Spine and Spinal Cord: A Neurosurgical Approach* (pp. 585-600). Cham: Springer International Publishing.

van den Berg, B., & Buitenweg, J. R. (2021). Observation of Nociceptive Processing: Effect of Intra-Epidermal Electric Stimulus Properties on Detection Probability and Evoked Potentials. *Brain Topography*.

van den Berg, B., Doll, R. J., Mentink, A. L. H., Siebenga, P. S., Groeneveld, G. J., & Buitenweg, J. R. (2020). Simultaneous tracking of psychophysical detection thresholds and evoked potentials to study nociceptive processing. *Behavior Research Methods*.

Venables, W. N., & Ripley, B. D. (2002). *Modern Applied Statistics with S* (4 ed.): Springer-Verlag New York.

Vuilleumier, P. H., Biurrun Manresa, J. A., Ghamri, Y., Mlekusch, S., Siegenthaler, A., Arendt-Nielsen, L., & Curatolo, M. (2015). Reliability of Quantitative Sensory Tests in a Low Back Pain Population. *Regional Anesthesia & Pain Medicine, 40*(6), 665.

Wylde, V., Sayers, A., Odutola, A., Gooberman-Hill, R., Dieppe, P., & Blom, A. W. (2017). Central sensitization as a determinant of patients' benefit from total hip and knee replacement. *European Journal of Pain, 21*(2), 357-365.

Chapter 7

Combining Psychophysical and EEG Biomarkers Using Machine Learning for Improved Observation of Altered Nociceptive Processing in Individual Failed Back Surgery Syndrome Patients

Published as:

Van den Berg, B., Berfelo, T., Verhoeven, E.M.H., Krabbenbos, I.P., & Buitenweg, J. R. (2021). Combining psychophysical and EEG biomarkers for improved observation of altered nociceptive processing in failed back surgery syndrome. Proceedings of the 43rd Annual International Conference of the IEEE Engineering in Medicine and Biology Society (EMBC), Guadalajara, Mexico.

DOI: https://www.doi.org/10.1109/EMBC46164.2021.9630906

Abstract

Diagnosis and stratification of chronic pain patients is difficult due to a lack of sensitive biomarkers for altered nociceptive and pain processing. Recent developments enabled to preferentially stimulate epidermal nerve fibers and simultaneously quantify the psychophysical detection probability and neurophysiological EEG responses. In this work, we study whether using one or a combination of both outcome measures could aid in the observation of altered nociceptive processing in chronic pain. A set of features was extracted from data from a total of 66 measurements on 16 failed back surgery syndrome patients and 17 healthy controls. We assessed how well each feature discriminates both groups. Subsequently, we used a random forest classifier to study whether psychophysical features, EEG features or a combination can improve the classification accuracy. It was found that a classification accuracy of 0.77 can be achieved with psychophysical features, while a classification accuracy of 0.65 was achieved using only EEG features.

7.1 Introduction

Clinical assessment, diagnosis and stratification of chronic pain patients is difficult due to a lack of objective pain biomarkers (Mouraux & Iannetti, 2018). Current diagnostic guidelines largely rely on the identification of structural abnormalities using imaging, and assessment of the perceived pain using questionnaires. However, it remains unclear to which extent these structural abnormalities contribute to the perceived pain as these abnormalities are often observed in both painful and non-painful conditions (Jordan, Konstantinou, & O'Dowd, 2009; van den Bosch, Hollingworth, Kinmonth, & Dixon, 2004). Furthermore, if no structural abnormality could be identified, one is left without objective information about the underlying alterations in nociceptive processing that cause the pain. Development of methods to measure a composition of various sensitive biomarkers to observe altered nociceptive processing could aid clinicians with monitoring and diagnosis of chronic pain patients.

Recently, we developed a method with the aim of improving monitoring of chronic pain patients by measuring the sensitivity to electro-nociceptive stimuli and brain evoked potentials in response to those stimuli (van den Berg et al., 2020). The method uses intra-epidermal electric stimulation around the detection threshold to preferentially active nociceptive afferents in the skin (Mouraux, 2010; Poulsen, Tigerholm, Meijs, Andersen, & Mørch, 2020). An adaptive procedure is used to continuously center stimulation intensities around the detection threshold. The scalp EEG is measured simultaneously to analyze the brain activity evoked by nociceptive stimulation. The result of this procedure is a large heterogeneous collection of stimulus-response and stimulus-EEG pairs which can be used to effectively assess input-output relations of that patients' nociceptive system.

Using this heterogeneous dataset, the effects of stimulus amplitude, stimulus types (i.e., single-pulse and double-pulse stimuli) and the number of administered stimuli (i.e., habituation) on the EEG can be quantified using linear (mixed) models (Van den Berg & Buitenweg, 2018). Simultaneously, effects of the same stimulus properties on the detection probability can be

quantified using generalized linear (mixed) models. A recent study (van den Berg & Buitenweg, 2021) used this method to show that the various steps of processing a nociceptive stimulus, including peripheral nerve fiber recruitment, central synaptic summation, and habituation to a repeated stimulus are reflected by these effects of stimulus properties on detection probability and the evoked potential.

As a next step, we want to know whether we could use this method to observe altered nociceptive processing in individual chronic pain patients. We recently started combined sensitivity and brain activity measurements in patients suffering from failed back surgery syndrome (FBSS). In this work, we use individual features of detection probability and EEG obtained in this study to determine if a combination of these features could aid future monitoring and diagnosis of FBSS patients.

7.2 Method

The experimental procedures described in this paper were approved by the local Medical Review and Ethics Committee and all participants provided written informed consent prior to participation.

7.2.1 Participants

Psychophysical and brain activity features were extracted from a larger dataset of 16 FBSS patients (9 males; age: 50.1 ± 9.1 years; NRS: 7.0 ± 2.1; CSI: 44.6 ± 13.9) and 17 healthy controls (3 males, age: 35.9 ± 11.9 years; NRS: 0.0 ± 0.0; CSI: 14.6 ± 8.8) measured at the St. Antonius Hospital in Nieuwegein.

7.2.2 Procedure

Participants were seated in a comfortable chair and instructed to focus their gaze at a fixed point on the wall. Intra-epidermal electric stimuli were applied to the back of the hand via a custom made electrode with 5 microneedles

(Steenbergen et al., 2012) and centered around the detection threshold using an adaptive psychophysical procedure (Doll, Veltink, & Buitenweg, 2015). Participants were instructed to release a response button whenever they detected a stimulus. Each stimulus was randomly chosen from an equidistant vector of 5 amplitudes. When a stimulus was reported as detected, all amplitudes were decreased by 0.025 mA. When a stimulus remained undetected, all amplitudes were increased by 0.025 mA. This procedure continued until a total of 450 stimuli was applied (Figure 7.1). The total procedure had a duration of 35-45 minutes and was repeated on each hand.

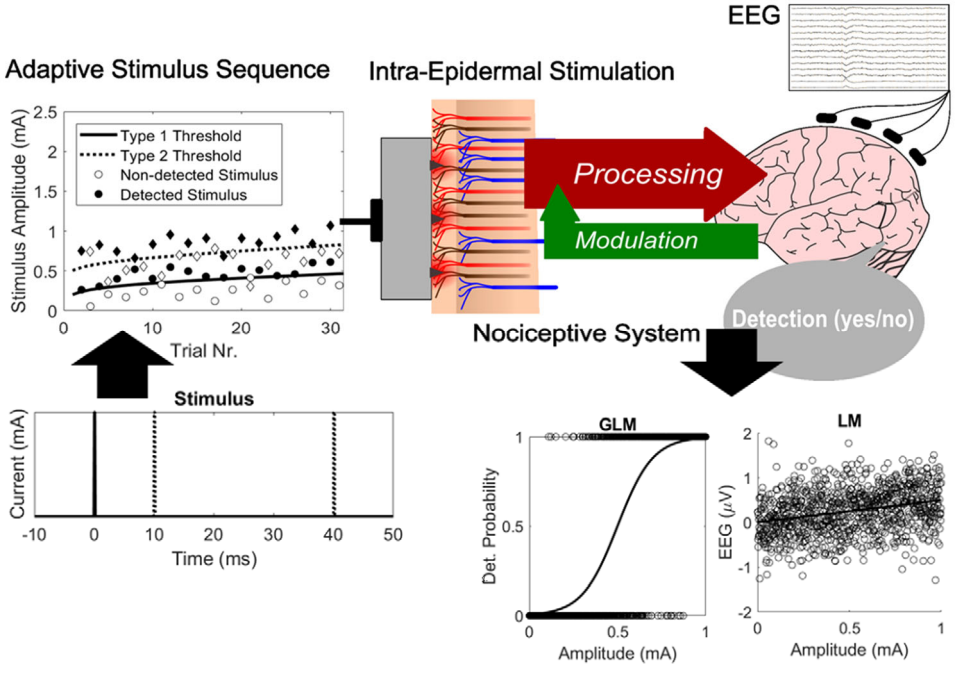

***Figure 7.1**: Simultaneous measurement of the nociceptive detection threshold (NDT) and evoked potential (EP), referred to as the NDT-EP method. In this method, the detection probability and threshold of multiple stimulus types (here with one or two pulses, 10 or 40 ms inter-pulse interval) is tracked using an adaptive algorithm while recording EEG. The effect of stimulus properties on the detection probability is quantified using a generalized linear model (GLM) and on the EEG using a linear model (LM). In this way, one might observe altered nociceptive processing (e.g., in FBSS patients) through a change of the relation between stimulus properties, detection probability and brain activity.*

7.2.3 Psychophysical Features

The 450 stimulus-response pairs obtained during each measurement were used to compute an average detection rate (R_{det}), average response time (RT_{mn}) and the standard deviation of the response time (RT_{std}). The generalized linear model in (1) was fit to the stimulus-response pairs to compute the effects of stimulus properties on the detection probability. The model quantified the effects of amplitude of the first pulse ($PU1$), amplitude of a second pulse with 10 ms inter-pulse interval ($PU2_{10}$), amplitude of a second pulse with 40 ms inter-pulse interval ($PU2_{40}$), trial number (TRL) a model intercept (INT) on the log-odds of stimulus detection. The guess rate and lapse rate were both assumed to be zero for robust estimation of coefficients. Subsequently, model coefficients were used to compute the average detection thresholds and slopes of single-pulse and double-pulse stimuli with inter-pulse intervals of 10 and 40 ms (T_{SP}, T_{DP10}, T_{DP40}, S_{SP}, S_{DP10} and S_{DP40}).

$$\ln\left(\frac{P}{1-P}\right) \sim 1 + PU1 + PU2_{10} + PU2_{40} + TRL \quad (1)$$

7.2.4 Brain Activity Features

The EEG was recorded at 1000 Hz using a 64-channel Ag/AgCl electrode cap (10-20 system) during the entire experiment. The signal was divided into epochs -0.5 to 1.0 s with respect to stimulus onset and bandpass filtered between 0.1 and 40 Hz using the Fieldtrip toolbox (Oostenveld, Fries, Maris, & Schoffelen, 2011) in Matlab. Latencies of the N1 and P2 component of the evoked potential were estimated to be 190 and 440 ms respectively based on the grand average global field power. At both latencies the average and standard deviation of the evoked potential for each stimulus type and overall were computed. The linear model in (2) was fit at both latencies to compute the effects of stimulus properties on the evoked potential. The model quantified the effects of amplitude of the first pulse ($PU1$), amplitude of a second pulse with 10 ms inter-pulse interval ($PU2_{10}$), amplitude of a second pulse with 40 ms

inter-pulse interval ($PU2_{40}$), trial number (TRL), stimulus detection (D) and a model intercept (INT) on the evoked potential amplitude.

$$U_{EEG} \sim 1 + PU1 + PU2_{10} + PU2_{40} + TRL * D \quad (2)$$

7.2.5 Random Forest Classification

A random forest classification model was fit separately on all psychophysical features, all brain activity features and all features combined using the 'Scikit-learn' toolbox (Pedregosa et al., 2012) in Python. A full list of these features is shown in Table 7.1.

Random forests are an accurate classification technique that is able to use complex nonlinear combinations of features for classification and is robust to outliers and noise (Breiman, 2001). As such, this classifier was expected to find an optimal combination of features for classification with an accuracy close to the Bayes rate. The number of estimators for random forest classification was fixed to 1000 estimators. Other parameters were optimized using grid search with 10-fold cross-validation. These optimized parameters included a maximum depth of 3, a minimum number of samples per split of 15 and a minimum number of samples per leaf of 5. Classification performance was evaluated using 10-fold cross-validation in terms of accuracy, sensitivity, specificity, and area under the curve (AUC). We also added a performance metric for consistency, which was defined as the percentage of subjects of which both measurements were assigned the same class. Minimum redundancy maximum relevance (MRMR) feature selection based on the F-test correlation quotient was used to select a subset of all features (Zhao, Anand, & Wang, 2019). Shapley values of the random forest classifier were computed using the 'shap' toolbox (Lundberg et al., 2020) to identify the top 6 features of interest in multiple sets of features.

Nr.	Feature	Category
1	detection rate	psychophysics
2	response time: mean	psychophysics
3	response time: standard deviation	psychophysics
4	GLM: intercept	psychophysics
5	GLM: pulse 1	psychophysics
6	GLM: pulse 2, 10ms IPI	psychophysics
7	GLM: pulse 2, 40ms IPI	psychophysics
8	GLM: trial number	psychophysics
9	detection threshold: single-pulse (log-transform)	psychophysics
10	detection threshold: double-pulse, 10ms IPI (log-transform)	psychophysics
11	detection threshold: double-pulse, 40ms IPI (log-transform)	psychophysics
12	psychometric slope: single-pulse (log-transform)	psychophysics
13	psychometric slope: double-pulse, 10ms IPI (log-transform)	psychophysics
14	psychometric slope: double-pulse, 40ms IPI (log-transform)	psychophysics
15	LM of N1: intercept	brain activity
16	LM of N1: pulse 1	brain activity
17	LM of N1: pulse 2, 10ms IPI	brain activity
18	LM of N1: pulse 2, 40ms IPI	brain activity
19	LM of N1: trial number	brain activity
20	LM of N1: detection	brain activity
21	LM of N1: detection x trial number	brain activity
22	mean N1: all stimuli	brain activity
23	mean N1: single-pulse	brain activity
24	mean N1: double-pulse, 10ms IPI	brain activity
25	mean N1: double-pulse, 40ms IPI	brain activity
26	standard deviation N1: all stimuli	brain activity
27	standard deviation N1: single-pulse	brain activity
28	standard deviation N1: double-pulse, 10ms IPI	brain activity
29	standard deviation N1: double-pulse, 40ms IPI	brain activity
30	LM of P2: intercept	brain activity
31	LM of P2: pulse 1	brain activity
32	LM of P2: pulse 2, 10ms IPI	brain activity
33	LM of P2: pulse 2, 40ms IPI	brain activity
34	LM of P2: trial number	brain activity
35	LM of P2: detection	brain activity
36	LM of P2: detection x trial number	brain activity
37	mean P2: all stimuli	brain activity
38	mean P2: single-pulse	brain activity
39	mean P2: double-pulse, 10ms IPI	brain activity
40	mean P2: double-pulse, 40ms IPI	brain activity
41	standard deviation P2: all stimuli	brain activity
42	standard deviation P2: single-pulse	brain activity
43	standard deviation P2: double-pulse, 10ms IPI	brain activity
44	standard deviation P2: double-pulse, 40ms IPI	brain activity

***Table 7.1**: List of all features used for classification and their category. Note that some psychophysical features were computed using the generalized linear model (GLM) in Section 7.2.3, and some brain activity features were computed using the linear model (LM) in Section 7.2.4.*

7.3 Results

7.3.1 Psychophysical Features

All psychophysical features extracted from this dataset were found to demonstrate a significant difference between both groups (Figure 7.2). The difference between FBSS patients and healthy controls is most clearly demonstrated by the logarithm of psychophysical slopes and detection thresholds (T_{SP}, T_{DP10}, T_{DP40}, S_{SP}, S_{DP10} and S_{DP40}), effects of trial number and amplitude of the second pulse in the psychophysical model (TRL, $PU2_{10}$ and $PU2_{40}$), the detection rate (R_{det}) and standard deviation of the reaction time (RT_{std}) which all were significant with p<0.001.

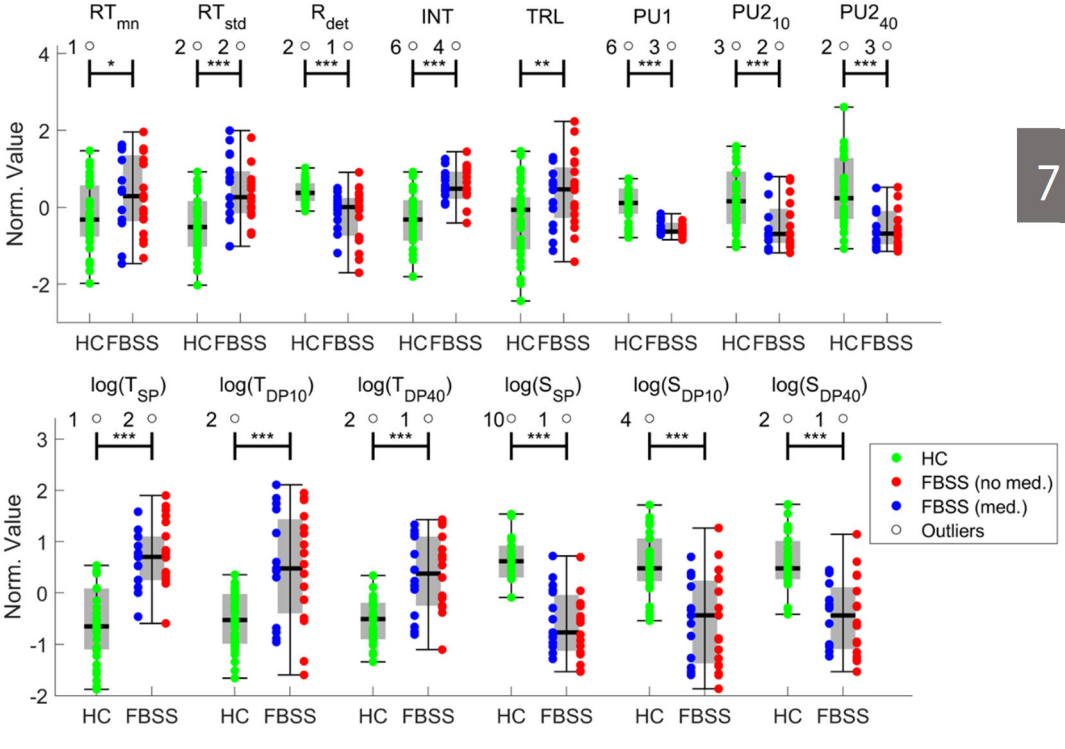

***Figure 7.2**: Psychophysical features with a significant difference between FBSS patients and healthy controls (HC). All psychophysical features were found to differ significantly between both groups, independent of used medication.*

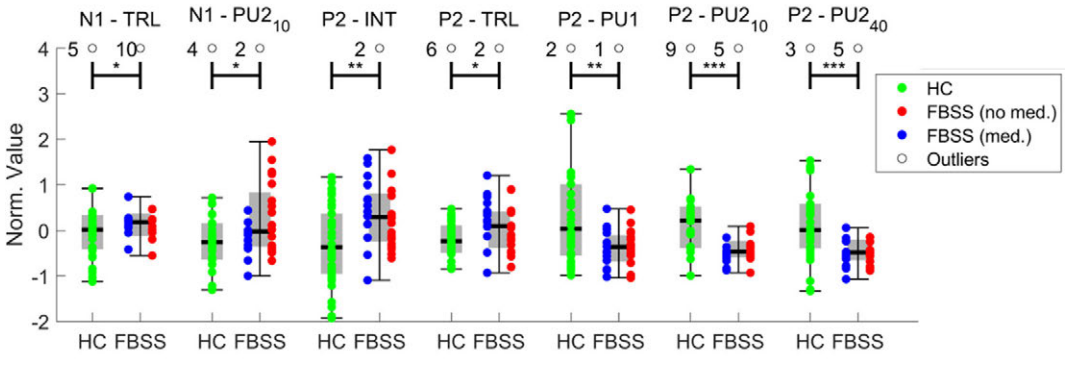

Figure 7.3: EEG features with a significant difference between FBSS patients and healthy controls (HC). The average and standard deviation of the evoked potential for each stimulus type and overall were not significant, and therefore not included in this figure.

7.3.2 EEG Features

Most EEG features did not demonstrate a significant difference between both groups. None of the averages or standard deviations at the N1 or P2 latency were significant. However, fitting a linear mixed model to the EEG data led to the observation of significant effects by successfully accounting for the multivariate experimental design (Figure 7.3). The difference between FBSS patients and healthy controls is most clearly demonstrated by the effect of the amplitude of the second pulse with either a 10 ms or 40 ms inter-pulse interval ($PU2_{10}$ and $PU2_{40}$) on the P2.

7.3.3 Random Forest Classification

Assessment of the random forest classification performance using 10-fold cross-validation led to an overall accuracy of 0.75, with 0.78 sensitivity, 0.72 specificity, 0.82 AUC and 0.72 consistency (Table 7.2). The accuracy improved to 0.78, with 0.78 sensitivity, 0.76 specificity, 0.89 AUC and 0.72 consistency when using only the top 5 features from MRMR feature selection. The accuracy also improved to 0.77, with 0.76 sensitivity, 0.76 specificity, 0.83 AUC and 0.73 consistency when using only the psychophysical features. The accuracy

decreased to 0.65, with 0.63 sensitivity, 0.73 specificity, 0.71 AUC and 0.60 consistency when using only EEG features.

An overview of the top 6 Shapley values for each model fit shows the features with the largest contribution to the each predicted class (Figure 7.4). The model fit using all features and the model fit using only psychophysical features both use the same psychophysical values as their most important features for classification: the effect of the first pulse amplitude in the psychophysical model ($PU1$), and log-transformed detection thresholds and slopes (T_{SP}, T_{DP10}, T_{DP40}, S_{SP}, S_{DP10} and S_{DP40}). The model fit using only EEG features uses mostly the features obtained by fitting a linear model: the model intercept and effect of the first and second pulse amplitudes on the P2 ($PU1, PU2_{10}, PU2_{40}$), the effect of the second pulse amplitude with 10 ms inter-pulse interval ($PU2_{10}$) on the N1, and the mean P2 amplitude for single-pulse stimuli (μ_{SP}). MRMR feature selection uses a combination of EEG and psychophysical features.

	Features			
	All	***MRMR***	***Psychophysical***	***EEG***
Accuracy	0.75	**0.78**	0.77	0.65
Sensitivity	**0.78**	**0.78**	0.76	0.63
Specificity	0.72	**0.76**	**0.76**	0.73
AUC	0.82	**0.89**	0.83	0.71
Consistency	0.72	0.72	**0.73**	0.60

Table 7.2: Performance of classifying FBSS patients and healthy controls using all, psychophysical and EEG features. The largest value of each metric is highlighted in ***bold****.*

7.4 Discussion

In this work, we extracted individual psychophysical and EEG features of FBSS patients and healthy controls to study whether a combination of these features could aid the observation of altered nociceptive processing in chronic pain patients. Note that the influence of the experimental procedure parameters on outcomes has been discussed previously by Van den Berg & Buitenweg (van den Berg & Buitenweg, 2021), and is therefore not studied here.

It was found that all psychophysical features differed significantly between all FBSS patients, with and without medication, and healthy controls. As such, stimulus detection behavior in FBSS patients, was completely different with respect to healthy controls. Differences included much larger detection thresholds and much lower slopes of the psychometric curve. Furthermore, the patients were characterized by a much lower detection rate and more variation in their reaction times. Each of these results indicates that FBSS patients had more trouble distinguishing nociceptive stimuli. Larger detection thresholds show that a larger stimulus intensity was required to elicit a detectable sensation. Lower psychometric slopes show that when a stimulus was reported as detected, patients were much less certain about their detection. Larger variation in response times might also be explained by the extra difficulty patients experienced in determining whether or not they detected a nociceptive stimulus.

It was also found that some EEG features obtained by fitting a linear model differed significantly between all FBSS patients and healthy controls. However, none of the features obtained by averaging or computing standard deviation of the EEG at a single latency differed significantly between both groups. This demonstrates that the effect of stimulus properties on the response is more important than the average response. As such, it was found that the most significant differences of EEG activity between FBSS patients and healthy controls were at the effect of the pulse amplitudes on the EEG.

Multiple features were combined into one classifier using a random forest model. Using all features resulted in an accuracy of 0.75. Using MRMR feature selection improved the accuracy towards 0.78. Using only psychophysical features resulted in a similar accuracy of 0.77, as well as a similar sensitivity, specificity, and consistency. Using only EEG resulted in a much lower accuracy of 0.65, and a lower score on all metrics. This suggests that the information included in the EEG features in this dataset was largely redundant with the information included in the psychophysical features. As such, classification using only the psychophysical features led to a similar accuracy as a classification that also included the informative but noisy EEG features.

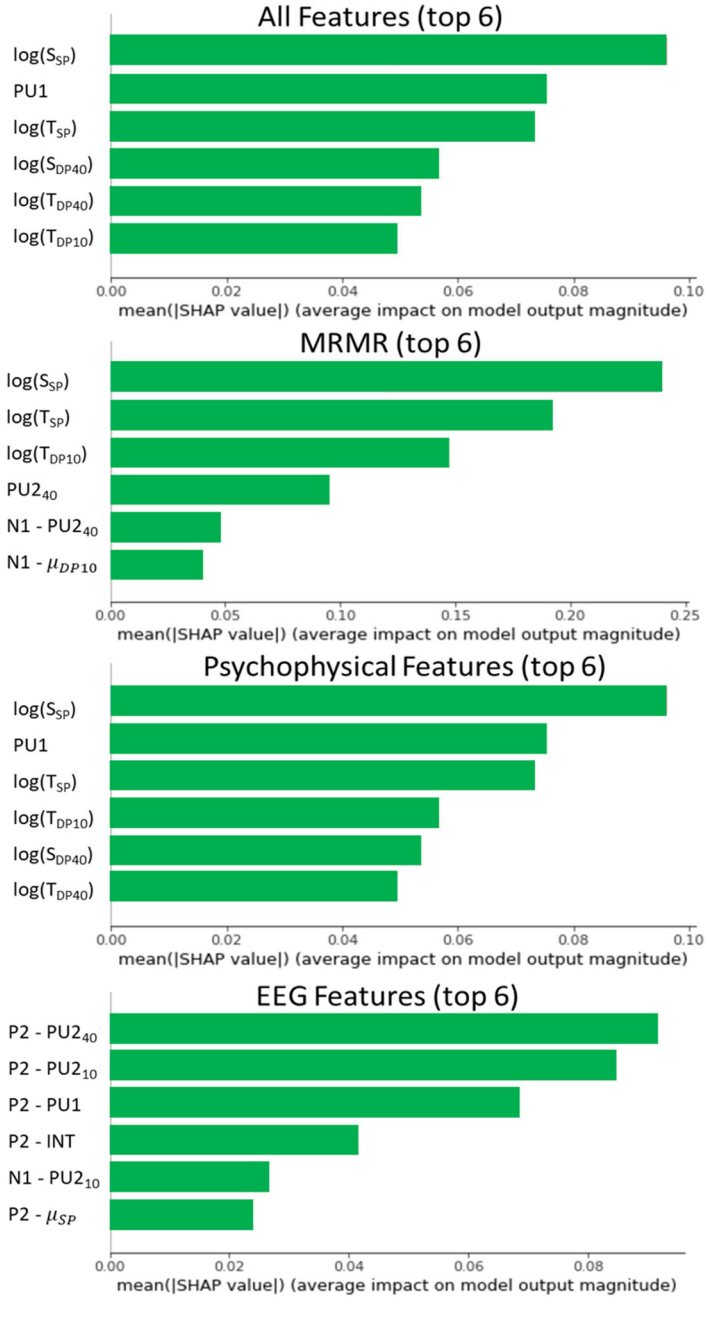

***Figure 7.4**: Shapley values of the 6 most important features for random forest classification when using all features (top), the top 6 features based on minimum redundancy maximum relevance (MRMR, middle), only psychophysical features (middle) and only EEG features (bottom).*

7.5 Conclusion

Combining EEG and psychophysical biomarkers only leads to minor improvements for the classification of FBSS patients with respect to healthy controls. For the sole purpose of monitoring patients, information about the detection thresholds and slopes might be sufficient. Indeed, all psychophysical outcome measures were shown sensitive to FBSS, and some differed between both groups with a high significance ($p<0.001$). We also found in this study that EEG features could be used separately for identification of altered nociceptive processing in the FBSS patients, although with a lower accuracy. As EEG is a measure of brain activity rather than the resulting behavior, this method might prove beneficial in situations where a more objective outcome measure is required. Some of the EEG features differed with a high significance ($p<0.001$) between both groups and are useful to observe altered nociceptive processing on group level.

7.6 Acknowledgements

The authors would like to thank Imre Krabbenbos and Tom Berfelo at the Department of Anesthesiology, Intensive Care and Pain Medicine at the St. Antonius Hospital in Nieuwegein, the Netherlands, for providing the patient data used in this study.

7

7.7 References

Breiman, L. (2001). Random Forests. *Machine Learning, 45*(1), 5-32.

Doll, R. J., Veltink, P. H., & Buitenweg, J. R. (2015). Observation of time-dependent psychophysical functions and accounting for threshold drifts. *Attention, Perception, and Psychophysics, 77*(4), 1440-1447.

Jordan, J., Konstantinou, K., & O'Dowd, J. (2009). Herniated lumbar disc. *BMJ clinical evidence, 2009*, 1118.

Lundberg, S. M., Erion, G., Chen, H., DeGrave, A., Prutkin, J. M., Nair, B., . . . Lee, S.-I. (2020). From local explanations to global understanding with explainable AI for trees. *Nature Machine Intelligence, 2*(1), 56-67.

Mouraux, A., & Iannetti, G. D. (2018). The search for pain biomarkers in the human brain. *Brain, 141*(12), 3290-3307.

Mouraux, A., Iannetti, G. D., & Plaghki, L. (2010). Low intensity intra-epidermal electrical stimulation can activate Aδ-nociceptors selectively. *Pain, 150(1)*, 199-207.

Oostenveld, R., Fries, P., Maris, E., & Schoffelen, J. M. (2011). FieldTrip: Open source software for advanced analysis of MEG, EEG, and invasive electrophysiological data. *Computational Intelligence and Neuroscience, 2011*.

Pedregosa, F., Varoquaux, G., Gramfort, A., Michel, V., Thirion, B., Grisel, O., . . . Louppe, G. (2012). Scikit-learn: Machine Learning in Python. *Journal of Machine Learning Research, 12*.

Poulsen, A. H., Tigerholm, J., Meijs, S., Andersen, O. K., & Mørch, C. D. (2020). Comparison of existing electrode designs for preferential activation of cutaneous nociceptors. *Journal of Neural Engineering*.

Steenbergen, P., Buitenweg, J. R., Trojan, J., van der Heide, E. M., van den Heuvel, T., Flor, H., & Veltink, P. H. (2012). A system for inducing concurrent tactile and nociceptive sensations at the same site using electrocutaneous stimulation. *Behavior Research Methods, 44*(4), 924-933.

Van den Berg, B., & Buitenweg, J. R. (2018). *Analysis Of Nociceptive Evoked Potentials During Multi-Stimulus Experiments Using Linear Mixed Models*. Paper presented at the 40th Annual International Conference of the IEEE Engineering in Medicine and Biology Society (EMBC), Honolulu, United States.

van den Berg, B., & Buitenweg, J. R. (2021). Observation of Nociceptive Processing: Effect of Intra-Epidermal Electric Stimulus Properties on Detection Probability and Evoked Potentials. *Brain Topography*.

van den Berg, B., Doll, R. J., Mentink, A. L. H., Siebenga, P. S., Groeneveld, G. J., & Buitenweg, J. R. (2020). Simultaneous tracking of psychophysical

detection thresholds and evoked potentials to study nociceptive processing. *Behavior Research Methods*.

van den Bosch, M. A., Hollingworth, W., Kinmonth, A. L., & Dixon, A. K. (2004). Evidence against the use of lumbar spine radiography for low back pain. *Clin Radiol, 59*(1), 69-76.

Zhao, Z., Anand, R., & Wang, M. (2019, 5-8 Oct. 2019). *Maximum Relevance and Minimum Redundancy Feature Selection Methods for a Marketing Machine Learning Platform.* Paper presented at the 2019 IEEE International Conference on Data Science and Advanced Analytics (DSAA).

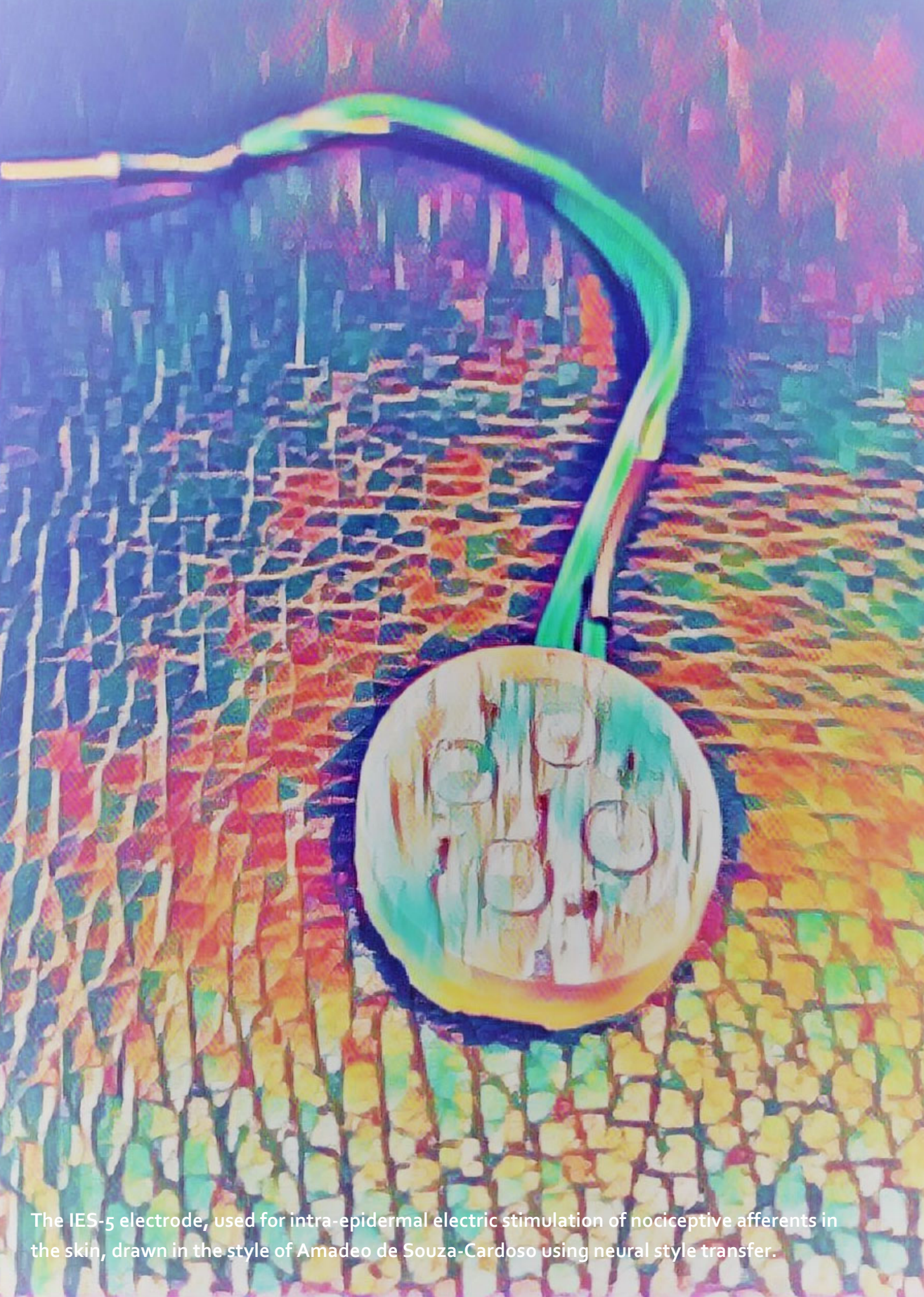

The IES-5 electrode, used for intra-epidermal electric stimulation of nociceptive afferents in the skin, drawn in the style of Amadeo de Souza-Cardoso using neural style transfer.

Part III:

Mechanisms for Altered Intra-Epidermal Detection Thresholds and Evoked Potentials

"Every act of perception, is to some degree an act of creation, and every act of memory is to some degree an act of imagination."

Oliver Sacks, Musicophilia: Tales of Music and the Brain

Chapter 8

Observation of Nociceptive Detection Thresholds and Cortical Evoked Potentials: Go/No-Go Versus 2-Interval Forced Choice

Published as:

Van den Berg, B., Vanwinsen, L., Pezzali, G., & Buitenweg, J. R. (2022). Observation of nociceptive detection thresholds and cortical evoked potentials: go/no-go versus 2-interval forced choice. *Attention, Perception, & Psychophysics*.

DOI: https://www.doi.org/10.3758/s13414-022-02484-5

Abstract

Pain scientists and clinicians search for objective measures of altered nociceptive processing to study and stratify chronic pain patients. Nociceptive processing can be studied by observing a combination of nociceptive detection thresholds and evoked potentials. However, it is unknown whether the nociceptive detection threshold measured using a Go-/No-Go (GN) procedure can be biased by a response criterion. In this study, we compared nociceptive detection thresholds, psychometric slopes and central evoked potentials obtained during a GN procedure with those obtained during a 2-interval forced choice (2IFC) procedure to determine 1) if the nociceptive detection threshold during a GN procedure is biased by a criterion and 2) to determine if nociceptive evoked potentials observed in response to stimuli around the detection threshold are biased by a criterion. We found that the detection threshold was higher when assessed using a GN procedure in comparison with the 2IFC procedure. During a GN procedure, the average P2 component increased proportionally when averaged with respect to detection probability but showed on-off behavior when averaged with respect to stimulus detection. During a 2IFC procedure, the average P2 component increased nonlinearly when averaged with respect to detection probability. These data suggest that nociceptive detection thresholds estimated using a GN procedure are subject to a response criterion.

8.1 Introduction

Pain scientists and clinicians search for objective criteria to identify impaired nociceptive processing for the purpose of stratification and treatment of chronic pain patients (Mouraux & Iannetti, 2018). With this aim, nociceptive processing of patients is usually evaluated using a combination of neurophysiological and psychophysical testing. In this field, there is a recent renewed interest in the assessment of mechanical, thermal, and electric detection thresholds. However, the interpretation of these thresholds could alter depending on the procedure through which these thresholds are measured.

Recently, we developed a method to assess nociceptive processing by quantifying the effect nociceptive stimulus properties on detection probability and cortical evoked potentials (EPs). In this method, we stimulate nociceptive afferents in the skin by intra-epidermal electric stimulation with a specialized electrode (Steenbergen et al., 2012). This method selectively activates nociceptive afferents in the skin provided that low stimulation currents are used, for which a limit of twice the detection threshold was proposed as a rule of thumb (Mouraux, 2010). Stimulus amplitudes are centered around the detection threshold by an adaptive psychophysical method of limits (Doll, Veltink, & Buitenweg, 2015) and the electroencephalogram (EEG) is recorded in response to each stimulus. This allows us to record the combination of nociceptive detection thresholds and evoked potentials in response to nociceptive stimulation. We recently showed that nociceptive detection thresholds of single-pulse and double-pulse intra-epidermal electric stimuli can be used to observe peripheral and central changes of nociception following deafferentation by capsaicin (Doll et al., 2016). Nociceptive evoked potentials can be used as a marker for altered central nociception, e.g. in central sensitization (van den Broeke et al., 2015), attentional modulation (Legrain, Guérit, Bruyer, & Plaghki, 2002) or placebo analgesia (Wager, Matre, & Casey, 2006). The combination of both methods allowed us to evaluate the effect of temporal stimulus properties on nociceptive detection threshold and evoked potentials in healthy participants (van den Berg & Buitenweg, 2021; van den

Berg et al., 2020), and could be used to study impaired nociceptive processing in chronic pain patients in future studies.

Although nociceptive detection thresholds appear sensitive to induced changes in peripheral and central nociceptive processing, it remains unclear how observed detection threshold are related to the underlying physiological systems. In all of our studies, we have used an adaptive method of limits with a Go-/No-Go (GN) procedure to approach and estimate the detection threshold, i.e.: 1) an adaptive series of stimuli is presented, 2) the participant has to indicate when a stimulus was detected and 3) the stimulus amplitude is increased or decreased depending on stimulus detection. Subsequently, logistic regression was used to estimate the detection threshold and slope based on all available data. Although the obtained detection threshold is used to probe central or peripheral nervous function, most studies appear to disregard the fact that these thresholds could also be modulated by a sensory, perceptual or decision criterion (Georgeson, 2012), which we will refer to more generally as a 'response criterion'. We can describe the role of such a response criterion during a GN procedure using signal detection theory (Kingdom & Prins, 2016), by assuming that the response of a participant is based on the quantity of sensory evidence, defined as any type of sensory neural activity that is available for decision making in the brain. During a GN procedure, the participant will report a stimulus as detected when the sensory evidence exceeds the response criterion (Figure 8.1). It remains unknown whether nociceptive detection thresholds estimated using a GN procedure indeed depend on such a response criterion.

In addition, it remains unexplored how evoked cortical activity, measured in some studies as a more 'objective' measure of altered nociceptive or somatosensory processing, is affected by the potential dependence on a response criterion in a GN procedure. The perception of a (change in) visual stimulus results in the generation of the famous P3 (also referred to as P300) peak in the event-related potential (Picton, 1992), which is considered a key marker of conscious access to visual information (Rutiku, Martin, Bachmann, & Aru, 2015; Salti, Bar-Haim, & Lamy, 2012). The P2 in response to nociceptive stimulation represents multi-modal brain activity similar to the visual P3, with

an important role in the generation of conscious perception (Mouraux & Iannetti, 2009). The P2 in response to nociceptive stimulation is also described as a response to stimulus salience (Legrain, Iannetti, Plaghki, & Mouraux, 2011). This interpretation of the P2 is closely related to the other (i.e., a marker of conscious access), as a more salient stimulus will have a higher probability of being consciously detected but is not the same. It therefore remains unknown how the P2 in response to near-threshold stimuli can be interpreted. And if the P2 is a marker of conscious access to information, will there be a P2 when there is sufficient sensory evidence to support decision making (i.e., to correctly classify the interval during the 2IFC procedure) or only when sensory evidence exceeds the response criterion (i.e., when stimulus detection is reported during the GN procedure)?

The potential influence of a response criterion can be omitted by using a 2-interval forced choice (2IFC) procedure (Kingdom & Prins, 2016), where participants are asked to choose during which of two observation intervals a stimulus was applied. During the 2IFC procedure, the interval is reported correct if the sensory evidence during an interval with a stimulus, i.e., with both spontaneous and stimulus-evoked neural activity, is larger than the sensory evidence during an interval without a stimulus, i.e., with only spontaneous neural activity (Figure 8.1). In this study, we compared nociceptive detection thresholds, psychometric slopes and the evoked P2 obtained during a GN procedure with those obtained during a 2IFC procedure with two objectives. Our first objective was to determine if the nociceptive detection threshold during a GN procedure is dependent on a response criterion, i.e., resulting in a different detection threshold with respect to the 2IFC threshold. Our second objective was to explore how the evoked P2 during each procedure is related to the detection probability and to stimulus detection itself.

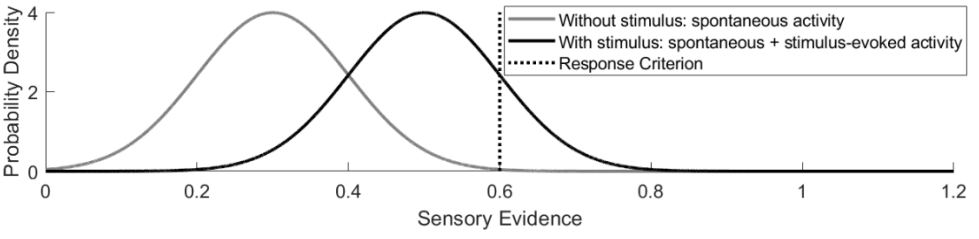

***Figure 8.1**: Stimulus detection as viewed by signal detection theory. Sensory evidence consists of random noise (e.g., spontaneous neural activity) and sensory information (e.g., stimulus-evoked activity). The total amount of sensory evidence during one time interval can be described by a probability density function. During a GN procedure, the stimulus is reported as detected when the sensory evidence during one interval exceeds a response criterion. During a 2IFC procedure, the interval is correctly classified when the sensory evidence during the interval with stimulus, exceeds sensory evidence of the interval without stimulus.*

8.2 Methods

The results presented in this work include measurements of the detection threshold using a GN and a 2IFC procedure in randomized order. A total of 25 participants was included and performed both procedures. In the last 15 participants, also the EEG was recorded during task performance. The experiments were performed at the University of Twente, the Netherlands, and were approved by the local Medical Review and Ethics Committee. All experiments were performed in accordance with the declaration of Helsinki.

8.2.1 Participants

A total of 25 healthy participants (12 males and 13 females, age 19-30) were included in this study. The inclusion criterion was an age between 18 and 40 years old. Exclusion criteria were skin abnormalities at the site of stimulation, diabetes, implanted stimulation devices, pregnancy, usage of analgesics within 24 hours before the experiment, the consumption of alcohol or drugs within 24 hours before the experiments, pain complaints at the time of the experiment, a medical history of chronic pain or any language problems that would impede

communication with the participant. All participants provided written informed consent before participation in the experiment.

8.2.2 Stimuli

Each stimulus consisted of cathodic square wave electric pulses generated by a constant current stimulator (NociTRACK AmbuStim, University of Twente, Enschede, The Netherlands). Stimuli were delivered to the epidermis at the back of the right hand via a custom-made electrode consisting of 5 inter-connected microneedles protruding 0.5 mm from the electrode surface. Intra-epidermal electric stimulation preferentially activates nociceptive afferents in the skin, provided that stimuli remain below twice the detection threshold (Mouraux, 2010; Poulsen, Tigerholm, Meijs, Andersen, & Mørch, 2020). A previous validation study of the electrode used in this study demonstrated that electric pulses resulted in a sharp pricking sensation (Steenbergen, 2012).

Previous studies noted that two intra-epidermal electric pulses repeated at a short inter-pulse interval (between 5 and 40 ms) result in a much lower detection threshold than a single intra-epidermal electric pulse (Doll, Maten, Spaan, Veltink, & Buitenweg, 2016; Mouraux, Marot, & Legrain, 2014; van den Berg & Buitenweg, 2021), suggesting an effect of temporal summation on detection probability. In this study, we therefore investigated the potential influence of response criterion on both single- and double-pulse stimuli. Two stimulus types were used during the experiment, which were both shown to result in similar latencies of response times and evoked N1, N2 and P2 peaks in comparison with earlier studies using intraepidermal and laser stimulation (van den Berg & Buitenweg, 2021):

- One square pulse with a pulse width of 210 µs.
- Two square pulses with a pulse width of 210 µs and an inter-pulse interval of 10 ms.

8.2.3 Familiarization

Participants were instructed to press and hold a button. For familiarization with the sensation of intra-epidermal stimuli, participants were stimulated with a series of pulses with a stepwise (0.025 mA) increasing amplitude and instructed to release the button when a stimulus was clearly perceived for at least two times. For an initial estimate of the detection threshold for each stimulus type, participants were stimulated with a series of pulses with a stepwise (0.025 mA) increasing amplitude and instructed to release the button when any sensation was perceived that they ascribed to stimulation.

8.2.4 Go/No-Go Procedure

Participants were seated upright in a chair and asked to focus on the site of stimulation. Detection thresholds were estimated and tracked using an adaptive procedure (Doll, Veltink, & Buitenweg, 2015). Participants were instructed to press and hold a button, and to briefly release the button when any sensation was perceived that they ascribed to stimulation (Figure 8.2). For the adaptive procedure, the stimulus amplitude was randomly picked from a vector of 5 stimulus amplitudes with a step size of 0.025 mA initialized around the initial estimate of the detection threshold. The vector of amplitudes was decreased by 0.025 mA when a stimulus was reported as detected and increased by 0.025 when the participant did not release the response button. This process was repeated independently for every stimulus type, with the order of stimulus type randomized, for a total of 130 stimuli per type.

8.2.5 2-Interval Forced Choice Procedure

Participants were seated upright in a chair and asked to focus on the site of stimulation. Detection thresholds were estimated and tracked using an adapted version of the adaptive procedure in previous version. Participants were stimulated during one out of two time intervals (Figure 8.2), marked by an auditory cue. After each set of two time intervals, participants were asked to indicate during which time interval they were stimulated. For the adaptive

procedure, the stimulus amplitude was randomly picked from a vector of 5 stimulus amplitudes with a step size of 0.025 mA initialized around the initial estimate of the detection threshold. The vector of amplitudes was decreased by 0.075 mA when the reported time interval was incorrect and increased by 0.025 when the reported time interval was correct. Note that the decrease after an incorrect answer [$d_{incorrect}$] is 3 times larger than the increase after a correct answer [$d_{correct}$], as this ratio is governed by the value of the detection threshold, $\frac{d_{incorrect}}{d_{correct}+d_{incorrect}} = p_{threshold}$, where $p_{threshold}$ is equal to 0.5 for a GN procedure and equal to 0.75 for a 2IFC procedure. This process was repeated independently for every stimulus type, with the order of stimulus type randomized, for a total of 130 stimuli per type.

8.2.6 Electroencephalography

The scalp EEG was recorded at 32 channels (international 10/20 system) using a REFA amplifier (TMSi B.V., Oldenzaal, the Netherlands) with a sampling rate of 1024 Hz. Participants were asked to fix their gaze at a spot on the wall. Electrode impedance was kept below 20 kΩ.

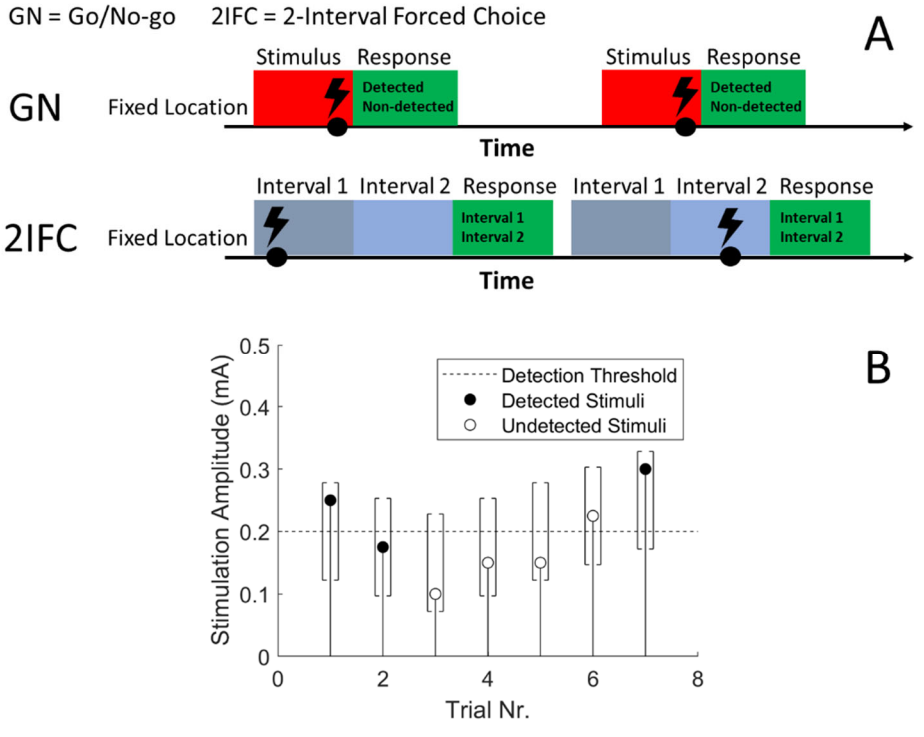

Figure 8.2: The Go/No-Go and the 2-Interval Forced Choice (2IFC) procedure used measure the nociceptive detection threshold for single-and double pulse intra-epidermal electric stimuli (left), and the adaptive procedure used to converge to the detection threshold in both procedures (right). The stimulus is randomly selected from a vector of 5 equidistant stimulus amplitudes (with a step size of 0.025 mA, indicated by []). When a stimulus is not detected (indicated by open markers), this vector is decreased by 0.025 mA (GN) or 0.075 mA (2IFC). When a stimulus is detected (indicated by closed markers), this vector is increased by 0.025 mA (both procedures).

8.2.7 Nociceptive Detection Threshold

The nociceptive detection probability was estimated by global optimization of the negative log-likelihood using an implementation of the GlobalSearch algorithm (Ugray et al., 2007) in combination with an interior-point algorithm to find local minima (Coleman & Li, 1996) in Matlab. In the case of the GN procedure (Equation (1)), the detection probability was modeled using a cumulative normal distribution as a function of an intercept [β_0], additive

temporal summation of the first pulse [$\beta_{A1}A$] and the second pulse [$\beta_{A2}A$], and a linear drift over time [$\beta_t t$]. In the case of a 2IFC procedure (Equation (2)), this function was adapted to account for a 50% guessing rate at low stimulus amplitudes. The lapse rate was assumed to be zero for robust estimation of function parameters. Differences between thresholds estimated using a 2IFC and a GN procedure were assessed based on Bland-Altman analysis (Bland & Altman, 1986), using the BlandAltmanPlot function available on the Matlab file exchange.

Detection probability for a go/no-go procedure:

$$P_{GN} = \Phi(-\beta_0 - \beta_t t + \beta_{A1}A + (n-1)\beta_{A2}A) \quad (1)$$

Detection probability for a 2-interval forced choice procedure:

$$P_{2IFC} = \frac{1}{2} + \frac{1}{2}\Phi(-\beta_0 - \beta_t t + \beta_{A1}A + (n-1)\beta_{A2}A) \quad (2)$$

8.2.8 Evoked Brain Activity

The EEG was preprocessed using the FieldTrip toolbox (Oostenveld, Fries, Maris, & Schoffelen, 2011). Eye-blinks, eye movement and movement artefacts were corrected using independent component analysis (Delorme, Sejnowski, & Makeig, 2007). Epochs with excessive EMG activity or remaining movement artefacts were removed by visual inspection. Grand average EP waveforms of detected and non-detected stimuli (GN), and of correct and incorrect stimuli (2IFC) were computed at T7-F4 and CPz-M1M2 and tested for significance with respect to baseline and with respect to the other condition using cluster-based nonparametric permutation tests (Maris & Oostenveld, 2007). In addition, grand average EP waveforms were computed for four levels of detection probability (.00-.25, .25-.50, .50-.75 and .75-1.0) for both procedures. Significance of the effect of detection probability on the EEG was assessed by fitting a linear mixed model (3) to the EEG at each latency and obtaining the t-value of effect coefficients using Satterthwaite's approximation of the degrees of freedom. The t-values were corrected for retesting over time using the Benjamini-Hochberg correction (Hochberg & Benjamini, 1995). The average P2

amplitude for each of the four levels of detection probability was determined by averaging over time between 380 ms and 420 ms post-stimulus.

$$U_{eeg} \sim 1 + detection\ probability + trial\ number + (1 + detection\ probability + trial\ number \mid subject) \quad (3)$$

8.3 Results

8.3.1 Nociceptive Detection Threshold

A typical example of an experiment with the GN and the 2IFC procedure is displayed in Figure 8.3. During the GN procedure, the detection threshold for single-pulse stimuli was larger than the detection threshold for double-pulse stimuli. Both thresholds showed a small increasing drift over time. During the 2IFC procedure, the thresholds were equal for single-pulse and double-pulse stimuli. Drift over time was small or not present.

Detection thresholds and slopes estimated using a GN procedure were compared to detection thresholds and slopes estimated using a 2IFC procedure. Note that 4 participants were excluded from comparison, because the optimizer failed to converge to a solution for either the GN or 2IFC procedure, and one participant was excluded because of inadequate task performance, defined as a detection rate lower than 0.2 during the GN procedure. Detection thresholds and slopes for the remaining 20 participants are displayed on the left in Figure 8.4. The detection threshold for single-pulse stimuli during a 2IFC procedure was significantly lower than the detection threshold for single-pulse stimuli during a GN procedure. The psychometric slope for single-pulse stimuli during a 2IFC procedure was significantly larger than the psychometric slope for single-pulse stimuli during a GN procedure. Bland-Altmann plots for analysis of the individual differences between threshold and slopes estimated using a GN procedure, and threshold and slopes estimated using a 2IFC procedure, are displayed on the right in Figure 8.4. For single-pulse stimuli, detection thresholds are positively biased, and slopes are negatively biased when estimated using a GN procedure. This bias of estimated thresholds appears to increase with respect to the estimated value. For double-pulse stimuli, thresholds and slopes were unbiased.

8.3.2 Evoked Brain Activity

Grand average evoked potentials at Cz-M1M2 acquired during both procedures are displayed in Figure 8.5. There was a significant contrast between evoked potentials in response to detected and non-detected stimuli in the GN procedure and correct and incorrect trials in the 2IFC procedure. For the GN procedure, the evoked potential was significantly larger than baseline for detected as well as non-detected stimuli. For the 2IFC procedure, the evoked potential was only significantly larger than baseline for correct trials. Note that the average evoked potential for correct trials (2IFC) was lower than the average evoked potential for detected stimuli (GN) but might be confounded by inclusion of trials that were not consciously perceived but simply guessed correctly.

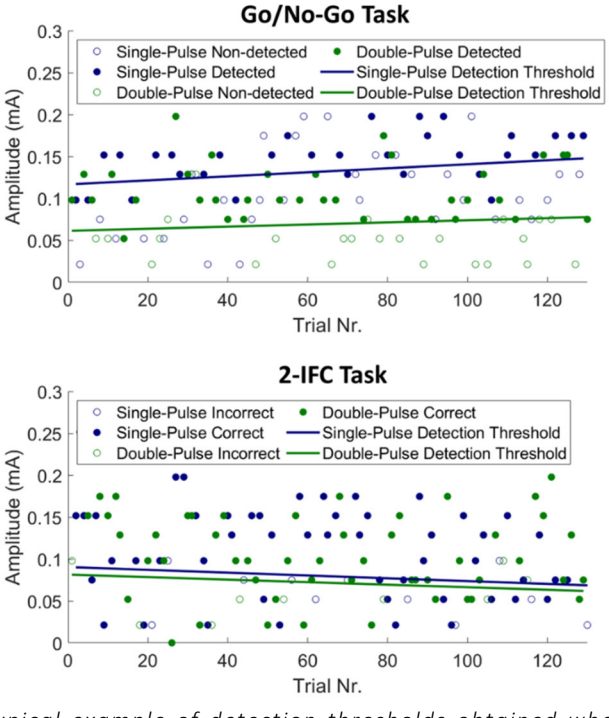

Figure 8.3: Typical example of detection thresholds obtained when performing a GN procedure (top) and when performing a 2IFC procedure (bottom). Detected and non-detected (GN) or correct and incorrect (2IFC) stimuli are depicted by closed and open circles respectively. When performing a 2IFC procedure, detection thresholds appeared to equalize for both stimulus types.

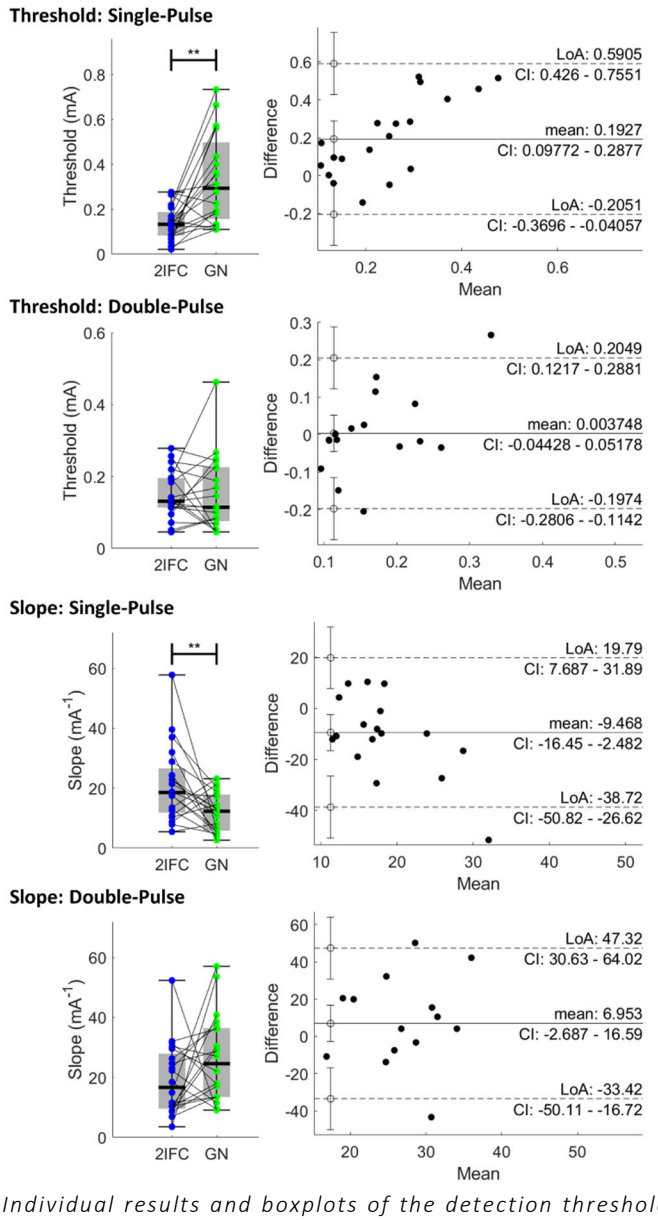

*Figure 8.4: Individual results and boxplots of the detection thresholds and slopes for single-pulse (SP) and double-pulse (DP) stimuli during the go-/no-go (GN) and the 2-interval forced choice (2IFC) procedure for a total of 20 participants. Significance is indicated with * (p<.05), ** (p<.01) and *** (p<.001). Detection thresholds for single-pulse stimuli were significantly lower and psychometric slopes were significantly larger when assessed in a 2IFC procedure in comparison with the GN procedure. Bland-Altmann plots are shown on the right and indicate that single-pulse detection thresholds and slopes are significantly biased and show that the difference between GN and 2IFC threshold estimates increases as the mean value of the estimates increases.*

Grand average evoked potentials at Cz-M1M2 for several levels of detection probability are displayed in Figure 8.6. There was a significant effect of detection probability on the evoked potential during both procedures and for both stimulus types. While the average evoked potential during a GN procedure appears graded with stimulus intensity, the average evoked potential during a 2IFC procedure remains low until high levels of detection probability are reached, i.e., a detection probability larger than 0.875. Both phenomena are more clearly visible in Figure 8.7, where the average amplitude of the major positive peak between 380 and 420 ms, the P2, is displayed. Here, the average P2 appears to increase almost proportional with respect to detection probability during the GN procedure. Note that this proportional increase with detection probability can be attributed to two phenomena: 1) The average P2 for detected stimuli is at almost every point significantly larger than the average P2 amplitude for non-detected stimuli, leading to an increased average P2 over all stimuli when more stimuli are detected. 2) There is an increasing trend in the average P2 for both detected and non-detected stimuli, leading to a further increase in the average P2 over all stimuli with respect to detection probability. Similar to previous figure, the average P2 during the 2IFC procedure remains low until a probability larger than 0.875 is reached.

8.4 Discussion

In this study, we observed nociceptive detection thresholds, psychometric slopes and central evoked potentials obtained during a GN and a 2IFC detection procedure. The differences observed between both procedures in nociceptive detection threshold and in evoked responses include important clues about how nociceptive detection might work, and how the threshold obtained during these procedures can be interpreted.

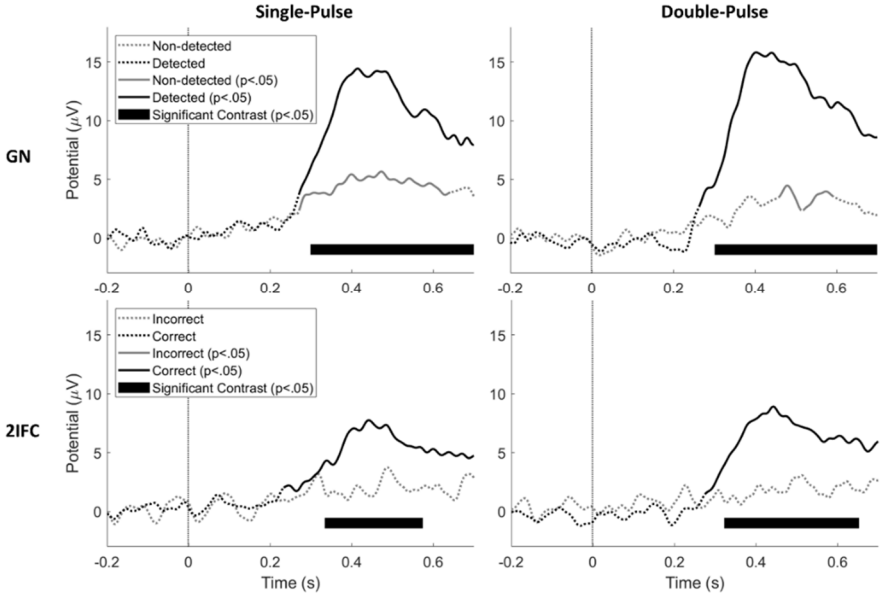

Figure 8.5: *Grand average evoked potential at Cz-M1M2 for stimuli acquired during both procedures. Significance with respect to baseline (p<.05) is indicated by a solid line, while insignificant parts are indicated by dotted lines. Latencies with a significant contrast (p<.05) between detected and non-detected (in GN procedure) and between correct and incorrect (in 2IFC procedure) are marked with a black bar.*

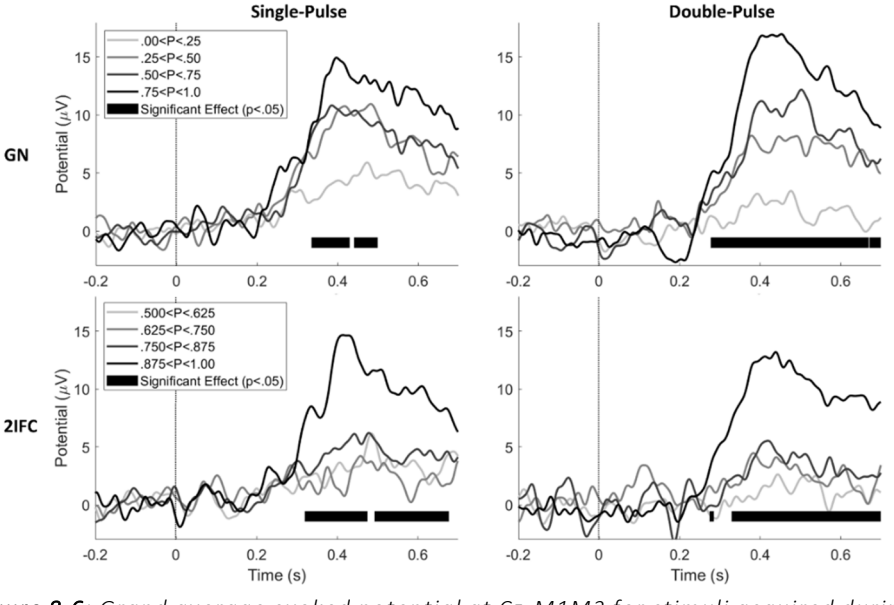

Figure 8.6: *Grand average evoked potential at Cz-M1M2 for stimuli acquired during both procedures at 4 levels of detection probability. Latencies with a significant effect of detection probability (p<.05) are marked with a black bar.*

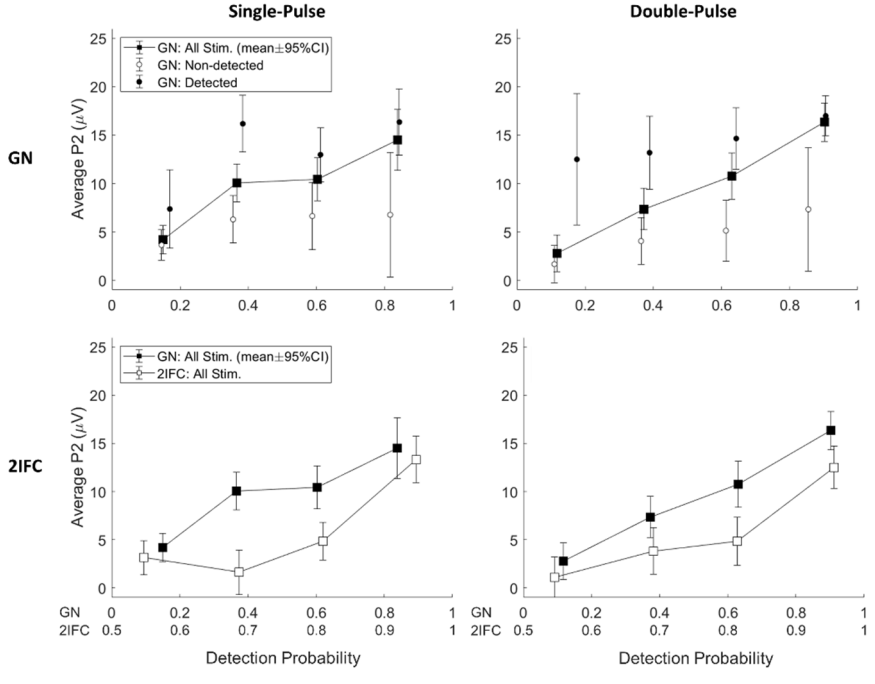

Figure 8.7: Average amplitude of P2 peak in the evoked potential (and 95%CI) with respect to detection probability. There is an almost proportional relation between the average P2 amplitude and detection probability. Average P2 amplitude is significantly larger for detected stimuli in comparison with non-detected stimuli and shows an increasing trend with respect to detection probability for both detected and non-detected stimuli. In the 2IFC procedure, the average P2 amplitude remains at very low levels (comparable with or even lower than non-detected stimuli) until a high detection probability (>0.8 for GN and >0.9 for 2IFC) is reached.

The first objective of this study was to determine if the nociceptive detection threshold during a GN procedure is biased by a response criterion. We found that the detection threshold for single-pulse intra-epidermal electric stimuli is significantly higher, and the psychometric slope significantly lower, during a GN procedure in comparison with a 2IFC procedure. In addition, this difference between both procedures appears to increase as the value of the estimated threshold or slope increases. In contrast, we found that the threshold for double-pulse stimuli does not differ significantly between procedures. In contrast, we found that the threshold for double-pulse stimuli does not differ

significantly between procedures. This result implies that for some types of stimuli the nociceptive detection threshold measured during a GN procedure reflects evoked neural activity exceeding a response criterion, rather than the presence of sensory evidence itself. Equal detection thresholds for double pulse stimuli between the GN and the 2IFC procedure indicate that the extent to which the observed detection threshold is influenced by the response criterion also depends on stimulus properties, and that the bias of the detection threshold introduced by a criterion might be lower for high signal-to-noise ratio stimuli such as the double-pulse stimulus in this experiment. In addition, a significant difference was observed between single- and double-pulse stimuli during a GN procedure, while no significant difference was observed between detection thresholds for single- and double-pulse stimuli during a 2IFC procedure. Although a small difference between the single- and double-pulse threshold might go unnoticed due to estimation errors, it is clear that the large difference between both stimulus types in a GN procedure almost completely disappears during 2IFC. The reason for this discrepancy between both tasks remains unclear without more sophisticated psychophysical modeling, which is out of the scope of this study. However, these results warrant the development of novel psychophysical models that are tailored to the process of nociception in future studies. One of the potential factors that might help explaining such a difference would be the presence of spontaneous neural activity influencing both the response criterion and psychometric slope of the participant. More importantly, formulation of psychophysical models that are connected to neurophysiological mechanisms can lead to more insight in the interpretation of the detection thresholds measured in a clinical or research setting.

The second objective of this study was to determine if the presence of a response criterion is reflected in the nociceptive evoked potentials observed in response to stimuli around the detection threshold. We measured a significant central evoked response at Cz-M1M2 during both procedures for detected stimuli (GN) and correctly reported trials (2IFC). We also measured a significant evoked response to non-detected stimuli (GN), which was absent for incorrectly reported trials (2IFC). We found that the evoked P2 response is proportionally graded with detection probability during a GN procedure. At the same time, we

observed that the P2 response during a 2IFC procedure for stimuli with the same detection probability (corrected for guessing rate), remains low until a large detection probability is reached. The P2 response to detected and non-detected stimuli show that we might be looking at a mostly dichotomous response, where the response is much larger for detected stimuli than for non-detected stimuli. The visual evoked P3 response is considered a key marker of conscious access to sensory evidence (Rutiku, Martin, Bachmann, & Aru, 2015; Salti, Bar-Haim, & Lamy, 2012), and the high degree of overlap in activated brain regions suggests a similar functional significance of the nociceptive P2 (Iannetti & Mouraux, 2010; Mouraux & Iannetti, 2009). Our observation that the P2 shows an on-off behavior with respect to reported conscious perception is in accordance with this theory.

Assuming that we are looking at an entirely dichotomous response, we can explore how the detection probability in both procedures relates to the stimulus amplitude and the associated probability of evoking a central brain response at Cz-M1M2. Figure 8.8 shows that the difference between detection probability and evoked response probability determines the observed pattern of the average P2 response in Figure 8.7. When there is no difference between the detection threshold and the threshold for evoking a brain response at 0.5 probability, both curves will overlap leading to a proportional relation between the evoked response probability (or average P2) and the detection probability, as we observed for the GN procedure. When the detection threshold is lower than the threshold for evoking a brain response, we expect a bended curve which predicts that the evoked response probability (or average P2) remains low until a high detection probability is reached, as we observed for the 2IFC procedure. As such, our results suggest that the evoked response probability is equal to the detection probability in the GN procedure, but lower than the detection probability in the 2IFC procedure, implying that the probability of evoked a P2 response was approximately equal to the probability of a stimulus being detected in the GN procedure. Our data indicates that the P2 might be modulated by both conscious stimulus detection and detection probability, however, the effect of stimulus detection appeared to be much larger. If we interpret this increase of the P2 with respect to stimulus detection as a marker

for conscious access to sensory evidence, the response criterion observed in this experiment could be interpreted as a perceptual criterion, i.e., only stimuli above this criterion are perceived. This also implies that the average P2 responses observed during a GN procedure are affected by a response criterion just like the participant responses itself, when they are not corrected for stimulus detection.

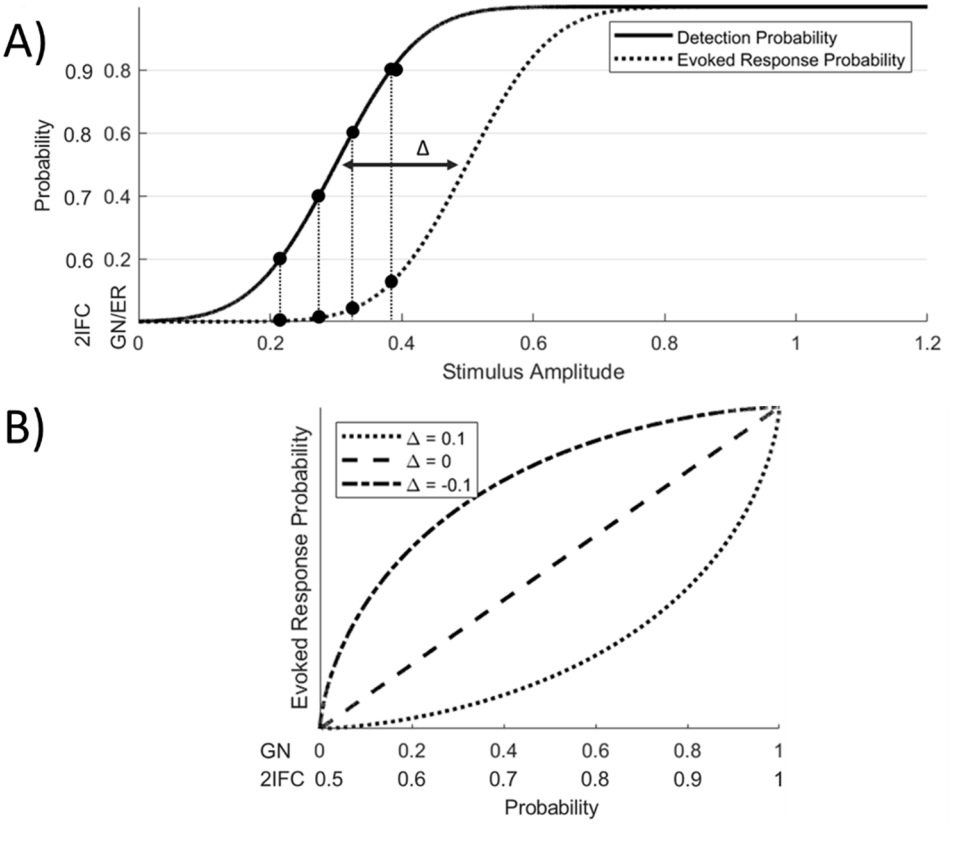

***Figure 8.7**: The difference between detection probability and evoked response probability (A) determines the relation between detection probability and average evoked response (B).*

These observations show that when the nociceptive detection threshold is assessed using a GN procedure, one might observe the effect of an adjusted perceptual criterion rather than altered nociceptive processing following an intervention. This has important consequences for studies using nociceptive detection thresholds to assess altered central and peripheral nociceptive processing. The mechanical and thermal detection threshold are increased in patients with neuropathic pain and signs of central sensitization (Maier et al., 2010). Thermal heat and cold detection thresholds show a high sensitivity to potential peripheral nerve damage by diabetes (Courtin et al., 2020) as well as painfulness in diabetic neuropathies (Krämer, Rolke, Bickel, & Birklein, 2004). Intra-epidermal electric detection thresholds are increased following deafferentation by capsaicin (Doll et al., 2016) and following diabetic neuropathy (Suzuki et al., 2016). Our current results emphasize that these nociceptive detection thresholds can in some cases reflect a central criterion that determines if the stimulus is consciously perceived, rather than the threshold for activation of the nociceptive system itself. This criterion does not only affect participant report, but also the central P2 response, which appeared to be generated only when the stimulus was reported as consciously perceived, i.e., when the stimulus exceeded a perceptual criterion. The notion that we can measure the potential influence of a perceptual criterion by comparing detection thresholds in a GN and 2IFC procedures opens up new avenues of research into the role of perception in nociceptive processing and (chronic) pain.

8.5 References

Bland, J. M., & Altman, D. G. (1986). Statistical methods for assessing agreement between two methods of clinical measurement. *Lancet, 1*(8476), 307-310.

Coleman, T. F., & Li, Y. (1996). An Interior Trust Region Approach for Nonlinear Minimization Subject to Bounds. *SIAM Journal on Optimization, 6*(2), 418-445.

Courtin, A. S., Maldonado Slootjes, S., Caty, G., Hermans, M. P., Plaghki, L., & Mouraux, A. (2020). Assessing thermal sensitivity using transient heat and cold stimuli combined with a Bayesian adaptive method in a clinical setting: A proof of concept study. *European Journal of Pain, 24*(9), 1812-1821.

Delorme, A., Sejnowski, T., & Makeig, S. (2007). Enhanced detection of artifacts in EEG data using higher-order statistics and independent component analysis. *NeuroImage, 34*(4), 1443-1449.

Doll, R. J., Maten, A. C. A., Spaan, S. P. G., Veltink, P. H., & Buitenweg, J. R. (2016). Effect of temporal stimulus properties on the nociceptive detection probability using intra-epidermal electrical stimulation. *Experimental Brain Research, 234*(1), 219-227.

Doll, R. J., van Amerongen, G., Hay, J. L., Groeneveld, G. J., Veltink, P. H., & Buitenweg, J. R. (2016). Responsiveness of electrical nociceptive detection thresholds to capsaicin (8 %)-induced changes in nociceptive processing. *Experimental Brain Research, 234*(9), 2505-2514.

Doll, R. J., Veltink, P. H., & Buitenweg, J. R. (2015). Observation of time-dependent psychophysical functions and accounting for threshold drifts. *Attention, Perception, and Psychophysics, 77*(4), 1440-1447.

Georgeson, M. (2012). Sensory, perceptual and response biases: the criterion concept in perception. *Journal of Vision, 12*(9), 1392-1392.

Hochberg, Y., & Benjamini, Y. (1995). Controlling the false discovery rate: A Practical and powerful approach to multiple testing. *J.Roy.Statist.Soc., 57*, 289-300.

Iannetti, G. D., & Mouraux, A. (2010). From the neuromatrix to the pain matrix (and back). *Experimental Brain Research, 205*(1), 1-12.

Kingdom, F. A. A., & Prins, N. (2016). Chapter 6 - Signal Detection Measures∗. In F. A. A. Kingdom & N. Prins (Eds.), *Psychophysics (Second Edition)* (pp. 149-188). San Diego: Academic Press.

Krämer, H. H., Rolke, R., Bickel, A., & Birklein, F. (2004). Thermal thresholds predict painfulness of diabetic neuropathies. *Diabetes Care, 27*(10), 2386-2391.

Legrain, V., Guérit, J. M., Bruyer, R., & Plaghki, L. (2002). Attentional modulation of the nociceptive processing into the human brain: Selective spatial attention, probability of stimulus occurrence, and target detection effects on laser evoked potentials. *Pain, 99*(1-2), 21-39.

Legrain, V., Iannetti, G. D., Plaghki, L., & Mouraux, A. (2011). The pain matrix reloaded: A salience detection system for the body. *Progress in Neurobiology, 93*(1), 111-124.

Maier, C., Baron, R., Tölle, T. R., Binder, A., Birbaumer, N., Birklein, F., . . . Treede, D. R. (2010). Quantitative sensory testing in the German Research Network on Neuropathic Pain (DFNS): somatosensory abnormalities in 1236 patients with different neuropathic pain syndromes. *Pain, 150*(3), 439-450.

Maris, E., & Oostenveld, R. (2007). Nonparametric statistical testing of EEG- and MEG-data. *Journal of Neuroscience Methods, 164*(1), 177-190.

Mouraux, A., & Iannetti, G. D. (2009). Nociceptive Laser-Evoked Brain Potentials Do Not Reflect Nociceptive-Specific Neural Activity. *Journal of Neurophysiology, 101*(6), 3258-3269.

Mouraux, A., & Iannetti, G. D. (2018). The search for pain biomarkers in the human brain. *Brain, 141*(12), 3290-3307.

Mouraux, A., Iannetti, G. D., & Plaghki, L. (2010). Low intensity intra-epidermal electrical stimulation can activate Aδ-nociceptors selectively. *Pain, 150(1)*, 199-207.

Mouraux, A., Marot, E., & Legrain, V. (2014). Short trains of intra-epidermal electrical stimulation to elicit reliable behavioral and electrophysiological responses to the selective activation of nociceptors in humans. *Neuroscience Letters, 561*(Supplement C), 69-73.

Oostenveld, R., Fries, P., Maris, E., & Schoffelen, J. M. (2011). FieldTrip: Open source software for advanced analysis of MEG, EEG, and invasive electrophysiological data. *Computational Intelligence and Neuroscience, 2011*.

Picton, T. W. (1992). The P300 wave of the human event-related potential. *Journal of Clinical Neurophysiology, 9*(4), 456-479.

Poulsen, A. H., Tigerholm, J., Meijs, S., Andersen, O. K., & Mørch, C. D. (2020). Comparison of existing electrode designs for preferential activation of cutaneous nociceptors. *Journal of Neural Engineering*.

Rutiku, R., Martin, M., Bachmann, T., & Aru, J. (2015). Does the P300 reflect conscious perception or its consequences? *Neuroscience, 298*, 180-189.

Salti, M., Bar-Haim, Y., & Lamy, D. (2012). The P3 component of the ERP reflects conscious perception, not confidence. *Conscious Cogn, 21*(2), 961-968.

Steenbergen, P., Buitenweg, J. R., Trojan, J., van der Heide, E. M., van den Heuvel, T., Flor, H., & Veltink, P. H. (2012). A system for inducing concurrent tactile and nociceptive sensations at the same site using electrocutaneous stimulation. *Behavior Research Methods, 44*(4), 924-933.

Steenbergen, P., Buitenweg, J. R., Trojan, J., van der Heide, E. M., van den Heuvel, T., Flor, H., & Veltink, P. H. (2012). A system for inducing concurrent tactile and nociceptive sensations at the same site using electrocutaneous stimulation. *Behavior research methods, 44(4)*, 924-933.

Suzuki, C., Kon, T., Funamizu, Y., Ueno, T., Haga, R., Nishijima, H., . . . Baba, M. (2016). Elevated pain threshold in patients with asymptomatic diabetic neuropathy: an intraepidermal electrical stimulation study. *Muscle Nerve, 54*(1), 146-149.

Ugray, Z., Lasdon, L., Plummer, J., Glover, F., Kelly, J., & Martí, R. (2007). Scatter Search and Local NLP Solvers: A Multistart Framework for Global Optimization. *INFORMS Journal on Computing, 19*(3), 328-340.

van den Berg, B., & Buitenweg, J. R. (2021). Observation of Nociceptive Processing: Effect of Intra-Epidermal Electric Stimulus Properties on Detection Probability and Evoked Potentials. *Brain Topography*.

van den Berg, B., Doll, R. J., Mentink, A. L. H., Siebenga, P. S., Groeneveld, G. J., & Buitenweg, J. R. (2020). Simultaneous tracking of psychophysical detection thresholds and evoked potentials to study nociceptive processing. *Behavior Research Methods*.

van den Broeke, E. N., Mouraux, A., Groneberg, A. H., Pfau, D. B., Treede, R.-D., & Klein, T. (2015). Characterizing pinprick-evoked brain potentials before and after experimentally induced secondary hyperalgesia. *Journal of Neurophysiology, 114*(5), 2672-2681.

Wager, T. D., Matre, D., & Casey, K. L. (2006). Placebo effects in laser-evoked pain potentials. *Brain, Behavior, and Immunity, 20*(3), 219-230.

8

Chapter 9

Psychophysical Models for Detection of Single- and Double-Pulse Electronociceptive Stimuli: Implications for Interpretation of Clinical Observations

To be submitted as:

Van den Berg, B., Berfelo, T., Jansen, N., & Buitenweg, J. R., Psychophysical models for detection of single- and double-pulse electronociceptive stimuli: implications for interpretation of clinical observations.

Abstract

Observation of altered nociceptive processing is key to increase our understanding of underlying mechanisms and diagnostic abilities in chronic pain syndromes. In recent studies, we observed increased psychometric detection thresholds and decreased slopes in patients with failed back surgery syndrome (FBSS), in response to single- and double-pulse electro-nociceptive stimuli. It remains unknown how changes in nociceptive detection thresholds can be related to known mechanisms of nociceptive dysfunction. In this work, our first objective was to derive a conceptual psychophysical model for detection of both single- and double-pulse nociceptive stimuli and to compare this model with simpler alternatives based on additional assumptions, to justify the choice of model parameters. Our second objective was to use this model for retrospective analysis of FBSS patient data, to explore potential mechanisms. We derived a model for stimulus detection during a Go-/No-Go procedure at a single location, assuming that a stimulus is detected when maximum neural activity exceeds a response criterion. Performance of the model and alternative models was compared using AIC, accuracy, and optimizer convergence in 25 healthy university participants, 17 healthy hospital participants and 16 FBSS patients. Model parameters were compared between healthy participants and patients. We found that the derived model performed better than alternative models with less parameters in terms of preselected criteria. Model simplification might increase sensitivity to altered nociceptive processing in FBSS by increasing parameter significance. A decrease in parameter value in all models in patients suggests that increased detection thresholds and decreased slopes are potentially caused by increased spontaneous neural activity.

9.1 Introduction

New techniques for observation of altered nociceptive processing in human subjects could help to shed more light into underlying mechanisms, like central sensitization, and the development of chronic pain. Recently, we developed a method to explore peripheral and central nociceptive processing mechanisms using a rich set of single- and double-pulse nociceptive stimuli applied around the detection threshold (Doll, Maten, Spaan, Veltink, & Buitenweg, 2016; van den Berg & Buitenweg, 2021; van den Berg et al., 2020). Afferent nociceptive nerve fibers in the skin are targeted selectively by intra-epidermal electric pulses of less than twice the detection threshold (Mouraux, 2010). By measuring the detection threshold, we assess the quantity of neural activity required for stimulus perception. By varying the number of applied pulses and the interval between pulses, we can differentially activate peripheral and central mechanisms in the nociceptive system and study the properties of those mechanisms based on the observed detection probability of each stimulus type.

Recently, we started to apply this technique in a clinical setting to explore whether chronic pain is associated with local and generalized changes in nociceptive processing in patients with failed back surgery syndrome (FBSS) eligible for neurostimulation treatment, as these patients suffer from long-term neuropathic pain with a potential shift towards nociplastic pain. A first study on FBSS patients explored the feasibility of using the technique in a small sample of patients with unilateral limb pain treated by DRG stimulation. It was found that the NDT method can be applied successfully. In addition, the study explored if it was possible to observe a difference in single-and double-pulse stimuli in the affected and unaffected limb. It was found that the nociceptive sensitivity dramatically decreased in the affected limb, leading to a significant increase of single- and double-pulse detection thresholds and a significant decrease of both psychometric slopes. Subsequently, the study explored in the same patients whether pain relief by stimulation with an implanted dorsal-root-ganglion (DRG) stimulator would normalize sensitivity. It was found that detection thresholds and psychometric slopes normalized to the same level in

the affected and unaffected limb, suggesting that the technique seems to measure DRG treatment effects, which corresponded with patient reports (Berfelo, Doll, Krabbenbos, & Buitenweg, 2022). In a recent study, we investigated if chronic pain in FBSS was also associated with a generalized reduction in nociceptive sensitivity. We found that the nociceptive sensitivity was dramatically decreased in FBSS patients in comparison to healthy controls, again leading to a significant increase of single- and double-pulse detection thresholds and a significant decrease of both psychometric slopes (Berfelo, Van den Berg, Krabbenbos, & Buitenweg, 2021). These results indicate that measuring nociceptive sensitivity to single- and double-pulse nociceptive stimuli could be a useful tool to evaluate nociceptive processing in a clinical setting.

Despite these remarkable differences observed between the affected and unaffected limb and between chronic pain patients and healthy controls, we do not yet understand how changes in nociceptive detection thresholds can be related to known mechanisms of nociceptive dysfunction. It is necessary to derive models of the association between neural activity evoked by a single- or double-pulse stimulus and detection probability to understand how altered nociceptive processing might lead to differences in detection thresholds and psychometric slopes in chronic pain patients.

In this work, we aim to formulate and explore a psychophysical model for observation of altered nociceptive processing of single- and double-pulse intra-epidermal electric stimuli in chronic pain patients. Our first objective was to derive a conceptual psychophysical model for detection of both single- and double-pulse nociceptive stimuli and to compare this model with simpler alternative models based on additional assumptions, to justify the choice of model parameters. Our second objective was to use these models for retrospective analysis of data from patients with FBSS, to explore if we can observe maladaptive nociceptive mechanisms through estimation of psychophysical model parameters.

9.1.1 Conceptual Model

We model nociception at a single location of the body as a stochastic psychophysical channel followed by a decision unit (Figure 9.1), and study nociceptive processing by characterizing the properties of this channel. Channel properties are observed by applying a rich set of nociceptive stimuli and observing stimulus-response relations. Information on this channel is encoded by neural activity. Where this channel ends, and where the decision unit is located, remains an open question. In earlier modeling studies such as Yang et al. (Yang, Meijer, Doll, Buitenweg, & van Gils, 2015) and Tanaka et al. (Tanaka et al., 2021) the decision unit is defined as the central neurons after the first synapse, and in Tigerholm et al. (Tigerholm, Poulsen, Andersen, & Mørch, 2019) the decision unit is defined as the peripheral neuron itself. Meanwhile, other literature indicates that the decision unit might be in our brain (Dehaene & Changeux, 2011). Also, the scope of this channel remains unclear, and could range from a few neuronal fibers having the receptive field of a single patch of skin to the collection of fibers on the entire body surface. Furthermore, we stress that the scope of the channel under investigation can potentially be modulated by top-down attentional modulation.

Instantaneous neural activity is defined by the firing rate, which has a lower limit of zero. Instantaneous firing rate tends to be distributed as log-normal or normal depending on if neurons follow a mean-driven or fluctuation-drive regime (Buzsáki & Mizuseki, 2014; Petersen & Berg, 2016; Roxin, Brunel, Hansel, Mongillo, & van Vreeswijk, 2011). Also note that the average instantaneous firing rate will converge to a normal distribution when considering a very large population of neurons, according to the central limit theorem. Importantly, the channel does not only contain neural activity related to the stimulus, but also spontaneous activity, which is a potential driving force of central sensitization associated with neuropathic pain (Devor, 2009; Latremoliere & Woolf, 2009; North et al., 2019). A necessary but not sufficient condition for stimulus perception is the presence of neural activity in terms of an instantaneous neural firing rate larger than zero, assuming that no perception can occur when no action potentials are generated. Each pulse

delivered to the system results in a temporary increase of neural activity. We assume that neural activity in response to a second pulse adds up to neural activity generated by the first pulse. Mathematically, each pulse generates an arbitrary impulse response on the channel, which sums up to the impulse response of a previous pulse.

Stimulus detection takes place by estimating if a stimulus was applied within a fixed period of time by observing average neural activity, modeled by a stochastic channel $Y(x(t))$ (Figure 9.1). We assume that reported stimulus detection by the decision unit follows the maximum rule, i.e., a stimulus is reported as detected when the maximum value of neural activity within the interval exceeds the detection threshold. Therefore, when evoked neural activity at time t, $Y(x(t))$, is larger than a response criterion $D(t)$, this will result in sufficient firing rate to result in conscious stimulus perception. The probability that the potential exceeds the response criterion at a single point in time, is equal to one minus the probability that a stimulus is lower than the response criterion at this time point, which is described by the cumulative density function of $Y(x(t))$, denoted as $F_Y(x(t), D(t))$. As a consequence, we can model the probability that a stimulus is detected using the geometric integral in Equation (1).

$$P_d = P(\max(Y(x(t)) > D(t)) = 1 - P(\max(Y(x(t)) < D(t)) \quad (1)$$
$$= 1 - \prod_{t=t_1}^{t_2} F_Y(x(t), D(t))^{dt}$$

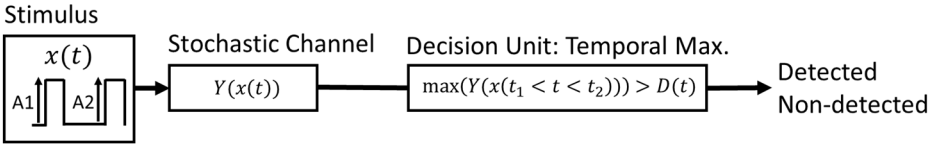

Figure 9.1: *Conceptual model where a stimulus x(t) results in an average neural firing rate through a random process Y(x(t)). Stimulus detection follows the maximum rule, i.e., a stimulus is detected if the average neural firing rate Y(x(t)) exceeds a response criterion D(t) within a fixed interval of time.*

9.1.2 Psychophysical Model

Equation (1) has to be reduced to a finite number of parameters which can be estimated during a single psychophysical experiment. We consider simplifications based on the assumption that each pulse only leads to a local peak in neural activity. When observing only spontaneous activity, which we will refer to as noise, the maximum over the observed interval will approach an extreme-value distribution when the observed interval goes to infinite. We will assume that the observed interval is long enough to result in an extreme value distribution of maximum noise, which is a Gumbel distribution in the case of a normal or log-normal distribution.

Under these assumptions, when only a single peak is present in the waveform that is much higher than the level of noise, this peak will determine the detection probability of the stimulus, as the peak maximum will always be larger than the maximum over the rest of the trial (Figure 9.2a and 9.2e). However, when this single peak is close to noise level, the detection probability will depend on the maximum between peak amplitude and maximum noise, resulting in a generalized extreme value distribution (Figure 9.2b and 9.2e). If one of two peaks is significantly larger than the other, the maximum of this peak will always be larger than the rest of the trial and determine detection probability (Figure 9.2c and 9.2e). However, if two peaks are of approximately equal amplitude, detection probability will depend on the distribution of each of those two peaks (Figure 9.2d and 9.2e). Note that a crucial insight here, is that the distribution of evoked neural activity depends on stimulus amplitude, the number of pulses, and the amount of spontaneous neural activity. The resulting detection probability can be modeled by plugging the cumulative density function(s) of the maximum of one or multiple peaks, and the cumulative density function of maximum noise, into Equation (1).

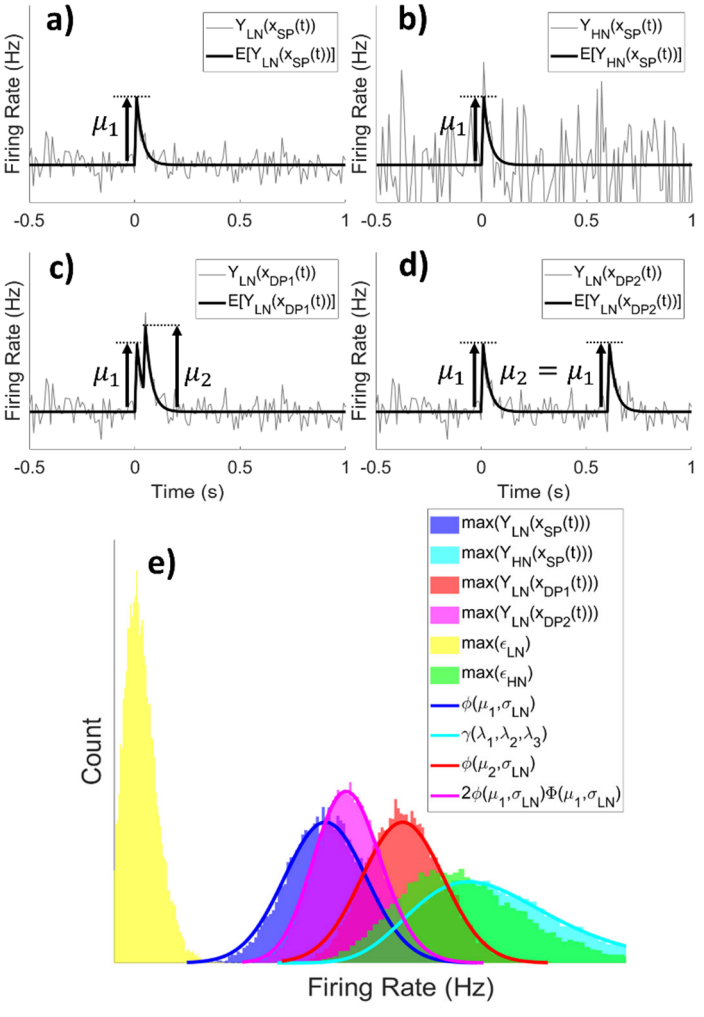

Figure 9.2: *Simulated waveforms of neural firing rate where the random process has a normal distribution, for the scenario that a) the noise is low (LN) with respect to the peak evoked by a single pulse (SP), b) the noise is high (HN) with respect to the peak evoked by a single pulse (SP), c) the noise is low (LN) with respect to the peaks evoked by a double-pulse with short inter-pulse interval (DP1), and d) the noise is low (LN) with respect to the peaks evoked by a double-pulse with long inter-pulse interval (DP2). In e) the histogram of maximum values for each waveform over 20000 realizations is displayed. Note that the maximum value distribution of a) and c is described by the normal probability density functions* $\phi(\mu_1, \sigma_{low})$ *and* $\phi(\mu_2, \sigma_{low})$ *respectively. The maximum value distribution of b, where the stimulus is close to noise levels is described by a generalized extreme value density function* $\gamma(\lambda_1, \lambda_2, \lambda_3)$*. The maximum value distribution of d where both peaks have a similar value is described by the distribution of the maximum of both peaks, which is given by the product of the probability and cumulative density function,* $2\phi(\mu_1, \sigma_{low})\Phi(\mu_1, \sigma_{low})$*, in the case of two normal distributions with equal means.*

The amplitude of each stimulus-evoked peak is a function of the average neural activity before stimulation [β_0] and the increase of neural activity due to stimulation [$\psi_1(A)$] with an amplitude [A] (Equation (2.1)). The amplitude of a second peak can be increased by activity caused by the first peak [$\psi_1(A)\xi(\delta)$], dependent on the inter-pulse interval [δ] (Equation (2.2)). The probability that stimulus-evoked neural activity is lower than the response criterion is modeled by the cumulative distribution of the evoked peak [$F_Y(x(\tau_1), D)$]. The probability that the maximum of a large number of samples of spontaneous activity is lower than the response criterion [D] is described by the product of the cumulative distribution of noise at each time instant (Equation (2.3a)). In case of a cumulative normal or log-normal distribution, this probability is described by a cumulative Gumbel distribution (Equation (2.3b)).

We can simplify Equation (1) to an observable psychophysical model by assuming that the detection probability is determined by the amplitude of each peak and the maximum of spontaneous activity. By using these terms in Equation (1), we arrive at the psychophysical model in Equation (2.4a), where the probability that a stimulus is detected is modeled as one minus the probability that the stimulus is not detected, i.e. one minus the probability that instantaneous neural activity evoked by the first pulse is lower than D [$F_Y(x(\tau_1), D)$] times the probability that instantaneous neural activity evoked by the second pulse is lower than D [$F_Y(x(\tau_1), D)$] time the probability that the maximum of spontaneous activity is lower than D [η]. In case of a normal distribution of evoked neural activity, this can be rewritten to the form in Equation (2.4b).

Peak amplitude after one pulse:

$$\mu_{\tau 1} = \beta_0 + \psi_1(A) \tag{2.1}$$

Peak amplitude after a second pulse:

$$\mu_{\tau 2} = \beta_0 + \psi_1(A)\xi(\delta) + \psi_2(A) \tag{2.2}$$

Probability of spontaneous activity being lower than time dependent response criterion $D(t)$:

$$\eta(t) = \lim_{k\to\infty} \prod_{i=1}^{k} F_{noise}\left(\boldsymbol{\varepsilon}(t_i), D(t_i)\right) \tag{2.3a}$$

with $t_i = i\frac{T}{k}$ and $k \in \mathbb{Z}^+$ and $\boldsymbol{\varepsilon}$ the parameters defining the cumulative distribution function

$$\eta = \lim_{k\to\infty} \prod_{i=1}^{k} \Phi\left(\frac{D-\mu_{noise}}{\sigma_{noise}}\right) = G\left(g_0 + g_1\left(\frac{D-\mu_{noise}}{\sigma_{noise}}\right)\right) = e^{-exp\left(-\left(g_0+g_1\left(\frac{D-\mu_{noise}}{\sigma_{noise}}\right)\right)\right)} \tag{2.3b}$$

Psychophysical model:

$$P_d = 1 - F_Y(x(\tau_1), D)F_Y(x(\tau_2), D)\eta \tag{2.4a}$$

$$P_d = 1 - \Phi\left(\frac{D-\mu_{\tau1}}{\sigma_{\tau1}}\right)\Phi\left(\frac{D-\mu_{\tau2}}{\sigma_{\tau2}}\right)\eta = 1 - \left(1 - \Phi\left(\frac{\mu_{\tau1}-D}{\sigma_{\tau1}}\right)\right)\left(1 - \Phi\left(\frac{\mu_{\tau2}-D}{\sigma_{\tau2}}\right)\right)\eta \tag{2.4b}$$

9.1.3 Further Considerations

At this moment, we do not know which form the transducer functions of both pulses [$\psi_1(A)$ and $\psi_2(A)$] might take and which distribution best describes spontaneous and evoked neural activity. In this work, we will use a linear transducer function for each pulse [$\beta_{A1}A$ and $\beta_{A2}A$] and use a normal distribution for evoked neural activity, assuming that the distribution is normalized by activation of a large number of nerve fibers. Taking a linear term for each transducer function, we arrive at Equation (3.1). The response criterion is modeled as an initial value [β_D] plus an additional criterion drift over time [$\beta_t t$], as all of our recent studies showed a significant drift of the detection threshold over time (Van den Berg & Buitenweg, 2018, 2021; van den Berg et al., 2020).

In addition, we consider two alternative models based on Equation (2.5b), that might lead to a lower information criterion due to a lower number of parameters. The participant might set the response criterion much higher than the amplitude of spontaneous neural activity, effectively making the

probability that spontaneous activity ever exceeds the criterion negligible (Equation 3.2). This situation might occur when the amount of spontaneous activity is very low, for example, in healthy subjects where the number of spontaneous discharges in nociceptive dorsal-root-ganglion cells is very low (North et al., 2019). The peak in neural activity following the second pulse could be consistently larger than the peak of the first pulse or spontaneous neural activity, e.g., in case of temporal summation of neural activity evoked by the second pulse to neural activity evoked by the first pulse. Earlier studies suggest that such a temporal summation might occur, as the observed detection probability of double-pulse stimuli was consistently higher than the detection probability predicted based on probability multiplication alone (Doll, Maten, Spaan, Veltink, & Buitenweg, 2016). If this is the case, the detection probability is only a function of the amplitude of the dominant peak, i.e., the peak of the first pulse for a single-pulse stimulus and the peak of the second pulse in case of a double-pulse stimulus (Equation 3.3).

Complete model:

$$P_d = 1 - \left(1 - \Phi\left(\frac{-\beta_{D0} - \beta_t + \beta_{A1}A}{\sigma_{\tau 1}}\right)\right)\left(1 - \Phi\left(\frac{-\beta_{D0} - \beta_t + \beta_{A2}A}{\sigma_{\tau 2}}\right)\right)^{n-1} G(g_{D01} + g_{t1}t) \quad (3.1)$$

Where $\beta_{D0} = -\beta_D + \beta_0$ and $g_{D01} = g_0 + \frac{g_1\beta_D - \mu_{noise}}{\sigma_{noise}}$ and $g_{t1} = \frac{g_t\beta_t}{\sigma_{noise}}$

High criterion:

$$P_d = 1 - \left(1 - \Phi\left(\frac{-\beta_{D0} - \beta_t + \beta_{A1}A}{\sigma_{\tau 1}}\right)\right)\left(1 - \Phi\left(\frac{-\beta_{D0} - \beta_t + \beta_{A2}A}{\sigma_{\tau 2}}\right)\right)^{n-1} \quad (3.2)$$

Single dominant peak:

$$P_d = \Phi\left(\frac{-\beta_{D0} - \beta_t + \beta_{A1}A + (n-1)\beta_{A2}A}{\sigma_{\tau 2}}\right) \quad (3.3)$$

9.2 Methods

The experiments presented in this work included measurements of the detection threshold and the electroencephalogram (EEG) with respect to intra-epidermal stimuli in experiments at the University of Twente and the St. Antonius Hospital Nieuwegein, the Netherlands. For this work, only the stimulus-response pairs acquired for detection threshold measurement were used. All experiments were approved by the local Medical Review and Ethics Committee and in accordance with the declaration of Helsinki. All participants provided written informed consent prior to participation.

9.2.1 Participants

The first study (University of Twente) included a total of 25 healthy participants (16 males, age 23.0 ± 3.6). In this study, one experiment was conducted to estimate the detection threshold on the right hand in each participant. The second study included a total of 17 healthy participants (3 males, age 35.9 ± 11.9) and a total of 16 patients with a diagnosis of FBSS (9 males, age 50.1 ± 9.1). In this study, two experiments were conducted to estimate the detection threshold in the right hand and the detection threshold in the left hand in each participant. For more details about the study populations, please refer to (van den Berg & Buitenweg, 2021) and (Berfelo, Van den Berg, Krabbenbos, & Buitenweg, 2021).

9.2.2 Stimuli

Participants were stimulated with intra-epidermal electric stimuli on the dorsal hand using an electrode consisting of 5 interconnected microneedles (Steenbergen, 2012). Electric stimuli were generated using a constant current stimulator (NociTRACK AmbuStim, University of Twente, Enschede, The Netherlands). Intra-epidermal electric stimulation activates nociceptive afferent nerve fibers in the skin when applied at intensities of less than twice the nociceptive detection threshold (Mouraux, 2010; Poulsen, Tigerholm, Meijs, Andersen, & Mørch, 2020). Stimuli consisted of either 1) a single cathodic

square-wave pulse with a pulse width of 210 µs, 2) a double cathodic square-wave pulse with a pulse width of 210 µs and an inter-pulse interval of 10 ms, or 3) a double cathodic square-wave pulse with a pulse width of 210 µs and an inter-pulse interval of 40 ms.

9.2.3 Procedure

Participants were seated in a comfortable chair and instructed to focus their attention on the stimulation electrode. For familiarization, stimulus amplitude was increased in steps of 0.025 mA until participants reported to clearly perceive a stimulus below the electrode. An initial estimate of the detection threshold was obtained for each stimulus type by increasing the stimulus amplitude in steps of 0.025 mA until participants reported to perceive a sensation around the electrode that they ascribed to stimulation. Subsequently, stimuli were selected using an adaptive probing procedure designed to estimate and track the detection threshold (Doll, Veltink, & Buitenweg, 2015; van den Berg & Buitenweg, 2021) (Figure 9.3). For each stimulus type, an initial set of five equidistant stimulus amplitudes with a step size of 0.025 mA was initialized around the initial estimate of the detection threshold. Participants were instructed to press and hold a button and to release the button whenever any sensation was perceived that they ascribed to stimulation. For each stimulus, one of the five stimulus amplitudes was randomly selected. If the participants released the button within 1 s of stimulation, the stimulus was recorded as detected, after which the set of stimulus amplitudes was decreased by 0.025 mA. If the participants did not release the button within 1 s of stimulation, the stimulus was recorded as non-detected, after which the set of stimulus amplitudes was increased by 0.025 mA. This procedure was used to estimate and track detection thresholds for all three different stimulus types independently, with a total of 150 stimuli per stimulus type.

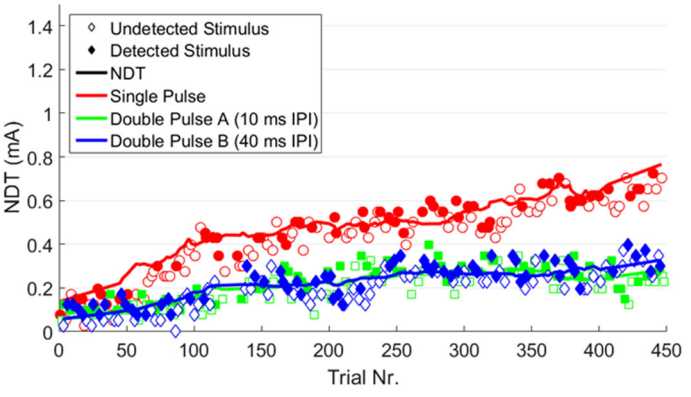

Figure 9.3: *Example of an experiment using adaptive probing (Doll, Veltink, & Buitenweg, 2015) with three stimulus types. Single-pulse stimuli, double-pulse stimuli with 10ms IPI, and double-pulse stimuli with 40ms IPI, are indicated by circles, squares, and diamonds respectively. Each nociceptive detection threshold (NDT) is tracked by random selection of an adaptive set of 5 equidistant (0.025 mA) stimulus amplitudes. The set of stimulus amplitudes is decreased by 0.025 mA when a stimulus is detected and increased by 0.025 mA when a stimulus was not detected.*

9.2.4 Analysis

To compare the models described by equations (3.1) to (3.3), models were optimized for each measurement by global optimization of the negative log-likelihood using an implementation of the GlobalSearch algorithm (Ugray et al., 2007) in combination with an interior-point algorithm to find local minima (Coleman & Li, 1996) in Matlab. Models were compared in each population and for each inter-pulse interval based on 4 criteria, of which the first two were derived from the Akaike information criterion (AIC) (Akaike, 1974):

- The median AIC scores.
- The percentage of experiments where the model achieved the lowest AIC scores.
- The prediction accuracy.
- The percentage of measurements where the optimizer converged to a solution.

The models in Equations (3.1) to (3.3) were used to derive model parameters for each stimulus type in each participant to study detection behavior.

9.3 Results

9.3.1 Model Selection

The derived models are compared in each population for stimuli with an inter-pulse interval of 10 ms and stimuli with an inter-pulse interval of 40 ms in Tables 9.1 and 9.2 respectively. Tables 9.1 and 9.2 show that either the complete model, including both peaks in neural activity and the influence of spontaneous neural activity (Equation (3.1)), or the simplified high criterion model assuming spontaneous activity is negligible (Equation (3.2)) are preferred for an inter-pulse interval of 10 ms and 40 ms. However, also note that for a significant part of the participants, ranging from 15.2 to 30.3 %, the simplified model that assumes presence of a single dominant peak (Equation (3.3)) achieves the lowest AIC.

IPI: 10ms Group & Model	Median AIC	Lowest AIC (%)	Accuracy (%)	Converged (%)
Healthy (university):				
Complete Model	**349.2**	32.0	**70.7**	100
High Criterion	349.8	**40.0**	69.8	100
Single Dominant Peak	363.0	28.0	68.9	100
Healthy (hospital):				
Complete Model	354.9	**38.2**	**72.2**	100
High Criterion	**351.2**	**38.2**	71.5	100
Single Dominant Peak	360.9	23.5	70.5	100
FBSS (hospital):				
Complete Model	**377.7**	**45.5**	**68.1**	100
High Criterion	379.8	24.2	67.4	100
Single Dominant Peak	387.7	30.3	66.2	100

*Table 9.1: Model comparison for stimuli with an inter-pulse interval of 10 ms. The lowest median AIC values, and the highest percentages for lowest AIC and accuracy, are marked in **bold**. Models including the contribution of each pulse to detection probability through probability summation (Equations (3.1) and (3.2)) perform better than a simplified model based on the assumption that the amplitude of the second peak determines detection probability (Equation (3.3)).*

IPI: 40ms Group & Model	Median AIC	Lowest AIC (%)	Accuracy (%)	Converged (%)
Healthy (university):				
Complete Model	**359.1**	**48.0**	**69.0**	100
High Criterion	369.0	28.0	68.5	100
Single Dominant Peak	374.2	24.0	67.6	100
Healthy (hospital):				
Complete Model	**351.8**	35.3	**72.7**	100
High Criterion	352.8	**44.1**	72.0	100
Single Dominant Peak	361.0	20.6	70.7	100
FBSS (hospital):				
Complete Model	**383.5**	**42.4**	**67.5**	100
High Criterion	391.5	**42.4**	66.9	100
Single Dominant Peak	389.7	15.2	65.5	100

Table 9.2: Model comparison for stimuli with an inter-pulse interval of 40 ms. The lowest median AIC values, and the highest percentages for lowest AIC and accuracy, are marked in ***bold****. Models including the contribution of each pulse to detection probability through probability summation (Equations (3.1) and (3.2)) perform better than a simplified model based on the assumption that the amplitude of the second peak determines detection probability (Equation (3.3)).*

9.3.2 Detection Behavior

The median model parameters in each group are shown in Table 9.3 (10 ms inter-pulse interval) and Table 9.4 (40 ms inter-pulse interval). Both tables show a positive effect of both pulse amplitudes and a (pulse-dependent) negative effect of the number of received stimuli on the detection probability in each model. Comparison of parameters from FBSS patients with healthy controls in the hospital shows a decreasing trend in the magnitude of most parameters, which is confirmed by a significant decrease in $sum\left(\left|\frac{\boldsymbol{\beta}}{\boldsymbol{\sigma}}\right|\right)$, suggesting that there are larger values for σ in patients. The comparison also shows a significant decrease of g_{D0} in FBSS patients, which is associated to a larger standard deviation of the Gumbel distribution associated with the maximum of spontaneous activity or a smaller difference between spontaneous activity and

the response criterion. Note that all models show a similar trend in stimulus parameters but differ in terms of significance when comparing patients with healthy controls, where the model with the lowest number of parameters (assuming a single dominant peak) shows the most significant differences between both groups.

IPI: 10ms Group & Model	$-\frac{\beta_{D0}}{\sigma_{\tau 1}}$	$-\frac{\beta_{D0}}{\sigma_{\tau 2}}$	$\frac{\beta_{A1}}{\sigma_{\tau 1}}$ *or* $\frac{\beta_{A1}}{\sigma_{\tau 2}}$	$\frac{\beta_{A2}}{\sigma_{\tau 2}}$	$-\frac{\beta_t}{\sigma_{\tau 1}}$	$-\frac{\beta_t}{\sigma_{\tau 2}}$	$sum\left(\lvert\frac{\boldsymbol{\beta}}{\boldsymbol{\sigma}}\rvert\right)$	g_{D0}	g_{t1}
Complete Model:									
Healthy (university)	**-3.42**	**-3.93**	**10.05**	**22.14**	**-0.69**	**-0.54**	**42.51**	**8.66**	-0.35
Healthy (hospital)	**-4.14**	**-6.11**	**9.86**	**24.44**	**-0.76**	**-0.67**	**47.35**	**15.81**	0.40
FBSS (hospital)	**-4.44**	**-4.86**	**5.67**	**12.66*** **	**-0.70**	**-0.49**	**30.49***	**6.55***	0.00
High Criterion:									
Healthy (university)	**-2.64**	**-3.37**	**5.81**	**17.62**	**-0.42**	**-0.49**	**35.82**		
Healthy (hospital)	**-3.28**	**-5.84**	**9.11**	**23.02**	**-0.64**	**-0.64**	**41.72**		
FBSS (hospital)	**-3.01**	**-4.57**	**3.44****	**10.38*** **	**-0.30**	**-0.42**	**28.68*** **		
Single Dominant Peak:									
Healthy (university)		**-2.22**	**4.36**	**6.02**		**-0.43**	**14.53**		
Healthy (hospital)		**-3.45**	**9.12**	**5.81**		**-0.55**	**18.56**		
FBSS (hospital)		**-2.30***	**2.86*** **	**2.90***		**-0.43***	**10.38*** **		

Table 9.3: *Median model parameters in each group for single-pulse and double-pulse stimuli with an inter-pulse interval (IPI) of 10 ms. Parameters that were significantly different from 0 are shown in* ***bold****. Parameters of the FBSS population that were significantly different from healthy controls at the hospital are marked with * (p<0.05), ** (p<0.01) or *** (p<0.001).*

IPI: 40ms **Group & Model**	$-\frac{\beta_{D0}}{\sigma_{\tau 1}}$	$-\frac{\beta_{D0}}{\sigma_{\tau 2}}$	$\frac{\beta_{A1}}{\sigma_{\tau 1}}$ *or* $\frac{\beta_{A1}}{\sigma_{\tau 2}}$	$\frac{\beta_{A2}}{\sigma_{\tau 2}}$	$-\frac{\beta_t}{\sigma_{\tau 1}}$	$-\frac{\beta_t}{\sigma_{\tau 2}}$	$sum\left(\left\lvert\frac{\boldsymbol{\beta}}{\boldsymbol{\sigma}}\right\rvert\right)$	g_{D0}	g_{t1}
Complete Model:									
Healthy (university)	-4.09	**-3.24**	**11.31**	**16.36**	**-0.98**	**-0.53**	**43.04**	**10.61**	-0.82
Healthy (hospital)	**-4.34**	**-5.77**	**10.53**	**24.88**	**-0.75**	**-0.66**	**48.23**	**14.40**	**-0.70**
FBSS (hospital)	**-4.69**	**-5.39**	**5.41**	**11.93*** **	**-0.69**	**-0.73**	**38.14***	**4.24**	-0.29
High Criterion:									
Healthy (university)	**-2.81**	**-3.02**	**5.78**	**13.16**	**-0.44**	**-0.48**	**28.29**		
Healthy (hospital)	**-3.33**	**-5.35**	**9.57**	**20.50**	**-0.67**	-0.58	**42.44**		
FBSS (hospital)	**-3.01**	**-4.01**	**3.37****	**10.31*** **	**-0.30**	-0.56	**26.26*** **		
Single Dominant Peak:									
Healthy (university)		**-2.37**	**4.46**	**5.89**		**-0.32**	**14.12**		
Healthy (hospital)		**-3.49**	**9.89**	**5.73**		**-0.50**	**18.76**		
FBSS (hospital)		**-2.10****	**2.33*** **	**2.72*** **		**-0.42***	**8.73*** **		

Table 9.4: *Median model parameters in each group for single-pulse and double-pulse stimuli with an inter-pulse interval (IPI) of 40 ms. Parameters that were significantly different from 0 are shown in* ***bold****. Parameters of the FBSS population that were significantly different from healthy controls at the hospital are marked with * (p<0.05), ** (p<0.01) or *** (p<0.001).*

9.4 Discussion

In this study, we derived a set of equations describing stimulus detection for single- and double-pulse electro-nociceptive stimuli. We showed that detection behavior can change dependent on physiological parameters as well as on stimulus properties. A crucial insight obtained through theoretical analysis, was that the distribution of maximum neural activity within a limited interval depends on the distribution of spontaneous neural activity, and the distribution of neural activity evoked by each pulse, and that this distribution can change parameters and shape based on the stimulus properties. We derived a set of equations to describe the detection probability, based on this distribution of maximum neural activity. We analyzed two populations of healthy participants, and one population of chronic pain patients, to observe which parameters are

justified based on an information criterion, and how information from the psychophysical model could be used in a clinical context.

9.4.1 Model Selection

We found that for all groups, the detection behavior for both stimulus types are best described using the complete derived psychophysical model on a group level. The effect of model simplification by assuming that spontaneous activity is negligible with respect to the response criterion differed per group and stimulus type, leading in some cases to a decrease of AIC. For each of the models, there was a significant subset of the participants in which the model performed best, i.e., achieved the lowest AIC on an individual level. As such, on the individual level, there is not a single model that outperforms the other models on all participants and for both stimulus types. Note that all participants might behave according to the generic model presented in (1). All other models derived in this article, and many other models in psychophysics, can be regarded as simplifications of this generic model with the goal of arriving at a model with observable parameters. Nevertheless, the reality is that participants behave on the continuum described by (1), meaning that in some cases a more complex model is required as in Equation (3.1), while in other cases detection behavior can be described using a model with less parameters as in Equation (3.3). The model in Equation (3.1) describes the most generic observable model within this continuum, within the current framework, and is a safe choice if one wants to make sure no potentially relevant parameters are ignored. On the other hand, including too many parameters could impede model fitting, or parameter significance when trying to observe changes in detection behavior.

9.4.2 Detection Behavior

The ultimate goal for model selection is to derive a meaningful model which describes detection behavior in terms of observable physiological parameters.

We analyzed our data using the three proposed models. The major difference between the three models is the level of simplification, in terms of the parameters included in the model. The models are compared in terms of parameters from complex (complete model) to simple (model of a single dominant peak) in Figure 9.4. The complete model essentially identifies the same parameters of evoked nervous activity as the alternative models but contains more degrees of freedom for additional parameters such as the influence of the first peak and the influence of spontaneous neural activity. As a result, we identified similar values and similar trends for the same parameters among different models in Tables 9.3 and 9.4. Note that the model smallest number of parameters (single dominant peak) shows the most significant differences in parameters when comparing FBSS patients and healthy controls. This suggests that in this case a model with less parameters might be more sensitive to altered nociceptive processing in FBSS, by explaining total variance based on a smaller number of parameters.

We found that in all models and all groups, that all parameters except some values of g_{t1} and $-\frac{\beta_t}{\sigma_{\tau 2}}$ significantly differed from zero implicating that they significantly modulated the detection probability. Each model showed a positive influence of pulse amplitudes, which is related to the increased recruitment of peripheral nerve fibers with increasing pulse amplitudes, where the detection probability of a double-pulse stimulus is always higher than the detection probability of a single-pulse stimulus. Each model also showed a negative influence of the number of received stimuli on the detection probability, indicating a significant threshold drift during the experiments, as was already observed in previous studies (Berfelo, Van den Berg, Krabbenbos, & Buitenweg, 2021; Doll, Maten, Spaan, Veltink, & Buitenweg, 2016; van den Berg & Buitenweg, 2021). A comparison was made between FBSS patients and healthy controls in the hospital to observe how detection behavior could be altered as a result of chronic neuropathic pain. Most parameters, and most notably $\frac{\beta_{A2}}{\sigma_{\tau 2}}$ and $\frac{\beta_{A2}}{\sigma_{\tau 2}}$, decreased in average magnitude and as a result the overall magnitude of coefficients $sum\left(\left|\frac{\boldsymbol{\beta}}{\boldsymbol{\sigma}}\right|\right)$ decreased significantly in all models. An overall decrease of coefficient magnitude indicates that the dividers $\sigma_{\tau 1}$ and $\sigma_{\tau 2}$ increased in magnitude, suggesting an increase in spontaneous neural activity

in FBSS patients. This result is also supported by the observation of a decreased g_{D0} for stimuli with an inter-pulse interval of 10 ms. As spontaneous neural activity in peripheral and central nociceptive neurons is an important feature of neuropathic pain (Devor, 2009; Latremoliere & Woolf, 2009), quantifying this increase using psychophysical methods could be an important addition to patient assessment. It is important to note that previous studies were based on an explorative study design. As such, demographic differences between populations, such as age and gender, were present in the dataset analyzed in this study. Further research should evaluate if we can consistently quantify spontaneous neural activity in patients by means of psychophysical methods.

9.4.3 Limitations

Several assumptions and corresponding model simplifications were required to derive an observable psychophysical model, including the assumptions that stimulus detection is based on maximum neural firing rate and the assumption that neural firing rate increases proportional to stimulus amplitude. It remains unknown whether stimulus detection is governed by the maximum of instantaneous neural firing rate, the integral of neural firing rate over a limited time window, or the integral of neural firing rate over the entire detection interval. In the second case, spontaneous neural activity will be correlated over time, but with a sufficiently long detection interval the extreme value distribution used in this work will still apply. In the third case, the decision will be based on the addition of spontaneous neural activity and both pulses, in which case the model in Equation (3.3) would apply as long as spontaneous neural activity is negligible. Considering the good performance of the complete model in comparison with the simpler model in Equation (3.3), we believe that temporal integration of the entire detection interval is unlikely, and that a maximum detection rule is preferred.

Significant advantages of the current approach with respect to detailed neurophysiological models are the limited number of model parameters and the ability to model the influence of spontaneous neurophysiological activity.

Complete Model, Equation (3.1):

$$P_d = 1 - \left(1 - \Phi\left(\frac{-\beta_{D0} - \beta_t + \beta_{A1}A}{\sigma_{\tau 1}}\right)\right)\left(1 - \Phi\left(\frac{-\beta_{D0} - \beta_t + \beta_{A2}A}{\sigma_{\tau 2}}\right)\right)^{n-1} G(g_{D01} + g_{t1}t)$$

High Criterion, Equation (3.2):

$$P_d = 1 - \left(1 - \Phi\left(\frac{-\beta_{D0} - \beta_t + \beta_{A1}A}{\sigma_{\tau 1}}\right)\right)\left(1 - \Phi\left(\frac{-\beta_{D0} - \beta_t + \beta_{A2}A}{\sigma_{\tau 2}}\right)\right)^{n-1}$$

Single Dominant Peak (SDP), Equation (3.3):

$$P_d = \Phi\left(\frac{-\beta_{D0} - \beta_t + \beta_{A1}A + (n-1)\beta_{A2}A}{\sigma_{\tau 2}}\right)$$

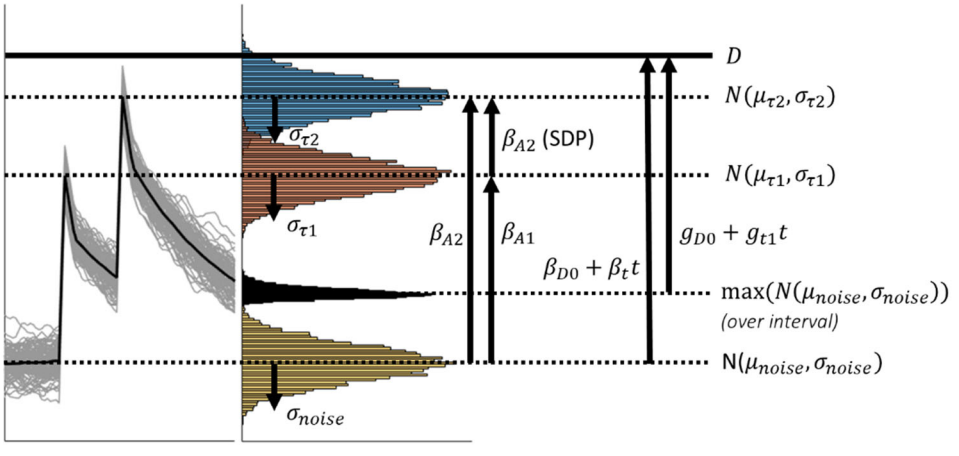

Figure 9.4: Model parameters can be interpreted as properties of the neural activity on the observed psychophysical channel. The parameter β_{A1} is proportional to the difference between average baseline activity and activity as a result of the first pulse. The parameter β_{A2} is proportional to the difference between average baseline activity and activity as a result of the second pulse, while in a model assuming a single dominant peak (SDP) this parameter is proportional to the difference between activity as a result of the second pulse and activity as a result of the first pulse. The sum of parameters $\beta_{D0} + \beta_t t$ is proportional to the difference between baseline activity and the response criterion at trial t. The sum of parameters $g_{D0} + g_t t$ is proportional to the difference between the maximum of spontaneous activity and the response criterion at trial t.

However, the assumption of a proportional increase of neural activity with respect to stimulus amplitude is a major limitation of the models presented in this study. The choice of potential transducer functions could be supported by using models of peripheral fiber activation as in (Tanaka et al., 2021; Tigerholm, Poulsen, Andersen, & Mørch, 2019; Yang, Meijer, Doll, Buitenweg, & van Gils, 2015), where modeling studies should focus on the number of activated

peripheral neurons and the average firing rate, rather than the minimum stimulus amplitude required to activate a single peripheral or central neuron.

9.5 Conclusion

In this work, we aimed to investigate how nociceptive processing could influence detection probability of single- and double-pulse stimuli, and if we could derive observable models to identify altered nociceptive processing. Stimulus detection might depend on average neural activity resulting in conscious detection when this activity reaches a response criterion. The distribution of this neural activity differs in shape and parameters depending on physiology and, importantly, depending on stimulus properties. Formulation of psychophysical models for nociception helps to identify physiological parameters in standard and impaired nociception. The optimal psychophysical model in terms of AIC, depends on which model simplifications are justified based on the persons nociceptive system. Nevertheless, as most models directly or indirectly share a common set of parameters, impaired nociceptive processing can be observed across models. Currently it is difficult to clarify altered detection behavior in FBSS patients with nociceptive dysfunctions using other clinical measurement techniques. However, our results suggest that spontaneous neural activity is increased in this population. Further studies should investigate if this phenomenon in present in other populations suffering from nociceptive dysfunctions.

9.6 Acknowledgements

The authors would like to thank Imre Krabbenbos and the Department of Anesthesiology, Intensive Care and Pain Medicine at the St. Antonius Hospital in Nieuwegein, the Netherlands, for supporting us with clinical studies on chronic pain patients.

9.7 References

Akaike, H. (1974). A new look at the statistical model identification. *IEEE Transactions on Automatic Control, 19*(6), 716-723.

Berfelo, T., Doll, R.-J., Krabbenbos, I. P., & Buitenweg, J. R. (2022). Observing Altered Nociceptive Detection Thresholds in Patients With Persistent Spinal Pain Syndrome Type 2 With a Dorsal Root Ganglion Stimulator. *Neuromodulation: Technology at the Neural Interface*.

Berfelo, T., Van den Berg, B., Krabbenbos, I. P., & Buitenweg, J. R. (2021). *Observing nociceptive detection thresholds and brain evoked potentials in persistent spinal pain syndrome type 2 patients*.

Buzsáki, G., & Mizuseki, K. (2014). The log-dynamic brain: how skewed distributions affect network operations. *Nature Reviews Neuroscience, 15*(4), 264-278.

Coleman, T. F., & Li, Y. (1996). An Interior Trust Region Approach for Nonlinear Minimization Subject to Bounds. *SIAM Journal on Optimization, 6*(2), 418-445.

Dehaene, S., & Changeux, J.-P. (2011). Experimental and Theoretical Approaches to Conscious Processing. *Neuron, 70*(2), 200-227.

Devor, M. (2009). Ectopic discharge in Abeta afferents as a source of neuropathic pain. *Exp Brain Res, 196*(1), 115-128.

Doll, R. J., Maten, A. C. A., Spaan, S. P. G., Veltink, P. H., & Buitenweg, J. R. (2016). Effect of temporal stimulus properties on the nociceptive detection probability using intra-epidermal electrical stimulation. *Experimental Brain Research, 234*(1), 219-227.

Doll, R. J., Veltink, P. H., & Buitenweg, J. R. (2015). Observation of time-dependent psychophysical functions and accounting for threshold drifts. *Attention, Perception, and Psychophysics, 77*(4), 1440-1447.

Latremoliere, A., & Woolf, C. J. (2009). Central sensitization: a generator of pain hypersensitivity by central neural plasticity. *The Journal of Pain, 10*(9), 895-926.

Mouraux, A., Iannetti, G. D., & Plaghki, L. (2010). Low intensity intra-epidermal electrical stimulation can activate Aδ-nociceptors selectively. *Pain, 150(1)*, 199-207.

North, R. Y., Li, Y., Ray, P., Rhines, L. D., Tatsui, C. E., Rao, G., . . . Dougherty, P. M. (2019). Electrophysiological and transcriptomic correlates of neuropathic pain in human dorsal root ganglion neurons. *Brain, 142*(5), 1215-1226.

Petersen, P. C., & Berg, R. W. (2016). Lognormal firing rate distribution reveals prominent fluctuation-driven regime in spinal motor networks. *eLife, 5*, e18805.

Poulsen, A. H., Tigerholm, J., Meijs, S., Andersen, O. K., & Mørch, C. D. (2020). Comparison of existing electrode designs for preferential activation of cutaneous nociceptors. *Journal of Neural Engineering*.

Roxin, A., Brunel, N., Hansel, D., Mongillo, G., & van Vreeswijk, C. (2011). On the Distribution of Firing Rates in Networks of Cortical Neurons. *The Journal of Neuroscience, 31*(45), 16217.

Steenbergen, P., Buitenweg, J. R., Trojan, J., van der Heide, E. M., van den Heuvel, T., Flor, H., & Veltink, P. H. (2012). A system for inducing concurrent tactile and nociceptive sensations at the same site using electrocutaneous stimulation. *Behavior research methods, 44(4)*, 924-933.

Tanaka, S., Gomez-Tames, J., Wasaka, T., Inui, K., Ueno, S., & Hirata, A. (2021). Electrical Characterisation of Aδ-Fibres Based on Human in vivo Electrostimulation Threshold. *Frontiers in Neuroscience, 14*(1305).

Tigerholm, J., Poulsen, A. H., Andersen, O. K., & Mørch, C. D. (2019). From Perception Threshold to Ion Channels-A Computational Study. *Biophys J, 117*(2), 281-295.

Ugray, Z., Lasdon, L., Plummer, J., Glover, F., Kelly, J., & Martí, R. (2007). Scatter Search and Local NLP Solvers: A Multistart Framework for Global Optimization. *INFORMS Journal on Computing, 19*(3), 328-340.

Van den Berg, B., & Buitenweg, J. R. (2018). *Analysis Of Nociceptive Evoked Potentials During Multi-Stimulus Experiments Using Linear Mixed Models*. Paper presented at the 40th Annual International Conference of the IEEE Engineering in Medicine and Biology Society (EMBC), Honolulu, United States.

van den Berg, B., & Buitenweg, J. R. (2021). Observation of Nociceptive Processing: Effect of Intra-Epidermal Electric Stimulus Properties on Detection Probability and Evoked Potentials. *Brain Topography*.

van den Berg, B., Doll, R. J., Mentink, A. L. H., Siebenga, P. S., Groeneveld, G. J., & Buitenweg, J. R. (2020). Simultaneous tracking of psychophysical detection thresholds and evoked potentials to study nociceptive processing. *Behavior Research Methods*.

Yang, H., Meijer, H. G. E., Doll, R. J., Buitenweg, J. R., & van Gils, S. A. (2015). Computational modeling of Adelta-fiber-mediated nociceptive detection of electrocutaneous stimulation. *Biological Cybernetics, 109*(4-5), 479-491.

The TMSi REFA amplifier, used for recording the electroencephalogram, drawn in the style of Amadeo de Souza-Cardoso using neural style transfer.

Part IV:

Novel Technological Steps for Improved Observation of Impaired Nociceptive Processing

"Men are only as good as their technical development allows them to be."

George Orwell, Inside the Wale and Other Essays

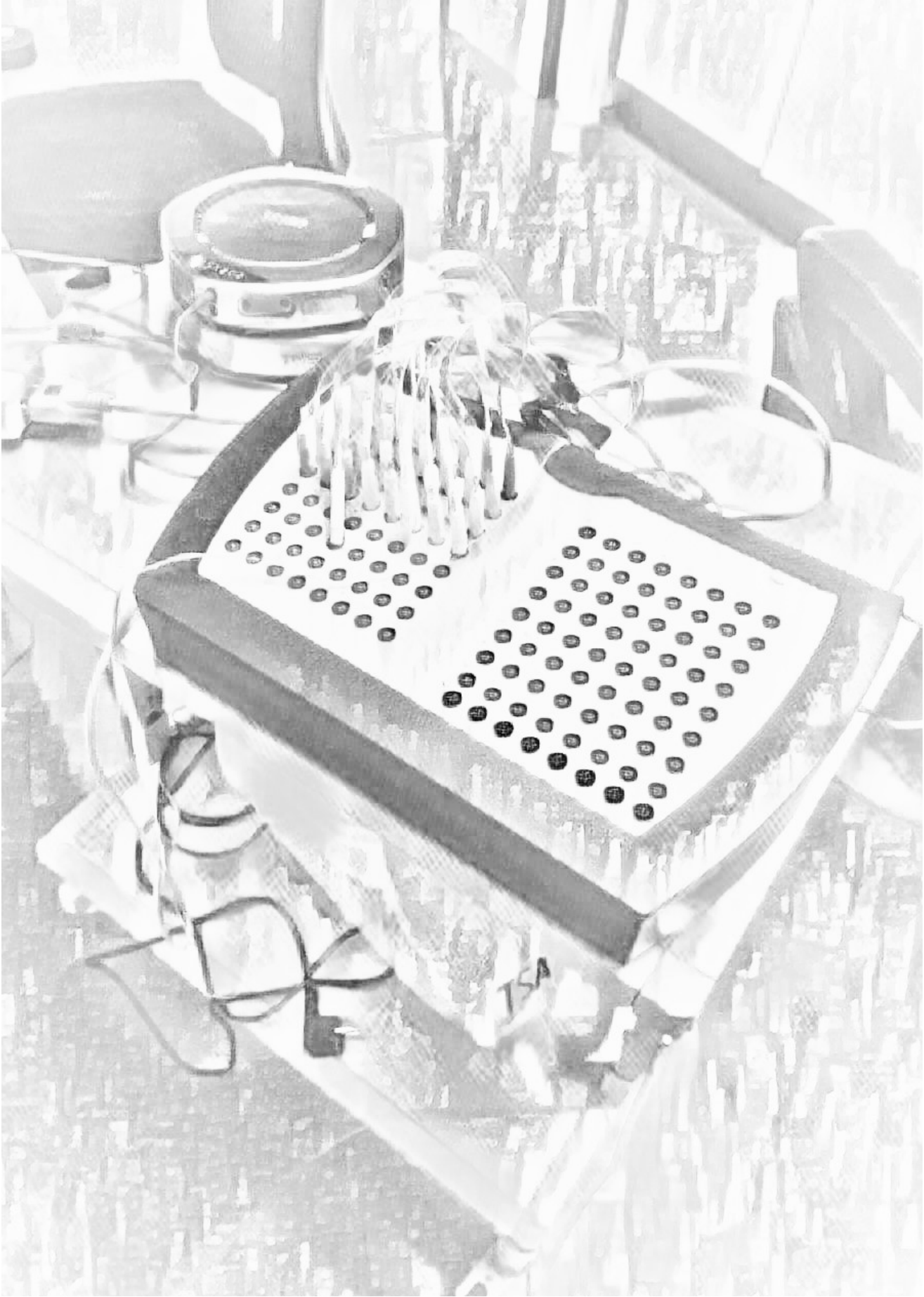

Chapter 10

Estimation of Perceptual Thresholds Based on the Electroencephalogram using a Deep Neural Network

Published as:

Van den Berg, B., Vanwinsen, L., Jansen, N., & Buitenweg, J. R. (2022). Real-time estimation of perceptual thresholds based on the electroencephalogram using a deep neural network, *Journal of Neuroscience Methods*, 374, 109580.

DOI: https://www.doi.org/10.1016/j.jneumeth.2022.109580

Abstract

Perceptual thresholds are measured in scientific and clinical setting to evaluate performance of the nervous system in essential tasks such as vision, hearing, touch, and registration of pain. Current procedures for estimating perceptual thresholds depend on the analysis of pairs of stimuli and participant responses, relying on the commitment and cognitive ability of subjects to respond accurately and consistently to stimulation. Here, we demonstrate that it is possible to measure the threshold for the perception of nociceptive stimuli based on non-invasively recorded brain activity alone using a deep neural network.

For each stimulus, a trained deep neural network performed a 2-interval forced choice procedure, in which the network had to choose which of two time intervals in the electroencephalogram represented post-stimulus brain activity. Network responses were used to estimate the perceptual threshold in real-time using a psychophysical method of limits.

The neural network successfully separated trials containing brain responses from trials without and could consistently estimate perceptual thresholds in real-time during a Go-/No-Go procedure and a counting task. Network classification was able to match participants in reporting stimulus perception, resulting in average network-estimated perceptual thresholds that matched perceptual thresholds based on participant reports.

Deep neural networks monitoring non-invasively recorded brain activity are now able to accurately predict stimulus perception and estimate the perceptual threshold in real-time without any verbal or motor response from the participant.

10.1 Introduction

In 1860, the psychologist Gustav Fechner first recognized that inner consciousness could be measured in terms of behavior, and since then methods have been developed and refined for the systematic exploration of sensory systems (Leek, 2001). The evaluation of perceptual thresholds plays a crucial role in the evaluation of human sensory function in vision, hearing, touch, and nociception. Evaluation of the perceptual threshold is also increasingly popular in pain research as stimulus perception can be used to assess altered central and peripheral nociceptive processing. For instance, mechanical and thermal perceptual thresholds are increased in patients with neuropathic pain and signs of central sensitization (Maier et al., 2010), or as a result of peripheral nerve dysfunction in diabetes (Courtin et al., 2020; Krämer, Rolke, Bickel, & Birklein, 2004). More recently, studies have suggested the use of intra-epidermal electric stimulation to assess nociceptive function by measuring the perceptual threshold to nociceptive specific stimulation (Doll, Veltink, & Buitenweg, 2015; Hennings et al., 2017; Tanaka et al., 2021; Van den Berg & Buitenweg, 2018, 2021; van den Berg et al., 2020; van den Berg et al., 2022).

The evaluation of perceptual thresholds using psychophysical procedures relies on the commitment and cognitive ability of participants to respond accurately and consistently to stimulation regardless of long and sometimes boring experiments. The complex adaptive psychophysical procedures used to measure an unbiased perceptual threshold often preclude usage in non-standard adult populations or children (Smith, Cesana, Farran, Karmiloff-Smith, & Ewing, 2018). In some cases, estimation of the perceptual threshold based on report is not possible because subjects are unable to reliably communicate stimulus perception. In other cases, the physician cannot rely on reported perception, due to potential simulation or malingering while no organic reason for sensory loss can be identified (Austen & Lynch, 2004; Bruce & Newman, 2010). Even in standard healthy adult participants, perception report (i.e., behavior) is not always equal to perception (i.e., conscious access to sensory information), as participants might fail to report a perceived stimulus (also known as lapsing) or might report stimulus perception while actually no stimulus was perceived (also known as guessing). To potentially enable the

accurate and objective assessment of perceptual thresholds in a wide variety of patient groups, we propose a fully automated approach that relies on non-invasive recordings of cortical brain activity rather than reported perception, to estimate the perceptual threshold.

When a (change in) visual stimulus is perceived during a psychophysical procedure, this results in the generation of the famous P300 peak in the event-related potential (Picton, 1992). The P300 is a positive peak in the human event-related potential and is considered a key marker of conscious access to sensory information (Rutiku, Martin, Bachmann, & Aru, 2015; Salti, Bar-Haim, & Lamy, 2012). A similar peak with the same functional significance, referred to as the P2, can be observed in experiments using nociceptive stimulation (Mouraux & Iannetti, 2009). Peaks like the P300 and P2 are easily identified in averaged EEG responses but remain difficult to detect on a single-trial basis. One of the best performing feature-based decoding and classification approaches (winner of the 2015 Kaggle BCI competition) consisting of a combination of xDAWN spatial filtering (Rivet, Souloumiac, Attina, & Gibert, 2009) and Riemannian geometry classification (Barachant, Bonnet, Congedo, & Jutten, 2012) achieves an area-under-the-curve (AUC) of around 0.8 for cross-subject classification of visual evoked potentials. An even higher AUC of 0.9 is achieved for the same dataset of visual evoked potentials using an end-to-end decoding and classification approach using a deep neural network (Lawhern et al., 2018). Such end-to-end decoding approaches using a deep neural network have the drawbacks of a high computational complexity, and a large number of trainable model parameters. Nevertheless, provided that one has sufficient computational resources and access a large amount of reliably labeled training data, a deep neural network could discover informative features and potentially find superior solutions to the classification problem by itself (Gemein et al., 2020; Roy et al., 2019). Although visualization and interpretation of the learned features inside such neural networks remains a challenge and topic of ongoing research, several approaches exist to visualize which parts of the recorded EEG contribute most to the neural network classifications, such as visualization of the network's sensitivity to the occlusion of parts of the input (Zeiler & Fergus, 2014).

In this work, we used a deep neural network to detect stimulus perception based on the EEG, and we used the neural network classification scores to control adaptive stimulation and compute perceptual thresholds in real-time (Figure 10.1). We hypothesized that when a stimulus is perceived, task-related neural activity associated with the conscious access to sensory information will be present in the EEG and detectable by a deep neural network. Therefore, a sequence of stimulus-classification pairs could be used to estimate the perceptual threshold. The first challenge in this work, was to use a deep neural network for the detection of brain responses to stimuli close to the perceptual threshold, i.e., stimuli that were difficult to perceive or sometimes not even reported as perceived by the participant. The second challenge was that the direct classification of perception using a deep neural network or other machine learning methods can suffer from an unknown calibration bias, introduced by the cross-subject application of the neural network (i.e., the classification score cannot be calibrated for an unseen subject) and non-stationarity of the EEG. We addressed this potential calibration bias in classification scores by performing a 2-interval forced choice (2IFC) classification task, where we compare the score of each post-stimulus interval to the score of each pre-stimulus interval. In the next sections, we will show that we can accurately estimate perceptual thresholds based on these classifications (*pre-stimulus* or *post-stimulus*) post-hoc, and we will provide a proof-of-concept that we might use this classification to control an adaptive stimulus sequence and estimate the perceptual threshold in real-time.

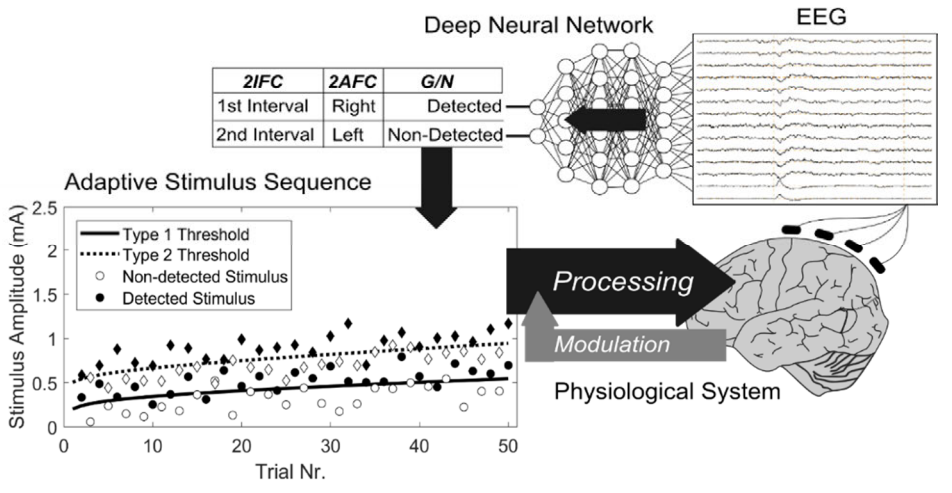

Figure 10.1: *Closed-loop estimation of perceptual thresholds based on neurophysiological activity using the presented methods. Stimuli are applied using an adaptive procedure to approach the perceptual threshold. Brain responses to those stimuli are measured using electroencephalography (EEG) and fed to a deep neural network to perform a psychophysical classification task. Subsequently, the stimulus sequence adapts based on classification of the network.*

10.2 Methods

10.2.1 Data

The study made use of three different datasets for training and validation of the method. Here we will briefly describe the general outline of each dataset and proceed with providing the implementation details. The experiments presented here were approved by the university ethical review committee (nr. RP 2021-05 and RP 2021-176) and in accordance with the 1964 declaration of Helsinki and its later amendments and all participants provided written informed consent prior to participation in these experiments. The three different datasets are described in the text below and summarized in Table 10.1.

Dataset 1 (DS1)

Initial network training, validation, calibration and performance testing was done using a collection of data obtained from previous studies (Van den Berg,

Berfelo, Verhoeven, Krabbenbos, & Buitenweg, 2021; van den Berg & Buitenweg, 2021) and an ongoing study (registered as NL66136.100.18 at toetsingonline.nl) at the Department of Anesthesiology, Intensive Care and Pain Medicine of the St. Antonius Hospital (Nieuwegein, the Netherlands), and at the University of Twente (Enschede, the Netherlands). This dataset includes a total of 38 healthy participants (16 male, age 18-73), which we will refer to as DS1. Participants were electrically stimulated on the back of the right or left hand using an electrode for preferential activation of nociceptive afferents in the skin. Participants had to perform a go-/no-go (GN) task by pressing a button and briefly releasing the button when a stimulus was perceived. Stimulus amplitudes were selected by an adaptive psychophysical method of limits to center amplitudes around the perceptual threshold. Each participant received a total of 450 (on one hand) or 900 (on both hands) stimuli of three types, resulting in 150 or 300 stimulus-response pairs per type:

- A single square-wave cathodic pulse with a pulse-width of 0.21 ms.
- A double square-wave cathodic pulse with a pulse-width of 0.21 ms and an inter-pulse interval of 10 ms.
- A double square-wave cathodic pulse with a pulse-width of 0.21 ms and an inter-pulse interval of 40 ms.

Note that the evoked potential waveforms in response to these stimulus types are very similar (van den Berg & Buitenweg, 2021; van den Berg et al., 2020). Therefore, we included all stimulus types for training, validation, and testing, to improve algorithm performance and generalizability of the results.

Dataset 2 (DS2)

Performance of the calibrated network in post-hoc EEG classification and threshold estimation was evaluated on a second independent dataset comprising 15 healthy participants (8 male, age 19-25), which we will refer to as DS2 (for more information, see (van den Berg, Vanwinsen, Pezzali, & Buitenweg, 2021)). Participants were electrically stimulated on the back of the

right hand using an electrode for preferential activation of nociceptive afferents in the skin. Participants had to perform a GN task by pressing a button and briefly releasing the button when a stimulus was perceived. Stimulus amplitudes were selected by an adaptive psychophysical method of limits to center amplitudes around the perceptual threshold. Each participant received a total of 130 stimuli of two types, resulting in 65 stimulus-response pairs per type:

- A single square-wave cathodic pulse with a pulse-width of 0.21 ms.
- A double square-wave cathodic pulse with a pulse-width of 0.21 ms and an inter-pulse interval of 10 ms.

Dataset 3 (DS3)

Performance of the calibrated network for real-time tracking and estimation of the perceptual threshold was evaluated in a proof-of-concept experiment on 8 healthy participants (5 male, age 19-24), which we will refer to as DS3. Participants were electrically stimulated on the back of the right hand with double-pulse stimuli (pulse-width: 0.21 ms, inter-pulse interval: 10 ms) using an electrode for preferential activation of nociceptive afferents in the skin.

Part I: The perceptual threshold based on reported stimulus perception was compared to the perceptual threshold estimated by the neural network. Participants had to perform a GN task by pressing a button and briefly releasing the button when a stimulus was perceived. The neural network performed a 2IFC classification task, where it had to classify which of two intervals (pre- and post-stimulus) contained post-stimulus brain activity (also see Section 10.2.2). Stimulus amplitudes were selected by two independent adaptive methods of limits (in randomized order) to center amplitudes around the perceptual threshold, where one used the neural network classification as feedback, and the other used button-release. Each participant received a total of 200 stimuli.

Part II: The perceptual threshold based on reported stimulus perception was compared to the perceptual threshold estimated by the neural network. In

contrast with the earlier experiments, participants had to perform a GN task by counting each stimulus when perceived. The neural network performed a 2IFC classification task, where it had to classify which of two intervals (pre- and post-stimulus) contained post-stimulus brain activity (also see Section 10.2.2). Stimulus amplitudes were selected by two independent adaptive methods of limits (in randomized order) to center amplitudes around the perceptual threshold, where each used the neural network classification as feedback. Each participant received a total of 200 stimuli.

10.2.2 Estimation of Perceptual thresholds

Perceptual thresholds were estimated by fitting a psychophysical model to stimulus-response pairs. Stimulus amplitudes were selected by an adaptive psychophysical method of limits aimed at tracking non-stationary perceptual thresholds. The original stimulation procedure from Doll et al. (Doll, Veltink, & Buitenweg, 2015) was designed for tracking perceptual thresholds using a GN task (Figure 10.2). Here, we adapted the procedure to track and estimate perceptual thresholds for either a GN task, executed by the participant by briefly releasing the response button, or a 2IFC task, executed by the neural network by classifying which interval of the EEG contains post-stimulus brain activity.

Nociceptive Stimulation

A custom-made electrode consisting of 5 microneedles (0.5 mm) embedded in a layer of flexible silicone (Steenbergen et al., 2012) was used to stimulate nociceptive afferents in the skin through intra-epidermal electric stimulation (Inui & Kakigi, 2012) using a constant current stimulator (NociTRACK AmbuStim, University of Twente, Enschede, the Netherlands). This type of electric stimulation was shown to preferentially activate nociceptive Aδ-fibers in the skin provided that the current remains below twice the perceptual threshold (Mouraux, 2010; Poulsen, Tigerholm, Meijs, Andersen, & Mørch, 2020). Stimuli were applied with a uniformly randomized inter-stimulus interval of 3.5 to 4.5 seconds.

Dataset	Stimulus Types	# Stimuli per Participant	# Participants	Participant Task	Network Task	Real-Time Network Classification	Adaptive Stimulation Based on:
DS1	SP, DP10, DP40	450 or 900	38	GN (release button when perceived)	2IFC (classify pre-/post-stimulus)	No	Participant responses
DS2	SP, DP10	130	15	GN (release button when perceived)	2IFC (classify pre-/post-stimulus)	No	Participant responses
DS3 Part I	DP10	200	8	GN (release button when perceived)	2IFC (classify pre-/post-stimulus)	Yes	Neural network classification
DS3 Part II	DP10	200	8 (same participants as in Part I)	GN (count stimulus when perceived)	2IFC (classify pre-/post-stimulus)	Yes	Neural network classification

***Table 10.1**: Summary of the datasets used in this study, the psychophysical task performed by the participant and the classification task performed by the neural network in each dataset. Stimulus types are abbreviated as SP (single-pulse, 0.21ms pulse-width), DP10 (double-pulse, 0.21ms pulse-width, 10ms inter-pulse interval) and DP40 (double-pulse, 0.21ms pulse-width, 40ms inter-pulse interval). Tasks are abbreviated as GN (go-/no-go) and 2IFC (2-interval forced choice).*

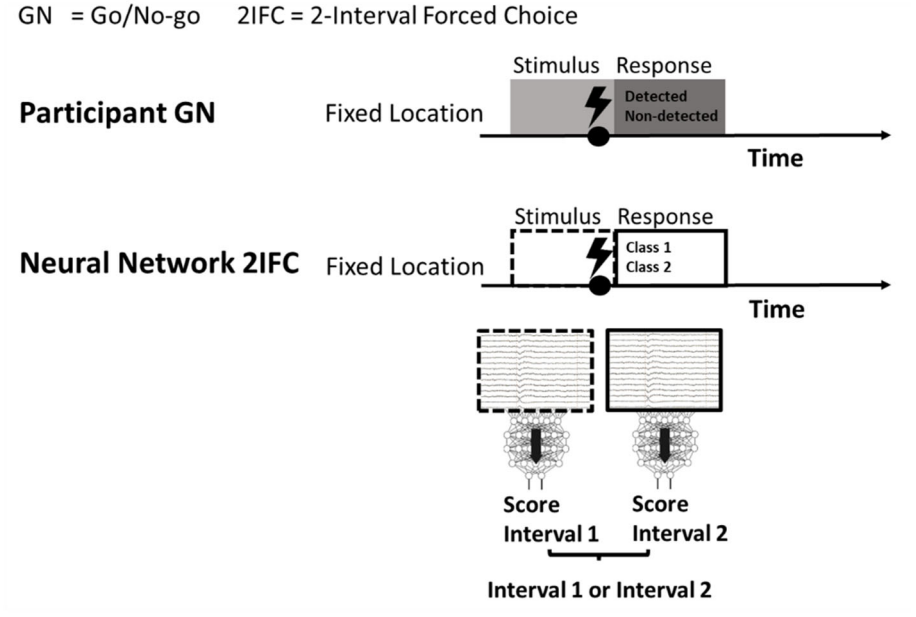

Figure 10.2: Psychophysical tasks executed by the participant or the neural network. During the Go/No-go (GN) task the participant receives a sequence of stimuli at a randomized interval and is instructed to report when a stimulus was detected, e.g., by releasing a response button. In the 2-Interval Forced Choice (2IFC) task the neural network classifies whether interval 1 or interval 2 contains post-stimulus brain activity. This classification task is repeated for each stimulus.

Stimulus Selection

Stimuli were selected using an adaptive randomized procedure developed by (Doll, Veltink, & Buitenweg, 2015). Such an adaptive procedure is necessary to center stimulus amplitudes around a (time-dependent) perceptual threshold, in order to estimate the psychometric curve and associated perceptual threshold based on stimulus-response or stimulus-classification pairs (Doll, Veltink, & Buitenweg, 2015; Leek, 2001; Treutwein, 1995). Randomization of the stimulus amplitude and inter-stimulus interval in this procedure is used to prevent an expectation bias.

One stimulus parameter (e.g., stimulus amplitude) is selected for threshold estimation. The value of this parameter is updated based on the response in the classification task as follows (Figure 10.3):

1) The parameter value is randomly chosen from a vector V consisting of an uneven number of k values separated by a fixed step size s.

2) If the stimulus is classified correctly, all vector values are increased with $d_{correct}$. If it is classified incorrectly all vector values are decreased with $d_{incorrect}$.

To let the mean of the applied parameter values converge to the perceptual threshold, it should hold that $\frac{d_{incorrect}}{d_{correct}+d_{incorrect}} = p_{threshold}$.

For a GN task, the perceptual threshold is defined as the parameter value where 50% of the stimuli is correctly classified, i.e., $p_{threshold} = 0.5$. For a 2IFC task, the perceptual threshold is defined as the parameter value where 75% of the stimuli is correctly classified, i.e., $p_{threshold} = 0.75$. For the adaptive stimulation procedure in DS1 and DS2, we used $k = 5$ values, $s = 0.025$ mA and $d_{correct} = 0.025$ mA. For the demonstration experiment (DS3), we explored which combination of the parameters k, s, $d_{correct}$ is optimal for estimating the perceptual threshold in each procedure through simulation. We found that the best estimates of the nociceptive perceptual threshold to double-pulse stimuli could be obtained in both procedures with $k = 7$ values, $s = 0.008$ mA and $d_{correct} = 0.008$ mA and used these settings for the adaptive stimulation procedure in DS3.

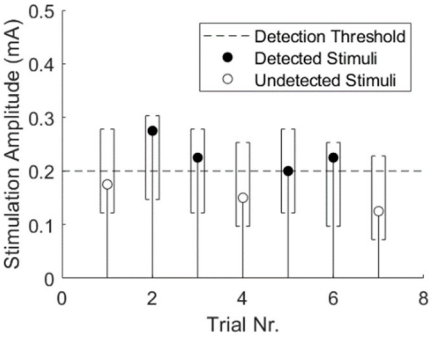

***Figure 10.3**: Randomized method of limits used to center stimulus amplitudes around the perceptual threshold (Doll, Veltink, & Buitenweg, 2015). A vector of k stimulus amplitudes separated by a stepsize s is initialized starting from 0 or centered around an initial estimate of the perceptual threshold. The stimulus amplitude is chosen randomly from this vector. The vector is increased with $d_{correct}$ if the stimulus is detected (in GN) or if the reported interval is correct (in 2IFC). The vector is decreased with $d_{incorrect}$ if the stimulus was not detected (in GN) or if the reported interval is incorrect (in 2IFC).*

Psychophysical Model

The probability of correct classification or detection of a sensory stimulus $p(\boldsymbol{\beta}, \boldsymbol{x})$ was modeled using the psychometric function described by Equation (1).

$$p(\boldsymbol{\beta}, \boldsymbol{x}, \lambda_{upper}, \lambda_{lower}) = \lambda_{lower} + (\lambda_{upper} - \lambda_{lower})\Phi(\beta_0 + \beta_1 x_1 + \beta_2 x_2 + \cdots + \beta_n x_n) \quad (1)$$

Where x denotes a vector of n stimulus parameters (e.g., stimulus amplitude, stimulus duration, number of previous stimuli), β denotes the vector of effects sizes of those stimulus parameters and Φ denotes the cumulative normal probability distribution function. Furthermore, λ_{upper} and λ_{lower} denote the upper and lower classification limit, respectively. The upper classification limit is the probability of correct classification when the value of stimulus parameters goes to infinite. The lower classification limit is the probability of correct classification when the values of stimulus parameters go to 0.

For post-hoc classification of DS2, with both single-pulse and double-pulse stimuli, we modeled classification/detection probability as a function of the first pulse amplitude (p_1), the second pulse amplitude (p_2) and the number of received stimuli (t) (Equation (2.1) and (2.2)). For real-time classification in DS3, we modeled classification/detection probability as a function of the pulse amplitude (p) and the number of received stimuli (t) (Equation (2.3) and (2.4)). Note that λ_{upper} and λ_{lower} were set to 1 and 0 respectively, in the case of a GN procedure, and set to 1 and 0.5 respectively, in the case of a 2IFC procedure.

DS2, participant GN:

$$p(\boldsymbol{\beta}, \boldsymbol{x}, 1{,}0) = \Phi(\beta_0 + \beta_{p1} p_1 + \beta_{p2} p_2 + \beta_t t) \quad (2.1)$$

DS2, neural network 2IFC:

$$p(\boldsymbol{\beta}, \boldsymbol{x}, 1{,}0.5) = 0.5 + 0.5\ \Phi(\beta_0 + \beta_{p1} p_1 + \beta_{p2} p_2 + \beta_t t) \quad (2.2)$$

DS3, participant GN:

$$p(\boldsymbol{\beta}, \boldsymbol{x}, 1{,}0) = \Phi(\beta_0 + \beta_p p + \beta_t t) \tag{2.3}$$

DS3, neural network 2IFC:

$$p(\boldsymbol{\beta}, \boldsymbol{x}, 1{,}0.5) = 0.5 + 0.5\ \Phi(\beta_0 + \beta_p p + \beta_t t) \tag{2.4}$$

Threshold Estimation

The psychometric function and corresponding perceptual thresholds were estimated based on the stimulus-classification pairs (SCPs) obtained using the adaptive procedure in Section 10.2.2. Parameters of the psychometric function were estimated by minimization the negative loglikelihood using an implementation of the GlobalSearch algorithm (Ugray et al., 2007) in combination with an interior-point algorithm to find local minima (Coleman & Li, 1996) in Matlab.

Performance of Threshold Estimation

Using DS2, the performance of post-hoc threshold estimation based on neural network classifications was 1) compared to the performance of threshold estimation using only the maximum value at the Cz channel during each interval for classification, and 2) compared to the performance of threshold estimation using a random score during each interval for classification. Differences between participant thresholds and neural network (or maximum value) estimated thresholds were assessed based on Bland-Altman analysis (Bland & Altman, 1986), using the BlandAltmanPlot function available on the Matlab file exchange. Differences in the limits of agreement between neural network and maximum value estimated thresholds, were tested by estimating the 95% confidence interval for the difference between limits of agreement (as the confidence interval between two sample means (Pfister & Janczyk, 2013)), and assessing whether the confidence interval included zero. The neural network classifications in DS2 were used to explain network classifications, which is further described in Section 10.2.3.

Using DS3, the performance of adaptive stimulation and real-time threshold estimation based on neural network classifications was assessed based on Bland-Altman analysis. In addition, the difference between stimulation amplitudes and estimated perceptual thresholds was assessed as a potential marker for the reliability of perceptual thresholds estimated using this paradigm.

10.2.3 Classification of EEG Data

EEG Recording

The EEG was recorded using a SAGA amplifier (TMSi, Oldenzaal, the Netherlands) with a sampling rate of 1024 Hz at 32 Ag/AgCl electrodes that were placed on the scalp according to the international 10-20 system.

Classification Task

Electroencephalography data were filtered by a causal high-pass filter of 0.1 Hz and a causal low-pass filter of 100 Hz, and downsampled to 512 Hz. Data were classified by a multilayer convolutional neural network performing a 2IFC classification task. The EEG was separated in an interval of pre-stimulus activity, ranging from -1.5 to -0.5 s, and an interval of post-stimulus activity, ranging from 0.05 to 1.05 s with respect to stimulus onset. Note that the first 50 ms following stimulation were excluded from the post-stimulus interval to rule out any influence of stimulation artifact. Each interval was centered by subtracting the mean and scaled by the standard deviation. The neural network was trained to label these EEG intervals as either pre-stimulus or post-stimulus activity. In the 2IFC classification task, the neural network computed a score for each interval, representing the probability that the interval represented post-stimulus activity. If the score of the second (post-stimulus) interval was higher than the score of the first (pre-stimulus) interval, the network classification was labeled as correct. Otherwise, the network classification was labeled as incorrect. The randomized method of limits described above was performed

based on if the interval classification by the neural network was correct or incorrect.

Note that the same neural network could also be used to classify if a stimulus was perceived or not by determining if the network score of the post-stimulus interval is higher than a cutoff value, which is equal to performing a GN task. However, this would introduce an estimation bias in the computed perceptual threshold, as network scores were calibrated based on the entire test set, but not for each individual new participant. Furthermore, as brain activity is non-stationary the potential calibration bias of neural network scores could vary over time. Therefore, the best reference we could compare the score of the post-stimulus interval with, is the score of the pre-stimulus interval. This comparison between post- and pre-stimulus interval scores is what we refer to as the 2IFC classification task.

Deep Neural Network for EEG Classification

An adapted version of a convolutional neural network developed for EEG-based BCIs, EEGnet (Lawhern et al., 2018), was used for EEG classification in Matlab. The epochs in DS1 that were reported as 'detected' by participants were used for training, validation, and testing. The detected epochs were split into a training set of 30868 intervals, a validation set of 3198 intervals and a test set of 4580 intervals, where half of the intervals were pre-stimulus and half of the intervals were post-stimulus. In the training and validation set, the intervals where no EEG was measured due to technical issues and the intervals where the maximum value over all channels was larger or smaller than 97.5% of all intervals were excluded. Intervals with technical issues or extreme noise were not excluded from the test set to have a representative distribution of test data, i.e., close to the distribution we would encounter with real-time classification. Recordings from the same subject were assigned to the same set (train, validation, or test), to prevent a bias through learning of subject-specific artefacts. The EEG intervals were shuffled within each set, and each interval was centered by subtracting the mean and scaled by the standard deviation.

Network and training parameters were explored using the training and validation set, resulting in the final network architecture is shown in Table 10.2. Training was done with a total of 9 epochs, a mini-batch size of 128, a gradient threshold of 2, and an initial learning rate of 0.1 with dropped with a factor of 0.2 every 3 epochs. Following training, the test set was used to evaluate classification performance, and to calibrate neural network scores with respect to the true classification probability using binomial regression with a complementary log-log link function. In addition, the accuracy and AUC of the calibrated neural network scores was evaluated using 10-fold cross-validation where in each non-overlapping fold 80% of DS1 was used for training, 10% for validation and 10% for testing.

Block	Layer	#Filter	Size	#Param	Output	Activation	Options
1	**Input**				(32,512)		
	Reshape				(32,512,1)		
	Conv2D	8	(1,128)	1024	(32,512,8)	Linear	Mode = same
	BatchNorm			16	(32,512,8)		
	DepthWiseConv2D	64	(32,1)	1024	(1,512,32)	Linear	Mode = valid Depth = 4 Max. norm = 1
	BatchNorm			64	(1,512,32)		
	Activation				(1,512,32)	ELU	
	AveragePool2D		(1,4)		(1,128,32)		
	Dropout				(1,128,32)		
2	**SeparableConv2D**	16	(1,16)	1024	(1,128,16)	Linear	
	BatchNorm			32	(1,128,16)		
	Activation				(1,128,16)	ELU	
	AveragePool2D		(1,8)		(1,16,16)		
	Dropout				(1,16,16)		
	Flatten				256		
Class.	**Dense**				2	Softmax	

Table 10.2: Neural network architecture, an adapted version of EEGnet (Lawhern et al., 2018).

Network Classification Explanations

Explanatory maps of the importance of each channel at several latencies for classification were obtained by computing the occlusion sensitivity (Zeiler & Fergus, 2014). In this technique, parts of the original input are systematically ablated to compute how much the output score changes by missing that part of the input signal. Occlusion sensitivity was computed for each channel in each interval using a mask of 50 samples and a stride of 10 samples. Nearest neighbor interpolation was used to resize the computed occlusion sensitivity to the original input size. Outliers were removed from the set of occlusion sensitivity maps where the standard deviation was larger than 0.05 or lower than 0.001. Overall occlusion sensitivity was determined by computing the median occlusion sensitivity over all intervals at each latency.

10.2.4 Analysis of EEG data

Electroencephalography data were processed using Fieldtrip, a Matlab toolbox for EEG and MEG signal analysis (Oostenveld, Fries, Maris, & Schoffelen, 2011). Similar to the data used for classification, continuous EEG data were filtered by a causal high-pass filter of 0.1 Hz and a causal low-pass filter of 100 Hz. Artefacts caused by eye movements and blinking were removed using independent component analysis (Delorme, Sejnowski, & Makeig, 2007). Epochs with excessive EMG activity or other remaining artefacts were removed through visual inspection. The averages shown in the results section either show filtered data at Cz, or data that was filtered, cleaned, and re-referenced at Cz-M1M2, which will be indicated explicitly. Contrasts between detected and non-detected and between correct and incorrect intervals, as well as the contrast between post-stimulus and baseline, were evaluated using cluster-based non-parametric statistical testing (Maris & Oostenveld, 2007).

10.3 Results

10.3.1 Neural Network Performance

Classification performance was initially evaluated on a single original test set in DS1 (also see Section 10.2.3). The classification performance of the neural network on this test set and calibrated network scores are shown in Figure 10.4. Here, the network classified post-stimulus and pre-stimulus EEG with an accuracy of 0.84 and AUC of 0.92. The network performed better classifying pre-stimulus EEG in comparison with classifying post-stimulus EEG.

Classification accuracy and AUC were also evaluated using 10-fold cross-validation, which was used to obtain more accurate estimates of network performance by averaging across multiple folds. Classification accuracy and AUC during 10-fold cross-validation are shown in Table 10.3. Although some folds show a similar classification performance as on the original test set, the average classification performance is lower with an average accuracy of 0.75 (± 0.05 std.) and an average AUC of 0.82 (± 0.06 std.).

Calibrated network scores should ideally be equal to the true probability of an interval being post-stimulus brain activity, corresponding to the diagonal line in Figure 10.4. Calibrated network scores were almost diagonal, showing that network scores after calibration were a good estimator of the average probability, and therefore suitable for EEG classification in a psychophysical procedure.

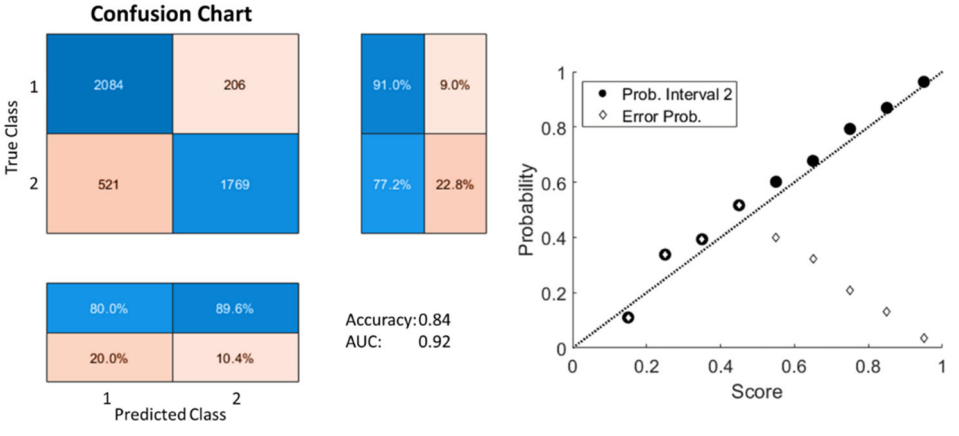

Figure 10.4: Neural network performance of classifying pre-stimulus and post-stimulus activity in the test set (left) and neural network classification scores in comparison with the average probability of an interval being post-stimulus brain activity (right). The confusion chart on the left shows the numbers and percentages of intervals of each class that were predicted correctly (blue) or incorrectly (red). The graph on the right shows the calibration of neural network classification scores. The neural network classification scores lie almost on the diagonal midline, showing that they were a good estimator of the true probability in this dataset.

Fold	Training Participants	Training Intervals	Test Participants	Test Intervals	Acc.	AUC
1	51	30326	6	4556	0.69	0.77
2	51	30948	6	3938	0.81	0.89
3	51	30198	6	3892	0.77	0.85
4	51	30856	6	4760	0.72	0.80
5	51	32038	6	3200	0.75	0.84
6	51	31498	6	3482	0.75	0.81
7	51	31208	6	3748	0.66	0.71
8	51	31540	6	3822	0.83	0.90
9	51	31888	6	3416	0.74	0.81
10	51	30450	6	3506	0.75	0.84
Average (±Std.)	51	31095	6	3832	0.75 (±0.05)	0.82 (±0.06)

Table 10.3: Classification accuracy and AUC during 10-fold cross-validation.

10.3.2 Post-hoc Estimation of Perceptual Thresholds

Perceptual Thresholds

The second dataset (DS2) was used to evaluate network performance in post-hoc estimation of the perceptual threshold. Two participants were excluded from this dataset due to failure to perform the detection task, defined as a detection rate of below 0.2 for one or both stimulus types. Performance of post-hoc threshold estimation based on neural network classifications was compared 1) to the performance of threshold estimation using only the maximum value at the Cz channel during each interval, and 2) to the performance of threshold estimation using a random score during each interval. An estimate of the perceptual threshold was considered invalid if the optimizer failed to converge to a solution, or if the estimated perceptual threshold was below 0 mA or above the maximum limit of stimulus amplitude in the experimental setup of 1.6 mA. As is shown in Table 10.4, using a random classifier almost always led to an invalid estimate of the perceptual threshold, while using the maximum value at Cz or using neural network scores returned more valid estimates.

The boxplot in Figure 10.5 shows that using the maximum value at Cz for interval classification, usually leads to a threshold estimate that is larger than the reference value (based on participant responses). Bland-Altman analysis in Figure 10.5 shows that using the maximum value at Cz for interval classification, leads to relatively large limits of agreement (LoA) of -0.30 and 0.56 for single-pulse stimuli and of -0.04 and 0.12 for double-pulse stimuli. The estimate of the perceptual threshold for double-pulse stimuli is significantly biased as the 95% confidence interval (CI) of the mean is above 0.

The boxplot in Figure 10.6 shows that using the neural network score for interval classification, usually leads to a threshold estimate that is similar to the reference value (based on participant responses), except for one exception marked with a red circle. Bland-Altman analysis in Figure 10.6 shows that using the neural network score for interval classification, leads to limits of agreement (LoA) of -0.08 and 0.05 for single-pulse stimuli and of -0.03 and 0.05 for double-pulse stimuli, with no significant estimation bias. The upper limits of agreement

of single- and double-pulse threshold estimates based on neural network scores, were significantly lower (i.e., closer to zero) than the upper limits of agreement of estimates based on maximum values ($p<.05$). The lower limit of agreement of single-pulse threshold estimates based on neural network scores, was significantly higher (i.e., closer to zero) than the lower limit of agreement of estimates based on maximum values ($p<.05$).

Method	Invalid Threshold Estimates Single-Pulse	Invalid Threshold Estimates Double-Pulse
Random	9	7
Maximum	3	2
Neural Network	1	1

Table 10.4: The number of invalid threshold estimates (out of a total of 13 estimates) for each type of classifier, where the optimizer failed to converge to a solution, or the estimated threshold was below 0 or above 1.6 mA.

Typical Examples

Tracked perceptual thresholds and average filtered EEG activity at Cz (not cleaned for artefacts) for an exceptional case (marked by red circles in Figure 10.6) are shown in Figure 10.7. Note that this participant showed a very large difference between the threshold computed based on participant responses, and the threshold computed based on brain activity. Averaged EEG activity shows that central evoked responses were also present for stimuli reported as non-detected. As a consequence, the neural network managed to successfully classify post-stimulus brain activity in 123 out of 130 epochs. Note that this resulted in an inaccurate estimate of the perceptual threshold due to the low amount of incorrectly classified stimuli available for threshold estimation.

Tracked perceptual thresholds and average filtered EEG activity at Cz (not cleaned for artefacts) for a typical participant are shown in Figure 10.8. Stimulus amplitudes were distributed around the estimated perceptual thresholds and the perceptual thresholds based on neural network classification were close to the perceptual thresholds based on participant responses. Note that the brain activity to non-detected or incorrectly classified stimuli remained close to baseline.

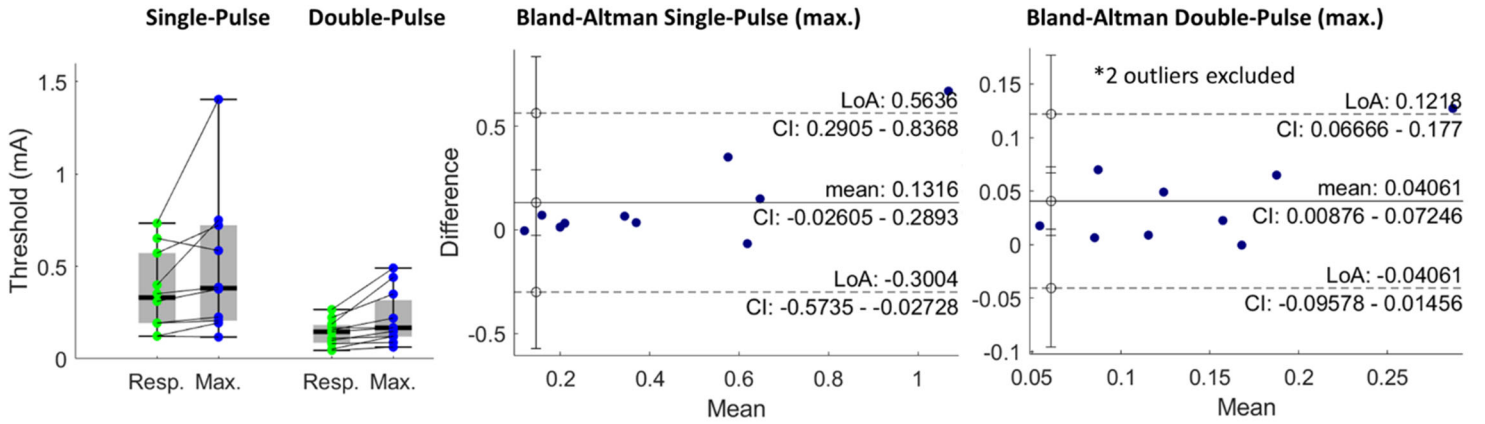

Figure 10.5: *Left: Perceptual thresholds based on participant responses (Resp.) and based on interval classification using the maximum value at Cz (Max.). Thresholds in the same participant are connected by a line. In each case, equal threshold estimates would indicate a good performance of automated threshold estimation. Right: Bland-Altman analysis of the difference between thresholds estimated based on maximum values and reference thresholds based on participant responses. Differences at more than 1.5 times the interquartile range above the upper quartile or below the lower quartile were excluded from Bland-Altman analysis as outliers. There was a significant bias in the thresholds estimated for double-pulse stimuli.*

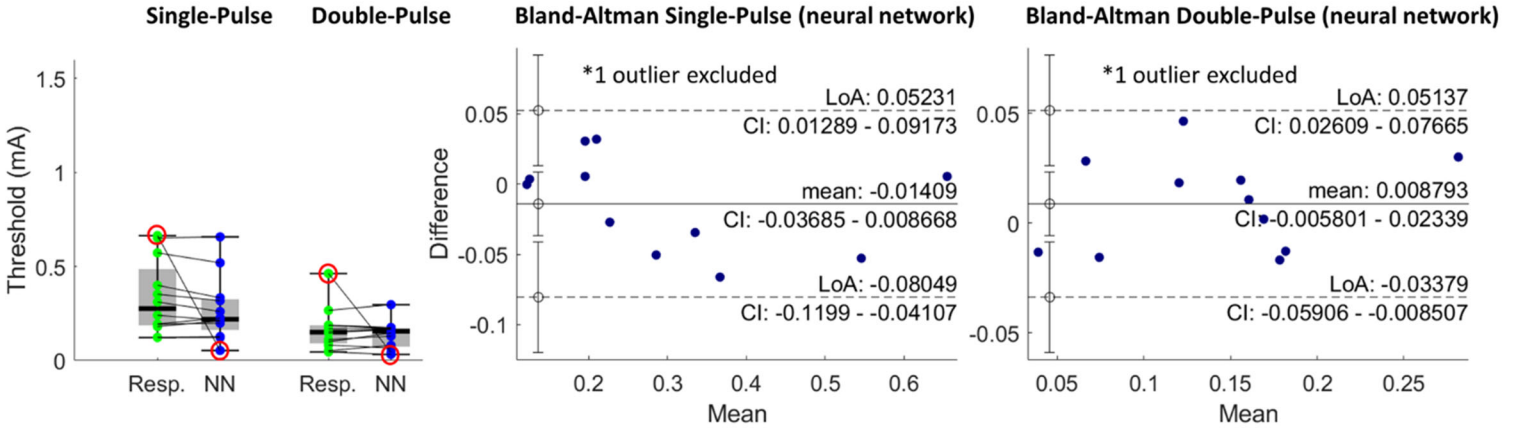

Figure 10.6: *Left: Perceptual thresholds based on participant responses (Resp.) and based on interval classification using the neural network score (NN). Thresholds in the same participant are connected by a line. In each case, equal threshold estimates would indicate a good performance of automated threshold estimation. One exceptional case, marked by red circles, is discussed in Section 10.3.2. Right: Bland-Altman analysis of the difference between thresholds estimated based on maximum values and reference thresholds based on participant responses. Differences at more than 1.5 times the interquartile range above the upper quartile or below the lower quartile were excluded from Bland-Altman analysis as outliers. There was no significant estimation bias and relatively narrow limits of agreement.*

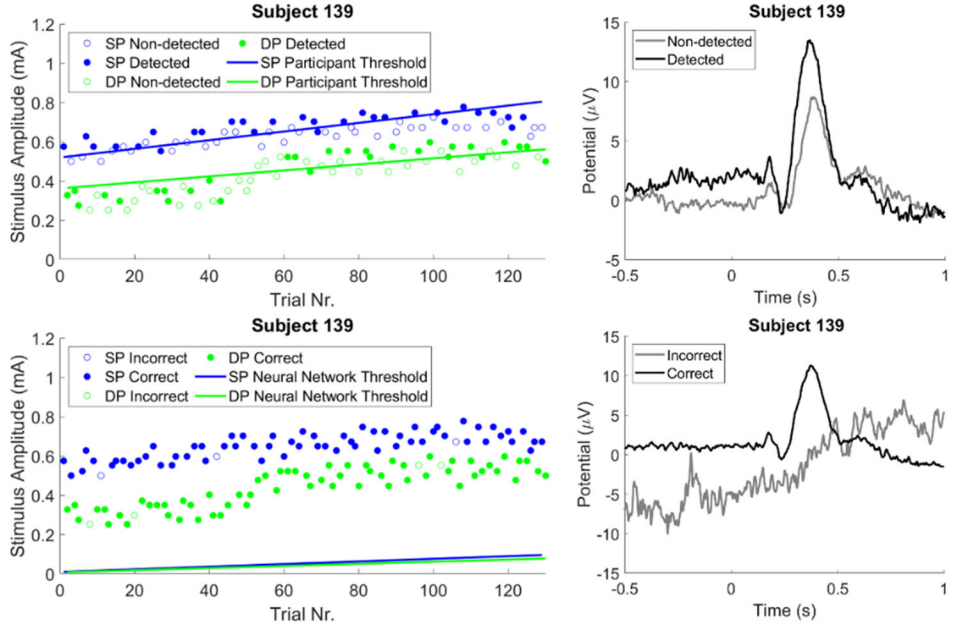

Figure 10.7: *Exceptional case. Detected (top) or correctly classified stimuli (bottom) are indicated by filled circles. Non-detected (top) or incorrectly classified stimuli (bottom) are indicated by open circles. The participant showed a very large difference between the threshold computed based on participant responses (top), and the threshold computed based on brain activity (bottom). Average evoked response at Cz (not cleaned for artefacts) shows a clear peak even for the stimuli reported as non-detected. The neural network did manage to correctly classify the interval of post-stimulus brain activity in all except 7 stimuli (bottom), leading to a very low estimate of the perceptual threshold which was likely inaccurate due to the low number of incorrect classifications available for threshold estimation.*

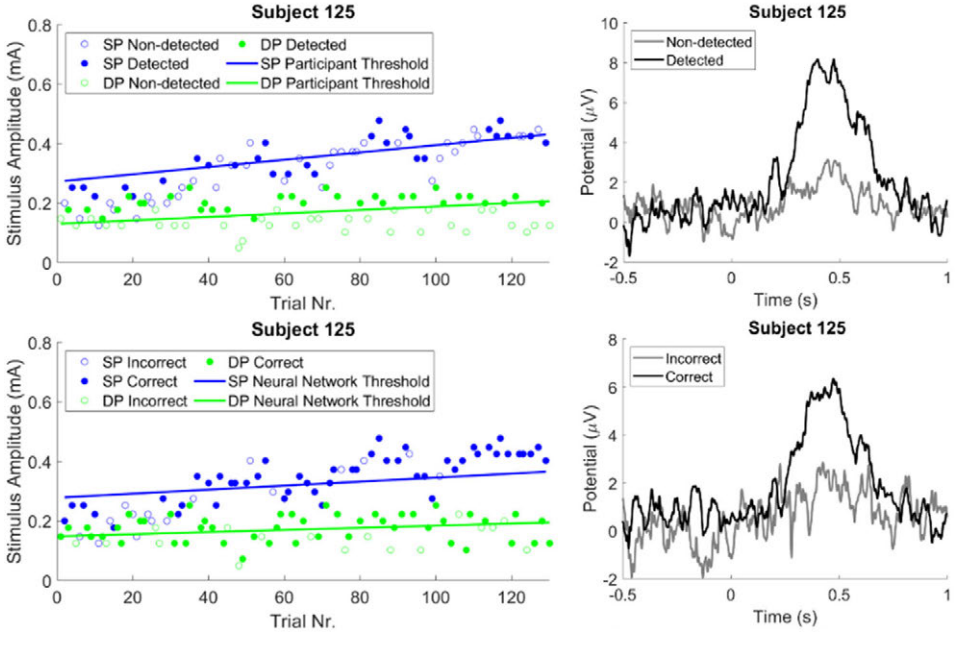

Figure 10.8: *Typical case. Detected stimuli are indicated by filled markers. The stimulus amplitudes were distributed around the estimated perceptual thresholds. There was a clear average evoked response at Cz (not cleaned for artefacts) to detected or correctly classified stimuli, while the evoked response to non-detected or incorrectly stimuli remained close to baseline. The perceptual threshold estimated by the neural network was close to the perceptual threshold estimated using participant responses.*

Evoked Potential

The average evoked potential at Cz-M1M2 (cleaned) in response to detected/correct and non-detected/incorrect stimulus-response and stimulus-classification pairs is shown in Figure 10.9. There was a significant contrast ($p<.05$) between detected and non-detected and between correct and incorrect epochs. Note that the average evoked potential in response to correctly classified epochs was lower than the average evoked potential in response to detected epochs, because of the lower limit on correct classification probability of 0.5 in a 2IFC task. As such, the average evoked potential of correctly classified epochs, could also include epochs with little or no brain activity. Also note that the average evoked potential in response to non-detected and incorrectly classified epochs was significant with respect to baseline at some latencies.

The average amplitude of the peak between 380 and 420 ms for several detection probabilities is displayed on the right. In order to compare detection probability during the GN task that was performed by the participant (ranging from 0 to 1) with detection probability during 2IFC classification task that was performed by the neural network, detection probability values during 2IFC were transformed to the same range of 0 to 1. The average peak amplitude appears to increase proportionally with respect to detection probability for participant as well as neural network responses.

Network Classification Explanations

Average occlusion sensitivity topographies in Figure 10.10 show that the neural network mainly focuses on several electrodes with a maximum at CP1 and a minimum at P3. The average evoked potentials at Cz, CP1 and P3 (not cleaned for artefacts) are compared to the occlusion sensitivity at CP1 and P3 in Figure 10.11. The occlusion sensitivity at P3 is minimal and the occlusion sensitivity at CP1 is maximal around the peaks at Cz, CP1 and P3 occurring between 380 and 420 ms.

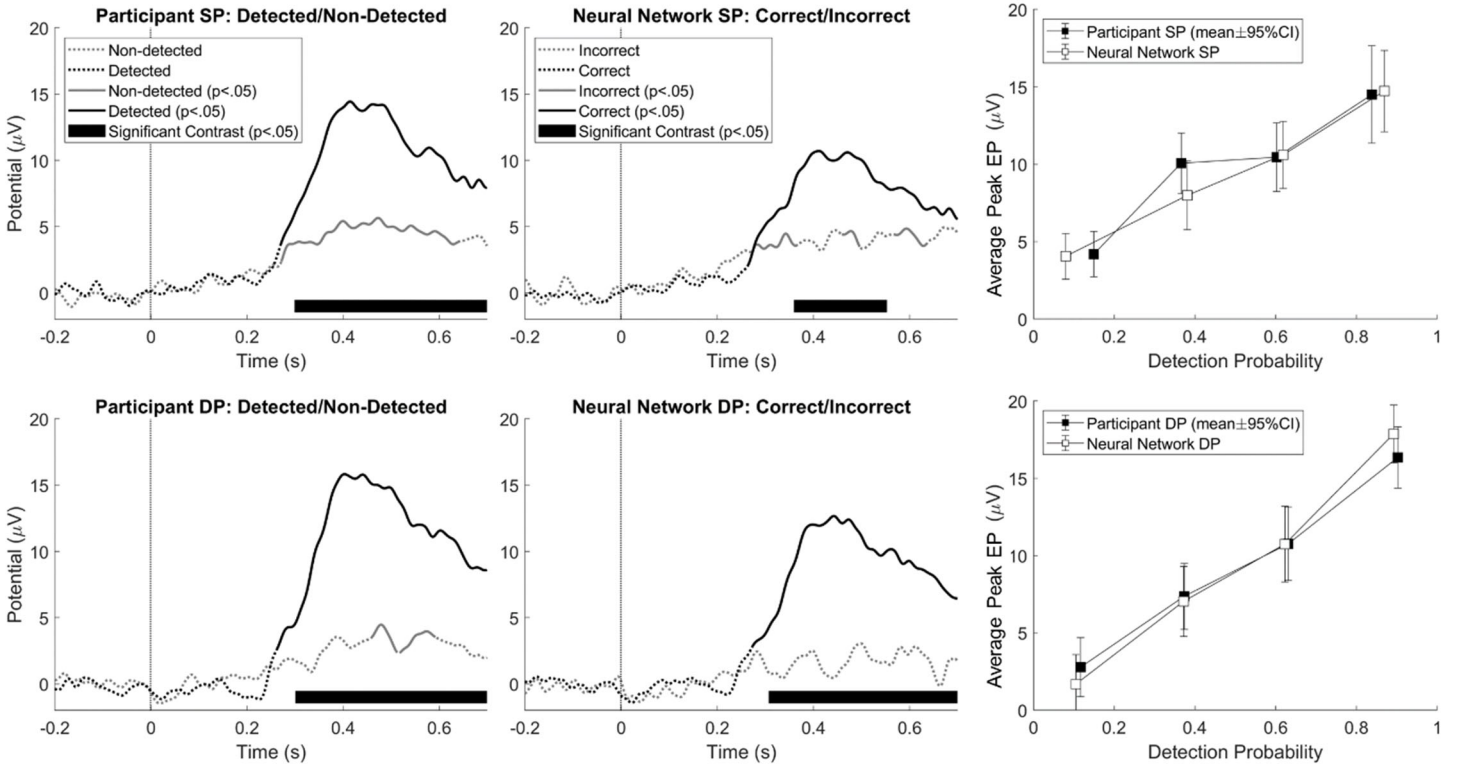

Figure 10.9: Average evoked potential at Cz-M1M2 (cleaned) for detected and non-detected (participant, go-/no-go), and for correct and incorrect (neural network, 2-interval forced choice) classified single-pulse (SP) and double-pulse (DP) stimuli. The was a significant contrast between detected and non-detected and between correct and incorrect. Average amplitude of the peak between 380 and 420 ms appears to increase proportional to detection probability.

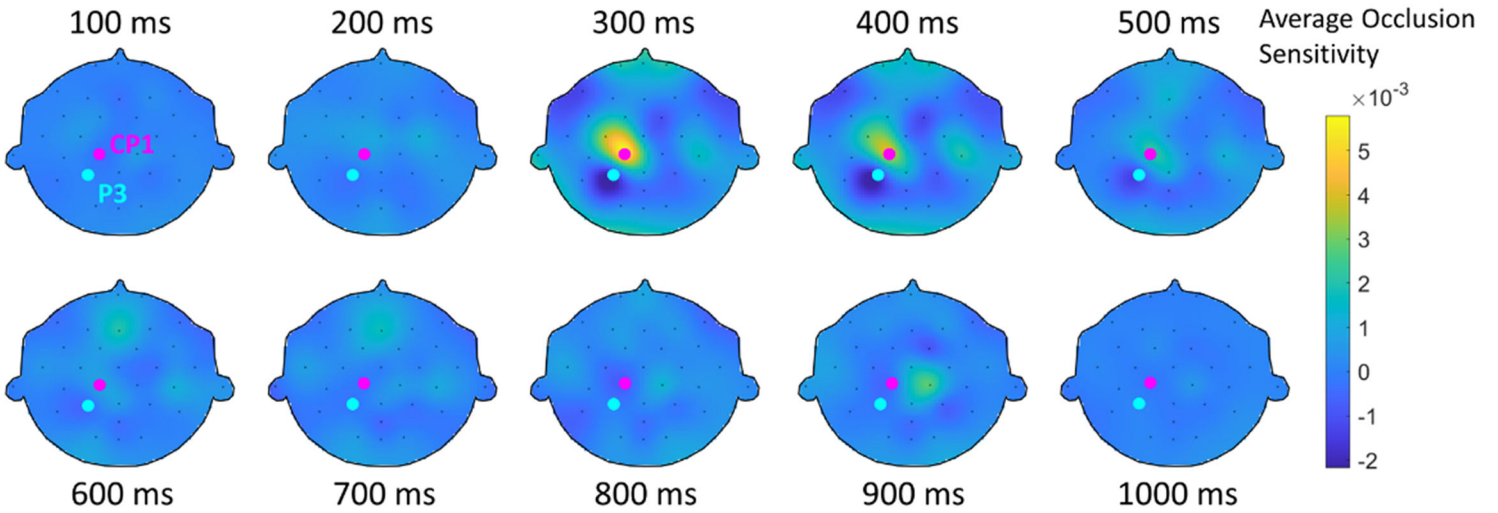

Figure 10.10: *Average occlusion sensitivity topographies for each 100 ms post-stimulus. The neural network appears to focus on CP1 (magenta) and P3 (cyan).*

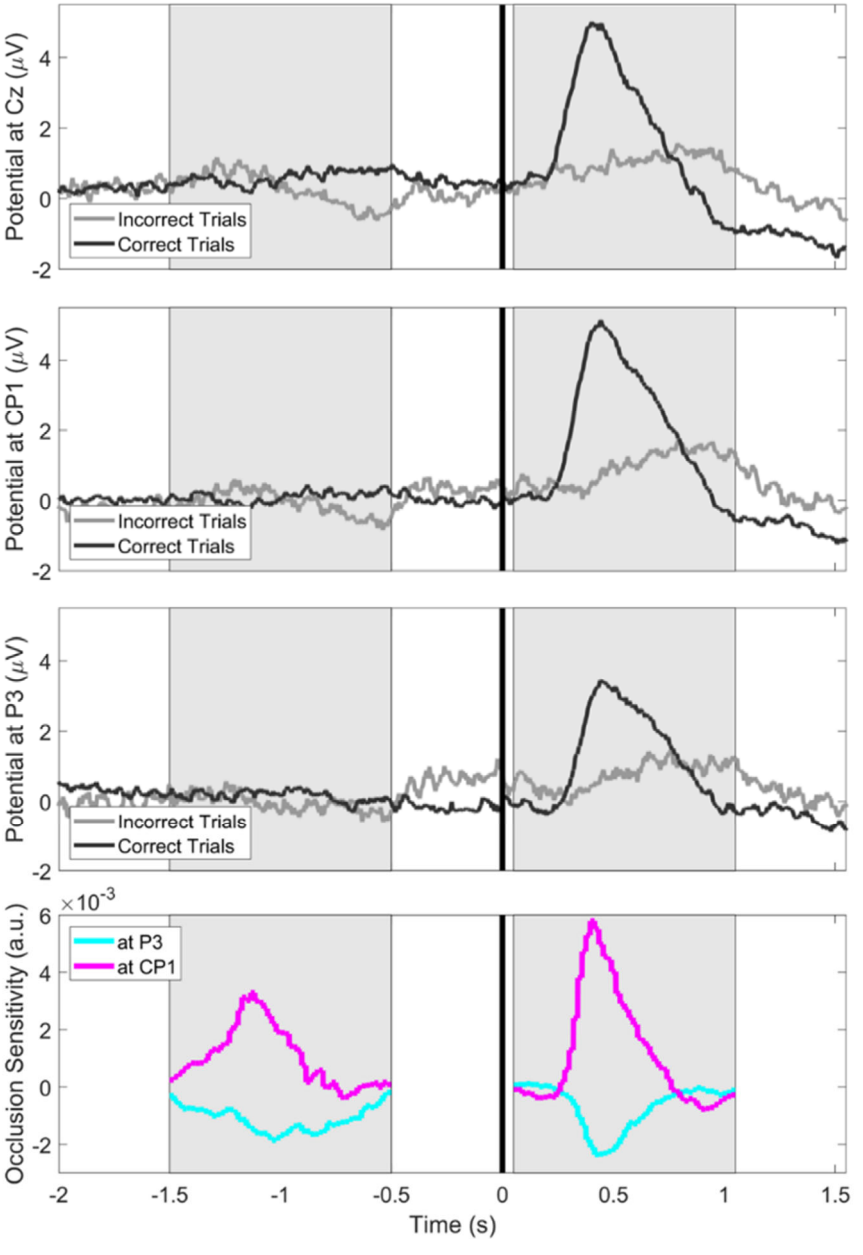

Figure 10.11: *Comparison between the average evoked potential waveforms observed at Cz, CP1 and P3 (not cleaned for artefacts, top) and the occlusion sensitivity at CP1 and P3 (bottom). Classification intervals are marked by a grey patch. Maxima and minima of the occlusion sensitivity coincide with the peak in evoked potential between 380 and 420 ms.*

10.3.3 Real-time Estimation of Perceptual Thresholds

Perceptual Thresholds

As a proof-of-concept, an experiment was performed (DS_3) where we used the neural network scores to control adaptive stimulation in real-time and to estimate the perceptual threshold based on the resulting stimulus-classification pairs. In part I, we simultaneously controlled stimulus amplitude based on an adaptive method of limits using participant responses and based on an adaptive method of limits using neural network classification. In part II, we simultaneously controlled stimulus amplitude based on two independent instances of the adaptive method of limits using neural network classification.

The boxplot in Figure 10.12 shows that using the neural network score for interval classification, usually leads to a threshold estimate that is similar to the reference value (based on participant responses) in Part I, where participants were assigned the task of releasing a response button when a stimulus was perceived. In Part II, where participants were assigned the task of counting the number of perceived stimuli, estimates by the two independent instances of the neural network appear less consistent in 2 participants. Table 10.5 shows a potential reason for inaccuracy in those estimates. The average absolute difference between stimulus amplitudes and the estimated perceptual threshold ($\overline{|\Delta|}$) tends to be larger when the estimates in Figure 10.12 are less consistent (marked in orange). Note that a large ($\overline{|\Delta|}$) indicates that the stimuli applied to the participant were far from the perceptual threshold, which could make it more difficult for optimization algorithms to find parameters of the psychometric function and the corresponding perceptual threshold.

Bland-Altman analysis in Figure 10.12 shows that using the neural network score for interval classification, leads to limits of agreement (LoA) of -0.09 and 0.06 with respect to estimates based on participant responses during a GN button-release task. Using two instances of the neural network for interval classification during a GN counting task, leads to limits of agreement of -0.09 and 0.10 between the estimates of both instances.

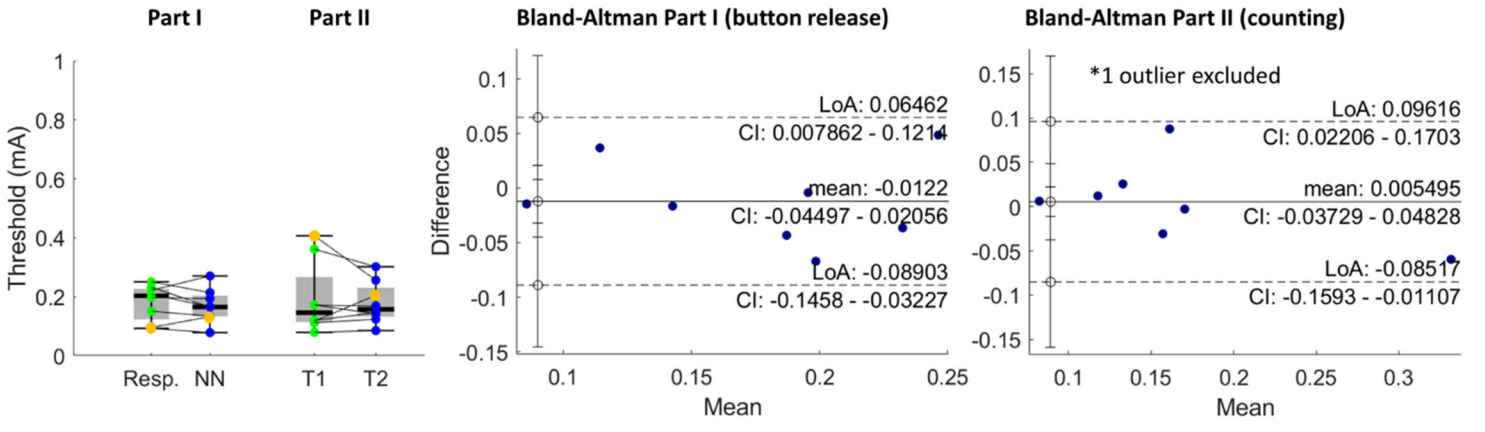

***Figure 10.12**: Left: Perceptual thresholds based on participant responses (Resp.) and based on interval classification using the maximum value at Cz (Max.). Thresholds in the same participant are connected by a line. In each case, equal threshold estimates would indicate a good performance of automated threshold estimation. Thresholds with an average absolute difference ($\overline{|\Delta|}$) between stimulus amplitudes and estimated perceptual threshold larger than 0.1 are marked in orange. Right: Bland-Altman analysis of the difference between thresholds estimated based on maximum values and reference thresholds based on participant responses. Differences at more than 1.5 times the interquartile range above the upper quartile or below the lower quartile were excluded from Bland-Altman analysis as outliers. There was a no significant bias of estimated thresholds.*

ID	Part	T_1 NN	S_1 NN	$\overline{\lvert\Delta\rvert}$	T_2 P	S_2 P	$\overline{\lvert\Delta\rvert}$	T_2 NN	S_2 NN	$\overline{\lvert\Delta\rvert}$
326	**I**	0.21	54.20	0.04	0.25	7.37	0.06			
416	**I**	0.27	24.74	**0.15**	0.22	7.77	**0.11**			
539	**I**	0.13	15.63	0.03	0.15	73.01	0.02			
595	**I**	0.08	53.63	0.02	0.09	91.10	0.02			
627	**I**	0.17	15.74	0.03	0.21	34.35	0.03			
655	**I**	0.13	17.80	0.03	0.10	70.97	0.02			
848	**I**	0.16	21.68	0.04	0.23	19.21	0.03			
926	**I**	0.19	8.56	0.07	0.20	12.43	0.04			
326	**II**	0.11	33.87	0.02				0.12	43.42	0.02
416	**II**	0.36	57.72	0.09				0.30	25.02	0.03
539	**II**	0.08	21.15	0.03				0.09	7.89	0.04
595	**II**	0.12	29.85	0.02				0.15	16.11	0.04
627	**II**	0.17	18.78	0.04				0.14	25.42	0.02
655	**II**	0.41	20.36	**0.18**				0.26	88.74	0.03
848	**II**	0.17	49.90	0.03				0.17	29.56	0.03
926	**II**	0.12	8.74	0.04				0.21	1.73	**0.28**

***Table 10.5**: Estimated perceptual thresholds (T) and slopes (S) based on participant (P) and neural network (NN) responses. The average absolute difference between stimulus amplitudes and the estimated perceptual threshold ($\overline{\lvert\Delta\rvert}$) is a potential marker for the quality of the estimated threshold. Participants where the $\overline{\lvert\Delta\rvert}$ is larger than 0.1 are marked in orange.*

Typical Examples

An exceptional case where estimation of the perceptual threshold was inaccurate in Part II is shown in Figure 10.13. The threshold estimates in Part I appear to be consistent and stable. A $\overline{|\Delta|}$ of 0.04 and of 0.06 for the neural network threshold and the participant threshold respectively (Table 10.5), indicates that the stimuli applied were close to the estimated perceptual threshold. Evoked responses at Cz (not cleaned for artefacts) that were incorrectly classified remain close to baseline, while a clear response is visible in the average of correctly classified stimuli. This confirms that the neural network performed well in the classification of evoked responses. Nevertheless, the estimate of threshold 2 in Part II is clearly inaccurate which is signaled by a large $\overline{|\Delta|}$ of 0.28 (Table 10.5).

Tracked perceptual thresholds and average filtered EEG activity at Cz (not cleaned for artefacts) for a typical participant in Parts I and II are shown in Figure 10.14. Stimulus amplitudes were distributed around the estimated perceptual thresholds. The perceptual thresholds based on neural network classification were close to the perceptual thresholds based on participant responses in Part I. Both independent estimates of the perceptual threshold based on neural network responses in Part II are consistent. Note that the average evoked response to incorrectly classified stimuli remained close to baseline, while an evoked response is visible in the average of correctly classified stimuli.

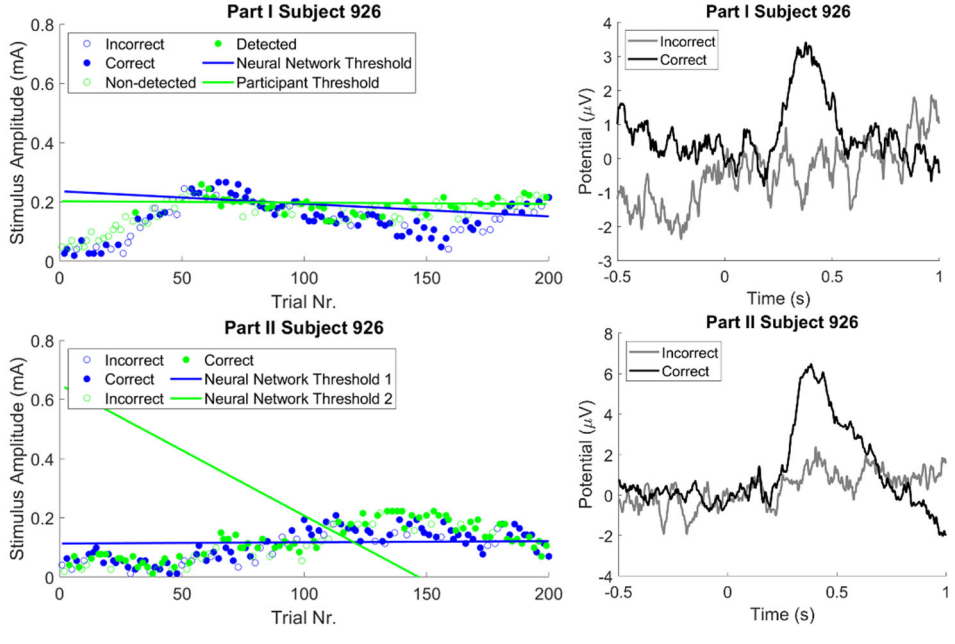

Figure 10.13: Exceptional case. Detected stimuli are indicated by filled markers. Estimated perceptual thresholds in part I are consistent and stable ($\overline{|\Delta|} = 0.04$ and $\overline{|\Delta|} = 0.06$). There was a clear average evoked response at Cz (not cleaned for artefacts) to correctly classified stimuli, while the evoked response to incorrectly classified stimuli remained close to baseline. However, the estimate of threshold 2 in part II appears to be inaccurate which is signaled by a large $\overline{|\Delta|}$ of 0.28.

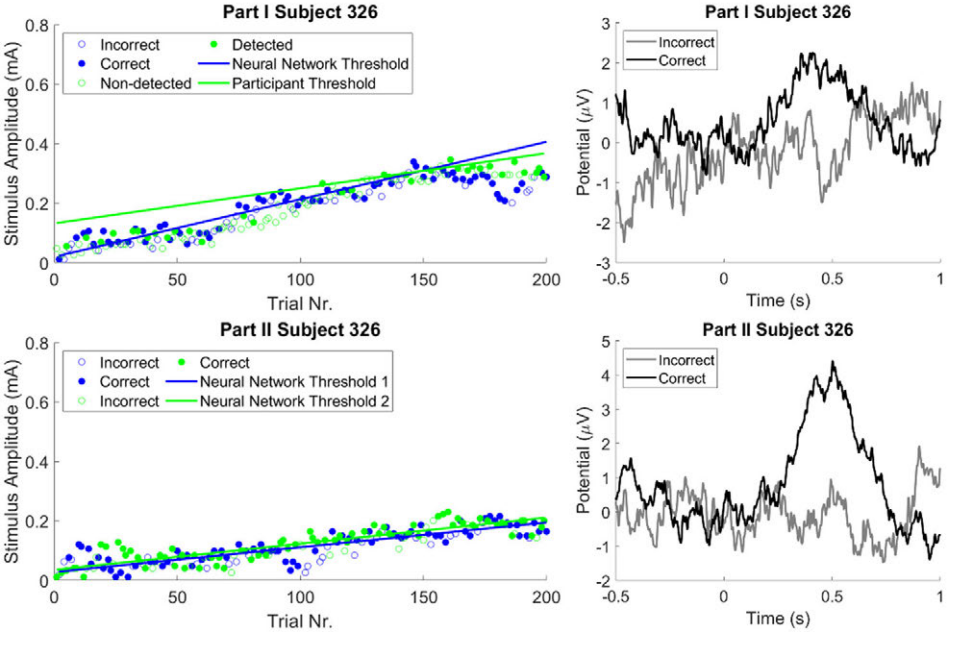

Figure 10.14: Typical case. Detected stimuli are indicated by filled markers. The stimulus amplitudes were distributed around the estimated perceptual thresholds. There was a clear average evoked response at Cz (not cleaned for artefacts) to correctly classified stimuli, while the evoked response to incorrectly classified stimuli remained close to baseline. The perceptual threshold estimated by the neural network was close to the perceptual threshold estimated using participant responses in part I, and both independent estimates of the perceptual threshold based on neural network classification in part II are consistent.

10.4 Discussion

In this work, we proposed a fully automated approach to estimate perceptual thresholds based on cortical brain activity rather than based on reported perception. To accurately estimate the perceptual threshold based on cortical activity, two challenges needed to be addressed. First, we needed the ability to accurately classify brain activity evoked by stimuli close to the perceptual threshold. Second, we needed to make sure that automated estimation based on neural network classification results in an unbiased estimate of the perceptual threshold.

We hypothesized that when a stimulus is perceived, task-related neural activity can be detected by a deep neural network and used for estimation of the perceptual threshold. In accordance with this hypothesis, neural network classification of post-stimulus EEG performed well with an accuracy of 0.84 and AUC of 0.92 on the test set, and an accuracy 0.75 and AUC of 0.82 during 10-fold cross-validation. In this study, we had the luxury of a large training set obtained through previous studies of nociceptive processing, which likely contributed to the success of deep learning. The deep neural network was most sensitive to occlusion of channel latencies around the observed P2 evoked response at Cz, associated with conscious access to sensory information. Topographies of the occlusion sensitivity show focus on a single dipolar source around these latencies. Importantly, these observations confirm that the neural network focusses on brain activity, rather than on artefacts such as eye-blinks or muscular activity. The difference between the observed dipolar topographies of occlusion sensitivity and the diffuse central topography associated with vertex potentials is not surprising: The occlusion sensitivity topography potentially represents the influence of any type of recorded neural activity on network scores, phaselocked and non-phaselocked, timelocked and non-timelocked, at these latencies as the neural network is able to use a combination of features spanning time, frequency and space using its three convolutional layers. On the other hand, the topography of the grand average vertex potential only represents timelocked and phaselocked neural activity (which also has to overlap between subjects). However, the exact reasons for the dipolar topography of occlusion sensitivity around 300 and 400 ms remain

unknown, although the spatial distribution could suggest involvement of the primary somatosensory cortex.

The challenge of obtaining unbiased estimates of the perceptual threshold was addressed by letting the neural network perform a 2IFC classification task. Although using this task helps us to deal with a potentially biased classification score due to cross-subject application of the neural network and the non-stationarity of EEG signals (also see Section 10.2.3), a few other potential reasons for error remain. For instance, presence of a readiness potential in pre-stimulus activity could have facilitated interval classification. Nevertheless, the experimental paradigm was designed to reduce expectation bias when participants perform a psychophysical task by randomizing stimulus amplitude and the inter-stimulus interval (Doll, Veltink, & Buitenweg, 2015), and this most likely reduced associated readiness potentials. In addition, these readiness potentials were not time-locked with the stimulus due to a 1s randomized inter-stimulus interval, further reducing the potential influence of readiness potentials. A remaining influence of readiness potentials could have negatively impacted the performance of threshold estimation by biasing estimated thresholds towards lower values. However, no evidence of such a negative bias was found in this study. Note that presence of an electrical stimulation artefact could be another reason for estimation bias, and the period between 0 and 50 ms was excluded from the post-stimulus interval to prevent a potential estimation bias.

We used the network classifications for estimation of the perceptual threshold by fitting a psychometric function to stimulus-classification pairs. If the neural network successfully classified post-stimulus brain activity by recognizing task-related brain activity, one would expect the estimated perceptual threshold to be equal to the perceptual threshold based on participant report. On the other hand, if the neural network classified post-stimulus brain activity by recognizing stimulus-evoked sensory-discriminative brain activity, one would expect the estimated perceptual threshold to be lower than the perceptual threshold based on participant report, based on the notion that sensory information is available for decision making before it is consciously perceived (Dehaene & Changeux, 2011).

During post-hoc estimation, the neural network estimate was remarkably close to the estimate based on participant responses with a difference of less than 0.1 mA in 11 out of 13 participants. Furthermore, Bland-Altman analysis showed that using a neural network for classification resulted in limits of agreement of -0.08 and 0.05 for single-pulse stimuli and of -0.03 and 0.05 for double-pulse stimuli, with no significant estimation bias. These limits of agreement are sufficiently small for clinical applications using nociceptive perceptual thresholds, such as observing the loss of intra-epidermal nerve fibers following capsaicin application (Doll et al., 2016), or the assessment of impaired nociceptive processing following sleep deprivation (van den Berg et al., 2022). In contrast, using the method of simply classifying the post-stimulus interval based on maximum values during both intervals, led to larger upper limits of agreement of 0.56 for single-pulse and 0.12 for double-pulse stimuli and a larger lower limit of agreement of -0.30 for single-pulse stimuli. Threshold estimates based on maximum values for double-pulse stimuli were significantly biased upwards. This shows that it is necessary to use neural networks or other similarly sophisticated classification methods within the protocol presented here, in order to obtain clinically relevant estimates of the perceptual threshold.

In a first proof-of-concept experiment on 8 healthy participants, we evaluated the performance of the neural network for real-time tracking and estimation of the perceptual threshold. When participants were assigned the GN task of releasing a response button when a stimulus was perceived (DS_3, Part I), 8 out of 8 neural network estimates were close to the estimate based on participant responses, with a difference of less than 0.1 mA. When participants were assigned the GN task of counting the number of perceived stimuli (DS_3, Part II), 7 out of 8 neural network estimates were close to the independent estimate of a second instance of the neural network, with a difference of less than 0.1 mA. Furthermore, Bland-Altman analysis showed that using a neural network for classification resulted in limits of agreement of -0.09 and 0.06 during the GN task based on button-release and of -0.09 and 0.10 during the GN task based on counting, with no significant estimation bias. Nevertheless, the average absolute difference between stimulus amplitudes and the estimated perceptual threshold ($\overline{|\Delta|}$), suggests that threshold estimation performed worse during the

counting task in two participants. A potential reason for this decrease in performance is the difference in task, which could mean that the brain activity used for classification during the experiment was different from the activity on which the neural network was trained. Also note that the neural network used in this study is unlikely to work for classifying perception of task-irrelevant stimuli. However, the network might still be retrained using transfer learning to achieve a better performance in classifying brain activity during counting or in response to task-irrelevant stimuli.

In addition, analysis of individual participants in DS2 and DS3 identifies two other potential reasons for error. First, in post-hoc estimation of the perceptual threshold, the estimate will be inaccurate if a clear P2 is present despite the participant reporting the stimulus as not perceived. As this dissociation between brain activity and reported perception resulted in a very high number of correctly classified epochs in one of the participants, optimization algorithms were unable to accurately estimate the psychometric function and associated perceptual threshold for this participant. Second, inaccurate estimates during real-time estimation of the perceptual threshold occur due to inability of the optimization algorithm to estimate parameters of the psychometric function based on the stimulus-classification pairs. However, these problems with threshold estimation are signaled adequately by a large difference between the applied stimulus amplitudes and the estimated threshold, which could be used as a quality control measure.

10.5 Conclusion

Deep learning enables accurate classification of EEG recordings in real-time, and thereby allows for non-invasive automated estimation of perceptual thresholds based on brain activity. While current BCI literature mainly focuses on the detection of visual evoked potentials, we found that neural networks can also be used as a reliable classifier of brain activity in response to nociceptive stimuli. In this work, we showed that deep neural network classification of the electroencephalogram leads to accurate estimates of the perceptual threshold post-hoc, and we provided a first proof-of-concept that we might use deep

neural network classification to control an adaptive stimulus sequence and estimate the perceptual threshold in real-time. Further studies should assess if the real-time method could accurately estimate the perceptual threshold in a larger group of participants outside the laboratory. Automated perceptual threshold estimation based on the electroencephalogram using deep neural network classification enables development of technology for accurate and objective assessment of perceptual thresholds in a wide variety of patient groups in which obtaining reliable perceptual reports can be difficult due to cognitive impairment, communication problems or potential simulation or malingering.

10.6 Acknowledgements

The authors would like to thank Imre Krabbenbos and Tom Berfelo at the Department of Anesthesiology, Intensive Care and Pain Medicine at the St. Antonius Hospital in Nieuwegein, the Netherlands, for providing a part of the training data (DS1) used in this study.

10.7 References

Austen, S., & Lynch, C. (2004). Non-organic hearing loss redefined: understanding, categorizing and managing non-organic behaviour. *International Journal of Audiology, 43*(8), 449-457.

Barachant, A., Bonnet, S., Congedo, M., & Jutten, C. (2012). Multiclass Brain–Computer Interface Classification by Riemannian Geometry. *IEEE Transactions on Biomedical Engineering, 59*(4), 920-928.

Bland, J. M., & Altman, D. G. (1986). Statistical methods for assessing agreement between two methods of clinical measurement. *Lancet, 1*(8476), 307-310.

Bruce, B. B., & Newman, N. J. (2010). Functional visual loss. *Neurologic clinics, 28*(3), 789-802.

Coleman, T. F., & Li, Y. (1996). An Interior Trust Region Approach for Nonlinear Minimization Subject to Bounds. *SIAM Journal on Optimization, 6*(2), 418-445.

Courtin, A. S., Maldonado Slootjes, S., Caty, G., Hermans, M. P., Plaghki, L., & Mouraux, A. (2020). Assessing thermal sensitivity using transient heat and cold stimuli combined with a Bayesian adaptive method in a clinical setting: A proof of concept study. *European Journal of Pain, 24*(9), 1812-1821.

Dehaene, S., & Changeux, J.-P. (2011). Experimental and Theoretical Approaches to Conscious Processing. *Neuron, 70*(2), 200-227.

Delorme, A., Sejnowski, T., & Makeig, S. (2007). Enhanced detection of artifacts in EEG data using higher-order statistics and independent component analysis. *NeuroImage, 34*(4), 1443-1449.

Doll, R. J., van Amerongen, G., Hay, J. L., Groeneveld, G. J., Veltink, P. H., & Buitenweg, J. R. (2016). Responsiveness of electrical nociceptive detection thresholds to capsaicin (8 %)-induced changes in nociceptive processing. *Experimental Brain Research, 234*(9), 2505-2514.

Doll, R. J., Veltink, P. H., & Buitenweg, J. R. (2015). Observation of time-dependent psychophysical functions and accounting for threshold drifts. *Attention, Perception, and Psychophysics, 77*(4), 1440-1447.

Gemein, L. A. W., Schirrmeister, R. T., Chrabąszcz, P., Wilson, D., Boedecker, J., Schulze-Bonhage, A., . . . Ball, T. (2020). Machine-learning-based diagnostics of EEG pathology. *NeuroImage, 220*, 117021.

Hennings, K., Frahm, K. S., Petrini, L., Andersen, O. K., Arendt-Nielsen, L., & Mørch, C. D. (2017). Membrane properties in small cutaneous nerve fibers in humans. *Muscle Nerve, 55*(2), 195-201.

Inui, K., & Kakigi, R. (2012). Pain perception in humans: Use of intraepidermal electrical stimulation. *Journal of Neurology, Neurosurgery and Psychiatry, 83*(5), 551-556.

Krämer, H. H., Rolke, R., Bickel, A., & Birklein, F. (2004). Thermal thresholds predict painfulness of diabetic neuropathies. *Diabetes Care, 27*(10), 2386-2391.

Lawhern, V. J., Solon, A. J., Waytowich, N. R., Gordon, S. M., Hung, C. P., & Lance, B. J. (2018). EEGNet: a compact convolutional neural network for EEG-based brain–computer interfaces. *Journal of Neural Engineering, 15*(5), 056013.

Leek, M. R. (2001). Adaptive procedures in psychophysical research. *Perception and Psychophysics, 63*(8), 1279-1292.

Maier, C., Baron, R., Tölle, T. R., Binder, A., Birbaumer, N., Birklein, F., . . . Treede, D. R. (2010). Quantitative sensory testing in the German Research Network on Neuropathic Pain (DFNS): somatosensory abnormalities in 1236 patients with different neuropathic pain syndromes. *Pain, 150*(3), 439-450.

Maris, E., & Oostenveld, R. (2007). Nonparametric statistical testing of EEG- and MEG-data. *Journal of Neuroscience Methods, 164*(1), 177-190.

Mouraux, A., & Iannetti, G. D. (2009). Nociceptive Laser-Evoked Brain Potentials Do Not Reflect Nociceptive-Specific Neural Activity. *Journal of Neurophysiology, 101*(6), 3258-3269.

Mouraux, A., Iannetti, G. D., & Plaghki, L. (2010). Low intensity intra-epidermal electrical stimulation can activate Aδ-nociceptors selectively. *Pain, 150(1)*, 199-207.

Oostenveld, R., Fries, P., Maris, E., & Schoffelen, J. M. (2011). FieldTrip: Open source software for advanced analysis of MEG, EEG, and invasive electrophysiological data. *Computational Intelligence and Neuroscience, 2011*.

Pfister, R., & Janczyk, M. (2013). Confidence intervals for two sample means: Calculation, interpretation, and a few simple rules. *Advances in cognitive psychology, 9*(2), 74-80.

Picton, T. W. (1992). The P300 wave of the human event-related potential. *Journal of Clinical Neurophysiology, 9*(4), 456-479.

Poulsen, A. H., Tigerholm, J., Meijs, S., Andersen, O. K., & Mørch, C. D. (2020). Comparison of existing electrode designs for preferential activation of cutaneous nociceptors. *Journal of Neural Engineering*.

Rivet, B., Souloumiac, A., Attina, V., & Gibert, G. (2009). xDAWN algorithm to enhance evoked potentials: application to brain-computer interface. *IEEE Trans Biomed Eng, 56*(8), 2035-2043.

Roy, Y., Banville, H., Albuquerque, I., Gramfort, A., Falk, T. H., & Faubert, J. (2019). Deep learning-based electroencephalography analysis: a systematic review. *Journal of Neural Engineering, 16*(5), 051001.

Rutiku, R., Martin, M., Bachmann, T., & Aru, J. (2015). Does the P300 reflect conscious perception or its consequences? *Neuroscience, 298*, 180-189.

Salti, M., Bar-Haim, Y., & Lamy, D. (2012). The P3 component of the ERP reflects conscious perception, not confidence. *Conscious Cogn, 21*(2), 961-968.

Smith, M. L., Cesana, M. L., Farran, E. K., Karmiloff-Smith, A., & Ewing, L. (2018). A "spoon full of sugar" helps the medicine go down: How a participant friendly version of a psychophysics task significantly improves task engagement, performance and data quality in a typical adult sample. *Behavior Research Methods, 50*(3), 1011-1019.

Steenbergen, P., Buitenweg, J. R., Trojan, J., van der Heide, E. M., van den Heuvel, T., Flor, H., & Veltink, P. H. (2012). A system for inducing concurrent tactile and nociceptive sensations at the same site using electrocutaneous stimulation. *Behavior Research Methods, 44*(4), 924-933.

Tanaka, S., Gomez-Tames, J., Wasaka, T., Inui, K., Ueno, S., & Hirata, A. (2021). Electrical Characterisation of Aδ-Fibres Based on Human in vivo Electrostimulation Threshold. *Frontiers in Neuroscience, 14*(1305).

Treutwein, B. (1995). Adaptive psychophysical procedures. *Vision Research, 35*(17), 2503-2522.

Ugray, Z., Lasdon, L., Plummer, J., Glover, F., Kelly, J., & Martí, R. (2007). Scatter Search and Local NLP Solvers: A Multistart Framework for Global Optimization. *INFORMS Journal on Computing, 19*(3), 328-340.

Van den Berg, B., Berfelo, T., Verhoeven, E. M. H., Krabbenbos, I. P., & Buitenweg, J. R. (2021). *Combining psychophysical and EEG biomarkers for improved observation of altered nociceptive processing in failed back surgery syndrome*. Paper presented at the 43rd Annual International Conference of the IEEE Engineering in Medicine and Biology Society (EMBC), Guadalajara, Mexico.

Van den Berg, B., & Buitenweg, J. R. (2018). *Analysis Of Nociceptive Evoked Potentials During Multi-Stimulus Experiments Using Linear Mixed Models*. Paper presented at the 40th Annual International Conference of the IEEE Engineering in Medicine and Biology Society (EMBC), Honolulu, United States.

van den Berg, B., & Buitenweg, J. R. (2021). Observation of Nociceptive Processing: Effect of Intra-Epidermal Electric Stimulus Properties on Detection Probability and Evoked Potentials. *Brain Topography*.

van den Berg, B., Doll, R. J., Mentink, A. L. H., Siebenga, P. S., Groeneveld, G. J., & Buitenweg, J. R. (2020). Simultaneous tracking of psychophysical detection thresholds and evoked potentials to study nociceptive processing. *Behavior Research Methods*.

van den Berg, B., Hijma, H. J., Koopmans, I., Doll, R. J., Zuiker, R. G. J. A., Groeneveld, G. J., & Buitenweg, J. R. (2022). Simultaneous measurement of intra-epidermal electric detection thresholds and evoked potentials for observation of nociceptive processing following sleep deprivation. *Experimental Brain Research*.

van den Berg, B., Vanwinsen, L., Pezzali, G., & Buitenweg, J. R. (2021). Influence of Response Criterion on Nociceptive Detection Thresholds and Evoked Potentials. *bioRxiv*, 2021.2011.2002.466896.

Zeiler, M. D., & Fergus, R. (2014). *Visualizing and Understanding Convolutional Networks.* Paper presented at the European Conference on Computer Vision 2014, Zurich, Switzerland.

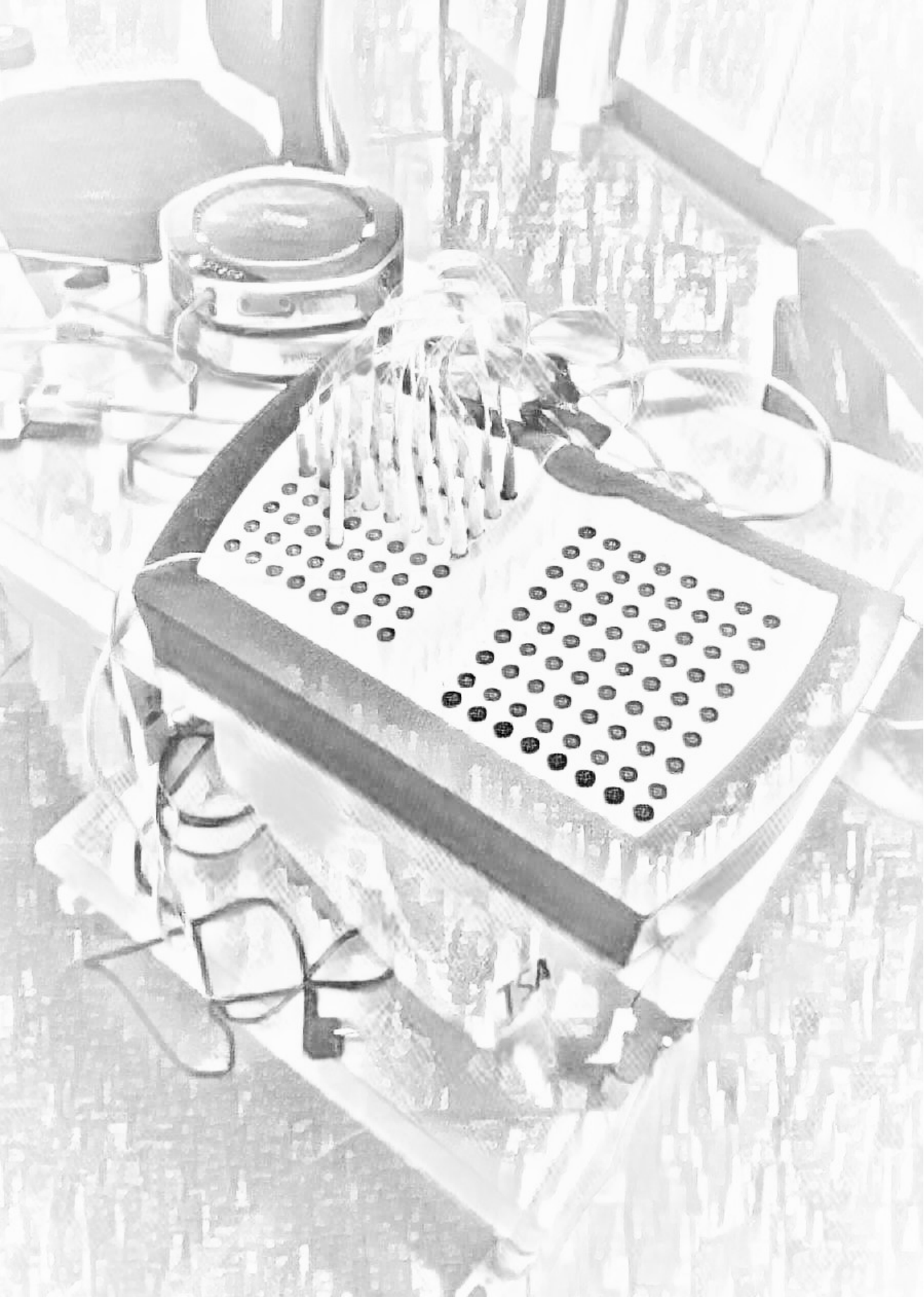

Chapter 11

Multisine Frequency Modulation of Intra-Epidermal Electric Pulse Sequences: A Novel Tool to Study Nociceptive Processing

Published as:

Van den Berg, B., Manoochehri, M., Kasting, M., Schouten, A. C., van der Helm, F. C. T., & Buitenweg, J. R. (2021). Multisine frequency modulation of intra-epidermal electric pulse sequences: a novel tool to study nociceptive processing. *Journal of Neuroscience Methods*, 353, 109106.

DOI: https://www.doi.org/10.1016/j.jneumeth.2021.109106

Abstract

A sustained sensory stimulus with a periodic variation of intensity creates an electrophysiological brain response at associated frequencies, referred to as the steady-state evoked potential (SSEP). The SSEPs elicited by the periodic stimulation of nociceptors in the skin may represent activity of a brain network that is primarily involved in nociceptive processing. Exploring the behavior of this network could lead to valuable insights regarding the pathway from nociceptive stimulus to pain perception.

We present a method to directly modulate the pulse rate of nociceptive afferents in the skin with a multisine waveform through intra-epidermal electric stimulation. The technique was demonstrated in healthy volunteers. Each subject was stimulated using a pulse sequence modulated by a multisine waveform of 3, 7 and 13 Hz. The EEG was analyzed for the presence of the base frequencies and associated (sub)harmonics.

Topographies showed significant central and contralateral SSEP responses at 3, 7 and 13 Hz in respectively 7, 4 and 3 out of the 9 participants included for analysis. As such, we found that intra-epidermal stimulation with a multisine frequency modulated pulse sequence can generate nociceptive SSEPs. The possibility to stimulate the nociceptive system using multisine frequency modulated pulses offers novel opportunities to study the temporal dynamics of nociceptive processing.

11.1 Introduction

Despite decades of research, it remains unclear how our brain creates the perception of pain based on a combination of peripheral nociceptive input and central nervous activity. To study the relation between peripheral nociceptive input and brain activity, researchers have extensively documented the brain potential evoked by a single painful stimulus. These pain evoked potentials provided one of the first tools to evaluate properties of nociceptive processing in both healthy and abnormal conditions. As such, pain evoked potentials have been used in a wide variety of contexts to study pain processing and modulation (e.g. (Liang, Lee, O'Neill, Dickenson, & Iannetti, 2016; Manresa, Andersen, Mouraux, & van den Broeke, 2018; Wager, Matre, & Casey, 2006)). These pain evoked potentials were shown to be associated with stimulus saliency (Iannetti & Mouraux, 2010) rather than any specific effects of stimulus modality (e.g. nociceptive or somatosensory).

An alternative technique to characterize stimulus-evoked brain activity is the measurement of steady-state evoked potentials (SSEPs). Instead of evoking brain activity using a single transient stimulus, SSEPs rely on sustained activation of brain areas by a continuous sensory stimulus. The tonic pain evoked by the continuous nociceptive stimulus leading to a nociceptive SSEP bears more similarity to the continuous and dynamic pain experienced by patients in daily life than the transient stimuli used to evoke brain potentials and reduces the effect of saliency. By modulating the intensity of this stimulus with one or multiple frequencies, evoked brain activity can be observed in the electroencephalogram (EEG) at these frequencies and their harmonics. Visual and auditory SSEPs have been widely used in cognitive and clinical neuroscience (Norcia, Appelbaum, Ales, Cottereau, & Rossion, 2015; Vialatte, Maurice, Dauwels, & Cichocki, 2010). Sensory transmission and processing can be further characterized by evoking SSEPs using multisine waveforms, perturbing the sensory system at multiple frequencies simultaneously. Some of the useful properties that could be quantified using this technique include the delay, nonlinearity and signal-to-noise ratio of a sensory system (Yang, Solis-Escalante, van der Helm, & Schouten, 2016). Recent studies have used the technique to observe fundamental properties of the sensorimotor system

(Yang, Dewald, Helm, & Schouten, 2017), and to demonstrate significantly altered transmission of sensory signals after stroke (Vlaar et al., 2017). Another important topic of current SSEP research is the (non)linearity of sensory processing. Modelling studies suggest that brain responses are highly nonlinear (Roberts & Robinson, 2012; Spiegler, Knösche, Schwab, Haueisen, & Atay, 2011) and investigating these nonlinear relations between sensory input and brain activity is essential for our understanding of sensory systems. Such nonlinear relations have been shown clinically relevant for motor disorders (Sanger, Pascual-Leone, Tarsy, & Schlaug, 2002), migraine (Nyrke & Lang, 1982) and epilepsy (Kalitzin, Parra, Velis, & Lopes da Silva, 2002). The (non)linearity of nociceptive processing and its potential clinical applications remains relatively unexplored, which is an area where multisine SSEP techniques might prove valuable as a relatively cheap and non-invasive technique to explore this topic.

Recently, Mouraux et al. (Mouraux et al., 2011) showed that it was possible to measure SSEPs related to specific nociceptive stimulation by applying a periodic sequence of laser pulses. This lab showed that the technique, also referred to as 'frequency tagging', could be used to dissociate cortical responses to nociceptive and tactile stimuli (Colon, Legrain, & Mouraux, 2014). More recently, the same lab has also demonstrated SSEPs generated by slow periodic variation of the heat in a contact thermode (Colon, Liberati, & Mouraux, 2017; Mulders et al., 2020), eliciting SSEPs with a similar topography, but limited to ultra-low stimulation frequencies. Nevertheless, a limitation of both thermode stimulation and laser stimulation is that nociceptive nerve fibers are activated through a nonlinear thermal transduction process (Xu, Lin, & Lu, 2010), which could limit the observability of central nociceptive processing.

The thermal transduction process can be bypassed by intra-epidermal electric stimulation, which has also been shown to preferentially activate nociceptive afferents, provided that stimulus intensity remains at or below twice the detection threshold (Mouraux, 2010). However, the benefit of bypassing transduction processes comes with an additional risk of eliciting stimulus artefacts in the EEG. A first study used square-wave modulated pulse sequences to elicit SSEPs through intra-epidermal stimulation (Colon,

Nozaradan, Legrain, & Mouraux, 2012) and successfully demonstrated the potential of intra-epidermal electric stimulation by measuring SSEPs with a large signal-to-noise ratio on a range of frequencies from 3 to 43 Hz. Another study successfully evoked SSEPs at 31 and 37 Hz by stimulation of superficial skin afferents using a concentric planar electrode (Blöchl, Franz, Miltner, & Weiss, 2015). However, both studies showed distinctly different SSEP topographies and lacked (description of) rigorous checks for stimulus artefacts and a description of the variability of elicited SSEPs among participants, making it difficult to anticipate potential applications. Furthermore, the square wave pulse train modulation used in these studies cannot be adapted for perturbing multiple frequencies simultaneously and already includes spectral peaks at harmonics in the input signal, which compromises usage of most system identification methods.

In this study, we developed a new procedure for eliciting multi-frequency nociceptive SSEPs through intra-epidermal stimulation. Accurate frequency modulated stimulation of nociceptive nerve fibers and measurement of the generated SSEPs creates many challenges with respect to hardware, stimulation procedures, recording procedures and analysis. As such, custom hardware was developed to modulate electric pulse sequences with sinusoid and multisine waveforms. We evaluated the performance and the limits of this method and outlined a procedure to accurately quantify and map stimulus artefacts. Subsequently, the effectiveness of multisine frequency modulation of a pulse sequence for generating and studying nociceptive SSEPs was evaluated in an experiment on ten participants. We tested our hypothesis that the technique would generate significant peaks in the power spectrum at the base frequencies and potentially at some of the harmonics. Furthermore, we used the evoked spectral components to estimate system delay and explore system nonlinearity.

11.2 Methods

11.2.1 Experiment

Participants

A group of ten healthy men (aged 23 to 27 years, nine right-handed) participated in this study. All participants provided written informed consent before participation. All experiments were approved by the local ethics committee and in accordance with the declaration of Helsinki.

Procedure

Experiments were performed in a dim and silent room shielded from external electromagnetic interference. Participants were seated upright in a chair facing a single neutral image. Stimulation was applied on the dorsum of the right hand on five different locations in separate stimulation blocks of 20 sequences each. Each pulse sequence had a duration of 8.5 seconds (Figure 11.1). Before every stimulation block, the detection threshold to a single 0.5 ms pulse was determined using a staircase paradigm and the pulse amplitude was set to twice this detection threshold. After the first stimulus sequence of each block, participants were asked to rate the pain on a visual analog scale (VAS) ranging from 0 (no sensation at all) to 5 (painful) to 10 (worst pain imaginable). The location order was chosen such that none of the locations were located directly next to each other to limit local (de)sensitization of the skin.

Nociceptive Stimulation

Participants were electrically stimulated using intra-epidermal electric stimulation at twice the detection threshold with a current controlled stimulator (AmbuStim, University of Twente, Enschede, the Netherlands). Cathodic square-wave pulses (pulse width: 0.5 ms) were applied using an electrode comprised of 5 microneedles in a layer of flexible silicone (Steenbergen et al., 2012) to selectively stimulate nociceptive afferent nerve fibers in the epidermis. Electrode dimensions are displayed in Figure 11.2. Each

microneedle protrudes 0.5 mm from the electrode surface. Experiments (Mouraux, 2010) and simulations (Motogi et al., 2016; Poulsen, Tigerholm, Meijs, Andersen, & Mørch, 2020) show that intra-epidermal stimulation preferentially activates nociceptive afferents, provided that the stimulus intensity remains at or below twice the detection threshold.

A validation study of the electrode used in this study showed that stimulation resulted in a sharp pricking sensation (Steenbergen et al., 2012). Average response time and evoked potential latency recorded using this electrode were similar to the average response time and evoked potential latency in previous studies using intra-epidermal stimulation (van den Berg & Buitenweg, 2021).

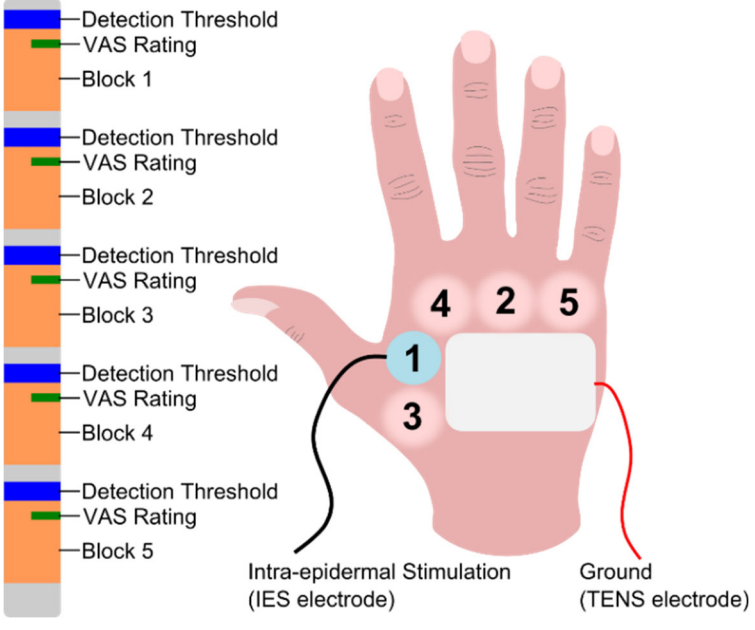

Figure 11.1: *Experiment outline. Participants were stimulated in 5 blocks of 20 sequences with a randomized interval of 10-15 seconds. For every block, the intra-epidermal stimulation (IES) electrode was moved to a different location on the dorsum of the right hand. Participants were allowed a small break in between every stimulation block. Before the start of every block, the detection threshold was measured which was used to set the amplitude of the pulse sequence to twice the detection threshold.*

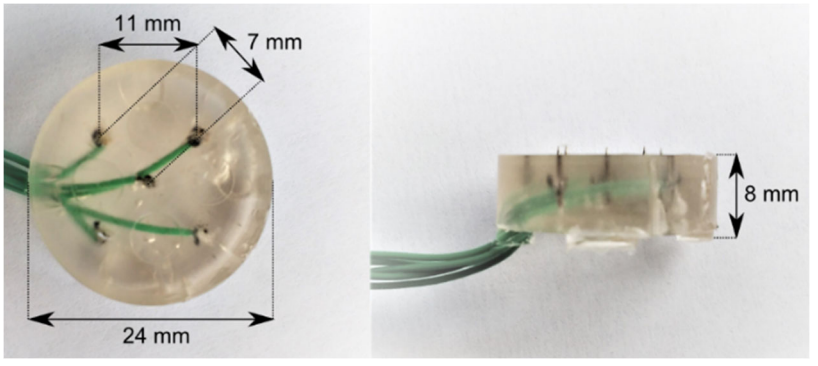

Figure 11.2: Electrode for intra-epidermal stimulation, consisting of 5 microneedles embedded in a layer of flexible silicone.

Multisine Frequency Modulation

Stimulation was controlled by a microcontroller connected to the trigger input of the stimulator. Each trigger pulse generated by the microcontroller resulted in a single stimulation pulse. Frequency modulated trigger sequences were generated by modulating the inter-pulse interval, which was computed based on (multi)sine frequency modulation, see Equation (1).

$$f_{pulse}(t) = C_{offset} + A_1 \sin(2\pi f_1 t + \phi_1) + A_2 \sin(2\pi f_2 t + \phi_2) + A_3 \sin(2\pi f_3 t + \phi_3) \quad (1)$$

Modulation frequencies (f_1, f_2, f_3) were chosen such that measured SSEPs are representative of the behavior of the studied sensory system. In a previous study using square wave intra-epidermal stimuli (Colon, Legrain, & Mouraux, 2012) brain responses were measured in a range from 3 to 43 Hz, where lower frequencies resulted in a more consistent response. To improve signal-to-noise ratio, frequencies with a large interference of EOG artefacts and alpha waves should be avoided. For multisine modulation, frequencies should be chosen such that the number of overlapping (sub)harmonics is minimized in order to apply nonlinear system identification techniques to the measured SSEP (Yang,

Solis-Escalante, van der Helm, & Schouten, 2016). In this study, 3, 7 and 13 Hz were used as modulation frequencies.

To avoid any transient brain activity to individual pulses within a sequence, the maximum inter-pulse interval should be well below the minimum detectable inter-stimulus interval. For nociceptive laser stimuli, stimuli can be individually perceived with an inter-stimulus interval as small as 200 ms (Lee, Mouraux, & Iannetti, 2009). As this interval could be even shorter for intra-epidermal stimuli, we chose to limit the minimum pulse frequency to 20 Hz (i.e., 50 ms inter-pulse interval). Furthermore, we chose a maximum pulse frequency of 200 Hz (i.e., 5 ms inter-pulse interval) to limit the effects of peripheral nerve repolarization on measured SSEPs.

The modulation amplitude is limited by practical constraints. The minimum pulse frequency ($\min\,(f_{pulse}(t))$, which is dependent on the offset (C_{offset}) and modulation amplitudes (A_1, A_2, A_3), cannot be smaller than can be measured given the duration of the stimulus sequence (T_{stim}), i.e. $\min\,(f_{pulse}(t)) > \frac{1}{T_{stim}}$. Observed power increases with modulation frequency. The observed power is lower, and less accurate, as the modulation frequencies (f_1, f_2, f_3) get closer to the minimum pulse frequency (Figure 11.3). For a multisine waveform the observed power at each frequency is dependent on the combination of frequencies (f_1, f_2, f_3), modulation amplitudes (A_1, A_2, A_3) and phases (ϕ_1, ϕ_2, ϕ_3). Simulations indicated that the selected frequencies 3, 7 and 13 Hz are a good trade-off between observed power and the physiological constrains ($20\ Hz < f_{pulse} < 200\ Hz$) with an offset ($C_{offset}$) of 110 Hz, a modulation amplitude of 30 Hz for each frequency and phases of $+\frac{1}{3}\pi$ and $-\frac{1}{3}\pi$ for 7 and 13 Hz respectively (Figure 11.3). Also note that as the total available bandwidth (90 Hz) is divided over three modulation frequencies, this leads to a reduction of power to one-ninth of the power when the full bandwidth is used for a single frequency (Figure 11.3).

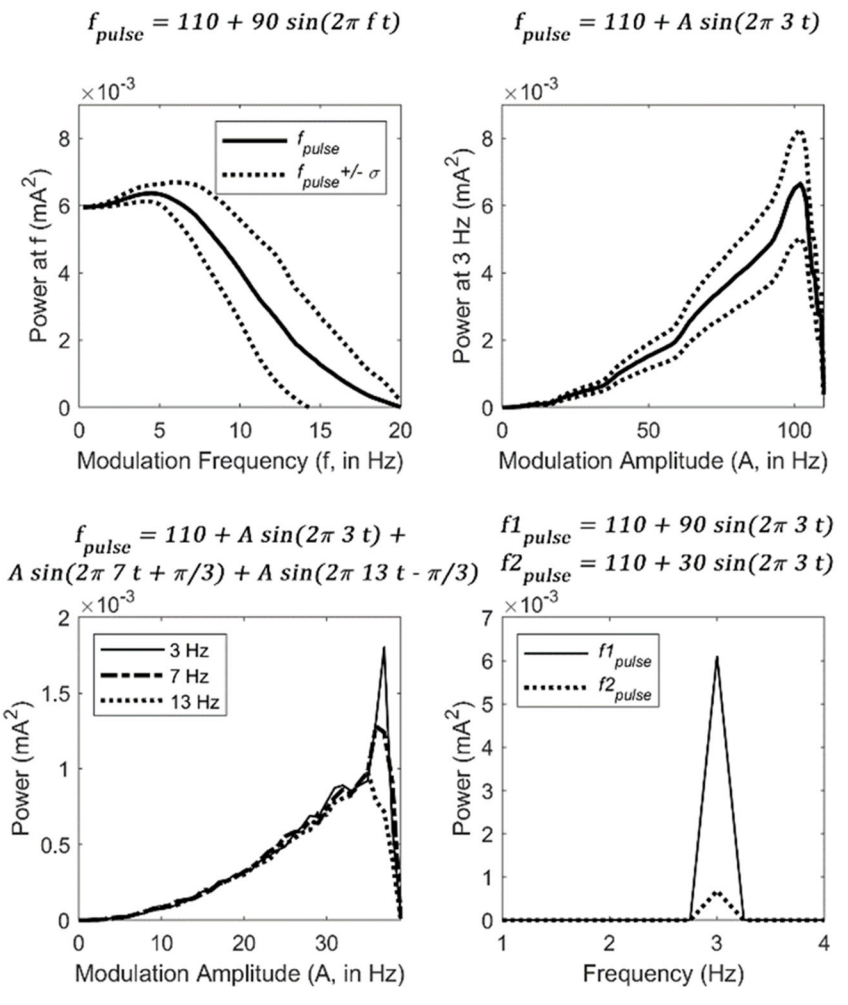

Figure 11.3: Simulation results of the observed power of a modulated pulse sequence when the modulation frequency is increased from 0 to the minimum pulse frequency (left), when the modulation amplitude is increased from 0 to the frequency offset when modulating at a single frequency (middle left) or at a combination of three frequencies (middle right). The observed power increases as the modulation amplitude increases. However, the observed power decreases as the stimulation frequency gets closer to the minimum pulse frequency. The last figure (right) shows the power spectrum of pulse sequences modulated at a frequency of 3 Hz with a modulation amplitude of 90 Hz and a modulation amplitude of 30 Hz. As the total modulation amplitude is divided over three frequencies in a multisine waveform, the total modulation amplitude per frequency is reduced to one-third and the power is reduced to one-ninth.

11.2.2 EEG Recording

Scalp EEG was recorded with a sampling rate of 1024 Hz using a REFA amplifier (TMSi B.V., Oldenzaal, the Netherlands) and 128 Ag/AgCl electrodes located according to the international 10/5 system (Oostenveld & Praamstra, 2001) with a common average reference. Electrodes were gelled with an impedance below 10 kΩ. A tubular net bandage was placed over the EEG cap for improved fixation of the electrodes and reduction of potential movement artefacts. Impedances were checked before each stimulation block and decreased if necessary by adding gel. Channels of which the impedance did not decrease to a value below 10 kΩ were disconnected.

11.2.3 Data Preprocessing

The recorded EEG was pre-processed using EEGlab (Delorme & Makeig, 2004), a Matlab toolbox for EEG signal processing and used for identification of stimulation artefacts and SSEPs. For identification of stimulation artefacts, the EEG recording was high-pass filtered with a cutoff frequency of 60 Hz and extracted in epochs from -10 to 30 ms with respect to each pulse applied during the experiment. For identification of SSEPs, the EEG recording was high-pass filtered with a cutoff frequency of 0.5 Hz and low-pass filtered with a cutoff frequency of 40 Hz. Channels were re-referenced to common average after removing channels with flat or excessive EMG activity. Epochs were extracted from 0.5 to 8.5 seconds with respect to stimulation onset. Epochs with excessive EMG activity or eye movement artefacts were removed by visual inspection. Subsequently, any residual contamination of the EEG by eye blinking, eye movements or EMG activity was removed using adaptive mixture independent component analysis (Palmer, Makeig, Kreutz-Delgado, & Rao, 2008).

11.2.4 Identification and Analysis of Stimulation Artefacts

To inspect the stimulation artifact, the average over all epochs in all sequences and blocks was computed for each participant, with approximately 80 000

epochs per participant as an epoch was extracted around each pulse. Consequently, we were able to detect and map the stimulation artefact on a nanovolt scale. Based on this analysis, one participant was excluded due to an excessive stimulation artefact, defined as a stimulation artefact larger than 100 nV at the Cz channel.

11.2.5 Identification and Analysis of Steady State Evoked Potentials

For spectral analysis, epochs were divided in segments of two seconds, and each segment was Fourier transformed. To identify potential SSEPs on an individual level the T^2_{circ} value (Victor & Mast, 1991) was computed for every channel on every stimulated frequency using Equation (2). The T^2_{circ} is the ratio between the power ($|\widehat{X}(f)|^2$) and the variance ($\sigma^2(f)$) of the segments in the frequency domain ($X_m(f)$) multiplied by the number of segments (M) minus one and is therefore a scaled version of the signal-to-noise ratio. This value is distributed according to the F-statistic and can be statistically tested accordingly (Victor & Mast, 1991).

$$T^2_{circ} = (M-1)\frac{|\widehat{X}(f)|^2}{\sigma^2(f)} \qquad (2)$$

Where $\hat{X}(f) = \frac{1}{M}\sum_{m=1}^{M} X_m(f)$

and $\sigma^2(f) = \sum_{m=1}^{M}(X_m(f) - \hat{X}(f))^2$

On a group level T^2_{circ} was averaged over all participants to determine the average scalp distribution of observed SSEPs. In each subject and on a group level, the 7 central midline electrodes (C5, C3, C1, Cz, C2, C4, C6) were tested for significance by testing the T^2_{circ} against the F-statistic with a significance level of 0.05 as these are the locations where most nociceptive SSEP activity was observed in previous studies (Blöchl, Franz, Miltner, & Weiss, 2015; Colon, Nozaradan, Legrain, & Mouraux, 2012; Mouraux et al., 2011). Subsequently, we computed the power ($|\widehat{X}(f)|^2$), phase ($Arg(\hat{X}(f))$) and noise level ($\frac{\sigma^2(f)}{M}$) of

time-locked activity at all (sub)harmonic frequencies for all contralateral central midline electrodes with a significant T^2_{circ} at one of the base frequencies.

To estimate the overall time delay, the time delay of each significant frequency at the corresponding electrode was estimated based on the phase. The time delay (τ) was computed based the phase delay (ϕ) using Equation (3). As phases wrap over a period of 2π and SSEP responses could be both positive and negative (Norcia, Appelbaum, Ales, Cottereau, & Rossion, 2015), time delay estimates are repeated at $\frac{k}{2f}$, in which f is the stimulated frequency and k is an integer number

$$\tau = \frac{(\phi + k\pi)}{2\pi f} = \frac{\phi}{2\pi f} + \frac{k}{2f} \quad with \quad k \ni \mathbb{Z} \quad for \quad \tau > 0 \qquad (3)$$

11.3 Results

11.3.1 Pain Rating

Nociceptive detection thresholds remained between 0.1 and 0.5 mA (Figure 11.4) with an average of 0.43 ± 0.17 mA. Pain ratings were reported on a VAS Scale ranging from 0 (no sensation at all) to 5 (painful) to 10 (worst pain imaginable). The VAS line mentioned 0, 5 and 10 and measured 12 cm in length. One of the nine included participants did not report pain ratings. Participants reported a continuous mild sensation with an average VAS score of 3.0 ± 1.9 (Figure 11.4). A single subject did report a strong sensation of pain (VAS>7) in the 1st, 3rd and 5th block. Participants also reported that the perceived intensity of each sequence decreased across sequences within each block. Redness of the skin around the needle locations was observed after each stimulation block.

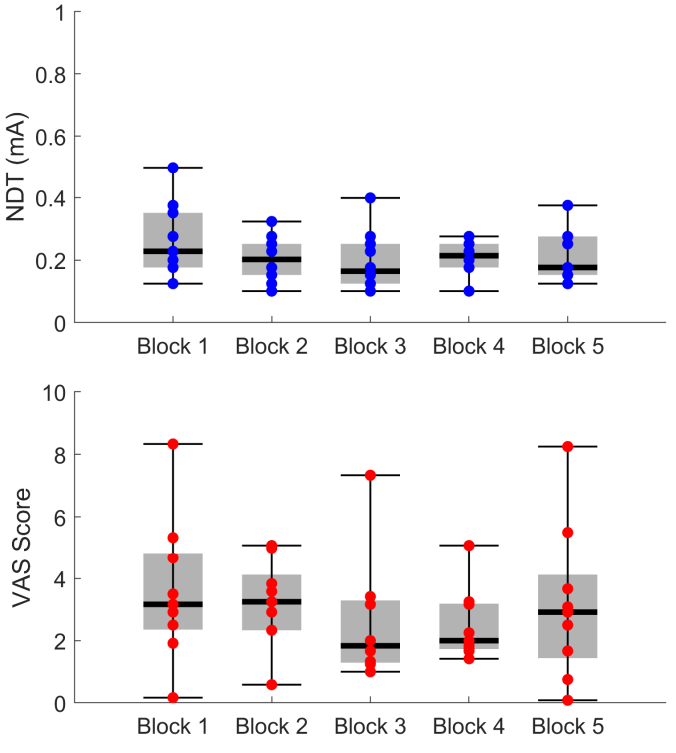

***Figure 11.4**: Nociceptive detection thresholds (NDTs) in mA and pain ratings on a visual analog scale (VAS) ranging from 0 (no sensation at all) to 5 (painful) to 10 (worst pain imaginable) at each stimulation block (see also Figure 11.1). Detection thresholds remained between 0.1 and 0.5 mA. Participants were stimulated at twice the NDT. In general, participants reported a mild sensation with an average score of 3 in response to this stimulation.*

11.3.2 Stimulation Artefacts

A stimulation artefact was observed in all participants (Figure 11.5). In 8 out of 9 participants, the stimulation artefact was concentrated around the ground electrode on the right mastoid, indicating that the observed stimulation artefact was caused by displacement currents toward this electrode. In all included participants the stimulation artefact at Cz was limited to a maximum of 50 nV and occurred between 0 and 10 ms after each pulse. The topographical distribution of the artefact is ipsilateral to the side of stimulation and therefore contralateral to any expected brain activity.

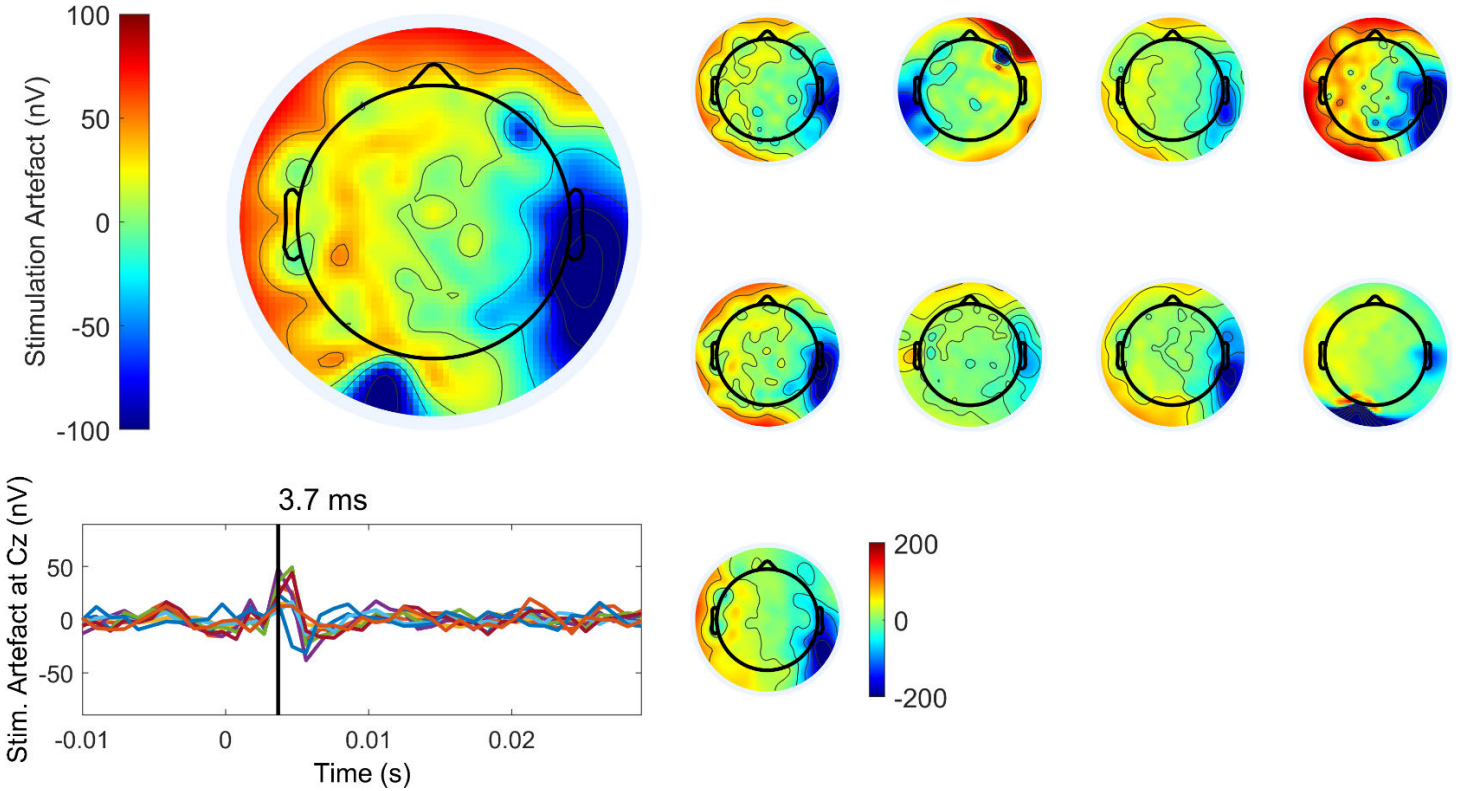

***Figure 11.5**: Maps and amplitude of the stimulation artefact. Most stimulation artefacts were centered around the ground electrode on the right mastoid. As such, the observed stimulation artefact was likely due to displacement currents. The stimulation artefact at Cz remained limited to below 50 nV in all included participants and occurred between 0 and 10 ms after each pulse.*

11.3.3 Multisine SSEP Topographies

The group and individual level topographies of the T^2_{circ} statistic at 3, 7 and 13 Hz are shown in Figure 11.6. At 3 Hz, a total of 7 participants showed a significant SSEP response on at least one of the central midline electrodes. At 7 Hz a significant SSEP response was observed in 4 participants and at 13 Hz only in 3 participants. At 13 Hz, significant electrodes were located ipsilateral in 2 participants. On a group level, significant 3 Hz and 7 Hz spectral components were mostly observed central/mid-parietal and slightly shifted towards the contralateral side, centered around the Cz, C1, C3 and C5 channels. At 13 Hz, the group level topography shows activity in similar areas as 3 and 7 Hz in addition to other regions ipsilateral with respect to stimulation.

11.3.4 Multisine SSEP Spectra

Of the central midline electrodes, a significant spectral component of one or more of the base frequencies was observed at C5, C3, C1, Cz, C2 and C6. At the contralateral electrodes (C5, C3, C1 and Cz), the spectra were analyzed to investigate the base frequencies and (sub)harmonics, see Figure 11.7. At 3 Hz, 3 participants had a significant spectral component at Cz, 4 participants had a significant spectral component at C1 and C3, and 2 participants had a significant spectral component at C5. Furthermore, the group level averages at Cz, C1 and C3 had a significant spectral component ($p<0.05$). At 7 Hz, 3 participants had a significant spectral component at C5 and with a significant group level average ($p<0.05$) at the same electrode. At 13Hz, 1 participant had a significant spectral component at Cz, C1 and C3 and no significant spectral component was observed at C5. At all other frequencies, a few significant individual spectral components were incidentally found on 2nd and 3rd order harmonics at both electrodes.

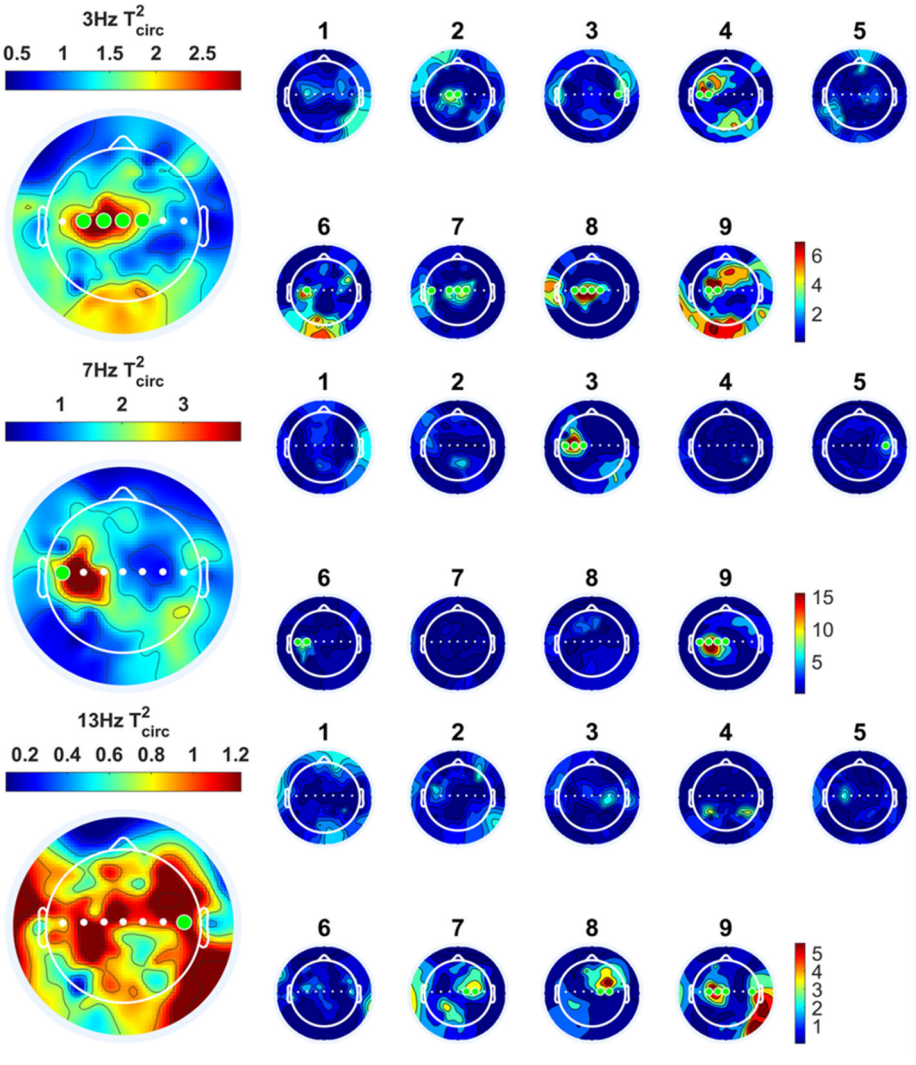

***Figure 11.6**: The group and individual level topographies of the T^2_{circ} statistic at 3, 7 and 13 Hz. The SSEP response was tested for significance at the central midline electrodes (C5, C3, C1, Cz, C2, C4, C6). Significant electrodes (p<0.05) are indicated by green dots. At 3 Hz, a significant SSEP response was observed in 7 participants on at least one of the central midline electrodes. The group level average has a central/mid-parietal distribution and is significant at C2, Cz, C1 and C3. At 7Hz, a significant SSEP response was observed in 4 participants on at least one of the central midline electrodes. The group level average also has a central/mid-parietal distribution and is significant at C5. At 13 Hz, a significant SSEP response was observed in 3 participants on at least one of the central midline electrodes. The group level average shows activity at the same area as 7 Hz stimulation and several other areas, with significance at C6.*

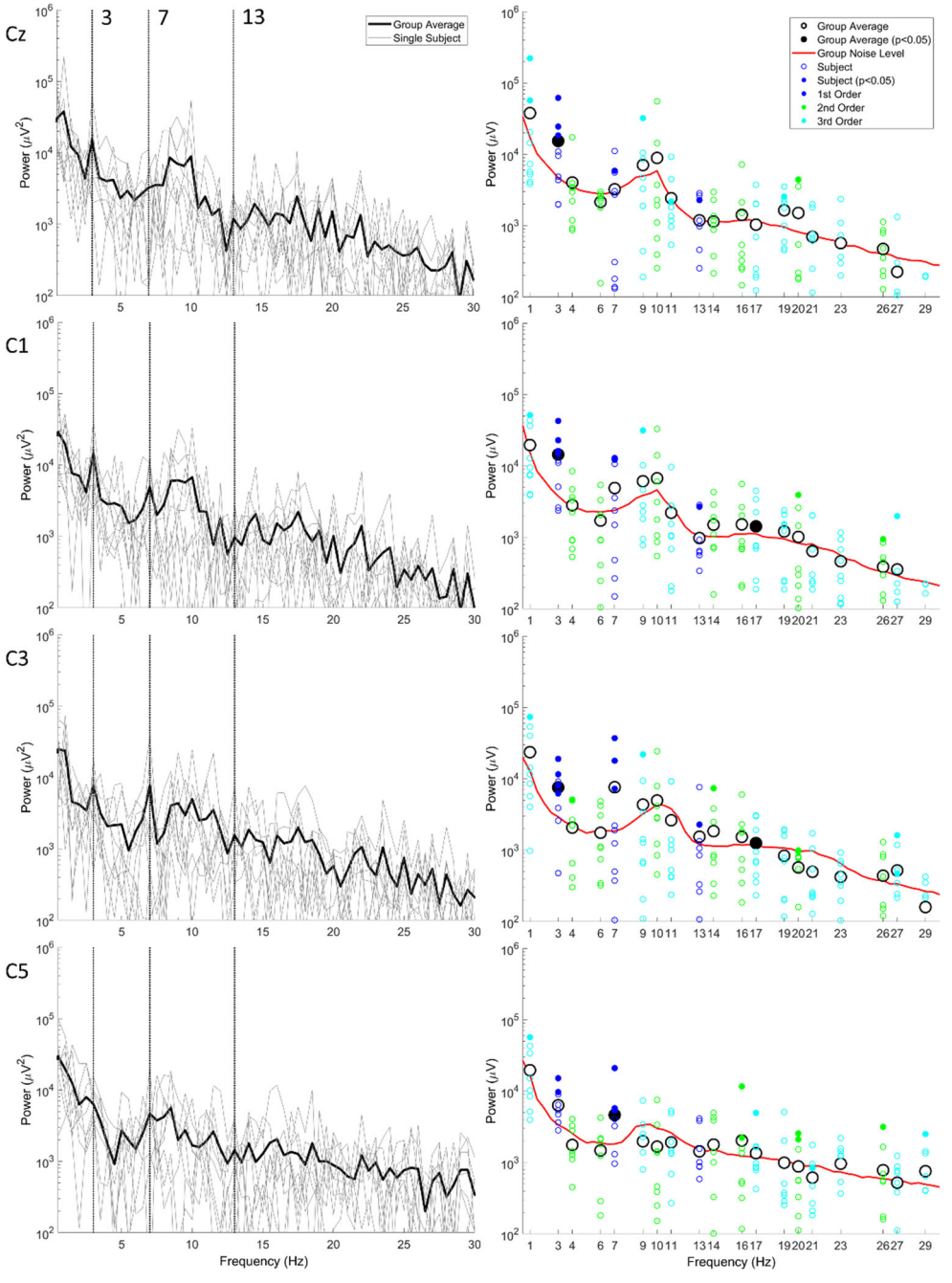

***Figure 11.7**: Group and subject power spectra (left) and the power and noise level of (sub)harmonics (right) at Cz, C1, C3 and C5. Larger circles indicate group average, smaller circles indicate individual participants. Multiple participants showed significant spectral components at 3 and 7 Hz. A single subject also had a significant spectral component at 13 Hz.*

11.3.5 Time Delay

Time delay was estimated for 3 and 7 Hz in individual participants and on a group level at the electrodes with significant SSEP on a group level (C2, Cz, C1 and C3 for 3 Hz, C5 for 7 Hz). As for 13 Hz, no electrodes were significant on group level, this frequency was not used for time delay estimation. For the group level estimate, only the participants with a significant spectral component at those frequencies were averaged.

The resulting estimates are shown in Figure 11.8. Multiple subject and group level estimates are displayed in each column due to the 2π wrapping effect. Group level estimates align around an average time delay of 168 ms.

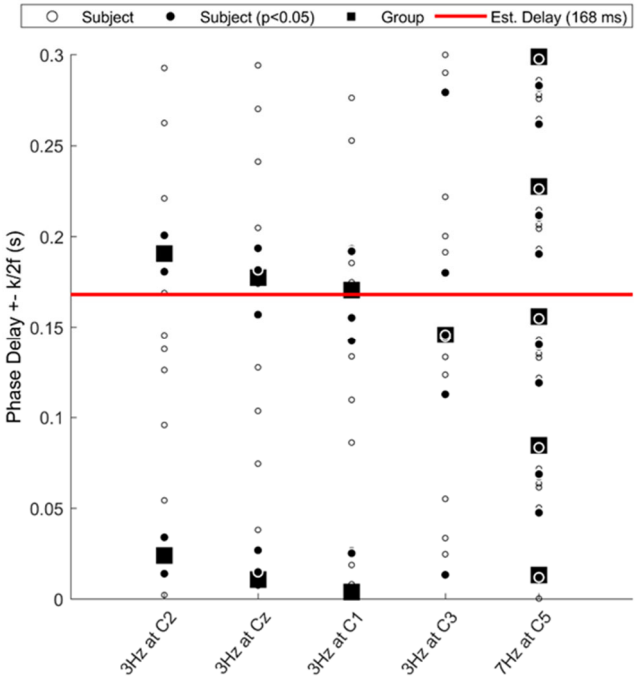

***Figure 11.8**: Group-level and individual time delay estimates of 3 Hz at C2, Cz, C1 and C3, and of 7 Hz at C5. Due to phase wrapping and EEG polarity, time delay estimates are repeated every k/2f seconds, leading to multiple estimates for each subject and the group. Group-level time delay estimates align around an average time delay of 168 ms.*

11.4 Discussion

This study outlined a method to directly stimulate nociceptive afferents in the skin to evoke SSEPs in order to study nociceptive processing. In contrast to previous studies, using square waveforms at a single frequency to modulate electrical stimulation (Blöchl, Franz, Miltner, & Weiss, 2015; Colon, Nozaradan, Legrain, & Mouraux, 2012), we used a multisine waveform (Figure 11.9). The use of specific combinations of base frequencies in this multisine waveform allows for system identification techniques to explore system properties such as delay, signal-to-noise ratio and (non)linearity.

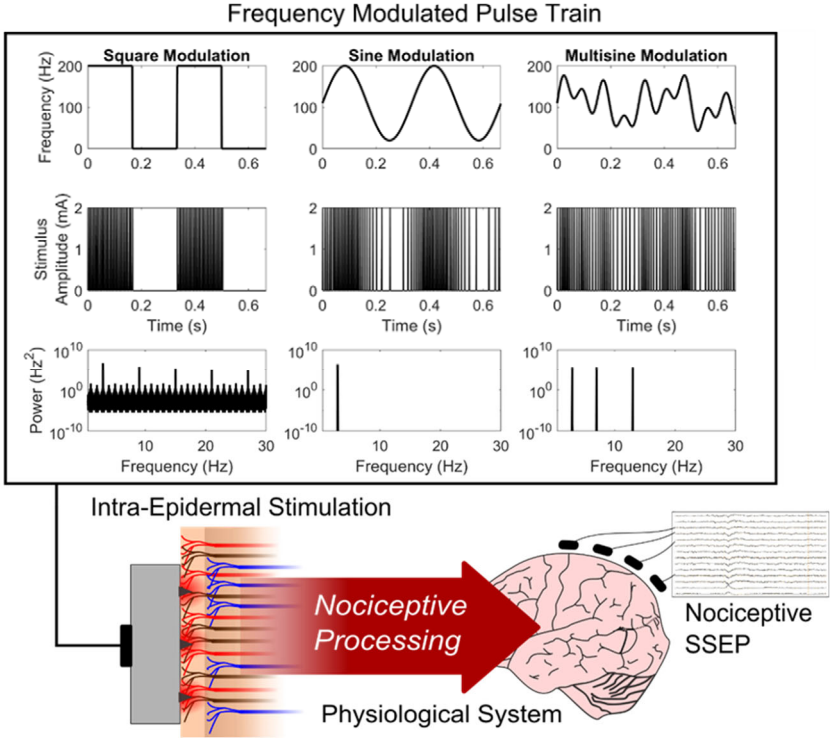

Figure 11.9: Examples of frequency modulated intra-epidermal stimulation using pulse sequences. The aim is to preferentially stimulate nociceptive afferents in the skin and therefore measure SSEPs related to nociception. Earlier studies aimed at generating SSEPs by stimulation of nociceptors using square wave modulation (left). Theoretically, this type of stimulation does not only elicit the stimulated frequency, but also its harmonics. In this work, we proposed to stimulate nociceptors using sinusoid or multisine frequency modulated pulse sequences.

11.4.1 Technical Challenges

A number of challenges were addressed to reliably measure SSEP brain activity in response to intra-epidermal electric stimulation. Low pulse amplitudes were a requirement for preferential activation of superficial nociceptive afferents in the skin leading to a low signal-to-noise ratio of any observable brain activity. In addition, the total available bandwidth for frequency modulation was divided in three to achieve multisine modulation, leading to a ninefold decrease of the power of single stimulation frequencies in the input signal. As such, the implementation of the paradigm in terms of hardware and procedures was optimized to reduce noise and augment any potential SSEP activity. This involved 1) optimizing the temporal accuracy of stimulation hard- and software, 2) strategically choosing stimulation parameters, 3) reducing stimulation artefacts by strategic electrode placement and lowering electrode impedances and 4) reducing EOG, EMG and movement artefacts as much as possible. We observed that incorrect implementation of any of these steps could lead to a substantial loss of power of the observed SSEP and an increase of background noise during several pilot recordings.

Special care was taken to identify and reduce potential stimulation artefacts. Stimulation artefact would have a similar frequency content as the input signal and overlap with potential brain activity related to stimulation. Three potential sources of electric stimulation artefacts are identified in literature: volume conduction current, displacement current and electromagnetic coupling (McLean, Scott, & Parker, 1996). In this study, the volume conduction current artefact was reduced by limiting the electric field of the stimulation (i.e., using multiple intra-epidermal needles, scrubbing the skin, using a low stimulation intensity). Electromagnetic coupling was reduced by lowering the impedance of EEG scalp electrodes as much as possible and keeping stimulation and EEG electrode leads as far apart as possible. The displacement current artefact (Figure 11.10) was reduced by scrubbing the location of stimulator ground before application and using a large surface TENS electrode as a ground proximal with respect to the stimulation electrode. As displacement currents could nevertheless occur, the EEG ground was placed on the mastoid bone

ipsilateral to stimulation to prevent any interference with brain activity, which was expected on central or contralateral locations.

Stimulation artefacts are usually much faster than the dynamics of neural systems. While an electric stimulation artefact usually occurs in the range of a few milliseconds (McLean, Scott, & Parker, 1996) a neural response takes several tens to hundreds of milliseconds. We made use of this property to design an accurate procedure for identification of potential stimulus artefacts by averaging the EEG with respect to each pulse. The resulting waveforms showed that a small stimulation artefact remained in most participants with an amplitude of up to 50 nV at Cz and concentrated around the EEG ground electrode on the right mastoid. Fortunately, it is unlikely that the stimulus artefact interferes with any observed central and contralateral brain activity due to the small amplitude at Cz and its ipsilateral distribution.

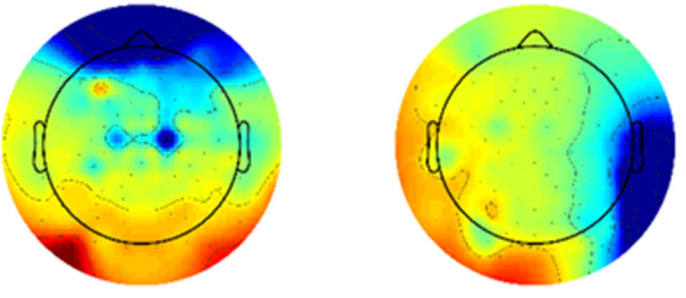

***Figure 11.10**: Examples of two stimulation artefacts observed in pilot sessions. In A) and B) the artefact was concentrated around the EEG ground electrode, which was located on the forehead and right mastoid respectively. As such, these artefacts were likely caused by the displacement current.*

11.4.2 Multisine SSEP Responses

We observed brain activity in response to multisine intra-epidermal stimulation with significant spectral components at the base frequencies 3, 7 and 13 Hz. On average, stimulation was perceived as a mild sensation, rated 3.0 on a VAS. Stimulation caused a slight redness of the skin around needle locations after each stimulation block, which was potentially caused by the release of substance P by stimulated nociceptors. No other signs of potential tissue damage were observed. Crucially, the stimulus intensity was high enough to be clearly perceived by most participants, but low enough to allow the participant to relax during the stimulation and EEG recording. At 3 Hz, we observed significant central midline electrodes for a majority of the participants and a clear group level topography. At 7 Hz and 13 Hz, we observed significant central midline electrodes in four and in three participants respectively. There is a considerable variation in topographies among individual participants, which could be due to a larger amount of background activity in some of the participants. However, this might also reflect anatomical variation and the large diversity in which participants tend to respond to nociceptive stimulation.

To the best of our knowledge, this is the second study to demonstrate SSEP responses to intra-epidermal stimulation. The first demonstration of this technique was done by Colon et al. (Colon, Nozaradan, Legrain, & Mouraux, 2012) where SSEP responses were shown at 3, 7, 13, 23 and 43 Hz. Similar to the study of Colon et al., we observed SSEP responses to 3, 7 and 13 Hz intra-epidermal stimulation. However, the observed signal topographies are markedly different. In the study of Colon et al. a frontal topography was observed which centers around AFz as the stimulation frequency is increased. Another recent study by Blöchl et al. (Blöchl, Franz, Miltner, & Weiss, 2015) used a concentric planar electrode in an attempt to generate nociceptive specific SSEPs with 31 and 37 Hz stimulation. They reported contralateral activation similar to the topographies observed in this study for 7 and 13 Hz stimulation.

In both these studies it remains unclear whether stimulus artefact could have contributed to observed topographies. In the first study, the fact that the topography was centering around the ground of the EEG cap as stimulation frequency increased might suggest that not all stimulation artefact was

removed by the independent component analysis algorithm used for artefact removal. Furthermore, the average stimulus intensity in that study was 0.23 (±0.08) mA applied on a single intra-epidermal needle, while the average stimulus intensity in this study was 0.43 (±0.17) mA applied over five intra-epidermal needles, effectively resulting in a much lower current density and smaller electric field in this study. In the second study, no method of dealing with stimulation artefacts was reported.

A recent study to observe purely nociceptive SSEP topographies was done by Mouraux et al. (Mouraux et al., 2011). They used laser stimulation, which selectively activates nociceptive afferents in the skin and generates no electric stimulation artefacts. In response to 7 Hz periodic stimuli, they reported a topography centered around Cz similar to the topography observed in response to 3 Hz stimulation in this study. Although stimuli were applied through intra-epidermal needles, the observation of contralateral activation in response to 7 Hz and 13 Hz stimuli in the current study could imply concurrent activation of tactile large diameter Aβ-fibers in the skin. As it remains uncertain whether this difference is caused by concurrent activation or simply by the fact that the brain responds differently to a different stimulus modality, the intra-epidermal stimulation in this study should be considered 'preferentially' but not 'specifically' nociceptive.

11.4.3 System Behavior

To the best of our knowledge, this is the first study demonstrating SSEP responses to multisine frequency modulated electric stimulation of superficial afferents in the skin. Compared to previous studies using square wave modulation at a single frequency, the multisine modulation used in this study allows for exploration of system (non)linearity by observation of the combination of (sub)harmonics associated with the three stimulation frequencies in the power spectrum. The observed brain activity also allows for estimation of other properties such as the delay and order of the stimulated system.

An estimate of time delay was obtained by unwrapping the phase delay of the SSEP at multiple frequencies (Norcia, Appelbaum, Ales, Cottereau, & Rossion, 2015). The average time delay of participants with significant spectral components at the significant base frequencies aligned around a latency of 168 ms. This is markedly later than the latency observed in an earlier study using laser stimulation by Mouraux et al. (Mouraux et al., 2011), where delays between 30 and 50 ms were observed in response to 7 Hz stimulation. However, it should be noted that Mouraux et al. used the average potential over each stimulation period to compute the time delay. This implies that the true value of the time delay observed in that study could also be $\pm\frac{k}{2f}\ [\mathrm{s}] = k \cdot 71\ [\mathrm{ms}]$ larger due to phase wrapping (where $k = 0, 1, 2, \ldots$), indicating that their time delay could actually be similar to the one measured in this study. The observed delay corresponds with the latency of the N2 component observed in evoked potentials in response to intra-epidermal electric stimuli during earlier studies (van den Berg & Buitenweg, 2021; van den Berg et al., 2020), and supports that the observed signal is indeed related to brain activity.

The distribution of signal power in base frequencies and (sub)harmonics provides information on the linearity of the system. Studying system (non)linearity could have important implications for the way we model nociceptive processing. While base frequencies were significant, we did not find any significant (sub)harmonics on a group level. As such, we did not find any indications that nociceptive processing is nonlinear. Nevertheless, further studies replicating these findings in a larger sample size are required to determine if nociceptive processing could be modeled as a linear system.

11.5 Conclusion

Intra-epidermal stimulation of superficial nociceptive afferents in the skin using a multi-sine modulated pulse sequence of 3, 7 and 13 Hz, results in SSEPs at central electrodes. Significant SSEPs at the base frequencies 3, 7 and 13 Hz were found in a majority of participants. Such multisine SSEPs can be used to study the temporal dynamics of nociceptive processing in terms of delay and nonlinearity. Phase analysis indicated an average time delay of 168 ms. No indications for nonlinearity of nociceptive processing were observed in the current exploratory dataset.

11

11.6 References

Blöchl, M., Franz, M., Miltner, W. H. R., & Weiss, T. (2015). Captured by the pain: Pain steady-state evoked potentials are not modulated by selective spatial attention. *Brain Research, 1603*, 94-100.

Colon, E., Legrain, V., & Mouraux, A. (2012). Steady-state evoked potentials to study the processing of tactile and nociceptive somatosensory input in the human brain. *Neurophysiologie Clinique, 42*(5), 315-323.

Colon, E., Legrain, V., & Mouraux, A. (2014). EEG Frequency Tagging to Dissociate the Cortical Responses to Nociceptive and Nonnociceptive Stimuli. *Journal of cognitive neuroscience, 26*(10), 2262-2274.

Colon, E., Liberati, G., & Mouraux, A. (2017). EEG frequency tagging using ultra-slow periodic heat stimulation of the skin reveals cortical activity specifically related to C fiber thermonociceptors. *NeuroImage, 146*, 266-274.

Colon, E., Nozaradan, S., Legrain, V., & Mouraux, A. (2012). Steady-state evoked potentials to tag specific components of nociceptive cortical processing. *NeuroImage, 60*(1), 571-581.

Delorme, A., & Makeig, S. (2004). EEGLAB: An open source toolbox for analysis of single-trial EEG dynamics including independent component analysis. *Journal of Neuroscience Methods, 134*(1), 9-21.

Iannetti, G. D., & Mouraux, A. (2010). From the neuromatrix to the pain matrix (and back). *Experimental Brain Research, 205*(1), 1-12.

Kalitzin, S., Parra, J., Velis, D. N., & Lopes da Silva, F. H. (2002). Enhancement of phase clustering in the EEG/MEG gamma frequency band anticipates transitions to paroxysmal epileptiform activity in epileptic patients with known visual sensitivity. *IEEE Trans Biomed Eng, 49*(11), 1279-1286.

Lee, M. C., Mouraux, A., & Iannetti, G. D. (2009). Characterizing the cortical activity through which pain emerges from nociception. *Journal of Neuroscience, 29*(24), 7909-7916.

Liang, M., Lee, M. C., O'Neill, J., Dickenson, A. H., & Iannetti, G. D. (2016). Brain potentials evoked by intraepidermal electrical stimuli reflect the central sensitization of nociceptive pathways. *Journal of Neurophysiology, 116*(2), 286-295.

Manresa, J. B., Andersen, O. K., Mouraux, A., & van den Broeke, E. N. (2018). High frequency electrical stimulation induces a long-lasting enhancement of event-related potentials but does not change the perception elicited by intra-epidermal electrical stimuli delivered to the area of increased mechanical pinprick sensitivity. *PLoS ONE, 13*(9).

McLean, L., Scott, R. N., & Parker, P. A. (1996). Stimulus artifact reduction in evoked potential measurements. *Arch Phys Med Rehabil, 77*(12), 1286-1292.

Motogi, J., Sugiyama, Y., Laakso, I., Hirata, A., Inui, K., Tamura, M., & Muragaki, Y. (2016). Why intra-epidermal electrical stimulation achieves stimulation of small fibres selectively: a simulation study. *Phys Med Biol, 61*(12), 4479-4490.

Mouraux, A., Iannetti, G. D., Colon, E., Nozaradan, S., Legrain, V., & Plaghki, L. (2011). Nociceptive Steady-State Evoked Potentials Elicited by Rapid Periodic Thermal Stimulation of Cutaneous Nociceptors. *The Journal of Neuroscience, 31*(16), 6079.

Mouraux, A., Iannetti, G. D., & Plaghki, L. (2010). Low intensity intra-epidermal electrical stimulation can activate Aδ-nociceptors selectively. *Pain, 150(1)*, 199-207.

Mulders, D., de Bodt, C., Lejeune, N., Courtin, A., Liberati, G., Verleysen, M., & Mouraux, A. (2020). Dynamics of the perception and EEG signals triggered by tonic warm and cool stimulation. *PLoS ONE, 15*(4), e0231698.

Norcia, A. M., Appelbaum, L. G., Ales, J. M., Cottereau, B. R., & Rossion, B. (2015). The steady-state visual evoked potential in vision research: A review. *J Vis, 15*(6), 4.

Nyrke, T., & Lang, A. H. (1982). Spectral analysis of visual potentials evoked by sine wave modulated light in migraine. *Electroencephalogr Clin Neurophysiol, 53*(4), 436-442.

Oostenveld, R., & Praamstra, P. (2001). The five percent electrode system for high-resolution EEG and ERP measurements. *Clin Neurophysiol, 112*(4), 713-719.

Palmer, J. A., Makeig, S., Kreutz-Delgado, K., & Rao, B. D. (2008, 31 March-4 April 2008). *Newton method for the ICA mixture model.* Paper presented at the 2008 IEEE International Conference on Acoustics, Speech and Signal Processing.

Poulsen, A. H., Tigerholm, J., Meijs, S., Andersen, O. K., & Mørch, C. D. (2020). Comparison of existing electrode designs for preferential activation of cutaneous nociceptors. *Journal of Neural Engineering*.

Roberts, J. A., & Robinson, P. A. (2012). Quantitative theory of driven nonlinear brain dynamics. *NeuroImage, 62*(3), 1947-1955.

Sanger, T. D., Pascual-Leone, A., Tarsy, D., & Schlaug, G. (2002). Nonlinear sensory cortex response to simultaneous tactile stimuli in writer's cramp. *Mov Disord, 17*(1), 105-111.

Spiegler, A., Knösche, T. R., Schwab, K., Haueisen, J., & Atay, F. M. (2011). Modeling Brain Resonance Phenomena Using a Neural Mass Model. *PLOS Computational Biology, 7*(12), e1002298.

Steenbergen, P., Buitenweg, J. R., Trojan, J., van der Heide, E. M., van den Heuvel, T., Flor, H., & Veltink, P. H. (2012). A system for inducing concurrent tactile and nociceptive sensations at the same site using electrocutaneous stimulation. *Behavior Research Methods, 44*(4), 924-933.

van den Berg, B., & Buitenweg, J. R. (2021). Observation of Nociceptive Processing: Effect of Intra-Epidermal Electric Stimulus Properties on Detection Probability and Evoked Potentials. *Brain Topography*.

van den Berg, B., Doll, R. J., Mentink, A. L. H., Siebenga, P. S., Groeneveld, G. J., & Buitenweg, J. R. (2020). Simultaneous tracking of psychophysical detection thresholds and evoked potentials to study nociceptive processing. *Behavior Research Methods*.

Vialatte, F. B., Maurice, M., Dauwels, J., & Cichocki, A. (2010). Steady-state visually evoked potentials: Focus on essential paradigms and future perspectives. *Progress in Neurobiology, 90*(4), 418-438.

Victor, J. D., & Mast, J. (1991). A new statistic for steady-state evoked potentials. *Electroencephalogr Clin Neurophysiol, 78*(5), 378-388.

Vlaar, M. P., Solis-Escalante, T., Dewald, J. P. A., van Wegen, E. E. H., Schouten, A. C., Kwakkel, G., . . . on behalf of the, D. E. E. G. c. (2017). Quantification of task-dependent cortical activation evoked by robotic continuous wrist joint manipulation in chronic hemiparetic stroke. *Journal of NeuroEngineering and Rehabilitation, 14*(1), 30.

Wager, T. D., Matre, D., & Casey, K. L. (2006). Placebo effects in laser-evoked pain potentials. *Brain, Behavior, and Immunity, 20*(3), 219-230.

Xu, F., Lin, M., & Lu, T. J. (2010). Modeling skin thermal pain sensation: Role of non-Fourier thermal behavior in transduction process of nociceptor. *Computers in Biology and Medicine, 40*(5), 478-486.

Yang, Y., Dewald, J. P. A., Helm, F. C. T., & Schouten, A. C. (2017). Unveiling neural coupling within the sensorimotor system: directionality and nonlinearity. *European Journal of Neuroscience, 48*(7), 2407-2415.

Yang, Y., Solis-Escalante, T., van der Helm, F. C. T., & Schouten, A. C. (2016). A Generalized Coherence Framework for Detecting and Characterizing Nonlinear Interactions in the Nervous System. *IEEE Transactions on Biomedical Engineering, 63*(12), 2629-2637.

11

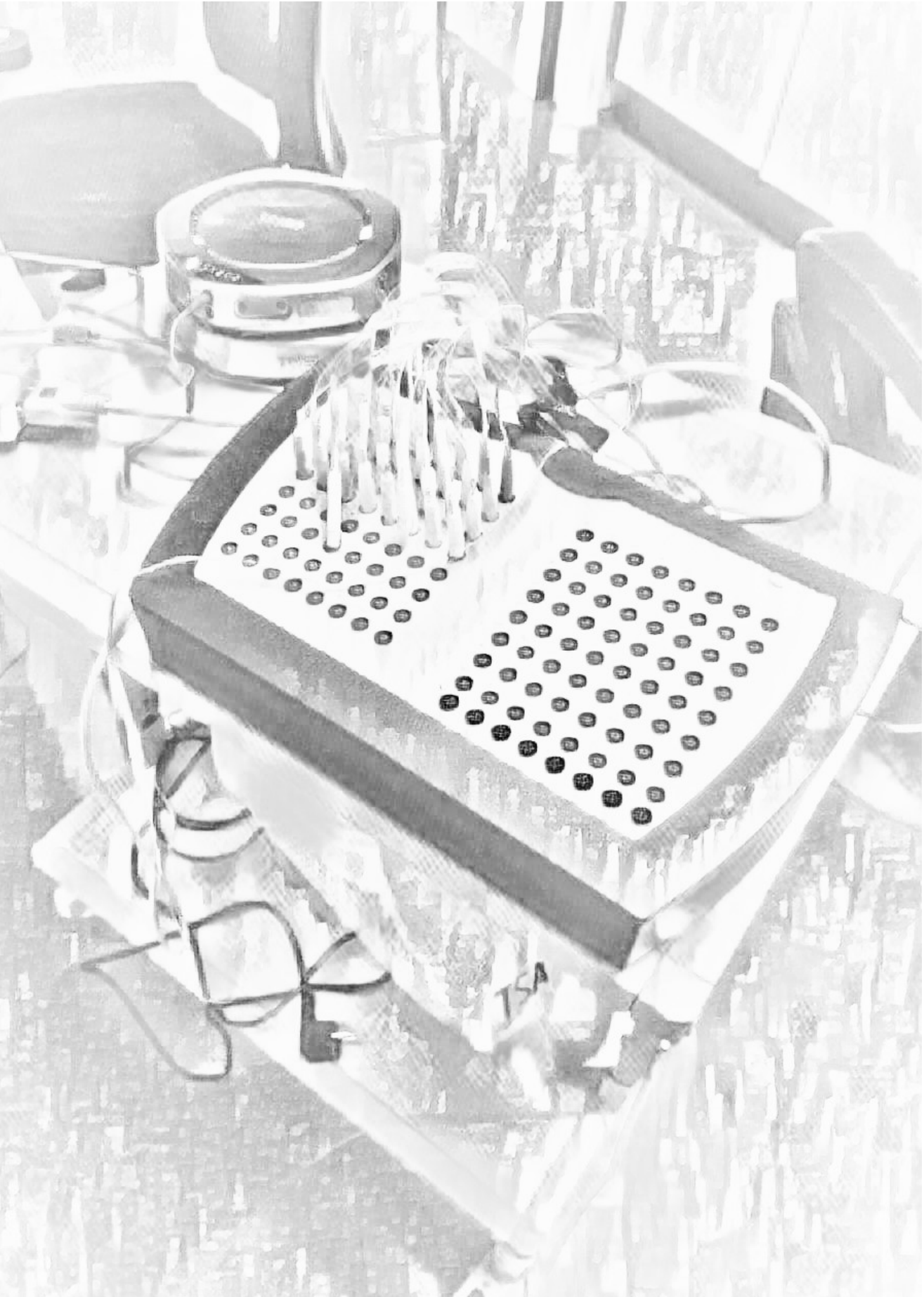
TSA

Chapter 12

Nociceptive Intra-Epidermal Electric Stimulation Evokes Steady-State Responses in the Secondary Somatosensory Cortex

Published as:

Van den Berg, B., Manoochehri, M., Schouten, A. C., van der Helm, F. C. T., & Buitenweg, J. R. (2022). Nociceptive intra-epidermal electric stimulation evokes steady-state responses in the secondary somatosensory cortex. *Brain Topography*, 35(2), 169-181.

DOI: https://www.doi.org/10.1007/s10548-022-00888-y

Abstract

Recent studies have established the presence of nociceptive steady-state evoked potentials (SSEPs), generated in response to thermal or intra-epidermal electric stimuli. This study explores cortical sources and generation mechanisms of nociceptive SSEPs in response to intra-epidermal electric stimuli. Our method was to stimulate healthy volunteers (n=22, all men) with 100 intra-epidermal pulse sequences. Each sequence had a duration of 8.5 s and consisted of pulses with a pulse rate between 20 and 200 Hz, which was frequency modulated with a multisine waveform of 3, 7 and 13 Hz (n=10, 1 excluded) or 3 and 7 Hz (n=12, 1 excluded). As a result, evoked potentials in response to stimulation onset and contralateral SSEPs at 3 and 7 Hz were observed. The SSEPs at 3 and 7 Hz had an average time delay of 137 ms and 143 ms respectively. The evoked potential in response to stimulation onset had a contralateral minimum (N1) at 115 ms and a central maximum (P2) at 300 ms. Sources for the multisine SSEP at 3 Hz and 7 Hz were found through beamforming near the primary and secondary somatosensory cortex. Sources for the N1 were found near the primary and secondary somatosensory cortex. Sources for the N2-P2 were found near the supplementary motor area. Harmonic and intermodulation frequencies in the SSEP power spectrum remained below a detectable level and no evidence for nonlinearity of nociceptive processing, i.e., processing of peripheral firing rate into cortical evoked potentials, was found.

12.1 Introduction

Nociceptive stimulation leads to an organized response in multiple sensory and cognitive-evaluative brain areas, which is used to study the neurophysiological basis of pain. A temporally well-defined response can be measured when recording the cortical potential on the scalp evoked by a single nociceptive stimulus. This nociceptive evoked potential has a distinct temporal pattern including an early contralateral negative peak (N1), a subsequent central negative peak (N2), and a late central positive peak (P2). This pattern has consistently been reproduced for both laser (Carmon, Dotan, & Sarne, 1978) and intra-epidermal electric (Inui, Tran, Hoshiyama, & Kakigi, 2002) stimulation of nociceptive afferents. A large body of studies of this temporal pattern found that the N1 is generated by the simultaneous activation of the primary (S1) and secondary (S2) somatosensory cortex (Ploner, Schmitz, Freund, & Schnitzler, 1999, 2000; Tarkka & Treede, 1993; Valeriani, Rambaud, & Mauguière, 1996), while the N2-P2 complex appears to be associated with activation of the anterior cingulate cortex (ACC) (Bentley, Youell, & Jones, 2002; Garcia-Larrea, Frot, & Valeriani, 2003). Although this pattern is consistently observed in response to nociceptive stimulation, similar activation patterns could be observed in response other stimulation modalities. While the N1 was found to be associated with mostly nociceptive and somatosensory-specific activity, the N2-P2 complex was found to be associated with multimodal activity occurring in response to visual, auditory, somatosensory and nociceptive stimulation (Mouraux & Iannetti, 2009). As such, recent studies suggest that the N2-P2 complex is related to the temporal saliency of a stimulus rather than somatosensory or nociceptive specific brain activity (Iannetti & Mouraux, 2010).

An alternative approach uses a series of stimuli that are applied at a specific frequency in order to generate a steady-state evoked potential (SSEP). The continuous application of a series of stimuli downregulates the effect of temporal saliency and is thought to result in the entrainment of a network of cortical neurons involved in sensory processing of the stimulus, or the superposition of a series of transient neural responses (Norcia, Appelbaum, Ales, Cottereau, & Rossion, 2015; Picton, John, Dimitrijevic, & Purcell, 2003;

Regan, 1966). A seminal study by Mouraux et al. used this approach to study pain processing by stimulating participants with blocks of nociceptive laser pulses with the hypothesis that the SSEPs elicited by this rapid thermal stimulation would result in "the activation of a network that is preferentially involved in processing nociceptive input" (Mouraux et al., 2011). Later studies showed that it is also possible to record such a nociceptive SSEP in response to blocks of intra-epidermal electric pulses (Colon, Nozaradan, Legrain, & Mouraux, 2012) and sinusoidal ultra-slow temperature modulation of the skin (Colon, Liberati, & Mouraux, 2017; Mulders et al., 2020).

In a recent study, we showed that it is also possible to evoke nociceptive SSEPs using frequency modulation of intra-epidermal pulses to further downregulate saliency effects (i.e. by decreasing the maximum distance between pulses and avoiding the rapid variations in pulse rate associated with blocks of pulses), and to enable multisine frequency modulation for probing system properties such as system delay, linearity and order (van den Berg et al., 2021). Frequency analysis showed significant peaks at stimulation frequencies (3 and 7 Hz) but did not find any significant harmonic or intermodulation frequencies that would confirm nonlinearity of nociceptive processing. Using the phase delay of significant nociceptive SSEPs at 3 and 7 Hz stimulation, we showed that there was an average time delay for both frequencies on the contralateral central midline electrodes (C_5, C_3, C_1 and C_z) of 168 ms which is similar to the average delay of the N1 (160 ms) in previous studies measuring evoked potentials to single intra-epidermal pulses (van den Berg & Buitenweg, 2021; van den Berg et al., 2020), suggesting that the nociceptive SSEP might result from the activation of similar neural pathways.

It remains unknown which mechanism and which cortical sources are responsible for the generation of nociceptive SSEPs. In this work, the first objective is to explore if we can identify sources of nociceptive SSEPs and stimulus onset EPs in response to intra-epidermal electric stimulation. In addition, SSEP time delays and EP latencies are compared to explore whether these sources are activated through similar neural pathways. The second objective is to study the (non)linearity of these brain responses based on harmonic and intermodulation frequencies. Comparison of nociceptive SSEP

and stimulus onset EP topographies, sources and latencies helps to gain more insight in the functional differences and similarities between transient and steady-state evoked responses in response to nociceptive stimulation.

12.2 Methods

The results presented in this work are based on data from two experiments. The first set of experiments on 10 participants were reported in (van den Berg et al., 2021). Another set of experiments on 12 participants was recorded to extend the original dataset for improved signal-to-noise ratio and source localization.

12.2.1 Experiment

Participants

A total of 22 healthy male volunteers between 18 and 40 years old participated in this study. Only male volunteers were used to prevent potential sex-based differences within the group. All participants provided written informed consent before participation. All experiments were approved by the ethics committee at the Delft University of Technology (approval nr. 1238) and are in accordance with the declaration of Helsinki.

Procedure

Participants were seated upright facing a single neutral image in a dim and silent room. The room was shielded from external electromagnetic interference. Participants were stimulated on the dorsum of the right hand on five different locations (Figure 12.1) to reduce potential habituation or sensitization effects induced by repeated stimulation on the same location. On each location, a block of 20 pulse sequences was applied. Each pulse sequence had a duration of 8.5 s. The pulse amplitude during each block was set to twice the detection threshold to a single 0.5 ms pulse. This detection

threshold was measured in advance of each block using a staircase paradigm, in which the participant was asked to press and hold a response button, and a single 0.5 ms pulse was applied repeatedly and increased with a step size of 0.025 mA (starting from zero) until the participant reported stimulus detection by releasing the response button.

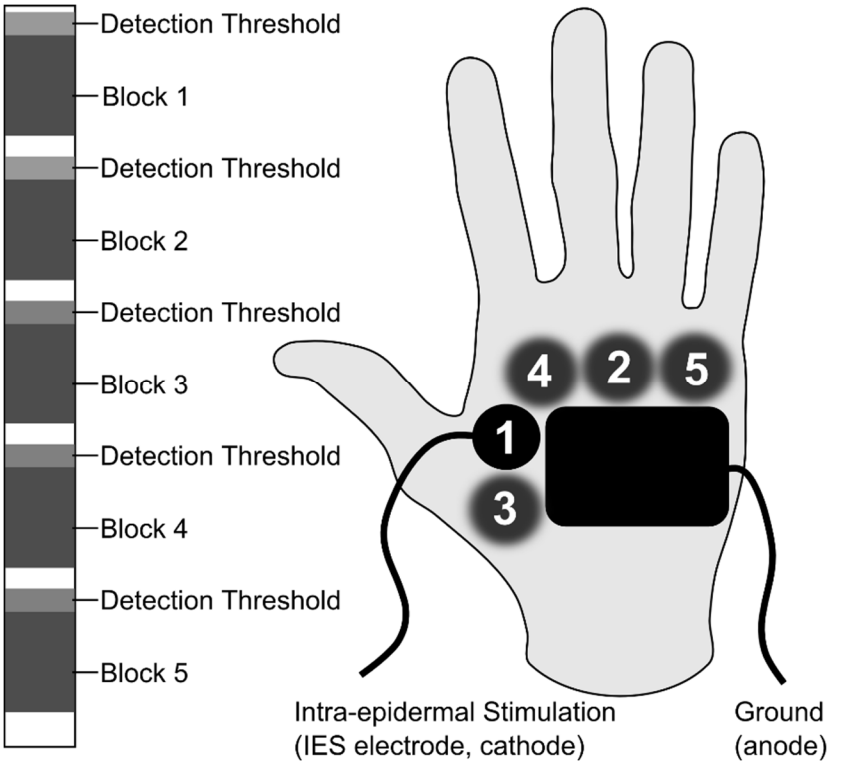

Figure 12.1: *Participants were stimulated in 5 blocks of 20 frequency modulated pulse sequences. Each block was applied at a different location, indicated by numbers in the figure. In each block, the pulse amplitude was set to twice the detection threshold of a single pulse, measured before the start of each block.*

Nociceptive Stimulation

Intra-epidermal electric stimulation was applied to participants with a current controlled stimulator (AmbuStim, University of Twente, Enschede, the Netherlands) at twice the detection threshold (on average 0.35 ± 0.28 mA). This type of stimulation preferentially activates nociceptive afferents in the epidermis (Mouraux, 2010; Poulsen, Tigerholm, Meijs, Andersen, & Mørch, 2020). The stimulation electrode consisted of 5 microneedles in a layer of flexible silicone (Steenbergen et al., 2012), protruding 0.5 mm from the electrode surface (Figure 12.2). Stimulation with this electrode results in a sharp pricking sensation (Steenbergen et al., 2012). The recorded responses using this electrode are similar to other studies using intra-epidermal stimulation (van den Berg & Buitenweg, 2021). The electrode was sterilized by autoclave before each measurement.

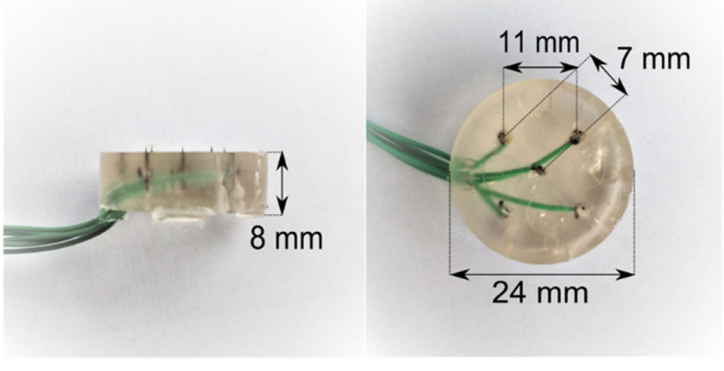

Figure 12.2: *Electrode for intra-epidermal stimulation, consisting of an array of 5 inter-connected microneedles embedded in a flexible layer of silicone.*

Frequency Modulation

Stimulation consisted of frequency modulated sequences of square wave cathodic electric pulses, using the same method as was used earlier in (van den Berg et al., 2021). Stimulation was controlled by a microcontroller connected to the trigger input of the stimulator. Each trigger pulse generated by the

microcontroller resulted in a single stimulation pulse. Pulse sequences were frequency modulated through modulation of the inter-pulse interval (Figure 12.3). Inter-pulse intervals were based on a multisine frequency modulation function, see Equation (1).

$$F_{pulse}(t) = C_{offset} + A_1 \sin(2\pi F_1 t + \phi_1) + A_2 \sin(2\pi F_2 t + \phi_2) + A_3 \sin(2\pi F_3 t + \phi_3) \quad (1)$$

Applying this multisine frequency modulation function (Figure 12.3, top left) to a sequence of electric pulses (Figure 12.3, middle left) leads to a stimulus with power at the three modulation frequencies (F_1, F_2, F_3) (Figure 12.3, bottom left). Modulation frequencies (F_1, F_2, F_3) were chosen such that measured SSEPs are representative of the behavior of the nociceptive system. In a previous study using square wave intra-epidermal stimuli (Colon, Nozaradan, Legrain, & Mouraux, 2012) brain responses were measured in a range from 3 to 43 Hz, where lower frequencies resulted in a more consistent response. Furthermore, the frequencies were chosen such that the number of overlapping harmonics and intermodulation frequencies were minimized in order to apply nonlinear system identification techniques to the measured SSEP (Yang, Solis-Escalante, van der Helm, & Schouten, 2016), while avoiding frequencies with a large interference by alpha waves. To avoid transient brain activity due to perception of individual pulses within the sequence, the maximum inter-pulse interval was set to 50 ms, i.e., a minimum pulse frequency (F_{pulse}) of 20 Hz. To limit the effects of peripheral nerve repolarization on measured SSEPs, the minimum inter-pulse interval was set to 5 ms, i.e., a maximum pulse frequency (F_{pulse}) of 200 Hz.

For the first 10 participants, modulation frequencies (F_1, F_2, F_3) of 3, 7 and 13 Hz were used, and each modulation amplitude (A_1, A_2, A_3) was set to 30 Hz and phase delays (ϕ_1, ϕ_2, ϕ_3) were set to 0, $\frac{1}{3}\pi$ and $-\frac{1}{3}\pi$. For the last 12 participants, only the modulation frequencies of 3 and 7 Hz were used to improve SNR by increasing the modulation amplitudes from 30 to 43 Hz, with phase delays set to $-\frac{1}{2}\pi$ and $\frac{1}{2}\pi$.

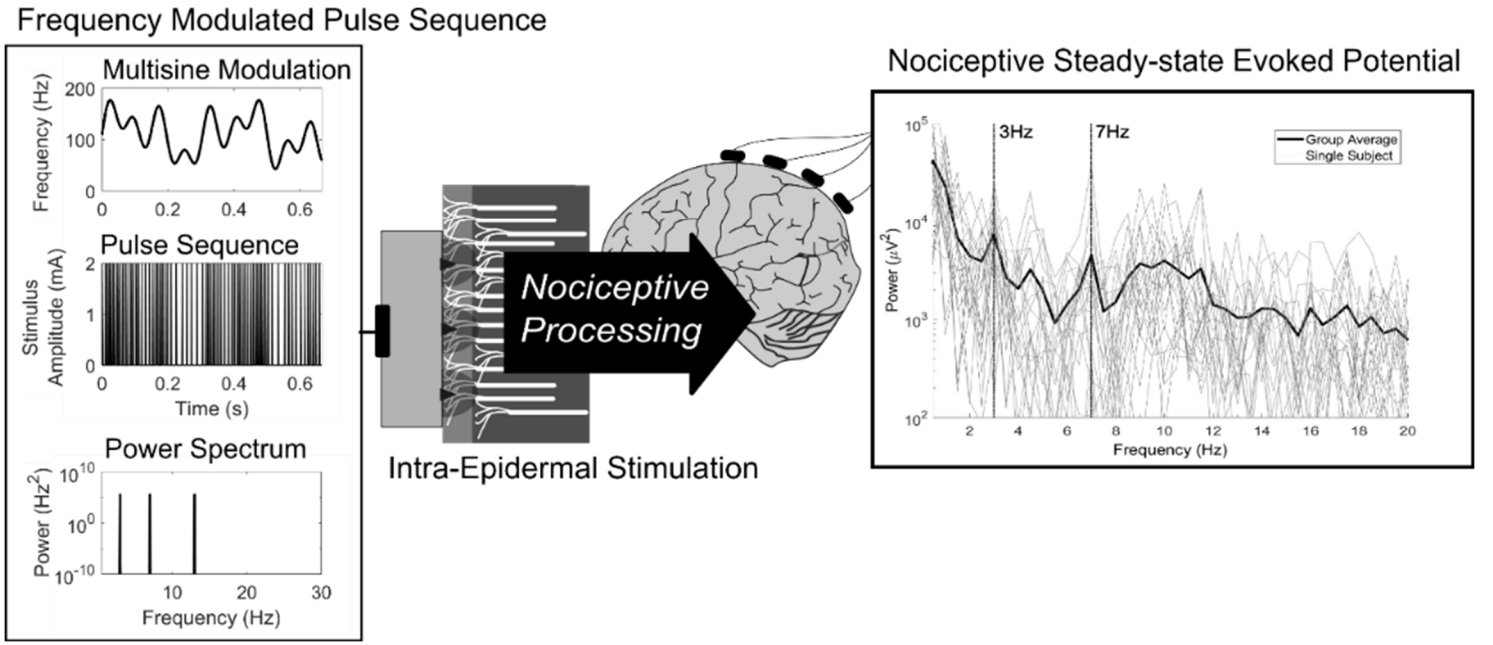

Figure 12.3: *Nociceptive afferents are stimulated with a sequence of intra-epidermal electric pulses. Applying a multisine frequency modulation function (top left) to the frequency of a sequence of electric pulses (middle left) leads to a stimulus with power at the modulation frequencies (bottom left). Stimulation using a multisine frequency modulated pulse sequence leads to a SSEP with peaks at the fundamental stimulation frequencies, harmonics, or intermodulation frequencies (right), which can be used to study system (non)linearity and time delay.*

EEG Recording

The scalp EEG was recorded using a TMSi REFA amplifier (TMSi B.V., Oldenzaal, the Netherlands) at a sample rate of 1024 Hz. The signal was recorded at 128 Ag/AgCl electrodes, which were located on the scalp according to the international 10/5 system (Oostenveld & Praamstra, 2001). A common average reference was used for recording. In the first 10 participants, the ground electrode was located on the right mastoid. In the last 12 participants, the ground electrode was located on the right wrist to minimize possible displacement current artifacts, i.e. artefacts due to the flow of stimulation current to the EEG ground instead of the stimulator ground (McLean, Scott, & Parker, 1996). Electrodes were gelled with an impedance below 10 $k\Omega$.

12.2.2 Data Analysis

Identification of stimulation artifacts

To inspect for stimulation artifacts, a time-locked epoch was extracted around each pulse, with approximately 80 000 to 100 000 epochs per participant, and high-pass filtered with a cutoff frequency of 60 Hz. The average over all epochs in all sequences and blocks was computed for each participant to obtain the stimulation artifacts. Participants with an average stimulation artifact larger than 100 nV at the Cz channel were excluded.

Data Preprocessing

The recorded EEG was pre-processed using EEGlab (Delorme & Makeig, 2004). The EEG was high-pass filtered with a cutoff frequency of 1 Hz and low-pass filtered with a cutoff frequency of 40 Hz. To reduce distortion by potential EMG, EOG and movement artifacts, channels in front of the head, on the mastoids and on the lower back of the head were symmetrically removed (M1, M2, FT9, FTT9h, TP7, TPP9h, P9, FT10, FTT10h, TP8, TPP10h, P10, T7, T8, Fp1, Fpz, Fp2, I1, Iz, I2, OI1h, OI2h, AFp3h, AFp4h). In addition, channels with flat

or excessive EMG activity were removed from the data (on average 2 channels per subject). The remaining channels were re-referenced to the common average. Epochs were extracted from -10.0 to 10.0 s with respect to stimulation onset. Epochs with excessive EMG activity or eye movement artifacts were removed by visual inspection. Any residual contamination by EOG, EMG or movement artifacts was removed using adaptive mixture independent component analysis (Palmer, Makeig, Kreutz-Delgado, & Rao, 2008). No contamination by ECG artifacts was found during visual inspection or during independent component analysis.

Identification of EPs

For each participant, epochs were averaged across all sequences to identify the evoked potential in response to sequence onset. Channels for EP analysis were selected based on previous publications using intra-epidermal electric stimulation (Liang, Lee, O'Neill, Dickenson, & Iannetti, 2016; Mouraux, Marot, & Legrain, 2014; van den Berg & Buitenweg, 2021). A first negative peak (N1) was defined as the most negative peak at T3-Fz between 80-180 ms after stimulus onset. A second negative peak (N2) was defined as the most negative peak at Cz between 100-300 ms after stimulus onset. A positive peak (P2) was defined as the most positive peak at Cz between 200-500 ms after stimulus onset. To study the average EP waveform across all participants, a grand average EP was computed at T3-Fz and Cz. The grand average EP was tested for significance at N1, N2 and P2 latencies at T3, Cz and T4, and at the T3-Fz derivation. Participants that did not show an N1, i.e., a negative peak between 80-180 ms at T3-Fz, were excluded from the grand average and source localization of the N1 waveform. Participants that did not show an N2 or P2, i.e., a negative peak between 100-300 ms or a positive peak between 200-500 ms at Cz, were excluded from the grand average and source localization of the N2-P2 waveform.

Identification of SSEPs

Epochs were limited to 0.5-8.5 s with respect to sequence onset to remove activity evoked by stimulus onset. Epochs were split into 4 segments of 2 s, giving a total of 400 segments per participant, allowing for additional reduction of spectral noise by averaging, while limiting the frequency resolution to 0.5 Hz. For each participant, the power ($\widehat{|X(f)|^2}$), phase ($Arg(\hat{X}(f))$) and noise level ($\frac{\sigma^2(f)}{M}$) of time-locked activity across all segments for all central midline electrodes (C3, C1, Cz, C2, C4) were computed. The T^2_{circ} value (Victor & Mast, 1991) was computed across all segments for every channel on every stimulated frequency using Equation (2).

$$T^2_{circ} = (M-1)\frac{\widehat{|X(f)|^2}}{\sigma^2(f)} \quad (2)$$

Where $\hat{X}(f) = \frac{1}{M}\sum_{m=1}^{M} X_m(f)$

and $\sigma^2(f) = \sum_{m=1}^{M}(X_m(f) - \hat{X}(f))^2$

Here, the T^2_{circ} value is described in terms of the average $\hat{X}(f)$ and the variance $\sigma^2(f)$ of the Fourier transformed segments $X_m(f)$ at frequency f with a total of M segments. The group level power spectrum was tested for significance at fundamental stimulation frequencies, harmonics and intermodulation frequencies by testing the T^2_{circ} against the F-statistic with a significance level of 0.05, as was initially proposed by (Victor & Mast, 1991).

Source Localization of EPs

Sources of the N1 and the N2-P2 were reconstructed with a linearly constrained minimum variance (LCMV) beamformer (Van Veen, van Drongelen, Yuchtman, & Suzuki, 1997) using Fieldtrip (Oostenveld, Fries, Maris, & Schoffelen, 2011) with a workflow similar to Popov et al. (Popov, Oostenveld, & Schoffelen, 2018). A forward model was computed using the default volume conduction model provided by Fieldtrip. The average EP

waveform was obtained using the full epoch and the covariance matrix was based on the pre-stimulus activity. Subsequently, LCMV source analysis was performed using ft_sourceanalysis with normalization of the weights to account for the center of the head bias and a regularization parameter of 20%. The individual source reconstructions were averaged over the participants to obtain the grand average brain activity. A mask was used to visualize the top 0.1% of the voxels.

Source Localization of SSEPs

Sources of 3 Hz and 7 Hz SSEPs were reconstructed with dynamic imaging of coherent sources (DICS) (Gross et al., 2001), using Fieldtrip (Oostenveld, Fries, Maris, & Schoffelen, 2011) with a workflow similar to Popov et al. (Popov, Oostenveld, & Schoffelen, 2018). A forward model was computed using the default volume conduction model provided by Fieldtrip. A dummy signal at the modulation frequency is created for coherence computation. Cross-spectral density matrices are computed for the entire epoch, pre-stimulus, and post-stimulus data. A common spatial filter is computed using the cross-spectral density matrix of the entire epoch. Subsequently, source coherence is computed based on pre-stimulus and post-stimulus data using a regularization parameter of 1%. Individual source reconstructions are obtained by computing the coherence difference between pre-stimulus and post-stimulus activity. The individual source reconstructions were averaged to obtain the grand average brain activity. A mask was used to visualize the top 0.1% of voxels.

12.3 Results

A total of 10 participants participated in the first set of experiments and a total of 12 participants participated in the second set of experiments included in this study. Two of the 22 participants were excluded: one due to an excessive stimulation artifact and one due to excessive movement artifacts throughout the experiment.

12.3.1 Identification of SSEPs

Steady state evoked potential power spectra and topographies are shown in Figure 12.4 and 12.5. Fundamental, harmonic and intermodulation frequencies were tested for significance based on the T^2_{circ}. In addition, significance of 3 Hz and 7 Hz at electrodes was tested for significance based on the T^2_{circ} (see Section 2.2.4). Electrode C3 had significant power ($p<0.05$) at 3 Hz and 7 Hz. Other frequencies, including harmonics and intermodulation frequencies, did not have significant power at a group level. For 3 Hz, significant power was found at C2, Cz, C1 and C3. For 7 Hz, significant power was found only at C3. The estimated SSEP delays at C3 was 137.3 ± 22.6 ms at 3 Hz and 143.4 ± 13.7 ms at 7 Hz. For the N1, N2 and P2 there was an average time delay of 142.6 ± 11.9 ms, 192.1 ± 23.0 ms and 459.3 ± 41.8 ms respectively.

12.3.2 Identification of EPs

Evoked potential waveforms at T3-Fz and Cz are shown in Figure 12.6. No N1 was found for a total of five participants. For the remaining 15 participants, a significant ($p<.01$) negative peak between 80 and 180 ms at T3-Fz (N1) was found at 115 ms. The average latency of the N1 was found to be 136.1 ± 30.0 ms. No N2 or P2 was found in one participant. For the remaining 19 participants, a second significant ($p<.001$) negative peak between 100 and 300 ms at Cz (N2) was found at 140 ms. The average latency of the N2 was found to be 165.8 ± 38.6 ms. A significant ($p<.001$) positive peak between 200 and 500 ms at Cz (P2) was found at 300 ms and the average latency of P2 was found to be 323.9 ± 34.7 ms. Grand average topographies of the N1, N2 and P2 in Figure 12.7 are showing a contralateral negative potential, a central contralateral potential, and a central vertex potential respectively. The N1, N2 and P2 latencies are compared with the SSEP time delay at 3 Hz and 7 Hz in Figure 12.8. The P2 latency was significantly later ($p<.001$) than the latencies at 3 and 7 Hz.

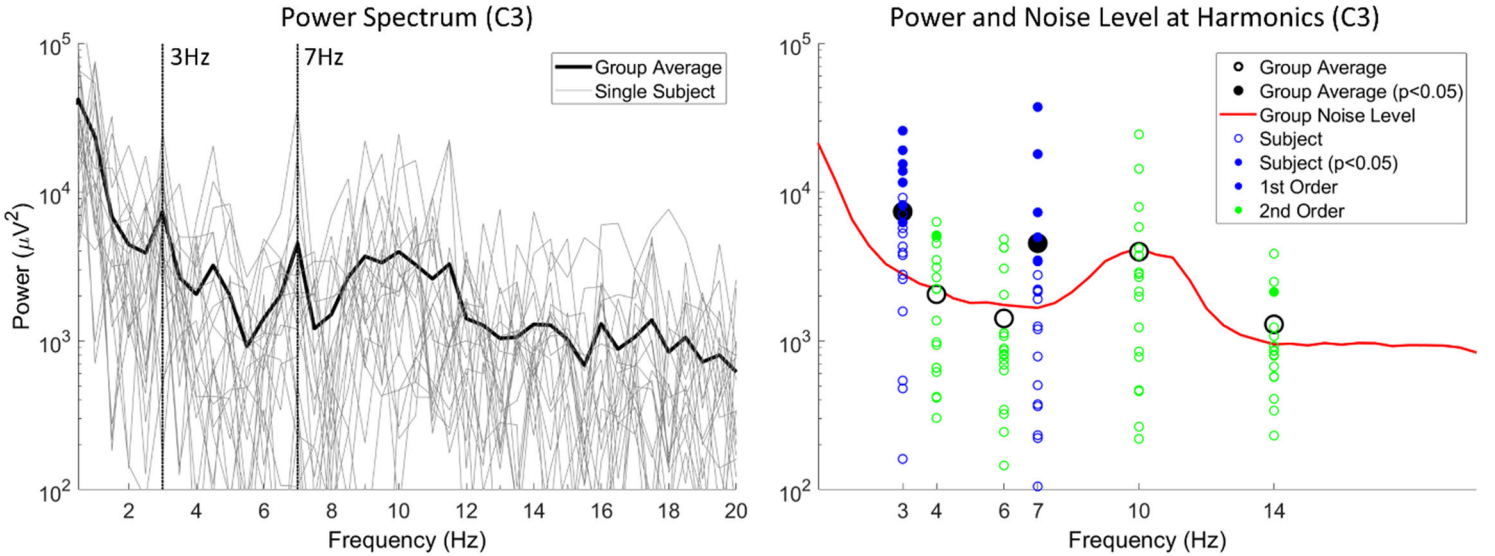

Figure 12.4: *Group and individual steady state evoked potential power spectra at all frequencies (left), and at harmonic and intermodulation frequencies (right) at C3. The power at first order and second order harmonics and intermodulation frequencies in individual participants is shown as blue and green circles, respectively. Group average power at harmonics and intermodulation frequencies is shown in black. Fundamental, harmonic and intermodulation frequencies were tested for significance based on the* T^2_{circ}*. Significant frequencies at individual and group level (p<0.05) are marked with a filled circle. The group average power was significant at 3 Hz and 7 Hz.*

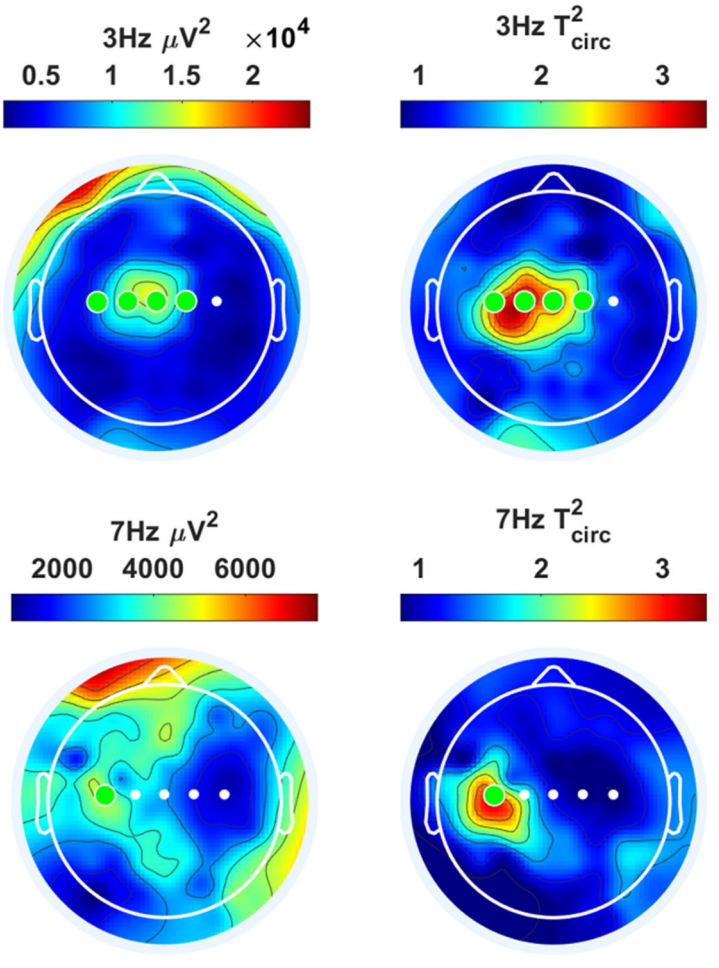

Figure 12.5: *Steady state evoked potential power (left) and T^2_{circ} (right) topographies at 3 Hz (top) and 7 Hz (bottom). The T^2_{circ} is an efficient statistic for detecting true SSEP activation out of noise (Norcia, Appelbaum, Ales, Cottereau, & Rossion, 2015). Significance of 3 Hz and 7 Hz at electrodes was tested for significance based on the T^2_{circ}. Significant electrodes ($p<0.05$) are marked by a green dot.*

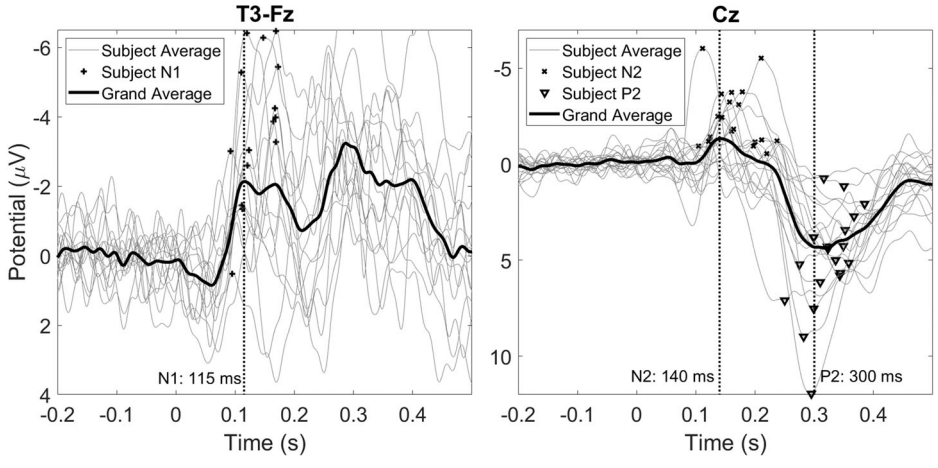

Figure 12.6: Grand average evoked potential waveforms at T3-Fz and Cz, and the average waveform of each subject. Evoked potential components were defined as the most negative peak on T3-Fz between 80 and 180 ms (N1), the most negative peak at Cz between 100 and 300 ms (N2) and the most positive peak at Cz between 200 and 500 ms (P2). In the grand average, a significant N1 was found at 115 ms (p<.01), a significant N2 was found at 140 ms (p<.001) and a significant P2 was found at 300 ms (p<.001).

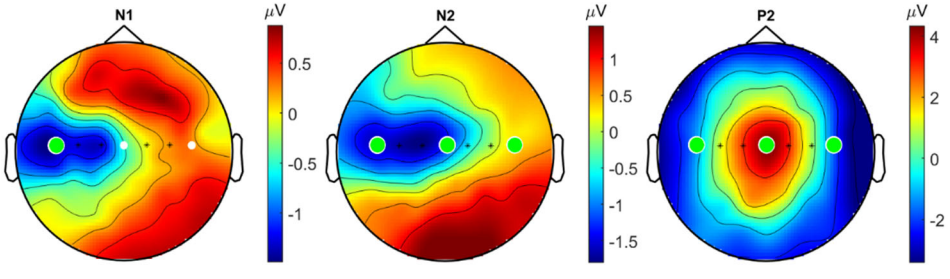

Figure 12.7: Grand average evoked potential topographies at 115 ms (N1), 140 ms (N2) and 300 ms (P2). The channels T3, Cz and T4 were tested for significance. Significant channels (p<.05) are marked by green dots.

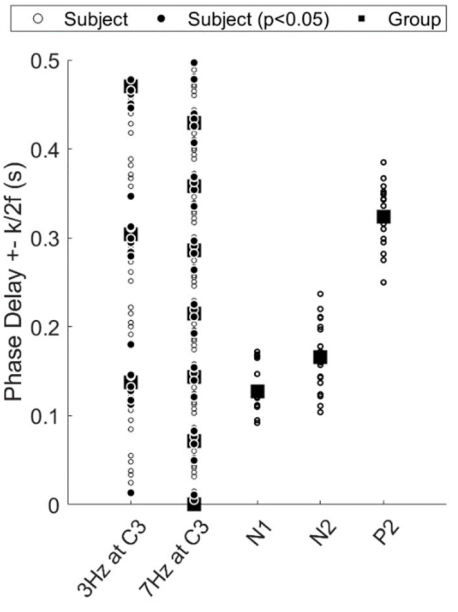

Figure 12.8: Estimated steady state evoked potential time delay at C3 for 3 Hz and 7 Hz, and the individual and average time delays of N1, N2 and P2 for comparison. There was an average time delay of 137.3 ± 22.6 ms at 3 Hz and an average time delay of 143.4 ± 13.7 ms at 7 Hz. For the N1, N2 and P2 there was an average time delay of 136.1 ± 30.0 ms, 165.8 ± 38.6 ms and 323.9 ± 34.7 ms respectively.

12.3.3 Source Localization of SSEPs

Coronal, transversal, and axial slices of reconstructed 3 Hz and 7 Hz activity are shown in Figure 12.9. Position of the slices is indicated by blue crosshairs. The top 0.1% of voxels is shown in color. For 3 Hz, maximum activation was found in the secondary somatosensory cortex and no other sources were found. For 7 Hz, maximum activation was found around the primary motor cortex and no other sources were found.

12.3.4 Source Localization of EPs

Coronal, transversal, and axial slices of reconstructed N1 and N2-P2 activity are shown in Figure 12.10. Position of the slices is indicated by blue crosshairs. The top 0.1% of voxels is shown in color. For the N1, maximum activation was found in the secondary somatosensory cortex. For the N2-P2, maximum activation was found in the left and right supplementary motor area.

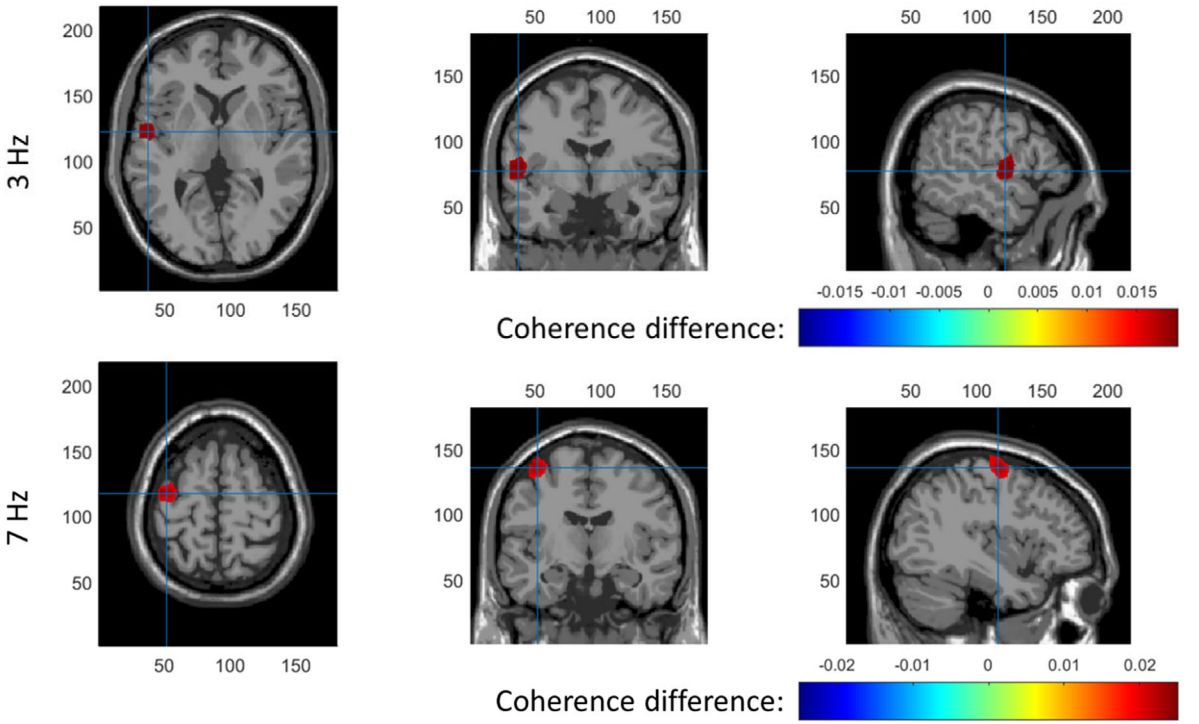

Figure 12.9: *Coronal, transversal, and axial slices of reconstructed 3 Hz (top) and 7 Hz (bottom) activity. The top 0.1% of voxels is shown in color and the position of the slices is indicated by blue cross hairs.*

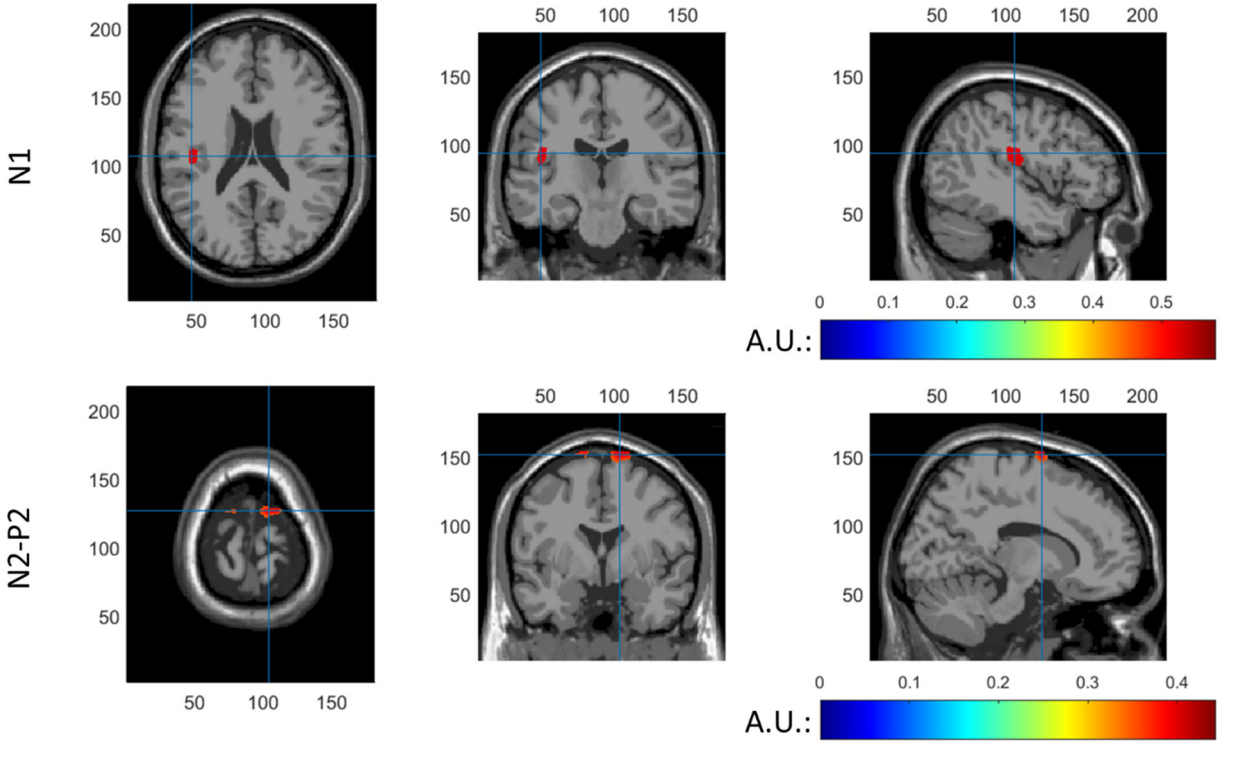

Figure 12.10: *Coronal, transversal, and axial slices of reconstructed N1 activity (top) and N2-P2 activity (bottom). The top 0.1% of voxels is shown in color and the position of the slices is indicated by blue cross hairs.*

12.4 Discussion

In this study data from over 2000 trials in 20 subjects were combined to study which mechanism and which cortical sources are responsible for the generation of nociceptive SSEPs. The first objective was to explore if we could identify sources of nociceptive SSEPs and stimulus onset EPs in response to intra-epidermal electric stimulation. The second objective was to study the (non)linearity of these brain responses based on harmonic and intermodulation frequencies. We used a multisine waveform of 3 and 7 Hz for frequency modulation of an intra-epidermal electric pulse sequence. We found evoked responses in the time-domain and steady-state evoked responses at 3 and 7 Hz in the frequency domain. We used beamforming to reconstruct sources of nociceptive SSEPs and stimulus onset EPs and studied system (non)linearity based on the power spectrum.

12.4.1 Intra-epidermal SSEPs and EPs

Significant group-level SSEPs at 3 and 7 Hz were observed central and contralateral with respect to the side of stimulation, showing that multisine frequency modulation of an intra-epidermal pulse sequence leads steady-state evoked potentials at the stimulated frequencies. Special care was taken to identify and reduce potential stimulation artefacts. Participants with stimulation artifacts larger than 100 nV at Cz were excluded and the remaining stimulation artifact in the first 10 participants was centered around the EEG ground (on the right mastoid) and no larger than 50 nV at Cz, while no stimulation artifact was observed in the last 12 participants. As such, the observed SSEPs at 3 Hz and 7 Hz can be attributed to cortical activation in response to intra-epidermal electric stimulation.

The additional value of using multisine modulation instead of modulation at a single frequency, is the possibility to study system nonlinearity and estimate system delay more accurately. As harmonic and intermodulation frequencies remained below a detectable level in the current study, no evidence for nonlinearity of nociceptive processing was found. This is opposite to several SSEP studies in other sensory modalities which clearly demonstrated the

presence of nonlinear effects in sensory processing (e.g. in proprioception (Vlaar, Solis-Escalante, Vardy, der Helm, & Schouten, 2016), in vision (Regan & Regan, 1989) and in hearing (Wang, Noordanus, & van Opstal, 2021)). In these studies, stimuli were applied to sensory organs that act as a transducer by transforming a form of energy (e.g., work in proprioception, photons in vision, sound waves in hearing) to a neural firing rate. In contrast, in our study the neural firing rate in intra-epidermal electric stimulation is directly modulated through a series of electrical pulses, effectively bypassing nonlinear sensory transduction processes occurring in other sensory modalities. Significant nonlinear effects were absent in this study, potentially as a result of bypassing these sensory transduction processes. Stimulation type and parameters play an important role in system (non)linearity. In the current study, a maximum pulse rate of 200 Hz was used to avoid potential nonlinearities due to the refractory period of nociceptive afferents. The pulse amplitude was kept constant to avoid nonlinear system behavior arising from modulation of the number of recruited nociceptive afferents. Nonlinear behavior could still occur due to nonlinear central neural processing (Roberts & Robinson, 2012). The absence of nonlinear behavior in the current experiment implies that central neural processing might be linear around the used stimulation parameters, e.g. due to a linearizing effect of corticothalamic feedback (Song et al., 2021). However, absence of any type of nonlinearity remains difficult to prove, and further research is needed to explore the dynamics of central nociceptive processing.

Earlier SSEP studies hypothesized that SSEPs either originate from the entrainment of neural oscillators or the linear superposition of transient responses (Norcia, Appelbaum, Ales, Cottereau, & Rossion, 2015). There is compelling evidence that, in contrast with the neural entrainment hypothesis, auditory (Bohórquez & Ozdamar, 2008; Bohorquez, Ozdamar, Acikgoz, & Yavuz, 2007; Galambos, Makeig, & Talmachoff, 1981; Santarelli et al., 1995) and visual (Capilla, Pazo-Alvarez, Darriba, Campo, & Gross, 2011) SSEPs are generated by the linear superposition of transient responses to the stimuli. As such, it is not unlikely that nociceptive SSEPs could also be explained by the linear superposition of N1 responses. The current results cannot be used to

confirm one of both hypotheses (e.g. as is done in (Capilla, Pazo-Alvarez, Darriba, Campo, & Gross, 2011)), due to absence of jittered control sequences. However, observation of an overlap in location and delay of SSEP and transient responses could warrant further investigation of the linear superposition hypothesis. The transient response evoked by intra-epidermal electric stimulation was analyzed by averaging trials around stimulus onset. A significant N1 wave and N2-P2 wave were found. Topographies and timing of both waves match earlier articles involving intra-epidermal electric stimulation (Mouraux, Marot, & Legrain, 2014; van den Berg & Buitenweg, 2021). Whereas the delay of the P2 was significantly later ($p<.001$) than the delay of 3 and 7 Hz SSEPs, the delays of the N1 (136.1 ± 30.0 ms) and the N2 (165.8 ± 38.6 ms) were close to the delay observed at 3 (137.3 ± 22.6 ms) and 7 Hz (143.4 ± 13.7 ms), suggesting that similar neural processing pathways are involved in the generation of the nociceptive intra-epidermal SSEPs and EPs.

12.4.2 Source Localization of Intra-epidermal SSEPs

For the first time, this study localized cortical sources of SSEPs in response to intra-epidermal electric stimulation. A major obstacle for accurate source localization was the low signal-to-noise ratio of the signal caused by both the low stimulus amplitude required to preferentially stimulate nociceptive afferents and the division of bandwidth over multiple stimulation frequencies to probe system (non)linearity. For a more elaborate discussion of parameters involved in the signal-to-noise ratio, please refer to (van den Berg et al., 2021). As a result, individual source estimates (not reported) suffered from noise and were not accurately depicting a single source location. However, by averaging individual source estimates, group-level sources converged to areas at the secondary somatosensory cortex (3 Hz) and the primary motor cortex (7 Hz).

The source of the SSEP at 7 Hz was located around the primary motor cortex (M1). Earlier nociceptive and pain studies did occasionally report M1 activation, suggesting that this activation could be related to suppression of movement or pain-evoked movements (Apkarian, Bushnell, Treede, & Zubieta, 2005). Both explanations seem unlikely in this study, as participants

generally experience intra-epidermal SSEPs as non-painful (van den Berg et al., 2021). Earlier nociceptive and pain studies using EEG and MEG did consistently report sources in S1 and S2. As such the source observed in M1 could also be explained by a biased estimate of S1 location. A potential bias in source locations in this study is caused by the use of a standard leadfield and MRI model. Further evidence about potential involvement of the S1 in intra-epidermal SSEPs might be obtained by comparing the topographical distribution and source localization for stimulation of the upper and lower limbs in future studies.

The source of the SSEP at 3 Hz was located at the secondary somatosensory cortex. Activation of S2 is frequently observed in both EEG, MEG, and fMRI studies, in response to both phasic and tonic stimulation. Both S1 and S2 are thought to be involved in parallel in upstream nociceptive sensory processing before the signal is passed on to the ACC for the cognitive-evaluative stages of pain processing (Apkarian, Bushnell, Treede, & Zubieta, 2005; Ploner, Schmitz, Freund, & Schnitzler, 1999). The identification of the S2 as a generator of nociceptive intra-epidermal SSEPs suggests that these reflect sensory-discriminative rather than cognitive-evaluative aspects of nociceptive processing.

A comparison was made between the aforementioned SSEP sources and sources of the stimulus onset EP. Source localization using a LCMV beamformer identified the S2 as a primary source of the N1. Several previous MEG studies reported parallel activation of both S1 and S2 in response to nociceptive stimulation, e.g., (Ninomiya et al., 2001; Ploner, Schmitz, Freund, & Schnitzler, 1999, 2000). Although some EEG studies also observe activation of both sources, as in (Valentini et al., 2012), many other EEG studies observe sources in only the S2 (Apkarian, Bushnell, Treede, & Zubieta, 2005). One possible reason for not observing both sources is the high correlation between both sources, which does not only make it more difficult to observe distinct sources using beamforming (Belardinelli, Ortiz, & Braun, 2012), but also violates the independence assumption of independent component analysis. In the current study, we did not observe N1 sources in S1, but the reconstruction of sources in the S1 could have been impeded by the presence of highly

correlated sources in the S2. Source localization using a LCMV beamformer identified bilateral activity in the supplementary motor area as a potential source of the N2-P2 waveform. Several earlier studies reported activation of the supplementary motor area in response to painful stimulation (Christmann, Koeppe, Braus, Ruf, & Flor, 2007; Peyron, Laurent, & García-Larrea, 2000), which might be attributed to preparation or inhibition of motor reactions. While earlier studies also identified the ACC as a primary generator of the N2-P2 waveform (Bentley, Youell, & Jones, 2002; Garcia-Larrea, Frot, & Valeriani, 2003), the current study could not find evidence for contribution of the ACC to the N2-P2 waveform. One potential reason is that ACC activation by painful stimuli could be confounded by supplementary motor activity (Apkarian, Bushnell, Treede, & Zubieta, 2005), in which case activity from the superficial supplementary motor area might contribute more to the observed EEG waveform than deep sources like the ACC. As such, source analysis suggests that sources of the N1 waveform and of the SSEP at 3 Hz are located in the same region, while the N2-P2 waveform associated with stimulus onset appears to originate from different regions of the brain.

12.4.3 Limitations

This was one of the first studies to reconstruct sources of nociceptive SSEPs. Despite the interesting possibilities nociceptive SSEPs might offer to study nociceptive processing, few studies have been performed on this topic as it remains challenging to reliably generate nociceptive SSEPs. In the case of intra-epidermal electric stimulation, stimulation parameters are adjusted for preferential activation of nociceptive afferents. In the first studies using intra-epidermal stimulation, preferential activation was achieved by a concentric needle electrode (Inui & Kakigi, 2012; Inui, Tran, Hoshiyama, & Kakigi, 2002). In the current study, we used a silicone needle electrode together with a separate planar ground electrode to stimulate nociceptive afferents. Stimulation using this configuration was shown to result in a sharp pricking sensation (Steenbergen, 2012) and to result in reaction times and evoked response latencies similar to earlier studies using laser or intra-epidermal stimulation (van den Berg & Buitenweg, 2021), indicating preferential

activation of nociceptive afferents. However, in order to remain preferential, both configurations require a limitation of stimulus intensity to twice the detection threshold (Mouraux, 2010; Poulsen, Tigerholm, Meijs, Andersen, & Mørch, 2020) to reduce concurrent activation of tactile afferents, which leads to a reduction in signal-to-noise ratio of the SSEP and challenges conventional signal analysis and source localization approaches. Therefore, the current techniques demand for ideal experimental circumstances to reliably observe nociceptive brain responses, including optimized setup and stimulation parameters, as well as a homogeneous study population.

The aim of this study was to explore whether it is possible to reconstruct sources of the nociceptive SSEP under these ideal circumstances. These ideal circumstances include a homogeneous study population, as it is well-known that age or sex can influence pain outcomes (Bartley & Fillingim, 2013) and might potentially affect evoked brain potentials (Monciunskaite, Malden, Lukstaite, Ruksenas, & Griksiene, 2019), and as a consequence reduce significance on a group level in a mixed population. For this reason, the current study was done with a homogeneous population of young healthy males. It is therefore important to note that the generalizability of these results might be limited, and that these results should be reproduced in populations of different age, sex, and ethnicity to provide more inclusive evidence of the effects observed in this study.

12.5 Conclusion

This study aimed to explore sources of nociceptive SSEPs and stimulus onset EPs following intra-epidermal electric stimulation, and to study the (non)linearity of these brain responses. We found that potential sources of nociceptive SSEPs can be studied through beamforming, and that these sources are located at or near the somatosensory cortices. We observed EPs in response to stimulation onset that were similar to the EPs evoked by a single electric or laser pulse, and the sources of these EPs were located at the secondary somatosensory cortex and the supplementary motor area. Multisine frequency modulation of the applied intra-epidermal pulse

sequences leads to cortical activation at the stimulated frequencies. As harmonic and intermodulation frequencies remained below a detectable level in the current study, no evidence for nonlinearity of nociceptive processing was found.

12.6 References

Apkarian, A. V., Bushnell, M. C., Treede, R.-D., & Zubieta, J.-K. (2005). Human brain mechanisms of pain perception and regulation in health and disease. *European Journal of Pain, 9*(4), 463-463.

Bartley, E. J., & Fillingim, R. B. (2013). Sex differences in pain: a brief review of clinical and experimental findings. *British Journal of Anaesthesia, 111*(1), 52-58.

Belardinelli, P., Ortiz, E., & Braun, C. (2012). Source activity correlation effects on LCMV beamformers in a realistic measurement environment. *Comput Math Methods Med, 2012*, 190513.

Bentley, D. E., Youell, P. D., & Jones, A. K. P. (2002). Anatomical localization and intra-subject reproducibility of laser evoked potential source in cingulate cortex, using a realistic head model. *Clinical Neurophysiology, 113*(8), 1351-1356.

Bohórquez, J., & Ozdamar, O. (2008). Generation of the 40-Hz auditory steady-state response (ASSR) explained using convolution. *Clin Neurophysiol, 119*(11), 2598-2607.

Bohorquez, J., Ozdamar, O., Acikgoz, N., & Yavuz, E. (2007, 22-26 Aug. 2007). *Methodology to Estimate the Transient Evoked Responses for the Generation of Steady State Responses.* Paper presented at the 2007 29th Annual International Conference of the IEEE Engineering in Medicine and Biology Society.

Capilla, A., Pazo-Alvarez, P., Darriba, A., Campo, P., & Gross, J. (2011). Steady-State Visual Evoked Potentials Can Be Explained by Temporal Superposition of Transient Event-Related Responses. *PLoS ONE, 6*(1), e14543.

Carmon, A., Dotan, Y., & Sarne, Y. (1978). Correlation of subjective pain experience with cerebral evoked responses to noxious thermal stimulations. *Experimental Brain Research, 33*(3-4), 445-453.

Christmann, C., Koeppe, C., Braus, D. F., Ruf, M., & Flor, H. (2007). A simultaneous EEG-fMRI study of painful electric stimulation. *NeuroImage, 34*(4), 1428-1437.

Colon, E., Liberati, G., & Mouraux, A. (2017). EEG frequency tagging using ultra-slow periodic heat stimulation of the skin reveals cortical activity specifically related to C fiber thermonociceptors. *NeuroImage, 146*, 266-274.

Colon, E., Nozaradan, S., Legrain, V., & Mouraux, A. (2012). Steady-state evoked potentials to tag specific components of nociceptive cortical processing. *NeuroImage, 60*(1), 571-581.

Delorme, A., & Makeig, S. (2004). EEGLAB: An open source toolbox for analysis of single-trial EEG dynamics including independent component analysis. *Journal of Neuroscience Methods, 134*(1), 9-21.

Galambos, R., Makeig, S., & Talmachoff, P. J. (1981). A 40-Hz auditory potential recorded from the human scalp. *Proc Natl Acad Sci U S A, 78*(4), 2643-2647.

Garcia-Larrea, L., Frot, M., & Valeriani, M. (2003). Brain generators of laser-evoked potentials: From dipoles to functional significance. *Neurophysiologie Clinique, 33*(6), 279-292.

Gross, J., Kujala, J., Hamalainen, M., Timmermann, L., Schnitzler, A., & Salmelin, R. (2001). Dynamic imaging of coherent sources: Studying neural interactions in the human brain. *Proc. Natl. Acad. Sci. U.S.A., 98*(2), 694-699.

Iannetti, G. D., & Mouraux, A. (2010). From the neuromatrix to the pain matrix (and back). *Experimental Brain Research, 205*(1), 1-12.

Inui, K., & Kakigi, R. (2012). Pain perception in humans: use of intraepidermal electrical stimulation. *Journal of Neurology, Neurosurgery and Psychiatry, 83*(5), 551.

Inui, K., Tran, T. D., Hoshiyama, M., & Kakigi, R. (2002). Preferential stimulation of Aδ fibers by intra-epidermal needle electrode in humans. *Pain, 96*(3), 247-252.

Liang, M., Lee, M. C., O'Neill, J., Dickenson, A. H., & Iannetti, G. D. (2016). Brain potentials evoked by intraepidermal electrical stimuli reflect the central sensitization of nociceptive pathways. *Journal of Neurophysiology, 116*(2), 286-295.

McLean, L., Scott, R. N., & Parker, P. A. (1996). Stimulus artifact reduction in evoked potential measurements. *Arch Phys Med Rehabil, 77*(12), 1286-1292.

Monciunskaite, R., Malden, L., Lukstaite, I., Ruksenas, O., & Griksiene, R. (2019). Do oral contraceptives modulate an ERP response to affective pictures? *Biol Psychol, 148*, 107767.

Mouraux, A., & Iannetti, G. D. (2009). Nociceptive Laser-Evoked Brain Potentials Do Not Reflect Nociceptive-Specific Neural Activity. *Journal of Neurophysiology, 101*(6), 3258-3269.

Mouraux, A., Iannetti, G. D., Colon, E., Nozaradan, S., Legrain, V., & Plaghki, L. (2011). Nociceptive Steady-State Evoked Potentials Elicited by Rapid Periodic Thermal Stimulation of Cutaneous Nociceptors. *The Journal of Neuroscience, 31*(16), 6079.

Mouraux, A., Iannetti, G. D., & Plaghki, L. (2010). Low intensity intra-epidermal electrical stimulation can activate Aδ-nociceptors selectively. *Pain, 150(1)*, 199-207.

Mouraux, A., Marot, E., & Legrain, V. (2014). Short trains of intra-epidermal electrical stimulation to elicit reliable behavioral and electrophysiological responses to the selective activation of nociceptors in humans. *Neuroscience Letters, 561*(Supplement C), 69-73.

Mulders, D., de Bodt, C., Lejeune, N., Courtin, A., Liberati, G., Verleysen, M., & Mouraux, A. (2020). Dynamics of the perception and EEG signals triggered by tonic warm and cool stimulation. *PLoS ONE, 15*(4), e0231698.

Ninomiya, Y., Kitamura, Y., Yamamoto, S., Okamoto, M., Oka, H., Yamada, N., & Kuroda, S. (2001). Analysis of pain-related somatosensory evoked magnetic fields using the MUSIC (multiple signal classification) algorithm for magnetoencephalography. *NeuroReport, 12*(8), 1657-1661.

Norcia, A. M., Appelbaum, L. G., Ales, J. M., Cottereau, B. R., & Rossion, B. (2015). The steady-state visual evoked potential in vision research: A review. *J Vis, 15*(6), 4.

Oostenveld, R., Fries, P., Maris, E., & Schoffelen, J. M. (2011). FieldTrip: Open source software for advanced analysis of MEG, EEG, and invasive electrophysiological data. *Computational Intelligence and Neuroscience, 2011*.

Oostenveld, R., & Praamstra, P. (2001). The five percent electrode system for high-resolution EEG and ERP measurements. *Clin Neurophysiol, 112*(4), 713-719.

Palmer, J. A., Makeig, S., Kreutz-Delgado, K., & Rao, B. D. (2008, 31 March-4 April 2008). *Newton method for the ICA mixture model.* Paper presented at the 2008 IEEE International Conference on Acoustics, Speech and Signal Processing.

Peyron, R., Laurent, B., & García-Larrea, L. (2000). Functional imaging of brain responses to pain. A review and meta-analysis (2000). *Neurophysiologie Clinique, 30*(5), 263-288.

Picton, T. W., John, M. S., Dimitrijevic, A., & Purcell, D. (2003). Human auditory steady-state responses. *International Journal of Audiology, 42*(4), 177-219.

Ploner, M., Schmitz, F., Freund, H. J., & Schnitzler, A. (1999). Parallel activation of primary and secondary somatosensory cortices in human pain processing. *J Neurophysiol, 81*(6), 3100-3104.

Ploner, M., Schmitz, F., Freund, H. J., & Schnitzler, A. (2000). Differential organization of touch and pain in human primary somatosensory cortex. *Journal of Neurophysiology, 83*(3), 1770-1776.

Popov, T., Oostenveld, R., & Schoffelen, J. M. (2018). FieldTrip Made Easy: An Analysis Protocol for Group Analysis of the Auditory Steady State Brain Response in Time, Frequency, and Space. *Frontiers in Neuroscience, 12*(711).

Poulsen, A. H., Tigerholm, J., Meijs, S., Andersen, O. K., & Mørch, C. D. (2020). Comparison of existing electrode designs for preferential activation of cutaneous nociceptors. *Journal of Neural Engineering*.

Regan, D. (1966). Some characteristics of average steady-state and transient responses evoked by modulated light. *Electroencephalography and Clinical Neurophysiology, 20*(3), 238-248.

Regan, M. P., & Regan, D. (1989). Objective investigation of visual function using a nondestructive zoom-FFT technique for evoked potential analysis. *Can J Neurol Sci, 16*(2), 168-179.

Roberts, J. A., & Robinson, P. A. (2012). Quantitative theory of driven nonlinear brain dynamics. *NeuroImage, 62*(3), 1947-1955.

Santarelli, R., Maurizi, M., Conti, G., Ottaviani, F., Paludetti, G., & Pettorossi, V. E. (1995). Generation of human auditory steady-state responses (SSRs). II: Addition of responses to individual stimuli. *Hear Res, 83*(1-2), 9-18.

Song, Y., Su, Q., Yang, Q., Zhao, R., Yin, G., Qin, W., . . . Liang, M. (2021). Feedforward and feedback pathways of nociceptive and tactile processing in human somatosensory system: A study of dynamic causal modeling of fMRI data. *NeuroImage, 234*, 117957.

Steenbergen, P., Buitenweg, J. R., Trojan, J., van der Heide, E. M., van den Heuvel, T., Flor, H., & Veltink, P. H. (2012). A system for inducing concurrent tactile and nociceptive sensations at the same site using electrocutaneous stimulation. *Behavior Research Methods, 44*(4), 924-933.

Steenbergen, P., Buitenweg, J. R., Trojan, J., van der Heide, E. M., van den Heuvel, T., Flor, H., & Veltink, P. H. (2012). A system for inducing concurrent tactile and nociceptive sensations at the same site using electrocutaneous stimulation. *Behavior research methods, 44(4)*, 924-933.

Tarkka, I. M., & Treede, R. D. (1993). Equivalent electrical source analysis of pain-related somatosensory evoked potentials elicited by a CO2 laser. *J Clin Neurophysiol, 10*(4), 513-519.

Valentini, E., Hu, L., Chakrabarti, B., Hu, Y., Aglioti, S. M., & Iannetti, G. D. (2012). The primary somatosensory cortex largely contributes to the early part of the cortical response elicited by nociceptive stimuli. *NeuroImage, 59*(2), 1571-1581.

Valeriani, M., Rambaud, L., & Mauguière, F. (1996). Scalp topography and dipolar source modelling of potentials evoked by CO2 laser stimulation of the hand. *Electroencephalography and Clinical Neurophysiology/Evoked Potentials Section, 100*(4), 343-353.

van den Berg, B., & Buitenweg, J. R. (2021). Observation of Nociceptive Processing: Effect of Intra-Epidermal Electric Stimulus Properties on Detection Probability and Evoked Potentials. *Brain Topography*.

van den Berg, B., Doll, R. J., Mentink, A. L. H., Siebenga, P. S., Groeneveld, G. J., & Buitenweg, J. R. (2020). Simultaneous tracking of psychophysical detection thresholds and evoked potentials to study nociceptive processing. *Behavior Research Methods*.

van den Berg, B., Manoochehri, M., Kasting, M., Schouten, A. C., van der Helm, F. C. T., & Buitenweg, J. R. (2021). Multisine frequency modulation of intra-epidermal electric pulse sequences: A novel tool to study nociceptive processing. *Journal of Neuroscience Methods, 353*, 109106.

Van Veen, B. D., van Drongelen, W., Yuchtman, M., & Suzuki, A. (1997). Localization of brain electrical activity via linearly constrained minimum variance spatial filtering. *IEEE Trans Biomed Eng, 44*(9), 867-880.

Victor, J. D., & Mast, J. (1991). A new statistic for steady-state evoked potentials. *Electroencephalogr Clin Neurophysiol, 78*(5), 378-388.

Vlaar, M., Solis-Escalante, T., Vardy, A., der Helm, F. V., & Schouten, A. (2016). Quantifying Nonlinear Contributions to Cortical Responses Evoked by Continuous Wrist Manipulation. *IEEE Transactions on Neural Systems and Rehabilitation Engineering, PP*(99), 1-1.

Wang, L., Noordanus, E., & van Opstal, A. J. (2021). Estimating multiple latencies in the auditory system from auditory steady-state responses on a single EEG channel. *Scientific Reports, 11*(1), 2150.

Yang, Y., Solis-Escalante, T., van der Helm, F. C. T., & Schouten, A. C. (2016). A Generalized Coherence Framework for Detecting and Characterizing Nonlinear Interactions in the Nervous System. *IEEE Transactions on Biomedical Engineering, 63*(12), 2629-2637.

12

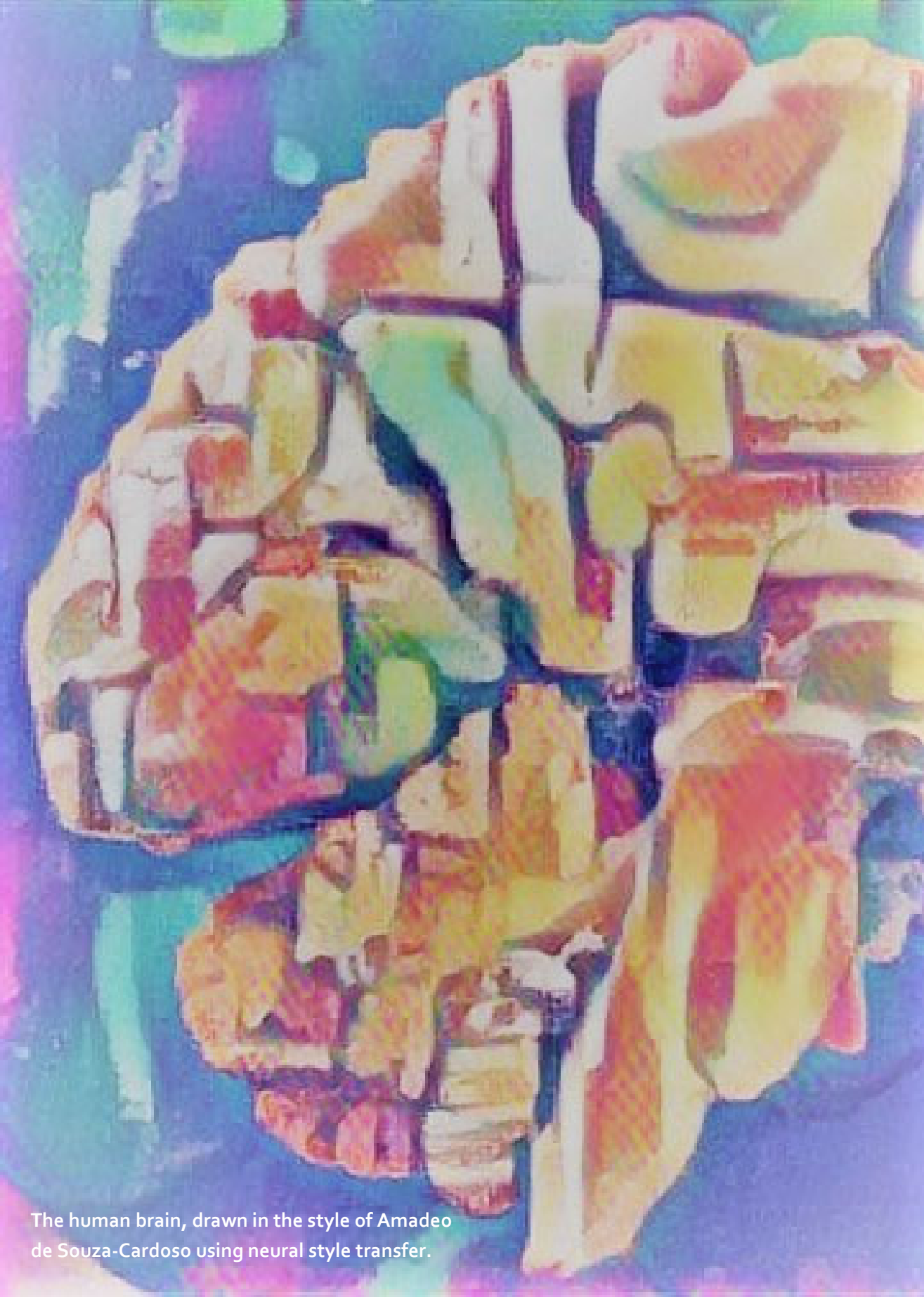

The human brain, drawn in the style of Amadeo de Souza-Cardoso using neural style transfer.

Chapter 13

General Discussion

"You can't connect the dots looking forward; you can only connect them looking backward. So you have to trust that the dots will somehow connect in your future. You have to trust in something -- your gut, destiny, life, karma, whatever. This approach has never let me down, and it has made all the difference in my life."

Steve Jobs, Stanford University commencement speech, 2005

This dissertation is about the development of combined psychophysical and neurophysiological tools for mechanism-based observation of impaired nociceptive processing in patients with chronic pain. Chronic pain is sustained and amplified by impaired nociceptive processing. In patients with chronic neuropathic pain, spontaneous ectopic activity causes long episodes of pain and drives central sensitization. In patients with chronic nociplastic pain, sensitization, and reduced inhibition of nociception lead to pain amplification and the generation of pain by activation of other sensory modalities, often for unknown reasons. It remains difficult for clinicians to effectively treat neuropathic, nociplastic or mixed chronic pain because it is difficult to observe the underlying physiological mechanisms and predict the effect of treatments on those mechanisms. A mechanism-based approach could enable early diagnosis and selection of effective treatments to improve the outlook for neuropathic, nociplastic and mixed pain patients (Baron, Binder, & Wasner, 2010; Fitzcharles et al., 2021). Therefore, researchers and clinicians search for novel tools for mechanism-based observation of impaired nociceptive processing. The development of such tools has been impeded because it remains difficult to selectively activate the nociceptive system in human participants using a stimulus that can be accurately controlled in terms of location and time. Furthermore, observation of physiological responses to nociceptive stimulation without potential bias by psychological states remains a current challenge for pain science. This dissertation presents the next steps towards the development of new assessment methods, by improving the observability of nociceptive processing mechanisms in a research or clinical setting. This discussion will evaluate the progress made in this dissertation towards the development of clinical tools for mechanism-based observation of impaired nociceptive processing.

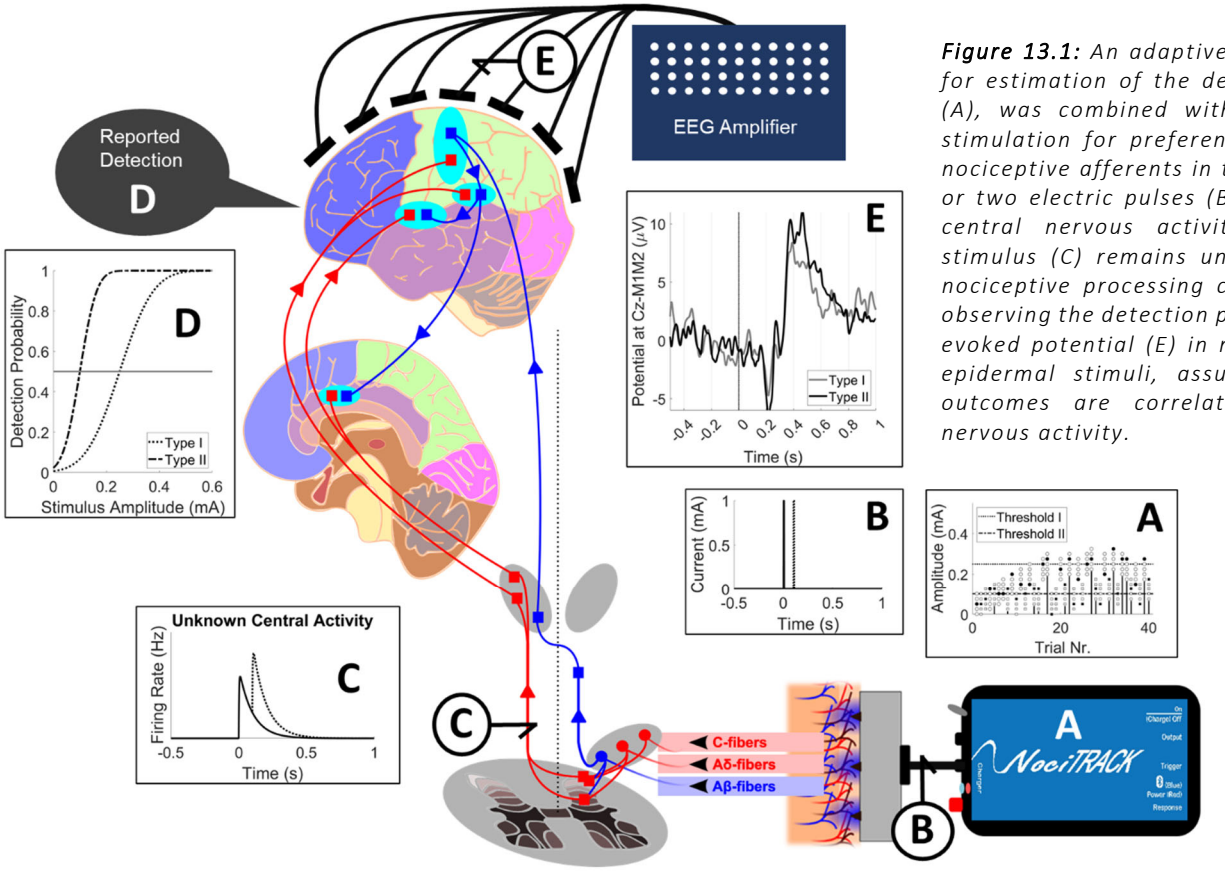

Figure 13.1: *An adaptive method of limits for estimation of the detection threshold (A), was combined with intra-epidermal stimulation for preferential activation of nociceptive afferents in the skin using one or two electric pulses (B). The amount of central nervous activity evoked by a stimulus (C) remains unknown. However, nociceptive processing can be studied by observing the detection probability (D) and evoked potential (E) in response to intra-epidermal stimuli, assuming that these outcomes are correlated with central nervous activity.*

13.1 Observation of Nociceptive Processing

The strategy in this project was to combine psychophysical methods for the observation of nociceptive processing with neurophysiological techniques to provide objective mechanism-based information on nociceptive function. This was implemented by combining an adaptive psychophysical method of limits to measure detection probability and the detection threshold (Figure 13.1A) with intra-epidermal stimulation for controlled activation of nociceptive afferents in the skin, and an EEG recording setup to measure cortical activity evoked by stimulation. To differentially activate peripheral and central mechanisms, single- and double-pulse electric stimuli were used with one or more settings for inter-pulse interval (Figure 13.1B). The amplitude of the electric pulse modulates the number of recruited peripheral nociceptive afferents in the skin. Addition of a second pulse leads to a temporal summation of both pulses in first, second or third order neurons (Figure 13.1C). The impulse response function in those neurons modulates the output of temporal summation as a function of the inter-pulse interval. The effect of these mechanisms on the nociceptive information arriving in the brain was measured in terms of the detection probability (Figure 13.1D) and the evoked cortical response recorded by EEG (Figure 13.1E).

13.1.1 Can we quantify aspects of nociceptive processing?

One of the problems involved in assessing nociceptive detection probability and evoked potentials, is that nociceptive processing is not stationary, and can adapt during a single experiment, the number of received stimuli or experimental conditions. It was shown by Doll et al. that non-stationary detection probability can be evaluated by using a windowed estimate, or by including a parameter for time in generalized (mixed) regression (Doll, Veltink, & Buitenweg, 2015). It was shown in Chapter 2 of this thesis, that non-stationary evoked potentials can be evaluated by including parameters of stimulus detection and time (or the number of received stimuli) in linear (mixed) regression. Importantly, this provided us with a method to analyze evoked brain activity during measurement of nociceptive detection thresholds with an

adaptive psychophysical algorithm, by incorporating all potentially confounding trial parameters into a single linear mixed model.

The next step was to use the combination of intra-epidermal detection probability and evoked potentials to assess nociceptive processing in healthy participants. The feasibility of simultaneously recording both outcomes in a clinical research setting was explored in Chapter 3. Using mixed regression, it was possible to estimate the effect of stimulus parameters on detection probability and the evoked potential. This allowed us to quantify aspects of nociceptive processing, such as the effect of pulse amplitudes on detection probability and the evoked potential, and the effect of trial number on detection probability and the evoked potential, in addition to basic measures such as the detection threshold and average evoked potential amplitudes. It was found that both detection probability and evoked potentials were modulated by stimulus parameters such as stimulus amplitude, i.e., peripheral recruitment, number of pulses, i.e., temporal summation, and the number of received stimuli, i.e., habituation. Note that mechanism(s) causing the observed habituation remain unknown and might be attributed to learning effects, loss of attention, or changes in central or peripheral nerve excitability.

13.1.2 Can we objectively quantify aspects of nociceptive processing using evoked potentials?

Before the start of this project, little was known about the properties of intra-epidermal evoked potentials during these experiments. Major questions about intra-epidermal evoked potentials were addressed in Chapter 4 to enable acquisition of high-quality signals in a clinical setup, including: 'Which peaks are visible in the evoked potential?', 'Which of these peaks are modulated by stimulus parameters?', 'At which electrodes do these peaks have an optimal signal-to-noise ratio?', and 'How many trials are required to achieve an acceptable signal-to-noise ratio?'. This study allowed us to explore how we might improve observation of intra-epidermal detection thresholds and evoked potentials and provided reference values for the effect of intra-epidermal stimulus properties on both outcomes in a healthy population. We found that

an N1 and N2 component can be observed with a maximum positive and negative potential at F4 and T7 respectively. The P2 component can be observed with maximum positive and negative potentials at CPz and A1 respectively. Statistical analysis showed that the N1 and N2 components observed in this experiment were mainly influenced by stimulus detection, while the P2 as well as the detection probability of a stimulus are also significantly influenced by stimulus properties such as the pulse amplitudes and the trial number. The results in this chapter suggested that the various steps of processing of a nociceptive stimulus, including peripheral nerve fiber recruitment, central synaptic summation, and habituation to a repeated stimulus are reflected by the detection thresholds as well as the evoked potential.

While detection thresholds are measured based on the detection of stimuli reported by participants, evoked potentials measure brain activity evoked by a stimulus. Could we study nociceptive processing more objectively by observing evoked potentials instead of detection thresholds? Earlier studies have shown that the N1 is associated with mostly nociceptive and somatosensory-specific activity, while N2-P2 complex is associated with multimodal activity occurring in response to visual, auditory, somatosensory and nociceptive stimulation (Mouraux & Iannetti, 2009) and that the N2-P2 complex is related to the temporal saliency of a stimulus rather than the stimulus intensity itself (Iannetti & Mouraux, 2010). The P2 amplitude in Chapter 4 was correlated to pulse amplitudes, as these amplitudes might increase or decrease stimulus saliency. However, stimulus detection had a much larger effect on the P2 amplitude, potentially because stimulus detection is more closely related to stimulus saliency, i.e., a stimulus that is not salient will not be detected and will result in a much lower P2, while a stimulus that is salient with respect to its spatial and temporal environment (including spontaneous neural activity) will result in conscious detection and generation of a P2 peak.

The P2 amplitude is therefore an indirect measure of nociceptive processing and perception, as it does not directly represent neural activity generated in the dorsal horn and somatosensory cortices as a result of nociceptive stimulation, but rather stimulus saliency and subsequent stimulus detection. Although

measuring the P2 amplitude might remove some subjectivity by removing the need for participants to report whether a stimulus was detected, the P2 amplitude remains dependent on the subjective comparison of a stimulus with respect to its environment. The N1 amplitude might be a more objective measure of afferent nociceptive input but remains too noisy to identify potential correlations between stimulus properties and the N1.

An alternative approach to evoking brain potentials uses a series of stimuli that are applied at a specific frequency in order to generate a steady-state evoked potential (SSEP). The continuous application of a series of stimuli downregulates the effect of temporal saliency and is thought to result in the entrainment of a network of cortical neurons involved in sensory processing of the stimulus, or the superposition of a series of transient neural responses (Norcia, Appelbaum, Ales, Cottereau, & Rossion, 2015; Picton, John, Dimitrijevic, & Purcell, 2003; Regan, 1966). By activating sensory brain areas while reducing the effect of saliency, nociceptive SSEPs might provide a method to objectively sensory-discriminative aspects of nociceptive processing. A novel method of eliciting nociceptive SSEPs was described in Chapters 11 and 12, which is discussed in Section 13.5.2.

13.2 Towards Point-of-Care Clinical Tools

To enable development of an effective method for observation of impaired nociceptive processing in a clinical setting, it was essential to start applying the method for observation of differences between clinical populations from early on. The first steps in bringing the method from laboratory towards clinical practice were 1) to assess if outcome measures are sensitive to impaired central nociceptive processing and 2) to evaluate if we can use the method on a typical population of chronic pain patients. Studies were performed to investigate method feasibility and sensitivity in a setting for pharmacological testing and at the hospital: at the Centre for Human Drug Research (Leiden, the Netherlands), an institute for early-stage clinical drug research, and at department of Anesthesiology, Intensive Care and Pain Medicine of the St.

Antonius Hospital (Nieuwegein, the Netherlands), which runs one of the largest outpatient pain clinics in the Netherlands.

13.2.1 Can we observe altered nociceptive processing in a clinical setting?

The sensitivity of intra-epidermal detection probability and evoked potentials to impaired central nociceptive processing was assessed by studying a population of healthy participants before and after sleep deprivation. Sleep deprivation in human participants is a potential pain model that could be used to study impaired central nociceptive processing in chronic pain patients (Schuh-Hofer et al., 2013). Sleep deprivation studies could also be used as proof-of-concept studies for pharmacological compounds acting on the central nervous system for chronic pain relief. Such pharmacological studies require accurate measures of impaired central nociceptive processing following sleep deprivation. In Chapter 5, it was shown that intra-epidermal detection probability and evoked potentials can be used to identify and quantify impaired nociceptive processing following sleep deprivation, but that there are strong differences in outcomes dependent on sex. More specifically, intra-epidermal detection thresholds and evoked potentials were decreased following sleep deprivation in a male population, while this decrease was not observed in a female population. It remained unclear whether this difference between the sexes reflected a difference in task performance between the male and the female population. However, the observed difference between male and female was more likely caused by a sex-specific response of the nociceptive system to sleep deprivation, as has been documented in previous studies (Eichhorn, Treede, & Schuh-Hofer, 2018; Smith et al., 2019).

The feasibility of measuring intra-epidermal detection probability and evoked potentials in a clinical setting was evaluated in a group of patients with failed back surgery syndrome with a control group of healthy participants in Chapter 6. The effect of stimulus properties on intra-epidermal detection probability and evoked potentials observed in a laboratory setting in Chapter 5 were replicated on the group of healthy participants in a clinical setting in Chapter 6.

Patients with failed back surgery syndrome showed striking differences compared to healthy controls. First, the detection threshold of single-pulse and double-pulse intra-epidermal stimuli of patients was almost twice the value in healthy controls. Second, the effect of pulse amplitudes on evoked potential amplitude was more than halved, indicating a loss of sensory encoding in these brain responses. These findings showed an excellent sensitivity of both outcomes to impaired nociceptive processing in failed back surgery syndrome. Post-hoc analyses showed that increased detection thresholds were mainly associated with pain intensity (NRS), while loss of sensory encoding was associated with both pain intensity (NRS) and score on the central sensitization inventory (CSI) (Neblett et al., 2013). Post-hoc analyses also showed a significant effect of diagnosis and sex on individual detection thresholds, and a significant effect of diagnosis, age, and sex on individual average evoked potentials, which means that care should be taken for potential confounding by age or sex.

Currently, new studies are ongoing to extend our observations in FBSS patients, and to show feasibility and potential sensitivity of the method in other chronic pain syndromes. A first analysis of intra-epidermal electric detection thresholds and evoked potentials in patients with neuropathic pain as a consequence of diabetic polyneuropathy shows that we can use the method in this group of patients, and that the outcomes might be very sensitive in detecting polyneuropathy (Berfelo, Krabbenbos, Van den Berg, Gefferie, & Buitenweg, 2021). Recent analyses of a larger dataset with age- and sex-matched controls seem to confirm that we might use intra-epidermal electric detection thresholds and evoked potentials to detect diabetic polyneuropathy and are currently being incorporated into journal publication.

13.2.2 Can we improve observation of altered nociceptive processing using evoked potentials?

Provided that significant differences were observed between patients and healthy controls in intra-epidermal detection thresholds, sensory encoding in the evoked potential and a number of other secondary measures, combining

these features might aid identification of impaired nociceptive processing. In Chapter 7, these features were combined using a random forest classifier (Breiman, 2001). Performance of the random forest classifier using 1) all features, 2) minimum redundancy maximum relevance (MRMR) selected features (Zhao, Anand, & Wang, 2019), 3) only psychophysical features and 4) only evoked potential features was used to evaluate the value of each feature set for observation of impaired nociceptive processing in patients with failed back surgery syndrome. Classification using the full set of features (Accuracy: 0.75, AUC: 0.82) performed worse than classification using only psychophysical features (Accuracy: 0.77, AUC: 0.83), showing that using a combination of all psychophysical and evoked potential features does not improve classification, and might even reduce performance by overfitting. Selecting the top 6 features based on MRMR improved performance of classification based on a combination of psychophysical and evoked potential features (Accuracy: 0.78, AUC: 0.89). The improvement of performance by combining evoked potential and psychophysical features remains marginal, showing that information in the evoked potential was mostly redundant with the information provided by psychophysical features in patients with failed back surgery syndrome. Nevertheless, the added value of evoked potentials and other EEG features (e.g., event-related (de)synchronization) to the clinical workup of patients with chronic pain might depend on the patient group and should be further explored in clinical research.

13.2.3 Can we improve observation of altered nociceptive processing using machine learning?

Although it remains uncertain whether EEG features are useful to combine with psychophysical features to improve observation of impaired nociceptive processing in FBSS patients, Chapter 7 does show an increase of classification accuracy and AUC when we use a combination of features instead of just a single feature for classification. Classification of FBSS patients based on a selection from all features led to an average accuracy of 0.78 and an AUC of 0.89, whereas classification using only the best feature (the logarithm of the single-pulse detection threshold, determined by MRMR selection) leads to an

accuracy of 0.75 and an AUC of 0.84. Classification of FBSS patients based on the combination of EEG features led to an average accuracy of 0.65 and an AUC of 0.71, whereas classification using only the best EEG feature (the effect of stimulus amplitude on the P2, determined by MRMR selection) leads to an average accuracy of 0.5 and an AUC of 0.71.

As such, traditional machine learning approaches such as the random forest classification applied in Chapter 7, can lead to an improvement of classification accuracy, and might aid diagnosis in a clinical setting, by combining multiple features. Nevertheless, the performance of such traditional methods remains limited by the Bayes error rate (Tumer & Ghosh, 1996). Such a fundamental limit to the performance is present because the input features or the labels are inherently stochastic. For example, if we would select the EEG at a random latency and a random location of the scalp, the signal is most likely stochastic and unrelated to any physiological condition we might want to classify, and therefore the error rate will be high. On the other hand, we might have great input features, but random labels when no golden standard method exists for determining the true physiological condition of a patient. In this case the error rate might be high due to stochastic labels.

Both problems can be frequently encountered when using machine learning in a clinical context and will certainly limit the performance when we try to use machine learning to assess nociceptive processing in patients. For example, we might eventually want to use machine learning to determine if a patient suffers from central sensitization based on a set of psychophysical and EEG features. However, the meaning of the term 'central sensitization' in a clinical context remains debated (van den Broeke, 2018; van den Broeke, Torta, & Van den Bergh, 2018), and there is no golden standard by means of which we could label patients as sensitized or not. We might partly circumvent this problem by using a multitude of methods to determine the correct label, and only use a patient in our training and test data if all methods agree. Unfortunately, the presence of a condition such as central sensitization is difficult to establish objectively, and it is unlikely that all methods will agree on its presence or absence.

Stochasticity of input features can also increase the error rate and therefore decrease the limit of machine learning performance. To achieve a high classification performance, it is key to select a good set of orthogonal input features for classification, with ideally a high correlation with the classification labels and a low unexplained variance. In Chapter 7, we tried to find such features by manually selecting a large set of 44 features (e.g., N1 amplitude, N1 latency, P2 amplitude, P2 latency, etc.), and subsequently selecting a smaller optimized set based on MRMR feature selection. When dealing with such a large set of features, feature selection, dimensionality reduction, or regularization techniques can improve classification performance by reducing overfitting but cannot increase the limit imposed by the Bayes error rate.

We might increase this limit if we know how to select better features. When sufficient data is available for training, validation and testing, deep learning can be used to automatically identify and combine a set of features. Recent work using deep learning for EEG classification has shown that the method successfully identifies and integrates features in the time-, frequency- and spatial domains to solve clinical neurophysiological classification problems including automated detection of epileptic seizures (Acharya, Oh, Hagiwara, Tan, & Adeli, 2018; Tjepkema-Cloostermans, de Carvalho, & van Putten, 2018) and the early diagnosis of Parkinson's disease (Oh et al., 2020) and Alzheimer's disease (Bi & Wang, 2019). The most important limitation of deep learning is that it requires large amounts of data for training. The dataset acquired for the NOCICEPT project currently consists of over 200 000 trials on over 200 healthy participants and chronic pain patients and might be a good starting point.

Several deep learning architectures developed for EEG classification are available (Heilmeyer et al., 2018; Lawhern et al., 2018; Schirrmeister et al., 2017), and could eventually support identification of patterns in time, frequency and space that might improve observation of impaired nociceptive processing. To study which EEG features are targeted by these neural networks, top layers can be decomposed into narrow-band frequency filters and frequency-specific spatial filters (Lawhern et al., 2018). Relevance of features in time, frequency and space can also be visualized using occlusion sensitivity as was done in Chapter 10, or gradient-based relevance attribution methods such as DeepLIFT

(Shrikumar, Greenside, & Kundaje, 2017). Currently, a starting collaboration between the Biomedical Signals and Systems group and the Data Management and Biometrics group aims to work on novel approaches for explainable deep learning to identify EEG patterns associated with the development of chronic neuropathic pain using these and other recent methods in explainable artificial intelligence.

13.2.4 Can clinicians start using the developed procedure for patient assessment?

Assessing a patient using a total of 450 stimulus-response pairs and corresponding evoked potentials as described in Chapter 6 (where this was done on each hand), requires about 1.5 hours of time of the patient and the clinician (or researcher), which is a severe limitation for potential large-scale implementation of the method in a clinical setting. A typical breakdown of these 1.5 hours would be 5 minutes introduction, 25 minutes preparation of the EEG cap, 5 minutes preparation of stimulation electrodes, 45 minutes for performing the experiment and 10 minutes for clean-up. In this procedure, mainly the application of EEG required time and significant expertise of the clinician in conducting EEG recordings.

Chapter 7 revealed that most of the information currently extracted from EEG recordings is redundant with the information in psychophysical outcomes, when studying healthy controls and patients with failed back surgery syndrome. As such, a convenient simplification would be to exclude EEG from the experiment, as this could reduce duration of the total procedure from 1.5 hours to approximately 30 minutes. However, note that EEG could include important information in other conditions than failed back surgery syndrome. For example, if the function of nociceptive nerve fibers in the skin is compromised by small-fiber neuropathy, one might observe a change in P2 latency due to the activation of Aβ-fibers rather than Aδ-fibers around the detection threshold. The potential of combining EEG with psychophysical data still remains quite unexplored, which warrants inclusion of EEG in the procedure

in a future research setting to explore whether EEG is of additional value in a clinical setting.

Besides requiring significant time and materials, the experiment also requires the cognitive ability and commitment of participants to perform the experimental task, which could last up to 45 minutes when measuring EEG for 3 different stimulus types. This requirement could mainly affect task performance in an elderly population, due to declining cognitive ability, and in patients with chronic pain, due to the continuous burden imposed by the presence of pain. A novel method that would only require counting the perceived stimuli and could be performed significantly faster due to not relying on participant responses, was outlined in Chapter 10, and is discussed in Section 13.5.1.

13.3 Mechanism-Based Interpretation

A necessary condition for utilization of the techniques developed in this project for the workup of chronic pain patients in the hospital is interpretability of the psychophysical and neurophysiological observations in terms of nociceptive processing mechanisms. Here, some of the underlying mechanisms that might give rise to nociceptive detection thresholds and cortical potentials in response to intra-epidermal electric stimuli are discussed.

13.3.1 Can we interpret nociceptive detection thresholds and evoked potentials in terms of nociceptive processing mechanisms?

The chapters in Part I aimed at investigating peripheral and central nociceptive processing by observing nociceptive detection thresholds and cortical potentials evoked by stimuli around the detection threshold, but it remains unclear how observed detection thresholds are related to the underlying physiological systems. As these studies (and many other, e.g. (Courtin et al., 2020; Hennings et al., 2017; Tanaka et al., 2021)) relied on a Go-/No-Go (GN) procedure to measure the detection threshold, this threshold could reflect an internal sensory, perceptual or cognitive response criterion (Georgeson, 2012)

rather than the threshold for activation of central nociceptive processing itself. This was investigated in Chapter 8 by comparing the detection threshold estimated using a GN procedure with the detection threshold estimated using a 2-Interval Forced Choice (2IFC) procedure. It was found that the detection threshold estimate for single-pulse stimuli was higher in a GN procedure in comparison with the threshold estimated in a 2IFC procedure. This observation confirmed that the nociceptive detection threshold is a measure of a response criterion rather than a measure of the presence of sensory evidence by itself.

The question naturally arises whether an increased detection threshold means that participants decide not to release the response button even though they felt a sensation, or if the sensation did not enter their consciousness at all. The evoked potentials recorded in Chapter 8 demonstrate that the P2 response, a component associated with emotional-affective aspects of nociception (Apkarian, Bushnell, Treede, & Zubieta, 2005) and a potential marker of conscious access, shows an on-off behavior with respect to reported stimulus detection and shows a strong correlation with detection probability during a GN procedure when averaged. In contrast, the average P2 response remained low up to a detection probability of 0.875 during a 2IFC procedure, suggesting that no P2 response was evoked by the majority of stimuli around the 2IFC detection threshold at a detection probability of 0.75. In other words, the threshold measured during a GN procedure can be interpreted as a threshold for conscious perception, the perceptual threshold, while the threshold during a 2IFC procedure might partly rely on subconscious information. Note that this is not a new result, as the integration of subconscious information in decision making is well documented (Dehaene & Changeux, 2011; Dehaene & Naccache, 2001), but it has large implications for how we might interpret increased nociceptive detection thresholds in chronic pain patients or decreased nociceptive detection thresholds following sleep deprivation.

How can we interpret an altered nociceptive detection threshold in terms of mechanisms, provided that this threshold depends on an internal subconscious perceptual criterion? In Chapter 9, a theoretical framework to model and interpret detection of intra-epidermal electric stimuli was constructed, building forth upon the traditional tools provided by signal detection theory. In this

framework, the detection probability was expressed as a function of a time-dependent response criterion, a system impulse response function and spontaneous neural activity. Implications of this framework are 1) that the difference between the detection probability of single- and double-pulse stimuli can be used to probe the system impulse response function at several intervals and 2) that the absolute amplitude of psychometric parameters can inform us about the presence and amplitude of spontaneous neurophysiological activity. In Chapter 6, it was found that the nociceptive detection threshold correlated with pain intensity (NRS). By re-analyzing data from Chapter 6, it was also found that spontaneous neurophysiological activity is a potential explanation for increased nociceptive detection thresholds in patients with failed back surgery syndrome.

13.3.2 Can we interpret altered nociceptive detection thresholds and evoked potentials in a clinical setting?

Spontaneous ectopic activity is identified by literature as one of the root causes of neuropathic pain due to peripheral nerve injury (Devor, 2013; North et al., 2019), as well as a potential generator of neuropathic pain due to central nerve injury (Lenz, Kwan, Dostrovsky, & Tasker, 1989; Rinaldi, Young, Albe-Fessard, & Chodakiewitz, 1991). Therefore, assessing neurophysiological noise based on the detection probability and evoked potentials in response to intra-epidermal electric stimuli, could be a useful addition to the clinician's toolkit for assessing neuropathic pain. The conceptual model in Chapter 6 implies that an increase of nociceptive detection threshold, and a general decrease of psychometric function parameters (including the psychometric slope), indicates increased neurophysiological noise.

We might have to adjust our terminology to correctly describe these new insights. An increase of sensory detection threshold is typically referred to as hypoesthesia. Note that in pain science algesia (sensitivity for pain) and esthesia (sensitivity) are treated as two separate concepts as both aspects are traditionally measured using mechanical stimulation, where an initial tactile sensation occurs at a low pressure and a pain sensation only occurs at higher

pressures when mechanically sensitive nociceptive afferents are activated. This distinction between the threshold for sensory activation and the threshold for the perception of pain is less clear when nociceptive afferents are stimulated selectively, which could be a reason for reconsidering the meaning of algesia and esthesia in current pain research. It is well-known among pain scientists that selective activation of nociceptive afferents through laser or intra-epidermal electric stimulation is not necessarily reported as 'painful' when a low stimulus intensity is used. If the threshold for this type of non-painful nociceptive stimulation increases: Should we talk about hypoalgesia or hypoesthesia? The word combination 'nociceptive hypoesthesia' might be a the most appropriate term as '-algesia' is typically used for stimuli that are painful by definition, and the word 'hypoesthesia' alone is mostly used for a decreased sensitivity to mechanical stimulation.

13.4 Methodological Remarks

13.4.1 Selectivity

Intra-epidermal electric stimulation was used throughout this thesis to preferentially stimulate nociceptive Aδ- and C-fibers. The word 'preferential' was used rather than 'selective', as it remained unknown whether coactivation of tactile Aβ-fibers could occur. Research has shown that intra-epidermal electric stimulation at a 'low' stimulus intensity can selectively activate nociceptive nerve fibers as these fibers are located superficially in the epidermis, while tactile fibers are located more deeply in the dermis. An experimental study of fiber selectivity with intra-epidermal stimulation confirmed that selective activation was achieved using electric pulses at less than twice the detection threshold (Mouraux, 2010), using an intra-epidermal concentric needle electrode with a needle protruding 0.1 mm from the base (Inui, Tran, Hoshiyama, & Kakigi, 2002) applied to the back of the hand. Modelling studies suggest that electrode shape and depth are important parameters for selective activation, where needle electrodes perform the best when it comes to selective nociceptive activation (Poulsen, Tigerholm, Meijs, Andersen, & Mørch, 2020). Optimal needle depth depends on the thickness of

the skin, and should ideally be just long enough to penetrate the stratum corneum, resulting in a point current source with a high electric field density around the tip of the needle (Motogi et al., 2016).

In this thesis stimulation was applied to the back of the hand and the volar forearm where the average thickness of the stratum corneum is estimated to be 29.3 ± 6.84 µm and 22.6 ± 4.33 µm, respectively (Egawa, Hirao, & Takahashi, 2007). The electrode used in this thesis was a custom-made needle electrode for preferential nociceptive fiber activation consisting of 5 needles protruding 0.5 mm from the electrode surface embedded in a layer of flexible silicone. As such, the electrodes were long enough to penetrate the stratum corneum on the volar forearm and the back of the hand, but short enough prevent the needle from protruding the epidermis, with a depth of 56.6 ± 11.5 µm (Sandby-Møller, Poulsen, & Wulf, 2003) in addition to the thickness of the stratum corneum. A validation study using this electrode confirmed that stimulation at 1.3 x the detection threshold resulted in a sharp pricking sensation, whereas stimulation using metal disc electrodes at the same intensity resulted in a dull sensation (Steenbergen et al., 2012). As such, stimulation using this electrode at low intensities is likely preferential for nociceptive afferents in the skin.

Nevertheless, fiber selectivity remains reason for debate due to two reasons:

- It was never determined up to which stimulus intensity the electrode remains selective for nociceptive afferents.
- It remains unknown what influence individual patient condition, including chronic pain, might have on fiber selectivity.

In chapter 6, it was observed that detection thresholds were increased, and psychometric slopes were reduced in patients with failed-back surgery syndrome and in Chapter 9 it was argued that this change in detection behavior is associated with an increase of spontaneous neural activity. Does the rule of thumb of selective nociceptive activation for stimuli below twice the detection threshold, still apply if detection thresholds are altered due to maladaptive central nociceptive processing?

This question remains to be answered by validation studies using an Aβ-fiber and an Aδ-fiber nerve block (as in (Mouraux, 2010)) or other sophisticated methods to assess selective activation. However, the current data supports that fiber activation is at least preferentially nociceptive. Response times for intra-epidermal stimulation at the hand dorsum in healthy subjects of 546 ± 161 ms (Chapter 4, not assessed in FBSS patients), and P2 latencies of 414 ms in healthy subjects (Chapter 4) and 440 ms in FBSS patients (Chapter 5) are consistent with the response time of 504 ± 105 ms and the P2 latency of 399 ± 57 ms reported by Mouraux et al. (Mouraux, 2010) for nociceptive specific laser stimulation at the hand dorsum.

13.4.2 Influence of Psychological Processes

Developing nociception biomarkers that remain unbiased by psychological states is a current challenge for pain science, which has not yet been solved satisfactorily. Like any method relying on participant report (e.g. questionnaires, QST), nociceptive detection thresholds could be influenced by attention (Bushnell, Duncan, Dubner, Jones, & Maixner, 1985) and potentially learning. Similarly, the evoked potential can also be modulated by attention (Legrain, Guérit, Bruyer, & Plaghki, 2002, 2003), emotion (Stancak, Ward, & Fallon, 2013) and potentially learning. Also other factors might influence perceived pain intensity, e.g. gender of the experimenter (Aslaksen, Myrbakk, Høifødt, & Flaten, 2007) and phase of the menstrual cycle (Kowalczyk et al., 2010), and it remains unknown whether these could also influence nociceptive detection thresholds or evoked potentials. As such, it remains important to standardize these factors as much as possible in any study design, and to neutralize potential attention and learning effects.

While it is not possible to remove any attention bias from outcomes, potential bias by spatial attention was reduced by asking the participants to focus on the stimulation electrode. In addition, attention drift was reduced, but not excluded, by reducing protocol time as much as possible. As learning might influence the detection threshold when the procedure is repeated several times, measurement order should be randomized in study designs.

13.4.3 Statistical Model

"Essentially, all models are wrong, but some are useful" (Box & Draper, 1987). In many chapters, a statistical model was formulated to analyze the effect of stimulus properties on detection probability or the evoked potential via (generalized) linear mixed regression. In the studies that were initiated first (Chapter 3 and Chapter 5), the statistical analysis model included all parameters required for a separate offset and a slope with respect to each stimulus type, regardless of the stimulus properties (number of pulses, stimulus amplitude, inter-pulse interval). In later studies (Chapter 4 and Chapter 6), an attempt was made to use a more parsimonious model, provided that the statistical model might be simplified based on several constraints that might exist for the data, e.g., the detection probability of a single-pulse stimulus can in theory not be any smaller than the detection probability of a double-pulse stimulus when the stimulus amplitude is zero. The balance between goodness-of-fit and parsimony was sought is Chapter 4 by selecting a model among other potential models based on the Akaike Information Criterion (AIC) (Akaike, 1974) and Bayesian Information Criterion (BIC, used in case both outcomes were contradictory) (Schwarz, 1978). The selected model for detection probability, modelled detection probability as a result of the independent contributions of a first pulse, a second pulse, and trial number (habituation). The selected model for evoked potentials, modelled the evoked potential as a result of the independent contributions of a first pulse, a second pulse, trial number (habituation) and stimulus detection.

Describing a new theoretical framework to describe the detection of intra-epidermal stimuli using psychophysical models in Chapter 9, led to new insights into which forms this statistical model could theoretically take. If detection probability is best described using an additive summation model (which was the optimal model for 12.0 % to 23.5 % of the participants in Chapter 9), detection behavior on a group-level is well described using the statistical model selected earlier in Chapter 4. However, if detection probability is best described using a probability summation model including noise (optimal for 28.0 % to 48.0 % of the participants in Chapter 9), no statistical model formulation exists to

accurately describe group-level detection behavior using mixed logistic or probit regression. Nevertheless, allowing a separate offset and a slope with respect to each stimulus type in mixed regression would in this case reduce the estimation error by including more degrees of freedom in the model.

13.5 Novel Technological Steps

13.5.1 Automated Estimation of Perceptual Thresholds using EEG

The visual evoked P_3 response (also known as the P300) is a positive peak in the human event-related potential which is considered a key marker of conscious access to sensory evidence (Rutiku, Martin, Bachmann, & Aru, 2015; Salti, Bar-Haim, & Lamy, 2012), i.e. visual perception. The high degree of overlap in activated brain areas and latencies is reason to assume a similar functional significance for the nociceptive evoked P2 response (Iannetti & Mouraux, 2010; Mouraux & Iannetti, 2009). The results in Chapter 8 confirmed that the nociceptive evoked P2 indeed shows an on-off response with respect to stimulus detection, and that the average P2 response of both detected and non-detected stimuli is proportional to the detection probability. This observation led to the hypothesis that instead of relying on participant report, we could directly measure the perceptual threshold based on brain activity.

A necessary condition for measuring the perceptual threshold based on brain activity was the availability of a potent method to classify EEG epochs as either detected or non-detected. While traditional approaches led to cross-subject classification of visual stimulus detection with an area-under-the-curve (AUC) of 0.8, recent advances in deep learning allow for cross-subject classification of visual stimulus perception using a deep neural network with an AUC of up to 0.9 (Lawhern et al., 2018). In Chapter 10, it was found that it is possible to classify nociceptive stimulus perception using a similar deep neural network with an even higher performance including an AUC of 0.92 and an accuracy of 0.84, indicating that deep neural network classification of EEG could allow for estimation of perceptual thresholds.

The challenge of removing potential threshold estimation bias by an internal classification criterion in the deep neural network was addressed using a unique approach: the deep neural network was deployed to perform a 2IFC procedure, where the network identifies the interval with the highest probability to contain post-stimulus brain activity. As a consequence, the network will guess the correct interval with a probability of 50% when no brain activity is present, and a probability of 75% if brain activity is present in 50% of the cases, i.e., around the perceptual threshold. The similarity between perceptual thresholds measured with a GN procedure and perceptual thresholds estimated by the neural network, warrant further research into potential clinical applications of the method, including the assessment of nociceptive detection thresholds in chronic pain patients. Validation of the method in other sensory modalities could allow for the development of a platform technology for the assessment of nociceptive, somatosensory, visual, and auditory perceptual thresholds based on brain activity.

13.5.2 Intra-epidermal Electric Steady-state Evoked Potentials

The nociceptive evoked potential is an excellent marker of stimulus perception, as was observed in Chapters 8 and 10. For suprathreshold stimuli, the P2 is determined by saliency of the perceived stimulus, rather than stimulus intensity itself (Iannetti, Hughes, Lee, & Mouraux, 2008). For stimuli around the perceptual threshold, it was shown that the P2 is much weaker when a stimulus is not detected, irrespective of the underlying detection probability (Chapter 8). As such, the nociceptive P2 marks stimulus perception or saliency rather than directly measuring the amount of sensory input, even though both will be correlated.

As some of the underlying mechanisms of chronic pain occur as early as the dorsal root ganglia, the dorsal horn and the thalamus, an ideal tool for observing those mechanisms should observe nociceptive activity as close to these mechanisms as possible. It is currently impossible to non-invasively and accurately observe nervous activity in these areas, but it might be possible to get more objective estimates of sensory input to the brain by observing activity

in the somatosensory cortices. With the aim of reducing the influence of stimulus salience and perception and getting a larger SNR from sensory brain areas Chapter 11 introduced a novel approach to measure the nociceptive steady-state evoked potential (SSEP), which is a neurophysiological response generated by neural entrainment, or by the superposition of transient responses to repeated stimulation in the activated brain areas.

Earlier studies showed the potential of nociceptive SSEPs evoked by blocks of laser pulses (Mouraux et al., 2011), electric pulses (Colon, Nozaradan, Legrain, & Mouraux, 2012), or sinusoidal thermal stimulation (Colon, Liberati, & Mouraux, 2017; Mulders et al., 2020). The unique approach in this thesis was to modulate the frequency of a continuous series of intra-epidermal electric pulses, with the benefit of directly stimulating nociceptive afferents in the skin without the effects of thermal or mechanical transduction mechanisms. This approach offers a lot of flexibility for experimental design, because it allows for frequency modulation with an arbitrary waveform. In Chapter 11, a multisine waveform was used to study system delay and nonlinearity. It was demonstrated that frequency modulated intra-epidermal electric stimulation elicited associated brain activity in the frequency domain at fundamental frequencies of the multisine waveform, 3, 7 and 13 Hz.

In Chapter 12, a second study was presented using frequency modulated intra-epidermal electric stimulation to study system delay and non-linearity and the location of sources that generate the observed nociceptive SSEP. It was found that a multisine waveform of 3 and 7 Hz, also led to cortical activation of 3 and 7 Hz, without significant activation of any harmonics or intermodulation frequencies. The delay of 3 Hz and 7 Hz activity was almost exactly equal to the delay of the N1 peak in the evoked potential. Source localization confirmed that both the N1 and 3Hz SSEP were generated in the secondary somatosensory cortex. The 7Hz activity, which had a much lower signal-to-noise ratio in these experiments, was reconstructed in the primary motor cortex. However, the use of a standardized head model and MRI for source localization could have caused some error in localization, and this activity is more likely generated by the adjacent primary somatosensory cortex. Further source localization studies are required to confirm whether nociceptive intra-epidermal electric SSEPs could

be used to observe neural correlates of nociceptive processing in the spinal cord.

13.6 Future Research Objectives

Based on the new insights outlined in this discussion, several avenues can be pursued in future research to improve the observation of impaired nociceptive processing in chronic pain patients and guide their treatment. Potential future research goals include:

Validity of intra-epidermal detection thresholds and evoked potentials for the observation of impaired nociceptive processing

- Identifying the reasons for within-subject and between-subject variability of nociceptive detection thresholds and evoked potentials.
- Identifying nociceptive mechanisms that alter intra-epidermal detection thresholds and evoked potentials (e.g., diffuse noxious inhibitory control, temporal summation, and wind-up).

Intra-epidermal detection thresholds and evoked potentials for stratification and treatment of chronic pain patients

- Assessing in which chronic pain conditions impaired nociceptive processing can be observed by means of intra-epidermal detection thresholds and evoked potentials, alone or in combination with other outcome measures.
- Determining if chronic pain mechanisms (such as ectopic nociceptive activity, central sensitization, reduced inhibitory control) can be observed in individual patients to guide pain treatment.

Machine learning for improved observation of impaired nociceptive processing

- Improving the classification of chronic pain conditions based on existing psychophysical and EEG biomarkers using explainable artificial intelligence.
- Mapping the patterns in neurophysiological activity associated with chronic pain conditions using deep learning and explainable artificial intelligence.

Intra-epidermal steady-state evoked potentials for observation of impaired nociceptive processing

- Assessing in which chronic pain conditions impaired nociceptive processing can be observed by means of intra-epidermal steady-state evoked potentials, alone or in combination with other outcome measures.

13.7 Concluding Remarks

This thesis provides the first steps towards development of a clinical tool to observe impaired nociceptive processing. The studies presented in this thesis show that the combined observation of intra-epidermal detection thresholds and evoked potentials allows for the observation of impaired nociceptive processing following sleep deprivation, in a setup for pharmacological testing, as well as the identification of impaired nociceptive processing in patients with failed back surgery syndrome at the hospital. Novel technologies that were invented during this thesis are still in a low technology readiness level but can aid observation of impaired nociceptive processing in future scientific and clinical applications. Automated measurement of perceptual thresholds based on brain activity could eventually lead to a more objective, faster, and accessible procedure for measuring the nociceptive perceptual threshold. Intra-epidermal electric steady-state evoked potentials provide a method to observe brain activity associated with the sensory-discriminative aspects of the pain

experience. The potential of these methods warrants further research to determine in which chronic pain conditions impaired nociceptive processing can be observed using these methods, and whether the observed values can be used to guide pain treatment.

13.8 References

Acharya, U. R., Oh, S. L., Hagiwara, Y., Tan, J. H., & Adeli, H. (2018). Deep convolutional neural network for the automated detection and diagnosis of seizure using EEG signals. *Computers in Biology and Medicine, 100*, 270-278.

Akaike, H. (1974). A new look at the statistical model identification. *IEEE Transactions on Automatic Control, 19*(6), 716-723.

Apkarian, A. V., Bushnell, M. C., Treede, R.-D., & Zubieta, J.-K. (2005). Human brain mechanisms of pain perception and regulation in health and disease. *European Journal of Pain, 9*(4), 463-463.

Aslaksen, P. M., Myrbakk, I. N., Høifødt, R. S., & Flaten, M. A. (2007). The effect of experimenter gender on autonomic and subjective responses to pain stimuli. *Pain, 129*(3), 260-268.

Baron, R., Binder, A., & Wasner, G. (2010). Neuropathic pain: diagnosis, pathophysiological mechanisms, and treatment. *The Lancet Neurology, 9*(8), 807-819.

Berfelo, T., Krabbenbos, I. P., Van den Berg, B., Gefferie, S., & Buitenweg, J. R. (2021). *Exploring nociceptive detection thresholds combined with evoked potentials in patients with diabetes mellitus*. Paper presented at the 43rd Annual International Conference of the IEEE Engineering in Medicine and Biology Society (EMBC), Guadalajara, Mexico.

Bi, X., & Wang, H. (2019). Early Alzheimer's disease diagnosis based on EEG spectral images using deep learning. *Neural Networks, 114*, 119-135.

Box, G. E. P., & Draper, N. R. (1987). *Empirical model-building and response surfaces*. Oxford, England: John Wiley & Sons.

Breiman, L. (2001). Random Forests. *Machine Learning, 45*(1), 5-32.

Bushnell, M. C., Duncan, G. H., Dubner, R., Jones, R. L., & Maixner, W. (1985). Attentional influences on noxious and innocuous cutaneous heat detection in humans and monkeys. *The Journal of Neuroscience, 5*(5), 1103.

Colon, E., Liberati, G., & Mouraux, A. (2017). EEG frequency tagging using ultra-slow periodic heat stimulation of the skin reveals cortical activity specifically related to C fiber thermonociceptors. *NeuroImage, 146*, 266-274.

Colon, E., Nozaradan, S., Legrain, V., & Mouraux, A. (2012). Steady-state evoked potentials to tag specific components of nociceptive cortical processing. *NeuroImage, 60*(1), 571-581.

Courtin, A. S., Maldonado Slootjes, S., Caty, G., Hermans, M. P., Plaghki, L., & Mouraux, A. (2020). Assessing thermal sensitivity using transient heat and cold stimuli combined with a Bayesian adaptive method in a clinical

setting: A proof of concept study. *European Journal of Pain, 24*(9), 1812-1821.

Dehaene, S., & Changeux, J.-P. (2011). Experimental and Theoretical Approaches to Conscious Processing. *Neuron, 70*(2), 200-227.

Dehaene, S., & Naccache, L. (2001). Towards a cognitive neuroscience of consciousness: basic evidence and a workspace framework. *Cognition, 79*(1), 1-37.

Devor, M. (2013). Neuropathic Pain: Pathophysiological Response of Nerves to Injury. In S. B. McMahon, M. Koltzenburg, I. Tracey, & D. C. Turk (Eds.), *Wall and Melzack's Textbook of Pain* (6th ed., pp. 861-888): Elsevier Saunders.

Doll, R. J., Veltink, P. H., & Buitenweg, J. R. (2015). Observation of time-dependent psychophysical functions and accounting for threshold drifts. *Attention, Perception, and Psychophysics, 77*(4), 1440-1447.

Egawa, M., Hirao, T., & Takahashi, M. (2007). In vivo estimation of stratum corneum thickness from water concentration profiles obtained with Raman spectroscopy. *Acta Derm Venereol, 87*(1), 4-8.

Eichhorn, N., Treede, R.-D., & Schuh-Hofer, S. (2018). The Role of Sex in Sleep Deprivation Related Changes of Nociception and Conditioned Pain Modulation. *Neuroscience, 387*, 191-200.

Fitzcharles, M. A., Cohen, S. P., Clauw, D. J., Littlejohn, G., Usui, C., & Häuser, W. (2021). Nociplastic pain: towards an understanding of prevalent pain conditions. *Lancet, 397*(10289), 2098-2110.

Georgeson, M. (2012). Sensory, perceptual and response biases: the criterion concept in perception. *Journal of Vision, 12*(9), 1392-1392.

Heilmeyer, F. A., Schirrmeister, R. T., Fiederer, L. D. J., Volker, M., Behncke, J., & Ball, T. (2018, 7-10 Oct. 2018). *A Large-Scale Evaluation Framework for EEG Deep Learning Architectures.* Paper presented at the 2018 IEEE International Conference on Systems, Man, and Cybernetics (SMC).

Hennings, K., Frahm, K. S., Petrini, L., Andersen, O. K., Arendt-Nielsen, L., & Mørch, C. D. (2017). Membrane properties in small cutaneous nerve fibers in humans. *Muscle Nerve, 55*(2), 195-201.

Iannetti, G. D., Hughes, N. P., Lee, M. C., & Mouraux, A. (2008). Determinants of laser-evoked EEG responses: Pain perception or stimulus saliency? *Journal of Neurophysiology, 100*(2), 815-828.

Iannetti, G. D., & Mouraux, A. (2010). From the neuromatrix to the pain matrix (and back). *Experimental Brain Research, 205*(1), 1-12.

Inui, K., Tran, T. D., Hoshiyama, M., & Kakigi, R. (2002). Preferential stimulation of Aδ fibers by intra-epidermal needle electrode in humans. *Pain, 96*(3), 247-252.

Kowalczyk, W. J., Sullivan, M. A., Evans, S. M., Bisaga, A. M., Vosburg, S. K., & Comer, S. D. (2010). Sex differences and hormonal influences on response to mechanical pressure pain in humans. *J Pain, 11*(4), 330-342.

Lawhern, V. J., Solon, A. J., Waytowich, N. R., Gordon, S. M., Hung, C. P., & Lance, B. J. (2018). EEGNet: a compact convolutional neural network for EEG-based brain–computer interfaces. *Journal of Neural Engineering, 15*(5), 056013.

Legrain, V., Guérit, J. M., Bruyer, R., & Plaghki, L. (2002). Attentional modulation of the nociceptive processing into the human brain: Selective spatial attention, probability of stimulus occurrence, and target detection effects on laser evoked potentials. *Pain, 99*(1-2), 21-39.

Legrain, V., Guérit, J. M., Bruyer, R., & Plaghki, L. (2003). Electrophysiological correlates of attentional orientation in humans to strong intensity deviant nociceptive stimuli, inside and outside the focus of spatial attention. *Neurosci Lett, 339*(2), 107-110.

Lenz, F. A., Kwan, H. C., Dostrovsky, J. O., & Tasker, R. R. (1989). Characteristics of the bursting pattern of action potentials that occurs in the thalamus of patients with central pain. *Brain Res, 496*(1-2), 357-360.

Motogi, J., Sugiyama, Y., Laakso, I., Hirata, A., Inui, K., Tamura, M., & Muragaki, Y. (2016). Why intra-epidermal electrical stimulation achieves stimulation of small fibres selectively: a simulation study. *Phys Med Biol, 61*(12), 4479-4490.

Mouraux, A., & Iannetti, G. D. (2009). Nociceptive Laser-Evoked Brain Potentials Do Not Reflect Nociceptive-Specific Neural Activity. *Journal of Neurophysiology, 101*(6), 3258-3269.

Mouraux, A., Iannetti, G. D., Colon, E., Nozaradan, S., Legrain, V., & Plaghki, L. (2011). Nociceptive Steady-State Evoked Potentials Elicited by Rapid Periodic Thermal Stimulation of Cutaneous Nociceptors. *The Journal of Neuroscience, 31*(16), 6079.

Mouraux, A., Iannetti, G. D., & Plaghki, L. (2010). Low intensity intra-epidermal electrical stimulation can activate Aδ-nociceptors selectively. *Pain, 150(1)*, 199-207.

Mulders, D., de Bodt, C., Lejeune, N., Courtin, A., Liberati, G., Verleysen, M., & Mouraux, A. (2020). Dynamics of the perception and EEG signals triggered by tonic warm and cool stimulation. *PLoS ONE, 15*(4), e0231698.

Neblett, R., Cohen, H., Choi, Y., Hartzell, M. M., Williams, M., Mayer, T. G., & Gatchel, R. J. (2013). The Central Sensitization Inventory (CSI): Establishing Clinically Significant Values for Identifying Central Sensitivity Syndromes in an Outpatient Chronic Pain Sample. *The Journal of Pain, 14*(5), 438-445.

Norcia, A. M., Appelbaum, L. G., Ales, J. M., Cottereau, B. R., & Rossion, B. (2015). The steady-state visual evoked potential in vision research: A review. *J Vis, 15*(6), 4.

North, R. Y., Li, Y., Ray, P., Rhines, L. D., Tatsui, C. E., Rao, G., . . . Dougherty, P. M. (2019). Electrophysiological and transcriptomic correlates of neuropathic pain in human dorsal root ganglion neurons. *Brain, 142*(5), 1215-1226.

Oh, S. L., Hagiwara, Y., Raghavendra, U., Yuvaraj, R., Arunkumar, N., Murugappan, M., & Acharya, U. R. (2020). A deep learning approach for Parkinson's disease diagnosis from EEG signals. *Neural Computing and Applications, 32*(15), 10927-10933.

Picton, T. W., John, M. S., Dimitrijevic, A., & Purcell, D. (2003). Human auditory steady-state responses. *International Journal of Audiology, 42*(4), 177-219.

Poulsen, A. H., Tigerholm, J., Meijs, S., Andersen, O. K., & Mørch, C. D. (2020). Comparison of existing electrode designs for preferential activation of cutaneous nociceptors. *Journal of Neural Engineering*.

Regan, D. (1966). Some characteristics of average steady-state and transient responses evoked by modulated light. *Electroencephalography and Clinical Neurophysiology, 20*(3), 238-248.

Rinaldi, P. C., Young, R. F., Albe-Fessard, D., & Chodakiewitz, J. (1991). Spontaneous neuronal hyperactivity in the medial and intralaminar thalamic nuclei of patients with deafferentation pain. *J Neurosurg, 74*(3), 415-421.

Rutiku, R., Martin, M., Bachmann, T., & Aru, J. (2015). Does the P300 reflect conscious perception or its consequences? *Neuroscience, 298*, 180-189.

Salti, M., Bar-Haim, Y., & Lamy, D. (2012). The P3 component of the ERP reflects conscious perception, not confidence. *Conscious Cogn, 21*(2), 961-968.

Sandby-Møller, J., Poulsen, T., & Wulf, H. C. (2003). Epidermal thickness at different body sites: relationship to age, gender, pigmentation, blood content, skin type and smoking habits. *Acta Derm Venereol, 83*(6), 410-413.

Schirrmeister, R. T., Springenberg, J. T., Fiederer, L. D. J., Glasstetter, M., Eggensperger, K., Tangermann, M., . . . Ball, T. (2017). Deep learning with convolutional neural networks for EEG decoding and visualization. *Human Brain Mapping, 38*(11), 5391-5420.

Schuh-Hofer, S., Wodarski, R., Pfau, D. B., Caspani, O., Magerl, W., Kennedy, J. D., & Treede, R. D. (2013). One night of total sleep deprivation promotes a state of generalized hyperalgesia: A surrogate pain model to study the relationship of insomnia and pain. *Pain, 154*(9), 1613-1621.

Schwarz, G. (1978). Estimating the Dimension of a Model. *The Annals of Statistics, 6*(2), 461-464.

Shrikumar, A., Greenside, P., & Kundaje, A. (2017). *Learning important features through propagating activation differences*. Paper presented at the Proceedings of the 34th International Conference on Machine Learning - Volume 70, Sydney, NSW, Australia.

Smith, M. T., Jr., Remeniuk, B., Finan, P. H., Speed, T. J., Tompkins, D. A., Robinson, M., . . . Irwin, M. R. (2019). Sex differences in measures of central sensitization and pain sensitivity to experimental sleep disruption: implications for sex differences in chronic pain. *Sleep, 42*(2).

Stancak, A., Ward, H., & Fallon, N. (2013). Modulation of pain by emotional sounds: A laser-evoked potential study. *European Journal of Pain, 17*(3), 324-335.

Steenbergen, P., Buitenweg, J. R., Trojan, J., van der Heide, E. M., van den Heuvel, T., Flor, H., & Veltink, P. H. (2012). A system for inducing concurrent tactile and nociceptive sensations at the same site using electrocutaneous stimulation. *Behavior Research Methods, 44*(4), 924-933.

Tanaka, S., Gomez-Tames, J., Wasaka, T., Inui, K., Ueno, S., & Hirata, A. (2021). Electrical Characterisation of Aδ-Fibres Based on Human in vivo Electrostimulation Threshold. *Frontiers in Neuroscience, 14*(1305).

Tjepkema-Cloostermans, M. C., de Carvalho, R. C. V., & van Putten, M. (2018). Deep learning for detection of focal epileptiform discharges from scalp EEG recordings. *Clin Neurophysiol, 129*(10), 2191-2196.

Tumer, K., & Ghosh, J. (1996). *Estimating the Bayes error rate through classifier combining.* Paper presented at the 13th International Conference on Pattern Recognition.

van den Broeke, E. N. (2018). Central sensitization and pain hypersensitivity: Some critical considerations. *F1000Research, 7*, 1325-1325.

van den Broeke, E. N., Torta, D. M., & Van den Bergh, O. (2018). Central Sensitization: Explanation or Phenomenon? *Clinical Psychological Science, 6*(6), 761-764.

Zhao, Z., Anand, R., & Wang, M. (2019, 5-8 Oct. 2019). *Maximum Relevance and Minimum Redundancy Feature Selection Methods for a Marketing Machine Learning Platform.* Paper presented at the 2019 IEEE International Conference on Data Science and Advanced Analytics (DSAA).

13

The Tre Cime di Lavaredo, Province of Belluno, Italy, drawn in the style of Pablo Picasso using neural style transfer.

Acknowledgements

"And, when you want something, all the universe conspires in helping you to achieve it"

Paulo Coelho, the Alchemist

Doing research, and writing a PhD Thesis about it, is not an easy undertaking. As a PhD candidate, you have to go through the first part of the so-called Dunning-Kruger Effect Curve. First, you learn that you know nothing. The only thing that you do know, is that the PhD Thesis should be finished within the next 3 to 4 years. The next years you acquire more skill, but by the time everything is starting to make sense, time is almost running out. Fortunately, the universe conspired to bring the right people on my path at the right moment to make my life during the past few years, despite these challenges, an enjoyable and enlightening experience.

First and foremost, I should thank all participants in scientific research, and especially the 205 persons who participated in the studies that were presented in this thesis. Many experiments are usually quite long and boring, often taking more than 2 hours, and I am grateful for the selfless effort these participants invested in science by participating in one or even multiple experiments.

I would like to thank Jan Buitenweg for being a great supervisor. The unique style of his supervision allowed me a lot of freedom, while guiding me in setting my own research goals, developing new methods, designing studies, and learning from my own mistakes. While doing this, Jan always managed to encourage me with his own enthusiasm for pain research. Crucially, he also corrected my often overly optimistic expectations when necessary. I am also grateful to Peter Veltink, my second promotor, for providing valuable input and creating a great working environment at the research group Biomedical Signals and Systems.

During the research project, I had the pleasure of collaborating with various organizations, and performing research in their labs and practices. I would like to thank the people at the St. Antonius Hospital in Nieuwegein, for their invaluable contribution to our research, and great collaboration. I am grateful for Imre Krabbenbos for keeping chronic pain research alive at the hospital. Especially, I would like to thank Tom Berfelo, a great colleague, teambuilder, organizer and friend working at the St. Antonius hospital, and continuing this research in a clinical setting. Besides organizing research at the hospital, Tom was a great organizer of drinks and snacks after work, making sure that I always

felt motivated to work at the hospital! Also, I would like to thank the many Technical Medicine Master and Bachelor students that supported our research at the St. Antonius hospital, which were great teammates and good company at the afternoon drinks, Silvano, Ruben, Eva, Marloe, Jelle and many others.

I would like to thank the people at the Centre for Human Drug Research (CHDR) in Leiden, for hosting some of the experiments and providing me with invaluable feedback and new insights. I would like to thank Geert-Jan Groeneveld for providing the opportunity to explore the potential of our methods in a pharmacological research setting, and for keeping innovation in pharmacological research alive. Especially, I would like to thank Robert-Jan Doll, for continuing to provide his support and valuable contribution to our research and for improving the quality of this work, by taking the time to discuss about key aspects. Also, I would like to give special thanks to Hemme, Titia and Ingrid for helping me to organize experiments at the CHDR and providing useful feedback on our scientific work.

This research started thanks to the combined vision of Jan Buitenweg at the University of Twente, and Frans van der Helm and Alfred Schouten at the Delft University of Technology. I would like to thank the people at the Delft University of Technology for working with me on developing new system identification methods for the nociceptive system. Alfred was always there, when I needed somebody to discuss about the several obstacles encountered when developing this method. Frans provided valuable insights in our discussion of the interpretation of the results and how we could utilize these methods. I would also like to thank Mana Manoochehri, for being a great colleague and collaborator in Delft, and also for perfecting my EEG skills and teaching me a lot about source localization. Last but not least, I want to thank Mindy Kasting, Master student in Delft, for her great work in organizing experiments in Delft to provide the proof-of-principle of this method.

I would also like to thank the people at the Center for Neuroplasticity and Pain, Aalborg University, Denmark, for the opportunity to learn from them. It was a great pleasure to collaborate with Aida Poulsen, Jenny Tigerholm and Carsten

Dahl Mørch on their work for the development of novel electrodes for selective nociceptive stimulation.

Importantly, I also need to thank my colleagues at the Biomedical Signals and Systems (BSS) group for helping me in this project and providing a great working environment. First of all, I would like to thank Niels Jansen for always being there as a great sparring partner to work out our theoretical understanding of nociceptive processing and develop new ideas, and for being a great colleague and a good office mate. I would also like to thank Mohamed Irfan Mohamed Refai for being another great office mate and being great company for the many symposia, conferences, and summer schools we attended. I also need to thank the technicians Ed Droog, Marcel Weusthof and Frodo Muijzer, for providing great technical support and great lunch walk partners. I am also grateful for all the nice colleagues at BSS, Xenia, Kostas, Carlijn, Yang, and many others, for being great company during lunch walks, lunches, and Friday afternoon drinks. Especially, I would like to thank the Bachelor students, Marleen van Hoorn, Saumitra Athlekar, Sylvana Wijers, and Master students, Luca Marotta, Mindy Kasting, Giacomo Pezzali, Elisa Verhoeven, and Leen Vanwinsen, which I had the honor to supervise during the past years and contributed directly or indirectly to the studies presented in this thesis.

I would like to thank all the great friends who have supported me throughout this journey. I am grateful to Martijn, Niek, Maikel and Jelmer for joining me in awesome climbing and mountaineering trips, and to Martijn for being a great training buddy! I am also grateful to Ruurd, Ruben and other people from the Arque crew for the regular climbing trips to Berdorf and Freyr, and a great holiday to Kalymnos. I would also like to thank Maiju and Stijn (and now also Pekka), Kitso and Orgita, Francesco and Fanny, Vincent, Gerardo, and Marieke for the nice dinners and/or weekend trips.

Last but not least, I would like to thank my family. First of all, I am eternally grateful to my parents, Ebart, and Annemarie, for always having supported me and believed in me, my brother Marnix, for being a great example as a fellow scientist, and my sister Hanna, for being a great example of entrepreneurship.

I am grateful for my grandmother Erica and my grandmother Ger, firstly for being great grandmothers, and secondly for their support throughout the past 29 years. I would also like to thank Els and Moniek for their kindness and support, and Jan and Eefje for being amazing additions to the family. Finally, I am eternally grateful to my fiancée, Mariangela. Without her, my life would be infinitely less fun. Thank you, Mariangela, for always being there for me, supporting me and filling my life with joy!

Public Dissemination

Journal Publications

Published

Van den Berg, B., Vanwinsen, L., Pezzali, G., & Buitenweg, J. R. (2022). Observation of nociceptive detection thresholds and cortical evoked potentials: go/no-go versus 2-interval forced choice. *Attention, Perception, & Psychophysics*. (included as **Chapter 8**)

Van den Berg, B., Vanwinsen, L., Jansen, N., & Buitenweg, J. R. (2022). Real-time estimation of perceptual thresholds based on the electroencephalogram using a deep neural network. *Journal of Neuroscience Methods*, 374, 109580. (included as **Chapter 10**)

Poulsen, A. H., **Van den Berg, B.**, Arguissain, F., Tigerholm, J., Buitenweg, J. R., Andersen, O. K., Mørch, C. D. (2022). Novel surface electrode design for preferential activation of cutaneous nociceptors. *Journal of Neural Engineering*, 19(1), 016010.

Van den Berg, B., Manoochehri, M., Schouten, A. C., van der Helm, F. C. T., & Buitenweg, J. R. (2022). Nociceptive intra-epidermal electric stimulation evokes steady-state responses in the secondary somatosensory cortex. *Brain Topography*, 35(2), 169-181. (included as **Chapter 12**)

Van den Berg, B., Hijma, H.J., Koopmans, I., Doll, R.J., Zuiker, R.G.J.A., Groeneveld, G.J., & Buitenweg, J. R. (2022). Simultaneous measurement of intra-epidermal electric detection thresholds and evoked potentials for observation of altered nociceptive processing following sleep deprivation. *Experimental Brain Research*, 240(2), 631-649. (included as **Chapter 5**)

Van den Berg, B., Manoochehri, M., Kasting, M., Schouten, A. C., van der Helm, F. C. T., & Buitenweg, J. R. (2021). Multisine frequency modulation of intra-epidermal electric pulse sequences: a novel tool to study nociceptive processing. *Journal of Neuroscience Methods,* 353, 109106. (included as **Chapter 11**)

Van den Berg, B., & Buitenweg, J. R. (2021). Observation of nociceptive processing: effect of intra-epidermal electric stimulus properties on detection probability and evoked potentials. *Brain Topography,* 34(2), 139-153. (included as **Chapter 4**)

Van den Berg, B.*, Doll, R. J.*, Mentink, A. L. H., Siebenga, P. S., Groeneveld, G. J., & Buitenweg, J. R. (2020). Simultaneous tracking of psychophysical detection thresholds and evoked potentials to study nociceptive processing. *Behavior Research Methods,* 52(4), 1617-1628. (included as **Chapter 3**) **authors contributed equally*

Submitted

Van den Berg, B., Berfelo, T., Jansen, N., & Buitenweg, J. R., Psychophysical models for detection of single- and double-pulse electronociceptive stimuli: implications for interpretation of clinical observations. (included as **Chapter 9**) **to be submitted*

Berfelo, T.*, **Van den Berg, B.***, Krabbenbos, I.P., Buitenweg, J.R., Observing nociceptive detection thresholds and brain evoked potentials in persistent spinal pain syndrome type 2 patients. (included as **Chapter 6**) **authors contributed equally*

Conference Proceedings

Van den Berg, B., Berfelo, T., Verhoeven, E.M.H., Krabbenbos, I.P., & Buitenweg, J. R. (2021). Combining psychophysical and EEG biomarkers for improved observation of altered nociceptive processing in failed back surgery syndrome. Proceedings of the 43rd Annual International Conference of the IEEE Engineering in Medicine and Biology Society (EMBC), Guadalajara, Mexico. (included as **Chapter 7**)

Jansen, N., Dollen, R., **Van den Berg, B.**, Berfelo, T., Krabbenbos, I.P., & Buitenweg, J.R. (2021). Combined evaluation of nociceptive detection thresholds and evoked potentials during conditioned pain modulation: a feasibility study. Proceedings of the 43rd Annual International Conference of the IEEE Engineering in Medicine and Biology Society (EMBC), Guadalajara, Mexico.

Berfelo, T., Krabbenbos, I.P., **Van den Berg, B.**, Gefferie, S., & Buitenweg, J. R. (2021). Exploring nociceptive detection thresholds combined with evoked potentials in patients with diabetes mellitus. Proceedings of the 43rd Annual International Conference of the IEEE Engineering in Medicine and Biology Society (EMBC), Guadalajara, Mexico.

Van den Berg, B., & Buitenweg, J. R. (2018). Analysis of nociceptive evoked potentials during multi-stimulus experiments using linear mixed models. Proceedings of the 40th Annual International Conference of the IEEE Engineering in Medicine and Biology Society (EMBC), Honolulu, United States. (included as **Chapter 2**)

Van den Berg, B., & Wanders, I. (2016). Windowed factorization and merging. Proceedings of the 2017 Symposium on Information Theory and Signal Processing in the Benelux, Delft, the Netherlands.

Presentations

Van den Berg, B., Berfelo, T., Verhoeven, E.M.H., Krabbenbos, I.P., & Buitenweg, J. R. (2021). Combining psychophysical and EEG biomarkers for improved observation of altered nociceptive processing in failed back surgery syndrome. 43rd Annual International Conference of the IEEE Engineering in Medicine and Biology Society (EMBC), Guadalajara, Mexico.

Jansen, N., Dollen, R., **Van den Berg, B.**, Berfelo, T., Krabbenbos, I.P., & Buitenweg, J.R. (2021). Combined evaluation of nociceptive detection thresholds and evoked potentials during conditioned pain modulation: a feasibility study. 43rd Annual International Conference of the IEEE Engineering in Medicine and Biology Society (EMBC), Guadalajara, Mexico.

Berfelo, T., Krabbenbos, I.P., **Van den Berg, B.**, Gefferie, S., & Buitenweg, J. R. (2021). Exploring nociceptive detection thresholds combined with evoked potentials in patients with diabetes mellitus. 43rd Annual International Conference of the IEEE Engineering in Medicine and Biology Society (EMBC), Guadalajara, Mexico.

Van den Berg, B., Berfelo, T., Verhoeven, E.M.H., Krabbenbos, I.P., & Buitenweg, J.R. (2021), Improved classification of chronic pain patients using a random forest classifier. NeuroControl Symposium October 2021, Den Dolder, the Netherlands.

Van den Berg, B., & Buitenweg, J.R. (2021), Combined measurement of nociceptive detection thresholds and electrical brain responses for observation of nociceptive processing. Neuroplasticity and pain in the transition from acute to prolonged pain (FRESCO workshop at the Centre for Neuroplasticity and Pain), Aalborg, Denmark.

Van den Berg, B., Jansen, N., Berfelo, T., & Buitenweg, J.R. (2021), Neurophysiological observation of chronification: system identification concepts for effective pain treatment (NOCICEPT). NeuroControl Symposium May 2021, Virtual.

Van den Berg, B., M. Manoochehri, M. Kasting, A.C. Schouten, F.C.T. van der Helm, & Buitenweg, J.R. (2021). Multisine frequency modulation of intra-epidermal electric pulse sequences to study nociceptive processing: Methods and Limitations. 8th Dutch Bio-Medical Engineering Conference 2021, Virtual.

Van den Berg, B., Hijma, H.J., Koopmans, I., Doll, R.J., Zuiker, R.G.J.A., Groeneveld, G.J., & Buitenweg, J.R. (2020). Observing the effect of sleep deprivation on nociceptive processing by simultaneous tracking of detection thresholds and evoked potentials. IASP Virtual Series on Pain & Expo 2020, Virtual.

Berfelo, T., **Van den Berg, B.**, Krabbenbos, I.P., & Buitenweg, J.R. (2019). Observing electrical brain responses around the nociceptive detection threshold. 11th Congress of the European Pain Federation EFIC, Valencia, Spain.

Van den Berg, B., Manoochehri, M., & Buitenweg, J.R. (2019). Measuring physiological nociceptive and tactile steady-state evoked potentials. NeuroControl Symposium 2019, Berg en Dal, the Netherlands.

Berfelo, T., **Van den Berg, B.**, Krabbenbos, I.P., & Buitenweg, J.R. (2019). Monitoring electrical brain responses during processing of nociceptive stimuli around the detection threshold. Technical Innovations in Medicine Conference 2019, Utrecht, the Netherlands.

Van den Berg, B., & Buitenweg, J.R. (2019). Psychophysical and neurophysiological correlates of nociceptive paired-pulse facilitation. 7th Dutch Bio-Medical Engineering Conference, Egmond aan Zee, the Netherlands.

Van den Berg, B., & Buitenweg, J.R. (2018). Analysis of nociceptive evoked potentials during multi-stimulus experiments using linear mixed models. 40th International Conference of the IEEE Engineering in Medicine and Biology Society 2018, Honolulu, United States.

Van den Berg, B., Marotta, L., & Buitenweg, J.R. (2018), Neurophysiological observation of chronification: system identification concepts for effective pain treatment (NOCICEPT). Ageing Brain – Medical Sciences Summer School 2018, Groningen, the Netherlands.

Van den Berg, B., & Buitenweg, J.R. (2018). Linear encoding of detected and undetected nociceptive stimuli in evoked potentials. NeuroControl Symposium 2018, Soesterberg, the Netherlands.

Van den Berg, B., & Buitenweg, J.R. (2018). Efficient analysis of evoked potentials using linear mixed-effects regression. Technical Innovations in Medicine Conference 2018, Utrecht, the Netherlands.

Van den Berg, B., & Buitenweg, J.R. (2017). Generalized additive mixed-effects modeling of evoked potentials during multiple threshold tracking. NeuroControl Symposium 2017, Zeist, the Netherlands.

Boudewijn van den Berg was born in Gouda, the Netherlands, in 1993. He obtained his Bachelor degree in Biomedical Engineering cum laude and with honors in 2014 at the University of Twente, the Netherlands. In 2018, he received his Master degrees in Electrical Engineering and Biomedical Engineering from the University of Twente, with an emphasis on signal processing, computer vision, pattern recognition and machine learning in his curriculum. He was awarded with the University of Twente Graduation Award for the best Master thesis of the faculty of Electrical Engineering, Mathematics and Computer Science in the year 2018 for his work on the analysis of electroencephalography data using linear mixed models. Between 2018 - 2021, he pursued his PhD as part of the Dutch NOCICEPT project at the Department of Biomedical Signals and Systems at the University of Twente. During his PhD, he worked on the development of tools to observe neural processing of pain based on bioelectric brain signals and reported pain perception.